Synthesis and Characterisation of Low-cost Biopolymeric/mineral Composite Systems and Evaluation of their Potential Application for Heavy Metal Removal

THE UNIVERSITY OF
WAIKATO
Te Whare Wānanga o Waikato

A thesis
submitted in fulfilment
of the requirements for the degree
of
Doctor of Philosophy in Chemistry
at
The University of Waikato
by
ZAHIDA ZIA
2022

Abstract

Heavy metal pollution and waste management are two major environmental problems faced in the world today. Anthropogenic sources of heavy metals, especially effluent from industries, are serious environmental and health concerns by polluting surface and ground waters. Similarly, on a global scale, thousands of tonnes of industrial and agricultural waste are discarded into the environment annually. There are several conventional methods to treat industrial effluents, including reverse osmosis, oxidation, filtration, flotation, chemical precipitation, ion exchange resins and adsorption. Among them, adsorption and ion exchange are known to be effective mechanisms for removing heavy metal pollution, especially if low-cost materials can be used.

This thesis was a study into materials that can be used to remove heavy metals from water using low-cost feedstock materials. The synthesis of low-cost composite matrices from agricultural and industrial by-products and low-cost organic and mineral sources was carried out. The feedstock materials being considered include chitosan (generated from industrial seafood waste), coir fibre (an agricultural by-product), spent coffee grounds (a by-product from coffee machines), hydroxyapatite (from bovine bone), and naturally sourced aluminosilicate minerals such as zeolite.

The novel composite adsorbents were prepared using commercially sourced HAp and bovine sourced HAp, with two types of adsorbents being synthesized, including two- and three-component composites. Standard synthetic methods such as precipitation were developed to synthesize these materials, followed by characterization of their structural, physical, and chemical properties (by using FTIR, TGA, SEM, EDX and XRD).

The synthesized materials were then evaluated for their ability to remove metal ions from solutions of heavy metals using single-metal ion type and two-metal ion type solution systems, using the model ion solutions, with quantification of their removal efficiency. It was followed by experimentation using the synthesized adsorbents for metal ion removal in complex systems such as an industrial input stream solution system obtained from a local timber treatment company.

Two-component composites were considered as control composites to compare the removal efficiency of the three-component composites against. The heavy metal removal experiments were conducted under a range of experimental conditions (e.g., pH, sorbent dose, initial metal ion concentration, time of contact). Of the four metal ion systems

considered in this study (Cd^{2+}, Pb^{2+}, Cu^{2+} and Cr as chromate ions), Pb^{2+} ion removal by the composites was found to be the highest in single-metal and two-metal ion type solution systems, while chromate ion removal was found to be the lowest. The bovine bone-based hydroxyapatite (bHAp) composites were more efficient at removing the metal cations than composites formed from a commercially sourced hydroxyapatite (cHAp).

In industrial input stream solution systems (containing Cu, Cr and As), the Cu^{2+} ion removal was the highest, which aligned with the observations recorded in the single and two-metal ion type solution systems. Arsenate ion was removed to a higher extent than chromate ion using the three-component composites, while the removal of chromate ion was found to be higher than arsenate ion when using the two-component composites (i.e., the control system).

The project also aimed to elucidate the removal mechanisms of these synthesized composite materials by using appropriate adsorption and kinetic models. The adsorption of metal ions exhibited a range of adsorption behaviours as both the models (Langmuir and Freundlich) were found to fit most of the data recorded in different adsorption systems studied. The pseudo-second-order model was found to be the best fitted to describe the kinetics of heavy metal ion adsorption in all the composite adsorbent systems studied, in single-metal ion type and two-metal ion type solution systems. The ion-exchange mechanism was considered as one of the dominant mechanisms for the removal of cations (in single-metal and two-metal ion type solution systems) and arsenate ions (in industrial input stream solution systems) along with other adsorption mechanisms. In contrast, electrostatic attractions were considered to be the dominant mechanism of removal for chromate ions.

Acknowledgements

Alhamdulillah! I am thankful to almighty ALLAH for blessing me with good physical and mental health to pursue PhD studies, and I owe HIM everything.

I am incredibly grateful to the Higher Education Commission of Pakistan (Pak-HEC) for granting me a prestigious scholarship to support my doctoral degree.

I want to express my heartfelt gratitude to my chief supervisor, Associate Professor Michael Mucalo, who accepted my application for being the chief supervisor and supported me throughout my PhD research. Michael's subject knowledge and expertise in research methods helped me innovate and improve my research work. His timely and developmental feedback helped me improve individual chapters and the overall thesis during the thesis writing phase. He is an adorable person, with a smiling face and a kind aura. Dear Michael, I am immensely thankful for your guidance, valuable feedback, and continuous belief in me throughout my PhD studies. I am also equally thankful to my co-supervisor, Associate Professor Adam Hartland, for his guidance and valuable feedback.

I am also thankful to all the laboratory staff and technical persons (Helen Turner, Jenny Stockdill and Annie Barker) for providing technical assistance in characterising materials (using FTIR, SEM and XRD) whenever required. I pay special thanks to Annie Barker, as she not only helped me to run the AAS analysis, but her smiling face and positive energy always boosted me up whenever I faced difficulties in the experimental research processes. Thanks to Dr Amanda French and Danielle Blackwell for their help in the ICP-MS analysis, Paul Brown from School of Computing and Mathematical Sciences for his help in data analysis and Dr Megan Grainger for her expert advice on ICP-MS analysis methods. I am grateful also to a local wood treatment company in Rotorua, NZ for the supply of the industrial input stream solution containing copper, chromium- and arsenic-based based ions with which the composite matrices in this study were tested.

After ALLAH, I owe my parents (*Meri pyari Ammi or Abbu*) everything in this world and could not find enough words to pay my gratitude to them. They showered their unconditional love and always trusted, supported, and guided me through thick and thin. My father wanted me to become a doctor, and his wish was the strongest motivation to do my PhD studies. My father's demise was the biggest setback I faced during this journey (in July 2020), but I continued to finish my studies on time. I am sure he will be

extremely happy and proud in the heavens (Insha Allah) when I get my doctorate, Insha Allah.

I could not thank my husband, Muhammad Salman Rashid, enough for his love, support, and guidance. During this taxing journey, he was my prime support and comfort. He shaded me like a “kind cloud” whenever I felt myself under a ruthless sun; he sheltered me when I faced stormy events and guided me like a firefly whenever I lost my path. Thank you, Salman! I could not have done this without you. Your kindness and unconditional love were my powerhouses to regain my energy. You kept me positive and confident whenever I doubted myself. I love you and pray for your success. May Allah (SWT) bless you with the best of health and wealth.

I am thankful to my brothers (Shahzad and Masood (late)), my sisters (Hina, Fakhra and Guriya (late)) for decorating my childhood with their affections and being part of my life. I express my love and appreciation to my nieces (Haram, Fatima and Bakhtawar) and nephews (Ali, Fahad, Zaid, Junaid and Masood) for making me smile with their beautiful innocent moves.

In the end, I pay my heartfelt gratitude to my teachers, especially Dr Muhammad Shahid, Dr Faiq Siddique and Sir Siraj Asim (late), who always encouraged me to achieve this milestone of my life. I also express my love and gratitude to all my friends (especially Dr Amna khan, Sobia Tufail, Dr Shazré and Hudda Riaz) and family members (Amma Ji, Tariq Bhai, Sidra Aapa, Sadia Aapa and Ejaz Bhai) who were always there to have my back.

Thank you to everyone who played a direct and indirect role in achieving this important milestone in my life.

Dedicated to

the memories of My father Zia ul Haq (late) and brother Masood Zia (late), to whom I could not say the last goodbye

&

To my beloved husband Salman Rashid for his unconditional love and support during this whole journey.

Table of Contents

List of Figures

List of Tables

Chapter 1
Introduction

The general theme of the research described in this thesis is the development of novel composite matrices for treating water through the removal by adsorption of metal ions and specifically heavy metal ions such as lead or cadmium and others. The function of this introductory chapter is to include the background of the research undertaken to explain the research problem (i.e., heavy metal pollution in water). Secondly, it discusses conventional methods targeted at solving that problem (i.e., the removal of heavy metals) that have been in use for several years and describes the use of adsorption materials based on low-cost composite matrices from waste materials for heavy metal removal. It identifies some research gaps relating to possible composite matrix combinations valuable to achieving water treatment by adsorptive removal of metal ions. Further, it describes some of the well-known adsorption and kinetic models which are extensively used to describe the mechanism of heavy metal removal and estimate the maximum adsorption capacity of such adsorption systems and finally concludes by describing the aim of the research embodied in this thesis and the selection of materials studied in light of these aims.

1.1 Water and water pollution as an environmental issue

Human society development shows that access to good, clean water is one of life's necessities. As our global population grows, there is international concern regarding the availability of clean water. The cleanliness of water supplies, as contamination of waterways (primarily through anthropomorphic activities and natural ones), becomes a matter of survival for society as the global population grows[1]. In the last century, water use increased globally at a rate of more than twice the population increase. Currently, it is estimated that approximately 1.1 billion people have no access to clean water worldwide, while about 2.7 billion people face water scarcity for at least one month of the year. It has been estimated that two-thirds of the world's population may face water shortages by 2025, and the impacts of this shortage could be even worse for ecosystems[2] (Worldwide Fund, WWF). As an example of the effect of rapidly rising populations, the urban population of Asia and the Pacific region more than doubled between 1950 and 2000, creating a massive

demand for new and improved wastewater treatment systems. As of 2009, 30% of this region's urban population were reported to live in slums, with over half of the regional rural residents lacking access to adequate sanitation, compared to 25% of urban residents. In addition to the water demand from the agricultural sector, which is currently responsible for 70% of water extraction worldwide, significant water demand increases are predicted shortly, particularly in industry and energy production[3].

Many pollutants can make their way into essential water bodies and deteriorate drinking water quality[4]. One of the most persistent water contaminants of concern is heavy metals[5]. "Heavy metal" is a term that refers to elements of relatively higher atomic densities among metals that have toxic effects even at low concentrations[6]. A group of elements (metals and metalloids) having a density of more than 4 g $cm^{-3,}$ i.e. with densities at least five times greater than water, are generally referred to as "heavy metals"[7]. In wastewater, the metals commonly found include cadmium, arsenic, lead, chromium, nickel, mercury, zinc, silver, and copper. A significant challenge of water purification processes is the presence of these heavy metals in excessive quantities, making it difficult to clean water to an acceptable level. Heavy metals originate from the earth's crust and are persistent contaminants in the environment due to their non-degradative properties. Bioaccumulation of heavy metals in any living body occurs in tiny quantities of soil, water, and food over a long period[6,8]. It can lead to serious consequences if these heavy metals exceed the permissible limits required to maintain the environment safe.

1.2 Sources of heavy metal pollution

Two primary sources of heavy metal contamination are described, including 1) natural and 2) anthropogenic sources. In anthropogenic sources, mining is considered the primary source of heavy metal emissions into the environment[9-11]. Heavy metal pollution can be prevalent in areas with excessive mining operations, and this pollution decreases with distance from the mining sites[12]. Acid mine drainage (AMD) is a phenomenon that generally happens in certain areas due to mining activities and geochemical processes. The AMD can produce metal ions, acidity, or a concentration of sulphate ions in the water body concerned[13]. The leaching of heavy metals from soil makes its way into streams through acidified water sources, facilitating the dissolution of heavy metals into their ions. These heavy metals can be converted into organometallic forms such as mono-methylmercury or

dimethyl-cadmium by bacterial action. Toxicity and non-biodegradability are the two significant characteristics of heavy metals, making them persistent in wastewater[14]. The major sources of heavy metals in the environment include volcanic eruptions, erosion, aerosols, and urban runoff. Dangerous heavy metal impacts from volcanic activity on the environment, climate and human health have also been reported. Volcanic eruptions can cause rapid deterioration of social and environmental conditions. The activity can release different air pollutants (e.g., hydrogen sulphide, carbon monoxide, carbon dioxide, sulphur dioxide), organic compounds (e.g., volatile halogenated compounds), and heavy metals (gold, lead, and mercury). The quality of water is hence affected adversely due to this sudden infusion of heavy metals. Volcanic rock erosion represents a critical source of heavy metal pollution in soil and water. This natural contamination can be an unavoidable source of heavy metals in the environment, with the metals making their way into natural waterways[15], where they accumulate and persist for very long periods and become distributed.

The metals commonly found in the environment (soil and water mainly) include cadmium, arsenic, lead, chromium, nickel, mercury, zinc, silver, and copper. It is crucial to treat industrial effluents before they can enter any water body from which potable water is extracted (i.e., lake, river or groundwater) or where aquatic life thrives. The contamination can be the leading cause of severe waterborne diseases, and medical problems like accelerated cancers of the kidney and liver can lead to organ failure[16]. Additionally, recycled and treated wastewater could be considered a potential water source for industrial and agricultural activities. A significant challenge of water purification processes is when these heavy metals in water are high, making them difficult to clean to the extent of providing potable water. This research focuses on removal strategies (in the form of materials) of some of the major heavy metals which can cause severe environmental damage from their excessive intrusion into the water bodies (such as rivers and lakes). The following section discusses the heavy metal ions targeted in this research project.

1.3 Major heavy metals included in this research and their sources

1.3.1 Arsenic (As)

Arsenic (As), a metalloid, and its inorganic compounds are highly poisonous and are classified as a Group 1 carcinogenic by the International Agency for Research on Cancer.

They hence pose a serious health concern for humans[17]. Chronic exposure to As present in drinking water may cause arsenicosis. Worldwide, a total of about 130 million people in different countries of the world, such as India (40 million), Bangladesh (>30 million exposed people), the United States (2.5 million) and China (1.5 million), are exposed to concentrations > 50 μg L^{-1} of this element[18]. Arsenic is a developmental neurotoxicant that affects brain functioning such as IQ and memory in adults and children[19,20]. In New Zealand, arsenic is also widespread in terrestrial and aquatic environments sourced by geochemical activities. In the Taupo volcanic zone (TVZ) in the North Island of New Zealand, some lakes and rivers contain As at levels exceeding the World Health Organisation (WHO)-permissible limit of 0.01 mg L^{-1}. Arsenic is abundant in all geothermal areas and waterways of the TVZ, which extends from Mt Ruapehu to White Island in the North Island of New Zealand[21]. In the Waikato river, the longest river in New Zealand, arsenic levels mostly exceed the WHO limit recommended for drinking water, i.e. > 0.01 mg L^{-1} [21]. In Pakistan, the Punjab and Sindh provinces also have water contaminated with more than 50 μg L^{-1} in 3% and 16% of their respective natural water resources[21]. Mineral dissolution, desorption occurring via redox chemistry and geothermally influenced groundwater are the significant sources of arsenic contamination in affected waterways[22]. The timber industry is another primary source of As because it is used as a timber preservative in a so-named copper-chromium-arsenate (CCA) cocktail[23]. The wastewaters generated in this industry have high As concentrations that require treatment costs before discharge into the environment. Otherwise, it can contaminate the water bodies if the effluents are discharged without proper treatment. Coal ash disposal sites and the mining industry are also sources of contamination in New Zealand, albeit to a lesser extent[24,25].

1.3.2 Cadmium (Cd)

Cadmium (Cd) is another heavy metal of concern because of its toxicity which destroys red blood cells in the body, causes bone fractures, renal disorders, high blood pressure and kidney damage[26]. Major cadmium sources include mining and electroplating industries, phosphate fertilizers, batteries, stabilizers, pigments and alloys[27]. In New Zealand, the main point of concern regarding cadmium contamination emanates from fertilisers imported from overseas, which are applied to soil for augmenting pasture growth. The average cadmium content in phosphate fertilizers is estimated to be 180 mg Cd kg^{-1} P from 2001 to

2005 in New Zealand. This has led to an accumulation of Cd in the soils of New Zealand, which makes it a matter of national concern with respect to possible food contamination that may breach food standards in New Zealand and overseas[28]. A significant amount of bioavailable Cd has been reported in the Waikato region due to the typically acidic nature of Waikato soils. For instance, in topsoil, the maximum net accumulation rate of Cd was reported[29] to be 18.3 μg kg^{-1} $yr^{-1,}$ while the net average accumulation rate of Cd was recorded to be 9.0 μg kg^{-1} yr^{-1}. In New Zealand pastoral soils, the mean concentration of Cd was reported as 0.43 mg $kg^{-1,}$ which is more than twice the natural background levels of 0.16 mg kg^{-1} [30].

Regarding waterway contamination, soil leaching is a possible way for cadmium to enter water bodies by washing out from the surface of the soil, posing a potential health risk. For the reduction of applied cadmium into the soil by superphosphate application, agriculturalists voluntarily limit the amount of fertiliser application so that the net amount of Cd is 280 mg Cd kg^{-1} P. It is estimated that superphosphate application accounts for an average of 8.3 tonnes of cadmium applied annually according to a report prepared by the Waikato Regional Council (New Zealand) in 2005 on cadmium contamination of agricultural soils of the region. As stated, this can eventually enter the water supply; hence there is an urgent need to determine ways of removing this potentially toxic element from the water. This could be achieved by subjecting any potentially contaminated water to suitable water treatment matrices.

1.3.3 Lead (Pb)

Lead (Pb) is a globally well-known toxic material that is extensively distributed and mobilized in soil and water. Although a non-essential element, its exposure and uptake in the human body have increased, causing serious health concerns. Anthropogenic sources primarily cause lead dispersion in the environment, including mining and smelting of ores, lead-containing products, coal and oil combustion, and incineration of waste. In the past, Pb-containing antiknock additives in petrol sold in New Zealand also contributed to environmental pollution from this element. Rain removes the lead present in the air in the form of particles that settle down gravitationally on the upper layer of soils. Natural sources such as windblown dust, volcanic activity and erosion can also contribute minor additions of lead to the environment. Mining and smelting of lead ores are the primary industrial sources of lead in the environment globally. Air is polluted by lead when the flue gases of

electrical utilities are emitted. For instance, a lignite fuel having $4.2x10^{-4}$ pounds of lead/ton of coal can emit about 420 pounds of lead when a million pounds of lignite coal is burned[31]. Aquatic pollution of lead is reported from lead production and processing and from iron and steel industries which emit lead into the air[32]. Atmospheric depositions bring this Pb to land, and urban runoff pollutes the water bodies. Lead poisoning can cause renal diseases, reproductive toxicity and neurological disorders[33]. In growing children, Pb was found responsible for preventing the absorption of iron, calcium, and zinc minerals into the blood, which are necessary minerals for developing nerve and brain function. The existence of violent behaviour in criminals has been linked to childhood lead exposure by medical researchers[34-36]. Several studies link attention deficit hyperactivity disorder (ADHD), aggression, delinquency, and destructive and criminal behaviour with elevated bone or blood lead levels[34,35,37]. Its removal from water bodies destined for human ingestion or that involved in hosting or producing food for animal or human consumption is hence vital.

1.3.4 Chromium (Cr)

Chromium (Cr) is a transition element and a heavy metal used extensively in industry. Metallic chromium is used to make steel, while its ionic forms Cr (III) and Cr (VI) are used in wood preservation, dyes and pigments, chrome plating and leather tanning. Among these forms, Cr (VI) is regarded as the most toxic form because of its carcinogenicity[38]. In New Zealand, leather is the seventh-largest industry in the country. Tanning is an essential part of leather processing. Yearly, about 2.5 million lambskins are tanned. Chemical processing in the leather industry uses water as a primary solvent, which adds chromium to wastewater outputs from the leather industry.

Most wastewater generated by tanneries is discharged into sewerage systems treated with other domestic water inputs. Chromium is challenging to treat in wastewater streams due to the many organic and inorganic pollutants that can interfere with the removal agents or surfaces to reduce extraction efficiency. Furthermore, chromium is undesirable in sewerage inputs because it is toxic to the microbes used to treat sewage. The other drawback of Cr in sewerage water is its conversion into chromium oxide compounds at neutral pH, which precipitate out and become part of the sewage sludge. Its presence in sludge makes it undesirable for using this waste product as an applied agricultural fertiliser. Hence, there is a need to treat industrial effluent for Cr removal *before* allowing it to enter sewerage systems[39].

1.3.5 Copper (Cu)

Copper (Cu) is a heavy metal of group IB in the periodic table with an atomic number 29 and a density of 8.96 g cm^{-3}. It is soft and malleable and has high electrical and thermal conductivity[40]. It takes part in several physiological processes in plants growth, including photosynthesis, oxidation, and cell wall metabolism. In plants, high Cu levels can lead to Cu toxicity, causing DNA and enzyme malfunctions, resulting in growth inhibition[41]. In humans, it is an essential micronutrient necessary for the growth of connective tissues and iron metabolism (Fe). Chronic Cu toxicity in humans can cause liver damage, while acute intoxication can lead to gastrointestinal problems[42].

High concentrations of Cu in the environment are harmful to organisms. It enters the environment through natural and anthropogenic sources. Natural sources of Cu pollution include volcanoes, forest fires, windblown dust, and vegetation decomposition. Anthropogenic sources involve Cu mining, domestic wastewater, fertilizer, and other industries such as batteries, pigments, and paint, which use Cu and Cu products. About 939,000 metric tonnes of Cu have been released into the environment in the past decades[43]. Cu enters the aquatic system through mine fly ash disposal, industrial wastewater and solid and municipal waste disposal[44]. Copper pollution in the soil is a secondary source of Cu in water bodies added via stormwater. The contaminated soil and water can cause Cu toxicity in plants and ultimately in humans if it exceeds a permissible limit in water and edible plants. It is crucial to control Cu pollution by treating wastewater before its disposal in water bodies. The above-mentioned heavy metals were selected as candidate metal ions in this research in which adsorption systems made from low-cost composites synthesised in this study were designed for their removal from aqueous solutions.

For the removal of metal ions, several conventional methods have been used, which are described in the following section.

1.4 Wastewater treatment and conventional heavy metal removal methods

Due to growing populations and the scarcity of potable water, there is a growing recognition that wastewater needs to be used as a water resource for different sectors. However, an estimated 80–90% of all wastewaters produced in the Asia and Pacific region are released untreated, polluting ground and surface water resources and coastal

ecosystems. A shift to using treated wastewater in different sectors, such as agriculture, is a growing trend[45], so there is a need to find out sustainable ways by using appropriate environmental technologies for treating wastewater for its potential reuse in such sectors.
Many conventional and novel treatments are being applied to remove heavy metals, including coagulation, chemical precipitation, adsorption, ion exchange, complexation, electro-deposition, and membrane operations.

Coagulation and flocculation may be simple methods to use superficially. Still, the major drawbacks include the use of excess materials and toxic solid waste generation, which are challenging to handle and not appropriate to dispose of in the environment. Electro-deposition represents a somewhat unfavourable method due to the need to use electricity, making it very costly for water treatment.
Ion exchange is an effective technique to remove heavy metal ions as it uses low-cost materials to prepare ion-exchange chambers. Still, its success in use is critically dependent on pH, which is a drawback for the technique[46].
Chemical precipitation involves using hydroxides or limes to coagulate and flocculate the dissolved pollutant. It requires adjusting the water media to specific pH values depending on the metal ions precipitated from the water[47].
Biologically based techniques such as the use of *microorganisms* for the removal of heavy metals also exist. *Activated sludge, trickling filters, stabilization ponds, and lagoons* are commonly used biological methods to treat industrial water, constituting relatively cheap removal methods and slow and inefficient ones. Adsorption is found the most appropriate due to simple operational procedures and low cost[48].
Among the existing treatment methods for wastewater treatment, particularly for heavy metal ions removal, adsorption is considered the most efficient, environmentally sustainable, economically feasible, and simple method[1]. In particular, the use of low-cost materials from the industrial and agricultural by-products, which are discarded into the environment, provides a promising source to synthesise low-cost adsorption systems for removing heavy metal ions from aquatic systems. Among these low-cost materials, several agricultural by-products such as rice straw and husk, maize cob, wheat straw, coconut fibre, and coconut pith have been successfully employed for heavy metal ions removal. Lignocellulosic (such as coir fibre and spent coffee grinds (SCGs) and biopolymeric materials (such as the chitosan) have also been employed and showed good potential for

heavy metal removal, as the constitutional functional groups of these materials, which include amidic, alcoholic, carbonyl, phenolic, and amino moieties possess high affinities for heavy metal ion immobilisation by chemical complexation[49]. The mechanisms of metal-complex formation by such functional groups present in the selected materials will be discussed in section 1.6.

1.4.1 Adsorption- as a promising wastewater treatment method

Adsorption is defined generally as the surface phenomenon in which adsorbate molecules are accumulated via binding to the surface of an adsorbent. The adsorption process can be explained by the chemisorption of adsorbate molecules using simple equations[50]. In 1918, Langmuir explained chemisorption by demonstrating the adsorption process of adsorbate on a surface with a limited number of adsorption sites (S). The bare sites (S_0) could be given as:

$$S_0 = S - S_1 \qquad (1\text{-}1)$$

In equation 1-1, S_1 is given as the sites occupied by the adsorbate molecules. Adsorption equilibrium is a dynamic state when the rate of adsorption is equal to the rate of desorption. The adsorption rate is non-activated and proportional to the frequency of the collisions between the adsorbate molecules and bare sites, and this collision frequency is proportional to the pressure P, so the rate of adsorption could be taken as follows:

$$\text{Rate of adsorption} = k_2 P S_0 = k_2 P (S - S_1) \qquad (1\text{-}2)$$

While the rate of desorption is proportional to the S_1 (number of occupied sites):

$$\text{Rate of desorption} = k_1 S_1 \qquad (1\text{-}3)$$

By taking the two rates to be equal, from equations 1-2 & 1-3, and then solving for S_1, the following equation 1-4 is obtained:

$$\frac{S_1}{S} = \theta = \frac{bP}{1 + bP} \qquad (1\text{-}4)$$

In equation 1-4, the fraction of surface coverage is equal to θ, and the k_2/k_1 equals b. The limiting value (ν_m) corresponds to θ =1, which means the ν/ν_m would be equal to θ, so the equation 1-4 could be re-written as follows:

$$\nu = \frac{\nu_m bP}{1 + bP} \qquad (1\text{-}5)$$

Equation 1-5 is known as the Langmuir isotherm model. It will be covered further in upcoming sections regarding the adsorption of heavy metal ions on solid-phase adsorbents from aqueous solutions (in section 1.7).

The rate of adsorption can be slow, depending upon the temperature. It could be increased by increasing the temperature, which indicates activation energy for the adsorption process. So, the adsorption would not be reversible in some cases. The better-performed adsorption systems exhibit a rapid adsorption process, and there will always be an equilibrium amount of adsorption for each adsorbate pressure. The *adsorption isotherm* is plotted as the amount of adsorbate adsorbed (denoted by υ) versus the pressure. In a normal adsorption process, the adsorbed amount of adsorbate (υ) increases with increasing the pressure of gas molecules (or concentration of metal ions) and approaches a limiting value υ_m, while decreasing by increasing the temperature but keeping the pressure constant[50].

The nature of interaction or bonding between the adsorbate (i.e. the metal ions) and the adsorbent (the substrate on which the adsorption would occur) depends upon the type of the species (adsorbate and adsorbent) involved in the adsorption process[51]. Broadly, the adsorption mechanisms are described as physisorption (physical adsorption) and chemisorption (chemical adsorption).

Physical adsorption is described as a non-specific binding process that does not involve specific functional groups in the adsorption of molecules on the adsorbent surface. It is reversible in nature due to the weak interactions (Van der Waals forces) involved. The Van der Waals forces are weak electric forces that allow the molecules of adsorbate and adsorbent to adhere to each other. When the adsorption cannot be explained by electrostatic or chemical interaction, it is classified as physisorption by these weak forces[52]. Hydrogen bonding could also be involved in the weak interaction of physisorption[53].

Chemical adsorption (chemisorption) is irreversible and very specific and describes a chemical interaction between the adsorbate and adsorbent molecules in terms of new bond

formation[54]. In contrast with physical adsorption, chemisorption involves (stronger) chemical interactions (or valence forces) by forming new bonds (e.g. covalent bonds) between the sorbate and sorbent molecules, which take part in the process of adsorption[55]. Generally, the adsorption is characterised as chemisorption when the activation energy is more than 20-30 kJ mol^{-1}. Metal-complexation (also termed metal-chelation) is described as a well-known mechanism for the removal of heavy metals and can also be classified as chemisorption. The detailed mechanism of metal-complexation is described in the upcoming section (1.6.2). The functional groups of lignocellulosic and biopolymeric adsorbents are reported to adsorb heavy metals by this mechanism.

Ion exchange (adsorption) on the surface of adsorbents is also included as a principal mechanism along with chemisorption for metal ion removal. The ion-exchange mechanism is described for the adsorption process, especially when involving the exchange between metal ions in aqueous solutions with ions present on the surface of inorganic adsorbents (minerals). Ion exchange is a reversible phenomenon (but not physical adsorption), which involves electrostatic interactions and could be stated as electrostatic adsorption[53]. Ion-exchange mechanisms can involve both cation and anion-exchange[56]. For instance, the ion-exchange mechanism is extensively reported for Pb^{2+} (a cation) which can exchange with the Ca^{2+} ions of HAp when HAp is used as an adsorbent for the removal of metal cations from aqueous solutions.

Similarly, arsenate (AsO_4^{3-}) is a water pollutant that is also removable by an ion-exchange mechanism by exchange with phosphate anions (PO_4^{3-}) present in hydroxyapatites. Potential adsorbents used for the removal of heavy metal ions are selected based on their potential to participate in the above-mentioned adsorption mechanisms.

Several characteristics of adsorbents make them valuable for applying heavy metal ions removal and are described as follows.

1.4.2 Characteristics of model adsorbents for the removal of heavy metal ions from the aqueous solutions

Adsorption using low-cost adsorbents is a sustainable solution for heavy metal removal. When using adsorption as an option for the removal of heavy metal ions from wastewater, the ideal adsorbent should have the following characteristics, namely:

- High adsorption capacity and large surface area

- Compatibility and mechanical stability
- High selectivity
- Cost-effectiveness and environmental friendliness

Adsorption capacity (or loading) is the amount of adsorbate taken up by the adsorbent per unit mass (or volume) of the adsorbent. It generally depends upon the nature of the adsorbent used or surface areas of the adsorbent[57]. For example, activated carbons are known to be materials that possess large adsorption capacities for treating wastewater due to their high surface area[58].

The surface area of the adsorbent is an important parameter to consider in studying this process, as adsorption is a process that depends on the surface area available. Highly porous engineered adsorbent materials generally have a surface area ranging from 10^2 to 10^3 m^2/g [59]. The surface area of an adsorbent influences adsorption capacity in that an adsorbent with a high surface area should have a higher adsorption capacity[60,61].

The mechanical stability and compatibility of adsorbents to apply in wastewater treatment systems is also a critical factor to consider. Wastewater treatment systems are complex and diverse because they contain various pollutants and are subject to variable environmental conditions. For instance, the pH values and temperature of the wastewater system could affect the adsorbents by dissolving them and ultimately affecting their removal efficiencies. The compatibility and stability of the material could be regulated by pre-treatment of the wastewater (by adjusting the pH or temperature) or by modification of the adsorbent materials, which could also assist in increasing the applicability of the potential material to water treatment systems. For this, the combinations of more than one material have been studied to improve the applicability of materials in wastewater treatment. For instance, hydroxyapatite has been used to make composites with chitosan and cellulosic materials to increase the removal efficiency of these materials[62]. Alternatively, the addition of chitosan to HAp in the form of a composite increases its applicability in fixed bed column systems where the powdered HAp causes pressure drops due to the high packing density of powdered material[63].

High selectivity is an important feature of the adsorbent for it to be an efficient removal agent of metal ions from the wastewater treatment systems. The presence of other chemical species (metal ions) could affect the adsorption of targeted metal ions. For instance, the removal of targeted cations such as Pb^{2+} and Cd^{2+} could be compromised by the presence

of other positive ions such as protons H^+, Na^+ and $Mg^{2+,}$ which could occupy the binding sites on the adsorbent surface and so decrease the removal efficiency of the adsorbents for the targeted metal ions[64].

Materials with ion-exchange abilities (e.g., HAp and zeolites) could favour cations (e.g., Pb^{2+}) adsorption. Lignocellulosic materials such as coir fibre and spent coffee grounds could be considered for the availability of negatively charged functional groups such as carboxyl and hydroxyl groups. Additionally, the HAp could be used in a composite with these materials to provide an additional removal mechanism (i.e., that of ion exchange) along with the electrostatic interactions and complexation. In this way, the removal ability of the lignocellulosic composite materials could be enhanced by adding the HAp to provide binding sites for ion exchange, particularly for cation removal.

Cost-effectiveness and environmental friendliness of materials are the most critical factors for selecting adsorbent materials for the adsorption of heavy metals ions. The cost of the raw materials and design of water treatment systems should be at a minimum to run an economically feasible water treatment system. For this purpose, agricultural and industrial by-products could be considered a potential resource for making adsorbents. The by-products could be selected by doing the literature review and by selecting the materials constituted with the functional groups that could participate in the aforementioned mechanisms (see *section 1.4.1*) for the effective adsorption of heavy metal ions.

1.4.3 Selection of candidate materials for synthesising the adsorbents for the heavy metal ions removal from aqueous solution

For this project, the raw materials chosen for synthesising adsorbents for heavy metal ion removal were selected after extensive literature research (summarised in section 1.5). The characteristics of the ideal adsorbents (*section 1.4.2*) were focused on selecting the materials for the synthesis of adsorbents. It was confirmed that the chemical composition of the selected raw materials effectively removes the heavy metal ions from the aqueous solution, as supported by literature studies. The materials which were selected include:

- Hydroxyapatite
- Chitosan
- Coir Fibre
- Spent coffee grounds (SCGs)

- Zeolite

The detailed literature review that provides the rationale for the selection of these materials is presented in section 1.5. Generally, all the materials represent potentially very low-cost matrices as most of them (i.e., chitosan, coir fibre and spent coffee grounds) are generated in excess as industrial or agricultural by-products. Similarly, zeolite is an aluminosilicate mineral that is plentiful in New Zealand. Hydroxyapatite is also an abundant calcium phosphate mineral that could be synthesised chemically or able to be sourced from mammalian bones (by-products of the meat industry).

Apart from the low cost of these materials, all of these materials can potentially remove heavy metal ions from aqueous solutions. The composition of these candidate materials (studied and confirmed by their detailed characterisation described in section 1.5) means they can act as effective adsorbents.

Generally, the hydroxyl groups (in all selected materials), amino and acetamide (chitosan), carboxyl (coir fibre), and phenolic groups (SCGs) can form metal-ligand complexes with the metal cations. Similarly, the cations of HAp and zeolite ($Ca^{2+,}$ Na^{+}, K^{+} and Mg^{2+}) can ion-exchange with the heavy metal cations ($Pb^{2+,}$ Cu^{2+} and $Cd^{2+)}$ found in aqueous solutions. Additionally, the phosphate groups of the hydroxyapatite could be potential sites for the anion exchange for arsenate ion due to their chemical similarity.

Most of the literature studies (discussed in section 1.5) concerning heavy metal ion removal discuss the combination of different materials into composite matrices to improve the metal ion removal efficiencies and increase the applicability of the materials in the water treatment systems.

1.4.4 Composite matrices to remove heavy metal ions from aqueous solutions

Composites: A composite is defined as a combined matrix of two or more materials with a unique set of properties. All the constitutional components of the composite matrix retain their fundamental characters while being a part of the composite. Composites are also explained as being heterogeneous multi-phase materials, which could be considered homogenous materials on a microscopic level due to the exhibition of similar physical properties[65-67].

In composites, one or more *discrete phases* (usually more complex materials such as fibres) are embedded in a *continuous phase* to obtain a superior material (a composite) than its

constituent material in terms of properties. The material that forms the continuous phase of the composite is present in a higher quantity and termed "matrix". The discrete phase is used to reinforce the composite material to improve its mechanical properties and is usually made up of fibrous material consisting of lignin, pectin and cellulose or biopolymeric materials.

1.4.5 The low-cost candidate material to synthesise composites for heavy metal ions removal

The stability and cost of material synthesis are challenges in the rapidly growing composite materials market, especially in wastewater treatment. So, achieving minimum cost to synthesise the composite systems for the effective removal of the metal ions was one of the most fundamental aims of this study, as described earlier. For this, biocomposites, using at least one bio-sourced material from an agricultural or industrial by-product, were selected to synthesise the adsorbent systems. The low cost of the materials was justified as they were bio-sourced materials, which originate from agricultural or industrial by-products, and are produced in bulk, which ultimately lowers their cost.

Additionally, most of the candidate materials selected for this study (such as chitosan, coir fibre and SCGs are normally regarded as discarded by-products; however, their employment in water treatment systems renders them beneficial. The double-fold benefit is achieved by employing these materials as safe disposal or discarding of these materials traditionally requires an additional cost which could then be avoided or minimised as a consequence. The effective management of the selected industrial and agricultural by-products could be one potentially beneficial side goal of this study, which is ultimately associated with their fundamental role in removing heavy metal ions from aqueous systems. The naturally sourced materials (e.g., zeolite minerals, which also justify the low cost, as they are available in bulk quantities due to local availability) and easy availability of agricultural and industrial by-products such as the CF and SCGs, make them attractive for composite preparation in heavy metal removal. Another source material is the biopolymeric polysaccharides studied widely for synthesizing adsorbents[68], which explains why chitosan was selected for this study.

1.4.6 Supporting literature to justify the addition of a third component into the CH/HAp composites

As mentioned above in the definition of composites, the discrete phase of the composite could include more than one material to add into the continuous phase. A third component added into the CH/HAp composite as additional material with chitosan (discrete phase) to enforce the continuous phase (HAp) was considered in this study. It was hypothesized that the addition of the third component could provide additional mechanical strength as the lignocellulosic materials (e.g., CF and SCGs) were considered to provide mechanical strength to the chitosan and HAp. Moreover, it was assumed that the addition of the third component could also enhance the removal efficiency of the CH/HAp composites. For instance, the zeolites were selected to add into the CH/HAp composites by assuming that the zeolites would provide the additional binding sites for the ion exchange of metal cations as literature studies into the ion-exchange abilities of the zeolites are well established. These hypotheses were based on the literature review (discussed in section 1.5), while the summary is given below.

Chitosan is one of the most widely used polysaccharides in water treatment due to its relatively greater natural abundance, biodegradability and non-toxicity (details in an upcoming chapter)[69] and found to be a promising adsorbent for metal removal due to the presence of hydroxyl and amine groups which provide active sites for metal adsorption[70,71]. However, there are some challenges to using chitosan directly in water treatment applications, such as low mechanical strength and dissolution in acidic media pH < 4)), which require some modifications to the chitosan before its use. Cellulosic materials have been studied extensively for strengthening the chitosan for increasing its applicability in low-cost wastewater treatment systems. For instance, commercially available microcrystalline cellulose has been extensively used to make a composite with chitosan for the purpose of its reinforcement, resulting in higher-cost materials. Similarly, Rahmi et al.[72] reported using palm-oil extracted cellulose to reinforce chitosan with the composite being used to remove Cd(II) ions. The cellulose used in this composite led to improved strength in the material. The results indicated that the increase in the tensile strength of chitosan was about 10% in part due to the inclusion of cellulose. The increase in mechanical strength was mentioned as the immobilization of the chitosan molecules and the presence of cellulose[73], which is made possible due to the excellent adhesion between

the two components via hydrogen bonding. The use of nano-cellulose to form chitosan and cellulose blends has also been reported to lead to a reinforced chitosan composite with the material[74].

Similarly, lignin, pectin, cellulose and hemicellulose-based biomaterials (such as coconut husk and coir pith) are other prominent examples studied for their adsorptive characteristics for several solutes, especially for the adsorption of metal cations[75]. These literature studies provide the foundation knowledge for selecting low-cost lignocellulosic materials such as the CF and SCGs to add into the CH/HAp composites to provide mechanical strength to these composites. These materials (CF and SCGs), as stated previously, also have adsorptive abilities related to the functional groups in their structures which can improve removal efficiency with respect to metal ions. The following sections are a detailed literature review of these candidate materials to show how the employment of these materials in heavy metal ion removal systems has proven worth.

1.5 Literature review of selected candidate materials used in this study to synthesise the composite adsorbents

1.5.1 Hydroxyapatite

Hydroxyapatite (HAp) or $[Ca_{10}(PO_4)_6(OH)_2]$ is a naturally occurring, non-toxic mineral from the apatite mineral family, which is the major inorganic component of bone and teeth. It possesses a hexagonal structure with a Ca:P mole ratio of 1.67 and is thermodynamically the most stable calcium phosphate to form under different physiological conditions (pH, temperature etc.)[76].

Calcium hydroxyapatite (HAp) is a promising material for metal ion removal from wastewater owing to several favourable characteristics such as its high adsorption capacity, low solubility in water, easy availability, low cost and chemical stability under redox conditions[77]. It has been shown to have high removal efficiency, especially for divalent metallic ions such as Cd(II), Cu(II), Pb(II), Zn(II) and Fe(II)[78]. There is extensive research demonstrating the application of HAp as an effective adsorbent for removing heavy metals from aqueous solutions.

In the literature studies, two types of calcium hydroxyapatite are discussed for the heavy metal ions removal, including the synthetic (or chemically sourced HAp synthesised using chemical reagents) and bio-sourced HAp (from animal bones). The following section

describes the literature studies for both types of HAps and their application in heavy metal ion removal systems.

1.5.1.1 Inorganic sourced hydroxyapatite for heavy metal ions removal

Phosphogypsum (calcium sulfate hydrate having a formula $CaSO_4.2H_2O$) is a mineral source of hydroxyapatite, with the phosphogypsum being used as a feedstock to prepare nano-sized HAp (n-CaHAp, particle size 50-57 nm) by using a method previously described by Mousa and Hanna[79]. The HAp synthesised using this mineral source (phosphogypsum) was applied to remove Pb(II) ions from model solutions of the lead salt. The removal efficiency of about 98.1% for Pb(II) was attained when the experiment was conducted in a pH range between 4.5 and 5.5. It was noted that the removal of Pb(II) increased gradually as solution pH was raised from 1.0 to 4.5, with removal efficiency stabilizing between pH 4.5 and 5.5. At pH values < 4.4, HAp is known to dissolve, and it was shown in this study that the dissolution of HAp was 49% at pH 1.0 but only 16% at pH 2.0, which affected the removal efficiency. At pH 3.0, there was no effect on removal efficiency from the dissolution of HAp. It was concluded from here that the adsorption might be suppressed at lower pH so, negatively affecting the adsorption of Pb(II)[80,81]. Moreover, it was revealed that the surface of n-HAp is predominantly positively charged at pH <3 which repels Pb(II) ions and decreases the adsorption, while above pH values of 3, the surface of the adsorbent is negatively charged so, favouring Pb(II) ion adsorption. Another study confirmed a similar effect of pH on Pb^{2+} ion adsorption by nanohydroxyapatite (i.e. nanorods of HAp), which reported 100% removal of lead from 200 mL of metal solution (100 ppm) at pH 5.6[82]. An electrostatic force of attraction between the adsorbent and adsorbate was described as a possible reason for the favourable adsorption for heavy metal removal[83] in the case of cationic heavy metal ions. Another study was done to evaluate the adsorption behaviour of nano-hydroxyapatite to remove Cd^{2+}, Ni^{2+} and Pb^{2+} using model solutions of (100 to 400 mg L^{-1}) of the heavy metal salt.
Some studies reported the use of chemically synthesised HAp in metal adsorption systems. For instance, the hydroxyapatite nanocrystals prepared by a simple precipitation method showed maximum adsorption of 1000, 142.857 and 40 mg g^{-1} on nano-hydroxyapatite for Pb^{2+}, Cd^{2+} and Ni^{2+} ions, respectively[84]. The Lewis acid-base concept can explain the higher removal of Pb^{2+} as compared to other divalent cations. The adsorbent contains hard Lewis bases (i.e., OH^-, PO_4^{3-} groups), which show a higher affinity for a hard Lewis acid

such as Pb^{2+} than for metal ions such as Ni^{2+} and Cd^{2+}, which are softer Lewis acids. It was concluded from this literature study that hydroxyapatite could be applied as an effective adsorbent for the removal of heavy metals (hard Lewis acids) from wastewater.

Some other studies (summarised in Table 1-1) reported the use of commercially sourced HAp application in heavy metal ions removal systems, which was found to be an excellent adsorbent showing >99% removal efficiency (summarised in Table 1-1). Apart from chemical precipitation and mineral sources of HAp, another vital source of hydroxyapatite is via chemical synthesis using low-cost feedstock reactants such as calcium carbonate and orthophosphoric acid, which eventually give HAp as a product in a one-step reaction in a 2.3 L glass U-form reactor as described by Minh et al.[85]. In this reaction, calcium carbonate powder (100 g) and deionised water (260-530 g) were introduced into the reactor, which was kept stirring (200-600 rpm). Orthophosphoric acid (69.2 g) was added at a 1 mL min^{-1} rate. The resultant suspension was filtered (using a 0.45 μm filter paper) followed by washing and drying of the solids at 105 ^{o}C leading to a powdered product. A study was conducted to evaluate the adsorption capacity of the CaHAp for the removal of lead (Pb) from a model solution prepared from the Pb salt. The reaction temperature was 25 to 80 ^{o} C. This study reported a good removal efficiency of this synthesised material up to 750 mg g^{-1} for Pb(II)[86].

The studies mentioned above illustrated the potential of synthetic/inorganic HAp to remove heavy metal ions from aqueous solutions. Hence, the HAp could be used to enhance the removal ability of other low-cost materials by making composite materials. Several studies described the employment of HAp with other materials to make composite materials for the removal of heavy metal ions (mentioned in the upcoming section).

1.5.1.2 Bone sourced hydroxyapatite as an adsorbent for heavy metal removal

Bone charcoal (BC) is an "organic" source of hydroxyapatite. It is the product of animal bone carbonization at 500-700 ◦C, consisting of 70-76% calcium hydroxyapatite (HAp), 9-11% carbonaceous material, and 7-9% calcium carbonate[87].

$$\text{Bovine bone} \xrightarrow{\text{500-700 °C/5h}} \text{BC residue + steam + oil + ammonia liquor} \quad (1\text{-}5)$$

Bone char is a mixed adsorbent that has been shown to exchange Ca^{2+} ions for Cd^{2+} Cu^{2+} and Zn^{2+} [88]. Bone-derived hydroxyapatite is used extensively in the sugar refining industry to decolourize the liquors from cane sugar crystals. Animal bone sourced charcoal has also been employed to adsorb cupric ions from an aqueous solution. Cupric ion solutions of different concentrations (0-500 mg L^{-1}) were prepared, and about 0.1 g of adsorbent was added to 50 mL of solution in a batch experimental set-up. The pH was maintained at a value < 5.5 to eliminate any possibility of the cupric ions precipitating. Bone charcoal was found to be an efficient adsorbent for the removal of cupric ions showing fast removal kinetics within 10 minutes of exposure[89].

Bone char also shows higher removal efficiency for arsenic (in the form of arsenate ion) at higher pH (9 to 13). A complex mechanism is implicated in removing As(V) by bone char which includes co-precipitation of hydroxyapatite and calcium hydrogen arsenate and ion exchange between hydroxyl ions and calcium hydrogen arsenate. It is evident that the divalent anions ($HAsO_4^{-2-}$) dominate at pH 8-11 [90]. Bone char particles provide a seed crystal for stimulating nucleation, leading to co-precipitation between calcium hydrogen arsenate and hydroxyapatite on the surface of the adsorbent. After adsorption of As(V) on the bone char, ion exchange occurs between anions where OH^- ions of Ca-OH groups are replaced by $HAsO_4^{2-}$ [91]. The adsorption and co-precipitation of As(V) can be summarized in the following equations:

Adsorption:

$$Ca_{10}(PO_4)_6(OH)_2 + Ca^{2+} + HAsO_4^{2-} \rightarrow Ca_{10}(PO_4)_6(OH)_2 \cdot Ca(HAsO_4) \quad (1\text{-}6)$$

Ion exchange:

$$Ca_{10}(PO_4)_6(OH)_2 + HAsO_4^{2-} \rightarrow Ca_{10}(PO_4)_6(HAsO_4) + 2OH^- \quad (1\text{-}7)$$

Increases in adsorbent dose cause a corresponding increase in arsenic adsorption, as expected due to the availability of greater surface area for the calcium arsenate salt to precipitate on. For 0.5 mg L^{-1} of arsenic, about 99.18% removal can be achieved at pH 10.0 by applying bone charcoal as an adsorbent[91]. Bone charcoal has also been used to remove radioactive isotopes of europium and antimony from radioactive wastes. In this system, chemical adsorption is the main suggested mechanism for metal (Eu^{3+}) removal from aqueous solution[92-94]. A batch study confirmed the findings of those authors. In another study, Moreno et al.[88] was performed to remove Cu^{2+}, Ni^{2+} and Fe from an aqueous

solution with bone charcoal. Different quantities of adsorbent ranging from 0.01 to 0.08 g were added to 100 mL of each metal solution to evaluate the removal potential of bone charcoal. Removal efficiency between 75% to 98% was attained by adding a dosage of adsorbent between 0.02 g to 0.03 g per 100 mL of metal solution. Afterwards, this experiment was repeated using industrial wastewater with the same metal components in quantifiable concentrations (i.e., more than 500 mg L^{-1}). A high removal capacity of up to 34.9 mg g^{-1} was attained for copper ions. Chemisorption was described as a mechanism for heavy metal removal, attributed to the presence of calcium phosphate as a major component of bone charcoal, providing adsorption sites for effective metal adsorption. Calcium phosphate also enables the ion exchange process demonstrated as a mechanism of metal removal in which the following reactions may occur[88].

Additionally, a mechanism described by Moreno et al.[88] showing the involvement of phosphate ("≡PO^-") and -OH groups of HAp to remove cations is given below:

For Cu^{2+}:

$$\equiv POH + Cu^{2+} \rightarrow \equiv POCu^{+} + H^{+} \quad (1\text{-}8)$$

$$\equiv PO^{-} + Cu^{2+} \rightarrow \equiv POCu+ \quad (1\text{-}9)$$

$$\equiv CaOH + Cu^{2+} \rightarrow \equiv CaOCu^{+} + H^{+} \quad (1\text{-}10)$$

The potential of bone sourced HAp to remove heavy metal ions was demonstrated in the literature studies as mentioned above. The chemical adsorption and ion exchange were the dominating mechanisms for removing metal ions using the bone sourced HAp. Additionally, a metal cations co-precipitation method (as described above in equations) was also described as a mechanism for removing metal ions. A few literature studies report the use of bone-sourced hydroxyapatite composites in heavy metal ions removal systems. Bazargan-Lari et al.[95] reported the synthesis of CH/HAp nanocomposites using bovine sourced HAp and crustacean shell sourced chitosan. The synthesised composite was used to remove Cu^{2+} ions from aqueous solutions and reported a maximum adsorption capacity of 1.776 mmol g^{-1} for Cu^{2+} ion adsorption. Other than this study, no related literature was found using the bovine sourced HAp *composites* to remove heavy metal ions.

Hydroxyapatite composites for heavy metal removal

Keeping in view the effectiveness and the efficiency of chitosan and HAp for heavy metal removal, combinations of these two materials have, in the past, been considered an

excellent option for increasing the efficiency of removal and its applicability in wastewater treatment processes. Moreover, a good mechanical strength has been reported for the composites themselves as a body. Moreover, they have been used in biomedical applications and have been said to possess good biocompatibility and biodegradability when employed in different applications[96]. A composite of chitosan and nanohydroxyapatite has also been shown to have good chemical and mechanical properties and was recommended for fluoride removal[97]. Another study that reported good mechanical and thermal stability of chitosan/HAp composites was one made up of krill-sourced chitosan for the removal of Cd(II), Cr(III) and Cu(II) ions and was demonstrated to have favourable metal ion removal efficiency (>90%). Aliabadi et al.[62] reported material of good mechanical strength made by using chitosan and hydroxyapatite in which hydroxyapatite was used as a binding material for the chitosan. It was used to remove lead, cobalt and nickel ions from an aqueous solution. It showed adsorption capacities of 296.7 mg g^{-1}, 213.8 mg g^{-1} and 180.2 mg g^{-1} for lead, cobalt and nickel ions, respectively. The stable and highly flexible crystal lattice of HAp allows easy substitution of different anions and cations, including Mn^{2+}, CO_3^{2-}, Fe^{2+}, Fe^{3+} and F^- [98], which combined with the additional adsorption ability of the chitosan, can further help enhance the removal efficiency of metal ions.

Chitosan utilises metal complexation as the dominant mechanism to remove heavy metals. It is further explained in two mechanisms: metal chelation versus ion-exchange depending upon the pH of the solution (as pH affects protonation of the polymer)[99]. Amine groups of chitosan take part in metal chelation to form metal complexes. In contrast, hydroxyl groups (especially in the C-3 position of the chitosan monomer unit) are responsible for the adsorption of heavy metals. Chitosan is a cationic polymer (with pK_a ranging from 6.2 to 7 for the amino groups) that is protonated in acidic solution and hence exhibits electrostatic properties on account of this. So, in this situation, it may involve the ion exchange mechanism to remove heavy metals[100] via the exchange of protons for metal cations. In another study, Fe-substituted HAp /chitosan-based composites were prepared to remove Pb (II) from an aqueous solution. A simple ion-exchange technique was used to synthesise the Fe-substituted HAp involving exchanging Ca^{2+} ions with Fe^{2+}. The prepared Fe-substituted HAp was then used to prepare a composite by embedding it into chitosan to remove a dye and a heavy metal. The prepared composite was used to remove methylene blue (MB) dye and lead (Pb(II)) ions under various experimental conditions. The results

revealed that the composite has an efficient adsorption capacity for removing the pollutants above from aqueous solutions[101].

Table 1-1: Hydroxyapatite-based adsorbents to remove heavy metals

Materials	Heavy Metal Removed	Adsorption Capacity	Reference
HAp (Synthetic)	Cd	1.22 mmol g^{-1}	105
HAp (Synthetic)	Uranium	> 99.5 %	106
Bone charcoal	Cu	34.9 mg g^{-1}	88
Bone charcoal	Cu	9615 mg g^{-1}	107
Nano Hydroxyapatite	Pb	769.23 mg g^{-1}	83
Nano Hydroxyapatite	Pb, Cd, Ni	20-430 mg g^{-1}	108
HAp gel	Pb	750 mg g^{-1}	109
HAp	Zn	3.99×10^{-6} mol g^{-1}	110
Hydroxyapatite/Chitosan	F	1560 mg kg^{-1}	97
Hydroxyapatite/Chitosan	Pb, Co, Ni	56.10-71.80 mg g^{-1}	62
Cellulose /hydroxyapatite	Cu	175 mg g^{-1}	104
Chitosan/Fe-hydroxyapatite	Pb	1385 mg g^{-1}	101
Cellulose acetate/HAp nanofibre	Pb and Fe	99.7 % (Pb), 95.46 % (Fe)	111
Hydroxyapatite/Fe_3O_4 nanocomposite	Pb	109.89 mg g^{-1}	112
Fe_3O_4/Hydroxyapatite	Fe, Mn	98% Fe, 95% Mn	113
Natural HAp	Ni, Cu	> 95 %	114
HAp (Synthetic)	Cd, Pb, Cu, Cr	> 60%	115
HAp (nano)	Pb, Cu, Zn. Cd	1352, 272, 285 and 304 mg g^{-1}	116
HAp (nano)	Pb	99.2 %	117
Chitosan/Ag-hydroxyapatite	Cu	40. 11 mg g^{-1}	118
Fluor-hydroxyapatite composite	Cd	236.41 mg g^{-1}	119
Chitosan/hydroxyapatite composite	Pb, Cu, Zn, Ni	100, 43.48, 62.5, 32.26 in mg g^{-1}	120
Hydroxyapatite-bentonite composite	Ni, Cd	29.46 mmol g^{-1}, 10.34 mmol g^{-1}	121
Hydroxyapatite attapulgite	Pb, Cu, Cd, Zn	3. 70, 1.99, 1.17, 0.98 mmol g^{-1}	122

The combination of chitosan and HAp in a composite matrix provides a highly efficient adsorbent for the heavy metal ions removal. The addition of HAp into the chitosan polymer could enhance the adsorption abilities of the chitosan in the chitosan/HAp composite by providing additional binding sites for the removal of metal ions. This composite (which already has been utilised and reported in the literature studies) was synthesised as a reference for the control composite system in the present study for the other base-three composite systems.

Hydroxyapatite composite in the form of hydrogels has also been studied for heavy metal ion removal. Hydrogels are three-dimensional hydrophilic polymers that absorb large amounts of water and swell to form a solid gel while maintaining their physical structure without dissolving[102]. There has been an increased effort to enhance these physical properties and functionalities by incorporating filler particles as physical cross-linkers into the hydrogel network. Such fillers can enhance the mechanical, optical, electrical and thermal conductivity properties of the hydrogel[103]. For example, hydroxyapatite was employed as a filler in a cellulose-grafted-polyacrylamide hydrogel, which was used as an adsorbent to remove Cu^{2+} ions from aqueous solutions. For this purpose, the hydroxyapatite powders were embedded into the hydrogel matrix through ionic crosslinking between the OH^-, Ca^{2+} and PO_4^{3-} moieties and amide groups of acrylamide and hydroxyl groups in the cellulose backbone. The hydrogel's ability to adsorb Cu(II) ions from aqueous solutions was investigated and found to have a maximum adsorption capacity of 175 mg g^{-1} [104]. Cellulosic materials such as coir fibre from the coconut industry and spent coffee grounds (as a low-cost by-product from the instant coffee machines or cafes) could be considered as potential materials to make composites with the hydroxyapatite in this study as no literature studies reported the use of these cellulose-based materials to make adsorbents in composite form with the HAp.

1.5.1.3 Heavy metal removal mechanism as used by hydroxyapatite

The studies mentioned above for applying commercial (synthetic) HAp and bone sourced HAp into the heavy metal ions removal use similar mechanisms for metal adsorption. These include 1) surface complexation involving the electron-donating ligand atoms such as oxygen of hydroxyl group 2) ion-exchange within the HAp lattice for Ca^{2+} ions during stirring 3) formation of metal phosphates by the dissolution of hydroxyapatite and its re-precipitation as either a wholly different metal hydroxyapatite compound or as a partially

substituted hydroxyapatite compound[123]. In low-pH systems (usually under 4.0), Ma et al.[124] described HAp dissolution followed by reprecipitation as the major mechanism occurring for heavy metal removal, which was confirmed by the observation of hydroxy pyromorphite (HP) [$Pb_{10}(PO_4)_6(OH)_2$ formed during Pb-immobilization study by HAp as shown in the following equations 1-11 and 1-12:

$$Ca_{10}(PO_4)_6(OH)_2 + 14H^+ \rightarrow 10Ca^{2+} + 6H_2PO_4^- + 2H_2O \quad \text{(Dissolution)} \quad (1\text{-}11)$$

$$10Pb^{2+} + 6H_2PO_4^- + 2H_2O \rightarrow 14H^+ + Pb_{10}(PO_4)_6(OH)_2 \quad \text{(Reprecipitation)} \quad (1\text{-}12)$$

Additionally, a study reported the removal of Cd(II) by HAp due to a substitution-diffusion process in which Cd(II) is taken up by incorporation into the crystal lattice of HAp ((substituting for Ca^{2+}), which leads to a more significant uptake[105]. In another study, Fuller et al.[106] reported the surface complexation as a metal removal mechanism by HAp during the removal of metal ions. In the adsorption of the metal ions from the aqueous solutions, which employ HAp as an adsorbent, ion exchange processes are the most reported and discussed mechanisms for removing heavy metal ions from wastewater through HAp as an adsorbent.

1.5.1.4 Hydroxyapatite -as an ion exchange material for heavy metal removal

As has been mentioned earlier, hydroxyapatite is found to be an efficient material for heavy metal removal due to its ion exchangeability via its lattice cationic and anionic groups (Ca^{2+}, PO_4^{3-} and OH^-). Its specific ability for heavy metal ion removal, such as those of Cd, Pb, Zn, As, U, Sb and V, has been studied[105,125-127]. Hydroxyapatite substitution within its lattice is possible due to its stable yet flexible or "hospitable" lattice with labile anions, cations or other functional groups[98]. Go´mez del R1´o et al.[110] reported the ion exchange mechanism for the removal of Cd^{2+}, Zn^{2+} and Co^{2+} from effluent in a column-based study. Similarly, an ion-exchange interaction between adsorbent and metal ions was reported in a column study in which HAp was used to remove different metal ions, including Cd^{2+}, Ba^{2+}, Zn^{2+}, Ni^{2+} and Mg^{2+} ions. The ion exchange mechanism was concluded by measuring the concentrations of removed metal and calcium ions in solution[128].

Ion-exchange mechanisms involving the phosphates (present in the hydroxyapatite) can also remove anions such as arsenates or chromates (as sorbate) from the solution. Chen et al.[91] explained that the ion-exchange mechanism for arsenate ion removal by bone char is

as follows. However, this involves more the exchange of hydroxyl ions instead of phosphate ions:

$$Ca_{10}(PO_4)_6(OH)_2 + HAsO_4^{2-} \longrightarrow Ca_{10}(PO_4)_6(HAsO_4) + 2OH^- \quad (1\text{-}13)$$

Arsenate ($HAsO_4^{2-}$) and phosphate (HPO_4^{2-}) have chemical similarities[129], which means that arsenate ion could exchange for phosphate ion on a hydroxyapatite surface. Liu et al.[130] proposed a mechanism of ion-exchange between arsenate and phosphate ion species for the removal of arsenic using synthetic hydroxyapatite as given in the following equation: ("≡" denotes a surface)

$$\equiv HAP\text{-}PO_4^{3-} + AsO_4^{3-} \longrightarrow \equiv HAP\text{-}AsO_4^{3-} + PO_4^{3-} \quad (1\text{-}14)$$

Like arsenate, no literature was found to report the ion exchange between phosphate and chromate anions. However, the possibility could be considered for chromate anions found in the solution containing the phosphate-containing substrate such as HAp. The effect of phosphate ions on the removal of Cr (as chromate ions) was reported[131] in a binary-solution removal system, using hydrotalcite $[Mg_2.Al(OH)_6]_2CO_3.3H_2O$ as the ion-exchange medium[131]. In this literature study[131], the co-existing chromate and phosphates ions in solution were found to be negatively affecting the ion-exchange ability of each other on the $[Mg_2.Al(OH)_6]_2CO_3.3H_2O$ substrate. Though there was no ion exchange between chromate and phosphate, it could be deduced from this finding that the phosphates of HAp present in the composites could affect the chromate ion concentrations in the solution. For the removal of chromate ions, an earlier study proposed the ion-exchange mechanism using HAp[132], which involves ion-exchange between the hydroxyl and chromate anions. This is described in the following equation:

$$\equiv Ca_x(PO_4)_x(OH)_x + H_3O^+ + xMe \equiv Ca_x(PO_4)_xMe + H_2O \quad (1\text{-}15)$$

Protonated hydroxyl groups on the surface of HAp attract negatively charged chromate ions to attach to the surface, which ultimately exchanges with negatively charged hydroxyl groups of the HAp. All the mechanisms described for the adsorption of metal ions (cations & anions) could be considered on the part of HAp to remove metal ions using the HAp-based composites systems in the present study.

1.5.2 Chitosan

1.5.2.1 Chitosan- a low-cost polymer for heavy metal ions removal

Chitosan (poly [(1,4)-β-linked 2 amino-2-deoxy-D-glucose] or (poly-glucosamine)) is the deacetylated form of chitin, a modified, N-containing polysaccharide (2-acetamide-2-deoxy-D-glucose). The precursor feedstock to chitosan is the second most abundant polysaccharide on earth after cellulose. Its derivative chitosan has several useful characteristics: low toxicity, chemically reactive, biodegradable, and versatility in chemical and physical characteristics. Hence, these characteristics make chitosan a promising material for several applications that can be extended to include the environmental and biomedical fields. Chitosan biopolymers, in particular, are beneficial for this purpose due to their unique properties such as hydrophilicity, non-toxicity and biodegradability[133]. Their abundance and easy availability make them appropriate materials in terms of cost, as economic viability is the key factor for designing and maintaining any adsorbent system.

Crustacea shells (crabs, prawns, and lobsters), fungi and crabs provide a source for chitin extraction[134]. A huge quantity of shrimp and crab shells is produced as a by-product of the seafood industry during seafood processing. Such normally cast-off quantities of these materials have attracted particular interest from a technological and scientific point of view for repurposing the chitin and chitosan in environmental applications. Crab and shrimp cuticles are the principal sources of chitin and, ultimately, chitosan[135]. Shrimp constitutes about 45% of the total processed matter in the seafood industry, which is the major chitosan[136]. In raw shrimp processing, about 50% to 70% of material is generated as a waste by-product after its processing. This by-product contains valuable materials such as chitin and protein, which offer themselves as prime candidates for repurposing.

1.5.2.2 Reactivity with metals- Mechanisms involved in metal ions removal using the chitosan as a metal adsorbent

Chitosan is a versatile and heterogeneous polymer due to the presence of glucosamine and acetylglucosamine units. At the same time, the amine group is very reactive due to the nitrogen atoms, which have free electron pairs available, which enables them to interact with metal cations to form chelate (metal complexes). The presence of acetylglucosamine

and glucosamine units in the chitosan structure contributes to its usefulness and versatility in the polymer.

Due to nitrogen atoms possessing spare electron pairs, amine groups of chitosan can interact with metal cations, forming metal complexes. This is known as *chelation* and allows metal ions uptake from wastewater and aqueous solutions. The protonation of these amine groups of chitosan leads to a different interaction, namely *electrostatic attraction* of anionic compounds (such as metal anions or anionic dyes)[71].

In chitosan, the hydrophilic nature of this polymer and the presence of many functional groups such as amide, amine and hydroxyl moieties provide easily chemically modifiable centres and this, together with the versatility of the polymer chain, explains the good metal adsorption performance of this biopolymer. The above characteristics of chitosan indicate it might be an appropriate adsorbent component to consider in designing novel composite materials for heavy metal adsorption in wastewater[137-141].

1.5.2.3 Physically modified chitosan used in heavy metal ions removal

Chitosan in its raw form (such as flakes and powder or in solution form) has been used to treat waster (Table 1-2). Chitin and chitosan have been modified physically in different forms such as membranes[142,143], hydrogels[144], beads[145], sponges[144], and scaffolds[146,147] to use them in environmental applications.

One effective method to increase the removal ability of chitosan is to immobilize it on a supporting medium. Immobilization does not necessarily hinder the molecular mobility of the material total. Instead, the number of active sites increases as the supporting medium (sand or mineral) also provide adsorption sites for metal adsorption. For instance, efficient inorganic arsenic removal was achieved using immobilized chitosan where inert support of sand[148] or ceramic alumina[149] was provided. Similarly, the adsorption ability of chitosan was also found to increase by the addition of eco-friendly fillers (such as clay minerals), which reinforce the chitosan.

1.5.2.4 Use of chitosan composites for heavy metal removal

As defined earlier in earlier section 1 (1.4.4), a composite comprises one or more component materials in its makeup. Some materials act as reinforcing fillers (discontinuous phase of composite) fixed in a matrix (known as the continuous phase of composite).

Natural or synthetic fibres such as (chitosan) can be used as a discontinuous phase of the composite to reinforce the fixed matrix, e.g. HAp (continuous phase)[150].

The use of chitosan-based composites (bio-adsorbents) has been reported extensively to remove heavy metals in wastewater streams[151] (summarised in Table 1-2). Studies about the wastewater treatment using the chitosan-based composites[71,99,139,146,152-155] and adsorption modelling data have also been summarised in Table 1-8. The summarised data illustrated that the modern literature focuses on preparing chitosan composites with novel materials, including low-cost adsorbents, which may enhance the removal efficiency of chitosan for heavy metal removal and provide mechanical strength to chitosan.

Apart from HAp, different materials have been employed in the literature studies to synthesise composites with chitosan for heavy metal removal. The materials used extensively to form composites with chitosan in past studies include polyurethane[156], montmorillonite[157], bentonite[158], activated clay[159], polyvinyl chloride, polyvinyl alcohol, kaolinite[160], perlite[161] and palm oil ash[162]. Among them, clay minerals are a good choice to make composites with chitosan, as clay is more useful as an adsorbent when it is compared with other adsorbents in terms of cost, availability, and effectiveness.

Clay is an adsorbent material of choice, having a nontoxic nature, high surface area, easy availability and remarkable adsorption properties, which show a high ion exchange potential. The special attention given to clay minerals is due to their exchangeability of cations and anions used extensively for water treatment. Clay minerals have been used effectively to make composites with chitosan for their application in heavy metal removal[163]. Perlite/chitosan composites were prepared and used to adsorb heavy metals such as chromium[164], cadmium[165], nickel and copper[166]. This composite was also applied in tertiary solutions of Co(II), Cu(II) and Ni(II) to evaluate the competitive adsorption of these metals on the composite[166]. It was reported that Cu(II) ions demonstrated the greatest affinity for the composite, with the order of adsorption capacity being Ni(II) < Co(II) < Cu(II). Montmorillonite is an example of a clay mineral that was used to synthesise composites with chitosan for water remediation. Chitosan-coated montmorillonite (CCM) beads were synthesised for the removal of Cr(VI)[167]. Bentonite is another aluminosilicate mineral clay that could serve as a material to combine with chitosan. Yang et al.[168] reported that Hg^{2+} ions were efficiently removed from aqueous solution by using a chitosan/bentonite composite. In other systems, it has been reported that a layered composite of silicate mineral and chitosan was prepared and used for the removal of Cd

(II), Cr(VI) and Cr(III) ions. The highest removal efficiency was obtained at neutral pH (7) for Cd(II) and Cr(III) while for Cr(VI) it was obtained at pH 4.0[169].

Similarly, aluminosilicate minerals can provide support for chitosan composites to allow the efficient removal of heavy metals. As mentioned above, chitosan's immobilisation on inert materials (such as clay and sand) can help to increase its removal efficiency by providing additional binding sites for metal ion adsorption. Additionally, the immobilisation of chitosan on aluminosilicate minerals can also increase its surface area, consequently increasing the adsorption ability of chitosan. For instance, alumina (Al_2O_3) has been used to synthesise ceramic alumina/chitosan composites. It is effectively used for the removal of heavy metals such as As(V) and As(III), Cu(II)[170], and Ni(II)[170].

Other polysaccharides also can form composites with chitosan, especially for environmental applications. Alginate is a polysaccharide obtained from brown seaweed[171], which can be made into porous, biodegradable materials. Such composites can be easily modified to form an efficient adsorbent for heavy metal pollutant removal[172]. Ngah et al.[173] reported alginate immobilisation on chitosan, with the resultant composite beads being used to adsorb heavy metals.

Cellulose is an abundant polysaccharide having a similar structure to chitosan. It is obtained from plant sources by using simple acid hydrolysis. It is an eco-friendly material that can be used to reinforce and fill biopolymers such as chitosan[174,175]. The structural similarities of cellulose and chitosan make it easy to form composites of the two. There is no need to add any coupling agent as there is the possibility of a good filler-matrix interface formation due to hydrogen bonding involving both chitosan and cellulose, which can provide enough adhesion for composite formation[176]. Cotton (a cellulosic fibre) has also been used to prepare a composite with chitosan to remove Pb(II), Ni(II), Cd(II), Cu(II), and Au(III)[177]. Microcrystalline cellulose is a type of cellulose that has a highly crystalline structure due to strong hydrogen bonding between glucans and exhibits unique chemical and mechanical properties. It can be used to synthesise highly efficient adsorbents for water treatment[178]. Commercially available microcrystalline cellulose has been extensively used to reinforce chitosan, but this results in higher-cost materials. Rahmi et al.[179] reported using palm-oil extracted cellulose for the reinforcement of chitosan, with the composite being used to remove Cd(II) ions. The cellulose used in this composite led to improved strength in the material.

Table 1-2: Chitosan-based adsorbents to remove heavy metals from water reported in the literature studies

Chitosan-based composites	Heavy Metal ions Removed	Adsorption Capacity	References
Chitosan/ Silica	Cu(II)	73.31 mg g^{-1}	181
Poly (acrylic acid) /chitosan	Pb(II)	734.3 mg g^{-1}	182
Chitosan/Acrylamide	Cu(II) and Co	150–220 mg g^{-1}	183
Pollen/chitosan	Cd(II), Cr(III), Cu(II), Ni (II) and Zn(II).	49.55-67.10 mg g^{-1}	184
Chitosan / Fe^0	Cu(II), Cd(II), Pb(II), Cr (VI)	44.8- 82.6 mg g^{-1}	185
Nano-chitosan	As(III), As(V)	-	186
Iron/chitosan	As(III), As(V)	86.87 -114.9 mg g^{-1}	187
Chitosan/Hydroxyapatite	Cd(II), Cu(II), Cr	_	188
Hydroxyapatite/Chitosan	Cd(II), Zn(II), Cr	_	189
Hydroxyapatite/ Chitosan	Cd(II)	_	189
Chitosan/hydroxyapatite	Pb(II), Co, Ni	_	62
Hydroxyapatite/chitosan	Cu(II)	1.776 mmol g^{-1}	190
Chitosan/Fe-hydroxyapatite	Pb(II)	_	101
Hydroxyapatite/Chitosan	Cd(II), Pb(II)	_	191
Hydroxyapatite/chitosan	Pb(II)	190 mg g^{-1}	192
Aniline/Chitosan	Cu II)	328.4 mg g^{-1}	193
Chitosan/sodium alginate/cellulose	Cu(II)	-	194
Chitosan/ cellulose	Cd(II)	204.082 mg g^{-1}	179
Magnetic/humic acid/chitosan	Cu(II), Cd(II), Pb(II)	105.15- 221.24 mg g^{-1}	195
Chitosan/ alginate beads	Cu(II), Cd(II)	207.0 -527.3mg g^{-1}	196
Chitosan/sodium alginate/calcium	Pb(II), Cu(II), Cd(II)	70-176 mg g^{-1}	197
Modified magnetic chitosan	Cr(VI)	163.93 mg g^{-1}	198
Biomimetic SiO_2@chitosan	Hg(II), As(V)	198.6 -204.1 mg g^{-1}	199
Chitosan/cysteine glutaraldehyde	Cu(II) and Cr(VI)	138.53-156.49 mg g^{-1}	200
Bacterial cellulose/chitosan	Cu(II) and Cr(VI)	152.1-200.6 mg g^{-1}	201
Chitosan / Leaf extract	Hg(I)	-	202
Cellulose/Chitosan	Cu(II)	75.8 mg g^{-1}	203
Porous poly (L–lactic acid)/chitosan	Cu(II)	111.66 ± 3.22 mg g^{-1}	204

The results indicated that the increase in the tensile strength of chitosan was about 10% in part due to the inclusion of cellulose. The increase in mechanical strength is due to the immobilization of the chitosan molecules and the presence of cellulose[180] , which is made possible due to the good adhesion between the two components via hydrogen bonding.

The applicability of the chitosan-based composites could be increased by increasing the mechanical strength of the chitosan. The strength of the chitosan could be increased by adding the cellulose-based materials, which could be used to increase the overall stability and strength of the CH/HAp (control) composites synthesised in this study. For this, the lignocellulosic materials such as coir fibre and spent coffee grounds could be selected as low-cost industrial and agricultural by-products, which have lignocellulosic composition and could serve the purpose of providing strength, ultimately increasing the applicability of the synthesised composite systems of the present study.

1.5.3 Coir Fibre (CF)

Coir fibre, as mentioned earlier section, can provide some mechanical strength in chitosan/HAp based composites. It is a well-known agricultural by-product that has been used to synthesise low-cost bio adsorbents to remove heavy metals like Cu, Cr, Hg, Cd and Ni[205]. Globally, millions of tonnes of coir fibres are produced as by-products each year. About 5 to 6 million tonnes of coir fibres are produced as by-products each year. Only 10% of this product is used commercially, while that remaining behind is discarded[206 207]. The management of such waste is a major environmental issue. Therefore, using this in an environmental application constitutes an effective way of managing/utilizing this considerable quantity of environmental waste and assists in cyclability of use. The removal abilities of the coir fibre could be enhanced by including it as a compositing material with other adsorbents such as hydroxyapatite, which is well known for its metal ion removal abilities, as discussed above.

1.5.3.1 Coir - a lignocellulosic fibre with the potential to form a composite with other materials

Coir is a natural fibre, which mainly constitutes cellulose, lignin and hemicellulose. It is generally regarded as an agricultural by-product, being the inner husk of coconut from the coconut palm. Coir pith is made up of 70% pith and 30% fibrous material. The pith is a

waste product, and its disposal is a serious environmental concern as large quantities are produced during coconut harvesting[205].The main constituent of coir pith includes cellulose (35.0%), lignin (25.2%), pentosane (7.5%), fats (1.8%), ash content (8.7.5%), moisture (11.9%) and other components (10.6%)[208]. As it has a high lignin content, coir is considered a tougher, stiffer and longer-lasting fibre among the natural fibres. This property makes it suitable as a reinforcing material for biopolymers such as chitosan.

Compared to manufactured fibres, naturally sourced fibrous materials such as jute, kenaf, palm and coir, etc., are more suitable for this purpose due to their being lightweight, low cost, and high biodegradability[209]. If being bonded to polymers, increased adhesion can be achieved through chemical modification of the natural fibre. It is difficult to elaborate on a definite mechanism for describing the bonding in composites. Generally, chemical modification optimizes the interface of the fibres by helping to increase the effectiveness of natural fibres in two ways. Firstly, the chemical modifying agent reacts with hydroxyl groups on cellulose and secondly, they react with functional groups on the fibres themselves in such a way as to facilitate chemical binding between the natural fibres and biopolymers[210].

1.5.3.2 Coir fibre potential to remove the heavy metal ions

Lignocelluloses (mainly plant biomass) in some naturally occurring materials such as coir fibre have adsorptive abilities and ion exchange capacities related to their basic constituent polymer and structure. Proteins, lignin, pectin, cellulose, and hemicellulose are prominent polymers studied for their adsorptive characteristics for several solutes, especially for the adsorption of metal cations[75]. Coir has been used to synthesise low-cost bio adsorbents to remove heavy metals like Cu, Cr, Hg, Cd and Ni[205] (summarised in Table 1-3). Coir materials have been applied to wastewater treatment in the past.

As mentioned above, it is a lignocellulosic material, and these materials can have a large surface area. About 1 $inch^3$ of this material and with a specific gravity of 0.4 may have about 15 square feet (1.393 m^2) of surface area; moreover, grinding it further helps to increase the surface area of these materials. Additionally, these fibres are hygroscopic and hence have higher water affinity, making them more suitable for an adsorption application[211], hence could be used to make a composite with suspended powdered adsorbents (such as HAp) to enhance their applicability in the water treatment systems.

Further, it is considered suitable for adsorption due to its lower bulk density and higher pore space volume. It possesses different carboxyl, phenolic, amino and hydroxyl groups that are further known for their efficient removal capabilities for different pollutants. Coir has been used to remove Ni, Cu and Zn from model solutions of these metals. Results have indicated that it was an effective adsorbent for removing these pollutants, but it showed lower efficiency than other adsorbents, which led to higher consumption of this adsorbent. The materials, like HAp, could be used to improve the removal efficiency of the coir fibre and could be used as a unique combination for making the composites for the removal of metal ions (as this was not studied earlier).

1.5.3.3 Literature studies employing coir-based adsorbents for the heavy metal ions removal

The following section discusses the literature studies that employed coir-based adsorbents to remove the heavy metal ions to demonstrate the potential of coir fibre for removing heavy metal ions.

Several literature studies have reported the application of coir for the removal of metal ions such as chromium (as chromate ion) in the past[212]. In a fixed-bed column experiment, a maximum adsorption of Cr(VI) up to 201.47 mg Cr(VI)/g adsorbent was reported at the highest bed depth of 60 cm and for the lowest flow rate of 10 mL/min[213]. Kadirvelu et al.[214] investigated the mechanism of Cr(VI) removal from wastewater by applying coconut coir. Results revealed that at pH 3.0, chromium reduction occurs, which produces Cr(III) ions from Cr(VI). The possible binding sites for Cr(III) could be provided by phenolic methoxyl and hydroxyl groups located on lignin which binds the Cr(III) and causes its removal. Another study reported the potential application of coir as a low-cost adsorbent for removing copper and lead ions[215]. An important parameter dictating the removal efficiency of this heavy metal was pH. It was noted that Pb ions were most efficiently removed at pH 4.5, with pH 5.0 being the best pH at which to remove copper ions. The adsorption capacity of coir (at pH 4.5) for the lead was 48.84 mg g^{-1}, although, for Cu ions, it was much lower, i.e., 19.30 mg g^{-1}. Quek et al.[216] used coir pith for the adsorption of Co(II), Cr(III) and Ni(II) ions from single-ion solutions as well as from a mixture of them. The pH at which maximum metal ion adsorption was observed for Cr(III) was at 3.3, for Co(II) 4.3, and Ni(II) 5.3. At these pH values, the adsorption capacity of coir pith was 12.82 mg g^{-1}, 11.56 mg g^{-1} and 15.95 mg g^{-1} for cobalt, chromium and nickel ions, respectively.

1.5.3.4 Coir based activated carbons for heavy metal removal

Activated carbons are the best-known adsorbent for removing heavy metal ions such as Ag(I), Au(I), V(VI, V), Ni(II), Zn(II), Fe(II, III), Cu(II), Hg(II), Cd(II) and Cr(III, VI). Commercially available activated carbons (also known as activated charcoals) are processed to produce materials with tiny low volume pores, which help increase surface area for adsorption. Generally, all organic materials can be processed by physical and chemical activation to synthesise activated carbons. Char is prepared by physical means (carbonization of the precursor at a temperature below 900 °C in an inert atmosphere) followed by activation of the carbonized precursor using activated agents. Activated agents, which are mostly used for activation, include acids or alkalis (e.g. KOH, NaOH, and H_3PO_4)[217,218]. Activated carbons are expensive to prepare, and it is not feasible economically to generate very cheap water treatment systems[219] from these.

Generally, low-density materials are processed to synthesise activated carbons, including rice husk, sugarcane bagasse, coir pith, etc. Coir pith carbons can be activated by mixing the coir pith with polyvinyl acetate to get a granular material. The prepared granular material has been applied to remove Zn, Cd, and Cu ions in a batch experiment to compare the removal efficiency of coir pith activated carbon to commercially available activated carbon for the removal of these heavy metals from an aqueous solution. For the treatment of large volumes of water on an industrial scale, continuous flow systems are preferred over batch systems. The batch experiment was extended to column studies by applying the optimum conditions developed from the batch studies. The results of this study indicated the removal of heavy metal ions increases with an increase in pH.

Column scale studies revealed that the activated carbon in coir is superior to commercially available activated carbon materials. They can be used to treat large volumes of industrial effluents with different heavy metals[220]. Coconut shell fibre was used as a source of low cost activated carbon to remove Cr(III) ions from water and wastewater and was compared with carbon fabric cloth (commercially available activated carbon fabric cloth) to evaluate removal efficiency. Results indicated that the adsorption capacity for removing Cr(III) ions was 39.56 mg g^{-1} and 12.2 mg g^{-1} for activated carbon from coconut fibre and carbon fibre cloth, respectively[221].

Activated carbon in coir pith was also used to remove Cd(II) ions. It was activated by using a procedure described by Namasivayam et al.[222] and was found to be effective for removing cations from aqueous solution[223]. Adsorption of Ni(II) ions was also reported by the

application of carbonized coir pith[224]. Coir pith carbon was activated (by using concentrated sulphuric acid and ammonium persulphate [$(NH_4)_2S_2O_8$)] as activating agents. Activated coir pith was found to be more effective than unmodified coir pith. Adsorption capacities of 38.9 and 9.5 mg $g^{-1,}$ respectively, were noted for the activated and non-activated systems[225]. All these studies show that low-cost organic materials (such as coir) can be used as "activated carbons" to replace the more expensive commercially available activated carbon adsorbents.

1.5.3.5 Coir-based composites for the heavy metal removal

As described earlier, a composite might have more than one discrete phase to reinforce the continuous phase (such as the HAp). The coir fibre, as a biopolymer, could be included as a discrete phase to make composites with other materials.

Composites are formally defined as materials made by mixing two or more materials of different physical or chemical properties to create a hybrid material. The product material will have both properties, but the individual components tend to retain their distinctive properties. Chemical composition is very important for synthesizing a composite of natural fibres with other natural materials, as adhesive bonding is necessary for achieving adequate mechanical strength in the resultant composite. Materials of similar chemical compositions have a natural affinity for each other.

A way to use coir fibre more efficiently is through its binding with other natural polymers, which may enhance its properties. Hence, materials with known high efficiencies for removing heavy metal ions can be used to synthesise composites with coir, such as chitosan, hydroxyapatite and hemicellulose[226]. Modifications of coconut fibre can provide it with enhanced removal properties for wastewater treatment than unmodified fibres[227]. Coir pith, a by-product of the coir production industry and consisting of lignocellulosic polymers, may be used as a potential adsorbent to remove heavy metals. Swarnalatha et al.[205] investigated the coir pith to remove Zn, Cu, and Ni from model solutions of these heavy metals. It was found to be an effective removal agent for low and high concentrations of heavy metals in water.

For increasing the water adsorption property of coir, hemicellulose can be used to make a composite with coir, which can enhance its water adsorbing ability due to the presence of the cellulosic hydroxyl groups. This increases its utility in wastewater treatment applications. Moreover, modifications of composite materials can be enhanced further by

using strong oxidizing agents such as nitric acid. A composite adsorbent was prepared by modifying coconut shell charcoal with chitosan. This composite was further modified by using oxidizing agents (nitric acid and sulfuric acid). These materials were used to remove Cr(VI) from simulated electroplating wastewater. Results indicated a better adsorption capacity for Cr(VI) was obtained on the composite material that was further modified by nitric acid (10.88 mg g^{-1}) compared to a composite that was modified with sulfuric acid (adsorption capacity 4.05 mg g^{-1}). For the unmodified composite, the adsorption capacity was only measured to be 3.65 mg g^{-1}.

Table 1-3: Coconut Fibre (CF) based adsorbents to remove heavy metals reported in the literature studies

Coconut fibre-adsorbents	Metals removed	Adsorption capacity/Removal %	References
Coconut fibre	Zn, Ni,	0.31, 0.20, 0.42 in mg g^{-1}	211
Coir pith	Cr(VI)	76.3 mg g^{-1}	212
Coir pith	Cr(VI)	197.3 mg g^{-1}	213
Coir fibre	Cr(III), Cr(VI)	Not mentioned	229
Coir fibre	Pb, Cu	48.84 mg g^{-1} (Pb), 19.30 mgg^{-1} (Cu)	215
Coconut husk sawdust	Hg, Ni	100 %, 84.30%	
Coir pith	Cr(III)	11.56 mg g^{-1}	228
Coir pith	Ni	62.5 mg g^{-1}	224
Coir pith	Ni	9.5 mg g^{-1}	225
Coir pith (modified)	Ni	38.9 mg g^{-1}	225
Coir pith (modified)	Hg^0	956.282 ng g^{-1}	230
Coir pith	Ni, Cu, Zn	76.24 % (Ni), 85.12 % (Cu), 86.58 % (Zn)	205
Coir pith (modified)	Cd, Cu, Zn	93.2%, and 54.1% to 83.1 %	231
Coir pith	Co, Cr, Ni	12.82,11.56, 15.95 in mg $g^{-1,}$ respectively	232
Modified Coir	Ni, Zn, Fe	4.33, 7.88 and 7.49 in mg g^{-1}	233
Coir pith (modified)	Ni	24.39 mg g^{-1}	234
Esterified coir pith	Co	34.13 mg g^{-1}	235,236

1.5.3.6 Possible mechanisms involved in the adsorption of heavy metal ions using the coir-based adsorbent systems

Coir fibres have selective adsorption, cation exchange capacity, dehydration–rehydration, and catalysis properties that might make them effective in eliminating heavy metals. Adsorption is the dominant mechanism for heavy metal removal at pH values less than 7. However, in alkaline conditions, precipitation of the metal ions occurs preferentially due

to complex formation. In the pH range 3.0 to 9.0, removal of Zn(II), Cd(II) and Cu(II) ions increases from 54.1% to 83.1%, 68% to 93.2% and 70.8% to 97.6%, respectively, using the coir fibre as an adsorbent. This trend could be attributed to an increase in the negatively charged surface of the adsorbent with the increase in pH, which ultimately favours the adsorption of cations (M^{2+}). Parab et al.[228] reported that the combination of ion exchange and surface complexation of metal ions was the possible mechanism for the adsorption of Hg(II), Cd(II) and Cr(III) ions onto coconut husk.

1.5.4 Spent Coffee Grounds (SCGs)

1.5.4.1 Coffee-as a source of valuable by-products

Coffee is one of the most favourite caffeinated beverages worldwide and is cultivated in more than 70 countries. It is the second most largely traded product after petroleum[237]. Despite its popularity, its mass consumption is posing negative impacts on the environment. According to the International Coffee Organization (ICO), about 8.5 billion kg of coffee was produced in one year (2014) to consume in Brazil, the USA, Japan and the EU (European Union)[238]. After-harvest processing of such large volumes of coffee beans and consequently coffee-brewing on an industrial scale produces enormous by-products. The coffee industry produces 8.5 million tons of by-products as municipal waste, with an annual production of 9.34 million tons of coffee worldwide—such large quantities of by-products are responsible for economic and environmental issues linked with their management[239].

1.5.4.2 Composition of Spent Coffee Grounds (SCGs)

The spent coffee grounds (insoluble powder) are the primary by-product of coffee beans produced after dehydration, milling, and brewing coffee beans. Several components, including carbohydrates, proteins, lipids, nitrogenous compounds (e.g., peptides and alkalies), caffeine and phenolic compounds, constitute the coffee ground spent. Their quantities depend upon their source and processing methods[240]. Constituents of different spent coffee grounds from industrial sources were studied by some researchers and are summarized in the following Table (Table 1-4).

The spent coffee grounds (insoluble powder) are the primary by-product of coffee beans generated by two sources. One from the coffee-processing industries produces soluble or instant coffee products and consumes about 50% of coffee beans production worldwide.

The second source is the cafés and the public taking part to consume the remaining 50% of coffee production[241]. These by-products are dumped in landfills as municipal waste by industries, causing an alteration of local ecology[239]. In Sydney (Australia), 7% of the total 3000 tonnes of SCGs are reused in agricultural applications such as fertilizers or to feed worms. At the same time, the remaining is dumped as raw in land-fills, which are causing greenhouse gas emissions[242,243]. Australia could be considered the third-most carbon-emitting member after China and USA[244]; therefore, it demands a serious waste management strategy worldwide to deal with the detritus. Contrary to this, food waste (or organic waste) management can potentially benefit $700 billion if it successfully finds new markets that can accommodate organic waste[245].

Table 1-4: Composition of Spent Coffee Grounds (sourced from Brewing industry and commercial cafeterias)

Groups	Sub-groups	Composition	References
Carbohydrates	Mannose	46-57 %	246-248
	Galactose	26-30.4 %	
	Glucose	11-20 %	
	Arabinose	3.8-6 %	
Proteins	Total protein content	12.8-16.9 % (w/w)	241,249
	Coffee nitrogen compounds	8.5-13.6 %	
Caffeine (1,3,7-trimethyl-xanthine)	A purine alkaloid	0.734 to 41.3 µg mg^{-1} 0.007–31% 1.8 mg g^{-1}	241,250-253
Lipids	Oils consisting of linoleic, palmitic, stearic and oleic acids	7-25 %	254-256
Phenolic compounds	Gallic acid equivalent s (GAE)	16-399 mg g^{-1}	257,258
Minerals	K, P, Mg, Ca, Na, Fe, Cu, K as a major mineral	0.82-3.52 % 3.12-21.88 mg g^{-1}	241,257

1.5.4.3 Sources and application of spent coffee grounds (SCGs)

National regulations of many coffee-producing countries require a proper waste management plan for the by-products generated during the production of coffee products. For instance, in Europe, Nestlé pledged to reduce coffee grounds waste by employing spent coffee grounds in renewable energy production by 2020 in their >20 factories[240]. The

coffee grounds (spent) have been used in several applications, including biochar-production for consequent heavy metals and dye removal[259], biodiesel production[239] and as a subgrade construction material for roads[260]. In contrast, their use in animal feed is restricted due to toxic compounds such as caffeine, polyphenols and tannins[261]. SCGs are mainly composed of lignocellulosic material in which the core of cellulose is sheathed by covalently bonded lignin and hemicellulose. Organic compounds which constitute spent coffee grounds make it a potential material for activated carbon products[262], adsorbent for antibiotics[259], sugar[246] and compost[263].

1.5.4.4 Spent Coffee Grounds as a Bio-adsorbent for heavy metal removal

Generally, SCGs are described as organic particles with a large surface area (around 7.5 $m^2 g^{-1}$), making them useful for adsorption applications[264]. The presence of tannins in SCGs provides the polyhydroxy and polyphenol groups that take part in the adsorption of heavy metals[265,266]. Spent coffee grounds with and without treatment have been extensively used for heavy metal removal. For instance, spent coffee grinds without any treatment effectively removed Cr, Cd, Cu, Pb and Hg from water[264,267-269]. While in another study, spent coffee grounds were activated for their adsorption sites using HCl to remove Pb and F[270].

Similarly, Kim et al.[271] studied the effect of spent coffee grounds (SCGs) and charred spent coffee (SCG-char) grounds on ameliorating heavy metal contaminated water. They applied the SCGs and SCG-char to remove heavy metals from acid mine drainage (sourced from a gold mine) containing Cd, Pb, Cu and Zn. SCGs and SCG-char were highly efficient to remove these heavy metals giving a more than 80% removal efficiency.

SCGs have also been studied to prepare composites with other materials for metal removal, but the work is very limited to date. Coffee residues and a clay composite were prepared to remove heavy metals such as Pb, Cd, Cu, Zn and Ni[265]. Clay was used as a binding material for coffee residues to prepare coffee/clay granules. Before mixing, coffee residues and clay were pyrolyzed at different temperatures ranging from 300-800 °C before their mixing. The mixture was used to prepare a granular adsorbent of about 10 mm long and 1-6 diameter. Adsorption capacity order of heavy metals using these granules estimated by Langmuir adsorption model was given as $Ni^{2+} < Zn^{2+} < Pb^{2+} < Cu^{2+} < Cd^{2+}$. Another study reported the preparation of a magnetic composite of coffee waste using Fe_2O_3 nanoparticles and used this composite to remove Pb ions[272].

The adsorption capacities of spent coffee grounds (raw or treated) and coffee waste composites used for heavy metal removal are summarized in Table 1-5. According to our knowledge, only a few studies have been done on the composite synthesis of spent coffee grounds with other materials to use as adsorbents. To further explore the potential of spent coffee grounds as a low-cost adsorbent, spent coffee grounds were used to make composites with chitosan and hydroxyapatite. As described earlier, the HAp could increase the removal abilities of these low-cost by-products. The SCGs (as lignocellulosic materials) could provide mechanical strength to the CH/HAp composites for increasing their application in heavy metal ion removal applications.

Table 1-5: SCGs based adsorbents to remove heavy metals

Material	Source	Metals removed	Adsorption capacity	References
SCGs	Industry	Cr(VI)	10.2 mg g^{-1}	[264]
SCGs (activated)	Industry	Pb and F	61.6 mg g^{-1} Pb, 9.05 mg g^{-1} F^{-}	[270]
SCGs and SCG-char	Cafeteria	Cd, Cu, Pb, Zn	91%, 58%, >99%, 82% 99%, 88%,>99%, 99%	[271]
Untreated-coffee residues	Cafeteria	Cu and Cr	70 mg g^{-1} Cu, 45 mg g^{-1} Cr	[269]
SCGs	Cafeteria	Cd, Cu, Pb	0.12, 0.21, and 0.32 mmol g^{-1}, respectively	[268]
Magnetic-SCGs nanocomposite	Cafeteria	Pb	41.15 mg g^{-1}	[272]
SCGs	Cafeteria	Cu	0.214 mmol g^{-1}	[273]
SCGs/Silicon elastomer	Cafeteria	Pb, Hg	13.5 mg g^{-1} for (Pb) and 17.1 mg g^{-1} (Hg)	[274]
SCGs	Industry	Cu, Pb and Zn	8.2, 27.6, and 8.0 mg g^{-1}, respectively	[275]

1.5.5 Zeolites

Zeolites are naturally occurring hydrated aluminosilicates with a porous structure. There is a vast number of crystal structures reported for zeolites. According to a report in the Inorganic Crystal Structure Database (ICSD 1995), there are 273 zeolite crystal structures registered, with the number of cation exchanged zeolites being 409 [276].

Cost-effectiveness is the most important parameter before the application of any method for water treatment. This is especially so if it is to be used on a large scale. Among all available options, inherently low-cost materials (such as clay minerals) are hence the best option for water treatment. The use of locally available low-cost natural materials (e.g., zeolites) with a chemical structure that supports heavy metal removal (by adsorption and ion-exchange mechanisms) can economically provide a feasible option. It is proven in

literature (given below) that these materials could constitute an effective water treatment method due to the enhancement of metal ion removal abilities by the several mechanisms that would exist in any composite made with this and other materials that have the potential for being water treatment matrices.

1.5.5.1 Zeolites in the Taupo Volcanic Zone (TVZ) of New Zealand

In New Zealand, there is a presence of zeolite deposits in the TVZ, and their geology and mineralogy are well established[277]. In Ngakuru (TVZ), an extensive deposit of zeolites has been discovered, which is less than 50,000 years old.[278] In 1992, the first deposit was discovered at Mangatete Road (Rotorua), which was available for commercial use soon after its discovery. Deposits from this area have been used effectively to soak up oil, chemical spills and animal wastes and have shown excellent adsorption capacities[278]. Zeolite presence in lower temperature areas such as in Wairakei (a geothermal area in TVZ) has been known since the 1950s. The local availability of zeolites offers a low-cost option for the synthesis of adsorbents, especially for heavy metal ion removal.

1.5.5.2 Potential of Zeolites for heavy metal ion removal

A zeolite crystal is composed of three-dimensional frameworks of SiO_4 and AlO_4 connected through oxygen bridges[279]. Each tetrahedral unit contains at its centre an aluminium ion which is surrounded by four oxygen atoms. A negative charge is produced by the isomorphous replacement of Si^{4+} by Al^{3+} in the lattice. Exchangeable cations (e.g., sodium, potassium and calcium) balance out this negative charge.

The zeolites have potential industrial applications such as adsorbents, detergent builders, molecular sieves and ion exchangers[280,281]. The literature shows that heavy metals from industrial, municipal and agricultural wastewaters have been removed by the application of zeolite[282]. Easy availability and extraction make them low-cost adsorbents of great interest due to their high surface area and easy ion exchangeability. It has been shown that ion exchange is the major mechanism for heavy metal removal by zeolites[283,284]. In a study reporting the efficiency of three aluminosilicate minerals (perlite and vermiculite along with natural zeolites)[285], natural zeolites were reported to be the most efficient agents for lead ion removal from wastewater.

1.5.5.3 Modifications of Zeolites to remove heavy metals

Clay minerals (e.g., zeolites) have negatively charged surfaces, which hence show a low affinity for anions. Inorganic cations, mainly Fe(II) ions and other cationic species (e.g. of $Pb^{2+,}$ $Ba^{2+,}$ and Ag^{+}), have been used to modify clay minerals for using the modified clays to remove anionic species from water[286-288]. Pb-modified minerals (such as zeolite, perlite and vermiculite) have been used to remove Cr(VI) (in the form of chromate anions). Among these clay minerals, zeolites and vermiculite (another silicate mineral) show a higher removal efficiency with respect to Cr(VI), i.e. 86% and 60% for zeolite and vermiculite, respectively[289]. A proposed mechanism to account for this ion removal property suggests that a re-exchange process between the potassium ion of potassium chromate (K_2CrO_4) and lead takes place initially. In other words, insoluble lead chromate is formed by the combination of Pb^{2+} and CrO_4^{2-} which deposits on the surface of the lead-modified minerals[290]. Therefore, surface modification of minerals helps to increase their ion exchange and adsorption ability.

Chitosan has been reported as a potential material to remove heavy metals, as mentioned previously[151]. It can be used to make a biocomposite with the zeolites with enhanced properties for heavy metal ions removal from water. Chitosan-modified zeolites have been used to extract divalent metal ions ((Pb^{2+}, Cd^{2+}, and Cu^{2+}) from acidic media (i.e., H_3PO_4 solution, which has metal ions present as impurities). Modified zeolites have shown a remarkable removal efficiency of > 90 % for these cations after only 10 minutes of exposure. A study reported the synthesis of hydroxyapatite/zeolite nanocomposites by using a simple sol-gel method. This nanocomposite was used to remove Pb (II) and Cd (II) from aqueous solutions. Adsorption of cationic species on the surface of this composite was demonstrated to be the removal mechanism for ions in this study[291]. Literature studies have been summarized in Table 1-6 to illustrate the zeolite-based adsorbents' removal and adsorption abilities. It shows that the zeolites could be employed as a potential material to make composites with chitosan and HAp with enhanced properties and abilities for the heavy metal ions from the aqueous solutions.

Table 1-6: Zeolite-based adsorbents to remove heavy metals reported in the literature studies

Zeolite-based adsorbents	Metals Removed	Removal%/Adsorption capacity	References
Synthetic Mordenite (modified)	Cd	85 %	[292]
Zeolite (Natural)	Cu, Ni, Co, Fe	0.011-0.03 mg g^{-1}	[293]
Zeolite (Synthetic)	Zn, Cu, Pb, Cd	> 91 %	[294]
Clinoptilolite (Modified)	Chromate	9.83 mg g^{-1}	[295]
Zeolites (synthetic)	Cr, Cu, Cd	0.83, 0.79, 0.45 in mmol g^{-1}, respectively	[296]
Zeolites (Natural)	Cr, Cu, Cd	0.07, 0.09, 0.04 in mmol g^{-1}, respectively	[296]
Zeolites (synthetic)	Pb, U	20.1 (Pb), 37.6 (U) mg g^{-1}	[297]
Erionite (Natural)	Pb, Cd	26 mg g^{-1}, 3.8 mg g^{-1}	[298]
Clinoptilolite (Natural)	Pb, Cd	32 mg g^{-1}, 1.6 mg g^{-1}	[298]
Scolecite (Natural)	Pb, Cu, Cd	56 μeq g^{-1},130 μeq g^{-1}, 3.2 μeq g^{-1}	[299]
Fe-Zeolite (composite)	As	38.26 ± 3.59 mg g^{-1}	[300]
Clinoptilolite (modified)	Pb	0.537 mmol g^{-1}	[301]
Clinoptilolite (composite)	Pb	>99.9 %	[302]
Zeolite (Natural)	Pb	54 mg g^{-1}	[303]
Fe modified Zeolite	Pb	76 mg g^{-1}	[303]

1.6 Proposed mechanisms of selected materials for the removal of metal ions

The selected candidate materials (mentioned above) have been reported in the literature studies to use some fundamental adsorption mechanisms mentioned in their respective literature review sections. This mechanism has been summarised in the following section, as explained in the literature studies.

1.6.1 Electrostatic interactions for the metal ion removal from aqueous solutions

The first and the most common mechanism that could be considered for the removal of metal cations (Cd^{2+}, Pb^{2+} and $Cu^{2+)}$ is the electrostatic interactions between these positively charged metal ions and negatively charged functional groups (binding sites) on the surface of the composites[304]. The oppositely charged species attract each other leading to attachment and resulting in metal ion removal from aqueous solutions.

In the chosen adsorbent materials for this study, the hydroxyl groups are the most dominant functional groups which are found in all the selected materials, with a negative charge,

which principally plays a role in metal cations by electrostatic interactions[115]. The carbonyl (C=O) and carboxyl groups (COO^-), which are found in coir fibre (from hemicellulose)[305-307] and spent coffee grounds (SCGs), participate in the aforementioned mechanism for to remove cations. Similarly, negatively charged phosphate groups (PO_4^{3-}) are the fundamental components of the hydroxyapatite to assist the metal cations removal from the aqueous solutions by electrostatic attraction.

The positively charged functional groups (produced by the protonation of the active sites at lower pH values) of adsorbents (chitosan, coir fibre, SCGs etc.) and hydroxyapatite must remove anionic species (metal ions) such as chromate and arsenate by electrostatic interactions as documented in the literature studies[308-310]. The pH of the solution is an important parameter to accomplish the removal of the anionic metal species, as it is essential for the protonation and deprotonation of the functional groups to create a positive charge on the surface for removing the negatively charged metal ions from the solution by electrostatic interactions[311,312]. A lower pH (acidic) in the solution provides an excess of H^+ ions, which cause protonation of the functional groups, such as the hydroxyl, amino and carboxyl groups, to produce a positive charge on these functional groups so, allowing the removal of anions (chromate and arsenate) by electrostatic interactions[310].

1.6.2 The Metal-ligand complexation (metal chelation) mechanism for metal ions removal from the aqueous solutions

The metal chelation is an extensively reported mechanism for the removal of metal ions from the desired sites (e.g., an aqueous solution). This mechanism is founded on the coordination chemistry, involving the *chelating agents* to form a complex structure (chelate) with the metal ions to bind them for the removal[313]. The chelating agents could be organic or inorganic, possessing ligand(s) or chelating atoms that coordinate with the metal ions by covalent and coordinate linkages. The ligand atoms, primarily N, O, and S, are present in the chemical groups of the materials (such as bio-adsorbents). The most common functional groups involved in metal-chelation by their ligand atoms include $-NH_2$, =NH, -OH, and OPO_3H[314].

In the metal-chelation mechanism for the metal ions removal, the chelating agent acts as a Lewis base (electron donor) to bond with metal cations such as Pb^{2+}, Cd^{2+} and Cu^{2+}. In contrast, the metal ions act as Lewis acid (electron acceptors) to make covalent/coordinate

linkages with the chelating agents (Figure 1-1)[314]. In this process, the metal atoms are held a central place surrounded by neutral or ionic groups (ligand) to form a complex structure. In this way, the adsorbents' functional (chemical groups) immobilize or bind the metal ions on their surface to remove them. The metal-ligand complexes could be monodentate (involving one donor atom), bidentate (involving two donor atoms) or polydentate (involving more than two donor atoms)[314].

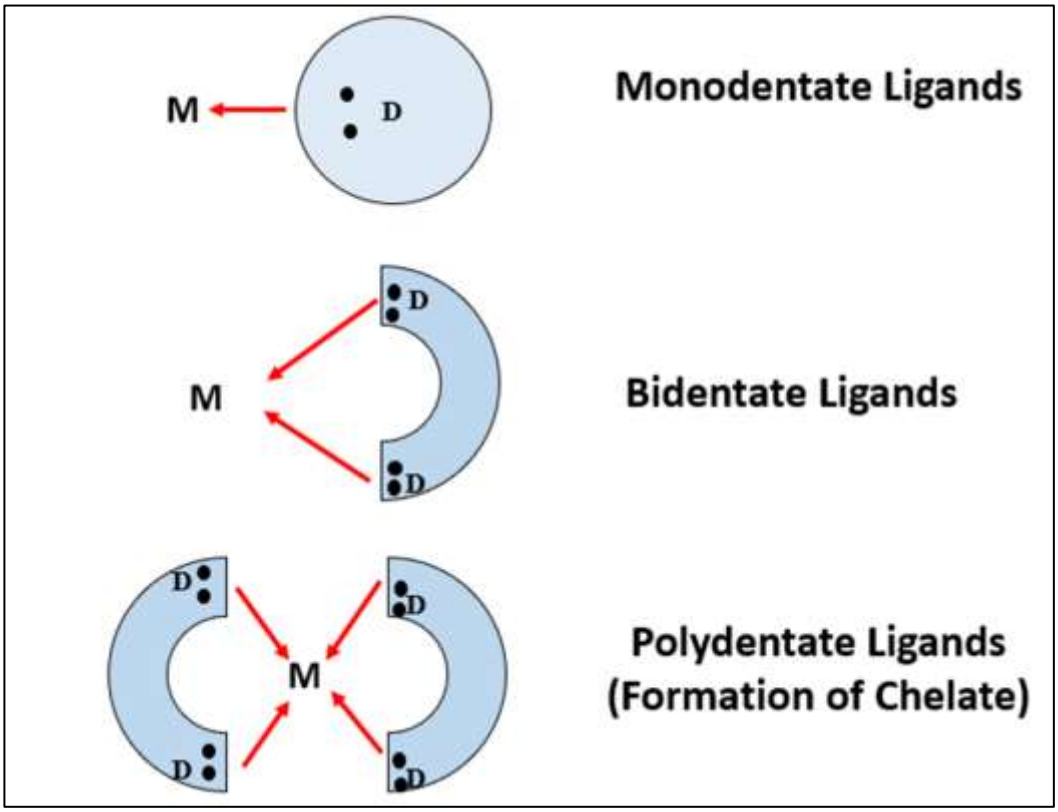

Figure 1-1: Synthesis and types of metal-ligand complexes[314] displayed with permission under a Creative Commons Attribution 4.0 International License.

The functional groups present in the chosen candidate materials, such as hydroxyl groups, carboxyl groups and amino groups, which are the constitutional part of the selected materials, contain the ligand atoms such as N and O and actively participate in metal-ligand complexation for their removal[315,316]. The literature studies extensively reported metal-chelation as one of the dominant mechanisms involved in metal ion removal (cations particularly) by the functional groups of biopolymers[317]. The biopolymers such as chitosan and lignocellulosic materials (coir fibre and SCGs) contain the hydroxyl, amino and carboxylic groups. They are reported to form metal complexes[71,318,319] for metal cation removal from aqueous solutions. Similarly, the hydroxyl groups are the fundamental part

of the hydroxyapatite and zeolites and could be considered to be involved in this mechanism[320].

To remove negatively charged metal ions such as chromates, the functional groups with ligand atoms (such as the amino groups of chitosan & carboxylic groups of the lignocellulosic materials) could work differently. The metal oxides, such as the oxides of Cr(VI), contain many H^+ ions, or at acidic pH conditions, there is an excess of H^+ ions in the solution. The H^+ ions can protonate the negatively charged or neutral functional groups to create an electron donor group[310]. The electron-donating group resulting from the H^+ ions' protonation can transfer electrons to Cr(VI) to reduce it into Cr(III). The Cr(III) could remain in the aqueous solutions or form complexes with binding groups of the bioadsorbents[321]. The reduction of Cr(VI) to Cr(III) is also mentioned in the literature to remove chromate ions using bioadsorbents[322] such as chitosan and coir fibre[323].

1.6.3 The ion-exchange mechanism for metal ions removal from the aqueous solution

Ion exchange is one of the fundamental mechanisms involved in metal ions removal by using the materials containing non-toxic metal cations or anions, which could exchange with toxic heavy metal cationic or anionic species. Hydroxyapatite and zeolites are well-reported materials using the ion-exchange mechanism to remove toxic heavy metal cations such as Pb^{2+}, Cu^{2+}, Cd^{2+}, Zn^{2+} and anions such as arsenate ion.

The Ca^{2+} ions present in the apatites are favoured as adsorption sites for the metal cations using the ion-exchange mechanism. The Ca^{2+} ions are exchanged by the metal cations (Pb^{2+}, Cd^{2+}) when they are removed from solution using the hydroxyapatite or HAp-based composites. Similarly, the metal cations in the zeolites, such as those of sodium, calcium and potassium, are the potential sites of removal for metal cations by ion exchange.

For removing heavy metals from industrial effluent, ion exchange is another very efficient and essential mechanism. For ion exchange purposes, a solid material must be used with ion exchange sites for either anions or cations through interaction with the targeted ions for removal. Ion exchange formally occurs by an ion of identical valency being released on acceptance into the resin's site of the "pollutant ion", so preserving net neutrality in solution. As stated above, calcium hydroxyapatite can remove heavy metal ions by exchanging calcium ions (Ca^{2+}) with heavy metal cations in the crystal lattice of HAp. Ion exchange between calcium and lead ions has been studied, and equimolar ion exchange was observed

by measuring the concentration of released calcium ions and consumed lead during all reaction times[109]. However, hydroxyapatite can also exchange out anionic species through replacement with OH^- or orthophosphate ion. A study reported removing copper, cadmium, lead and iron ionic species by using synthetic hydroxyapatite. The exchange of calcium ions with these metal ions was reported as a mechanism for heavy metal removal, which was concluded due to an observed increase of calcium ion concentration in solution during the experiment[324].

Synthetic and natural zeolites are well-known adsorbents for removing heavy metal ions by ion exchange[325]. These materials possess negatively charged tetrahedral SiO_4 and AlO_4 groups, which effectively remove cations through ion exchange. Natural and synthetic zeolites have been studied as removal agents for Cd(II), Cu(II), Zn(II), Ni(II) and Cr(VI) ion species, and results have shown that synthetic analogues of these zeolites have a higher removal efficiency compared to natural zeolites[326]. This is due to synthetic zeolites' higher H^+ exchange capacity and cation exchange capacity, which results from their lower Si/Al ratio (1.7) compared to natural zeolites (4.8). Studies have shown that zeolites with lower Si/Al ratios exhibit greater adsorption capacities[326]. The presence of harmless exchangeable ions (sodium, calcium, and potassium ions) makes zeolites suitable for removing heavy metals from wastewaters as these exchangeable ions are found naturally in waterways. The selectivity order of clinoptilolite was studied for a series of heavy metal ions for their removal, and it was found that the order of ion removal efficiency was as follows: Pb^{2+}>Cd^{2+} > Cs^+> Cu^{2+}> Co^{2+}> Cr^{3+}> Zn^{2+}> Ni^{2+}>Hg^{2+} [327].

There are different methods to interpret the adsorption mechanisms involved in the adsorption of metal ions when composite adsorbents are employed in water treatment systems to remove metal ions. One of the most studied and the most relied on methods is adsorption modelling, which involves fitting different adsorption models on the experimental data to interpret the adsorption behaviour of metal ions in adsorption systems. The following section discusses the adsorption models which are commonly used in composite adsorption systems for the evaluation of the mechanism involved in metal adsorption and also provides the ground for the selection of adsorption models which have been employed in this study to fit the experimental data of metal ions removal on the composite adsorbents.

1.7 Adsorption Modelling

The adsorption process is the fundamental technique applied using the low-cost synthesised composites for the heavy metal ions removal from the aqueous solutions in this study. It has been mentioned earlier (section 1.4.1) that adsorption could involve different mechanisms for the removal of the heavy metal ions mechanisms, such as the chemisorption (formation of new bonds), and the physisorption (by Van der Waals forces) and ion-exchange. The understanding of the adsorption mechanism is important for the design of the adsorption systems for the efficient application of wastewater treatment plants. Different methods have been employed to explore the possible mechanism of adsorption involved in the removal of heavy metal ions. These methods include the characterisation of adsorbent materials before and after the adsorption process, density functional theory, the molecular dynamics study[332] (using a computer simulation program) and the adsorption modelling of the experimental data of adsorption, which is recorded at adsorption equilibrium[333]. Among these methods, the adsorption modelling of the experimental adsorption data is the most common and widely used method, which also can assist in the evaluation of the removal efficiency of adsorbents (by some models) by calculating the maximum adsorption capacities of the adsorbent materials.

Adsorption modelling involves the application of different adsorption isotherms to elucidate the mechanism of metal removal or metal adsorption by adsorbents. When an adsorbent is employed in a solution, sorbate molecules (metal ions in this study) adsorb at the surface of the adsorbent depending upon their concentration present in the solution at a constant temperature. A graphical representation of this adsorbed quantity of sorbate in the solid phase (mg g^{-1} or mmol g^{-1}) vs sorbate quantity in the solution phase (mg L^{-1} or mmol L^{-1}) is called adsorption isotherm or adsorption isotherm. This isotherm is typically used to calculate the efficiency of adsorption. At equilibrium, a certain amount of adsorbent (g) adsorbs a certain amount of sorbate (mg) for a particular concentration of adsorbate (mg L^{-1}) for a constant volume of solution (L)[334].

Several adsorption isotherms have been reported to model the adsorption data, including the Langmuir, the Freundlich, the Temkin, the Sips and the Brunauer, Emmet and Teller (BET) models. These models are classified depending upon their isotherm shapes or the number of parameters calculated. However, this is not an effective way to classify these models, as the classification is not enough to describe the adsorption mechanism. For

instance, the Langmuir and the BET adsorption models are classified as two-parameter models. The Langmuir is used to mention chemical adsorption (monolayer adsorption), and the BET mostly involves physical adsorption[52].

Most of the adsorption models are empirical, such as the Freundlich isotherm model, the Temkin and the Sips isotherm models, which lack theoretical support to describe the adsorption mechanisms in the adsorption systems. Each adsorption model has its limitations, which limits its applicability to a wide range of adsorption systems. The physical meanings of the adsorption isotherm parameters offer a way to comment on possible adsorption mechanisms. The isotherm parameters are calculated by using the two methods.

The first one is the *linear regression method* applied using the linearized form of the adsorption isotherms. It is the simplest and most convenient method used extensively in published papers to report the adsorption mechanisms.

The second is the *non-linear regression method*, which employs the Microsoft Excel solver add-in using non-linear regression functions (error functions) to calculate the adsorption isotherm parameters. It is relatively more complex than the linear regression method and considered more reliable to calculate the accurate values for the isotherm parameters.

The linear regression is reported as a biased method that can cause errors in the estimated adsorption data. The actual model equation is converted into its linearised form, which possibly affects the dependent and independent variables of the model. In contrast, non-linear regression was found to report relatively more accurate calculations of the estimated isotherm model's parameters.

The following sections describe the different isotherm models, including the two-parameter isotherm models (e.g., the Langmuir and the Freundlich) and the three-parameter isotherm model (e.g., the Sips model). Both the linear and non-linear forms of the isotherm models have been given. However, the Langmuir and the Freundlich isotherm models were used in this study's experimental data due to their applicability to the vast variety of adsorption systems. Considering this study's extremely large data sets, only two models were selected to explore the possible adsorption mechanisms involved in heavy metal ion removal using the synthesised composite systems.

1.7.1 Langmuir Isotherm

The Langmuir isotherm is one of the most applied adsorption models used to describe the adsorption behaviour of adsorbents in adsorbent systems. It was initially established by Irving Langmuir (1916) to define the adsorption of gas at specific, confined sites of an adsorbent as a function of pressure and has been employed to explain both chemical and physical adsorption. It assumes monolayer formation of sorbate molecule on the homogenous surface of adsorbent by interacting with one active site of adsorbent with one molecule of sorbate[335]. It also holds that adsorption energy is constant, and there is no or negligible interaction between adsorbate molecules. The following equation applies:

$$q_e = \frac{K_L q_{max} c_e}{1 + K_L c_e} \qquad (1\text{-}16)$$

Where q_e is the experimental quantity of adsorbate at equilibrium (mg g^{-1}), C_e is the adsorbate concentration in solution at equilibrium (mg L^{-1}); qmax (mg g^{-1}) and K_L (L mg^{-1}) are the Langmuir constants related to estimated adsorbate quantity at equilibrium (mg g^{-1}) and affinity between sorbate and adsorbent, respectively. There are two constant quantities (parameters) calculated with the Langmuir adsorption isotherm (i.e., q_{max} and K_L), classified as a two-parameter model in the literature studies.

Equation 1-16 is used to calculate the Langmuir isotherm parameters using non-linear regression functions (error functions) as given in appendix 1A (section 1.3A).

The different linearised forms of Langmuir isotherm derived from equations 1-16 to represent and interpret model constants are given below in Table 1-7 [336]. These forms are used in the literature studies to calculate the parameters by a simple linear regression method using Excel. However, these methods to calculate the Langmuir isotherm parameters have been reported to produce biased and inaccurate results and the % errors were calculated to be up to 40% using these linearized equations (linearisation methods)[337].

Table 1-7: Different linearised forms of Langmuir isotherm model

Isotherms	Equation	Linear Form	Plot
Langmuir 1	$q_e = \frac{q_m K_L C_e}{1 + K_L C_e}$	$\frac{1}{q_e} = \frac{1}{q_m K_L C_e} + \frac{1}{q_m}$	$\frac{1}{q_e}\ vs. \frac{1}{C_e}$
Langmuir 2	$q_e = \frac{q_m K_L C_e}{1 + K_L C_e}$	$\frac{C_e}{q_e} = \frac{1}{q_m} C_e + \frac{1}{q_m K_L}$	$\frac{C_e}{q_e}\ vs. C_e$
Langmuir 3	$q_e = \frac{q_m K_L C_e}{1 + K_L C_e}$	$q_e = -\frac{1}{K_L}\frac{q_e}{C_e} + q_m$	$q_e\ vs. \frac{q_e}{C_e}$
Langmuir 4	$q_e = \frac{q_m K_L C_e}{1 + K_L C_e}$	$\frac{q_e}{C_e} = -K_L q_e + q_m K_L$	$\frac{q_e}{C_e}\ vs. q_e$
Langmuir 5	$q_e = \frac{q_m K_L C_e}{1 + K_L C_e}$	$\frac{1}{C_e} = K_L q_m \frac{1}{q_e} - K_L$	$\frac{1}{C_e}\ vs. \frac{1}{q_e}$

The Langmuir constant (K_L) is used to calculate a dimensionless parameter R_L which can be used to determine the favourability of the adsorption process[338]. It is given by equation 1-17:

$$R_L = \frac{1}{(1 + K_L C_0)} \qquad (1\text{-}17)$$

The extent of favourability of the adsorption process could be explained in terms of R_L value. When the R_L is closer to zero, i.e. R_L <<<1, then it demonstrates a more irreversible and more favourable adsorption process. In contrast, when the R_L values approach unity, it illustrates the reversibility of adsorption and also indicates less favourable adsorption process. It means that when the R_L > 1, it indicates unfavourable adsorption. Hence, R_L <<< 1 means irreversible adsorption, while generally 0 < R_L < 1 is indicated as a "favourable" adsorption process.

For the Langmuir isotherm model, "homogenous adsorption" is described on homogenous surfaces on a macroscopic level. However, literature studies also show the applicability of this model to describe adsorption on irregular or non-uniform surfaces, such as microplastics[339], modified minerals, shale[340] and naturally sourced activated carbons[341], which were examined using microscopic characterisation techniques.

The explanations for the Langmuir isotherm fitting on adsorption data recorded for heterogeneous surface-based systems were supported by a good number of literature studies. The studies have been summarized in tabular form (Table 1-8), showing the fitting

of the Langmuir adsorption isotherm on similar composite-based adsorption systems. The fitting of the Langmuir isotherm illustrates homogeneous adsorption of the adsorbate molecules on these heterogeneous surfaces, which appear homogenous at macroscopic levels but are irregular (heterogeneous) at the microscopic level.

The Langmuir model is also associated with the chemical adsorption mechanism[239]. It assumes the monolayer adsorption of the adsorbate molecules on specific adsorption sites at the homogenous surface of adsorbents. Suppose an adsorbent system follows the Langmuir model of adsorption on a surface; in that case, it is known that as the concentration of metal ions initially increases from zero to higher values, the adsorption rate of the ions on the surface of the adsorbent is first order with respect to the metal ion concentration. As a monolayer is established on the surface of adsorbed metal ions, adsorption slows down gradually to a constant rate so, exhibiting zero-order kinetics with the establishment of equilibrium. The initially faster rate of adsorption is attributed to the availability of more significant numbers of active (empty) sites on the adsorbent. At equilibrium, there is no more change in the adsorption capacity of the adsorbent even after increasing the metal ion concentration, as the rate of reaction exhibits zero-order kinetics for the metal ion concentrations at this stage. It is assumed that the adsorbate molecules/ions have occupied all the available adsorbent sites and will not adsorb any more until existing molecules/ions leave the surface (i.e., they exhibit a "waiting effect"). Hence after a certain amount of time allowed for adsorption on the composite samples, the equilibrium concentration measured in solution represents the situation where the rate of adsorption = the rate of desorption of the metal ions. The model is considered one of the most reliable adsorption isotherm models, which has the theoretical background to explain the physical meanings of the parameters and provides reasonable derivations. So, the Langmuir isotherm model was selected for the adsorption modelling of the experimental data in the present study.

1.7.2 Freundlich isotherm

Freundlich discovered a possible relationship between adsorbed sorbate and the sorbate concentration at equilibrium in 1906 while investigating material adsorption in animal-sourced coal adsorbents. He expressed this relationship in equation 1-18:

$$q_e = K_F C_e^{\frac{1}{n}} \quad (1\text{-}18)$$

Where q_e and C_e are the exact quantities described earlier in Langmuir isotherm, while K_F and 1/n are Freundlich isotherm constants related to Freundlich adsorption and the heterogeneity factor, respectively[342]. The linearized form of the Freundlich isotherm is given as follows:

$$log\, q_e = log\, k_F + \frac{1}{n} log\, C_e \quad (1\text{-}19)$$

A plot of log C_e vs log q_e was used to calculate 1/n and K_F by slope and intercept of the graph, respectively. The Freundlich adsorption isotherm is one of the most commonly used adsorption models, which is used to represent non-linear adsorption described as a two-parameter model due to the two parameters calculated using this model (1/n and K_F).

As described above, it has been considered as an empirical isotherm model that lacks the theoretical background to support the physical meaning of the parameters. In several research articles, it was used to represent the multi-layer adsorption on heterogeneous surfaces[343-345]. Adsorption intensity or surface heterogeneity is measured by a slope that lies between 1 and 0. The more the value of 1/n closer to zero indicates more heterogeneity of the surface. 1/n is also regarded as the measure of favourability of the isotherm. Suppose the value is $0 < 1/n < 1$ it shows the favourability. If 1/n is equal to zero, it is irreversible, and if the value is > 1, it represents the unfavourable condition of isotherms[346]. The value of K_F (Freundlich constant) is used to estimate adsorption capacity (mg g^{-1})[347].

The Freundlich isotherm is a commonly employed adsorption isotherm reported in most adsorption studies conducted to report heavy metal ion removal. Hence, it was also used to fit the adsorption data collected in the heavy metal ion adsorption systems in the present study, along with the Langmuir isotherm.

1.7.3 Sips Isotherm

The Sips isotherm, also known as the L-R isotherm, is a hybrid model which combines the Langmuir and Freundlich equations to explain the adsorption on homogenous or heterogeneous surfaces[52,348]. It is considered the most applicable 3-parameter adsorption

isotherm for monolayer adsorption of adsorbates on the adsorbent surface[349-351]. It also overcomes the drawback of the Freundlich isotherm related to increased adsorption capacity by increasing the sorbate concentration through the incorporation of finite adsorption for a sufficiently high concentration of adsorption. At low sorbate concentrations, it is predicted to be a Freundlich adsorption isotherm illustrating monolayer adsorption on a heterogeneous surface. In contrast, it is supposed to indicate monolayer adsorption on the homogenous surface (showing Langmuir adsorption behaviour).

$$q_e = \frac{k_s q_{max} C_e^{\frac{1}{n}}}{1 + k_s C_e^{\frac{1}{n}}} \qquad (1\text{-}20)$$

In the above equation, where q_e, q_{max} and C_e are the same quantities described earlier for the Langmuir adsorption isotherm (Eq.1-16), while K_s and 1/n represent the Sips adsorption model constants. The Sips isotherm model has the potential to be employed to explore the adsorption behaviour of the composite systems of the present study. The plots showing the fitting of the Sips isotherm on the adsorption data of metal ions for the CH/HAp/Zeolite composites are included in appendix 4, which indicates the applicability of the Sips model to these composites systems.

1.8 Adsorption Kinetics

Adsorption kinetics also has been used as a tool to predict the adsorption mechanisms of metal removal systems. The kinetic models which are generally employed to investigate the adsorption are given below. Like adsorption modelling, the non-linear regression method was used to do kinetic modelling of the kinetics data collected for heavy metal ion adsorption on the synthesised composite systems investigated in this study. The four non-linear regression functions (also called the error analysis functions) were used and given in Equations 1A to 1D *(Appendix 1, section 1.3).*

1.8.1 Pseudo-First Order Kinetics

In 1898, Lagergren described the rate of adsorption of a solute from a liquid solution by expressing an equation known as pseudo-first-order (PFO) kinetics, and its non-linearized and linearized forms are represented by the following equation[352]:

$$q_t = q_e(1 - exp^{-k_{1t}\, t}) \tag{1-21}$$

$$log(q_e - q_t) = log(q_e) - \frac{k_1}{2 \cdot 303} t \tag{1-22}$$

In the above equations, k_1 is the rate constant of the pseudo-first-order kinetics model, q_e and q_t are adsorption capacity (mg g^{-1}) at equilibrium and at a time "t". A graph of log (q_e – q_t) vs "t" should give a straight line to allow calculation of the k_1 and q_e from the slope and intercept of the graph, respectively.

If the adsorption kinetic data are well fitted by the PFO kinetic model (i.e., if R^2 is close to unity for the fit), then physisorption is considered the rate-limiting step in the adsorption process.

1.8.2 Pseudo-Second Order Kinetics

Ho and McKay [353] expressed the pseudo-second-order (PSO) equation in 1999 by analysing findings from 112 literature studies and providing evidence using correlation data that all the experimental observations (from the selected studies) followed pseudo-second-order kinetics. After the publication of the work done by Ho and McKay, the PSO kinetic model became popular, and several studies conducted in the past years showed the dominance of the PSO kinetic model over the PFO kinetic model, as most of the kinetic data were found to follow PSO kinetic model to a better extent than the PFO kinetic model.

The non-linear and linear forms of the pseudo-second-order kinetic model are described as below[336]:

$$q_t = \frac{k_2 q_e^2 t}{(1 + q_e k_2 t)} \tag{1-23}$$

$$\left(\frac{t}{q_t}\right) = \frac{1}{k_2 q_e^2} + \frac{t}{q_e} \quad (1\text{-}24)$$

Where k_2 is the rate constant for pseudo-second-order kinetics, a plot of t/q_t vs t should give a straight line to determine q_e and k_2 as determined from values of the slope and intercept of the plot, respectively. The PSO model fitted to the experimental data illustrates that the chemical interaction is involved in the adsorption process, and the chemical adsorption is the rate-limiting step for the adsorption process.

The present study used the non-linear regression method to fit the PSO kinetic model on the heavy metal ions removal kinetic data on the synthesised composite systems using equation 1A-1D. The method is described in appendix 1 (section 1.3) for the Langmuir adsorption model, using the HYBRID error function. A similar method was used for the kinetic models fitting to the experimental data using four different error (non-linear regression) functions to calculate the best-fitted parameters of kinetic models. The best-fitted model values were decided by the calculated values of R^2, which lie closer to one for the best-fitted model values.

1.8.3 Weber-Morris Intra-Particle Diffusion Model

Weber and Morris described the intra-particle diffusion model (IPD) to explain the adsorption kinetics in 1962, which is given below:

$$q_t = k_d t^{0.5} + C \quad (1\text{-}25)$$

Where q_t is the amount of adsorbent in the solid phase (mg g^{-1}), k_d is the diffusion constant (mg g^{-1} $min^{-0.5}$) of IPD and C (the intercept) is the adsorption constant for any experiment in (mg g^{-1})[354]. A plot of q_t vs t is employed in different ways to explain intra-particle diffusion.

A single linear line plot is used to force through the origin, assuming intra-particle diffusion as the only rate-limiting step. A multi-linear plot explains more than one step in the adsorption process that could be defined by adsorption boundary thickness. The value of C gives an insight into boundary thickness as calculated by the intercept of the linear plot. A significant value of C specifies an extraordinary boundary thickness effect[338].

Generally, this model explains that the adsorption capacity varies with the square root of the time ($t^{0.5}$), and the adsorption process is typically following more than one step (as rate-limiting steps).

The adsorption process can include more than one step, such as boundary diffusion (film diffusion), sorbate diffusion from solution to the adsorbent's external surface, and intra-particle diffusion. The slowest process controls the overall rate of adsorption, while more than one process is considered as a rate-limiting process for adsorption. Theoretically, in the IPD model, if the intra-particle diffusion is the only rate-limiting step, then the plot based on this model equation must be linear and pass through the origin[355]. Most adsorption processes have been found to follow two or three steps, with the fastest initial step, which is attributed to bulk diffusion, followed by slower rate-limiting step(s)[356]. The rate-limiting steps could include chemical adsorption (occurring at particular adsorption sites to form complexes) and the intra-particular diffusion in the pore spaces of the porous adsorbents.

In literature studies, three steps of the multi-linear graph are explained as follows[357-359]:

Step 1: The bulk diffusion step, indicated by the steep line, describes the mass transfer from liquid to the adsorbent surface. It is the fastest, giving the highest k_d (rate of diffusion in step one) value of all three steps, due to the availability of excess adsorbate molecules in the solution and active sites on the surface of the adsorbent. The value of C (boundary thickness) is the lowest for this step because the lowest hindrance for the sorbate molecules is at the start of the adsorption process.

Step 2: In this step, the sorbate molecules adsorbed on the surface (in step one) diffuse into intra-particle space to penetrate into the inner structure of the adsorbent. The value of C is relatively higher than step 1 due to the adsorbed molecules on the surface. In comparison, the value of k_d in this step (second) is lower than in step one due to slower intra-particle diffusion. The diffusion rate is slowed down because of interference caused by molecules adsorbed on the surface.

Step 3 describes the last step of the adsorption process when it reaches equilibrium due to the saturation of active sites on the surface. The intra-particle diffusion space becomes narrow or blocked to allow more diffusion, not inside of pores. The concentration of sorbate molecules is also decreased in the solution while reaching this stage. At this step, the C (boundary layer thickness) is the highest due to adsorbed molecules in steps one and two, and the k_d is the lowest due to hindrance caused by the boundary layer thickness.

This kinetic model is applicable and described for porous materials. The model was included to study the kinetics of metal cation adsorption on the CH/HAp/Zeolite composites systems (in Chapter 5, section 5.1.4), taking into consideration the porous nature of zeolite materials.

Table 1-8 Literature studies showing the adsorption and kinetic models fitted to the composite based-adsorption systems

Heavy metal ions	Composite systems	Best-fitted isotherm models	Best-fitted kinetic models	References
Hg(II)	Chitosan/cotton fibres	Langmuir & Freundlich	PSO	360
Cu^{2+}, Ni^{2+}, Cd^{2+}	Chitosan/cotton fibres	Langmuir & Freundlich	PSO	361
Pb^{2+}		Freundlich	PSO	
Cu^{2+}, Ni^{2+}	Chitosan/Perlite	Langmuir & Freundlich	PSO	161
Cr(VI)	Chitosan/Perlite	Langmuir	_	164
As(III) , As(V)	Chitosan/Ceramic alumina	Langmuir, Freundlich	_	362
Cr(VI)	Chitosan/Ceramic alumina	Langmuir, Freundlich	_	363
Cu^{2+}	Chitosan/Alginate	Langmuir	PSO	364
Cd^{2+}	Chitosan/Ceramic alumina	Langmuir	PSO	
Cr(VI), Cu(II)	Chitosan/Orange peel	Freundlich	PSO	365
Cd^{2+}	Chitosan/Mesoporous silica	Freundlich	PFO	
Cu^{2+}	Chitosan/Poly(Lactic Acid)	Langmuir	PSO	204
Cu^{2+}	Chitosan/Montmorillonite	Langmuir	PSO	366
Cu^{2+}, Zn^{2+}	HAp/naturalsnail shell/chitosan	Langmuir & Temkin	PSO	367
Pb^{2+}	HAp/Cellulose acetate	Freundlich	PSO	111
Pb^{2+}	HAp/Chitosan	Elovich	PFO &PSO	368
Cu^{2+}, Ni^{2+}	HAp/Lignin/Alginate	Langmuir	PFO	369
Pb^{2+}	HAp/Chitosan	–	PSO	370

Cu^{2+}, Pb^{2+}	HAp/Bisphosphonate	Langmuir	–	371
As(V)	HAp/Cellulose	Langmuir	PFO	372
Cr(VI)	HAp/Cellulose	Langmuir	PSO	373
Pb^{2+}	HAp/Activated carbon	Langmuir, Freundlich		374
Pb^{2+}	HAp/Calcium silicate	Langmuir	PSO	375
Pb^{2+}, Ni^{2+}, Co^{2+}	HAp/Chitosan	Langmuir	PSO	82
Cu^{2+}, Zn^{2+}, Cd^{2+}, Pb^{2+}	HAp/Cellulose	Langmuir	–	376
Cd^{2+}	HAp/Chitosan	Langmuir	PSO	377
Pb^{2+}	HAp/Polyurethane	Langmuir	PSO	378
Pb^{2+}	HAp/Polyacrylamide	Langmuir	PSO	379
Pb^{2+}, Ni^{2+}, Co^{2+}	HAp/Chitosan	Langmuir, Freundlich	PSO	380
Pb^{2+}	HAp/Magnitite	Langmuir, Freundlich	PSO	381

PFO = Pseudo-first order kinetic model
PSO = Pseudo-second-order kinetic model

1.9 Significance of the selected feedstock materials and this research

Heavy metals, by nature, are non-degradable and hence persistent in the environment. Moreover, they are easily soluble and able to make their way to cells in organisms. The real threat to ecosystems is imposed by the entry of these contaminants into the food chain. Globally, pure water availability is becoming crucial over time and with its increasing demand due to an expanding global population. Thus the re-use of industrial wastewater before its discharge into any local water body using efficient strategies to reduce heavy metal contamination is an important research goal in the water treatment and purification field[328].

As mentioned above, globally, water demand is predicted to increase significantly over the coming decades. In addition to the water demand from the agricultural sector, which is currently responsible for 70% of water extractions worldwide, large increases in water demand are predicted, particularly for industry and energy production. The above estimates support the often-cited approximation that, globally, it is likely that over 80% of wastewater is released into the environment without adequate treatment. Inadequate wastewater management also directly impacts ecosystems services (such as food and water availability)[3]. Discharge effluent from industrial and agriculture activities are high in volume so that heavy metals, including organic compounds and some effluents, can be disposed of without proper treatment. This directly impacts water quality[329]. It has been estimated that two-thirds of the world's population may face water shortages by 2025, and the impacts of this shortage could be even worse for ecosystems (Worldwide Fund, WWF). There is a growing recognition of using wastewater as a water resource for different sectors. A shift in using treated wastewater in different sectors, such as for agricultural purposes rather than discharging it as a by-product, is growing[45]. By paying serious consideration to the above-mentioned environmental problems, it will be crucial to treat wastewater for ensuring the quality of surface and groundwater. Additionally, treated wastewater may provide a source to reuse in industrial and agricultural industries. Cost-effectiveness is the most important parameter before the application of any method for water treatment. This is especially so if it is to be used on a large scale. Among all available options, the use of inherently low-cost materials is hence the best option for water treatment. For this purpose, agricultural or industrial by-products can be very promising sources for developing materials/material composite for water treatment. This

is because the management and repurposing of industrial and agricultural by-products are also serious environmental problems in every developed and developing country of the world.

There is a drive towards sustainability, developing processes that solve present problems without compromising future generations. One valuable opportunity to repurpose these by-products is by using these materials to develop products which may be reused to solve another environmental problem issue. Globally, 6-8 million tonnes of marine by-products are produced, in which Southeast Asia alone accounts for 1.5 million tonnes. In developed countries, the management of seafood waste is expensive, with its costing up to US$150 per tonne in Australia, while in developing countries, it may, unfortunately, be dumped in landfills or at sea. The extraction of useful materials (such as chitin) from these marine by-products will be one good solution to waste disposal[330]. In other areas worldwide, 5 to 6 million tonnes of coconut fibre are produced yearly, with only 10% of this amount having been used commercially and the remainder being discarded into the environment[331].

So, the use of materials derived from marine by-products or even agricultural sources would not only be desirable from a cost viewpoint but will also help to mitigate environmental impacts**.** As described in detail in the literature review section, these materials can serve as effective adsorbents for the removal of heavy metals from water. The chemical structure of these materials supports adsorption and ion exchange processes, especially heavy metals and their effectiveness, it is believed, may be increased by developing innovative composites of these materials and applying them in different operating systems under different conditions. It is hypothesized that these materials could constitute an effective method of water treatment due to the enhancement of metal ion removal abilities by the several mechanisms that would exist in the composite.

1.10 Aim of this study and the overview of synthesised composite materials

More broadly, this study was based on one fundamental aim, i.e., *"the removal of heavy metal ions using low-cost adsorbents*", which was achieved by selecting low-cost materials with the potential to remove heavy metal ions. Afterwards, the composite

matrices using the candidate materials were synthesised to evaluate the removal efficiencies of the composite materials.

The commercially supplied hydroxyapatite (cHAp) was added to commercially sourced chitosan to make a chitosan/HAp (CH/cHAp) composite (the first composite considered for this study), and it was expected that the HAp (commercial) would enhance the removal ability of the chitosan. It was evaluated by comparing the removal efficiency of the chitosan (from literature studies) with the CH/HAp composite (present study). This two component-based composite system (CH/cHAp) was used as a composite control system. As described earlier, animal bone sourced HAp (bHAp) can be used in place of commercial HAp, as literature reported using bio-sourced HAp in the water treatment systems. Hence, another chitosan and HAp based composite was synthesised using the bovine-derived HAp (bHAp), and this composite (CH/bHAp) was used to compare with the CH/cHAp composite for the adsorption of metal ions.

As the literature studies reported the use of chitosan/HAp (for commercial HAp) composites for the removal of heavy metal ions, but no study reported the use of bovine-sourced HAp in combination with chitosan to remove heavy metal ions, this was hence selected as a unique combination for application as a heavy metal ion removal system.

Additionally, the third component (as a discrete phase) was added to CH/HAp (either CH/cHAp or CH/bHAp) composites to make novel combinations of the composites. The selected combinations (mentioned below) were not reported earlier in the literature for heavy metal ion removal. It was hypothesised that the addition of the third component (e.g., coir, fibre, SCGs or zeolite) into the CH/HAp composite would help to improve the removal efficiency or improve the applicability of the composite by providing stability or mechanical strength to the composite. The detailed synthesis and characterisation of two-component-based and three-component-based composites are given in the upcoming chapter (Chapter 3). For the overview of these composite systems, the following combinations were selected and synthesised to remove the metal ions from the aqueous solutions.

(i) ***Two-component composite systems*** containing chitosan and hydroxyapatite only (termed as control composites), which included Chitosan/commercial hydroxyapatite (CH/cHAp) and Chitosan/bovine-derived hydroxyapatite (CH/bHAp)

(ii) ***Three-component composite systems*** were synthesised by adding a third component into the CH/HAp based control composites, either using CH/cHAp or CH/bHAp. The materials added as a third component included coir fibre (CF), spent coffee grounds (SCGs) and zeolite.

The combinations for base-3 component composite systems are given as:

- CH/HAp/CF
- CH/HAp/SCGs
- CH/HAp/Zeolite

In this way, two sets of 3 component composite systems were formed as:

- ***cHAp-based composites*** using commercial hydroxyapatite and for these systems, CH/cHAp (base-2 component system) would be considered as composite control systems
- ***bHAp-based composite systems*** using the bovine-sourced hydroxyapatite: For these systems, the CH/bHAp would be taken as control composite systems to compare the removal efficiencies for metal ion removal.

As mentioned earlier, the choice of these combinations was made after carrying out the literature review to fulfil the fundamental aims of this study, which include using low-cost materials to effectively adsorb heavy metal ions from an aqueous solution. The following section also includes a justification of the selected combinations, which also aligned with the fundamental aims of this study.

Overall, this research aimed to provide *environmentally sustainable* and *economically feasible* solutions to remediate water pollution to target heavy metal removal. It focused on developing effective material composites with their adsorption or ion-exchange capacities for selected heavy metals (i.e., Pb, Cd, Cr, Cu) being optimized. It was of interest to develop economically viable materials and provide a means to utilize customarily discarded industrial and agricultural by-products. The key goals of this study could be summarised as follows:

Adsorption: Adsorption is a popular technique used for wastewater treatment, as discussed above in detail. The study is aimed at the adsorption process used to remove the heavy metal ions from the aqueous solutions. Polymeric materials (e.g., chitosan) and lignocellulosic materials (e.g., coir fibre, spent coffee grounds) are known to be very good

adsorbents that were selected to synthesise the composite materials for the adsorption of the heavy metal ions. Previous studies have given special attention to the potential of biopolymers such as chitosan in various applications, including heavy metal ions removal. Similarly, other candidate materials selected for this study can also adsorb heavy metal ions.

Waste management: Responsible management of waste/by-products from various industries is needed to avoid their careless disposal into the environment leading to pollution. For instance, global seafood markets, including the processing of lobsters, crabs, crayfish, crabs, and prawns, discard 50% of their shell waste, which adds up to millions of tonnes of waste that annually end up in the environment[146]. Using these by-products to produce valuable materials helps manage this environmental waste and create more sustainable processes.

Low-cost materials: The precursor material cost and the cost of operation for applying adsorbents for water treatment are key parameters. When making adsorbents for application, the selection of materials must consider the environmental consequences; therefore, agricultural or industrial by-products were considered the most suitable materials as these by-products would have been discarded into the environment anyway. Hence, using industrial by-products would be a double advantage, one being their relatively low cost and the other being a repurposing of the material to prevent its pointless disposal into the environment. Additionally, disposal costs would be spared.

1.11 Experimental Set up for the removal of metal ions using the adsorbent systems

The removal experiments are conducted in different experimental setups in the literature studies. The batch adsorption experiments using the model solutions of metal ions, or the original wastewater/environmental samples are extensively used in the laboratory setup. For this, different experimental parameters are studied to evaluate their effect on the adsorption efficiencies of the adsorbent systems. One parameter (as an independent variable) is regulated or controlled by keeping all other parameters constant.

Batch experiments using the model solutions could be conducted using different compositions of solution. For instance, the model solutions could contain a single metal-ion type, containing only one metal ion type, to evaluate the effect of different

experimental parameters on the removal efficiencies of the employed adsorbent systems for that particular (one) metal ion. Similarly, the solutions containing two or three metal ion types were prepared to evaluate the competitive adsorption of these metal ions on the adsorbent systems. Similarly, multi-metal ion-type solutions have also been employed in the literature studies to evaluate the competitive adsorption of the metal ions on the given adsorbent systems.

In the present study, the batch experiments were conducted using *the one metal ion type* solution, containing only one type of metal ion (e.g., Cd^{2+} or Pb^{2+}), and *two-metal ion type* solution (containing two metal ions in equimolar concentration) to evaluate the removal efficiencies of the employed system. After carrying out the experiments using the single-metal ion type and two-metal ion type solutions, it was desired to test the performance of the composites by exposing them to an industrial type of solution consisting of three co-dissolved heavy metal species of relevance to the wood treatment industry. The sample supplied was not a sample of wastewater from the company but the actual input stream (i.e., before it was exposed to the wood). This, nevertheless, was regarded as a suitable mimic for an industrial wastewater sample, except that the concentrations of heavy metals present were higher than they would have been due to non-exposure to the wood. The other aspect of the sample was that it contained a metal that had not previously been tested in the solutions containing either one or two metal ion types (as it was not available as an element for analysis by AAS). This was arsenic (present as the arsenate ion).

The definitions of the three sampling scenarios are given below:

1.11.1 Single-metal ion type solution systems

A system having only one metal ion type (e.g., Cd^{2+}) dissolved in it to evaluate the removal efficiency of each composite is described as a “single metal ion type system” in this study. The single metal ions covered in these experiments include the divalent cations of Cd^{2+}, Pb^{2+} and Cu^{2+}) and the anionic system containing Cr (as chromate ion).

1.11.2 Two-metal ion type solution systems

The system that contained both the divalent metal cations of (Pb^{2+} and Cd^{2+}) in equimolar concentrations was termed a two-metal ion type system.

1.11.3 Industrial input stream sample system

This system was an industrial input stream sample that was kindly provided by a company that subjected wood to the copper chrome arsenate treatment. The solution effectively represented an environmental sample containing three co-dissolved three metal ion types. This was used to evaluate the utility of the synthesised composites to treat such solutions where competitive metal adsorption would be taking place.

This study is based on the adsorption process, which is modelled using different adsorption models. The following section describes the theoretical background and justifications for using the adsorption and kinetic models employed in the current study to explain the adsorption behaviours.

1.12 Summary

Global population growth has resulted in an increase in agricultural activities, industrialisation and urbanisation and ultimately increasing pressure on water resources. There is a need to treat wastewater arising from industrial processes by using low-cost and eco-friendly methods, as this water could be reused as a conventional source of water in different sectors like agriculture.

Heavy metal ions are one of the most persistent and toxic water pollutants. They are associated with the risk of bioaccumulation and cancer. Wastewater containing these heavy metal ions could be treated to remove them so that they may be reused in, say, the agricultural sector. Different conventional methods are used to remove metal ions, mostly linked with high energy consumption and cost. Adsorption is considered one of the most effective, simple and low-cost methods to treat wastewater for heavy metal ion adsorption. Agricultural and industrial by-products have been used as a low-cost feedstock material to make composite adsorbents for the removal of metal ions. Among these by-products, biopolymeric and lignocellulosic materials have been employed in water treatment systems for the removal of metal ions and are found to be potential materials to remove metal ions from water.

In the present study, after an extensive literature review was carried out on the above theme, chitosan, coir fibre, spent coffee grounds, and zeolites were selected as low-cost feedstock materials to synthesise composites that could be used to remove metal ions from wastewater by adsorption processes. The chemical compositions (functional groups

such as amino and hydroxyl groups) and physical properties (e.g., the higher surface area) of these materials have been demonstrated to have a high potential to remove the metal ions. Hydroxyapatite is an effective material for removing metal ions, as discussed in many literature studies. It was chosen to make composites with the selected feedstock materials in this study for use in water treatment systems for the removal of metal ions.

In this study, two types of composites were prepared; the first type was two-component composite systems, which included only chitosan and hydroxyapatite. The second type was a series of three-component composite systems where the third component was chosen from coir fibre, spent coffee grounds or zeolite and combined along with chitosan and hydroxyapatite in a composite. The two-component composite systems were considered as a control composite system to evaluate their potential to remove heavy metal ions from the solution, while the third component was added to this system to evaluate whether the additional component would enhance the removal efficiency of the control composite.

Further, each composite system (i.e., the two-component or three-component composite systems) was synthesised using two types of hydroxyapatites, from either a commercial source(cHAp) or from a bovine-derived source (bHAp). These were prepared to compare the removal efficiencies of the cHAp-based and bHAp-based composite systems.

Based on the chemical composition of the feedstock materials, metal-ligand complexation and ion exchange were considered the dominant mechanisms for the adsorption of metal ions. Additionally, different adsorption and kinetic models were also considered to fit the experimental data to demonstrate the adsorption behaviours exhibited by the metal ions when adsorbing on the synthesised composite adsorbent systems.

After selecting the feedstock materials, characterisation using different microscopic and spectroscopic techniques was carried out to determine their physical and chemical attributes, which assisted their characterisation when combined with the other materials in the composite systems. The next chapter comprehensively explains the methods used in the material characterisation and discusses the results of the characterisation of the selected materials.

Chapter 2

Raw Materials making up the Composite Matrices: Their Sources, Processing and Characterisation

The selected raw materials were initially characterised by a suite of instrumental techniques to provide a molecular fingerprint to aid comparison between the raw materials and when they were incorporated into the resulting composites. This chapter hence solely explains the methods and procedures of characterisation used to characterise the raw materials (and composite adsorbents in the next chapter) and discusses the results of such characterisation to set a foundation for discussing the characterisation of the composite adsorbents in Chapter 3.

2.1 Introduction

When considering the raw materials making up composites, several properties such as chemical composition (functional groups), the nature of materials employed (be they crystalline or amorphous), and surface characteristics all play a fundamental role in synthesising composites. It is essential to consider their suitability and efficiency when it comes to the uptake of heavy metals (see Chapter 1). Some source materials may require additional chemical or physical modification when they are used in a composite synthesis to produce the best possible composite matrices for water treatments. Physical changes may take the form of grinding, for instance, to achieve smaller particle sizes and to increase the surface area available for adsorption. It has been shown by Raghavendra et al.[382] that the hydration properties of coconut residue (coir fibre) improved after grinding, possibly due to the expected increase in surface area and pore volume[382]. This modification hence made these fibres an attractive candidate for employment in water treatment technology, where their efficiency in adsorbing heavy metal ions was expected to increase. Similarly, in Chapter 1 (section 1.5.3), it was discussed in detail how the

chemical and physical modifications of materials from past studies helped to improve their metal removal capacities.

The research described in this thesis employs six different raw materials, which are examined and characterised further in this chapter. These raw materials were considered in combinations (scheme of combination given in Chapter 1, section 1.8)) to make composite matrices with hydroxyapatite that were then tested to assess their adsorptive abilities for removing heavy metal ions from aqueous solutions (dealt with in Chapter 5). Most of the raw materials used in syntheses of composite systems were employed as received without modification or processing. However, some materials did require some simple processing, such as washing, drying, and grinding.

In addition, to discussing the experimental details of the raw materials used in composites in this study, the various instrumental techniques used in the characterization of materials in this chapter and subsequent chapters will also be introduced. Given the instrumental techniques used for characterization are highly standard in materials science characterization, only a brief introduction to these has been made. In general, these methods include scanning electron microscopy (SEM), elemental analysis by energy-dispersive X-ray spectroscopy (EDX), Thermogravimetric analysis (TGA), Fourier transform infrared spectroscopy (FTIR) and powder X-ray diffraction (XRD).

2.2 Experimental details of the raw materials used in this study

2.2.1 Chitosan

Chitosan (referred to as CH for composite identification) was purchased from TCI (Tokyo Chemical Industries, Japan). In appearance, these were white to light yellow, flaky crystals with a stated degree of deacetylation > 80%.

2.2.2 Hydroxyapatite sources

The hydroxyapatite used in these studies came from two sources. One was a commercial powder, while the other had been supplied as received from a previously conducted science project in which New Zealand cattle bone had been converted to hydroxyapatite by using a thermal calcination method.

2.2.2.1 Hydroxyapatite (Commercial) powder (cHAp)

Analytical grade "Fluka" hydroxyapatite synthetic powder (purum p.a ≥ 90%) was purchased from Sigma-Aldrich. The powder is referred to as **cHAp** in this study.

2.2.2.2 Bovine-sourced hydroxyapatite (bHAp)

The HAp sourced in this study was existing pre-processed material in the laboratory in the School of Science, University of Waikato. This material was prepared in a previous project involving thermal calcination of the defatted crushed bone (sourced from cattle bones obtained from an abattoir) in a muffle furnace at 1000 °C, which burnt out the collagen-producing a white crystalline powder with some visible specks of char present. It is referred to as **bHAp** in this study.

2.2.3 Coir Fibre (CF)

Coir fibre (CF) was purchased from a local hardware store "Mitre 10" in Hamilton, New Zealand. The material consisted of brown-coloured, lightweight fibres and had originally come from Vietnam.

2.2.4 Spent coffee grounds (SCGs)

Spent coffee grounds were collected from a commercial automatic-dispensing coffee machine (Café Direct: c008965) located at the University of Waikato (Science and Engineering tearoom). The grinds were further ground after drying at 50 ºC when used in composites with hydroxyapatite.

2.2.5 Zeolite pellets

The zeolite used in the study was provided by WIS Pty. Ltd. and purchased from a local hardware store. The zeolite (obtained commercially in a sack) was identified by powder X-ray diffraction to be mordenite, with the representative chemical formula being $Al_2Si_{10}O_{24}\cdot 7H_2O$. It was an odourless granular solid with specification sheets stating it to have less than 10% crystalline silica and a specific gravity of approximately 0.65 g cm^{-3}.

2.3 Instrumental Methods used in this study

2.3.1 Fourier Transform Infrared Spectroscopy (FTIR)

FTIR is a fundamental molecular characterization technique of materials in solid, liquid, or gaseous states. When presented in various forms to the spectrometer (e.g., disks, thin films, mulls, in gas cells or simply as-received), the samples are irradiated with IR radiation in the mid (4000-400 cm^{-1}) IR range. Radiation of these wavelengths is absorbed by stretching and bending vibrations undergone by the molecules which comprise the material under analysis. Peaks detected in the IR spectrum usually represent fundamental vibrational frequencies, with each molecule having a set of unique or characteristic fingerprint peaks. These peaks occur at vibrational frequencies, which are sensitive to the chemical functional groups contained within the molecule, which are well known and extensively tabulated in the literature. IR spectroscopy is hence highly useful for identifying unknown samples or detecting the presence of certain chemical functional groups in different materials[383].

Experimental: All samples analysed by FTIR in the current study were recorded as potassium bromide (KBr) disks prepared by adding the pre-ground (and dried) analyte of interest to oven-dried KBr (Merck) (in a 1:9 sample: KBr ratio) followed by grinding to make a fine, homogenized powder. The powder was then placed in a KBr sample die, pressed at 7 tons pressure to prepare the semi-transparent KBr disks, which were subsequently placed in a sample holder and scanned from 4000-450 cm^{-1} on a Perkin Elmer Spectrum 400 FT-Spectrometer using three scans acquired at 4 cm^{-1} resolution with a spectrum of the empty sample holder functioning as the background. Baseline correction was done for each resultant spectrum using the Perkin Elmer proprietary software, followed by peak picking.

2.3.2 Powder X-ray Diffraction (pXRD)

Powder X-ray Diffraction (pXRD) is used to gather information about a material's structure, phase, and texture, including other structural parameters such as grain size, strain, and crystal defects. During pXRD analysis, a polycrystalline solid sample is exposed to X-rays of known wavelengths which means X-rays are diffracted from the crystal lattice existing in the polycrystalline sample. This results in characteristic diffraction patterns consisting of peaks with differing intensities[384]. Bragg's law given as

$n\lambda = 2d\sin\theta$ can explain the patterns observed where "λ" is the wavelength of the X-ray, "d" corresponds to distances between the different planes of the crystal lattice and "θ" represents the angle of diffraction[385]. To identify the phase(s) of materials examined, a standard database (International Centre for Diffraction database ICDD) was used along with software (known as High Score)[386] that is associated with the instrument used and which can search the database for matches.

Experimental: All powder X-ray diffractograms presented in this study were recorded on a Panalytical Empyrean multi-purpose X-ray Diffractometer, which used Ni-filtered, Cu Kα radiation (λ = 1.5406 Å), a 10 mm beam mask and a 1° anti- scattering slit. Finely ground sample material was packed into the aluminium metal sample holders to ensure a flat surface. The complete list of instrumental settings used is given below:

Anode Material: Cu

K-Alpha1 wavelength: 1.540598 Å

K-Alpha 2 wavelengths: 1.544426 Å

Ratio K-Alpha2/K-Alpha1: 0.5

Divergent slit: Fixed (0.5) °

Receiving slit: 0.1 °

Generator voltage: 45 mV

Tube current: 40 mA

Scanning range: 2θ = 5° - 100°

Scan step size: 0.026

Time per step (ms): 236.64

The resultant X-ray diffractograms were further analysed using the "Xpert-High Score plus" software to elucidate phase or other structural information from the solid materials examined.

2.3.3 Scanning Electron Microscopy and Energy-dispersive X-ray spectroscopy (SEM & EDX)

SEM is a microscopy technique that uses a high energy electron beam to provide a detailed sample image at very high magnification. Areas ranging from approximately 1 cm to 5 microns in width can be imaged in the scanning mode using conventional SEM techniques (magnification ranging from 20X to approximately 30,000X, a spatial

resolution of 50 to 100 nm). In conjunction with SEM, another technique called Energy-dispersive X-ray spectroscopy (EDS or EDX) is routinely used to determine a sample's elemental composition. The essential working requirement for an SEM is to work in a vacuum to prevent any interaction between air molecules and the source's electron beam. Additionally, it is necessary to conduct electrons in the sample away from it to avoid any charging effect at the surface, which can lead to poor image quality characterised by extra brightness being seen in the image. Pre-coating the sample with metal like gold or platinum helps in the imaging of non-conductive materials like polymers or ceramics (e.g. hydroxyapatite) by providing readily conductive surfaces[387].

Experimental: All SEM/EDX analyses conducted in this study were performed using ground, dried powders and analysed using a Hitachi S-4700 Field Emission Scanning Electron microscope. Sampling involved applying a thin layer of powdered sample to double-sided adhesive tape mounted on a stainless-steel sample holder, which was then platinum coated to reduce charging whilst under the beam. Additional analysis for hydroxyapatite was conducted without the platinum coating to allow a more reliable measurement of the Ca:P ratio without interference from Pt signals. Different accelerating voltages (5 to 15 keV) and working distances (10 to 15 mm) were used to take images. EDX analysis of the powdered samples was always done using high voltage (15 keV) at a constant working distance of 15 mm. The method of EDX analysis used was standardless. Several EDX analyses (at least three) were acquired by randomly targeting different sites of the same sample to obtain a more reliable estimation of elemental percentages and to overcome the limitations of this analysis, such as the use of a small sample, surface interactions (i.e. effects of roughness in sample surfaces) and accelerating voltages that could produce different results[388,389].

2.3.4 Thermogravimetric Analysis (TGA)

TGA is used to determine the thermal stability of materials by measuring the recorded loss in weight of the material as a function of temperature or time. A TGA instrument has two modes of operation, depending on whether time or temperature measurements are of interest. When time is selected as a function, it is called the "isotherm thermal mode", and "scanning mode" is the terminology used when the temperature is chosen to determine weight losses. When TGA is performed under programmed conditions, weight losses can explain or determine various thermal events occurring within the sample, such

as dehydration, oxidation, reduction, vaporization, and sublimation. Additionally, thermograms can also be used to describe multiple gaseous losses from materials. The types of material examinable by this technique are polymers and biopolymers, nanomaterials, fibres, films and coatings[390].

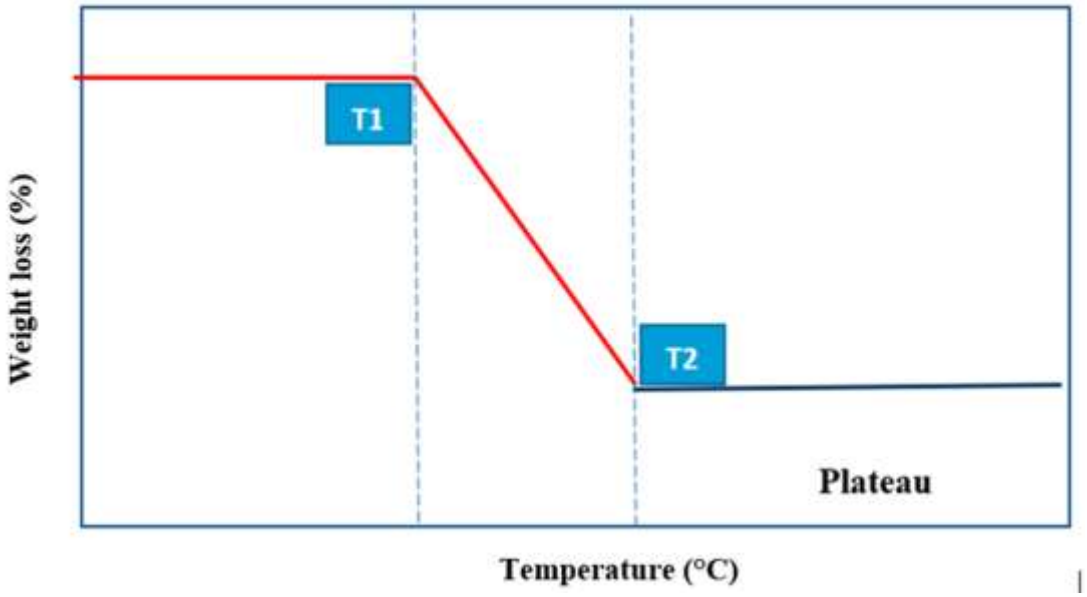

Figure 2-1: A typical thermogram with a single weight-loss event

A typical thermogram shown in Figure 2-1 represents weight loss (%) as a function of temperature, indicating a single decomposition event. T1 is the initial temperature where the decomposition starts, and T2 is the final temperature where it ends. The observed plateau shown in Figure 2-1 denotes a constant line region after the decomposition event, which occurs when no further weight loss to the material under examination occurs.

Experimental: In the present study, all the materials (be they raw or composite materials) were thermally analysed at different temperature ranges from 30 ºC to 1000 ºC under an air environment using PerkinElmer 8000 TGA analyser. About 20 mg of powdered sample was placed in the sample holder and placed in the sample holding pan. The analysis was done using a scanning speed of 10 º C min^{-1}.

One of the effective ways to interpret the TGA data is the "derivative curve of TG", otherwise known as the DTG curve[391,392]. The first derivative of % weight loss is calculated using OriginPro software 2021 (version 9.8.0.200), and the derivative data are then plotted against temperature. This highlights better the thermal events in TGA analyses of materials.

2.3.5 Specific Surface area estimation using the Mastersizer

In addition to the above characterisation methods, an estimation of the specific surface area of powdered raw materials and synthesised composite adsorbents was done by using the Malvern Mastersizer. This instrument uses a laser diffraction method (LDM) to measure the particle size distribution in terms of volume percentage. It was assumed in this method that the particles are treated as spherical. The particles cause the scattering of the light beam, which will scatter at an angle that would be directly related to particle sizes[481,587].

For this analysis, the materials were ground using a mortar and pestle, which produced a relatively heterogeneous sample in terms of grain sizes. Some of the raw materials could not be analysed easily due to their physical or chemical nature (e.g., chitosan, SCGs and coir fibre). Additionally, some of the composites were extremely heterogeneous in nature due to their composition. For instance, the CH/HAp/CF and CH/HAp/SCGs composites, which contained particles of the coir fibre and spent coffee grounds, as well as chitosan. In comparison, some other composites were relatively less heterogeneous, for instance, the CH/HAp composites.

As the instrument measures the particle sizes based on the assumption of spherical particles, it is therefore not very accurate for the true measurement of samples that may have irregular and angular shapes. The synthesised materials were not uniform in size, so this analysis was used at best estimate their particle sizes and the specific surface area of the composites. The results for the grain size and specific surface area of the composite adsorbents studied by this technique are included in appendix 3.

2.4 Results and Discussion: Raw materials Characterization

The following section provides a detailed characterization of the raw materials used in this project to prepare the composites under investigation. It is important to have a good idea of these characteristics when analysing combinations of such materials so that contributions from each material can be recognised without ambiguity in characterisations. This chapter will be referred back to in later sections of the thesis when

analysing the composites made up of combinations of the raw materials as characterised below.

An important point to note is that the y-axis scaling of the figures (such as FTIR spectra, XRD diffractograms and TGA thermograms) was determined automatically by OriginPro software used for plotting these figures in this study.

2.4.1 Characterization of chitosan

2.4.1.1 SEM/EDX characterization of chitosan

The micrographs of the chitosan (TCI) used in the current study are illustrated in Figure 2.2. The micrographs show the surface morphology of the flake-like material at two different resolutions (3 µm and 30.0 µm). At low voltage (Figure 2-2 a & b), it exhibited a non-porous multilayer structure with a fibrous surface. It appears as fragile-looking sheets with many microfibrils. The micrograph at high voltage (Figure 2-2 c) displays a close-up view of the flakes showing them to consist of a smooth sheet with some irregular orifices on the surface. This morphology of chitosan, as observed, is typical of that reported in previous studies [393,394].

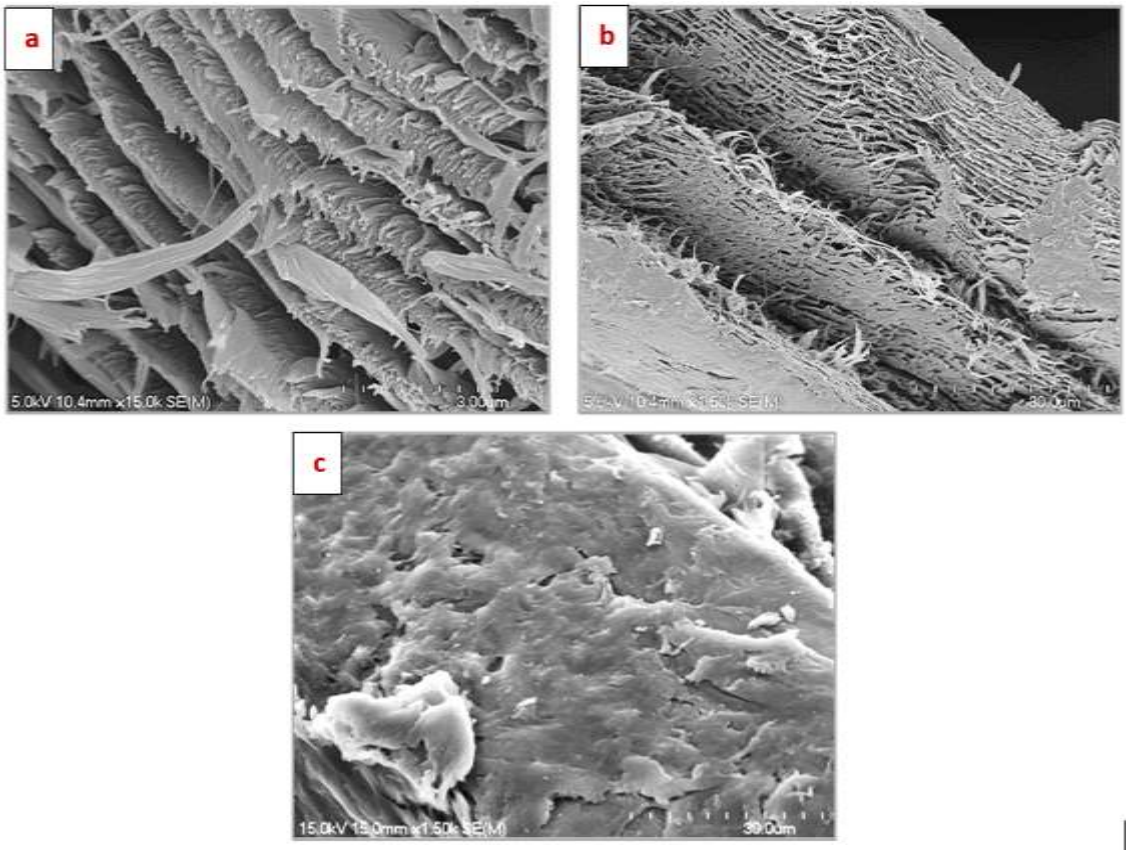

Figure 2-2: SEM micrographs of commercial chitosan 5.0 kV (a & b), 15 kV (c) used in the present study

The EDX elemental analysis of the chitosan is presented in Figure 2-3, which summarises the percentage amounts of the major elemental components of chitosan. These show expectedly that carbon and oxygen are the principal constituent elements of chitosan. Previous reports have shown that a low nitrogen level can also be present in these samples (due to unconverted chitin)[395]. A lower level of nitrogen could still be present (as DDA >80%) but is not detectable in the chitosan elemental analysis at this level of acetylation. The additional smaller peak at ca. 2 keV is due to the Pt coating on the specimen.

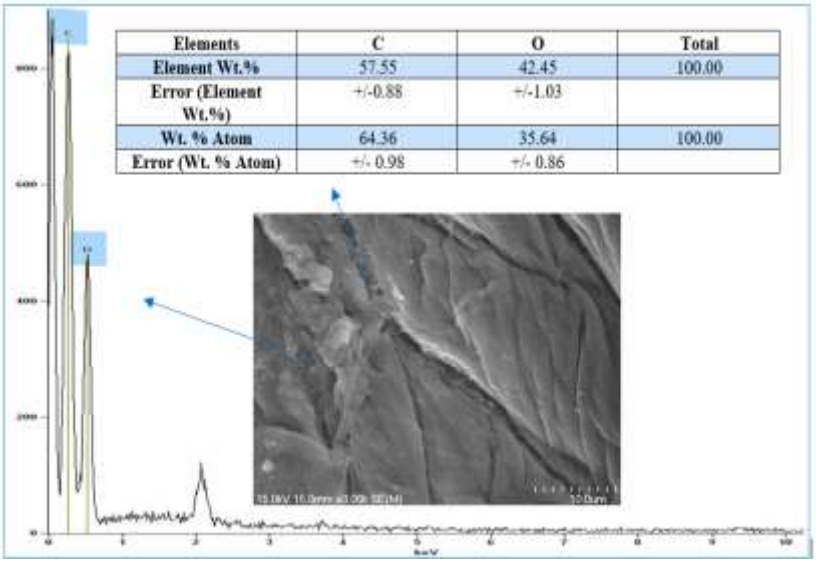

Figure 2-3: SEM micrograph and EDX analysis of the as-received TCI chitosan used in the present study

2.4.1.2 FTIR analysis of chitosan

The FTIR spectrum of chitosan as a KBr disk is shown in Figure 2-5. The range shows the characteristic absorption bands due to chitosan, which have been assigned as per Table 2-1. The features observed in Table 2-1 entirely agree with previous literature reports on the FTIR of chitosan.

Table 2-1: Characteristic IR absorption peaks of chitosan[396-398]

Assignment	**Wavenumber (cm^{-1})**
-OH and -NH stretching	3450-3500 (s)
C=O stretching	1638 (s)
C-H bending	1380 (m)
C-H stretching	2877 and 2921(m)
C-O-C stretching	1150 (w)
C-O stretching	1032 and 1074 (s)
C-H twisting	896 (w)
C-N stretching	1320 (m)

(s) = strong intensity, (m)= moderate, (w)=weak

The basic structural unit of chitosan polymer is given in Figure 2-4 to identify the corresponding absorption peaks in Figure 2.5.

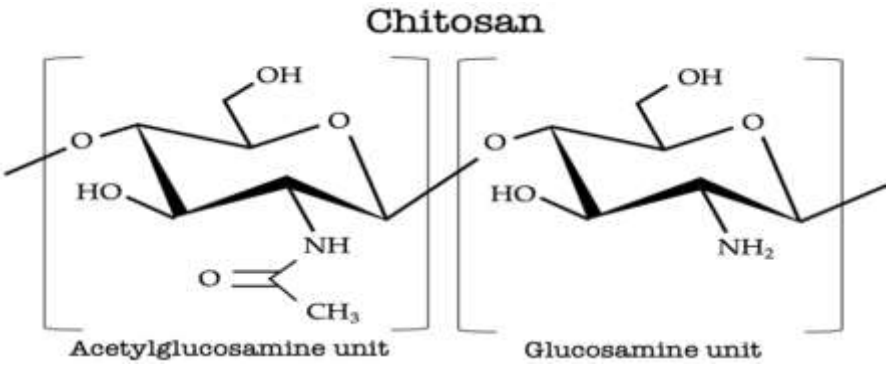

Figure 2-4: The basic structural unit of chitosan biopolymer [399]

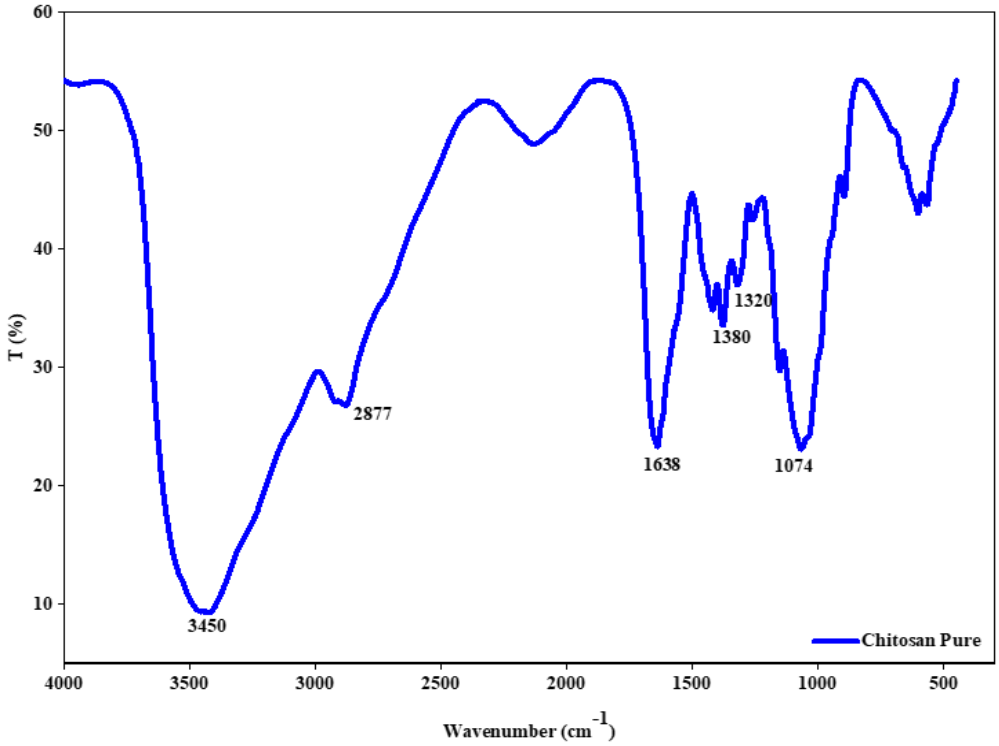

Figure 2-5: FTIR spectrum of TCI chitosan used in this study

2.4.1.3 Powder X-ray Diffraction of chitosan

The XRD diffractogram (Figure 2-6) of pure chitosan flakes displays two broad peaks around 2θ =10° and 2θ =20°, while another broad peak of very low intensity can be observed at 2θ =28-30º and 2θ =33-37º. The diffractogram with its broad peaks indicates

some low-level crystallinity in the chitosan and is entirely in line with what was previously reported in the literature for pure chitosan[377,400,401].

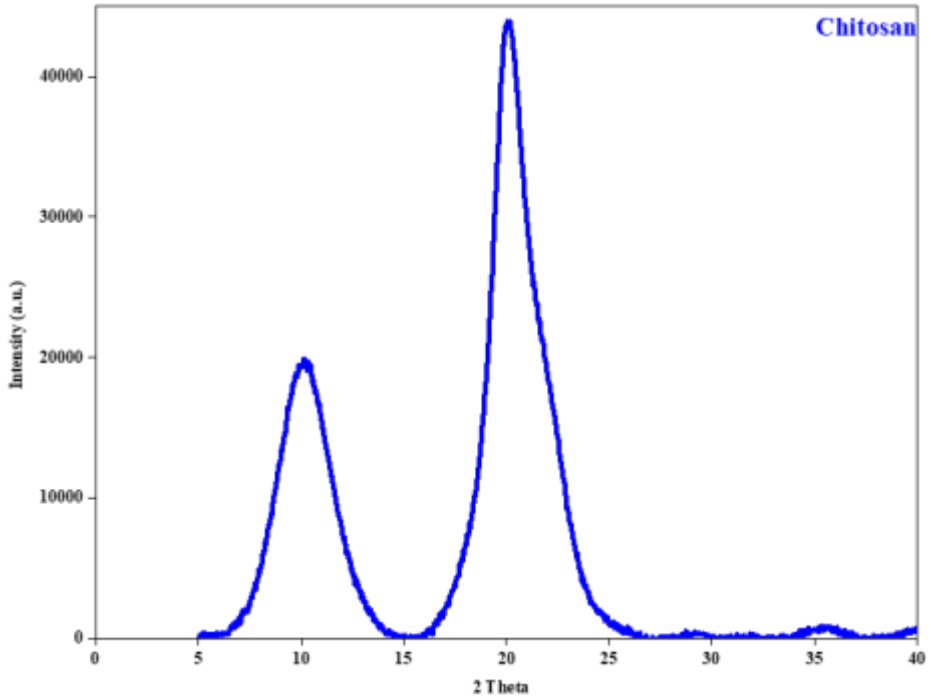

Figure 2-6: X-ray diffractogram of powdered TCI chitosan used in this study

2.4.1.4 Thermogravimetric analysis of Chitosan

Figures 2-7 and 2-8 represent the TGA data relating to the TCI chitosan, which was analysed over a temperature range of 30 ºC to 800 ºC. The thermogram curve (Figure 2-8) shows thermal degradation data, while the curve (Figure 2-7) represents the data for the first derivative of % weight loss (DTG).

No significant weight loss was observed before 100 ºC. The thermogram (Figure 2-8) shows three variations corresponding to three weight loss events, at around 150 ºC, 320 ºC and 600 ºC causing a weight loss of about 10.9%, 55% and 35%, respectively.

Weight losses recorded between 70 to 150ºC are attributed to the well-known dehydration of the polymer, while the significant degradation occurring around 300 ºC could be due to the deacetylation of chitosan. This dominant weight-loss event around this temperature range is directly related to the degree of deacetylation (DDA). With relatively low DDA, chitosan shows a lower weight loss in this region and vice versa[402]. A gradual weight loss continues to occur up to 650 ºC, finally reaching zero due to the burning of the remaining carbonaceous matter comprising the chitosan[403].

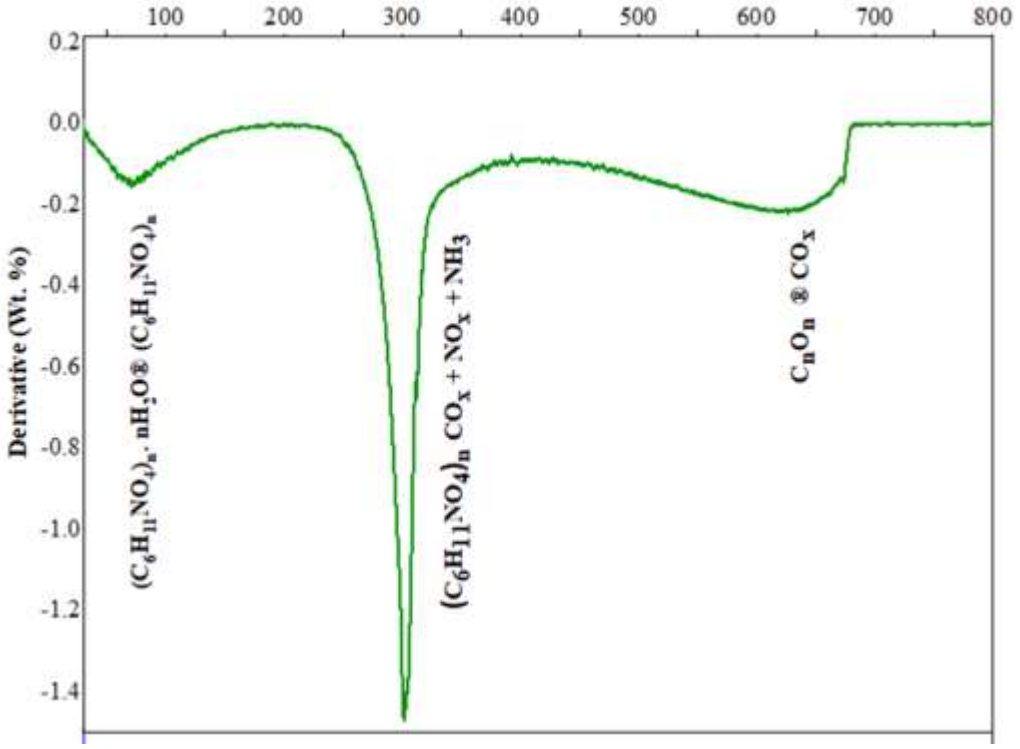

Figure 2-7: Thermogram of chitosan used in this study (Derivative % weight loss curve)

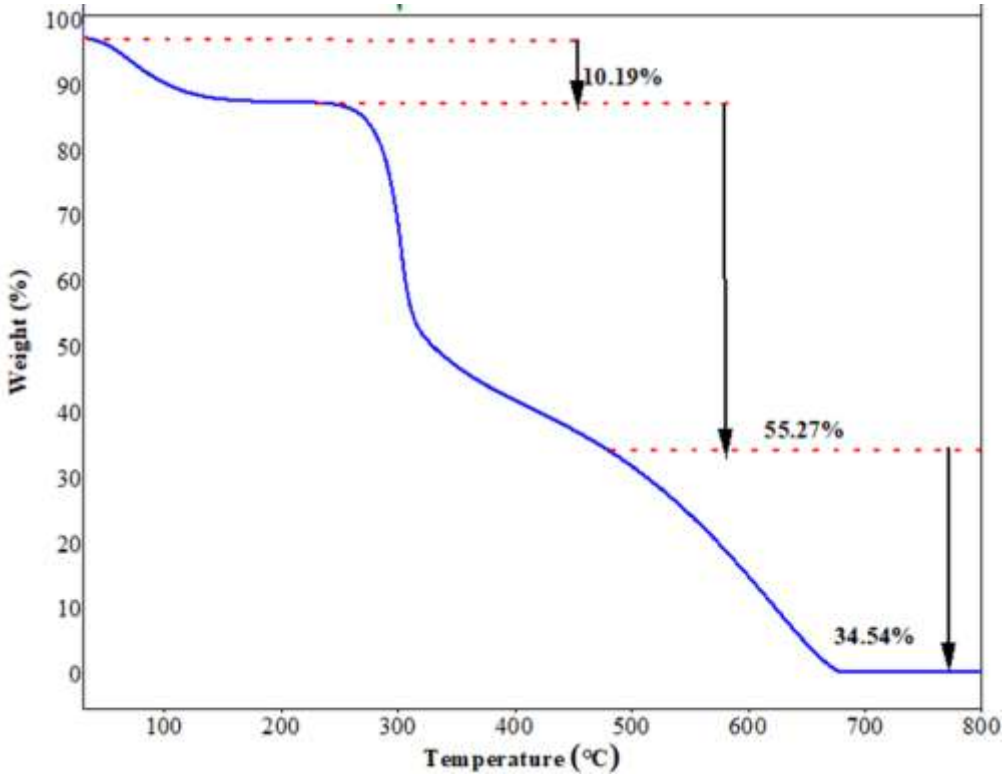

Figure 2-8: Thermogram of chitosan used in this study (Thermal degradation curve)

2.4.2 Characterization of the hydroxyapatites used in this study

2.4.2.1 SEM/EDX characterization of cHAp and bHAp

cHAp: An SEM micrograph and EDX analysis of cHAp are presented in Figure 2-9 (a and b). The morphology of cHAp has the appearance of rough surface aggregates of irregular particles. Similar morphology has been observed and reported in the literature[404,405] for synthetically prepared HAp, which was prepared using a sol-gel method, indicating that cHAp has been prepared commercially via similar methods.

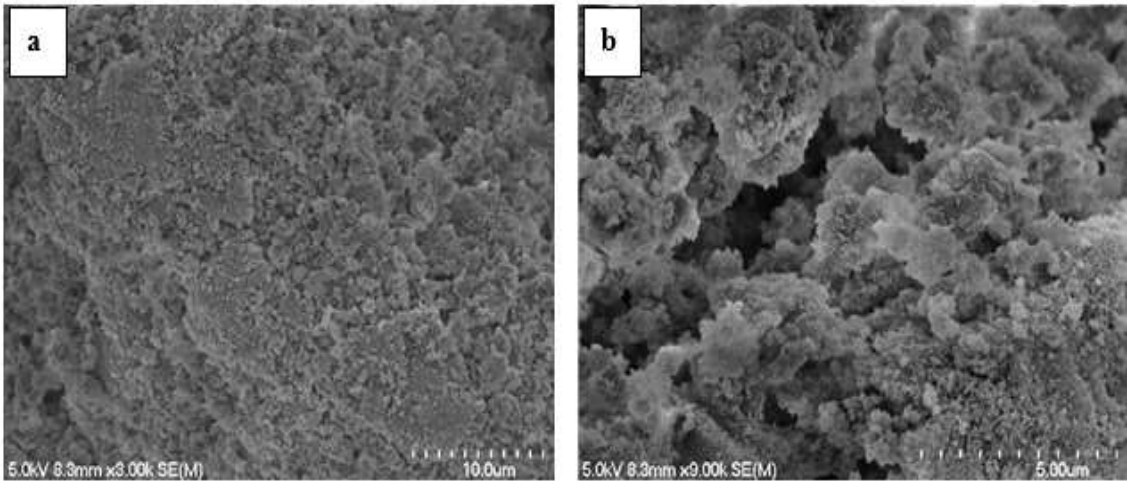

Figure 2-9: SEM micrographs of the commercial HAp (cHAp) used in this study

Elemental analysis (Figure 2-10) showed oxygen, phosphorus, and calcium as predominant elements at 22.67 %, 48.94 % and 33.75%, respectively. The Ca:P mole ratio is an important parameter to evaluate the phase purity of hydroxyapatite. Different Ca:P ratios in calcium phosphates correspond to different phases; for instance, the HAp and β-tricalcium phosphates (β-TCP) are two different phases of calcium phosphate, which give Ca:P mole ratios of 1.67 and 1.5, respectively.

In literature studies, the Ca: P mole ratio is calculated using the atomic % values measured by EDX analysis[406,407]. For the c-HAp in the present study, the Ca:P mole ratio was calculated using atomic % in at least three randomly measured spots on a given sample. The Ca:P mole ratio measured from these fell within the range of 1.67-1.8, with the c-HAp material falling within the range expected for stoichiometric HAp, which should have a Ca:P mole ratio of 1.67[407]. The Ca: P ratio variation could be due to systematic errors such as particle size or accelerating voltages used in the analysis[408]. Moreover, it is known that the phosphorus (P) and platinum (Pt) (from coating) peaks coincide in the

EDX spectrum. Hence the phosphorus peak could be affected by the platinum peak so giving variations in the Ca:P mole ratio.

To investigate the influence of any possible interaction between the two peaks (P and Pt) on the Ca:P mole ratio, the EDX measurements were repeated by using HAp samples without any platinum coating. The Ca:P ratio for these uncoated samples was 1.7-1.8, close to the range measured for the platinum-coated samples (i.e., 1.67-1.8); hence the effect of the Pt coating on the Ca:P mole ratio values was deemed negligible.

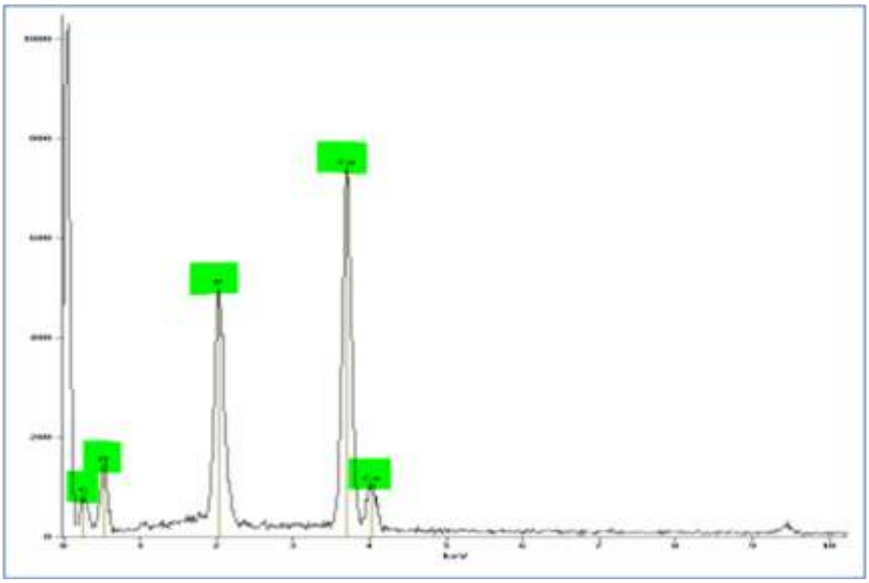

Elements	Carbon	Oxygen	Sodium	Phosphorus	Calcium	Total
Element Wt.%	5.47	22.67	0.46	22.46	48.94	100.00
Error (Element Wt.%)	+/-0.40	+/-0.77	+/- 0.10	+/-0.34	+/-0.61	
Wt. % Atom	11.86	36.19	0.53	18.89	31.81	100.00
Error (Wt. % Atom)	+/- 0.87	+/- 1.26	+/- 0.11	+/- 0.29	+/- 0.40	

Figure 2-10: EDX spectrum of commercial hydroxyapatite (cHAp)

bHAp: Figure 2-11 (a-d) shows the SEM micrographs for the bovine-derived hydroxyapatite (bHAp). The HAp from this was found to have a morphology consisting of irregular particles of different sizes. The magnified images (x5000 and x15000) of the larger particles showed interconnected semi-spherical particles and pores. The identical morphological characteristics were reported in an earlier study that discussed the bovine sourced synthesis of hydroxyapatite using thermal calcination as the method of preparation[409]. In this study, the porosity was attributed to the sintering of HAp powder and referred to the pores as arising from spaces occurring between the fine crystallites as

they formed agglomerates from the coalescence of particles during calcination[409,410]. Similar morphological features were also observed for bone-sourced hydroxyapatite sintered at 900-1000 °C[406]. This study described the HAp produced as possessing an interconnected network of pores which was considered helpful for bone tissue in-growth[411,412]. Similarly, in another study, HAp produced had been explained as being a mimic of the bone structure via its having a combination of pores and solid structures, making it desirable in orthopaedic applications[413]. Several studies on bovine sourced HAp[411,412,414-417] have reported an interconnected cumulus like structure with pores that appeared at >800 °C[409].

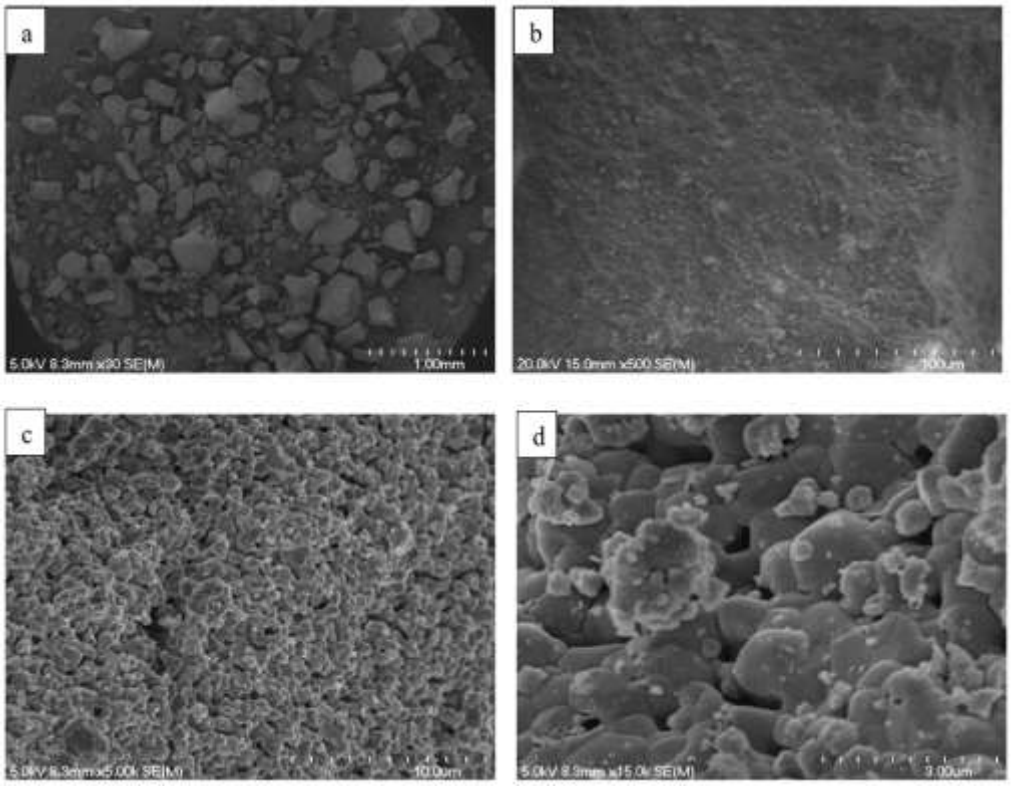

Figure 2-11: SEM micrographs of bHAp (a) x30 (b) x500 (c) x5.00k (d) x15.0k

Elemental analysis of bHAp by EDX (Figure 2-12) showed expectedly dominant Ca and P peaks in the sample. In addition, Mg and Na were observed, which characterises the HAp as being from a mammalian source because such elements are commonly found in the bone. The O, Ca, and P atomic percentages in bHAp were 42.43%, 31.50%, and 18.15%, respectively. The Ca:P mole ratio was calculated using the same method as mentioned above for calculating the Ca:P mole ratio for cHAp. The values ranged

between 1.80-1.84 for platinum-coated samples but were 2.03-2.48 for samples without platinum coating.

Others have reported Ca:P mole ratios in bovine sourced HAp prepared by thermal calcination up to 1000 ºC to be in the range of 1.58-1.93[417,418], while another study reported a weight % Ca:P ratio of 1.75-1.83 using EDX analysis for bovine sourced hydroxyapatite that was thermally calcined between 1000 °C and 1100 °C[419]. These findings of the literature study suggested that the hydroxyapatite produced from natural sources is non-stoichiometric with a Ca:P mole ratio greater than 1.67[420]. The carbonate substitution could be considered a possible reason to increase the Ca:P, as the P content would be less due to carbonate substitution resulting in an increase in the Ca:P ratio. It could be further explored in the FTIR analysis of the hydroxyapatites.

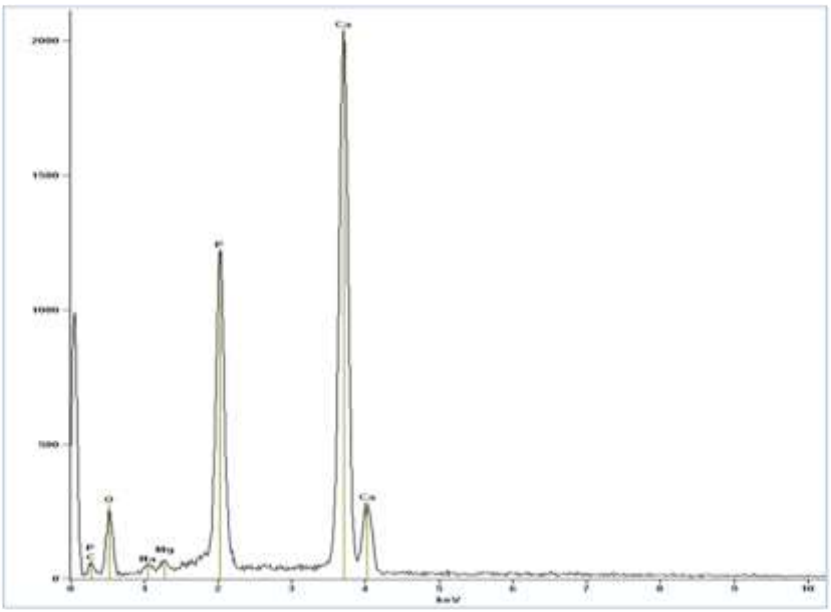

Elements	Carbon	Oxygen	Sodium	Magnesium	Phosphorus	Calcium	Total
Element Wt.%	4.16	19.53	0.69	0.49	18.73	56.40	100.00
Error (Element Wt.%)	+/-0.40	+/-0.55	+/- 0.12	+/- 0.08	+/-0.23	+/-0.51	
Wt. % Atom	9.55	33.64	0.83	0.55	16.66	38.77	100.00
Error (Wt. % Atom)	+/- 0.93	+/- 0.94	+/- 0.15	+/- 0.09	+/- 0.21	+/- 0.35	

Figure 2-12: EDX spectrum and analysis of bovine-sourced HAp (bHAp)

2.4.2.2 FTIR analysis of cHAp and bHAp

Figure 2-13 represents the FTIR spectra of both c- and bHAp as measured from KBr disks prepared from both samples. The IR absorption peaks observed in each spectrum are

summarised in Table 2-2 and generally agree with the reported literature on hydroxyapatite IR spectra.

The spectra of the two hydroxyapatite phases do have some differences in appearance from each other. The peaks in bHAp appear somewhat sharper compared to those from cHAp. This confirms the more crystalline nature of the bHAp, which is most likely due to the thermal calcination process used to produce it. In addition, there is relatively less moisture in the bHAp sample. This may be attributed to either less moisture inherently in the bHAp sample itself or in the KBr powder used to produce the disk. Some additional peaks were observed in the bHAp FTIR spectrum, which were absent in the cHAp spectrum. These were two lattice –OH stretching/liberational vibrations (weak) observed at 3570 cm^{-1} and 632 cm^{-1}. The presence of these vibrations is associated with a highly crystalline hydroxyapatite phase. This observation is additional evidence to support the fact that cHAp is less crystalline and indicates that its commercial preparation could have been via a precipitation process at lower temperatures and with relatively mild heating/drying[425].

Table 2-2: Observed IR absorption peaks in the FTIR spectra of hydroxyapatite (cHAp and bHAp)[406,412,421-424]

Assignment	**Wavenumber (cm^{-1})**
Asymmetric stretching of PO_4^{3-} (ν_3)	1050-1095 (s)
Asymmetric bending of PO_4^{3-} (ν_4)	570-604 (m)
-OH libration (shoulder on PO_4^{3-} (ν_4) peak))	632 (m/w)
-CO_3^{2-} (asymmetric stretching)	1415-1459 (m)
-OH, stretching from H_2O (moisture presence in powder or KBr)	3432 (s, broad)
HOH bending mode from H_2O (moisture presence in powder	1621 (w)
-OH stretching (structural (lattice) hydroxyl group of apatite in bHAp only)	3570 (m/w, sharp)
PO_4^{3-} (ν_1) symmetric stretch	960 (w)
-CO_3^{2-} (ν_2 bending mode)	840-900 cm^{-1} (w)

s=strong, m= moderate, w=weak, vw = very weak

An additional shoulder band (weak) was observed around 3640 cm^{-1} in the bHAp spectrum, which could be associated with an -OH stretching peak due to the presence of $Ca(OH)_2$. The observation of this peak in the bHAp is further proof of 1) the presence of carbonates in the bHAp and 2) their thermal breakdown after calcination, as this would produce CaO and CO_2. If some of this CaO is in the bHAp powder after calcination, then the interaction of the CaO with moisture (after cooling/during storage) can lead to the

formation of some Ca $(OH)_2$. Moreover, the bone apatite (such as bHAp) was reported as carbonated apatite due to carbonate ion substitution in the crystal lattice of apatite, which could affect the crystal lattice structure of apatite and affects the Ca:P ratio in hydroxyapatites. The carbonate substitution could occur at two different anionic sites of HAp, including type-A substitution (at -OH sites) or type-B substitution (at PO_4^{3-} sites). B-type substitution in bone sourced mineral (HAp) could be considered to cause a higher Ca:P ratio in the bHAp[426].

The weak peak assignments around at 1420 cm^{-1} and 1453 cm^{-1} in the below Figure could be assigned to antisymmetric stretching vibrations of carbonates (B-type substitution) in the bHAp spectrum, which is also used to justify the higher Ca:P ratio calculated earlier for bHAp in EDX analysis (Figure 2-11) of bHAp. Baxter et al.[427] observed the presence of the B-type carbonate substitution in bone-apatite minerals by indicating that the ν_3 (antisymmetric stretching vibration) was divided into two peaks, these being ν_{3a} and ν_{3b} at 1423 cm^{-1} and 1426 cm^{-1}, respectively.

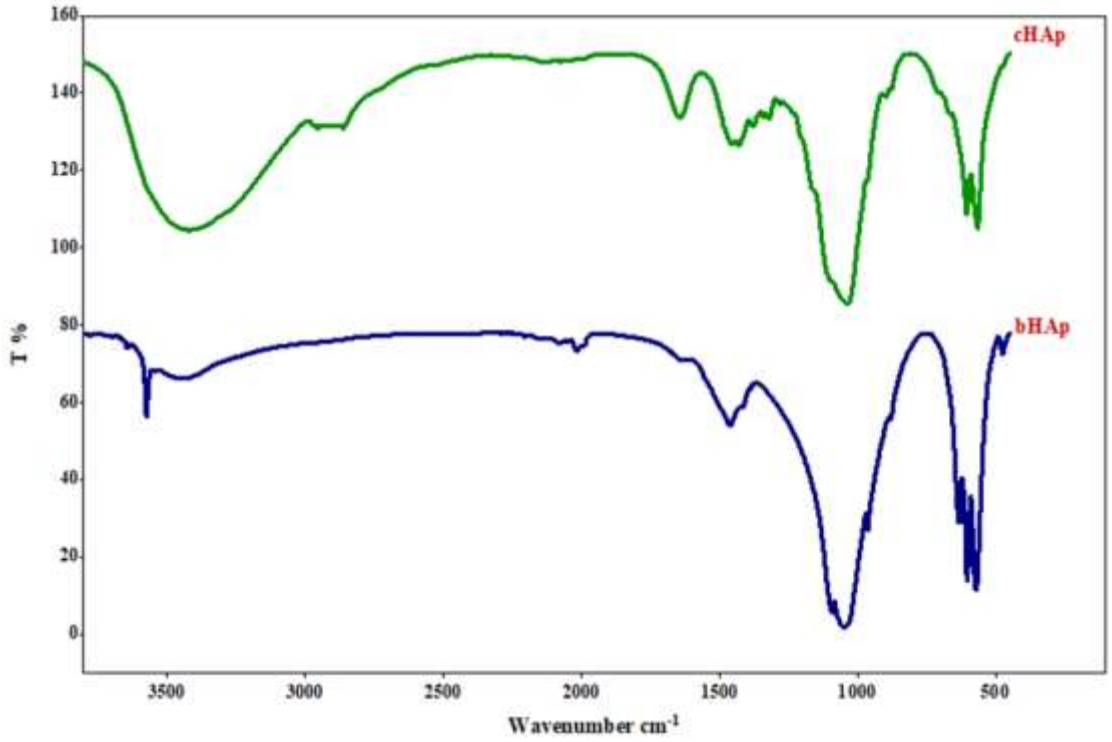

Figure 2-13: FTIR spectra of cHAp and bHAp

2.4.2.3 Powder X-ray Diffraction analysis of cHAp and bHAp

Figure 2-14 represents the powder X-ray diffractograms of the cHAp and bHAp powders used in this study. The observed peaks were found to be in good agreement with those reported in the reference diffraction patterns representing phase pure hydroxyapatite (ICDD no. 09-0432). This is given below in Figure 2-14 to compare with the other hydroxyapatites p-XRD patterns acquired.

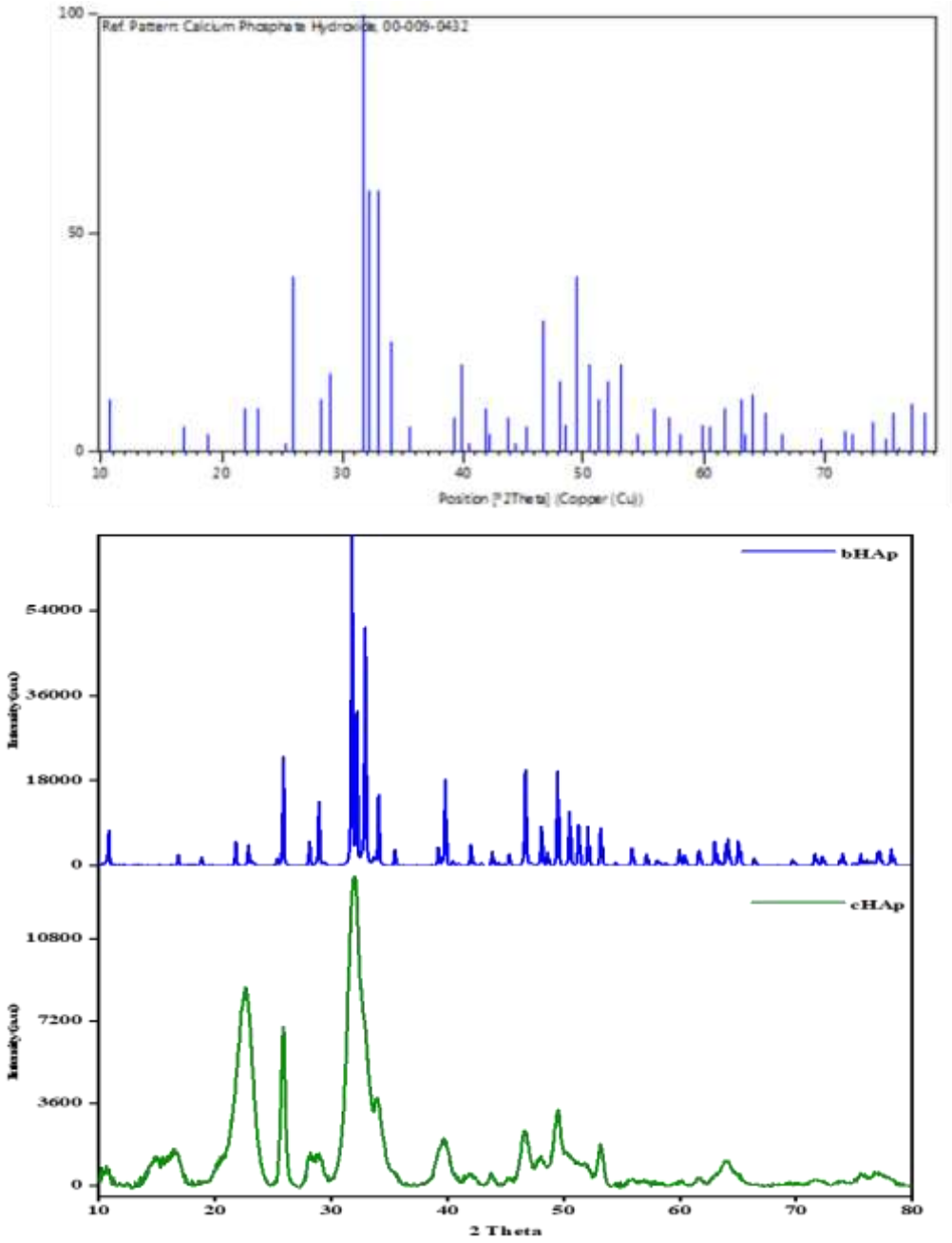

Figure 2-14: The reference diffraction pattern of stoichiometric hydroxyapatite ((ICDD no. 09-0432), and the diffractograms of bHAp and cHAp

The p-XRD for the cHAp (Figure 2-14 marked in green colour, bottom spectrum) showed fewer, broader, low-intensity peaks than what was observed in the p-XRD of bHAp (Figure 2-14, marked in blue colour, top spectrum), which could be attributed to its poorly crystalline nature as already observed in FTIR analysis. These peaks are in good agreement with what is observed in powder X-ray diffractograms of synthetic HAp samples as reported in the literature[428,429]. Moreover, hydroxyapatite shows clear peaks at 2 Theta =24° to 2 Theta =40° as observed and reported by Ergun et al.[430] for chemically precipitated hydroxyapatites using different Ca:P molar ratios. These characteristic peaks reported for chemically precipitated HAp are in good agreement with those exhibited in the p-XRD pattern of cHAp (Figure 2-13), indicating that the origin of this commercial material is possibly from chemical precipitation[430]. In contrast, the broader peaks were attributed to the likely smaller sizes of precipitated calcium phosphate particles present in the sample.

In contrast, the sintered bovine-derived hydroxyapatite (bHAp) was found to be more crystalline than cHAp, as evidenced from the sharper and more numerous XRD peaks observed in Figure 2-14, which are in good agreement with peaks exhibited in the reference powder XRD pattern (ICDD no. 09-0432 illustrated in Figure 2-14). The prominent peak positions (2 Theta) and respective d-spacings were recorded as 10.820 (8.17Å), 25.879 (3.44 Å), 29.967 (3.08 Å), 31.774 (2.81 Å), 32.197(2.77 Å), 32.902 (2.72 Å), 34.049 (2.63), 39.819 (2.26 Å), 46.713 (1.94 Å) and 49.469 (1.84 Å) for bHAp (Figure 2-14).

The preliminary characterization of the hydroxyapatite raw materials used in this study has shown a difference in crystallinity between cHAp and bHAp, which could be attributed to how they have initially been synthesised. The thermal calcination method produces HAp with high crystallinity compared to the chemical precipitation method[431]. Thermal calcination involves heating at a high temperature (1000-1400 °C) to crystallise the HAp. Venkatesan et al. reported that the thermal calcination produced a more crystalline HAp from fishbone than an alkaline heat treatment method[422]. The better (higher) crystallinity of bHAp is a direct result of its thermal treatment during its synthesis from bovine bone, and the outcomes of such treatments are well documented in the literature[416,417,424].

2.4.2.4 Thermogravimetric analyses of cHAp and bHAp

The characteristic TG thermograms of cHAp and bHAp are presented in Figures 2-15 & 2-16. The thermograms show phase transformations and weight losses in both HAps as a function of temperature. Total weight loss recorded for cHAp (Figure 2-15) was approximately 57%, while for bHAp, it was only about 2%, while heating samples up to 1000 °C.

Only two weight loss events were observed in the thermogram of bHAp (Figure 2-16). one with a minor weight loss around 100 to 250°C, which is indicative of dehydration of the bovine sourced HAp powder. According to previous reports, endothermic peaks observed at 425-560°C correspond to carbonate decomposition from the bovine bone, which is known to occur between 400 °C to 600 °C in an air atmosphere[432]. Gradual removal appears to continue up to 1000 °C. The same observation was reported in another study of bio-sourced hydroxyapatite isolated from bovine-bone[415]. The FTIR analyses discussed above support the presence of carbonate, as these were detected in the phases examined.

Weight losses observed for cHAp and bHAp differed from each other. cHAp exhibited a significant weight loss overall, with approximately 9.03% weight loss occurring on initial heating, which was attributed to dehydration. This was also observed by Chakravarty et al. in thermograms reported of nano-HAp[433]. However, over the temperature range of 350-530ºC, a more significant weight loss of 48.57% was observed due to the degradation of carbonate moieties in the cHAp.

In contrast, the weight loss exhibited by the bHAp sample was less relative to cHAp. This was interpreted as being indicative of the more crystalline nature of bHAp as the major weight loss, so as a result, when it is heated in TGA, it has already undergone its major weight changes. All the TGA process is doing is removing some adsorbed moisture, and possibly, if relevant, some surface adsorbed carbonate over the 400-650°C range of temperature. In general, all three characterisation techniques (EDX, FTIR and p-XRD) reinforce the fact that c-HAp is less crystalline and has been formed by some sort of milder chemical precipitation process followed by mild heating (but not to the extent that carbonate has been removed with crystallisation of the residual powder). In comparison, the bHAp has been formed by a higher temperature thermal calcination process which has led to the more highly crystalline materials observed in the case of bHAp[417,430].

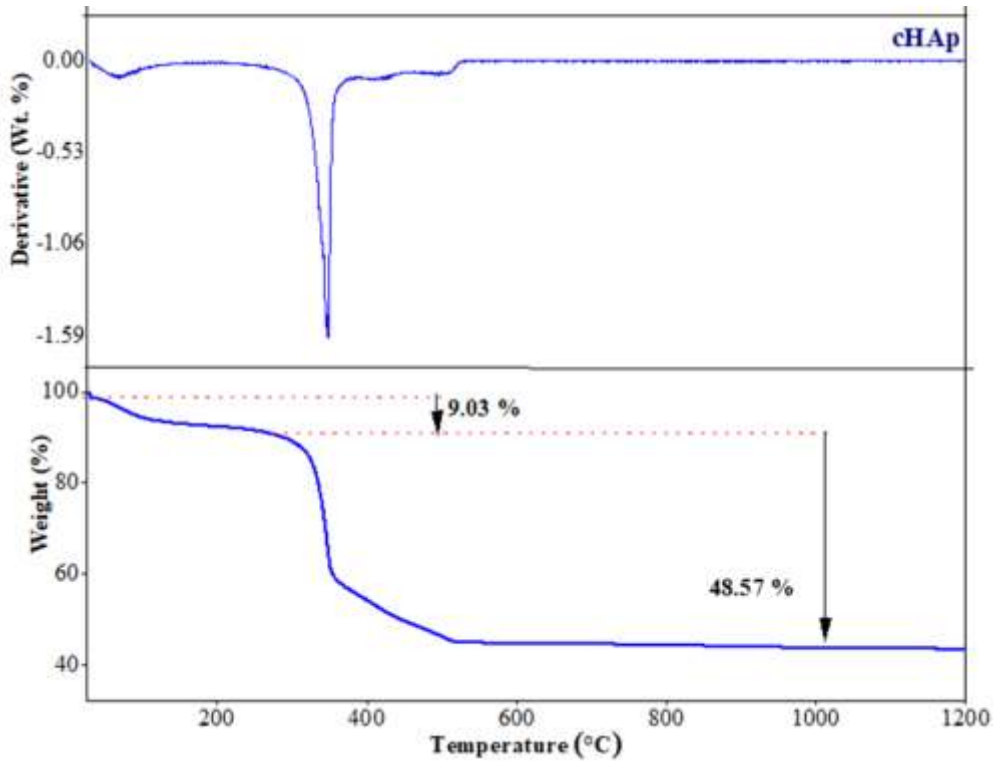

Figure 2-15: Thermogram of cHAp and corresponding DTG curve

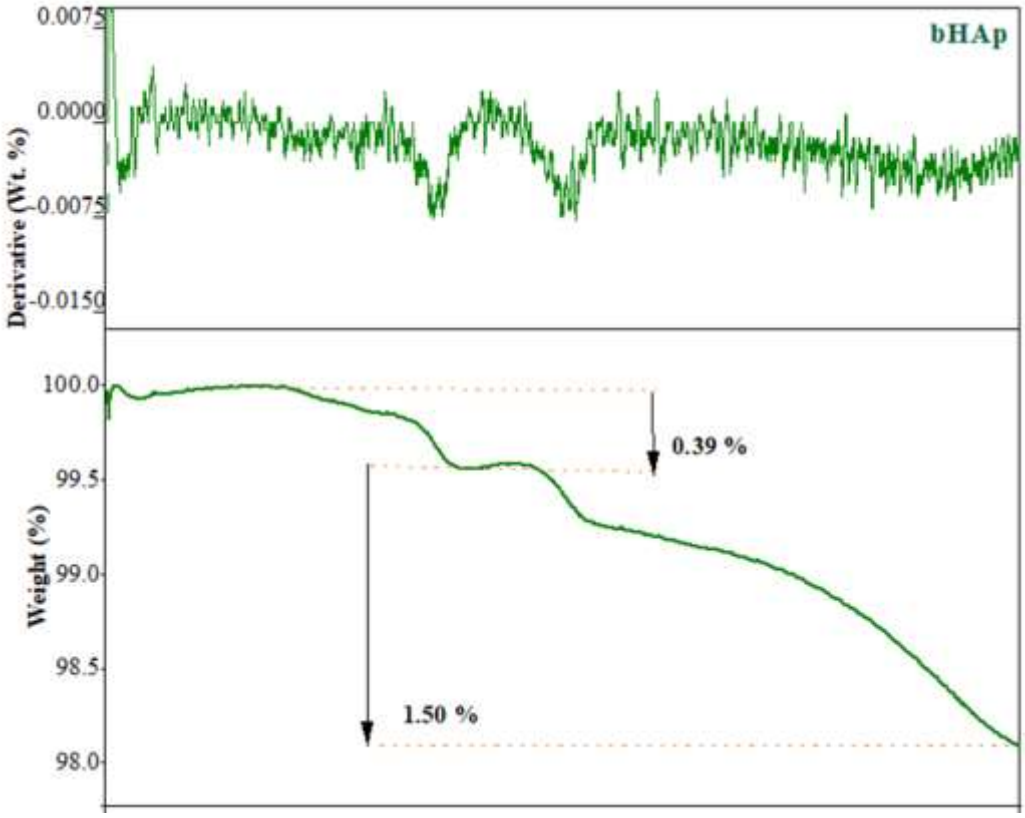

Figure 2-16: Thermograms of bHAp and corresponding DTG curves

2.4.3 Characterization of coir fibres used in the studies

2.4.3.1 SEM/EDX analysis of coir fibre

Figure 2-17 represents micrographs of SEM/EDX analyses of ground coir fibre. The tubular structure typical of natural coir fibre (Figure 2-17 a) is visible, which exhibits a large hole in the fibre centres and a smooth outer surface. The surface of the fibre appears flat, and this has been interpreted in the past as being due to the presence of surface waxes and oil[434]. Major constitutional elements include unsurprisingly carbon and oxygen, which make up 60.86% and 39.14 % of coir fibre, respectively, as shown by the detected EDX peaks (Figure 2-17 c). The peak at 2 keV is due to Pt coating for imaging purposes, as indicated earlier.

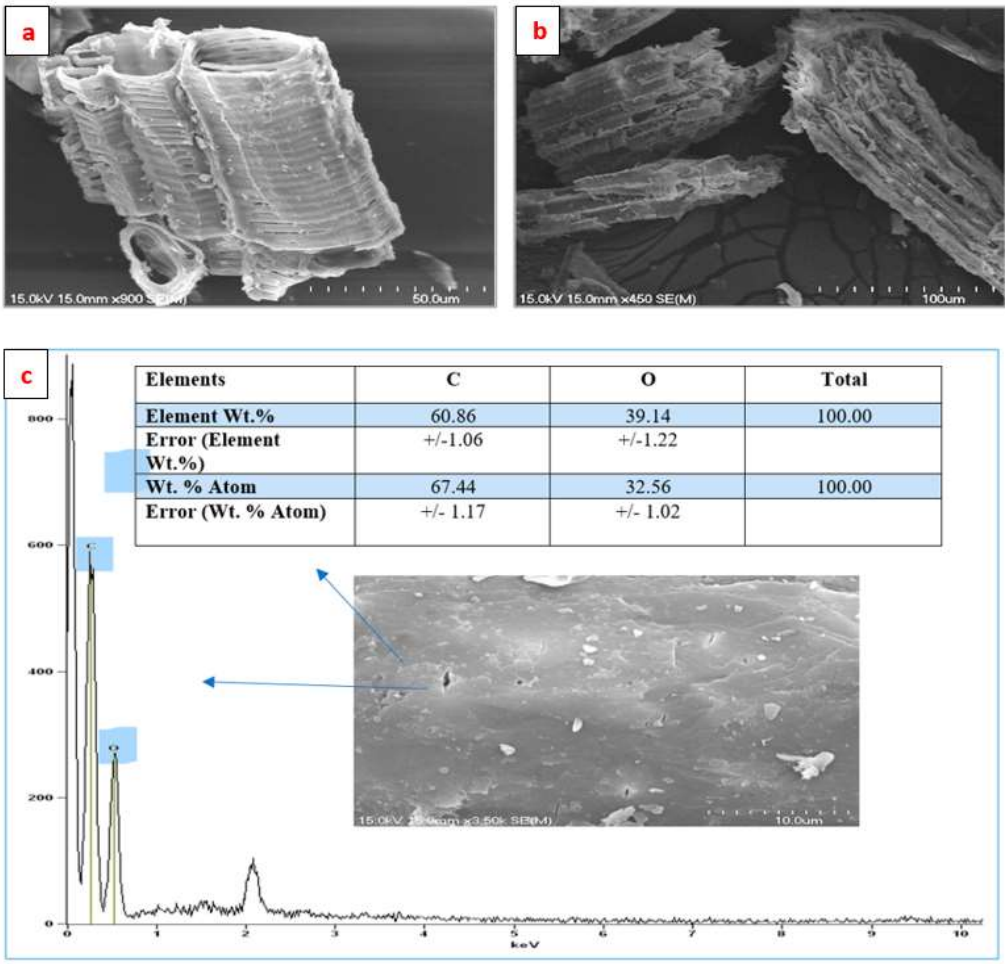

Figure 2-17: SEM micrograph of coir fibre with accompanying EDX analysis.

2.4.3.2 FTIR analysis of coir fibre

Figure 2-18 shows the FTIR spectrum of coir fibre (powdered consisting of smaller fractured fibres). The observed IR absorption peaks recorded for CF are given in Table

2-3. These peaks are reported for functional groups present in CF due to its constitutional components (such as cellulose, lignin). The observed peaks are entirely in line with what has already been reported in the literature for this material.

Table 2-3: Characteristic IR absorption peaks of Coir Fibre[435-437]

Vibrations	**Wavenumber (cm^{-1})**
C=O	1650, 1740 (m)
O-H stretching (hydroxyl group)	3407 (s)
C-H stretching	2918 (m)
-OH (aromatic deformation)	1241 and1377 (m)
-OH (primary and secondary alcohols)	1108 and ~1050 (s)

The carbonyl vibrations observed at 1650 cm^{-1} could be attributed to lignin and hemicellulose[435] in the CF, while a sharp peak around ~3400 cm^{-1} is associated with the -OH groups present in cellulose, lignin as well as adsorbed water (from moisture) in raw fibre[435], while a moderate intensity peak at 2900 cm^{-1} corresponds to -CH stretching vibrations due to the lignocellulosic constituents of coir fibre[436].

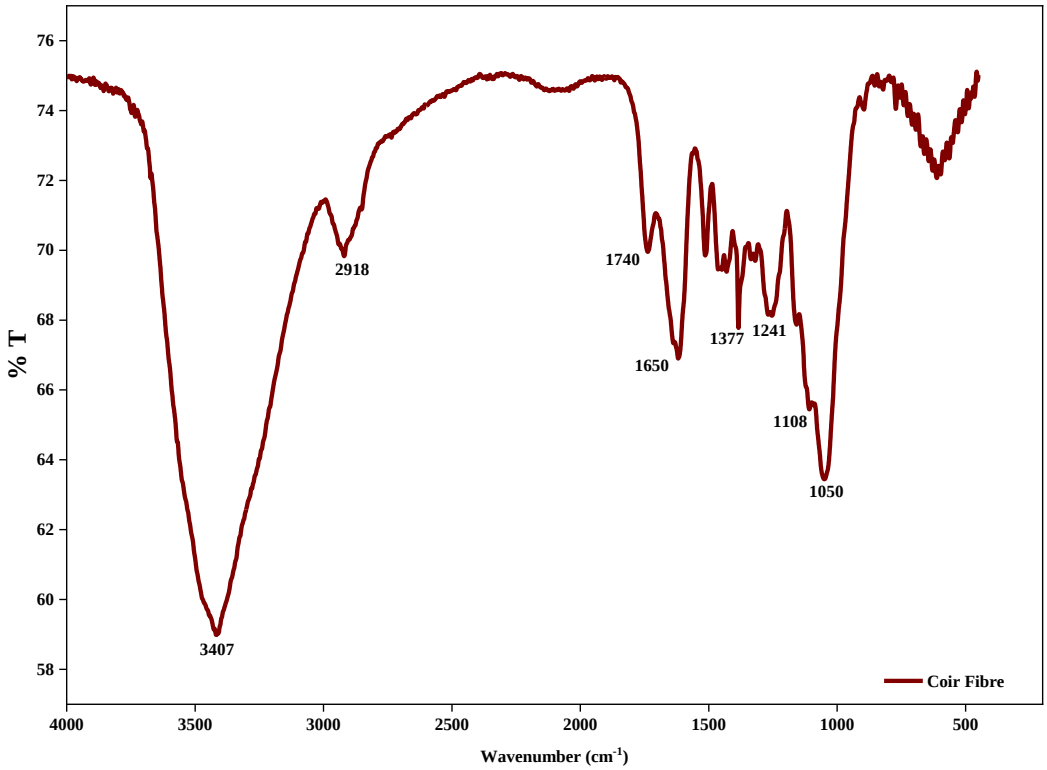

Figure 2-18: FTIR spectrum of coir fibre

2.4.3.3 Powder X-ray diffraction analysis of coir fibre

A typical coir fibre X-ray diffractogram is presented in Figure 2-19. Peak positions were assigned to 2 Theta= 10°, 16°, 22° and 35°. Generally, CF presents a poorly crystalline phase due to lignin and pectin components, as reported earlier[435]. The visible peak positions could be attributed to partially crystalline cellulose(I), which is embedded in the non-crystalline structural components of CF[438,439].

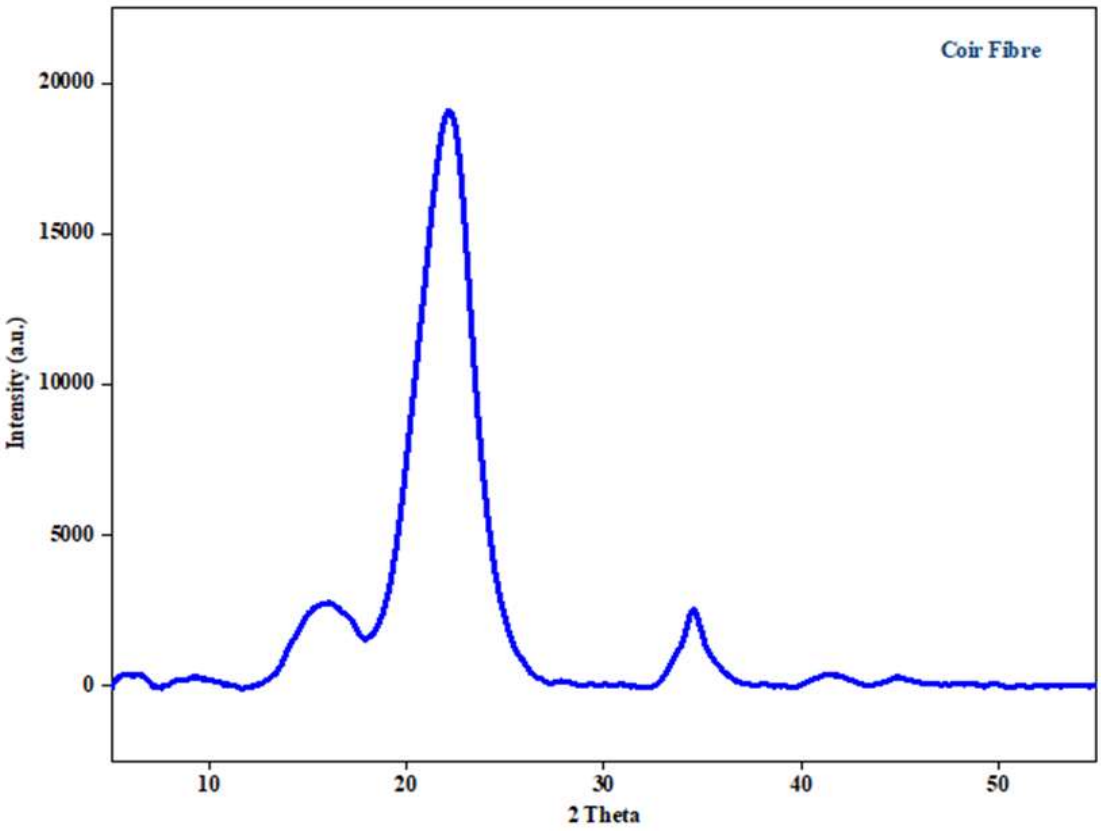

Figure 2-19: X-ray diffractogram of coir fibre

2.4.3.4 Thermogravimetric analysis of coir fibre

The thermogram of coir fibre and corresponding DTG curve (Figure 2-20 A & B) show the thermal decomposition of raw coir fibre (ground). Water loss due to evaporation from the sample counts for 9.27% weight loss occurring from 40-120 °C, while a significant weight loss occurs around 280 °C and 326 °C, which counts for a total of 50% weight loss of CF. A gradual weight loss continues after 300 °C and approaches zero around 500 °C.

The fact that water loss appears to start at lower temperatures in this sample may be due to its higher surface area caused by grinding. At the same time, other decomposition events may be occurring, including the thermal decomposition of lignin, α-cellulose and lignin. These observations are in line with results reported previously by Abraham et al.[435], who studied coir fibre extraction, with a slight change in endothermic temperature peaks. The decomposition pattern also confirms the presence of various compounds (such as lignin, lignin etc.) in coir fibre.

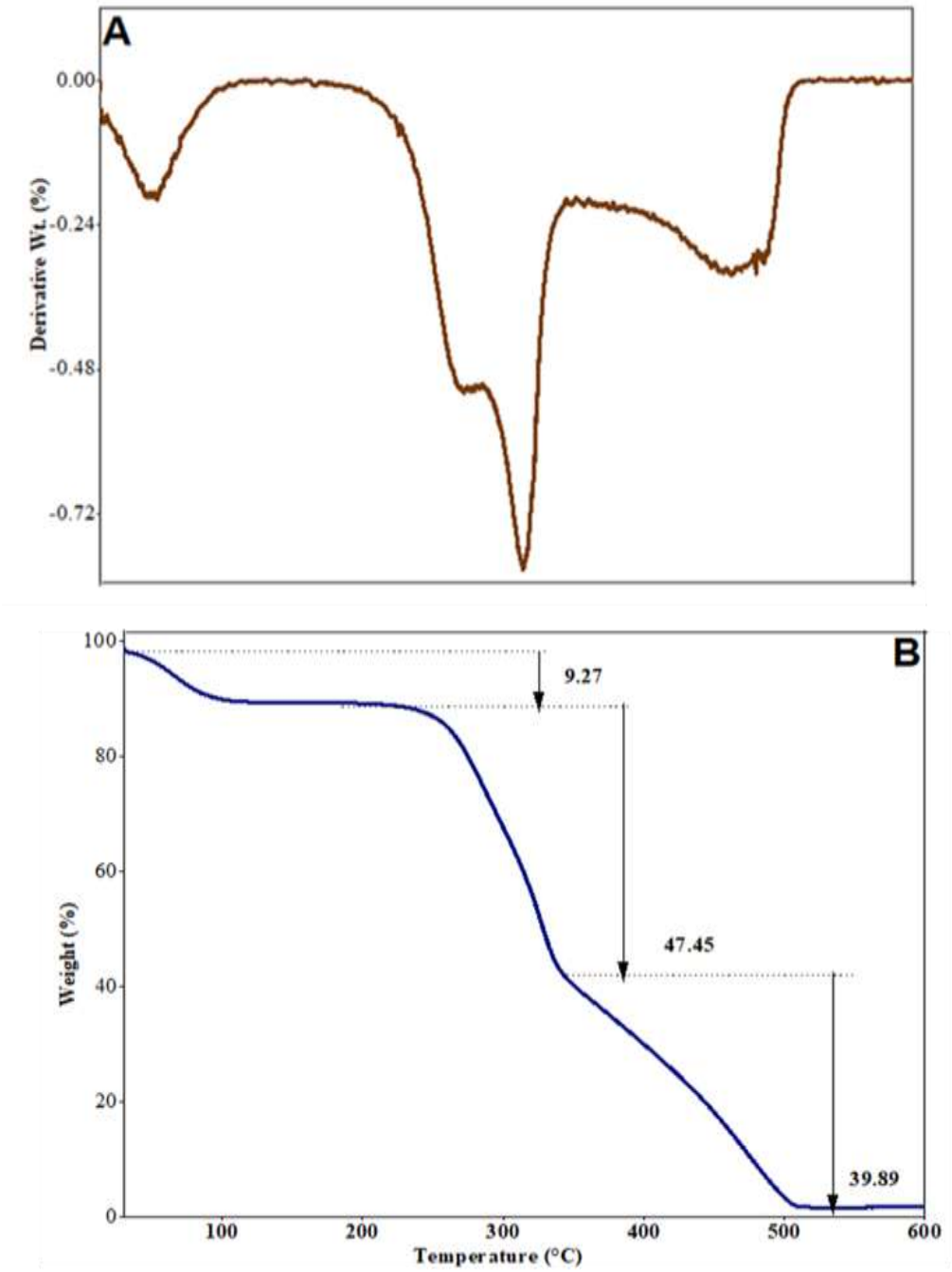

Figure 2-20: Thermograms of coir fibre (A) DTG curve (B) Thermogram of coir fibre

2.4.4 Characterization of the spent coffee grounds (SCGs) used in this study

2.4.4.1 SEM/EDX analysis of spent coffee grounds (SCGs)

Figures 2-21 & 2-22 show the SEM micrograph and EDX analysis of the spent coffee grounds material used. The SEM micrograph of spent coffee grounds shows an uneven surface that is full of irregular cavities. These cavities were observed as channels (not pores) onto the surface, as reported by other researchers who showed a similar morphology for the spent coffee grounds[269,440,441].

Elemental analysis of SCGs is presented in Figure 2-22. Carbon and oxygen were the major component elements 74.41% and 22.29% of spent coffee grounds, respectively, due to the abundance of polysaccharides in SCGs[240]. However, EDX also revealed the presence of K in the SCGs, which was reported as the most prominent mineral of spent coffee residues[240]. Ash is also present in SCGs, constituting about 1.6% reported by Mussatto, Ballesteros, et al.[442]. The ICP-AES analysis done in a study of ash from SCGs revealed potassium as the most abundant element of this ash[442], which is also evident from EDX analysis.

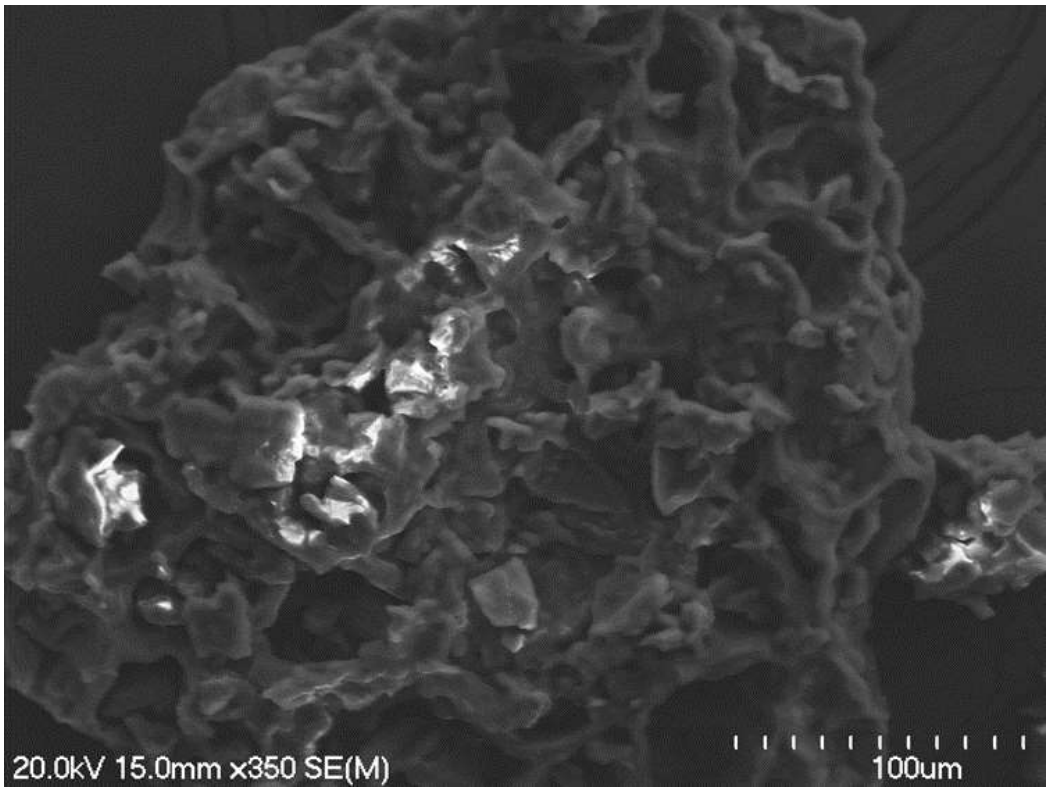

Figure 2-21: SEM micrographs of spent coffee grounds

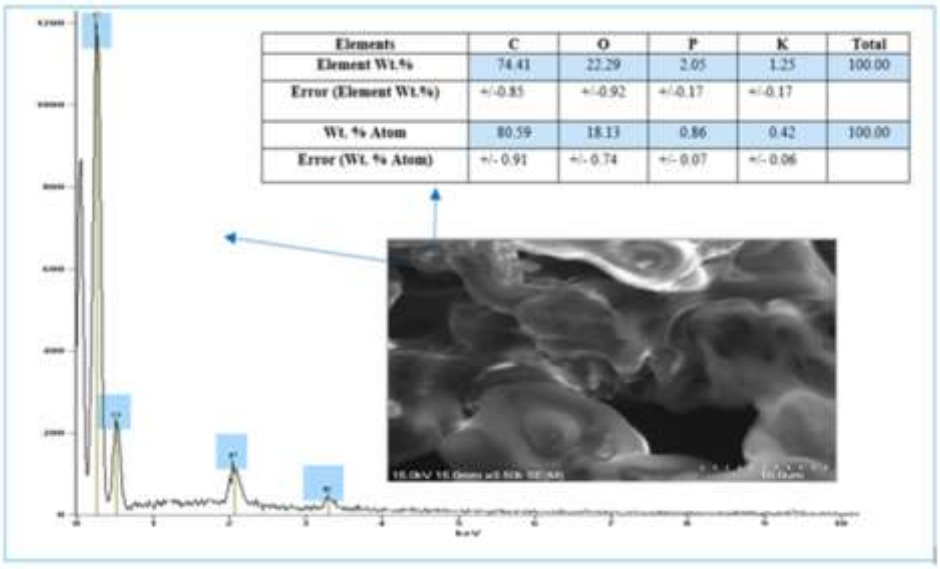

Figure 2-22: EDX micrographs of spent coffee grounds

2.4.4.2 FTIR analysis of spent coffee grounds

Figure 2-23 represents the IR spectrum of coffee grounds as a KBr disk. The characteristic IR peaks are given in Table 2-4.

Table 2-4: The characteristic IR absorption peaks of spent coffee grounds (SCGs)

Vibrations	**Wavenumber (cm^{-1})**
O-H and N-H stretching	3000-3600 (s) (broad)
C=O	1742 (s)
C=C	1653 (s)
C-H stretching	2923 and 2852 (s)
C-O stretching and N-H bending	1000-1100 (s)
C-O-C	1160 (m)
C-O-H bending	1380 (m)
C-H bending	1458 (m)
R-O-C-O-R (stretching in chlorogenic acid)	1247 (m)

Spend coffee grounds (SCGs) are complex materials containing various organic compounds, including polysaccharides, lipids, proteins, and phenols[240], as described in Table 1-4 (chapter 1). The SCGs constituents are composed predominantly of lignocellulosic polymers, containing various functional groups such as hydroxyl, methoxyl, and ether linkages[443]. Similarly, several functional groups are present in lipids, proteins, and phenols, which contribute to the appearance of the FTIR spectrum. These are listed in detail in the above Table.

Most of the vibrations of SCGs are very strong because they are associated with more than one functional group coming from different compounds of SCGs. For instance, C-H stretching vibrations around 2800-2900 cm^{-1} arise from both polysaccharides and lipids. Two sharper peaks in the same region have been previously reported in spectra of spent coffee grounds and attributed to the backbone structure of cellulose[444]. Simultaneously, similar stretching vibrations in this region were reported in caffeinated beverages such as coffee, tea, and soft drinks and attributed to asymmetric C-H stretching from the methyl group in caffeine molecules[445].

A strong band at 1742 cm^{-1} (C=O) is associated with ester linkages of triglycerides (lipids) and carboxyl groups present in both lignin (polysaccharides) and caffeine[446,447]. A wide band representative of O-H stretching of hydroxyl groups in polymeric components such as pectin, cellulose and lignin and N-H stretching of primary amines of proteins is also an essential part of SCGs IR spectra. A stretching vibration at 1247 cm^{-1} is associated with chlorogenic acid (CGA), indicating phenolic compounds in SCGs[448]. In general, all vibrations observed in the spectra have been well studied and well-reported for coffee wastes from coffee processing industries and spent coffee wastes from cafeterias[259,441,447,448].

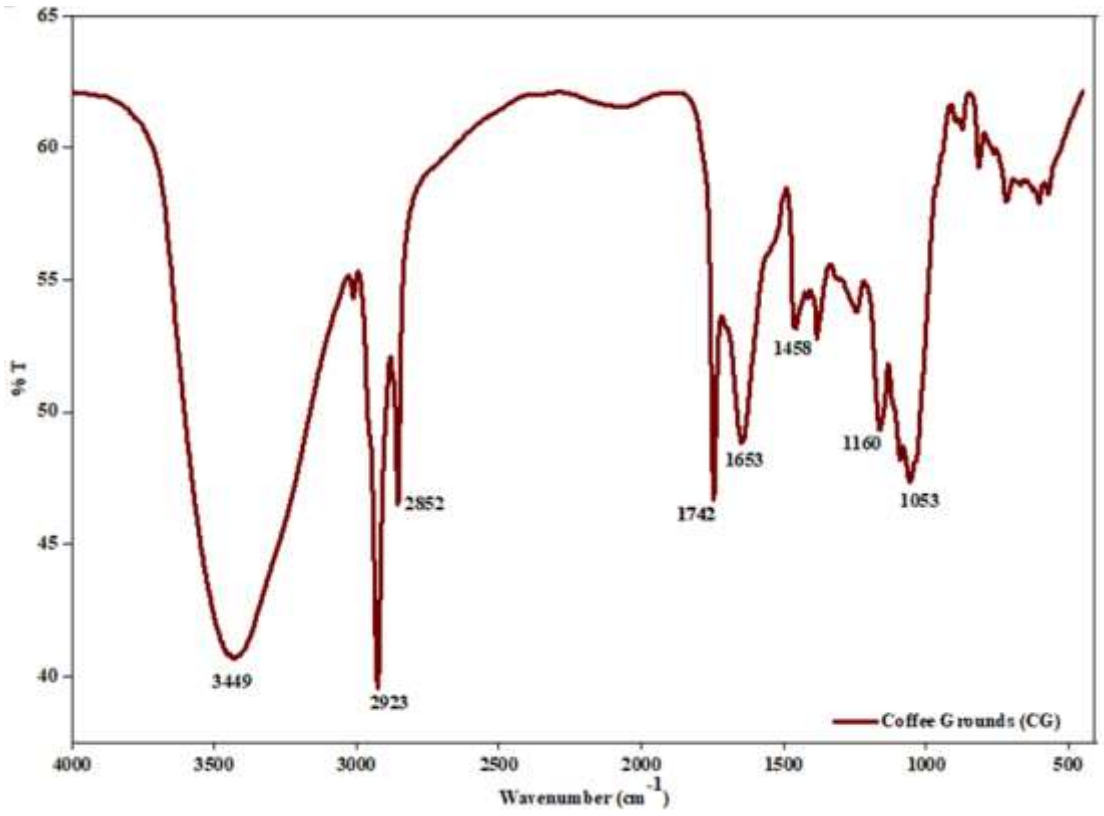

Figure 2-23: FTIR spectrum of spent coffee grounds (SCGs)

2.4.4.3 Powder X-ray diffraction analysis of spent coffee grounds (SCGs)

Figure 2-24 represents the p-XRD of SCGs. The broad peak exhibited showed SCGs were poorly crystalline materials, showing two peaks at 2θ=16 and 2θ = 20.8°and a small peak at 2θ = 35°. This pattern is comparable with the typical cellulose diffraction pattern ((ICDD card no. 00-003-0226) used by Ballesteros et al.[445] to explain the crystalline cellulosic phase of spent coffee grounds. The two peaks (2θ=16 and 2θ = 20.8°) observed in the present study and also reported for typical cellulosic biomass earlier in the literature studies, which indicate the presence of cellulose in SCGs[449,450]. A smaller peak at 2θ= 35 in Figure 2-23 was observed, and it was indicated for cellulose I lattice in the literature[451].

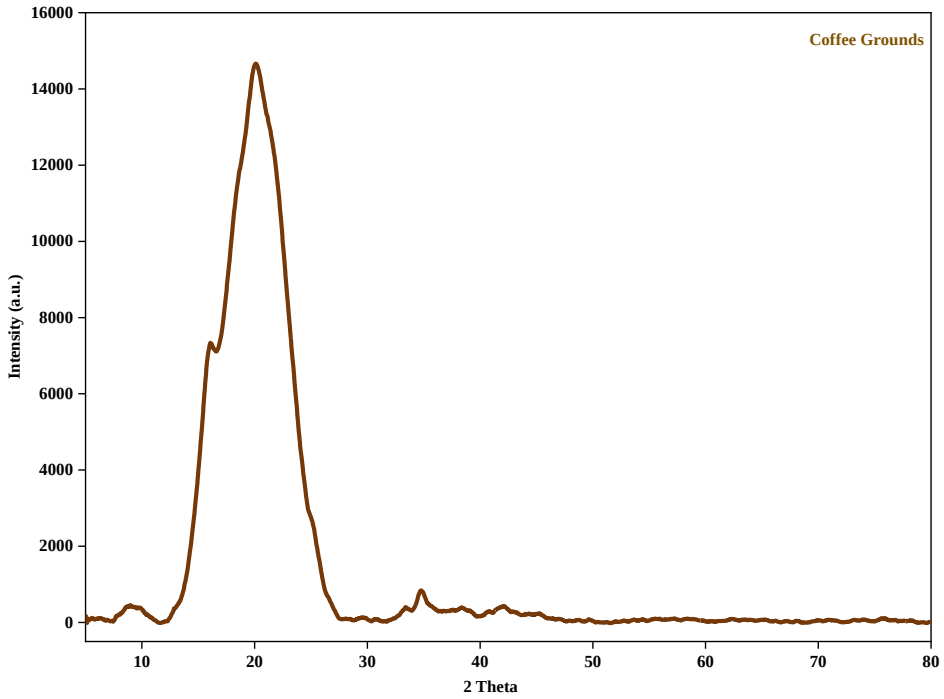

Figure 2-24: Powder X-ray diffractogram of spent coffee grounds used in the current study

2.4.4.4 Thermogravimetric analysis of spent coffee grounds (SCGs)

Figure 2-25 (A &B) represents the TGA of spent coffee grounds (SCGs), in which two weight loss events were observed. The first event occurs around 80-100 °C and counts for 11% weight loss and is attributed to the typical evaporation of the moisture present in the beans. The critical thermal event causing the 70% weight loss starts at 300°C. It continues up to 500 °C and has been attributed to the decomposition and depolymerization of the polymers present in SCGs (such as cellulose and lignin)

backbone structure[445] with only a greyish ash material remaining after complete combustion up to 1000 °C.

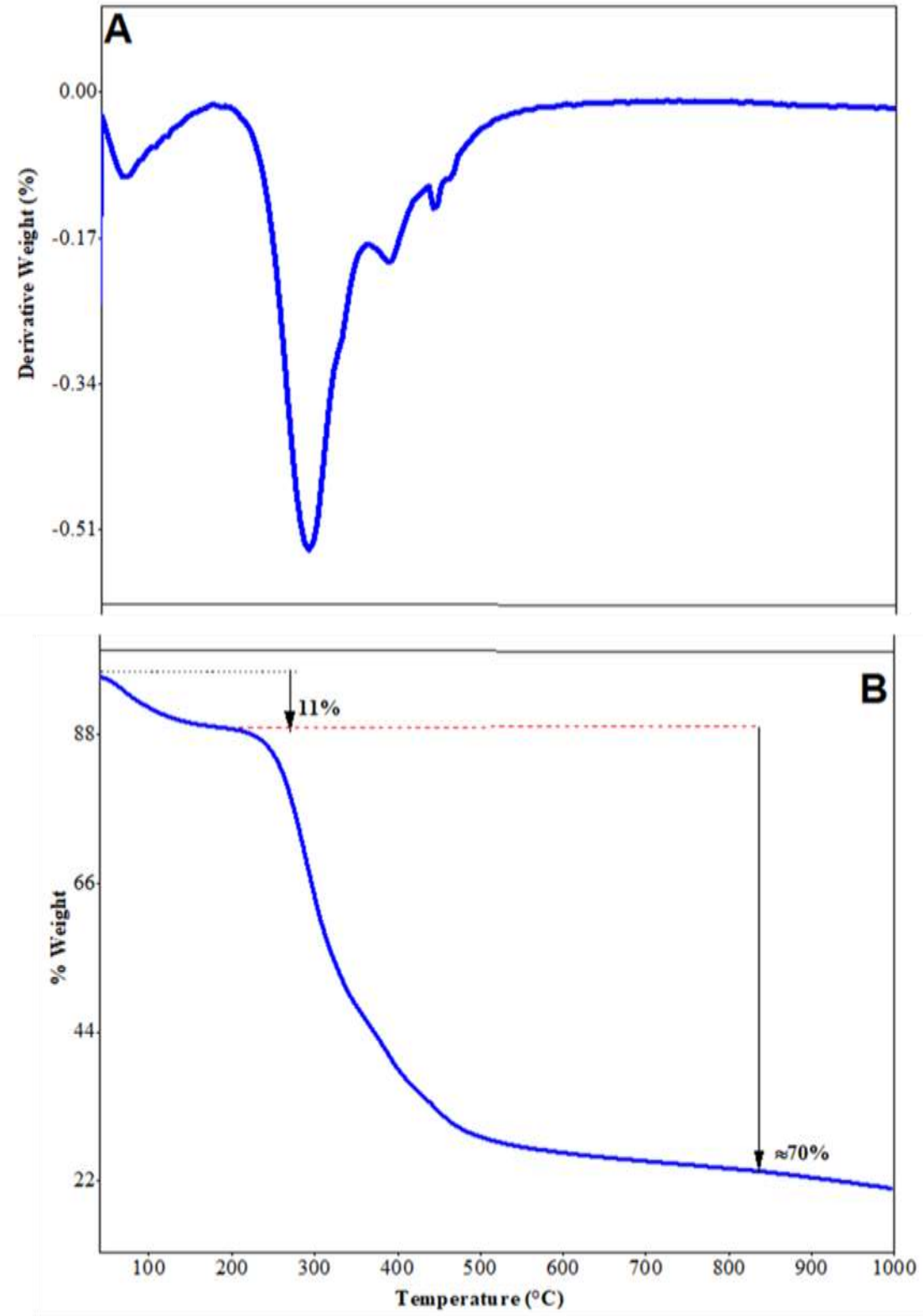

Figure 2-25: Thermograms of spent coffee grounds (SCGs) (A) DTG Curve (B) Thermogram

2.4.5 Characterization of the zeolite material (mordenite) used in this study

2.4.5.1 SEM/EDX analysis of mordenite

The SEM/EDX of the as-received commercial zeolitic material is shown in Figures 2-26 & 2-27. Later p-XRD analyses would identify this to be "mordenite". The surface morphology consisted of irregularly shaped needle-like structures with a fragile-looking, patchy surface which is in line with descriptions reported in previous literature reports (i.e., mordenite)[452-454].

The EDX analysis (Figure 2-27) of the zeolitic mordenite sample showed Si, Al and O elemental components at 40.79%, 6.08% and 37.88 %, respectively. The zeolite was a silicon-rich mordenite having a Si/Al ratio ranging between 6-7. Natural mordenite has a Si/Al range between 4.4-5.5 and is usually found in silica-rich rocks[453]. Dealumination occurs in strongly acidic conditions, which could cause an increase in the Si/Al ratio for mordenite zeolites[455]. Moreover, synthetic zeolites prepared using a hydrothermal method are known to have a Si/Al ratio of 5-10[456]. It has also been shown that in natural mordenite (from Greece), potassium content (K^+)[457] can also be found. This is evident in samples used in the present study (see Figure 2-2) which shows K to be the highest in wt. % (i.e., 3.63%) compared to the amounts of Na, Mg and Ca.

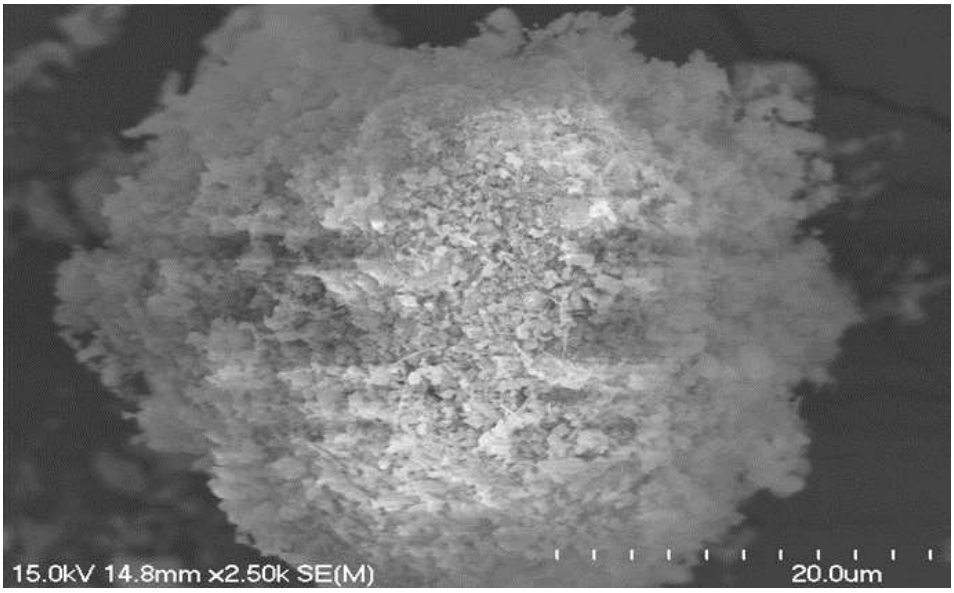

Figure 2-26: SEM micrograph of zeolite (mordenite)

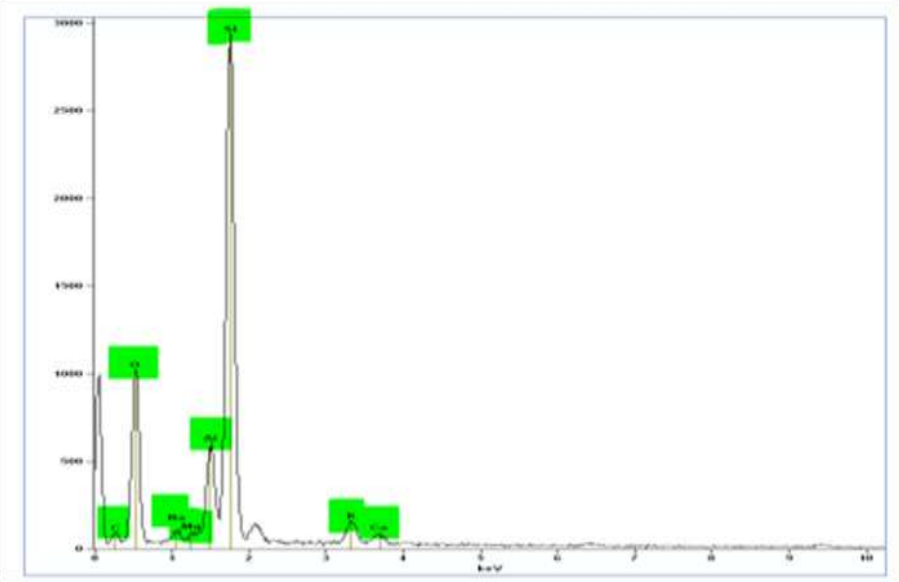

Elements	C	O	Na	Al	Si	K	Mg	Ca	Total
Element Wt.%	8.74	37.88	0.93	6.08	**40.79**	**3.63**	0.26	1.44	**100.00**
Error (Element Wt.%)	+/-1.03	+/-0.47	+/-0.07	+/-0.20	+/-0.34	+/-0.19	+/-0.07	+/-0.1	
Wt. % Atom	14.66	47.70	0.73	4.54	**29.26**	1.87	0.22	0.72	**100.00**
Error (Wt. % Atom)	+/-1.75	+/-0.59	+/-0.05	+/-0.15	+/-0.25	+/-0.10	+/-0.06	+/- 0.05	

Figure 2-27: EDX spectra and analyses of zeolite (mordenite)

2.4.5.2 FTIR analysis of mordenite

Figure 2-28 represents an FTIR spectrum of the zeolitic material used in the present study. Table 2-5 summarizes the main features observed in the spectrum. In general, the spectral features observed were in good agreement with previous literature reports where the FTIR spectrum of mordenite is discussed.

Table 2-5: The characteristics of IR peaks of zeolite (i.e., mordenite)[452,453,458-462]

Vibrations	**Wavenumber (cm^{-1})**
O-H stretching (w)	3620 (w)
O-H stretching (s)	3440 (s)
H-O-H bending	1639 (m)
Si-O-Si (symmetric)	790 (m)
T-O-T asymmetric stretching (s)	1052 (s)
Si-O-Si (bending)	470 (m)

* T= Si or Al

The structural framework of zeolites consists of AlO_4 and SiO_4 tetrahedra, connected through oxygen atoms forming rings (as described earlier in Chapter 1). One of the most important band vibrations of zeolites is the T-O asymmetric stretching vibration, where

"T" is Al or Si. This strong asymmetric stretching vibration appears in the region of 1200-950 cm^{-1} [462].

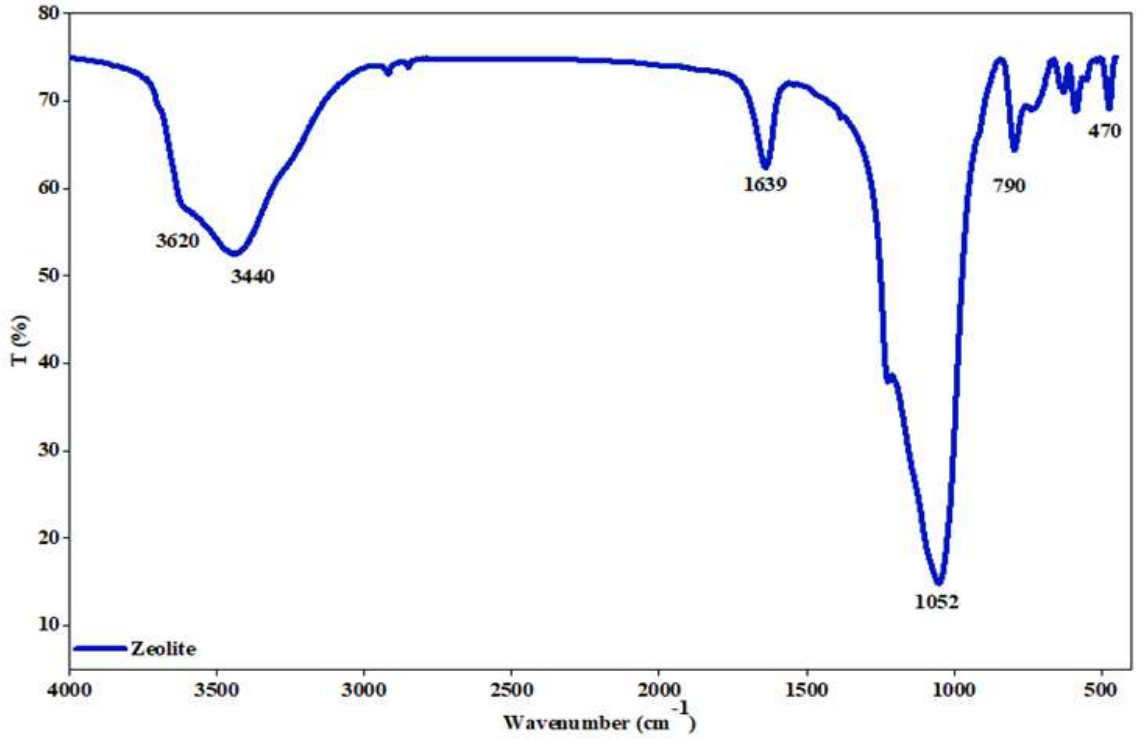

Figure 2-28: FTIR spectrum of zeolite (mordenite)

In the literature, a shift to a lower wavenumber is indicative of greater Al presence than Si in the structural framework of the zeolites, which was attributed to an increase in the Al-O bond length and a decrease in the T-O-T. This results in a lower observed vibrational frequency. For instance, heulandite has 9 Al atoms, and clinoptilolite has 6 Al atoms in a single formula unit. The higher number of Al atoms (in heulandite) gives a band vibration at a relatively lower frequency around 1022 cm^{-1} compared to clinoptilolite (which has only 6 Al atoms), which exhibits a stretching vibration at 1059 cm^{-1}[460]. Natural mordenite has been reported to show this band around 1046 cm^{-1} when it has a Si/Al ratio ranging between 4.4-4.5 [459], while in the present study, the mordenite examined gave a peak around 1052 cm^{-1} in the FTIR spectrum, which seems to indicate a somewhat lower aluminium content in agreement with the EDX analysis. Other important characteristic vibrations of mordenite in Fig. 2-26 were reported at 796 cm^{-1} (symmetric stretching of SiO_2) and at 1206 cm^{-1} which corresponds to the asymmetric stretching mode of SiO_4 or possibly quartz[462]. A peak at 470 cm^{-1} can be associated with a T-O bending mode[453]. Bands at 3300-3600 cm^{-1} and 1638 cm^{-1} are associated with physically adsorbed water on the zeolite[453,461].

2.4.5.3 Powder X-ray diffraction analysis of mordenite

The diffractogram of zeolite is shown in Figure 2-29. The XRD was a critically important characterization technique for this commercial material because it served to identify the main component present (as this is not otherwise indicated in the commercially supplied specifications of this material). The XRD data indicates that this zeolite is chiefly composed of mordenite through analysis of the data using the "Xpert-Highscore software". The recorded peaks agreed with the reference diffractogram for mordenite (i.e., ICDD-00-029-1257); see Figure 2-30. Mordenite is an orthorhombic mineral with the empirical formula $Al_2H_{14}Na_2O_{31}Si_{10}$.

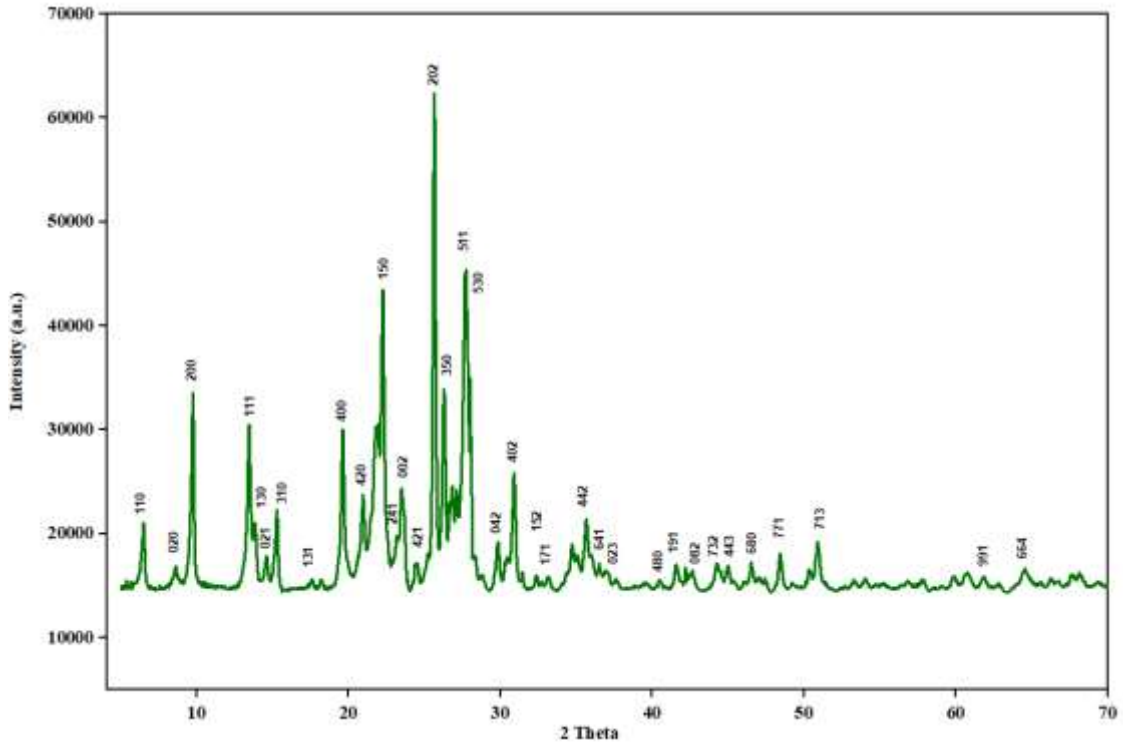

Figure 2-29: X-ray Diffractogram of zeolite (mordenite) used in this study

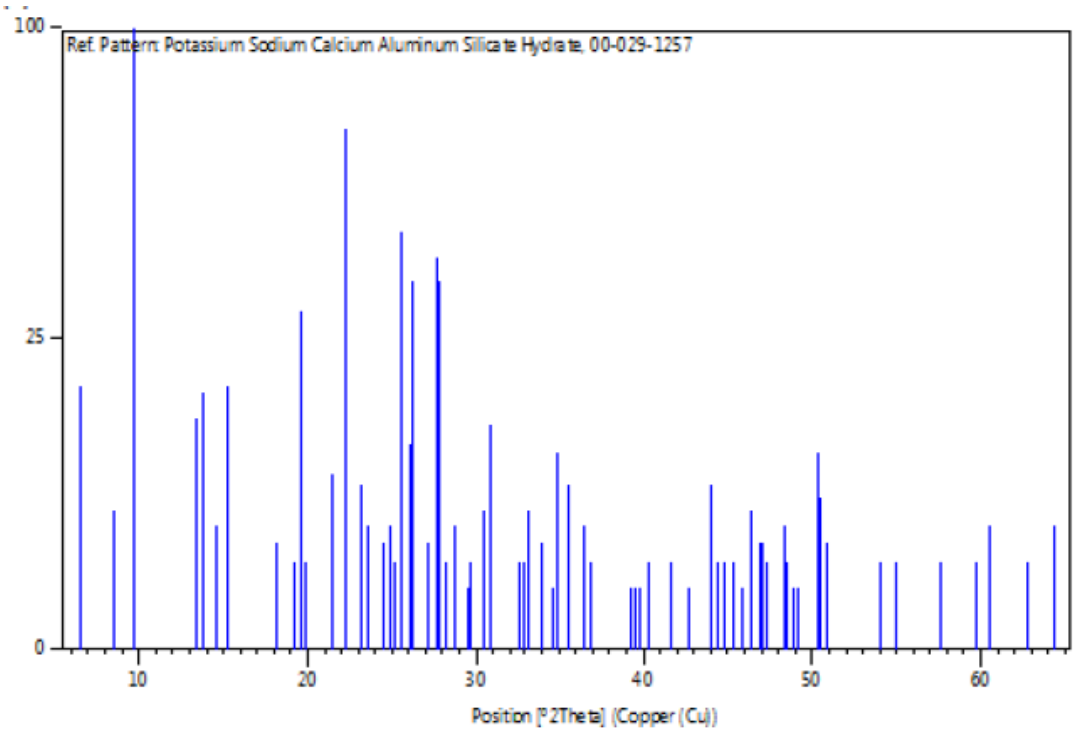

Figure 2-30: The reference diffraction pattern of mordenite (ICDD: 00-029-1257)

2.4.5.4 Thermogravimetric analysis of mordenite

Figure 2-31 (A & B) represents a typical thermogram of the zeolitic (mordenite) material used in the current study. This reveals a sharp weight loss starting from 30°C to 300 °C but with a value of 6 % only. A more gradual looking weight loss occurs with higher temperatures (> 300 °C), with the graph giving a plateau after 600 °C indicating no further weight loss in the zeolite on heating. A literature study reported the thermal decomposition of the mordenite, and thermal decomposition (weight loss) was reported up to 800 °C, illustrating no change in the structure of mordenite. At the same time, the heating beyond this temperature was found to cause structural changes[463].

This weight loss could be attributed to moisture removal from the surface and pore water molecules from mordenite. A total weight loss of approximately 8% was recorded by TGA analysis, which shows that the zeolitic material (consisting of mordenite) had relatively good thermal stability at the higher temperature ranges used in the TGA analysis[444,464]. Natural mordenite (studied in Turkey) was more stable than modified mordenite beyond 800 °C with this thermal stability is attributed to its high K content and Si/Al ratio, favouring the structural stability of zeolites[453]. So, the thermogram recorded for the natural mordenite used in this study illustrated the thermal stability showing a little

weight loss (%), which aligns with the literature reported for the natural mordenite stability.

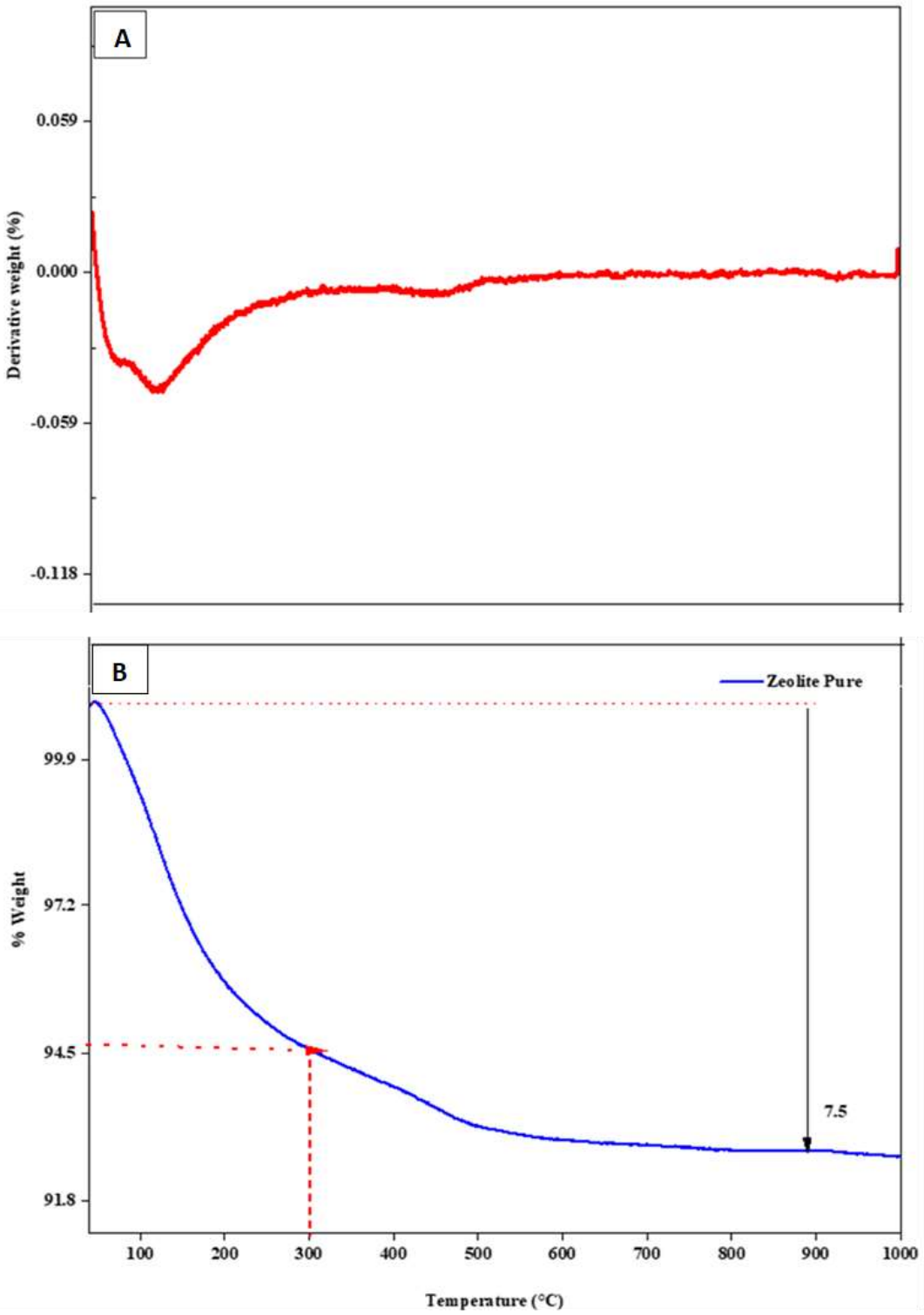

Figure 2-31: Thermograms of mordenite used in this study (A) DTG Curve (B) Thermogram

2.5 Summary

This chapter broadly demonstrated the methods used to characterise the feedstock materials. Similar methods would be used further in this study to characterise the synthesised composite materials using the selected feedstock materials.

The morphological characteristics of the feedstock materials were analysed using scanning electron microscopy (SEM). The SEM micrographs showed that the chitosan has a fragile sheet-like appearance. The commercially sourced HAp micrographs exhibited a non-porous and amorphous morphology, while the bovine-sourced HAp was porous, showing a network of interconnected pores. SEM analysis demonstrated that spent coffee ground exhibited an irregular surface full of cavities while the coir fibre appeared as a tubular structure with a central void. The zeolite powder micrographs showed that they had irregular, needle-like morphology.

EDX analysis was carried out to detect the principal elements of the raw materials. Carbon and oxygen were the major components of chitosan, coir fibre and spent coffee grounds as expected. In addition to C and O, SCGs also contained potassium and phosphorus in small quantities. The hydroxyapatite exhibited calcium and phosphorus as principal constitutional elements along with carbon and oxygen, while the bovine-sourced HAp also contained a small amount of Mg, which indicated its biogenic source.

The Fourier transform infrared spectrometry was used for the molecular analysis of the raw materials. All the raw materials exhibited the vibrations of the characteristic functional groups in the raw materials, which agreed with previously reported literature studies of the materials.

Powder X-ray diffractometry was used to determine the crystallinity of the raw materials. The diffractograms of chitosan, coir fibre and spent coffee grounds were found to be poorly crystalline as broad peaks were detected. HAp samples exhibited the characteristic peaks of Hap in agreement with those observed in the reference diffractogram of hydroxyapatite. When comparing cHAp and bHAp, the bHAp was found to be more crystalline in nature than the cHAp because of the sharp and narrow peaks observed in the diffractogram. The diffractogram of the zeolite used in the present study agreed with the reference diffraction pattern of mordenite.

The thermogravimetric analysis revealed that the chitosan and coir fibre decompose completely at temperatures < 700 °C. The bHAp was more thermally stable than cHAp as the residue of bHAp showed a lower % weight loss than cHAp when heated up to 1000 ° C. The zeolite was also very thermally stable, showing only *ca.* 8% weight loss in total when heated up to 1000 ° C.

As stated earlier, these materials were employed in the synthesis of the composite materials under study. The upcoming chapter comprehensively discusses the processing of the raw materials and the synthesis and characterisation of the composite adsorbents.

Chapter 3

Synthesis and Characterisation of Composite Systems to be trialled for Heavy Metal Removal

In the previous chapter, selected raw materials were characterised using different spectroscopic and microscopic techniques. These materials were subsequently used to synthesise the composite adsorbents in order that they can be trialled in treatment systems for the adsorption of heavy metal ions. Hence, this chapter exclusively discusses the synthesis and characterisation of the composite adsorbents, which were synthesised from the raw materials discussed in chapter 2.

3.1 Introduction

The modern literature (as discussed in Chapter 1 in detail) focuses on preparing bio-composites with novel materials, including low-cost adsorbents, for achieving a better removal efficiency for heavy metals from wastewater. The chosen raw materials (as discussed in Chapter 2) were believed to be the most appropriate choices for making composites that would be low cost, easily accessible in terms of raw materials and effective as heavy metal ion removal agents.

This chapter discusses the synthesis of the novel composites studied, including the pre-processing of the raw materials. Lastly, it also covers the characterisation of the composite matrices produced using the techniques and methods described earlier in Chapter 2).

3.2 Experimental Methods

3.2.1 Chemical Reagents

All chemical reagents were sourced commercially as analytical grade reagents and used as received without any further purification. The chemicals list, including their source and their respective use in the composite syntheses, is given below.

3.2.1.1 Acetic Acid (Glacial) 100% (CH_3COOH)

A 2% acetic acid solution (v/v) was used to dissolve chitosan. The 2% solution was prepared by adding 20 mL of Merck-grade glacial acetic acid to 250 mL of distilled water in a dropwise fashion, with the final volume being adjusted to the mark in a 1 L volumetric flask.

3.2.1.2 Hydrochloric Acid (HCl)

Analytical grade (Merck) HCl was used for two purposes in this study. The concentrated HCl (12.178 mol L^{-1}) and density 1.2 g mL^{-1} were diluted to 4 mol L^{-1} solutions used to dissolve the cHAp and bHAp. Secondly, the HCl was further diluted to prepare 0.1 mol L^{-1} HCl solutions in pH-related experiments to adjust pH. A fresh 0.1 mol L^{-1} solution was prepared each time for this purpose.

3.2.1.3 Sodium Hydroxide Pellets

Analytical grade NaOH pellets (Merk) were dissolved in distilled water to make a solution with a concentration of 4 mol L^{-1} NaOH. This solution was used to bring about the precipitation of composite materials from their solutions as a crucial part of their synthesis.

3.2.2 Processing methods of raw materials

Chitosan and HAp (cHAp or bHAp) were used in all composite matrices produced in this study, so the methodologies used to process these two materials were similar when synthesising the composite matrix systems.

3.2.2.1 Chitosan processing

The required quantity of fresh chitosan solution was prepared at the time of each composite synthesis. For this, 1 g of chitosan was dissolved in 2% acetic acid solution (100 mL) and was stirred until complete dissolution of chitosan had occurred (up to 8 to 12 hours). This resulted in a viscous solution which was then ready for composite synthesis.

3.2.2.2 Hydroxyapatite processing

Hydroxyapatite (cHAp or bHAp) was fully dissolved by addition to 4 mol L^{-1} HCl solution. Generally, 1g of HAp was added to 25 mL of diluted HCl and stirred for 15 to 30 minutes to effect dissolution, resulting in a clear, colourless solution. This solution could then be used immediately in composite synthesis.

3.2.2.3 Coir fibre processing for composite synthesis

Coir fibre was washed with distilled water thrice before use and then air-dried at room temperature (25 ºC). Grinding of the fibre was necessary and was accomplished using a mortar and pestle with the assistance (by embrittlement) of liquid nitrogen (N_2) (100 mL g^{-1} coir fibres) into a form consisting of small fibrous particles and fibre dust and stored until use for composite synthesis. Coir fibre was suspended in type I water when it was used in coir composite preparation (see later).

3.2.2.4 Spent coffee grounds processing

The spent coffee grounds (SCGs) were further ground with a mortar and pestle after drying at 50 ºC and used in a suspended form in distilled water without further processing when used to synthesise composites.

3.2.2.5 Zeolite (Mordenite) processing

The mordenite zeolite pellets were ground in their as-received state into finer powders and suspended in type I water, in which form they were further used in composite synthesis.

3.3 Synthesis of composites

The composite synthesis process was designed and carried out to make two sets of composites based on the hydroxyapatite used (as described in chapter 1, section 1.9).

Group A: cHAp containing composites (using commercial hydroxyapatite)

Group B: bHAp containing composites (using bovine powder as a source of hydroxyapatite)

The general scheme to prepare composite matrices system is given below (Figure 3-1):

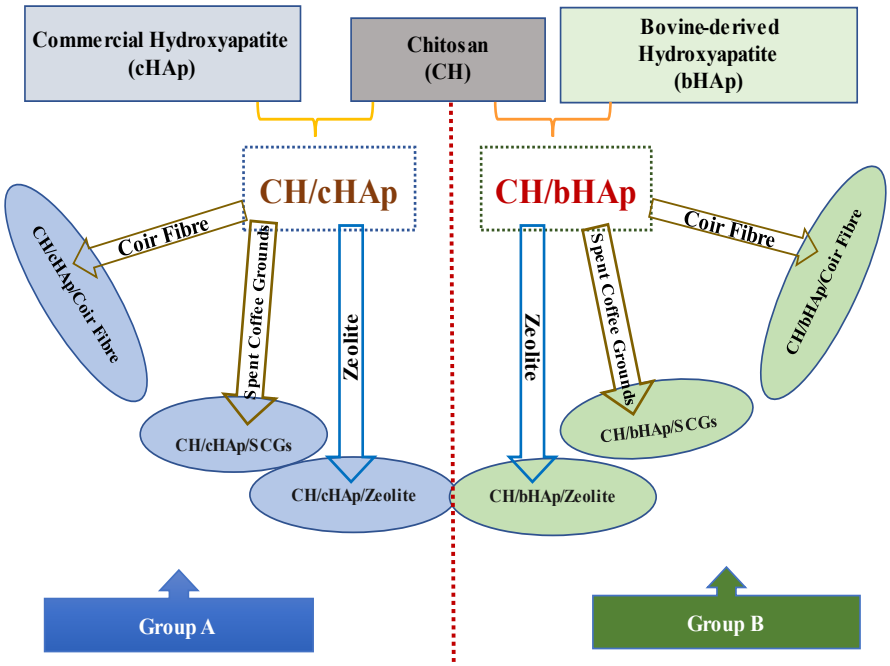

Figure 3-1: Schematic diagram showing the composite matrices synthesised in this study

In each composite synthesis, the chitosan and hydroxyapatite solution preparation was the first step of the synthesis, as shown in Figure 3-1. The first composite system was based on the two-component (chitosan and HAp) based systems, while the rest of the novel composites made in this study were three-component systems, with the third component being one of coir fibre, spent coffee grounds and zeolite (mordenite). These were added to the CH/HAp solution after pre-processing of the third component, as discussed above. Also, as mentioned earlier, the two-component composites would serve as the control composites (in section 1.9, Chapter 1) to evaluate the effect of the third component on the removal efficiencies of the control composite with respect to the metal ions trialled.

3.3.1 Synthesis of the Chitosan/Hydroxyapatite composites (CH/cHAp and CH/bHAp)

The base two-component chitosan/hydroxyapatite composites were synthesised using the chemical precipitation method described by Bazargan-Lari et al.[95] with minor modifications to the procedure. As mentioned earlier, the CH/cHAp composite (using synthetic HAp) has been synthesised and studied in earlier studies for its capacity to remove heavy metal ions from the solution (Table 1-1). In this study, this particular composite was synthesised as a control for the novel three-component composite systems

considered in this study. Similarly, the CH/bHAp composite has also been reported earlier, where it was considered as a removal agent for Cu^{2+} ions, although it is also of interest to explore its removal abilities for other heavy metal ions. Hence like the CH/cHAp composite, the CH/bHAp composite was synthesised in this study to not only compare the cHAp and bHAp based composite systems but also to serve as a control for the three-component systems. Hence the third composite component was added to both CH/cHAp and CH/bHAp composites.

CH/cHAp composite synthesis: Using the solutions of chitosan and cHAp described earlier (3.2.2.1 & 3.2.2.2), the combination was executed with stirring maintained for 48 hours. This resulted in a gel-like thick, white mixture that indicated the premature formation of the CH/CHAp composite. Further precipitation of the composite was facilitated by adding 1 L of NaOH solution (4 mol L^{-1}) to 500 mL of CH/HAp solution. After the addition of NaOH, the mixture was kept for three days to mature in an open atmosphere (under fumehood and beaker covered with watch glass). After three days, the mixture was centrifuged and washed with distilled water until a neutral pH was observed. The resultant product was a white jelly-like material, which was then dried in an oven at 50 ºC. The dried material was subsequently ground into a powder using an electric grinder and stored in an airtight jar until further use in adsorption experiments with heavy metal ions, with some set aside to allow for characterisation.

CH/bHAp composite synthesis: A similar procedure was repeated to synthesise the CH/bHAp composite. Similar observations were made to the CH/cHAp composite as to the physical appearance of the material.

3.3.2 Synthesis of Coir Fibre composites with chitosan and HAp (CH/cHAp/CF and CH/bHAp/CF)

CH/cHAp/CF: Coir fibre composites with chitosan and hydroxyapatite were formed following the method described by Rajesh et al.[438] with some modification, who synthesised the CH/HAp/CF composite specifically for its use as packaging materials and not for water treatment. There is no other literature study at the time of writing reporting the synthesis or application of this three-component composite in any other field.

The chitosan and cHAp solutions mixture were prepared as described in the earlier section (3.3.1). To make a 1:1:1 composite of coir, chitosan, and hydroxyapatite, 1 gram of

ground coir fibre was dispersed in 20 mL of type I water and immediately added into the CH/cHAp solution (1:1) with vigorous stirring. The even distribution of the coir dust/particles within the solution was ensured by a continuous stirring of the three-component mixture for 24 h, after which NaOH solution (4 mol L^{-1}) was added (1 L NaOH to a 500 mL mixture of CH/HAp/CF) to the mixture to reprecipitate the 3-component material composite. After reprecipitation, a similar procedure of centrifugation and washing was done to wash out the by-products from the composite, followed by drying and grinding of the composite material.

CH/bHAp/CF: The same procedure used for the CH/cHAp/CF composite synthesis was used, except that cHAp was replaced with bHAp to prepare the CH/bHAp/CF composite. Apart from some material set aside for characterisation, both CH/HAp/CF composites prepared were stored in airtight jars until adsorption experiments were carried out with heavy metal ions.

3.3.3 Synthesis of Spent Coffee ground composites with chitosan and HAp (CH/cHAp/SCGs and CH/bHAp/SCGs)

The oven-dried spent coffee grounds (SCGs) were suspended into type I water to add to the pre-dissolved chitosan/HAp solution (either cHAp or bHAp). Approximately 20 mL of water was used to disperse 1 g of SCGs powder which was then added to the chitosan/HAp solution with vigorous stirring to distribute the SCGs evenly into the mixture. Additional time (24 h) was used to allow the mixture to be optimally homogenized before re-precipitation. As described earlier, a similar re-precipitation method was used by using a 4 mol L^{-1} NaOH solution. However, in the case of the CH/HAp/SCGs composite syntheses, the volume of the NaOH utilised was at least double the volume of the materials mixture to ensure homogeneity of the composite formed. Hence, for a 500 mL mixture of three components, 1 L NaOH solution was added, followed by centrifugation and washing. It was dried and stored until its further use in metal ion adsorption experiments.

3.3.4 Synthesis of zeolite (mordenite) composites with chitosan and HAp (CH/cHAp/Zeolite and CH/bHAp/Zeolite)

Ground zeolite (mordenite) was suspended in type I water (20 mL) and then added to the pre-dissolved chitosan/HAp solution (either cHAp or bHAp). The mixture of chitosan, HAp and mordenite was stirred vigorously to allow the lump-like mordenite to be evenly distributed throughout the solution. Subsequently, NaOH (double the volume of the mixture) was added to the solution using high-speed stirring in order to ensure precipitation of the homogenized composite of the three components. After adding NaOH, the reprecipitated material was further left to mature for 4-5 days to ensure complete composite precipitation. The composite material produced was then washed, dried and ground for further use in metal adsorption experiments.

3.4 Results and discussion

The visual characterization of the synthesised composites was done by schematic diagrams and presented below (see Figures 3-2 to 3-5). Physiochemical characterization of the synthesised composite matrices is given in the following sections.

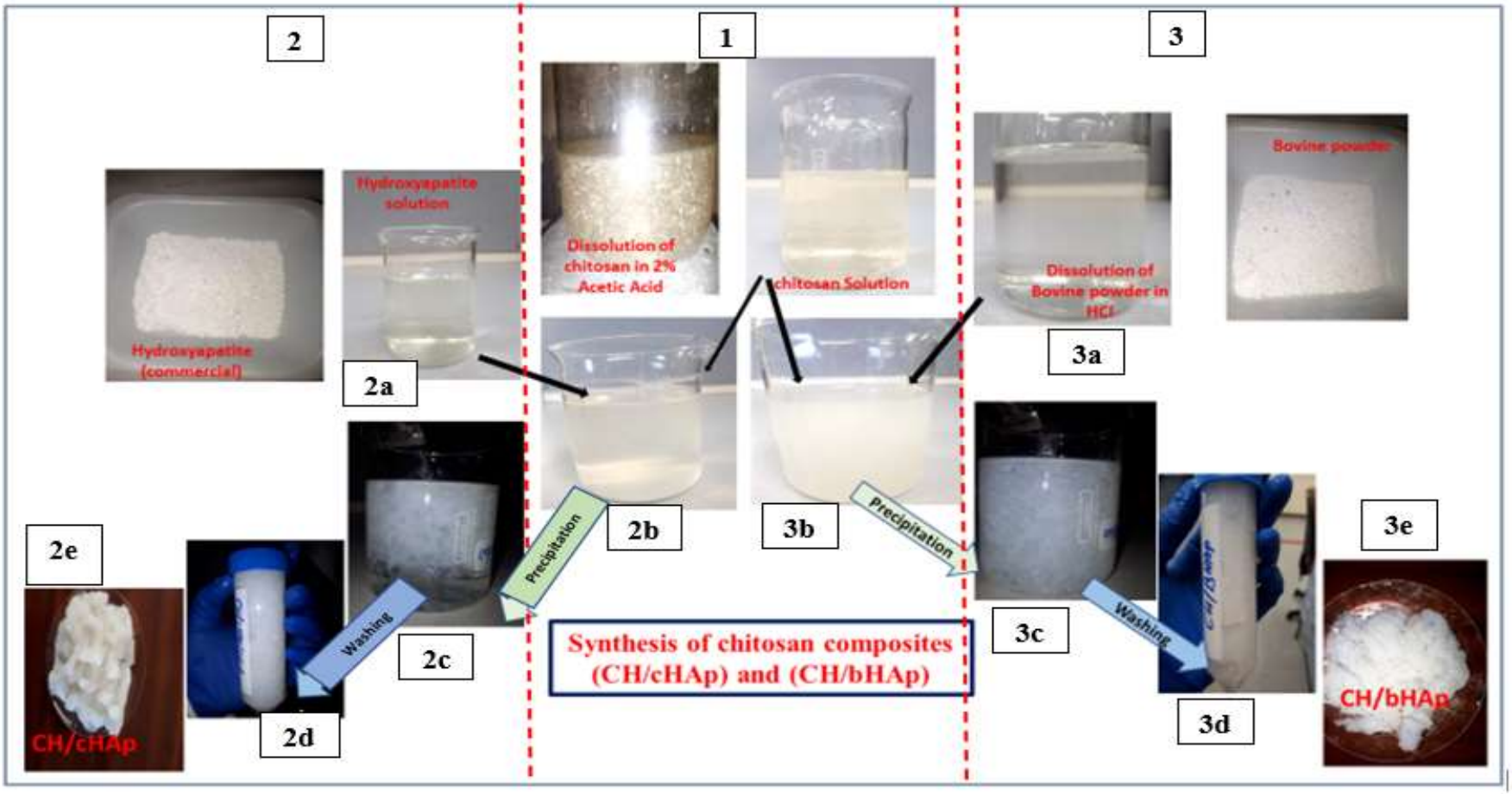

Figure 3-2: The synthesis of the CH/HAp composites

Figure 3-3: The synthesis of the CH/HAp/CF composites

Figure 3-4: The synthesis of the CH/HAp/SCGs composites

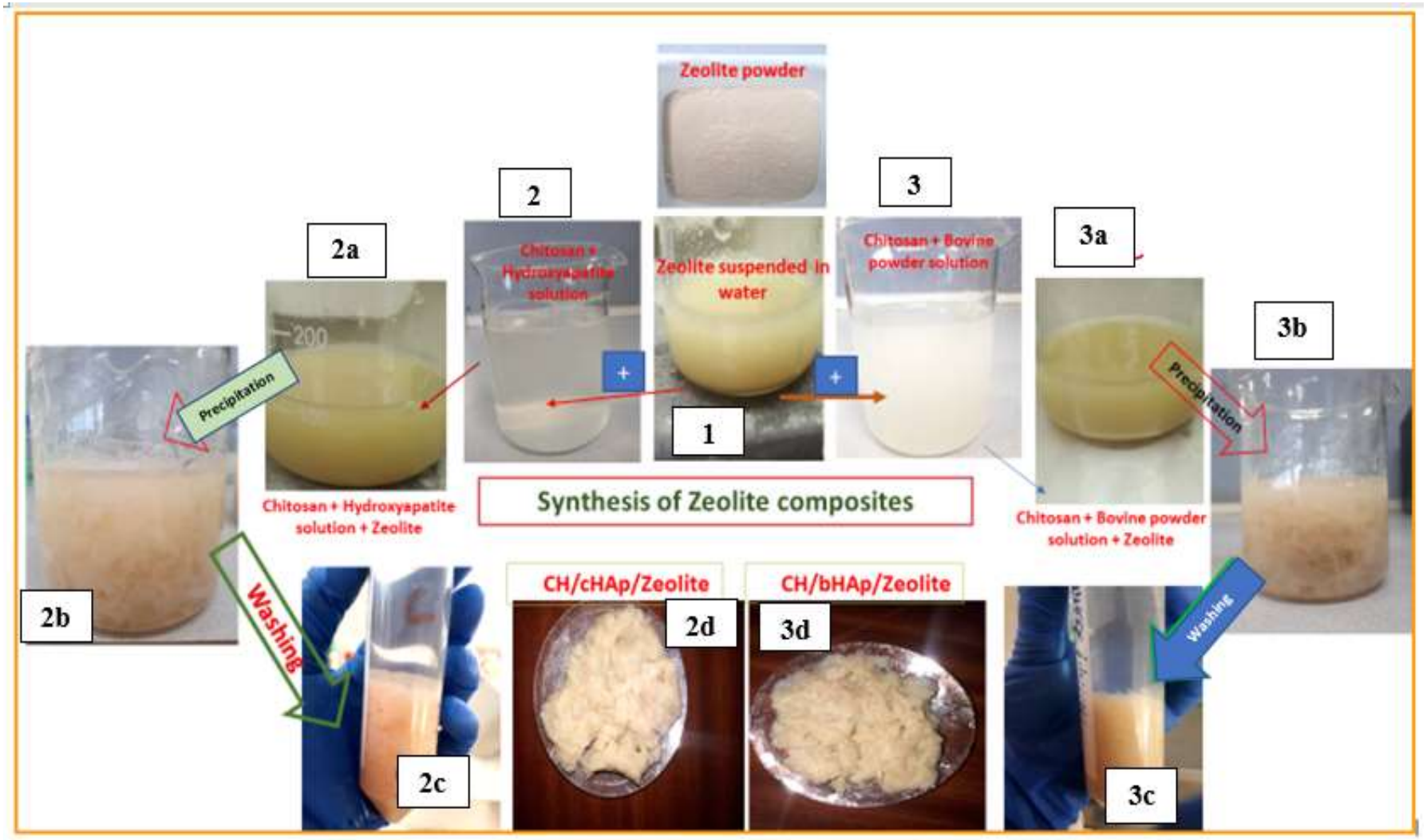

Figure 3-5: The synthesis of the CH/HAp//Zeolite composites

The following section describes the characterisation of the composite systems, which were synthesised by using the raw materials (studied in chapter 2). As mentioned earlier in chapter 2, the OriginPro software was used to plot the figures in this study which automatically selects the y-axis scales for FTIR spectra, XRD diffractograms and TGA and thermograms.

3.4.1 Characterization of the control two-component chitosan/cHAp and chitosan/bHAp composites

3.4.1.1 SEM/EDX analysis of CH/cHAp and CH/bHAp composites

CH/cHAp: In Figure 3-6, the SEM micrographs of the CH/cHAp composites are presented at high and low magnification. A high magnification view (X8000, Figure 3-6 A) exhibits a homogenized material having random macropores on the surface. The presence of macropores was confirmed by doing several repeat SEM measurements of the composite. Similar macropores were reported in the literature in the earlier reported synthesis of a chitosan and HAp nano-composite, which was prepared using a calcium-deficient source of hydroxyapatite[465].

A lower magnification SEM image of the partially ground composite is presented in Figure 3-6 B and shows aggregates made up of different sizes with irregular shapes. This would have been brought about by the mechanical breaking up of the dried caked mixture. The texture of these particles looked smooth when observed as low magnification images.

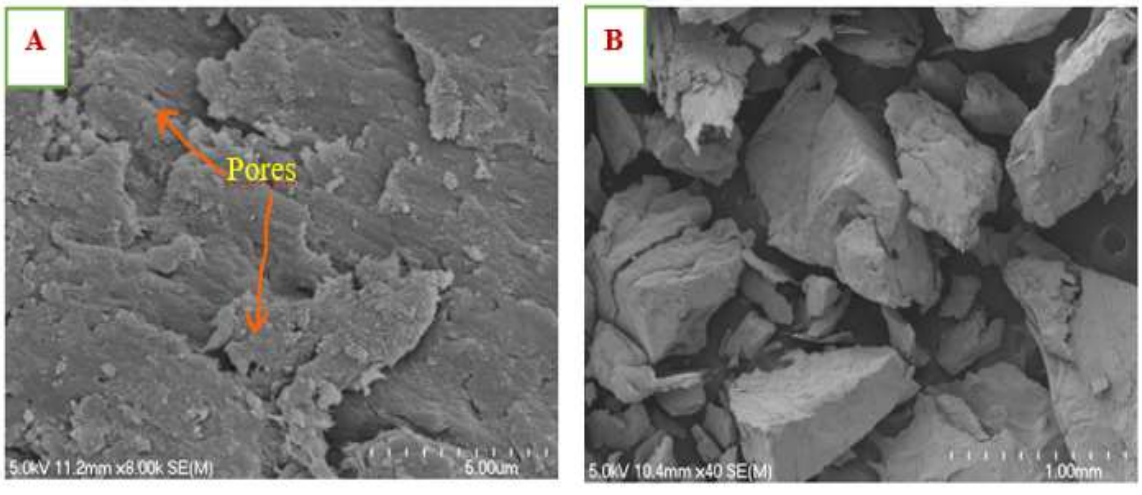

Figure 3-6: SEM micrographs of CH/cHAp composites at different magnifications

The EDX analysis of the CH/cHAp composite is shown in Figure 3-7. The graph featured prominent peaks due to carbon, oxygen, calcium and phosphorus, which are the principal elemental components of the precursor materials. The Ca:P ratio calculated for the various CH/cHAp composite samples was found to fluctuate between 1.6-1.7, which is similar to the Ca:P mole ratio of stoichiometric hydroxyapatite[96].

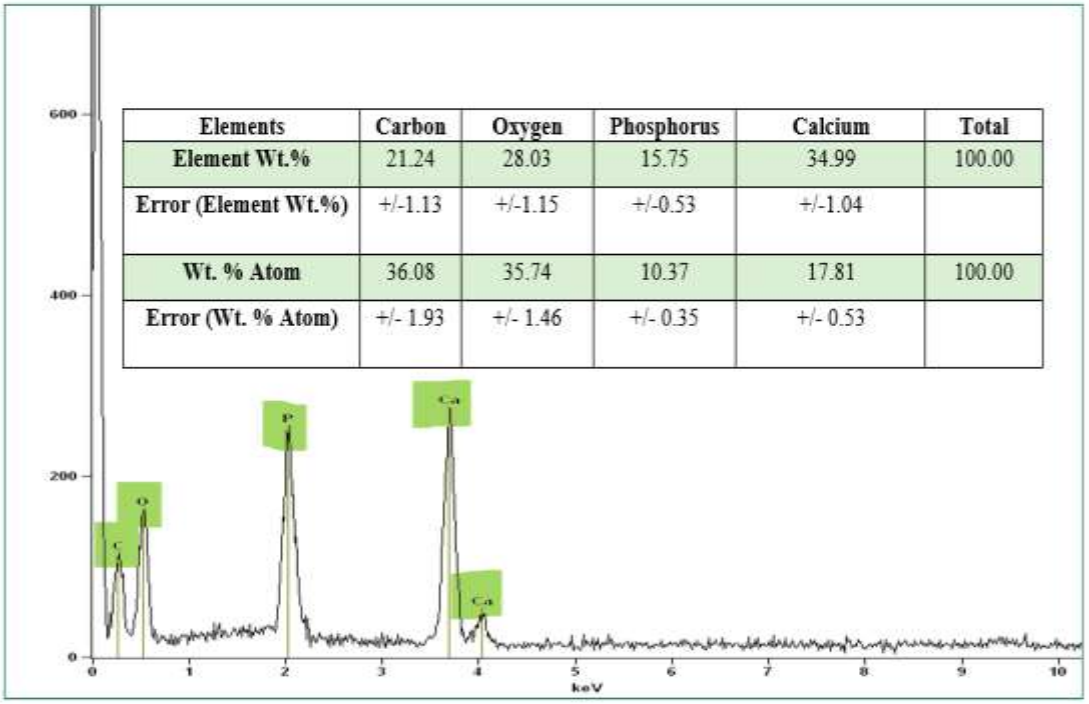

Figure 3-7: EDX analysis of the CH/cHAp composite

CH/bHAp: The SEM images in Figure 3-8 illustrate the morphology of a partially ground CH/bHAp composite. The CH/bHAp composite surface shows the deposition of fine particles (Figure 3-8 A). The surface of the composite was also observed to be rough, with some pits and cracks. The heterogeneous looking CH/bHAp composite morphology could be due to the deposition of HAp particles on the surface. Additionally, the heterogeneity and deposition could be attributed to the mechanical breaking up of the particles and intercalating the chitosan and the HAp. The particle deposition was observed and reported in another literature study[466] during the course of a hydroxyapatite/chitosan nano-composite synthesis, which was uniform in size and round in appearance and recognized as HAp particles. The literature study reported them as HAp particles that were dispersed in a biopolymeric matrix of chitosan. In the present study, the deposited particles could also be HAp deposition inside a biopolymeric matrix as reported in the literature or simply be a representation of the composite itself. The interpretation is

subject to some doubt because there was not enough data to confirm and conclude that this was the case.

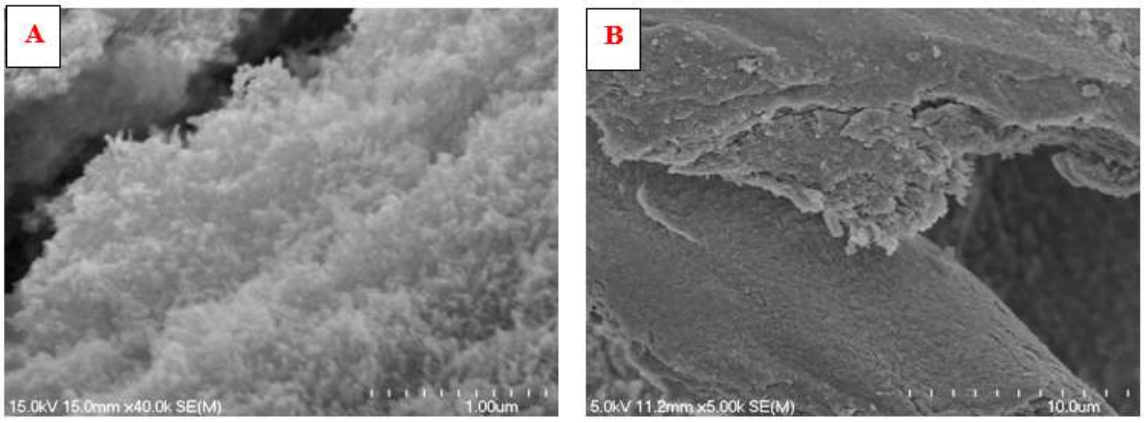

Figure 3-8: SEM micrographs of CH/bHAp (A) x40.0k magnification (B) x5.00k magnification.

The EDX microanalysis of the CH/bHAp composite is presented in Figure 3-9 and shows the expected major elemental components based on the raw material content. The Ca:P mole ratio calculated for measured samples ranged between 1.7- 1.8, while Mg was <0.5% in all measured samples. The presence of Mg in this composite confirms the bovine-derived source of the hydroxyapatite in the composite, as Mg is commonly found in HAp derived from bovine sources. The cHAp (synthetic), in contrast, shows no Mg in its analysis, confirming its synthetic origin.

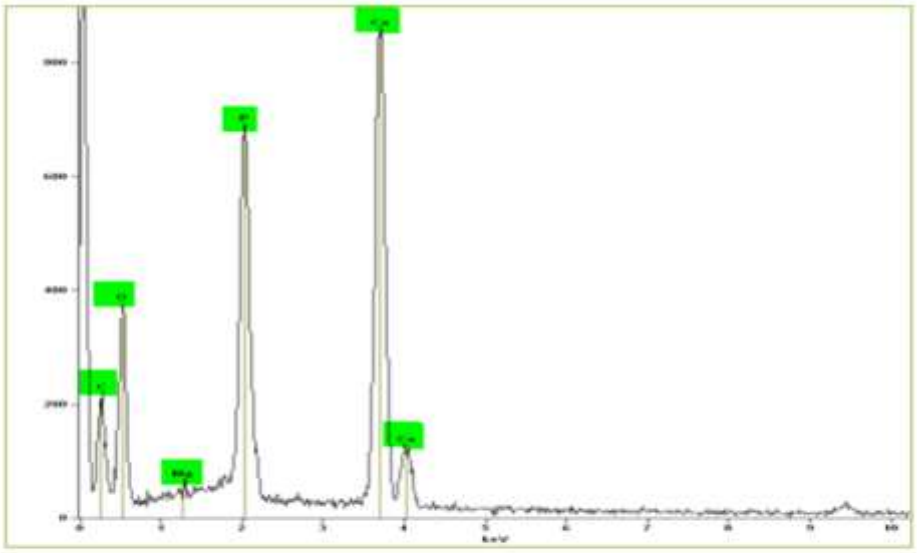

Elements	Carbon	Oxygen	Magnesium	Phosphorus	Calcium	Total
Element Wt. %	19.21	32.26	0.25	14.38	33.92	100.00
Error (Element Wt. %)	+/-0.83	+/-0.83	+/-0.05	+/-0.26	+/-0.47	
Wt. % atom	32.40	40.86	0.19	9.40	17.14	100.00
Error (Wt. % atom)	+/- 1.41	+/- 1.06	+/- 0.05	+/- 0.17	+/- 0.24	

Figure 3-9: EDX analysis of the CH/bHAp composite

Overall, the micrographs of the two composites were different in terms of the surface, as the fine deposition of particles was more apparent on the CH/bHAp composite surface. In contrast, the surface of the CH/cHAp composite was relatively homogenised/uniform in its appearance.

3.4.1.2 FTIR analysis of the CH/cHAp and CH/bHAp composites

Further probing of the molecular composition of the CH/HAp composites was achieved using FTIR analysis. The FTIR spectra of the KBr disks of both composites are shown in Fig 3.10, and assignments of peaks are summarised in Table 3-1, where the peaks due to chitosan and hydroxyapatite are denoted by "C" and "A" in Figure 3-10, these are in good accordance with characteristic peaks described earlier for chitosan (Figure 2-5) and hydroxyapatite in general as derived from the two sources (Figure 2-13).

Table 3-1: Characteristic IR absorption peaks observed in the spectra of the CH/cHAp and CH/bHAp composites[377,406,421-423,429,467,468]

Assignment	**Wavenumber (cm^{-1})**
-OH and -NH stretching (combined)	3420 (s)
C=O (Chitosan)	1632 (m)
C-H stretching (Chitosan)	2853-2926 (w)
C-N stretching (Chitosan)	1320 (w)
PO_4^{3-} (P-O-P bending) (Apatite)	550-600 (m)
PO_4^{3-} P-O asymmetric stretching (Apatite)	1040-1099 (s)
C-O stretching	1380 & 1417 (w)
CO_3^{2-} (asymmetric C-O stretching modes)	1413 & 1460 (w)

In the FTIR spectrum of the CH/bHAp composite, some peaks that had been observed in the bHAp spectrum (see Chapter 2 Figure 2-13) disappeared/changed their position when forming a composite. For instance, the OH stretching vibration of lattice OH around 3572 cm^{-1}(see Figure 2-13) and the librational mode of HAp at 632 cm^{-1} disappeared in the CH/bHAp composite FTIR spectrum, which confirmed the formation of poorly crystalline HAp in the composite with chitosan. The characteristic acetyl group vibration of chitosan at 1638 cm^{-1} exhibited a lower intensity in the spectra of the composite samples, which could be attributed to some further deacetylation occurring in chitosan re-precipitation using NaOH, which is known to act as a catalyst in such a process[469].

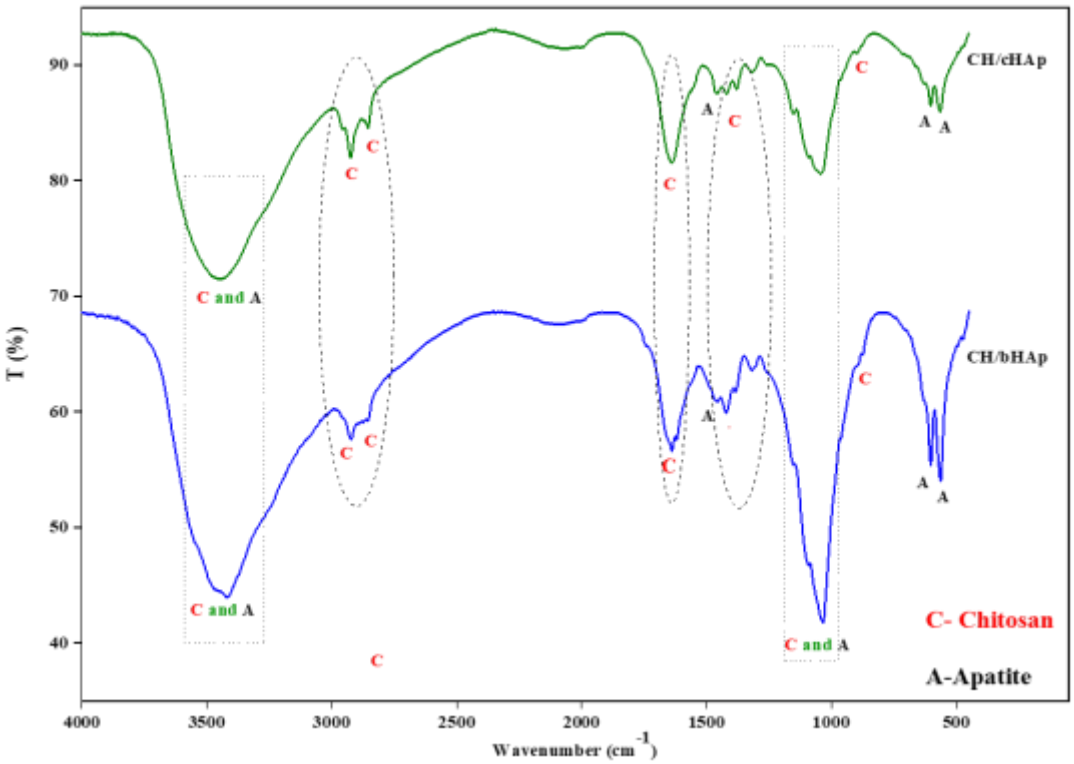

Figure 3-10: FTIR spectra of the CH/HAp composites

3.4.1.3 Powder X-ray diffraction analysis of CH/cHAp and CH/bHAp

Figure 3-11 represents the powder X-ray diffractograms of both the chitosan/hydroxyapatite composites. The features observed in the powder X-ray diffractograms of the two composites confirmed hydroxyapatite presence via peaks observed at 2θ = 26°, 31.7°, 32.9°, 34.04° and 39.8° (presented in Figure 3-11). HAp peaks were predominant in the diffraction patterns of the composites compared to chitosan, though the intensities of peaks are lower and broader than for the precursor hydroxyapatite sources. The broader peaks in the composites than the candidate HAp confirm the formation of a poorly crystalline HAp-chitosan composite. Similar low intensity and broad peaks were reported in powder XRD by Salah et al.[377], who studied the development of a nano-hydroxyapatite/chitosan composite.

The characteristic peaks of chitosan flakes[377,400,401]at around 2θ =10° and 2θ =20° was observed in the composites and additionally illustrated in Figure 3-12. A broad peak at 2θ =20° in the reported diffractogram of candidate chitosan flakes was found to exhibit three smaller peaks, which could be attributed to the overlapping of the HAp diffraction

peaks at 2θ=21.8° and 2θ= 22.9°. The diffractogram of composites (Figure 3-11) with its broad peaks indicates the formation of poorly crystalline composites, which was in accord with the observation recorded in the FTIR spectra of the composites.

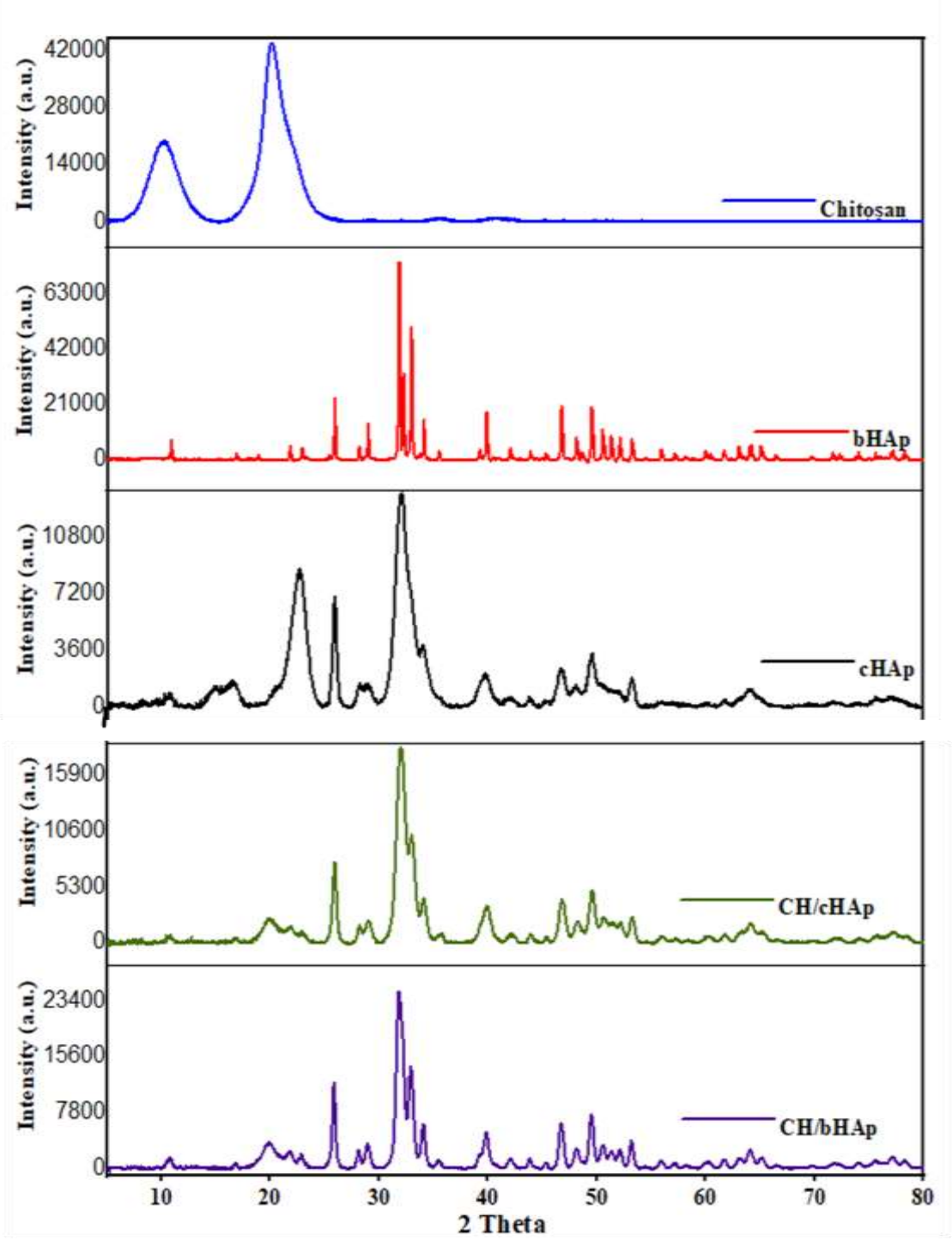

Figure 3-11: Diffractograms of CH/HAp composites and the candidate materials used to synthesise the composite

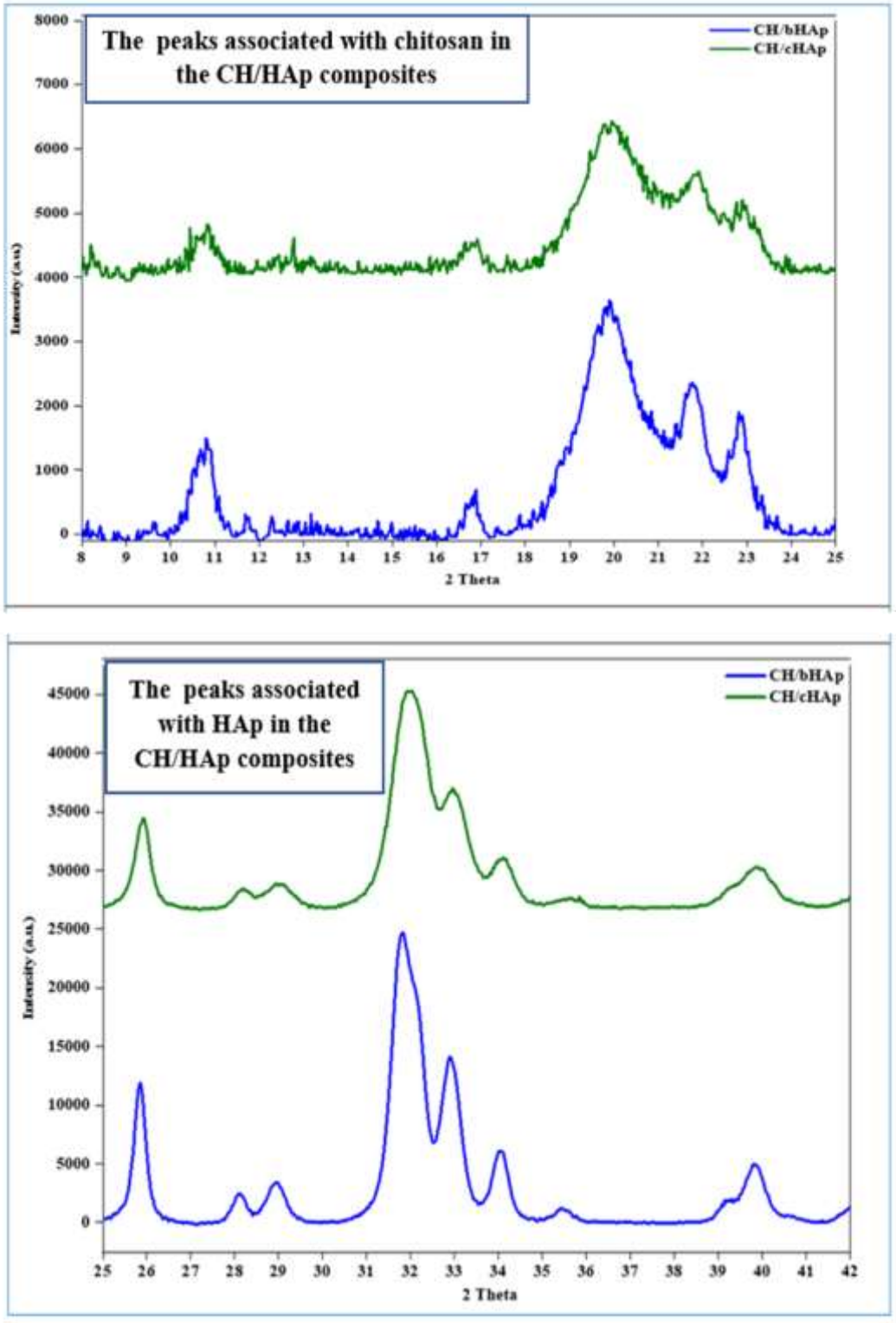

Figure 3-12: The characteristic diffraction peaks of chitosan and HAp recorded in the CH/HAp composites and presented as a detailed view

The peaks illustrated above in Figures 3-12 for the characterisation of chitosan and HAp were recorded for the CH/HAp (control) composites. These peaks are mentioned to demonstrate the presence of the CH/HAp part in the three-component composite systems.

3.4.1.4 Characterisation of the CH/cHAp and CH/bHAp composites by thermogravimetric analysis

Figure 3-13 represents the thermograms of the CH/cHAp and CH/bHAp composites measured over a temperature range of 30 to 1000 °C. In the thermogram for CH/cHAp, a 7.61% weight loss occurs around 200 °C, while a total weight loss of approximately 45% occurs in the range of 200 °C to 550 °C. There is no significant weight loss observed after 550 °C. The initial weight loss occurs because of dehydration of the composite matrix. A comparison of the CH/cHAp thermogram with that of chitosan (Figure 2-8 in chapter 2) revealed that the weight loss over the 200-550 °C temperature range is occurring due to the combustion of the chitosan itself.

A comparison of the thermogram in Fig. 3-13 of the CH/cHAp composite with those of the raw material thermograms (Figure 2-8 (chitosan) and 2-15 & 2-16 (HAp)) confirms that the residual mass is due to the apatite component only, as chitosan completely combusts up to 550 °C, leaving no mass behind in the pan. Furthermore, the white material counts for approximately 50% of total mass, as shown in Fig. 3-13, which shows that the composite was approximately 1:1 chitosan and HAp by weight. After the analysis was completed, the observation of a white residual powder in the sample holder confirmed that the organic chitosan had completely burnt out and that HAp remained.

The TGA of CH/bHAp is very similar in shape and form to that for CH/cHAp and indicates that similar processes are occurring in the CH/bHAp composite with the burning out of the chitosan. After 600 °C, a gradual weight loss up to 1000 °C was observed in the thermogram of the CH/bHAp, which counts for 11.35% and is probably due to the decomposition of carbonates contained within the HAp which were observed in the FTIR analysis of the as-received bHAp (Figure 2-13). After the TGA analysis, a similar-looking residual white powder was observed, which accounted for approximately 55% of the mass of the CH/bHAp composite.

A major difference between the two thermograms is the residual mass after burning up to 1000 °C. The total weight loss recorded for the CH/cHAp was 60%, while for the CH/bHAp, 45% weight loss was recorded. It is known that the chitosan is burnt out completely by 600-700 °C, as observed in the thermogram of chitosan alone (Figure 2-

8), while the cHAp itself showed a weight loss of 60% leaving behind 40% residual mass. According to these observations, the residual left behind after heating CH/cHAp composites up to 1000 °C is (decarbonated) cHAp.

In contrast, the bHAp thermograms showed a relatively smaller weight loss when heated up to 1000 °C (Figure 2-16). The residual mass of 60% after the combustion of chitosan in CH/bHAp is attributed to (decarbonated) bHAp. The higher residual weight could be due to the CH/bHAp composite containing more bHAp incorporated into the composites than cHAp. The more incorporation of bHAp in the bHAp-based composite could be attributed to the relatively higher purity (in terms of stoichiometry) of the bovine-sourced HAp (bHAp), as it represents sintered HAp and is "purer" in composition relative to the cHAp (which contains relatively more substituted carbonate)**.** So, the incorporation of carbonates in commercially sourced HAp (cHAp) could be the reason for there being lower incorporation of "HAp" in the cHAp-based composite. When the equal masses of cHAp or bHAp are used to make a composite with the chitosan (see section 3.3.1), it is possible that less HAp is deposited (as some mass is taken up by the carbonates, leading to less pure HAp) in cHAp-based composite compared to bHAp-based composites.

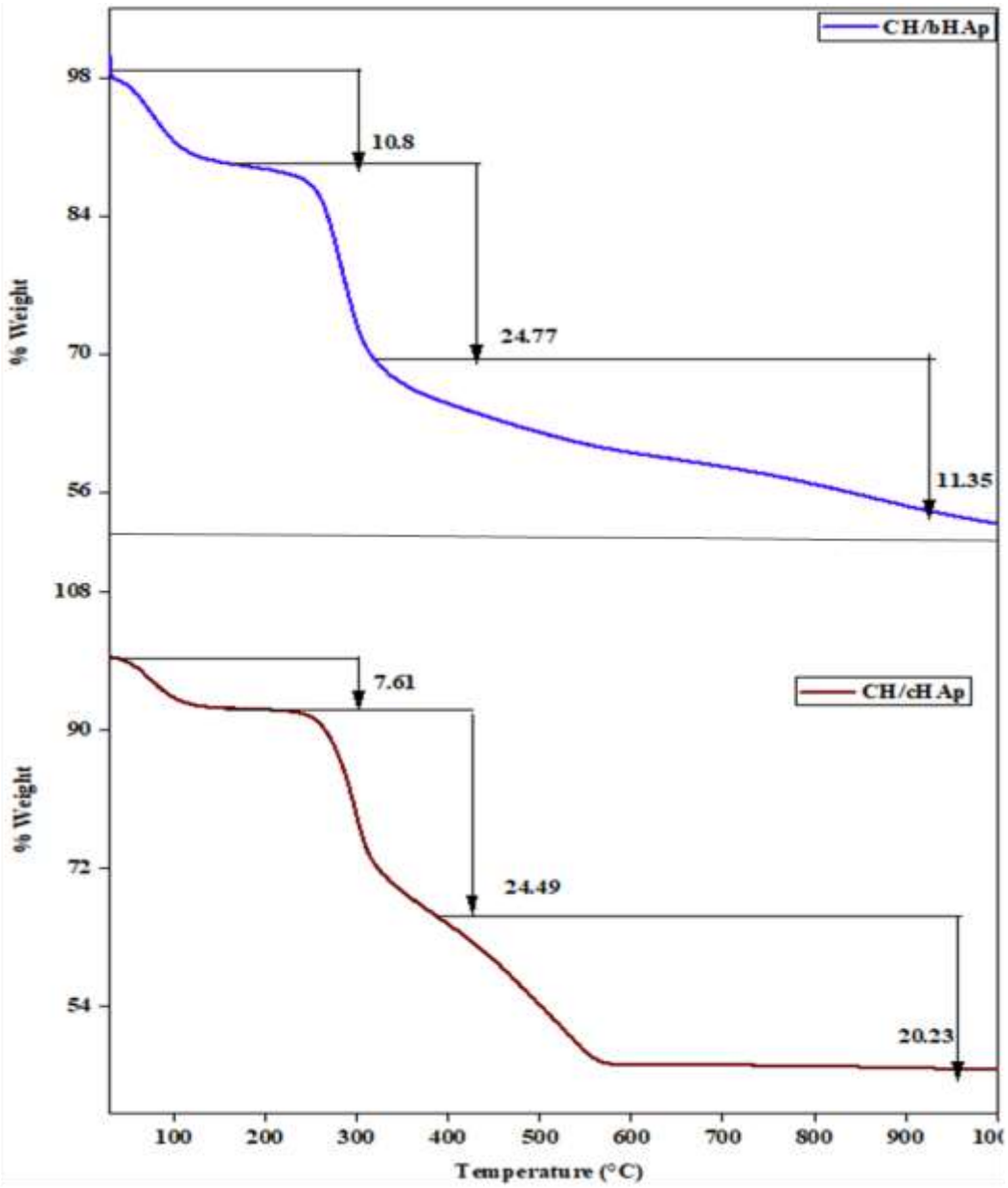

Figure 3-13: Thermograms of the CH/cHAp and CH/bHAp composites

3.4.2 Characterization of the Chitosan/cHAp/CF and Chitosan/bHAp/CF

3.4.2.1 SEM/ EDX analysis of CH/cHAp/CF and CH/bHAp/CF

CH/cHAp/CF: Figure 3-14 presents the SEM micrograph and EDX analysis of the CH/cHAp/CF composite. The micrographs generally showed an uneven and non-porous surface with deposition of very fine particles on it. The fine particles could be nanocrystals of HAp or coir fibre dust

The EDX analysis of the composite showed that the principal elements were Ca, P, C and O at atomic % values of 26.92 %, 13.56 %, 24.29 % and 35.24 %, respectively. A significant portion of C would be emanating from the presence of chitosan and the coir fibre, while the Ca and P signals would be coming from the presence of hydroxyapatite in the composite.

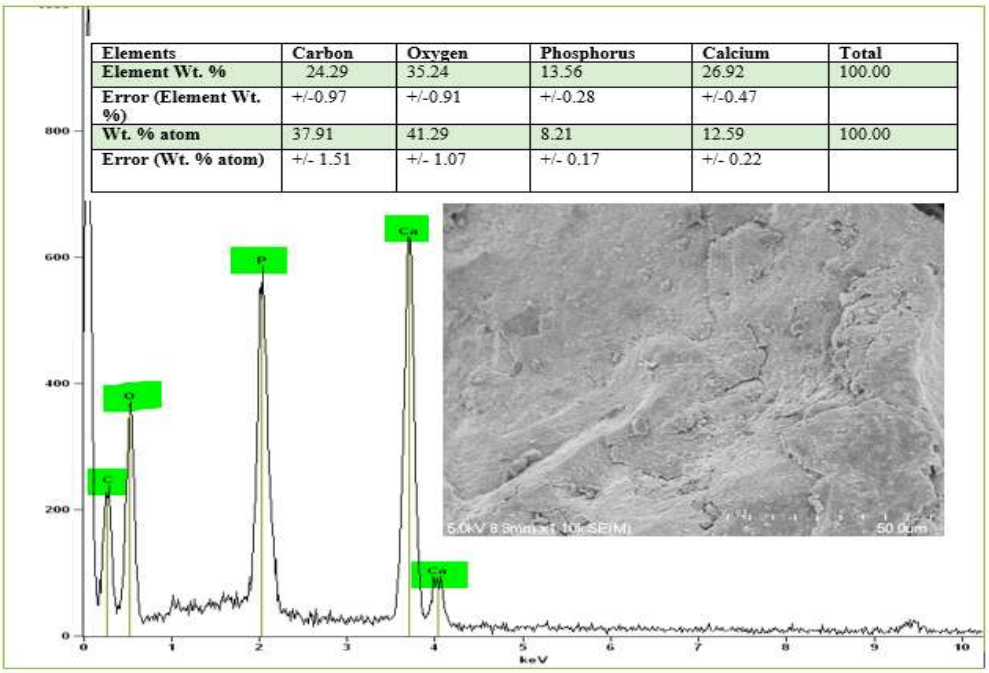

Figure 3-14: SEM micrograph and EDX analysis of CH/cHAp/CF composites

Figure 3-15 represents the micrograph of the CH/bHAp/CF composite, which shows similar uneven morphology as described for CH/cHAp/CF composite. It is not surprising that the morphology would be like that of CH/cHAp/CF composite. The EDX analysis (Figure 3-15) indicated C, O, Ca, P, and Mg and Na. The presence of Mg and Na is due to the biogenic (bovine) source of the HAp used to make the composite.

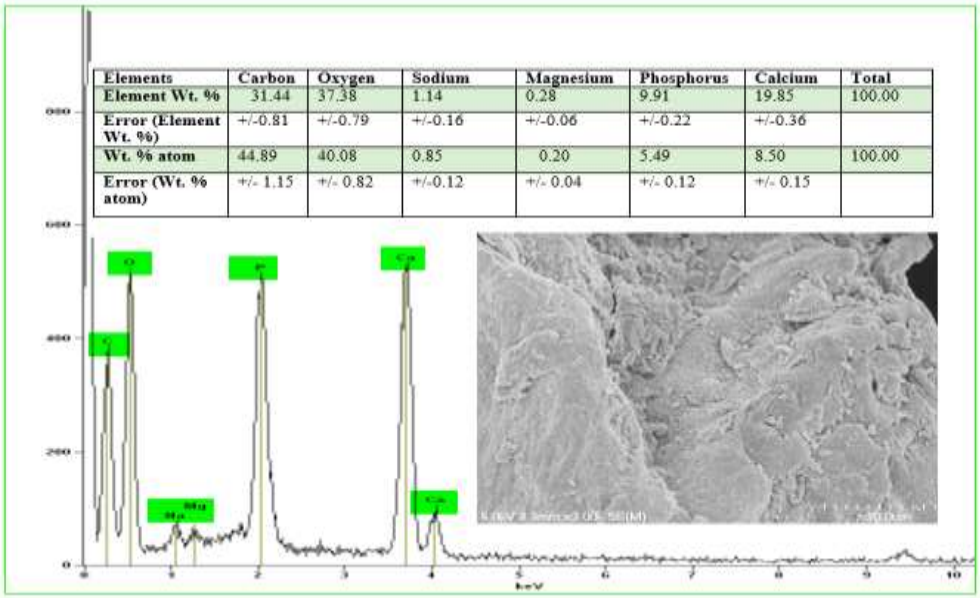

Figure 3-15: SEM micrograph and EDX analysis of the CH/bHAp/CF composite

3.4.2.2 FTIR analysis of CH/cHAp/CF and CH/bHAp/CF

The FTIR spectra of both coir composites are shown in Figure 3-16. Characteristic IR peaks in the composite and their assignments are summarized in Table 3-2.

Table 3-2: Characteristic IR absorption peaks of CH/cHAp/CF and CH/bHAp/CF composites[435,438]

Vibration	**Wavenumber (cm^{-1})**
Symmetric PO_4^{-3}	560-601
Asymmetric PO_4^{-3}	1032
-OH stretching	3443
-CH and -NH stretching	1380-1421
C=O stretching	1645-1647
C-H symmetrical stretching	2800-2920

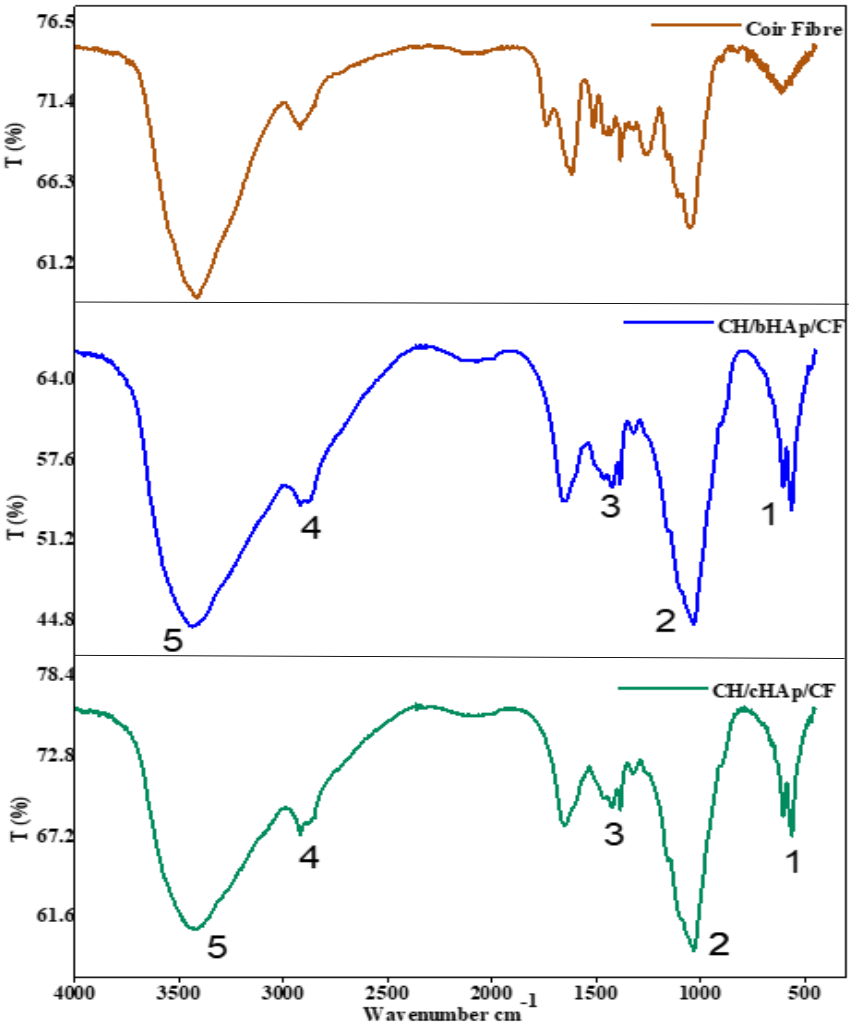

Figure 3-16: FTIR spectra of coir fibre (dust), CH/cHAp/CF and CH/bHAp/CF composites

In the spectra for both composites (Figure 3-16), the peaks in regions 1 and 2, the composites are dominated by the HAp, as the peaks are associated with the hydroxyapatite component (see Figure 2-13 for reference) and represent bending and stretching modes of the phosphates within the HAp. The IR absorption peaks in regions labelled 3, 4 and 5 are associated with the composite's coir fibre and chitosan components and represent C-O, C=O, CH and NH stretching vibrations. The dominant peak in region 6 is due to OH stretching of moisture and the chitosan and coir components.

Both IR spectra indicate the CH/cHAp/CF and CH/bHAp/CF composites are similar and successfully incorporated the chitosan, HAp, and CF, showing the characteristic peaks of all three components.

3.4.2.3 Powder X-ray diffraction analysis of CH/cHAp/CF and CH/bHAp/CF

Figure 3-17 represents the powder X-ray diffractograms for the CH/HAp/CF composites and raw chitosan, coir fibre and HAp. In both the composites, the XRD pattern is dominated by peaks from the hydroxyapatite component, which has characteristic peaks at 2θ= 25.87º (002), 32.197 º (112) and 34.049º (202) and 39.8 º (310). Similar peaks of HAp-content were observed in the X-ray diffractogram of the CH/HAp (control) composites (Figure 3-13) and were also in good agreement with the reference diffraction pattern for HAp (Figure 2-14).

For chitosan, a low-intensity peak signal at 2θ=10° was observed as well as a broad peak centred around 2θ=20° which was divided into three peaks as observed in the control composite diffractograms (Figure 3-11). A cellulose-associated peak from the coir fibre was not observed at 2θ= 22º, which was referred to as the cellulose pattern (ICDD = 00-050-2241) for the crystalline cellulose in the XRD diffractogram of coir fibre[458]. The actual reason of the disappearance of this peak is unknown. However, this could be due to the formation of poorly crystalline materials while being part of the composite.

The formation of the composites by reprecipitation led to a reduction in crystallinity for the raw components, particularly HAp. For instance, the intensity of characteristic peaks of HAp was reported to decrease when it is employed with biopolymeric materials (such as chitosan and coir fibre) due to reprecipitation and incorporation of polymers into the inorganic matrix of HAp[470].

In the XRD diffractogram of the CH/HAp composites (Figure 3-11), the bHAp characteristic peaks at 2θ=39-41° have been converted into a broader peak at 41.220 º in the diffractograms of CH/HAp/CF composites (Figure 3-17). Broad p-XRD peak patterns, as illustrated by the diffractograms of the CH/HAp/CF composites, can be attributed to the formation of poorly crystalline solids in the composite materials[470].

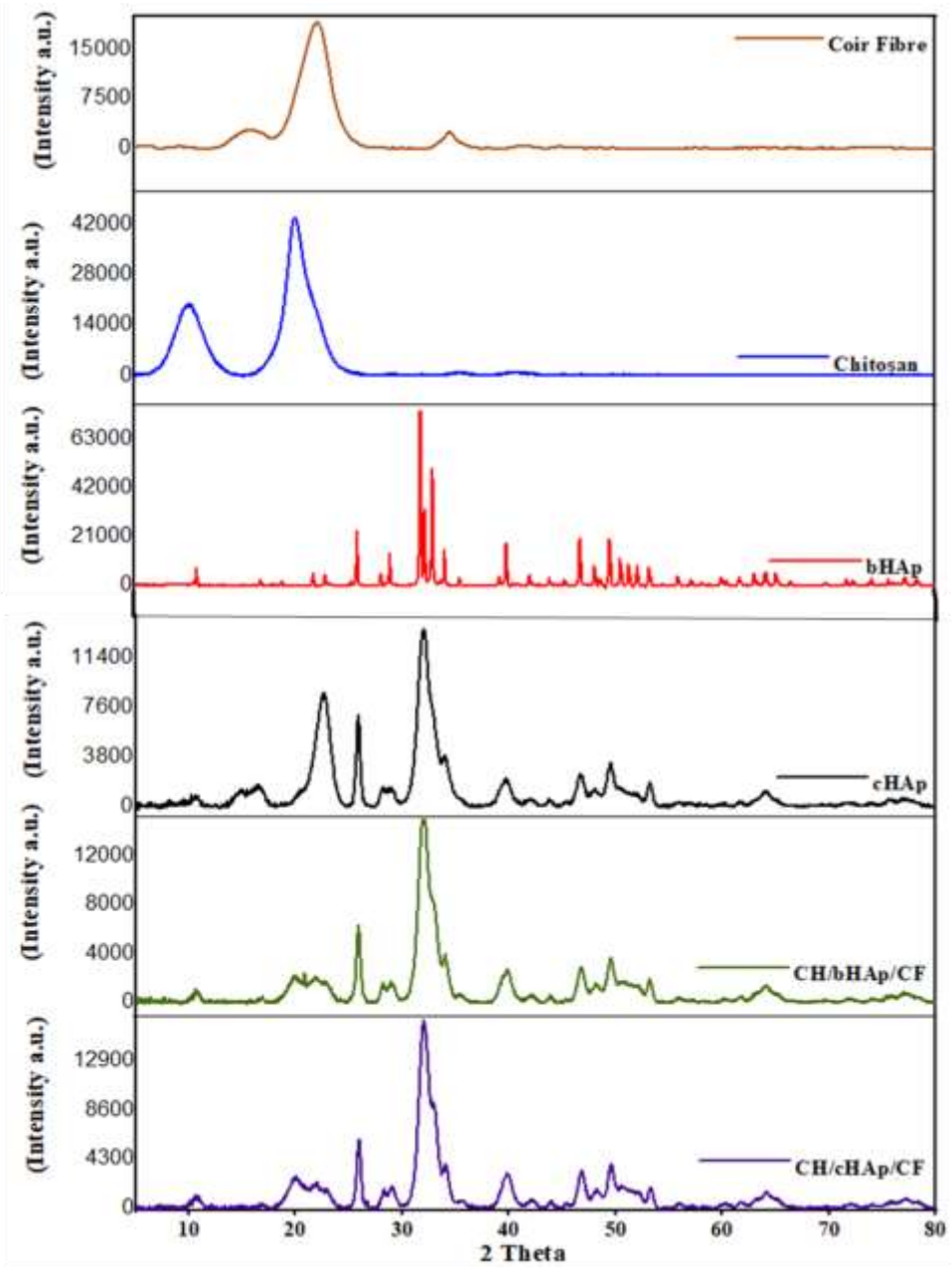

Figure 3-17: The X-ray diffractograms of CH/cHAp/CF and CH/bHAp/CF and the raw candidate materials of the composites

3.4.2.4 The thermogravimetric analysis of the CH/cHAp/CF and CH/bHAp/CF composites

Figure 3-18 exhibits the TGA thermograms of both the CH/HAp/CF composites. The thermograms showed features in three distinct regions. The first region lying below 200 °C led to approximately 9-11% weight loss in both composites. The second region is between 200-450 °C and is where significant weight loss (30-45 %) occurs in the composites. After 450 °C, only gradual weight loss is observed. The first weight-loss

event could be attributed to the dehydration of the composite. The second could be due to the breakdown of its carbonaceous component, i.e., chitosan and coir, which are known to decompose up to 500 °C as shown in Figures 2-8 (for chitosan) & 2-18 (for coir fibre). It infers that the weight loss occurring after 500 °C is mainly caused by changes occurring in the HAp solid component.

After heating up to 1000 °C, about 40% of the mass is left behind for the CH/bHAp/CF composite and about 20% for the CH/cHAp/CF composite, as shown in the following Figure 3-18. The higher residual mass % for the CH/bHAp/CF composite could be due to more incorporation of the bHAp into the CH/bHAp/CF composite material than cHAp in the CH/cHAp/CF composite.

These observations of more residual for the bHAp-based composites indicated that the bHAp was relatively more able to incorporate into the composite materials than cHAp. A similar mass of both the HAps was used to make composites with these materials. As 1 g of bHAp was used to make a composite with 1 g of chitosan, and similarly, 1 g of cHAp was added into chitosan to make the composite. Similarly, 1:1:1 of three components was used to form the CH/HAp/CF composites. It could be assumed that less cHAp incorporates into the composites than bHAp, as explained earlier in the TGA analysis of the control composite (see section 3.4.1.4 above).

Additionally, the comparison of the TGA analysis of the raw materials (chitosan, HAp and CF (Figure 2-8, 2-15 and 2-20, respectively) with their composite system (thermogram of CH/HAp/CF composites in Figure below) indicated that the chitosan and CF completely burnt off up to 550 °C, while beyond this temperature the residue in the pan is assumed to be HAp, indicating at least 20-40% weight of HAp in these composites (see Figure below).

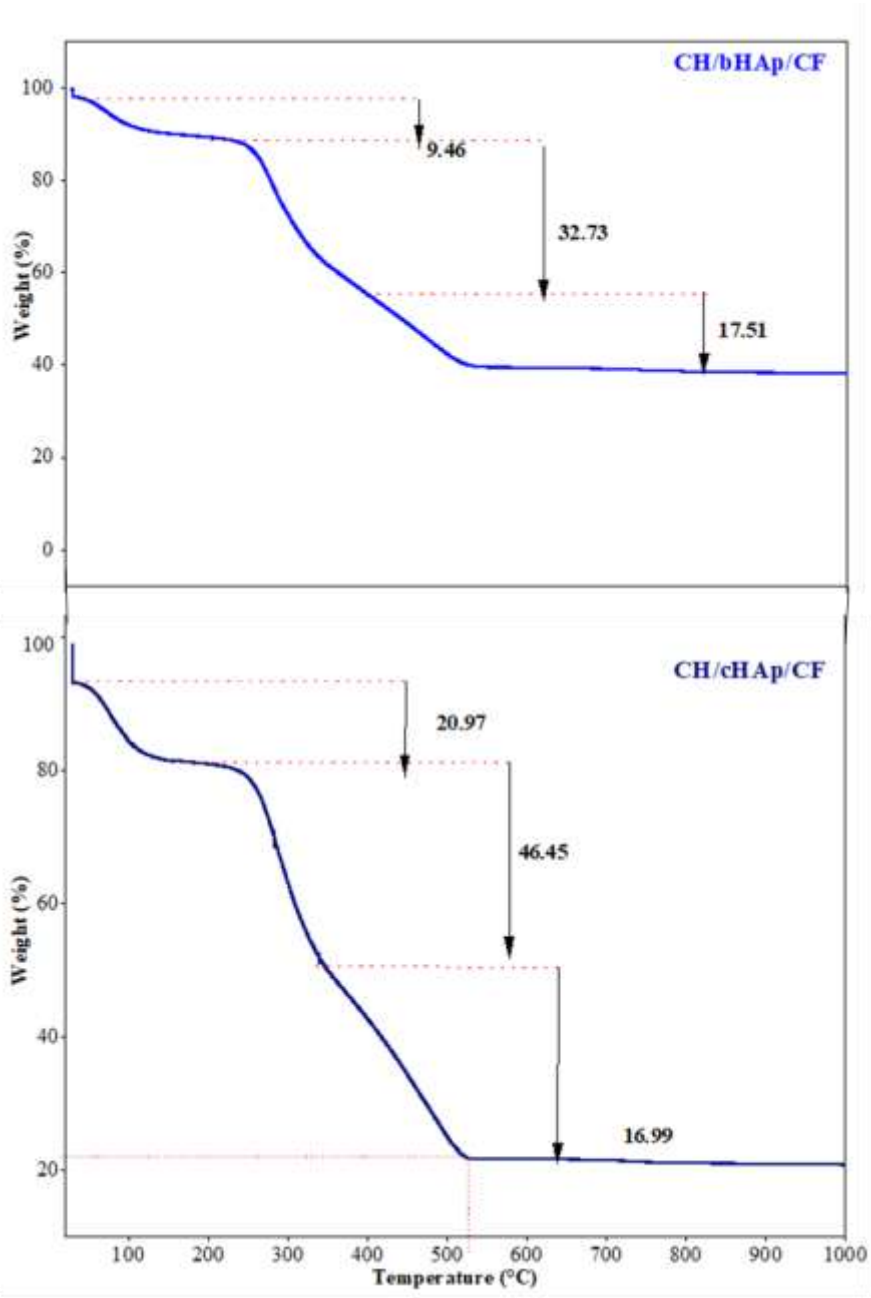

Figure 3-18: Thermograms of the CH/cHAp/CF and CH/bHAp/CF composites

3.4.3 Characterization of the Chitosan/cHAp/SCGs and Chitosan/bHAp/SCGs Composites

3.4.3.1 SEM/EDX analysis of the CH/cHAp/ SCGs and CH/bHAp/SCGs composites

Figure 3-19 and Figure 3-20 represent the SEM micrographs of the SCGs-based composites. These show a rough and pitted surface with rifts and cracks. The open

channels noted in Chapter 2 on the surface of the raw SCGs (Figure 2-19) are not visible in the SEM of the CH/HAp/SCGs composites. It could be due to the deposition of the SCGs with the chitosan/HAp solid mix, which possibly "fill voids" with co-deposited material. The literature available on the synthesis of such composites of SCGs with biopolymers or apatites is very sparse; hence interpretations of the nature of the morphology and why it is that way cannot be firmly concluded.

The EDX analysis is shown in Figures 3-19 & 3-20. Carbon is the principal element of these composites, accounting for 29-37% and also confirming the successful incorporation of the SCGs (as well as the chitosan) into the composite. Oxygen is the next most abundant element accounting for 31-34% by weight, with the remaining elements of Ca, P and Mg confirming the presence of hydroxyapatite into the composites. As observed in earlier analyses, Mg is present only in the bHAp composite due to its natural origins (bovine bone).

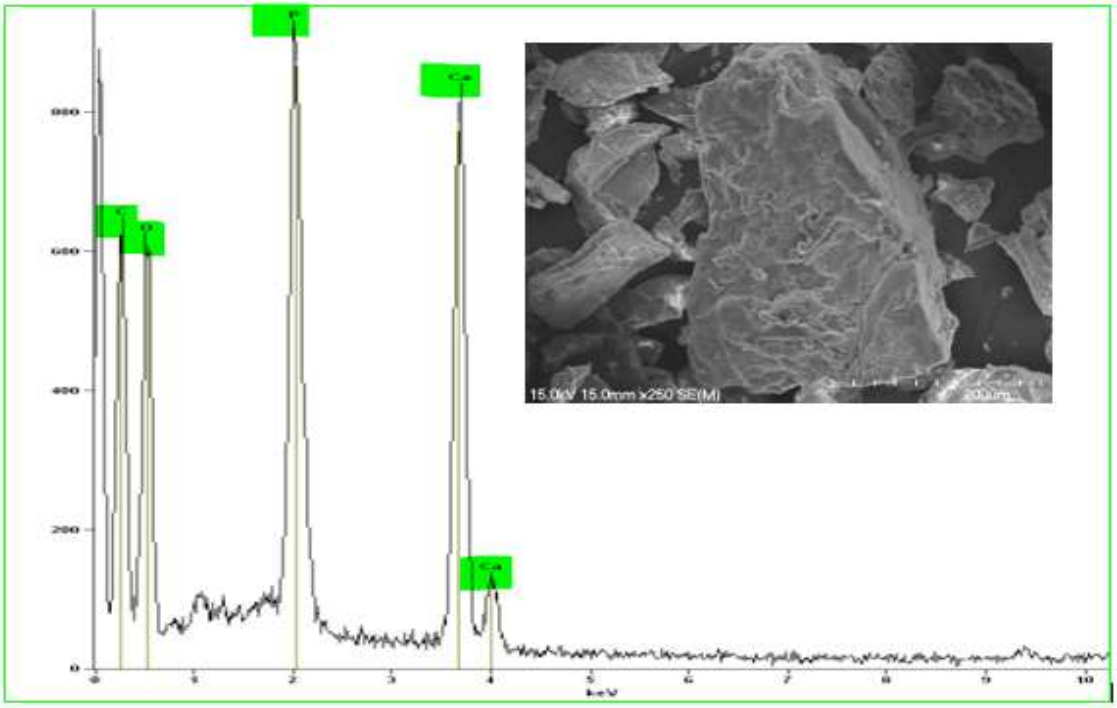

Elements	Carbon	Oxygen	Phosphorus	Calcium	Total
Element Wt. %	37.61	31.27	12.12	19.01	100.00
Error (Element Wt. %)	+/-0.75	+/-0.69	+/-0.20	+/-0.31	
Wt. % atom	52.62	32.84	6.57	7.97	100.00
Error (Wt. % atom)	+/- 1.05	+/- 0.73	+/- 0.11	+/- 0.13	

Figure 3-19: SEM micrograph and EDX analysis of the CH/cHAp/SCGs composite

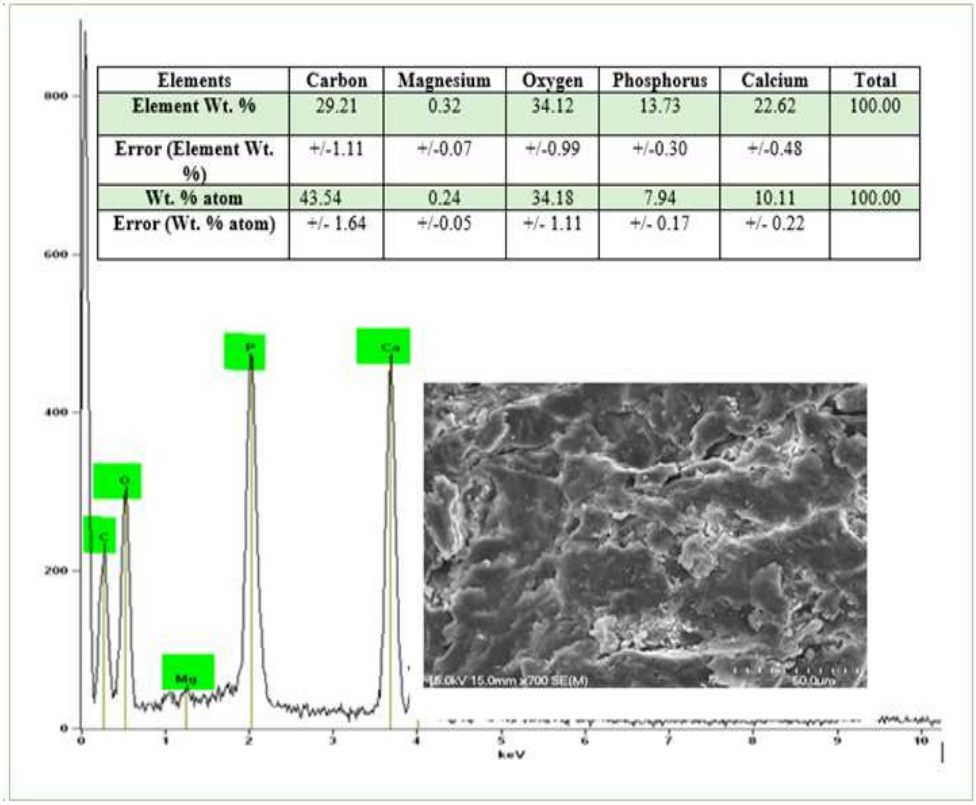

Figure 3-20: SEM micrograph and EDX analysis of the CH/bHAp/SCGs composite

3.4.3.2 FTIR analysis of the CH/cHAp/SCGs and CH/bHAp/SCGs composites

Figure 3-21 shows the IR spectra of the CH/cHAp/SCGs and CH/bHAp/SCGs composites. The characteristic IR absorption peaks observed in the spectra are summarised in Table 3-3 and assigned to chitosan, HAp or to vibrations associated with the spent coffee grounds.

Key changes in the IR spectra of the SCGs were observed when they became part of the composite. For instance, the characteristic vibration of the C=O stretching band (at 1742 cm^{-1}) associated with ester linkages (fatty acids) disappeared in the spectra of the composites. The C-O and C-O-C stretching vibrations of both chitosan and the SCGs were difficult to observe, possibly due to the overlapping of these peaks with the peak due to the phosphate group vibrations from hydroxyapatite in this region of the spectrum. However, the C=O vibration of amide I (in chitosan) and that of C=C (phenolic compounds of SCGs) are visible around 1650 cm^{-1}. The presence of hydroxyapatite is confirmed by peaks appearing in the spectra due to the phosphate groups in HAp around 550-600 cm^{-1} and 1038 cm^{-1}.

Table 3-3: Characteristic IR absorption peaks of CH/cHAp/SCGs and CH/bHAp/SCGs[444] [445] [443]

Assignments	Wavenumber (cm^{-1})
-OH (adsorbed water and -NH stretching (amino group of chitosan)	3430
CH stretching in backbone structure of cellulose (SCGs) and polysaccharides (chitosan)	2930-2850
CH bending (chitosan)	1320
PO_4^{3-} bending modes in HAp	620-550
C-O and C-O-C stretching of chitosan	1200-900
PO_4^{3-} (stretching modes) of HAp	1038
C=O (amide I) and C=C of phenols in SCGs	1650

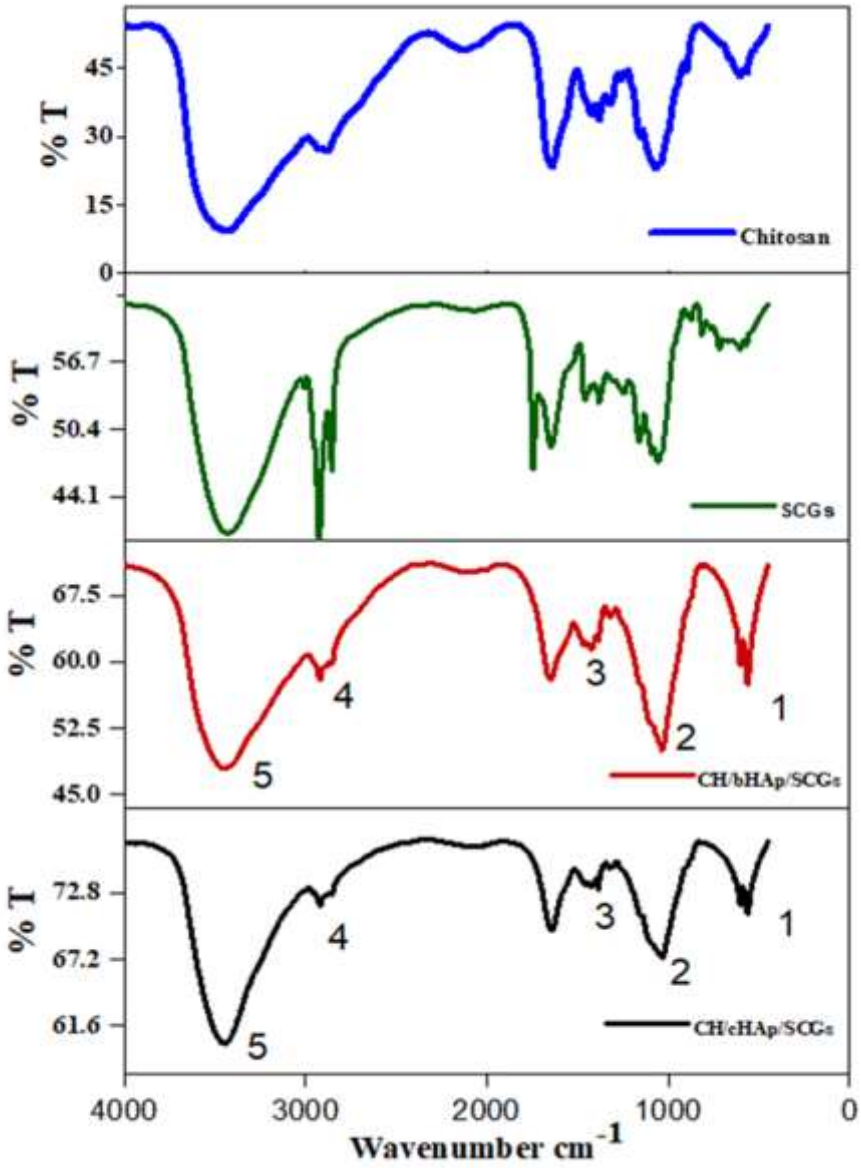

Figure 3-21: FTIR spectra of the CH/cHAp/SCGs and CH/bHAp/SCGs composites as well as those of the raw chitosan and SCGs materials

3.4.3.3 Powder X-ray diffraction analysis of CH/cHAp/SCGs and CH/bHAp/SCGs

The powder X-ray diffraction patterns of chitosan/hydroxyapatite/SCGs composites are given in Figure 3-22. The most prominent peaks in these are that of hydroxyapatite which was observed at 2θ= 25.8° and 2θ= 31.7° (as observed in the control composite Figure 3-12), while the presence of chitosan could be inferred from clear peaks at 2θ= 10° and 2θ= 20°[377,400,401]. A small diffraction peak at 2θ= 22.7° was attributable to crystalline cellulose present in SCGs, which agrees with the reference XRD for cellulose, ICDD =00-050-2241. Both composites showed similar diffraction patterns with broad peaks. The broader peaks are due to the poorer crystallinity of the reprecipitated HAp solid in the composites.

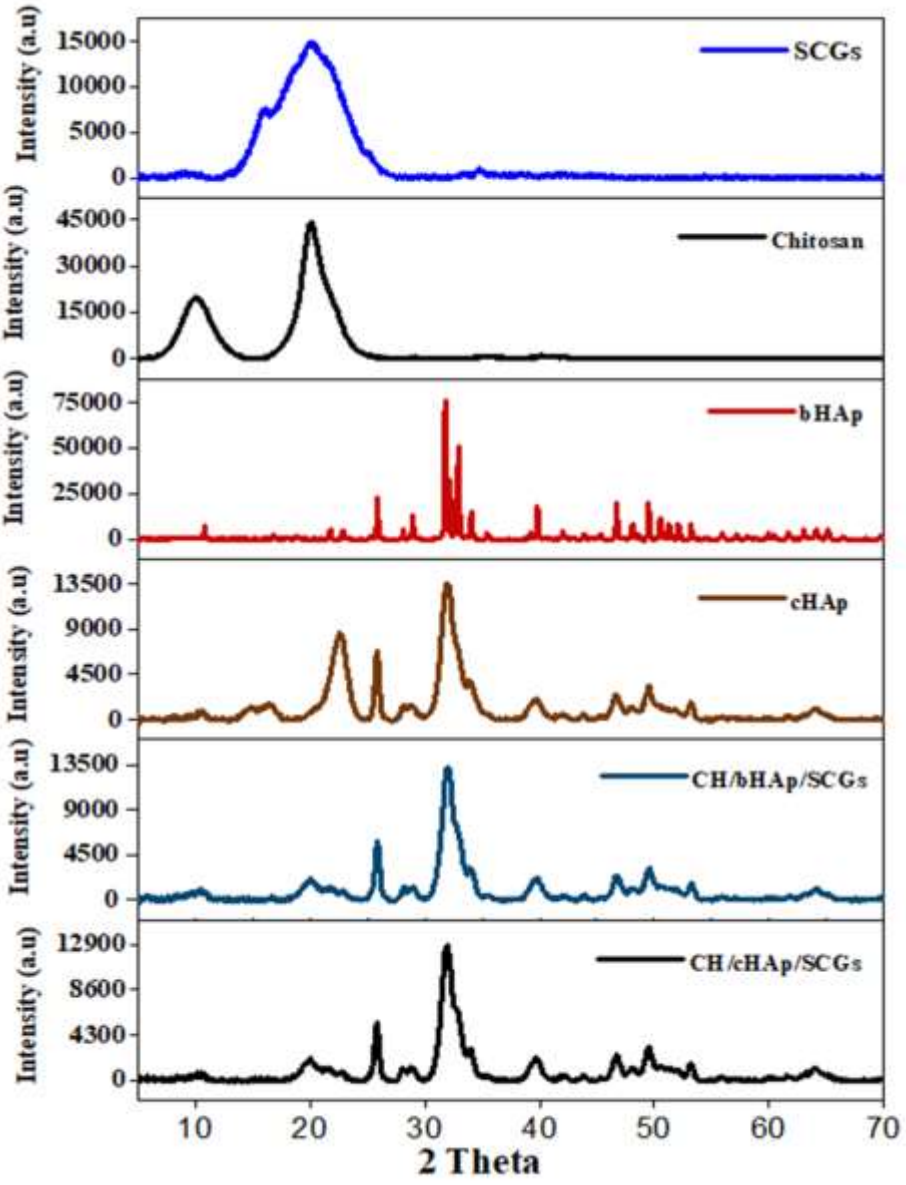

Figure 3-22: X-ray diffractograms of the CH/cHAp/SCGs and CH/bHAp/SCGs composites

3.4.3.4 Thermogravimetric analysis of CH/cHAp/SCGs and CH/bHAp/SCGs

The thermograms of the CH/cHAp/SCGs and CH/bHAp/SCGs composites are presented in Figure 3-23. Two weight-loss events were observed at approximately 100 °C and 300 °C and counted for about 13 % and 40% of the observed weight loss, respectively. No significant weight loss was observed after 550 °C.

The first weight loss is attributed (as seen in TGAs of other composites) to the dehydration of the composite material. The second weight loss is due to the oxidation and combustion of the carbonaceous components of the composite (i.e., chitosan and cellulose). Low weight losses were observed after 500°C and could be due to the decomposition of carbonates associated with the reprecipitated HAp. The HAp itself (both types) does not lose much mass in this region due to its thermal stability apart from carbonate decomposition. This is reflected in Chapter 2, when the individual HAp starting materials were characterised. The thermogram of CH/cHAp/SCGs composite is different from the thermograms recorded earlier for the cHAp-based composites. As the earlier cHAp-based composites showed a constant weight region starting from 550 °C or higher temperatures, the residual weight (in the pan) for the cHAp-based composites was always less than the bHAp-based composites of similar materials. The CH/cHAp/SCGs and CH/bHAp/SCGs show similar residual mass (47%). It could be due to an earlier mentioned reason (section 3.4.1.4) of more observed HAp incorporation in the bHAp-based composites than what occurred in the cHAp-based composites.

A white powder with a minute touch of greyish material was collected at the end of the TGA analysis (at 1000 °C), representing the composite's inorganic (HAp) part. Both composites show similar weight loss patterns in the TGA analysis and confirm XRD, SEM, and FTIR findings, which also show similar characteristics for both composites.

The comparisons of thermograms of the raw materials (chitosan (Figure 2-8), HAp (Figure 2-15) and SCGs (Figure 2-25) with the thermograms of the composites (given below) indicated that the chitosan decomposes completely under a temperature of 600 °C, while a major part of the SCGs also burnt off in a temperature range of 600-700 °C. The residual mass of the CH/HAp/SCGs could be attributed to the ash of the SCGs and HAp, constituting about 47% of the composite's mass. In this, the major part would be attributed to the HAp (at least >40%), keeping in view the thermogram of the HAp.

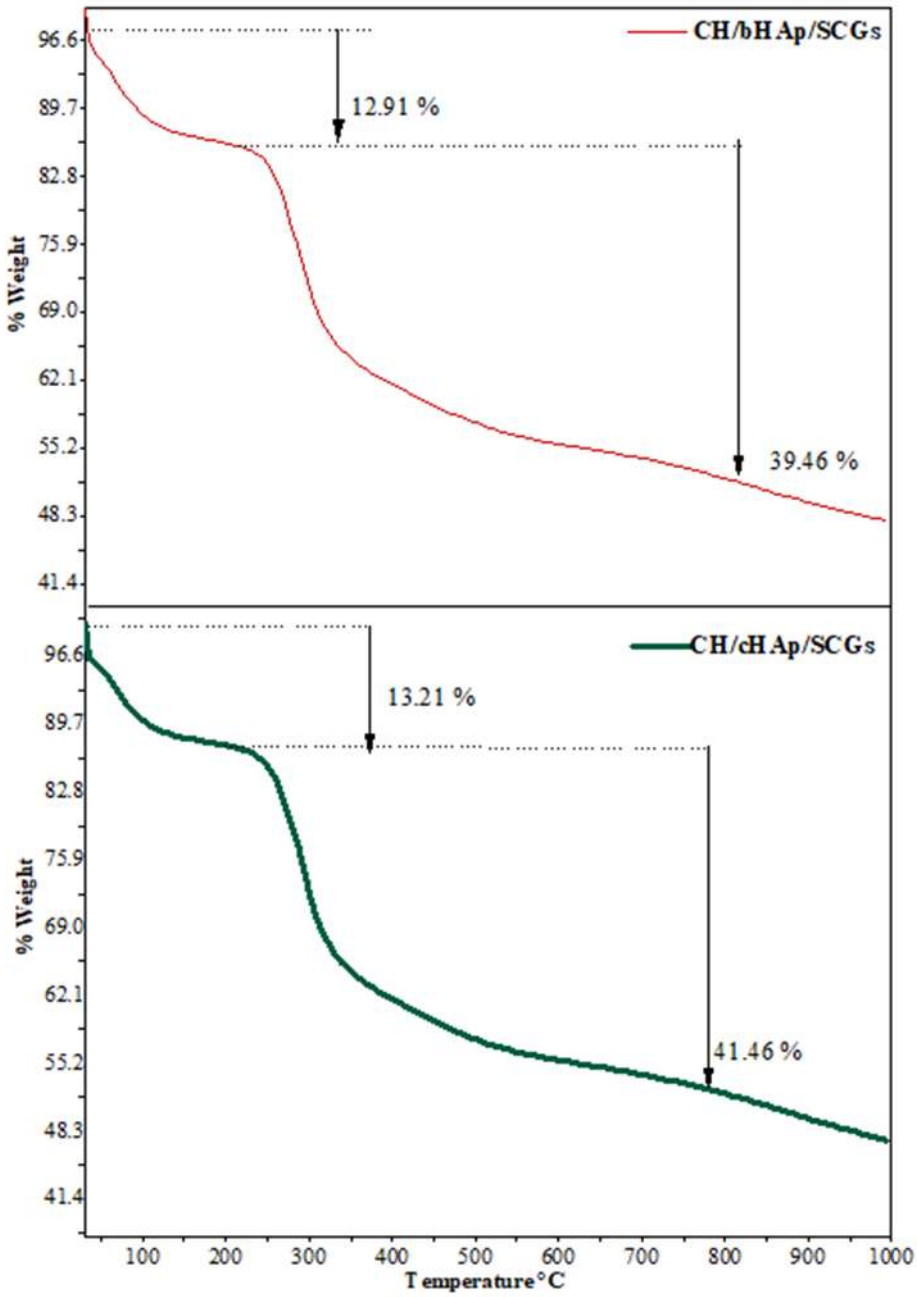

Figure 3-23: Thermograms of CH/cHAp/SCGs and CH/bHAp/SCGs

3.4.4 Characterization of the Chitosan/cHAp/Zeolite and Chitosan/bHAp/Zeolite Composites

3.4.4.1 SEM/EDX analysis of CH/cHAp/Zeolite and CH/bHAp/Zeolite composites

In SEM micrographs of the zeolite composites prepared for this study, i.e., Figure 3-24 & 3.25), similar surface morphology was observed for both composites. The typical

morphology shown was that of formation of large, homogenized particles having deposition of crystals on the surface. The surface deposition could be hydroxyapatite agglomerates covering the chitosan and zeolite composite, which aligns with the similar observations made in another study, where the HAp was reported to cover the surface where it was a part of a surfactant-modified hydroxyapatite/zeolite composite, which was synthesised as a copper removal agent[471].

In EDX microanalyses (Figure 3-24 & 3-25), prominent peaks of oxygen, carbon, calcium, aluminium, and silicon could be observed as expected. CH/bHAp/Zeolite is differentiated from CH/cHAp/Zeolite by the presence of the Mg (< 1%) peak, which arises from the biogenic source of the HAp. Some variation in elemental composition was observed between the two composites.

Oxygen was found to be the elemental component present by more than 35% by weight in both composites, followed by calcium from hydroxyapatite (16-17%), carbon from chitosan (14-15%), as well as Si (10-14%) and Al (1-2%) from the zeolite component of the composite. The minor elements such as K and Na emanate from the zeolite part of the composites.

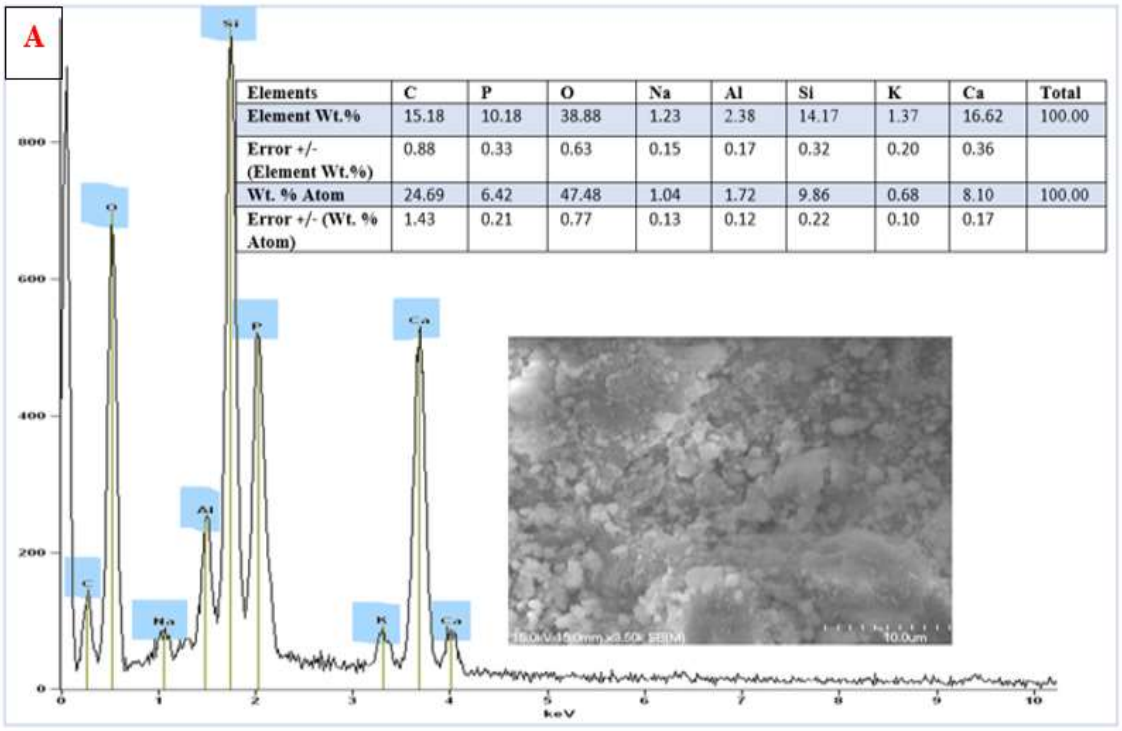

Elements	C	P	O	Na	Al	Si	K	Ca	Total
Element Wt.%	15.18	10.18	38.88	1.23	2.38	14.17	1.37	16.62	100.00
Error +/- (Element Wt.%)	0.88	0.33	0.63	0.15	0.17	0.32	0.20	0.36	
Wt. % Atom	24.69	6.42	47.48	1.04	1.72	9.86	0.68	8.10	100.00
Error +/- (Wt. % Atom)	1.43	0.21	0.77	0.13	0.12	0.22	0.10	0.17	

Figure 3-24: SEM micrograph and EDX analysis of the CH/cHAp/Zeolite composite

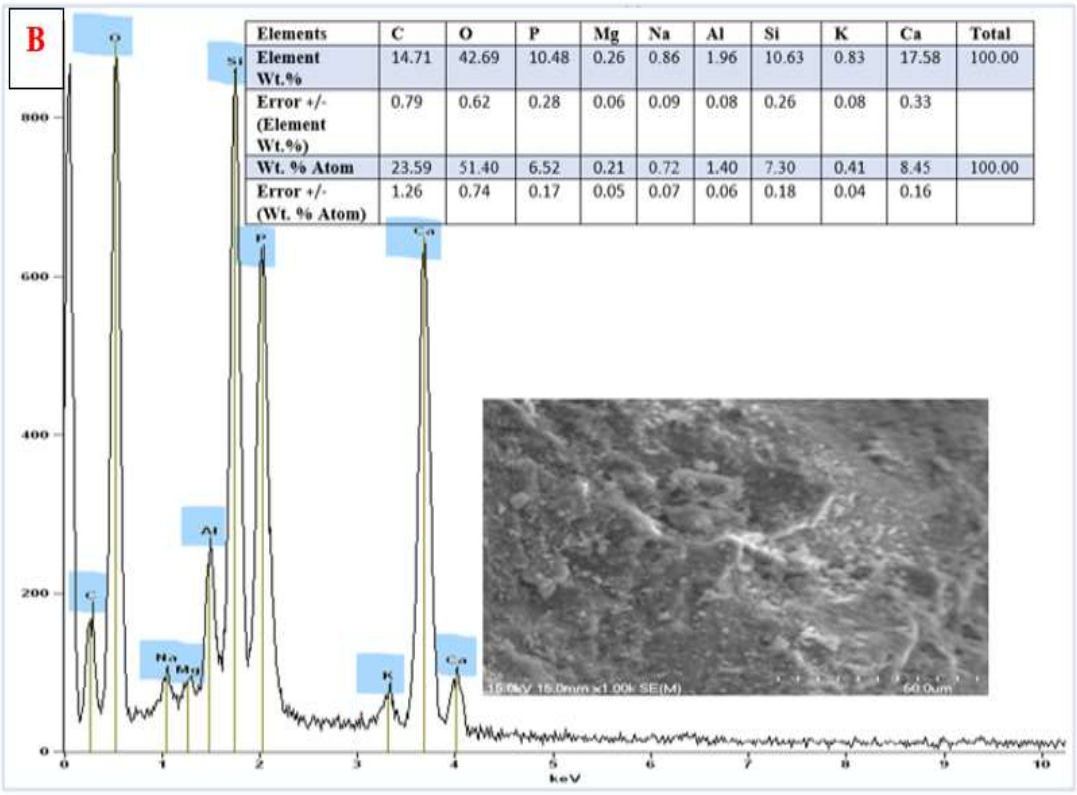

Figure 3-25: SEM micrograph and EDX analysis of the CH/bHAp/Zeolite composite

3.4.4.2 FTIR analysis of the Chitosan/cHAp/Zeolite and Chitosan/bHAp/Zeolite composites

Figure 3-26 shows the IR spectra of the CH/cHAp/Zeolite and CH/bHAp/Zeolite composites. All observed peaks in the spectra and assignments are summarised in Table 3-4.

Table 3-4: Characteristic IR absorption peaks of CH/cHAp/Zeolite and CH/bHAp/Zeolite composites

Assignments	**Wavenumber (cm^{-1})**
T-O-T bending	470
T-O-T stretching (overlapping PO_4^{-3})	1048
Si-O-Si stretching	792
CH stretching (chitosan)	2914
OH stretching	3440

*T refers to zeolite-associated IR vibrations

FTIR spectra of the zeolitic composites appear to be dominated by the spectra of the zeolite itself. It is evident that the characteristic peaks of PO_4^{3-} from hydroxyapatite are more challenging to find due to the overlapping of T-O-T framework peaks (*T= Si or Al) with those peaks due to the phosphate vibrations. The strong peak at around 1050

cm^{-1} corresponds to the asymmetric stretching vibration of T-O-T in mordenite. Similarly, biopolymeric peaks of chitosan are not visible in the spectra, while those related to CH stretching exhibited decreased intensity. The low-intensity peaks around 550-600 cm^{-1} are attributed to both mordenite and apatite. Both have characteristic peaks in this region because of the tetrahedral structural similarities of SiO_4^{4-} and PO_4^{3-} in the phosphate and silicate groups associated with the zeolite and hydroxyapatite[472]. A broad absorption peak in the region of 3300-3600 cm^{-1} was assigned to the characteristic OH stretching peak, which is merely due to adsorbed moisture on the composites.

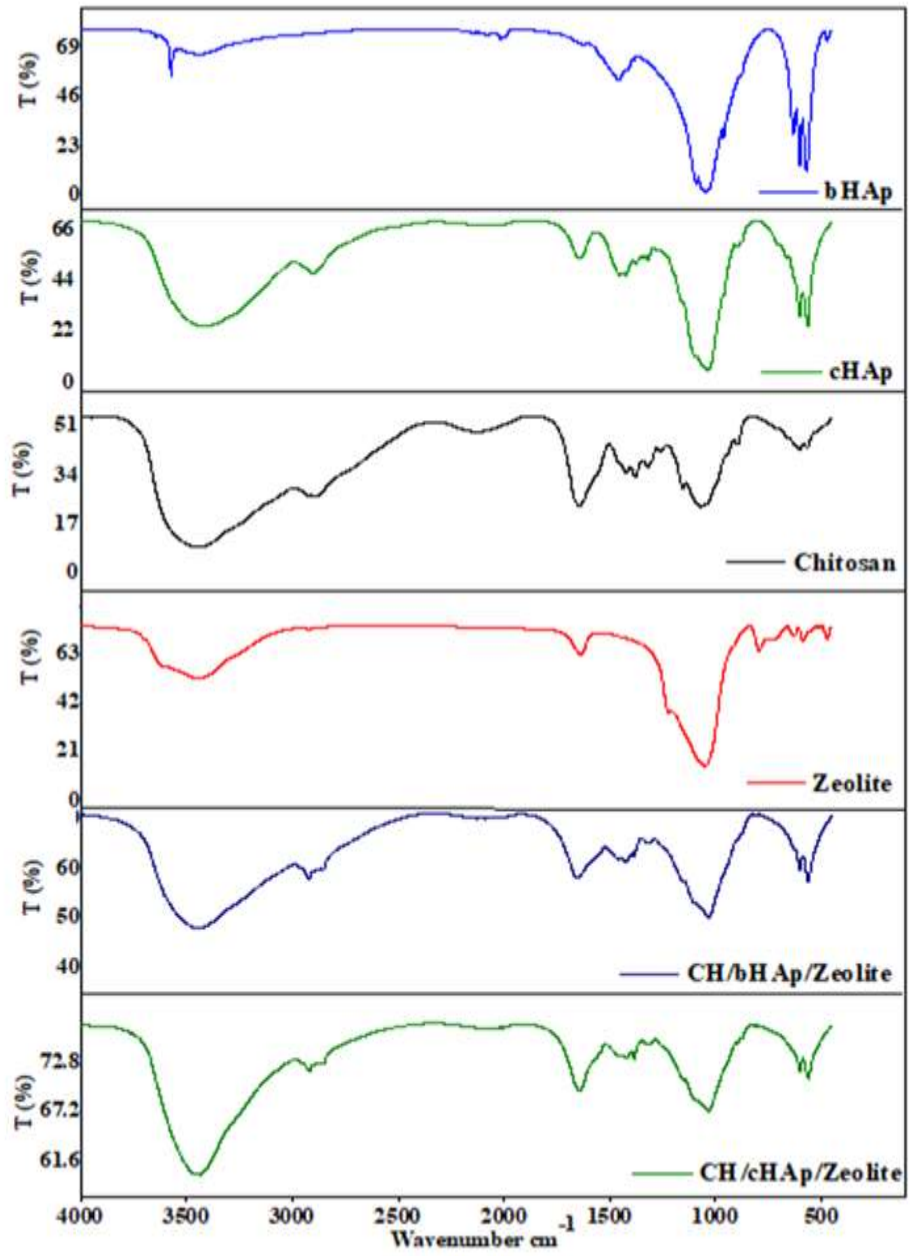

Figure 3-26: FTIR spectra of the CH/cHAp/zeolite and CH/bHAp/zeolite composites

3.4.4.3 Powder X-ray diffractogram analysis of the Chitosan/cHAp/Mordenite and Chitosan/bHAp/Mordenite composites

Figure 3-27 presents the powder X-ray diffractograms of the mordenite (zeolite)-based composites of chitosan/HAp. The diffraction patterns of mordenite and apatite were compared with the reference powder-diffraction pattern for HAp (ICDD = 00-009-0432) and mordenite (ICDD= 00-029-1257), as discussed in Chapter 3. The characteristic peaks of mordenite were recorded at 2θ = 9.75°, 22.2°, 25.5°, 26.2° and 27.6° and were in good agreement with the mordenite reference pattern.

As predicted from the FTIR spectra, the XRD pattern was more dominated by zeolite-associated features than with those coming from HAp. The most prominent XRD peaks of HAp at 2θ = 31.774, 32.197, 32.902 and 34.049 are hard to distinguish apart from one clear and broad peak at 31.8. [471]. Peaks at 2θ= 13° and 2θ = 23° confirm the presence of chitosan.

Iqbal et al.[473] reported that when the amount of zeolite powder is 10% or more in composite synthesis, it decreases the intensity of HAp peaks in the diffraction pattern of composite[473]. It probably implies that in the presence of a higher amount of zeolite, HAp crystallinity decreases, as shown by the weakness or non-observation of any XRD peaks due to HAp. Both composites produced showed similar crystallographic features so that these were unaffected by the source of the HAp.

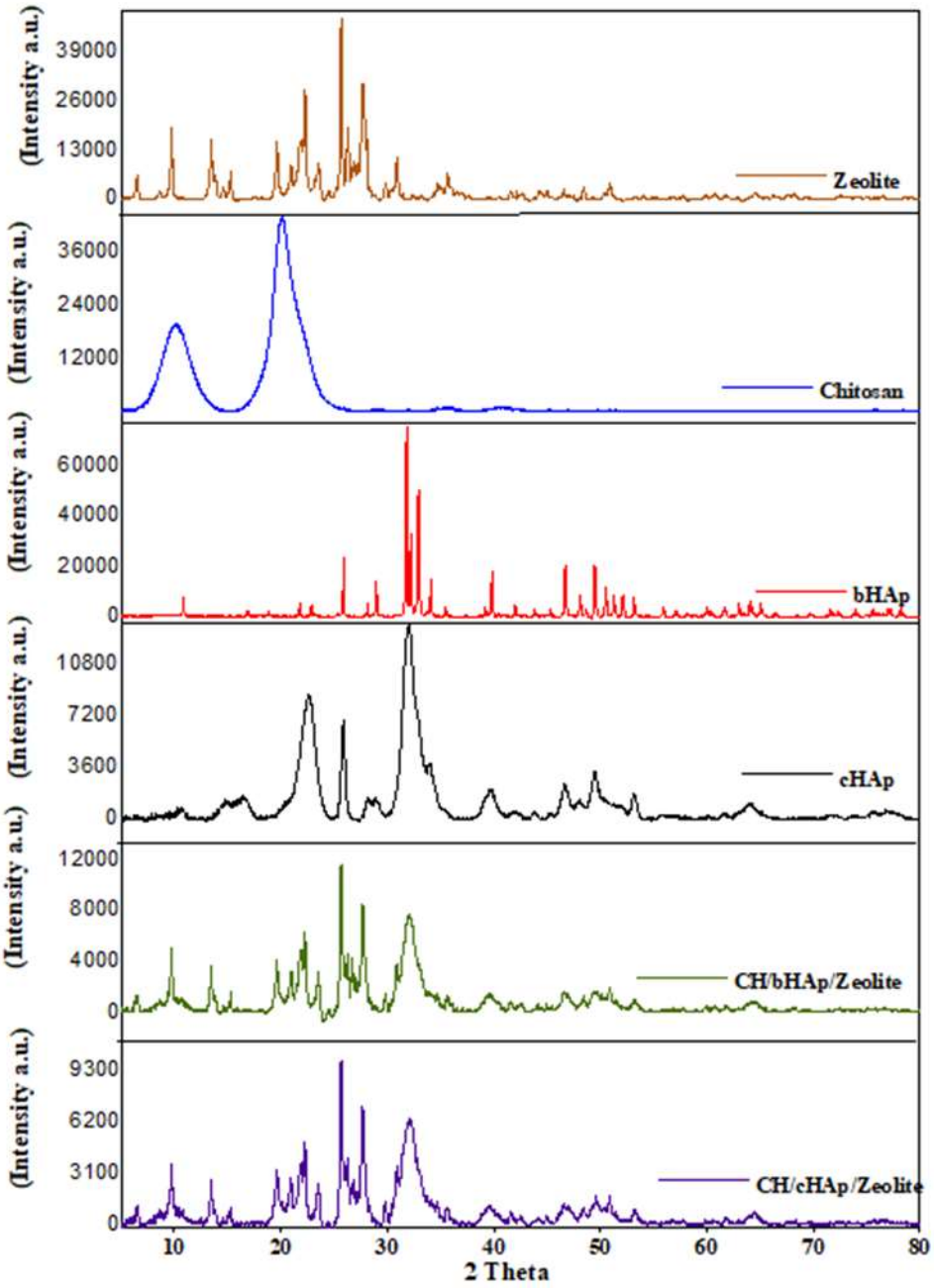

Figure 3-27: X-ray diffraction patterns of the CH/cHAp/Zeolite and CH/bHAp/Zeolite composites as well as those of the raw materials.

3.4.4.4 Thermogravimetric analysis of the Chitosan/cHAp/Zeolite and Chitosan/bHAp/Zeolite composites

The thermogravimetric analyses for both the CH/cHAp/Zeolite and CH/bHAp/Zeolite composites are shown in Figure 3-28. In both analyses, two weight-loss events were observed around 100 °C and another around 250 °C.

The weight loss temperatures were compared with thermograms of the component raw materials (i.e., chitosan, HAp and zeolite). As was typical, the first weight loss (about

10%) was attributed to the removal of moisture and dehydration of the powdered composite material. After 250 °C, decomposition of chitosan starts and structural dehydration of hydroxyapatite and mordenite zeolite occurs. About 32% and 28% weight loss was recorded for cHAp and bHAp based composites in this region, starting from 250 °C to 1000 °C, respectively. This confirms the thermal stability of bHAp more than cHAp, as we have already observed during their characterization.

After 500 °C, the cHAp-based composite did not show any weight loss, while a gradual weight loss was observed in bHAp based composite. It is already recorded that no weight loss occurs for raw cHAp (Figure 2-15, Chapter 2) and mordenite (Figure 2-31, Chapter 2) after 550 °C. While the bHAp continues to lose weight (although very little) up to high temperatures (1000 °C). The trends of weight loss are also visible in the respective composites of cHAp and bHAp. The residual material of these composites is made up of both zeolite and HAp.

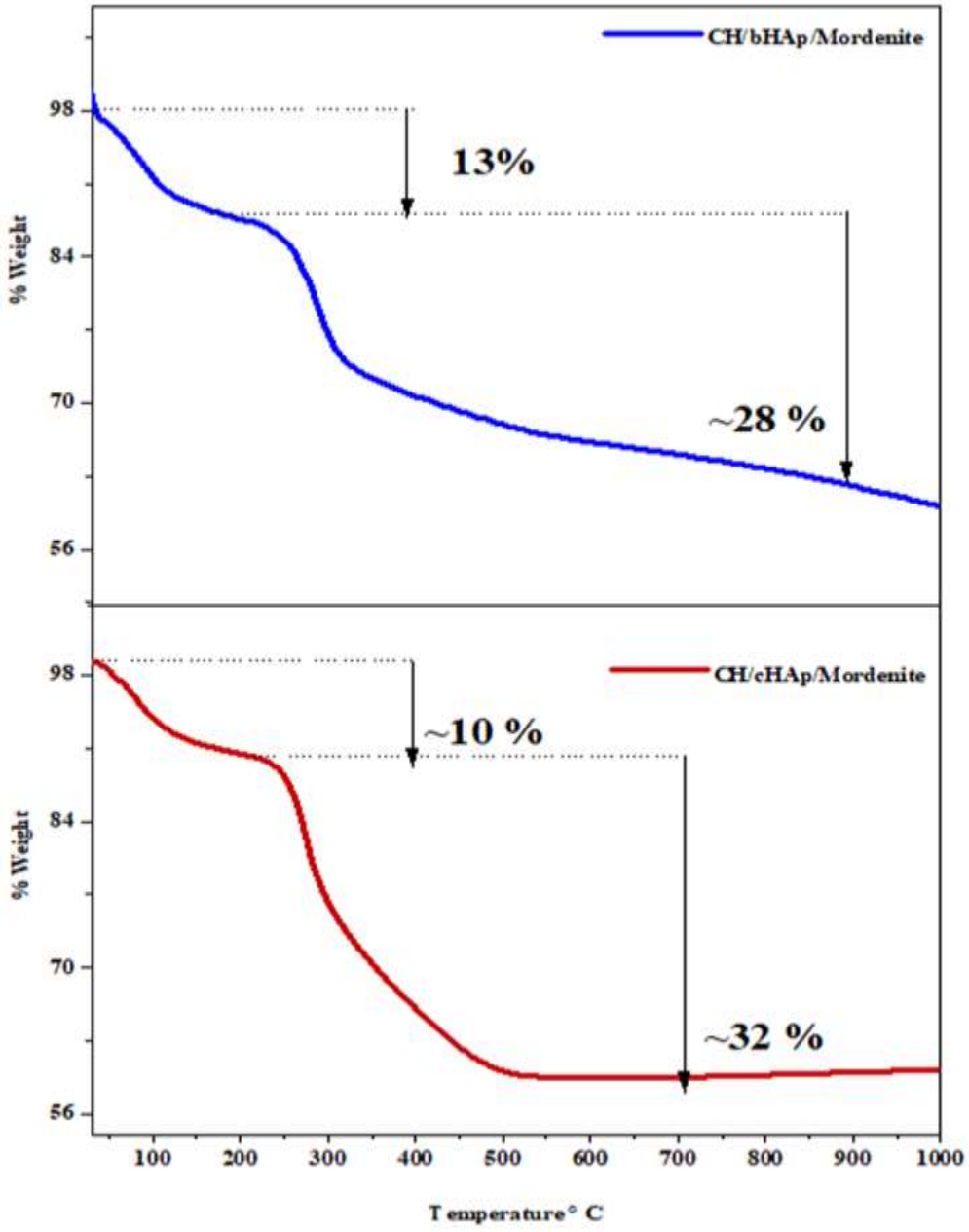

Figure 3-28: Thermograms of the CH/cHAp/Zeolite and CH/bHAp/Zeolite composites

3.5 Summary

The characterisation of the composite materials synthesised and discussed in this chapter is summarised as follows:

In SEM analysis of the CH/HAp (control) composites, CH/cHAp exhibited a homogenised surface. At the same time, the CH/bHAp was relatively heterogeneous, showing fine particles deposition at the surface attributed to the deposition of the nano-bHAp crystal or the composite matrix itself. Overall, both the composites exhibited

similar morphological characters as particles of irregular shapes. The EDX analysis showed that Ca, P, C and O were present. The bovine sourced HAp in CH/bHAp contained an additional feature in the form of a Mg peak in the micrograph. The FTIR spectra of the composites exhibited fewer peaks than the candidate materials (chitosan and HAp) after the formation of the composites, showing the poorly crystalline nature of the materials. Overall, both the composites showed similar morphological and spectroscopic characteristics, which were attributed to the re-precipitation of the materials during the synthesis of the composites, which could be a reason for similar HAp deposition in the composites. The differences between the two composite systems were recorded in the TGA analysis and XRD analysis. The XRD diffractogram of the CH/bHAp showed some additional peaks than CH/cHAp composites, attributed to the higher crystallinity of the bHAp.

Similarly, the residual mass for the CH/bHAp is higher than CH/cHAp. The white coloured powder residue was identified as HAp. It revealed the relatively less decomposition of HAp in the CH/cHAp composite, most likely due to its higher crystallinity of bHAp in the CH/bHAp composite or relatively higher mass deposition of bHAp than cHAp in their respective composites. Another possible reason could be the less deposition of cHAp in the CH/cHAp composites due to the lower purity in a stoichiometric sense of cHAp (as mentioned in section 3.4.1.4).

In the three-component composite systems, SEM analysis showed that the CH/HAp/CF and CH/HAp/SCGs composites exhibited highly amorphous and irregular surfaces. The deposition of finely powdered particles of coir fibre dust and spent coffee grounds were visible in their respective composites in SEM micrographs. The carbon content was high due to their constitutional components (coir fibre and SCGs along with chitosan), while the presence of the HAp was evident by the observation of Ca and P peaks. The Mg was present in the bHAp-based composites so, confirming its biogenic origins. Similarly, the FTIR and XRD analysis showed similar results for the cHAp and bHAp based composites. Like the control composites, the TGA analysis exhibited a higher weight loss (%) for cHAp-based composites (CH/cHAp/CF and CH/cHAp/SCGs) than the bHAp-based composites (CH/bHAp/CF and CH/bHAp/SCGs). It confirmed the higher thermal stability of the bHAp than cHAp in the composites. It may also be due to more HAp content per g when weighing out bHAp compared to cHAp due to the presence of carbonates in cHAp.

Chapter 4

Methods and Procedures for Studying the Removal of Heavy Metals via Novel Synthesised Composite Matrices

4.1 Introduction

This chapter is exclusively a methodology chapter, which only explains how the use of the novel synthesised composites in this study were studied in relation to their ability to remove heavy metal ions from the solution. As similar experimental parameters and experimental methods were used to analyse the composite systems, this chapter explains and summarises how the batch experiments used to remove metals were performed in three systems to evaluate the maximum adsorption capacity and removal efficiency of composite matrices. This chapter contained no experimental data and was included to avoid the repetition of mention of methods described in the next chapter (Chapter 5).

In the single metal ion type system, solutions containing only one metal ion were prepared. These solutions contained Cd, Pb, Cu, and Cr in either cationic (Cd^{2+}, Pb^{2+}, Cu^{2+}) form or in an anionic form (as chromate ion). Removal of these ions from the solution was studied for the composites produced. The two-metal ion type system used experimental parameters optimised through the studies of the single metal ion type systems and was tested with the composites using Cd^{2+} and Pb^{2+} co-dissolved in solution in cationic form. The third type of system is an "industrial input stream water" sample, which was taken from a real-life industrial input stream of a treatment chemical used to protect pine wood from decay or insect action. This input stream sample contained copper, arsenic (as arsenate ion) and chromium (as chromate ion). This sample represented a realistic environmental sample (i.e., containing more than one metal ion type) and tested the composites in terms of their removal abilities for such samples in a scenario, which was outside the model solutions prepared for this study.

4.2 Experimental

4.2.1 Batch experiments

As mentioned earlier in Chapter 1 (section 1.9), batch experiments are conducted to evaluate the effect of different experimental parameters on the removal efficiencies of the adsorbents.

In order to carry out the adsorption experiments for testing the ability of the individual composites to remove heavy metal ions from the solution, a series of batch experiments were executed by varying environmental conditions in each adsorbent system (i.e., the composite) when exposed to the selected metal ion solutions.

4.2.1.1 Heavy Metal salts

Analytical grade heavy metal salts were used to prepare the corresponding model solutions of metal ions that were exposed to the composites produced in this study to gauge heavy metal ion removal. Stock solutions of 1000 ppm concentration were prepared for each metal using the salts of metals with preparation details given in Table 4-1.

The following metal salts were used to prepare the respective stock solutions of metals:

Table 4-1: Metal ion salts used to prepare model solutions of metals

Reagent Name	Chemical Formula	Molar Mass (g mol^{-1})	Purity	Suppliers
Cadmium Chloride	$CdCl_2$. $2.5H_2O$	228.36	~ 99.5 %	BDH
Lead Nitrate	Pb $(NO_3)_2$	331.208	~99.0 %	MERCK
Cadmium Nitrate	Cd $(NO_3)_2$. 4 H_2O	308.47	~99.0 %	BDH
Copper Sulphate (Anhydrous)	$CuSO_4$	159.60	~ 98.0 %	AJAX Chemicals
Potassium Dichromate	$K_2Cr_2O_7$	294.185	~ 99.9 %	Merck

Working solutions used in adsorption experiments were prepared according to the requirement of each experiment by diluting the metal stock solutions. Concentrations and volumes of working solutions were calculated using $C_1V_1=C_2V_2$, where C_1 and V_1 represent the concentration and volume of the stock solution and C_2 and V_2 refer to the concentration and volume of the required solution.

4.2.1.2 Stock solutions preparations (1000 ppm)

The quantities of salts needed to prepare these are given in Appendix 2, Table 2-1. The concentrations and volumes prepared using these salts for conducting the metal removal experiments are also given in Appendix 2.

Given the hygroscopicity of some of the metal salts used to make the stock solutions, a minor error could be expected in making up the solutions. Some preventative measures were taken to minimize the errors in the concentration values, including:

- Storing the stock solutions in plastic containers instead of glass bottles to prevent any possible adsorption of metal ions that would occur if stored in glass vessels. This would have compromised the integrity of the concentrations.
- Preparing and using only freshly prepared solutions of required concentrations and required volumes at the times when experiments were actually conducted.
- Performing a 0.2% acidification of stock solutions using HNO_3. The acidification acts to prevent any unforeseen precipitation of the metal ion and also prevents surface deposition or adsorption on the walls of the containing vessels
- Measuring the initial metal ion concentrations in solutions before any adsorption experiments using an atomic absorption spectrometer to confirm the initial (nominal) concentrations as calculated in their preparation.

4.2.2 Types of metal ion removal experiments

Though the experimental set-up has been described earlier (section 1.8), the methodologies used to conduct the experiments with the synthesised composites in the present study are again described below to recap:

Single-metal ion type solution system – These experiments involved exposing the composites to solutions containing only one heavy metal ion type dissolved in solution and the adsorption behaviour (model of adsorption/kinetics) with the calculation of the removal efficiencies.

Two-metal ion type solution systems- These experiments involved exposure of the composites to solutions containing two types of heavy metal ion dissolved in solution and the adsorption behaviour (model of adsorption/kinetics) with the calculation of the removal efficiencies. This probed competitive binding.

Industrial input stream sample system

This system was an industrial input stream sample that was kindly provided by a company that subjected wood to the copper chrome arsenate (CCA) treatment. The solution effectively represented an environmental sample containing three co-dissolved heavy metal ion types. This was used to evaluate the utility of the synthesised composites to treat such solutions where competitive metal adsorption would likely be taking place.

Three replicates were used to conduct each batch experiment in order to assess reproducibility error. Two analytical instruments were employed to analyse the metal ion concentrations in solutions when the synthesised adsorbents were exposed to these solutions to study heavy metal ion removal. These analytical instruments included the atomic absorption spectrometer (AAS) and inductively coupled plasma mass spectrometer (ICPMS). AAS was used to analyse the metal ion concentration in single-metal ion type, and two metal ion type solutions. The ICPMS was used specifically to analyse the industrial input stream sample. The details of analysis using these instruments and the associated limitation of analysis of these instruments are discussed in the following section.

4.2.3 Atomic Absorption Spectrometry

Atomic Absorption Spectroscopy (AAS) is a technique used for qualitative and quantitative analysis of chemical samples by measuring the absorbed radiation by a specific elemental species of interest. Every atom has its own distinct absorption energy wavelength, which enables quantitative analysis of samples. Each element has several energy levels that give very narrow absorption lines in an atomic state. The principle by which AAS works is that the atoms (or ions) of an element can absorb light of a specific, unique wavelength. When the sample containing a specific element is exposed to a light source at the characteristic wavelength of that element, it absorbs the light. The concentration of the element in the sample is directly proportional to the amount of light absorbed by the atoms of that element. In AAS, when the sample is introduced to the flame, it atomises the atoms. The free atoms are exposed to the light (produced from a specific light source). The electronic transition from the ground state to the excited state occurs when atoms absorb light of their characteristic wavelength.

Quantitative analysis is achieved by obtaining a calibration curve via the analysis of standard solutions of known concentration for the elements of interest. These are prepared

from a stock solution. The AAS uses Beer's Law which states that absorbance is directly proportional to the concentration of the element. After preparing the calibration curves (given in appendices) for each element being tested, the curves were used to measure the actual test sample concentrations.

A weakness of AAS is that it is sensitive to the matrix of the sample. For instance, Ca^{2+} cannot be analysed in the presence of phosphate ions due to complex formation (insoluble solids), leading to calcium-associated signals being reduced[474]. The matrix must be modified by adding various complexing agents (e.g., ethylene diamine tetra-acetic acid, EDTA) to prevent compound formation, such as between calcium ions and phosphate ions. Fortunately, matrix effects are well known for the heavy metal ions of interest, so this was researched in advance and certain mixes avoided. For instance, similar salts of Pb and Cd (nitrates) were used in a two-metal ion type system.

Experimental: For metals of interest (Pb, Cd, Cu, Cr), no significant interferences were observed. Standard solutions of at least three known concentrations were prepared for preparing a calibration curve. The solutions were then analysed by a Flame atomic absorption spectrometer (GBC-Model: AVANTA G (Graphite furnace). Standard instrumental settings used in this for each metal analysis are given in Table 4-2.

Table 4-2: Instrumental settings to analyse metal ion solutions

Instrument settings table for metal analysis						
Metal	**Sensitivity**	**Flame type**	**Principal line**	**Lamp Current**	**Flame interferences**	**Correction**
Chromium (Cr)	0.05	Air/Acetylene (Fuel rich)	357.9 nm	12 mA	Transition elements could affect the response in fuel-rich flame	Use lean flame
Cadmium (Cd)	0.01	Air/Acetylene (Lean)	228.8 nm	6 mA	Silicates could affect the response	No interference
Copper (Cu)	0.035	Air/Acetylene (Lean)	324.8 nm	5 mA	Transition elements in the presence of mineral acids	No major interferences were observed
Lead (Pb)	0.1-0.2	Air/Acetylene (Lean)	217.0 or 283.3 nm	8 mA	No major interferences	283.3 nm line is used for a better signal to noise ratio

4.2.4 Inductively Coupled Plasma Mass-Spectrometry (ICP-MS)

The heavy metals of interest in industrial input stream samples, such as arsenic, were not amenable to the AAS technique due to a lack of lamps, or the technique could not be used for that element. In such a case, an alternative elemental analysis technique was employed, namely Inductively Coupled Plasma Mass-Spectrometry (ICP-MS). This technique is used to analyse and determine elements in different samples by combining an Inductively Coupled Plasma (a state of Argon at very high temperatures) with a mass spectrometer. The sample is typically converted into an aerosol for introduction into the ICP plasma by aspirating the sample through a nebulizer, or (in the case of ablation studies) a laser may be used to convert an initially solid sample directly into an aerosol. These aerosols are then converted into a gaseous state, followed by ionization (atoms convert to ionic form). After this, these ions are brought into the mass spectrometer to analyse where they are detected by separating them according to their mass-to-charge ratio. Arsenic is able to be analysed by using this technique as the correct lamps were not possessed to analyse this element by AAS.

ICP-MS has superior detection capability and offers many advantages over other analytical techniques such as atomic absorption spectroscopy (AAS), ICP-Atomic Emission Spectroscopy (ICP-AES), and Optical emission spectroscopy. Some of these advantages include

- Better detection limits for the various elements
- Minimum matrix interferences (though other “mass” interferences due to Ar gas combinations may occur, which can confound mass spectral analysis because their masses coincide with that mass of species being analysed)
- Superior detection abilities
- Provision of isotopic information which can be modelled and hence predicted for direct comparison and confirmation (however, only one isotope of each metal was selected (with the least number of mass spectral interferences), and the concentrations measured were employed to assess the metal ion removal efficiencies of the synthesised composites
- Capability to do multi-element determination compared to AAS, which is restricted to measurements of one element concentration at a time in samples.

A prime disadvantage of the technique (aside from the mass spectral interferences) is cost because the Argon gas used to create the plasma is relatively expensive.

4.2.5 Parameters for studying the removal of metal ions from single metal ion systems by the composites generated in this study

4.2.5.1 Initial metal ion concentration

Initial metal ion concentration is an important factor as it provides the initial driving force for an instantaneous adsorption process. When more metal ions are present in the solution, the more they tend to adsorb on the available binding sites of the adsorbent. However, after the equilibrium adsorption time or after the saturation of the active/binding sites (at adsorption equilibrium), a further increase in the initial metal ions does not affect the adsorption ability of the adsorbents.

Experimental: The initial concentrations of heavy metal ions exposed to the composite samples were calculated by the method as described by Mohammad et al.[192]. Initially, 0.1 g of adsorbent (composite sample) dose was added to aqueous solutions of the heavy metal ions of different concentrations (e.g., 5 to 50 ppm) at an optimum pH (initial pH of metal ion solution 4-6, see below) and time (minimum 2 h). The usual experimental procedure involved shaking of the composite with the metal ion solutions to effect adsorption, filtration of composite from the solution and analysis of the residual concentration of metal ions in the filtrate solution. The optimum initial metal concentration was selected by repeating the batch experiments using varying concentrations of metal ions. The optimized initial metal concentrations used to evaluate metal ion removal efficiency for the composites are summarised in Table 4-3.

Table 4-3: Initial metal ion concentrations used in batch experiments

Metals (in cationic or anionic form)	Initial Metal ion concentration (ppm)	Adsorbent dose (g)	Time (minutes)	Solution volume (mL)
Cadmium (Cd)	5, 10, 15, 20, 25			
Lead (Pb)	10, 20, 30, 40,50			
Copper (Cu)	5,10,15, 20, 25	0.01	120-180	20
Chromium (Cr)	10,20,30,40,50			

Trend recorded in the literature for the effect of initial metal ion concentration on adsorption capacity of adsorbents:

Generally, an increase in initial metal ion concentration was found to increase the adsorption ability of the adsorbents. The studies on heavy metal ion adsorption reported an increase in the adsorption capacity of the adsorbents with an increase in the initial metal ion concentration in solution, and the increase in adsorption was attributed to the availability of more metal ions to adsorb on available binding sites (or per unit mass of the adsorbent). In contrast, a lower concentration of metal ions causes a barrier in the mass transfer of metal ions between the liquid and solid phase surface by limiting ion diffusion. Contrary to this, higher concentrations of metal ions in the solution obviously help to overcome these limitations by providing a driving force for more metal ion adsorption by increasing the diffusion process[475,476].

4.2.5.2 Adsorbent Dose

Adsorption efficiency is affected by the number of available active sites or surface area of the adsorbent, especially for an adsorption-based mechanism, as it is a surface phenomenon[477].

Experimental: The effect of adsorbent dose on metal ion removal efficiency was evaluated for various adsorbent doses ranging from 0.01 to 0.05 g by keeping other parameters, e.g., metal ion concentration, contact time, and the volume of the metal ion solution exposed and pH constant. The procedure of shaking (solution exposed to adsorbent dose), centrifugation (at equilibrium time) and filtration were consistently followed prior to the analysis of metal ions using the atomic absorption spectrometer (AAS).

Trend recorded in the literature for the effect of adsorbent dose on adsorption capacity of adsorbents:

The literature studies reported that an increase in the dose of adsorbent exposed to the metal ion solutions (at a given constant concentration) was found to improve the removal efficiencies of the adsorbent. This can be obviously attributed to the availability of more binding/active sites for the adsorption of metal ions from the solution. In contrast, the adsorption capacity was always found to decrease with an increase in the adsorbent dose

as the adsorbent has an inverse relation with the quantity of adsorbate adsorbed, which is calculated as milligrams of adsorbate *per gram* of adsorbent.

4.2.5.3 Initial pH of the metal ion solution

The pH of the solution can be a critical factor in terms of its influence on the removal efficiency of heavy metals by a specific adsorbent. The pH value plays a vital role in the removal mechanism by changing the charge on the surface of the adsorbent. For instance, the protonation of the functional groups in acidic conditions pH <5.0 could affect the adsorption abilities of the adsorbent. The active sites are occupied by the protons in acidic conditions (at low pH) and can reduce the adsorption of the targeted metal cations. Alternatively, relatively less acidic conditions such as pH > 4.5-5.0 may favour the adsorption of the metal cations as a result of deprotonation of the binding sites as the proton concentration.

pH may also alter the solubility of the metal ion in the solution. Under some conditions, the metal ions targeted for removal from a solution may do so predominantly via a precipitation mechanism due to the formation of insoluble hydroxide salts due to the higher pH; hence, it is essential to be conscious of this phenomenon to account for it when studying metal adsorption on substrates. Thus, the pH range for different metals was selected and adjusted, keeping in mind the relative solubilities of the metal salts studied. For instance, a milky solution was observed for the solution containing Pb^{2+} ions at pH >5.5, which could be attributed to the formation of $Pb(OH)_2$, as reported in other studies[478]. Similarly, for copper ion removal, any solutions with pH above 6.0 were not studied in batch experiments involving composites due to their precipitation as a copper hydroxide salt above that pH value[479].

Experimental: A range of pH values from 4 to 8 for the cadmium and chromium-based solutions were used, while for copper and lead-based solutions, a pH range of between 4 and 5.5 was used. A constant amount of adsorbent (e.g., 0.01 g/20 mL of solution or 0.05 g/20 mL) for a constant initial concentration of metal ions (e.g., 50 ppm of Pb^{2+}) and a specific time of contact (2 h) were used for a range of pH values to evaluate the metal removal efficiency adsorbents. The pH was adjusted by using (0.1 M HCl or NaOH).

The suspensions were shaken, centrifuged and filtered after appropriate exposure times and then analysed to assess for metal ion removal efficiency by AAS. The optimal pH at

which removal efficiency is maximised was recorded for each composite material system tested.

4.2.5.4 Contact Time

It is evident from the literature that the contact time of adsorbent with adsorbate is also an important parameter influencing removal efficiency but, more importantly, from the point of view of knowing when equilibrium will be established in terms of surface adsorption/ion exchange. In the initial stages, due to the availability of a larger number of available active sites, the removal rate is high but slows down over time as the surface attains a monolayer[291], as the active sites become occupied through adsorption of heavy metal ions on the sites.

Experimental: The experiment was performed to test for the influence of contact time between the time ranges of 1 to 120 minutes by keeping other conditions (such as initial metal ion concentrations, pH, and adsorbent dose) constant. To give a degree of control and to allow for comparison, a constant amount of adsorbent was added to the metal ion solution (at a pre-decided initial concentration and optimum pH value for the solution). When the composite was mixed with the heavy metal ion solution in such experiments, it was kept under continuous magnetic stirring, followed by removal of the composite from the solution by filtration using 0.45 µm syringe filters and analysis by AAS at regular time intervals. For the first 5 minutes of exposure of the composite to the solution, readings of metal concentration in the stirred sample were taken every 1 minute; after that, readings were taken every 5 minutes up to 15 minutes total exposure time and, then after 15 minutes, solution measurements were taken every 30 and 60 and 120 minutes. The data recorded in the kinetics experiments were employed in kinetic modelling to explore the kinetic behaviour and adsorption mechanism by kinetic models mentioned in Chapter 1 (section 1.11).

Once an equilibrium time was established from the contact time experiments, the decision was made to use this determined exposure time in later soaking experiments where the desire was to determine adsorption capacities (adsorption modelling experiments).

4.2.6 Parameters studied for the two-metal ion type system

A two-metal ion type system was designed by using optimized parameters developed as a result of carrying out the single metal ion system experiments. In investigating these systems, only solutions containing Pb^{2+} and Cd^{2+} ions were studied due to limiting factors developing during this research, such as shortage of time due to the 2020 COVID-19 lockdown in New Zealand), instrument breakdown (centrifuge and AAS) and the cost factor due to the need to use an alternative, more expensive analysis technique such as ICP-MS.

Experimental: The desired combinations of Pb^{2+} and Cd^{2+} in equimolar concentration solutions were prepared. Two adsorbent doses, i.e. 0.01 g and 0.05 g, were used, taking them as a minimum and maximum quantity of adsorbent. After adding the composites, the samples were collected at different time intervals, allowing a maximum time of 180 minutes to attain equilibrium.

Single metal ion type and two-metal ion type systems helped to evaluate the optimum experimental parameters to remove heavy metals ions from water. However, the industrial input stream samples were a three-metal-ion-type system with high concentrations.

Experimental: An industrial input stream solution containing high concentrations of Cu^{2+}, Cr (as chromate ion) and As (as arsenate ion) was provided on request from a wood treatment industry. Initial characterization of this input stream solution was done prior to its use (as a diluted solution) in adsorption experiments.

The water pH was adjusted between 4-5 using 0.1 M NaOH. The dilution was done to make working solutions of the industrial input stream solution using Type I water.

4.2.7 Data Analysis

All experimental data were analysed using different equations to calculate the adsorption capacities and removal efficiencies. The removal efficiency (%) was calculated by using the following equation:

Equation 4-1:

$$\textbf{Removal} = \frac{C_o - C_e}{C_i} \times 100\%$$

In the above equation, Co and C_e are the initial and equilibrium concentrations of metal ions in solution (mg L^{-1}), which are analysed using an Atomic Absorption Spectrometer (AAS).

The quantity of adsorbate that is adsorbed by the adsorbent for a concentration and volume of solution is calculated experimentally using equation 4.2

Equation 4-2

$$q_e = \frac{(C_0 - C_e)V}{m}$$

In the above equation, C_o and C_e are adsorbate initial and equilibrium concentrations in the liquid phase (mg L^{-1}). V is the volume of the solution in L and m representing the mass of adsorbent added (g), while q_e is the equilibrium quantity of sorbate in the solid phase (mg $g^{-1)}$.

4.2.8 Statistical Analysis

It has been already mentioned that the experimentation involving soaking of composites in metal ion solutions to gauge removal efficiencies was done in triplicate to ascertain reproducibility error. For each optimised soaking experiment (from which AAS or ICP-MS data had been obtained), the standard error (SE) for recorded data was carried out by using the following formula in Microsoft Excel:

$$SE = \frac{\sigma}{\sqrt{n}}$$

Where "σ" is the standard deviation and "n" is the number of measurements/replications.

4.2.9 Non-Linear Regression Method

A method to overcome the limitations of the linear regression for the adsorption modelling (mentioned in section 1.7), is to use non-linearised regression functions by employing the true sorption modelling equations to fit the data to a model. It requires an assessment of the error analysis using the error functions (or non-linear regression functions) to optimise procedure[584].

Different non-linear regression functions have been used to determine the best-fit model in earlier literature by calculating the coefficient of determination (R^2) for non-linear regression functions[338,585]. Among them, a few that have been used in this study for adsorption and kinetic modelling of experimental data[336] are given in appendix 1.3 A.

Chapter 5

Results and Discussion: Metal Removal Experiments using Composite Matrices

After the detailed discussion of the characterisation of synthesised composites and confirmation of the successful incorporation of candidate components into the composite adsorbents, the next step was to employ the synthesised adsorbents into the metal removal systems. In the previous chapter (4), the experimental parameters studied to evaluate the removal efficiency of the composite adsorbents and methods employed to conduct the experiments were summarised. This chapter includes the results obtained in metal removal experiments using the composite matrices (the preparation of which was discussed in detail in chapter 3). The objective of this chapter is the evaluation of the removal efficiency of synthesised composites for the adsorption of metal ions in different removal systems. A comparison between cHAp-based components and bHAp-based composites was also studied to find out the better composite system between the two hydroxyapatites. Additionally, a comparison between two-component composite systems (regarded as a control) and three-component composite systems was also drawn to evaluate how the addition of a third component affected the removal ability of the control composites.

To recap, this study considered four novel composite systems, which were tested for their ability to remove heavy metals from model solutions and a real-life "environmental/industrial-style" sample. These composite systems were as follows:

- Chitosan/Hydroxyapatite (CH/cHAp and CH/bHAp)
- Chitosan/Hydroxyapatite/Coir Fibre (CH/cHAp/CF and CH/bHAp/CF)
- Chitosan/Hydroxyapatite/SCGs (CH/cHAp/SCGs and CH/bHAp/SCGs)
- Chitosan/Hydroxyapatite/Zeolite (CH/cHAp/Zeolite and CH/bHAp/Zeolite)

Chitosan/hydroxyapatite (CH/HAp) composites were considered as a "control" as these were composed of two components only (viz., chitosan and HAp), to compare the removal efficiencies of the other three systems studied, which were made up of an

additional third component *in addition to the chitosan and HAp*. This served to ascertain whether the addition of the third component (e.g., coir fibre, zeolite and spent coffee grounds (SCGs)) to the chitosan/hydroxyapatite "base composite" was increasing, decreasing, or having zero or a marginal effect on their removal efficiency toward heavy metal ions from aqueous solution.

Each composite system (in all, four studied) was made up of two different types of hydroxyapatite source (called “commercial” or “bovine”), which allowed comparison of "synthetically" derived or bovine-derived hydroxyapatite. In essence, given the characterisation results of Chapters 2 (i.e., the raw materials used in this study) and Chapter 3 (the synthesised composite systems), these experiments were effectively comparing "crystalline HAp" (the bovine-derived HAp) to "lower crystallinity/more carbonated HAp" (the “commercial” HAp).

All the synthesised composites (mentioned above) were investigated in three different sampling scenarios (mentioned in chapter 4, section 4.2.2) to test the heavy metal ion removal efficiency of the composite materials. These sampling scenarios related to how many metal ion types existed in the solutions to be treated. These are discussed in detail with respect to each composite system synthesised and studied.

5.1 Single-metal ion type solution system for the synthesised composites (commercial & bovine-derived)

5.1.1 Experiments involving the removal of metal ions by the CH/HAp composites (commercial & bovine-derived) from the single-metal ion type system

As mentioned earlier, this is the two-component composite system against which comparisons of the three-component composite matrices were made in this study.

Chapter 3 detailed the spectroscopic and microscopic characterization of the chitosan/hydroxyapatite (CH/HAp) composite system (section 0). In this section of Chapter 5, the CH/HAp composite system was tested for its heavy metal ion removal ability in the single-metal ion type solution systems, following the general experimental methodologies described in chapter 4. The specific methods used in each batch experiment are, however, described in their respective sections below.

The following describes the results of using this composite system to remove Cd^{2+}, Pb^{2+}, Cu^{2+} and Cr (as chromate ions) from various model solutions and their adsorption and kinetic modelling to understand better the adsorption mechanisms undergone by each metal ion and the kinetics of the adsorption process on the composite system. Given that the CH/HAp composite systems functioned as a reference system for the three-component systems, three-component composites studied (see later sections of thesis), comparisons of the adsorption behaviour and kinetics will be made with the data collected and conclusions drawn for these two-component composite systems.

The following sections discuss "the effects of the experimental parameters" on the removal efficiency of the CH/HAp composites for the removal of metal ions using the solution containing only one type of metal ions dissolved. It also includes the adsorption and kinetic modelling of the composites to understand better the removal mechanism involved in the metal ions removal and estimate the maximum adsorption capacity of the CH/HAp composites for the metal ion adsorption (in mg g^{-1}).

5.1.1.1 Effect of adsorbent dose on metal ions removal by the CH/HAp composites

Experimental: The effect of adsorbent doses on Cd^{2+}, Pb^{2+}, Cu^{2+} and Cr as chromate ions removal was measured by varying the adsorbent dose between 0.01g to 0.05 g for an initial metal ion concentration of 25 ppm for Cd^{2+} and Cu^{2+} adsorption and 50 ppm for the Pb^{2+} and Cr (as chromate ions) removal. The experiments were conducted without any pH adjustment at an initial metal ion solution pH of 4.0-6.0. The removal (%) and adsorption capacity (mg g^{-1}) of the CH/HAp composites were calculated using equations 4-1 and 4-2, respectively, in Chapter 4. No precipitation of the metal ions was noted in the solution at this pH.

Results: Table 5-1 (and *Figures 4-1 to 4-4, Appendix 4*) presents the metal ion adsorption capacity (mg g^{-1}) and removal efficiency (%) as measured by Atomic Absorption Spectroscopy (AAS) and calculated using equations 4-1 and 4-2 for the CH/HAp composite system with different adsorbent doses ranging between 0.01g to 0.05 g.

Table 5-1: The effect of the adsorbent dose on the removal efficiency (%) and adsorption capacity (mg g^{-1}) of the CH/HAp composites for the adsorption of the metal ions in the single-metal ion type solution systems

The effect of the adsorbent dose on removal (%) of metal ions using the CH/HAp composites						
	Dose	**0.01**	**0.02**	**0.03**	**0.04**	**0.05**
CH/cHAp	Cd^{2+}	31.78	49.50	60.25	67.37	72.40
	Pb^{2+}	49.57	85.38	94.88	96.12	96.59
	Cu^{2+}	26.84	48.59	61.45	70.44	80.25
	Cr (as chromate ions)	21.00	24.11	26.07	27.53	29.10
CH/bHAp	Cd^{2+}	39.45	69.03	87.28	95.22	97.89
	Pb^{2+}	87.99	99.75	99.83	99.89	99.95
	Cu^{2+}	34.68	66.89	83.24	86.06	87.93
	Cr (as chromate ions)	17.00	18.95	20.50	21.85	23.28
The effect of the adsorbent dose on the adsorption capacity (q_e in mg g^{-1}) of the CH/HAp composites with respect to the metal ions adsorbed						
CH/cHAp	Cd^{2+}	15.89	12.37	10.04	8.42	7.24
	Pb^{2+}	49.57	42.69	31.63	24.03	19.32
	Cu^{2+}	13.42	12.15	10.24	8.80	8.03
	Cr (as chromate ions)	21.00	12.05	8.69	6.88	5.82
CH/bHAp	Cd^{2+}	19.72	17.26	14.55	11.90	9.79
	Pb^{2+}	87.99	49.88	33.28	24.97	19.99
	Cu^{2+}	17.34	16.72	13.87	10.76	8.79
	Cr (as chromate ions)	17.00	9.47	6.83	5.46	4.66

As Table 5-1 shows, a gradual increase in removal efficiency and a gradual decrease in adsorption capacity (mg g^{-1}) of both the composites were observed with an increase in the adsorbent dose for all the metal ions studied. The CH/bHAp composite showed a higher removal of metal ions studied at equilibrium than the CH/cHAp composites.

The CH/bHAp showed >95% removal of Cd^{2+} ions at equilibrium (after 2 h) for 0.05 g of adsorbent, while the CH/cHAp composite achieved approximately 72% removal under the same conditions. Similarly, the % removal of Pb^{2+} was 96% and 99% for a 0.05 g adsorbent dose of CH/cHAp and CH/bHAp, respectively. The Pb^{2+} removal (%) is higher for CH/bHAp (99.75%) than CH/cHAp (85.37%) at lower adsorbent doses (0.01-0.02 g). The removal efficiency of Pb^{2+} plateaued for doses $\geq$ 0.03 g for both the composites. Hence, 0.03 g was found to be the optimum dose for realising the maximum removal (%), i.e., 96.58% and 99.95% for CH/cHAp and CH/bHAp, respectively. The removal% values for Cu^{2+} ions agree with the observations made for the Cd^{2+} and Pb^{2+} adsorption on the CH/HAp composites, which indicated that the removal of Cu^{2+} ions was better on the CH/bHAp composites than the CH/cHAp composites (Table 5-1).

The general trend of reduction in adsorption capacity (mg g^{-1}) with increasing the adsorbent dose could be explained mathematically by equation (4-2). The adsorption

capacity (q_e) is inversely proportional to the mass of adsorbent (m) in grams (g), affecting equilibrium between the metal ion concentration in solution and active sites when the dose increases (with metal ion concentration in the solution being kept constant)[480]. So, the increase in removal efficiency is attributable to there being more adsorption sites (such as amino and hydroxyl groups in chitosan and HAp (referring to FTIR analysis in Chapter 2) on the adsorbent surface with an increase in adsorbent dose. Hence when the adsorbent dose is increased for a constant concentration of adsorbing ion, there is a greater surface area provided by the CH/bHAp or CH/cHAp composites.

The different results shown by the CH/cHAp relative to the CH/bHAp composites (Table 5-1) can be understood by estimating the specific surface areas using average particle sizes from the Mastersizer analysis (included in appendix 3). The estimated specific surface area of the CH/bHAp composite was found to be higher (51.69 m^2/kg, *Appendix 3, Figure 3B*) than that of the CH/cHAp composite (27.98 m^2/kg, *Figure 3A).* Hence the better removal efficiency (%) of the CH/bHAp composite relative to the CH/cHAp composite can be directly attributed to this higher surface area of the bHAp-based composite system.

This was reasoned to be the best explanation for the difference even though the Mastersizer estimation of the specific surface area is at best approximate due to several factors such as the heterogeneity of composites and the dissolution or detachment of component materials making up the composites. The accuracy of measurement using this analysis is also compromised by the shape of the particles, as for the measurement of particle sizes, it assumes that the particles are spherical[481]. In addition, the specific surface area estimation by the Matersizer analysis is linked with the particle sizes of composites; for instance, the average particle size of CH/cHAp composites (the median given as Dv (50)) was 313 μm (*Figure 3A*), providing relatively less specific surface area than CH/bHAp composites (average particle size 282 μm). It illustrates that the heterogeneity in the particle sizes of the adsorbent doses exposed to the metal ions solutions could be a factor to influence the specific surface areas and affecting the adsorption abilities of the composite systems.

Besides the specific surface area, more incorporation of bHAp mass into the composite (CH/bHAp) than cHAp in CH/cHAp composite could be considered as a factor for the better adsorption ability of the bHAp-based composite system as mentioned earlier in

TGA analysis of the CH/HAp composites (section 3.4.1.4). The higher quantity of HAp in composite directly can influence the adsorption of metal cations by providing more adsorption sites, which could be favourable for their application in water treatment systems.

The optimum dose is an essential factor in improving the adsorbent's adsorption capacity. The adsorption capacity of the CH/cHAp composite could be enhanced by increasing the adsorbent dose up to an optimum level by keeping the ion concentration in the solution constant. This would cause greater metal ion removal by providing more adsorption sites for Cd^{2+} present in the solution, as observed in an earlier study[482], in which maximum adsorption (with a plateau in the graph) was achieved by increasing the adsorbent dose up to 1.0 g, with an optimum removal efficiency (value not mentioned) for Cd^{2+} removal. Further, it was noted that higher removal efficiencies (%) for Pb^{2+} ions were attained for adsorption on CH/bHAp composites at low adsorbent doses, which were attributed to its relatively higher surface area. Both composites performed well in terms of Pb^{2+} removal when doses exceeded 0.03 g. The adsorbent dose of the CH/HAp composites for attaining a maximum removal of at least >95% for Pb^{2+} was lower (0.03 g) than required for Cd^{2+} and Cu^{2+} ions (0.05 g). It illustrated that the CH/HAp composites were more efficient at removing Pb^{2+} than Cd^{2+} (See Figure in *appendix 4* for reference). The literature studies in this area have cited several mechanisms for explaining cation ($Cd^{2+,}$ Pb^{2+} and Cu^{2+}) uptake on adsorbents, such as ion exchange, chemisorption, complexation, and precipitation on hydroxyapatite based composite systems[352,483,484] (see section 1.6), additionally the Pb^{2+} ions were more preferentially adsorbed than Cu^{2+} and Cd^{2+} on such composite systems.

Table 5-1 also summarises the effect of adsorbent doses for chromate anion adsorption and removal on the CH/cHAp and CH/bHAp composites. A general trend of gradual increase in removal efficiency is in line with the observations recorded for cation removal. However, it was noted that the maximum removal of chromate ions did not increase beyond 30% for the batch experiments containing the maximum adsorbent dose of 0.05 g. In contrast, the composites were found to achieve approximately 80-99 % removal of the cations from those solutions (see Table 5-1).

The surface group charges of hydroxyapatite and ionic species of chromium present in the solution influence the specific behaviour relating to the removal of chromate by the

CH/HAp composites. Hokkanen et al.[132] explained the different possible mechanisms which could be involved in chromate ion removal by hydroxyapatite in particular which include 1) the ion-exchange between the negatively charged species (hydroxyl) in the crystal lattice of the HAp adsorbent and the chromate anion in solution 2) the electrostatic attraction between the chromate (anion) and positively charged species present on the surface of the HAp adsorbent, 3) the electrostatic attraction between the chromate (anion) and protonated hydroxyl groups present on the surface of the HAp adsorbent, in acidic conditions.

Hokkanen et al.[132] described these mechanisms assuming that the $-Ca^{2+}$, $-PO_4^{3-}$ and $-OH^-$ functionalities were the principal surface functional groups on the surface of HAp. The dominance of the species $HCrO_4^-$ for pH < 7.0 (and >5.0) could cause an ion-exchange reaction between hydroxyl groups (but not phosphates) of hydroxyapatites and this anionic species. Different chemical reactions occur in this pH range in solution to produce "HPO_4Ca^+" and "OH_2^+" (positively charged hydroxyl groups) on the surface of the HAp, resulting in the potential for electrostatic interactions and ion-exchange reactions to remove $HCrO_4^-$ [132] from the solution. The mechanisms for the removal of chromate ions using the HAp as an adsorbent, as given in the previously reported studies, are discussed below.

N.B. *($HCrO_4^-$ is denoted as "Me", and the ***surface of the adsorbent*** is indicated by the symbol "≡")

An ion-exchange mechanism involving hydroxyapatite to remove Cr (VI) ions from the solution

Ion-exchange between the hydroxyl groups and metal anions (Me) was presented as follows:

Equation 5-1:

$$\equiv Ca_x(PO_4)_x(OH)_x + H_3O^+ + xMe \equiv Ca_x(PO_4)_xMe + H_2O$$

Electrostatic interaction between positively charged surface groups and negatively charged Chromate ions

The most dominant ionic species in a chromate ion solution[485] are CrO_4^{2-} and $HCrO_4^-$ when considering a pH range of 2.0 < pH < 5.0. In this pH range, the high concentration of protons in the solution causes the protonation of the functional groups of chitosan and hydroxyapatite, producing ionic species such as $-NH_3^+$ and $-OH_2^+$. These positively

charged ionic species on the surface of the adsorbent can attract the negatively charged chromate ion species (i.e., CrO_4^{2-}, $HCrO_4^-$) by electrostatic interactions. The following equations demonstrate this process.

Equation 5-2:

$$\equiv HPO_4Ca^+ + Me \longrightarrow \equiv HPO_4Ca^+ \ldots\ldots Me \text{ (electrostatic interaction)}$$

Equation 5-3:

$$\equiv CaOH + H_3O^+ + Me \longrightarrow \equiv CaOH_2^+ \ldots. Me + H_2O \text{ (electrostatic interaction)}$$

Equation 5-4:

$$\equiv NH_3^+ + Me \longrightarrow \equiv NH_3^+ \ldots\ldots Me \text{ (electrostatic interaction)}$$

5.1.1.2 Effect of solution pH on metal ions removal by the CH/HAp composites

Experimental: In this experiment, the effect of the solution pH on the adsorption capacity (in mg g^{-1}) of the CH/HAp composites was measured using different environmental conditions for each metal ion removal experiment.

For instance, to record observations in this batch experiment, the pH of the Cd^{2+}-containing solutions was varied between 4.0 and 8.0 for an initial concentration of 25 ppm Cd^{2+} and a 0.01g dose of CH/HAp adsorbent. In contrast, the effect of pH on Pb^{2+} ion adsorption on the CH/HAp composites was examined via AAS measurements in only a restricted pH range from 4.0 -5.8 because of the risk of precipitation of Pb^{2+} ion[486,487] as $Pb(OH)_2$ at pH > 6.0. The solution concentration of Pb^{2+} was initially 50 ppm, and the adsorbent dose of the CH/HAp composite sample was 0.05 g. The effect of pH on Cu^{2+} ion removal by the composites was studied in the pH range of 4.0 - 6.5. The initial Cu^{2+} ion concentration in solutions exposed to adsorbent was 25 ppm, and the adsorbent dose was 0.05 g. A narrow pH range for Cu^{2+} adsorption was selected due to its risk of precipitation and forming copper hydroxide[488], which is usually reported to occur in the pH range 7-12. The influence of pH on the adsorption of chromate ion on the CH/HAp composites was studied over the pH range 4.0- 8.5 using a solution with an initial chromate ion concentration of 5.0 ppm, which was exposed to constant adsorbent dose samples of 0.01 g.

Results: AAS data in Table 5-2 shows the effect of pH (of the heavy metal ion solutions exposed to the CH/HAp composite samples) on the adsorption of metal ions (Cd^{2+}, Pb^{2+},

Cu^{2+} and chromate ions) on the CH/HAp composites. The results are also presented in appendix 4 (and in *Figure 4-5 to 4-8 in appendix 4*).

In general, an increase in cation (Cd^{2+}, Pb^{2+} and Cu^{2+}) adsorption was observed with increasing the pH from acidic to alkaline. For Cd^{2+} ions, the maximum adsorption (12.55 mg g^{-1} and 18.83 mg g^{-1} for the CH/cHAp and CH/bHAp composites, respectively) was recorded at pH 7.0. The literature studies reported that a pH range of 6-7 was optimum for Cd^{2+} ion removal by the chitosan composites prepared with cellulose[489] and hydroxyapatite[377]. However, the use of higher pH solutions would have led to precipitation from the solution as the cadmium hydroxide[490], which occurs around pH 11.0. No precipitation was expected in the pH range 4.0 to 8.0, which was confirmed through a calculation of the solubility product quotient (Q_{sp}) of $Cd(OH)_2$ in the solutions tested, which turned out to be (8.9×10^{-17}). It should be noted that this was less than the literature[491] K_{sp} value (2×10^{-14}) of $Cd(OH)_2$. Contrasting with literature studies, Kamiński and Modrzejewska[492] reported 100 % removal of heavy metal cations, including Cd^{2+}, for pH up to 5.6 when solutions were stirred with pure chitosan. Similarly, the optimum pH for Cd^{2+} ion removal on a multi-walled carbon/HAp composite was noted to be 5.0-6.0, according to other previous work[493]. Based on the current studies and judging from studies reported in the literature, a pH range of 5 to 7 was considered optimal for Cd^{2+} adsorption on various substrates. These substrates notably included biopolymers and hydroxyapatite.

For the adsorption of Pb^{2+} ions on the CH/HAp composites, a pH value of 5.0 was found to be optimal for giving maximum adsorption (35-40 mg g^{-1}) and a maximum removal % value of >95%. The optimum pH range aligns with what has been reported in the literature, which has stated that a pH range of 4.5-5.0 was found to be optimal for the uptake of Pb^{2+} ions on similar adsorbents previously studied. For instance, pH 5.0 was reported as the optimum pH for the adsorption of Pb^{2+} on a chitosan/femur bone extracted-HAp[494]. At this pH (5.0), the dominance of negatively charged functional groups on hydroxyl and phosphate groups of the composite to adsorb the Pb^{2+} ions in solution were thought to attain the maximum adsorption.

The Cu^{2+} ion adsorption was not greatly affected by adjusting the pH of the solution from 4.0 to 6.5 on both the composites. It was found that at a pH of 5-6, Cu^{2+} ion removal was observed at its maximum with an adsorption capacity of about 9 mg g^{-1} for both the

composites tested. A similar study in the literature showed that a composite made from chitosan and HAp and used to remove Cu^{2+} ion was optimised[95] for adsorption at pH 6.0, where a maximum adsorption value capacity of 1.443 mmol g^{-1} was observed.

In general, lower adsorption of cations measured at lower pH values (< 5.0) is most likely due to the hydrogen ion competition and protonation of the active sites on the CH/HAp composite surfaces such as amino and hydroxyl groups[495]. The protonation of active sites leading to a decrease in the overall adsorption capacity of adsorbents at lower pH values is a general trend observed in adsorption studies, especially for the adsorption of cations. Stirring the composite in higher pH metal ion solutions means there are lower concentrations of protons to compete with cations for the active sites provided by chitosan and HAp (i.e., $-NH_2$, -OH groups), which ultimately leads to higher uptake of cations[496]. In respect to HAp and chitosan, at lower (acidic pH, < 4.0)[484], the functional groups of hydroxyapatite and chitosan[494] are neutral (such as phosphates as ≡P-OH) or positively charged due to protonation (such as $\equiv Ca\text{-}OH_2^+$ and NH_3^+). The protonation of these binding sites at lower pH (<4.0) decreases the removal of positively charged metal ions by repelling the cations (e.g., Cd^{2+} Pb^{2+} ions), and protons instead occupy the active sites (such as $-NH_2$ groups). A gradual increase in pH >4.0 promotes the adsorption of these cations by deprotonation of these active sites and by creating negatively charged functional groups ($\equiv P\text{-}O^-$) for an overall negative charge to adsorb metal cations onto the surface of the CH/HAp composites[484,494]. Additionally, the Pb^{2+} is described as an intermediate Lewis acid that can sorb on a hard Lewis basis (such as $-OH^-$ and PO_4^{3-}) present in the CH/HAp composites[108]. This has support from hard and soft acid and base theory (HSAB theory)[497]. The amino groups (a functional group on the chitosan) were found to be 99% protonated at pH 4.3 in a literature study[498], where the chitosan was employed in a solution as the metal adsorbent, which could lead to a decrease in the adsorption of the metal cations (such as Cd^{2+}) on chitosan part of the CH/HAp composites. A slight decrease in adsorption capacity of the CH/HAp for the Cd^{2+} ions was recorded after pH 7.0 *(Figure 4-5, Appendix 4)*, which could be attributed to the speciation of the metal ions in this pH range. A study reported[499] the formation of hydroxyl Cd ion species such as $Cd(OH)^+$ in a pH range of 7.0-8.0 in a metal ion solution, which possibly decreases the free Cd^{2+} ion adsorption on negatively charged functional groups of

adsorbent and hence decreases the adsorption capacity (mg g^{-1}) at pH >7.0, which is evident in *Figure 4-5 (Appendix 4).*

Table 5-2: The effect of the solution pH on the adsorption capacity (in mg g^{-1}) of the CH/HAp composites for the adsorption of metal ions from solutions containing only one type of metal ion

	pH	**4.0**	**5.0**	**6.0**	**7.0**	**8.0**
Cd^{2+}	CH/cHAp	8.93	10.08	10.09	12.95	12.56
	CH/bHAp	13.58	14.52	17.81	19.80	18.83
	pH	4.5	5.0	5.5	6.0	6.5
Pb^{2+}	CH/cHAp	34.27	35.06	22.55	22.93	28.80
	CH/bHAp	38.76	39.13	32.42	33.12	37.80
	pH	**4**	**5**	**5.5**	**6**	**6.5**
Cu^{2+}	CH/cHAp	8.18	8.39	8.38	8.35	8.38
	CH/bHAp	9.18	9.17	9.17	9.18	9.18
	pH	**4.5-5**	**5-5.5**	**6-6.5**	**7-7.5**	**8-8.5**
Cr as chromate ions	CH/cHAp	2.44	1.63	1.32	1.00	0.88
	CH/bHAp	1.12	0.91	0.79	0.80	0.57

In contrast with the effect of pH on cation adsorption discussed above, a gradual decrease in chromate ion (an anion) adsorption was observed, as demonstrated in Table 5-2 *(Figure 4-8, Appendix 4),* when the solution pH was increased in both the composites tested. The pH of the chromate ion solution appears to be a key parameter influencing the extent of adsorption of chromate ions on the CH/HAp composites. Chromate ion was more readily removed from lower pH chromate solutions[485] exposed to the adsorbent. The most dominant chromium species are known to be $HCrO_4^-$ and CrO_4^{2-} in the pH range of 2.0-5.0. These anionic species could possibly interact with and be removed by protonated -NH_2 groups (see equation 5-4) on the chitosan and positively charged species on the HAp surface. Ion exchange with hydroxide or carbonate (in cHAp) in the HAp part of the composite could also occur but could not be confirmed as a mechanism for the removal of chromate ions[132,500,501]. Earlier reports state that the decrease in removal of chromate ions with increasing pH is due to the deprotonation of active sites (amino and hydroxyl groups) and a greater abundance of negative ions in solution (e.g. OH^-) which may create competition for anion adsorption[502] on the surface of the composites.

5.1.1.3 Effect of the initial metal ion concentration on metal ion removal by the CH/HAp composites

Experimental: The initial metal ion concentration was varied (between 5 ppm and 25 ppm for Cd^{2+} and Cu^{2+} ions and between 10 ppm and 50 ppm for Pb^{2+} and chromate ions) for a constant adsorbent dose of 0.01g, with initial solution pH at 4.5-6.0 to evaluate the effect of adsorbate concentration in solution on metal removal. Further, the data recorded in this experiment were used to study the adsorption mechanism by fitting adsorption models (discussed in the upcoming section) that are commonly proposed (and experimentally proven, Chapter 1, Table 1-8) for such adsorption systems. These were given with equations in Chapter 1. The results recorded using the AAS are presented in Table 5-3.

Results: Table 5-3 shows the AAS data recorded for the effect of the initial metal ion concentration on metal ion adsorption onto the CH/HAp composites (also presented in *Figures 4-9 to 4-12, Appendix 4*). A gradual decrease in removal efficiency with increasing metal ions concentration was observed for both the composites tested. At the same time, the adsorption capacity (mg g^{-1}) of the composites was noted to increase.

The lower adsorption capacity (in mg g^{-1}) of the adsorbent at low concentration values could be due to the lower concentration of metal ions present in the solution. The lower concentrations of ions cause a barrier in the mass transfer of metal ions between the liquid and solid phase surface by limiting ion diffusion. Contrary to this, higher concentrations of metal ions in the solution obviously help to overcome these limitations by providing a driving force for more metal ion adsorption by increasing the diffusion process[475,476].

The maximum adsorption of Pb^{2+} was recorded at 50 ppm, which was 49.08 mg $g^{-1}$and 84.19 mg g^{-1} on the CH/cHAp and CH/bHAp composites, respectively. At the same time, the highest removal (%) was recorded at 10 ppm initial Pb^{2+} ion concentration ranging between 88 and 99% for both composites. The explanation for these trends is similar, as described earlier (see above)[467]. The maximum adsorption of Cu^{2+} ions (at an initial ion concentration of 25 ppm) was found to be 12.22 mg g^{-1} and 16.01 mg g^{-1} on the CH/cHAp and CH/bHAp composites, respectively.

Table 5-3: The effect of the initial metal ion concentration on removal (%) and the adsorption capacity (in mg g^{-1}) of different metal ions adsorbed on the CH/HAp composites from a single-metal ion type solution system

The removal (%) of metal ions using the CH/HAp composites						
	Metal ion concentrations(ppm)	5.0	10.0	15.0	20.0	25.0
Cd^{2+}	CH/cHAp	50.37	44.61	40.40	35.77	30.69
	CH/bHAp	57.27	52.36	47.55	44.27	39.70
Pb^{2+}	Metal ion concentrations (ppm)	10.0	20.0	30.0	40.0	50.0
	CH/cHAp	88.75	87.33	72.00	58.71	49.09
	CH/bHAp	99.37	97.18	95.32	92.68	84.19
Cu^{2+}	Metal ion concentrations (ppm)	5.0	10.0	15.0	20.0	25.0
	CH/cHAp	50.33	44.51	37.36	30.46	24.44
	CH/bHAp	53.62	49.22	46.49	39.94	32.02
Cr as chromate ions	Metal ion concentrations (ppm)	10.0	20.0	30.0	40.0	50.0
	CH/cHAp	33.45	28.85	26.66	25.15	23.86
	CH/bHAp	32.31	26.90	23.27	22.72	22.00
The adsorption capacity (in mg g^{-1}) of the CH/HAp composite for the adsorption of the metal ions						
	Metal ion concentrations (ppm)	5.0	10.0	15.0	20.0	25.0
Cd^{2+}	CH/cHAp	5.04	8.92	12.12	14.31	15.35
	CH/bHAp	5.73	10.47	14.26	17.71	19.85
Pb^{2+}	Metal ion concentrations (ppm)	10.0	20.0	30.0	40.0	50.0
	CH/cHAp	17.75	34.93	43.20	46.97	49.09
	CH/bHAp	19.87	38.87	57.19	74.14	84.19
Cu^{2+}	Metal ion concentrations (ppm)	5.0	10.0	15.0	20.0	25.0
	CH/cHAp	5.03	8.90	11.21	12.19	12.22
	CH/bHAp	5.36	9.84	13.95	15.98	16.01
Cr as chromate ions	Metal ion concentrations (ppm)	10.0	20.0	30.0	40.0	50.0
	CH/cHAp	6.69	11.54	15.99	20.12	23.86
	CH/bHAp	6.46	10.76	13.96	18.18	22.00

Literature reveals that the adsorption capacity (in mg g^{-1}) of metal ions onto synthetic hydroxyapatite varies depending upon the initial metal ion concentrations. For instance, Cd^{2+} ion adsorption on synthetic nano-HAp was found to increase from 91.96 mg g^{-1} to 209.6 mg g^{-1} for 100 ppm Cd^{2+} and 500 ppm $Cd^{2+,}$ respectively[377]. Similarly, another study reported the maximum adsorption of about 30 mg g^{-1} for 100 ppm and around 70 mg g^{-1} for an initial Cd^{2+} concentration of 200 ppm. It reveals that the increase in ion concentration positively affects the adsorption capacity (mg g^{-1}) of adsorbents. Like the literature studies, in the present study, the maximum adsorption capacity of Cd^{2+} at 5 ppm initial concentration was 5-6 mg $g^{-1.}$ It increased up to 15.35 mg g^{-1} and 19.85 mg g^{-1} for the CH/cHAp and CH/bHAp composites, respectively, when the initial concentration was increased from 5 ppm to 25 ppm. It confirms that the initial metal ion concentration is also a crucial parameter for changing the efficiency of the adsorption system, and the

adsorption capacity of the adsorbent could be increased up to a particular level by increasing the initial metal ion concentration in solution for a constant dose.

The data presented in Table 5-3 revealed that the CH/bHAp composite exhibited a better removal efficiency for the metal ions removal than the CH/cHAp composite. The better removal ability trend for the bHAp-based composite is recorded for all the metal ions studied.

In common with cation adsorption, in Table 5-3, a continuous increase in adsorption capacity (mg g^{-1}) and a decrease in removal efficiency (%) were also observed with increases in the initial chromate ion concentration. The decrease in removal efficiency with an increase in the initial chromate ion concentration can naturally be attributed to the decrease in adsorption sites (as the adsorbent dose was kept constant in these experiments). The maximum adsorption of chromate ion on the CH/HAp composites ranges from 20-25 mg g^{-1} for an initial chromate ion concentration of 50 ppm.

Schmuhl et al. reported the adsorption capacity (mg g^{-1}) of chitosan for Cr(VI) to be 78 mg g^{-1} by using an initial chromate ion concentration of 1000 ppm[503]. The higher adsorption capacity reported in the literature study corresponds to a system that had been exposed to a higher initial metal ion concentration because it has been observed that the higher initial metal ion concentration helps to increase the adsorption capacity of the solution exposed to a constant amount of the adsorbent, providing more molecules in solution to adsorb on active sites of adsorbents. A study from the literature used a composite made from chitosan and hydroxyapatite to adsorb Cr (VI) (as chromate ion), and the adsorption capacity (mg g^{-1}) was found to be 3.45 mg g^{-1} at 0.01 g adsorbent dose of adsorbent when exposed to a 10 ppm solution of Cr(VI) at pH 4.0. A literature study discussed the electrostatic interactions between the negatively charged sorbate anions ($HCrO_4^-$) and the positively charged Ca^{2+} ions (HAp on its surface) as one of the possible mechanisms that may have been responsible for removing Cr(VI) using the chitosan/HAp based composite. The literature study[502] described the low pH of the solution (ranging between pH 4-5) as an assisting factor for encouraging uptake of the Cr(VI) species on the chitosan/HAp composite due to the protonation of the active sites such as amino groups which encourage electrostatic attractions to anions such as $HCrO_4^-$.

5.1.1.4 Adsorption modelling of the CH/HAp composites for the adsorption of metal ions

The adsorption modelling of the synthesised composite systems was carried out to explore the adsorption mechanisms and to estimate the maximum adsorption capacity (q_{max} in mg g^{-1}) of each composite system for each metal studied in this project. For this, the two-parameter adsorption models, including Langmuir and Freundlich (described in Chapter 1), are the most studied adsorption isotherm models for such biopolymeric composite systems. These two models were used to analyse the adsorption data of this study to determine which of these was the best-fit model for each composite system in terms of adsorption of metal ions. The theoretical background of these models (chapter 1, section 1.10) and supporting literature (Table 1-8) have been extensively described earlier.

To recap these non-linear adsorption models, the model equations and the explanation of their parameters are given as follows:

Non-Linear Langmuir isotherm:

Equation 5-5

$$q_e = \frac{K_L q_{max} C_e}{1 + K_L C_e}$$

In equations 5-5, q_e and C_e are quantities of adsorbate adsorbed to the solid (mg g^{-1}) and present (as ions) in the liquid phase (mg L^{-1}) at equilibrium. The term q_{max} (also termed as "b" in the literature) is the estimated maximum adsorption capacity of the system in mg g^{-1} calculated using the Langmuir model equation (5-5). K_L is the Langmuir equation constant that describes the affinity between the sorbate and the adsorbent, which indicates how favourable thermodynamically the adsorption of the species is on the composite surfaces. The K_L is used to calculate the dimensionless factor, R_L, of the Langmuir isotherm model using the following equation:

Equation 5-6:

$$R_L = \frac{1}{(1 + K_L C_0)}$$

R_L demonstrates the nature of the adsorption process as given in many literature studies[476,504-506]:

- Irreversible if $R_L = 0$ or maybe $R_L <<< 1$, i.e., it is almost equal to zero, indicating an irreversible adsorption process), which demonstrates a "really favourable" adsorption
- Unfavourable if $R_L > 1$
- Favourable if $1 > R_L > 0$ or could be described as "moderately favourable adsorption

Non-linear Freundlich isotherm:

Equation 5-7:

$$q_e = K_F C_e^{\frac{1}{n}}$$

In the Freundlich model equation, q_e (mg g^{-1}) and C_e (mg L^{-1}) are the same quantities as described above for the Langmuir isotherm model, while K_F and 1/n are Freundlich constants. The value of 1/n describes the adsorption process as follows: if 1/n is less than unity and greater than zero, it implies the adsorption process is favourable, while "1/n" > 1 describes an irreversible adsorption process[53,507].

In contrast with the adsorption modelling for the cations, linearized Langmuir and Freundlich isotherms were used in the adsorption modelling exercise in regard to the data obtained for chromate ion adsorption. The linearized Langmuir and Freundlich model equations used for chromate ion adsorption modelling are given as follows (see theory discussion in Chapter 1):

The linearized equation for the Langmuir isotherm: 5-8

$$\frac{1}{q_e} = \frac{1}{q_{max} K_L c_e} + \frac{1}{q_{max}}$$

In the above equation, q_{max} is the estimated maximum adsorption capacity of the adsorbent in mg $g^{-1,}$ q_e (mg g^{-1}) and C_e (mg L^{-1}) are sorbate quantities in the solid and liquid phases, respectively, after reaching equilibrium. Hence, the above equation is that of a straight line if $1/q_e$ vs $1/C_e$ is plotted, giving q_{max} through the y-intercept and K_L from the slope of the linearized equation.

The linearized equation for the Freundlich Isotherm: 5-9

$$\ln q_e = \ln K_F + \frac{1}{n} \ln C_e$$

With the linearized Freundlich model, a plot of $ln q_e$ vs $ln C_e$ should give a straight line from which the Freundlich equation constants "K_F" and 1/n can be calculated from the intercept and slope respectively of the straight-line plot.

The data collected from the studies into the effect of initial metal ion concentration on metal ion adsorption were analysed using the above-given adsorption models. The best-fitted adsorption model between Langmuir and Freundlich was then decided by comparing the R^2 values of the two fitted models. Similar methods (non-linear regression method for cations and linear regression for the chromate ions) were used to calculate the isotherm parameters in all the composite systems studied. For non-linear model fitting, non-linear regression functions (also called error functions) were used, which are given in *appendix 1 (section 1.3).*

Modelling of cation (Cd^{2+}, Pb^{2+}) adsorption on the CH/HAp composites

Experimental: An additional method of standardization for adsorption modelling, termed as the sum of normalized error (SNE), was used by employing the error functions for the adsorption modelling of Cd^{2+} and Pb^{2+} on the CH/HAp and CH/HAp/CF composite systems only and described in *Appendix 1, section 1.3B*. The importance of using this standardisation method is also explained in *Appendix 1.3B.*

Results:

Adsorption modelling of cations: The calculated isotherm parameters (using the non-linear regression method *Appendix 1, section 1.3*) for the two adsorption models for cation adsorption on the CH/HAp composites are given in Table 5-4. *(Figures 4.13 and 4-20 in Appendix 4)* show the fitting of non-linear adsorption isotherms for metal ion adsorption on the CH/HAp composites.

The comparison of R^2 values of Langmuir and Freundlich models revealed that the Langmuir isotherm model was the best-fitted model for explaining the adsorption of Cd^{2+} and Cu^{2+} onto the CH/HAp composites with $R^2 > 0.95$, which is in agreement with the modelling results recorded for these metal ions adsorption in similar adsorption systems [118,479]. The significance of the best-fit of the Langmuir isotherm model for both the composites (CH/cHAp and CH/bHAp) suggested a monolayer adsorption model for Cd^{2+}

and Cu^{2+} on a homogeneous adsorbent surface[494]. The finding is supported by the literature studies, which suggested the fitting of the Langmuir adsorption isotherm to adsorption data recorded for metal ion adsorption on similar heterogeneous composites (Table 1-8).

Table 5-4: Adsorption isotherm parameters for metal ion (Cd^{2+}, Pb^{2+} and Cu^{2+} and chromate ions) adsorption on the CH/HAp composites

Adsorption models		**Langmuir**				**Freundlich**		
Metal ions	Composites	q_{max} (mg g^{-1})	K_L	R^2	R_L	1/n	K_F	R^2
Cd^{2+}	CH/cHAp	24.338	0.106	0.996	0.274	0.560	3.309	0.969
	CH/bHAp	33.932	0.094	0.999	0.298	0.620	3.824	0.988
Pb^{2+}	CH/cHAp	52.422	0.588	0.965	0.064	0.240	23.804	0.858
	CH/bHAp	90.031	1.468	0.938	0.027	0.280	49.676	0.964
Cu^{2+}	CH/cHAp	15.910	0.217	0.156	0.973	0.373	4.405	0.896
	CH/bHAp	23.670	0.150	0.211	0.961	0.471	4.610	0.900
Chromate	CH/cHAp	45.045	0.026	0.436	0.996	1.666	0.731	1.000
	CH/bHAp	34.722	0.033	0.376	0.988	1.699	0.689	0.995

Both adsorption models (Langmuir and Freundlich) showed a good fit to the Pb^{2+} adsorption data on the composites with the goodness of fit, R^2 ranging between values of 0.86 to 0.96, and demonstrating a range of adsorption behaviour from monolayer adsorption on the homogenous surface to monolayer adsorption on heterogeneous surfaces. The Freundlich was a better fit to the adsorption data than the Langmuir model for the CH/bHAp composites with a relatively higher value of R^2 than calculated for the fitted Langmuir model R^2 (see Table 5-4). The better fitting of the Freundlich isotherm relative to the Langmuir one for Pb^{2+} adsorption on the CH/bHAp composites indicates that the adsorption is occurring on a heterogeneous surface. This was justifiable as the surface of the CH/bHAp was also found to be heterogeneous with visible fine particle deposition at the surface (SEM analysis of CH/bHAp, Chapter 3, Figure 3-8)). Overall, between the two adsorption isotherms modelled, the Langmuir isotherm could be considered the best-fitted model, as it gives more reliable maximum adsorption values (q_{max} mg g^{-1}) values (Table 5-4) for both composite systems, as the fitted (calculated) values for Pb^{2+} adsorption on the CH/HAp composites are numerically closer to the composite systems' *experimental values*. Additionally, the fitting of the Langmuir model is well-supported by the literature studies conducted for similar adsorption systems (Table 1-8).

Using the Langmuir model, the calculated q_{max} (in mg g^{-1}) of Cd^{2+} was 24.33 mg g^{-1} and 33.93 mg g^{-1} on CH/cHAp and CH/bHAp composites, respectively. The maximum adsorption capacity in relation to Cu^{2+} adsorption on the composites was 15.91 mg g^{-1} and 23.66 mg g^{-1} (calculated using the Langmuir model) for the CH/cHAp and CH/bHAp composites, respectively. The maximum capacity of the CH/HAp composites in relation to the Pb^{2+} adsorption is higher than the calculated q_{max} of Cd^{2+} and $Cu^{2+,}$ which indicated the higher adsorption of Pb^{2+} than the other two metal cations on this composite system. The values of the dimensionless factor R_L (calculated using equation 5-5) for all the three cations adsorption on CH/HAp composites given in Table 5-4 indicated a favourable adsorption process as $0 < R_L < 1$[505,508].

The literature studies reported that Langmuir adsorption was representative of Cd^{2+} ion adsorption behaviour on a hydroxyapatite/clay mineral composite[509] and on bone char[510], which lends support to the applicability of the Langmuir isotherm model to describing the Cd^{2+} adsorption on such biopolymeric (chitosan) and HAp based adsorption systems as used in the presently studied systems. Gandhi et al.[63] reported that Cu^{2+} adsorption on nano-HAp and n-HAp/Chitosan composites ranged from 4-6 mg g^{-1} when the composites were exposed to an initial concentration of 10 ppm Cu^{2+}. However, the adsorption capacity of the nHAp and nHAp/chitosan composites calculated in this literature study is lower than the Cu^{2+} adsorption calculated in the present study for the CH/HAp composites, illustrating the CH/HAp composites as a relatively more efficient adsorption system for Cu^{2+} removal. The better adsorption ability of the CH/HAp composites than the literature study conducted for similar composites could be due to better optimisation of the experimental conditions, such as the initial metal ion concentration, appropriate adsorbent dose and pH range in the present study, which could be the features to enhance the adsorption abilities of the systems.

The mode of uptake of metal ions, i.e., via exchange with Ca^{2+} and cations (e.g., Pb^{2+}) from the hydroxyapatite crystal lattice, is frequently discussed in literature[511-513]. In general, the ion exchange mechanism is believed to be the predominant mechanism for the adsorption of cations on HAp[117,370]. The ion-exchange activity is found to be higher for the composite samples having a higher surface area (i.e., the CH/bHAp composite).

As mentioned above, the linearised regression method was used for the adsorption modelling of chromate ions on the CH/HAp composites. Figures 4-19 and 4-20 (*Appendix*

4) illustrate respectively fitting of the linearized Langmuir and Freundlich isotherm equations to the chromate ion adsorption data on the CH/HAp composites. The equations generated from these linear fits using Microsoft Excel are given as follows:

Table 5-5: The linearized equations calculated for chromate ion adsorption on the CH/HAp composites using the linearized Langmuir and Freundlich isotherms

Composites	Linearized Langmuir Equation	Linearized Freundlich Equation
CH/cHAp	$y = 0.8583x + 0.0222$ ($R^2 = 0.995$)	$y = 0.7315x + 0.5107$ ($R^2 = 0.999$)
CH/bHAp	$y = 0.8679x + 0.0288$ ($R^2 = 0.988$)	$y = 0.6894x + 0.5298$ ($R^2 = 0.995$)

Hence, using the above equations, the Langmuir isotherm parameters were calculated as follows:

$1/q_{max}$ = intercept

q_{max} = 1/intercept

$1/(K_L * q_{max})$ = slope

$K_L = 1/\text{slope} * q_{max})$

The Freundlich isotherm parameters were calculated as follows:

lnK_F = intercept

$K_F = e^{\text{intercept}}$

1/n = slope

The calculated parameters for the systems tested and derived from both the adsorption models are given above in Table 5-4. By comparing the values of R^2 for both adsorption models, both the Freundlich and Langmuir adsorption isotherms were found to fit the data well. Although the Freundlich fit R^2 value is relatively higher than that calculated for the Langmuir fit (Table 5-4), it was obvious that the Langmuir model was also showing a reasonable fit with R^2 values of >0.98 being obtained from fits to data. Several authors have reported better fits of the Freundlich isotherm to chitosan-based systems in earlier studies. Kousalya et al.[502] reported the good fitting of both the Langmuir and the Freundlich isotherm model to chromate ion adsorption data when reporting results from using nHAp/chitosan-based composites to remove chromate ions from aqueous solutions. The value of the Freundlich isotherm constant "1/n" lies between 0 and 1 so, indicating favourable adsorption of chromate ion on both the composites[347].

The maximum adsorption capacity (mg g^{-1}) of the CH/cHAp and CH/bHAp composites for chromate ion adsorption, estimated by the Langmuir isotherm model, is 45.045 mg g^{-1} and 34.022 mg g^{-1}, respectively. The dimensionless factor R_L derived from the Langmuir isotherm fit to data shows that adsorption of chromate ion in both the composites is favourable as $0 < R_L < 1$.

The fitting of both the adsorption isotherms suggests that the chromate ion adsorption on the CH/HAp could include a range of behaviours, including homogeneous and heterogeneous surfaces. The literature studies equally favour the fitting of the Langmuir and Freundlich adsorption isotherms to describe the chromate ion adsorption on similar adsorption systems of biopolymers and hydroxyapatites.

5.1.1.5 Effect of contact time on metal ions removal by the CH/HAp composites

Experimental: The effect of contact time on metal ion removal (%) by the CH/HAp composites was measured by varying the contact time between 1 minute and 120 minutes for measuring adsorption on a 0.01 g dose of adsorbent. The experiment was conducted by exposing the 0.01 g of the adsorbent dose to the metal ion solutions at different concentrations. The initial metal ions concentration of Cu^{2+} and Cd^{2+} was 25 ppm exposed to 0.01 g of the adsorbent, while it was 5 ppm for Pb^{2+} and 50 ppm for chromate ions. The initial pH of the solution ranged from 4.0-6.0 to measure the removal efficiency per minute for the first 5 minutes, then at 10, 15, 30, 60 and 120-minute intervals.

Results: Table 5-6 presents the AAS data recorded to show the effect of contact time on metal ions removal (%) using the CH/HAp composites. The results for the effect of the contact time on the adsorption of the metal ions are plotted and presented in *Figures 4-21 to 4-24* in *Appendix 4.*

The Cd^{2+} adsorption was rapid in the initial 15 minutes. While reaching a plateau in 30 minutes which illustrates the adsorption equilibrium, it means the active sites on the adsorbent surface have been saturated, or monolayer adsorption of Cd^{2+} ions on the adsorbent surface has occurred. There was no considerable variation in removal efficiencies after 30 minutes. Maximum removal of 30% and 40% was recorded for Cd^{2+} on the CH/cHAp and CH/bHAp composites, respectively, at equilibrium.

A sharp increase in the removal % of Pb^{2+} ion from the solution was recorded in the initial 10 minutes for both the composites tested (*Figure 4-22, Appendix 4*). About 80-90% of

Pb^{2+} removal was achieved in just 30 minutes, with no significant change being observed after 30 minutes of exposure to the solution to the adsorbent. The maximum removal efficiency for both composites tested was calculated to be 97-98% over the 2 hours of exposure time. The optimum time for realising the highest Pb^{2+} ion removal with the CH/HAp composites was found to be 60 minutes.

The removal of Cu^{2+} ions by the composites was very efficient, as both the composites achieved more than 50-60% removal in just 15 minutes of exposure of the solution to the composites. The maximum removal efficiency measured for Cu^{2+} ion by the CH/cHAp and CH/bHAp composites was found to be 82.32% and 91.99%, respectively, after 120 minutes (which is considered the maximum time to achieve adsorption equilibrium for Cu^{2+} adsorption (mg g^{-1}) on the CH/HAp composite surface.

Compared to cation adsorption, both the composites removed up to 22% of chromate ion in solution within 10-15 minutes of contact time with the solution, with a plateauing of the uptake occurring after 60 minutes. The maximum removal was approximately 20-25% of the solution chromate ion by both composites. The rapid increase in removal (%) for both the composites for chromate ion adsorption in the initial 10-15 minutes of exposure is attributed to the excess availability of adsorption sites at the beginning of the adsorption process. The composites reached adsorption equilibrium for chromate ion adsorption at 60 minutes, which indicated that the saturation of the adsorption sites on the surface of adsorbents (as well as no further change in removal (%)) was recorded after 60 minutes for both the composites.

The CH/bHAp composite showed a relatively better removal efficiency for the cations than the CH/cHAp composite, which could be attributed to a relatively higher specific surface area of the CH/bHAp composite, as discussed earlier (see above *"*the effect of the adsorbent dose"). In contrast, the chromate (anion) adsorption was better on the CH/cHAp composite than on the CH/bHAp composite, which is in line with the observation recorded in earlier batch experiments for the chromate ion adsorption on these composites (see above).

Table 5-6: The effect of the contact time on the % removal of metal ions on the CH/HAp composites system from a single metal ion type solution system

Contact (minutes)	Time	1	2	3	4	5	10	15	30	60	120
Cd^{2+}	CH/cHAp	21.97	25.90	27.82	28.88	28.90	30.23	30.96	31.23	31.82	31.89
	CH/bHAp	21.59	22.60	26.56	26.61	27.09	29.58	33.24	39.23	39.70	39.75
Pb^{2+}	CH/cHAp	40.44	43.56	53.08	55.82	60.38	74.02	83.80	94.22	97.04	97.12
	CH/bHAp	36.92	50.98	70.46	70.66	73.50	88.96	92.34	96.36	97.20	97.80
Cu^{2+}	CH/cHAp	24.54	29.80	30.98	39.38	40.73	47.89	59.50	72.53	80.10	82.33
	CH/bHAp	36.66	42.71	54.47	58.65	67.49	79.62	84.90	90.38	91.74	92.00
Cr as chromate ions	CH/cHAp	9.72	12.18	13.52	14.27	14.94	17.87	19.97	21.80	23.24	23.25
	CH/bHAp	10.77	16.19	16.87	17.97	20.90	21.06	21.19	21.68	21.88	21.88

5.1.1.6 Kinetics modelling of metal ion adsorption on the CH/HAp composites

Kinetic modelling of metal ion adsorption on the CH/HAp composites was performed with testing done for non-linear pseudo-first-order (PFO) and pseudo-second-order (PSO) kinetics (described in Chapter 1, section 1.11). It was performed by employing the kinetics data recorded in "the contact time batch experiment" of each metal ion studied. The PFO and PSO are the most common kinetic models used to study the adsorption of metal ions on such composite systems. The non-linear kinetic model equations of PFO and PSO models are given in chapter 1 (section 1.11). The parameters of the kinetic models, including the rate constants k_1 and k_2 of PFO and PSO, respectively and the adsorption capacity at equilibrium (q_e in mg g^{-1}), were calculated using the non-linear regression method (*Appendix 1.3*) on the Microsoft Excel, using add-in solver function and given in Table 5-7. The best-fitted parameters set of each model was selected based on the maximum R^2 value calculated and realised for each error function. The best fit of the PFO or PSO kinetic models was decided upon by comparing the R^2 values calculated for both models and choosing the R^2 value closest to 1 calculated for each model.

Results: The calculated parameters of the kinetic models used for modelling the adsorption of metal ions on the CH/HAp composites are given in Table 5-7, and models fitted to the experimental data are presented in *Figures 4-25 to 4-32 in Appendix 4.* The comparison of the coefficient of determination values (R^2) calculated for both PFO and PSO kinetic models showed that the PSO kinetic model turned out to be the best-fitted model, with its R^2 value being greater than that for the PFO kinetic model for all four metal ions adsorption on both composite systems. The calculated adsorption capacities (q_{max} in mg g^{-1}) for the metal ions by PSO are given in Table 5-7.

Table 5-7: The parameters calculated for metal ion adsorption on the CH/HAp composites based on each kinetic model fitted.

Metal ions	Composite systems	PFO			PSO		
		k_1 (min^{-1})	q_e (mg g^{-1})	R^2	k_2 (g mg^{-1} min^{-1})	q_e (mg g^{-1})	R^2
Cd^{2+}	CH/cHAp	1.113	15.207	0.831	0.139	15.931	1
	CH/bHAp	0.49	17.675	0.561	0.039	19.071	0.992
Pb^{2+}	CH/cHAp	0.272	9.086	0.842	0.04	9.846	0.995
	CH/bHAp	0.391	9.424	0.955	0.059	10.112	0.999
Cu^{2+}	CH/cHAp	0.16	7.505	0.858	0.025	8.302	0.992
	CH/bHAp	0.317	8.836	0.935	0.049	9.518	0.999
Chromate	CH/cHAp	21.26	0.33	0.8	22.99	0.021	0.996
	CH/bHAp	21.34	0.62	0.94	22.56	0.049	0.998

The revelation that the PSO kinetic model was the best fit for data indicates that metal ions follow the "chemisorption" mechanism when interacting with the CH/HAp composites. The PSO fitting on experimental data of metal ion adsorption on both the composites confirms the chemisorption mechanism is the rate-limiting step for the CH/HAp composites for removing these metal ions. The literature studies have discussed the nature of the chemisorption of metal cations on chitosan and hydroxyapatite-based composites. "Chemisorption" could occur in various ways. For instance, cations (Cd^{2+}, Pb^{2+} and Cu^{2+}) may adsorb on the CH/HAp composites via metal-ligand complexation through the -NH_2 groups of chitosan (see mechanisms of removal section 1.6). Chitosan has an electron-donating atom (N) and could form stable complexes with cations[514], as discussed in the possible mechanism using the chitosan and HAp based composites in Chapter 1.

Similarly, the hydroxyl groups (on the surface of HAp and chitosan) and carboxyl groups (chitosan) could participate in the chemisorption of these metal cations by metal-ligand complexation[515,516]. Additionally, *ion exchange* could be considered while discussing the metal removal mechanisms using HAp (see sections 1.5.1 and 1.6.3). A study verified the ion-exchange mechanism of HAp for Pb^{2+} and Cd^{2+} adsorption while using synthetic hydroxyapatite. The literature confirmed it by structural changes in HAp (using XRD) and measuring Na^+ and Ca^{2+} concentrations in solution after Cd^{2+} adsorption[517]. As described in Chapter 1 (section 1.4.2), adding HAp into chitosan (and other low-cost materials) could introduce an additional removal mechanism (*ion exchange*) in biopolymer-based composite systems like chitosan-based adsorbents. So, this could be

one of the dominating mechanisms in the adsorption of cation on the part of the HAp in the CH/HAp composite systems. This finding of the rate-limiting chemisorption mechanism for chromate ion adsorption is also reported in other previous studies, which involved the removal of chromate ions using similar adsorbent systems based on chitosan/hydroxyapatite composites[189,310,312]. Similarly, the chemisorption of chromate ions on CH/HAp composites could occur in the pH range (5.0 -7.0) via electron-donating functional groups (-NH_2) of chitosan and also by hydroxyl groups (containing oxygen as an electron-donating ligand atom) to form metal-ligand complexes as described in section 1.6.2.

The findings of the kinetic modelling performed on the three data sets for metal cation adsorption on the CH/HAp composite systems (present study) generally agree with the results from literature studies (Table 1-8), which report metal ion adsorption on hydroxyapatite surfaces[110,518,519], carbon/hydroxyapatite composites[515], nano-HAp/chitosan composites[377] and on other similar composites made from chitosan and hydroxyapatite[83,368,483] and concluded that the pseudo-second-order kinetic model was the best fit kinetic model for explaining the mechanism of metal ion adsorption on these composites.

All of the composite systems in this study discussed in the upcoming sections include the CH/HAp component. So, the mechanisms that describe the adsorption of cations (Pb^{2+}, Cd^{2+}, Cu^{2+}) in this composite system, such as metal-complexation, ion-exchange, electrostatic interactions and physical adsorption by weak Van der Waals forces, would be considered fundamental mechanisms on the part of CH/HAp. The additional third components added to CH/HAp to synthesise the three-component composite systems could further be discussed (in the respective sections) to participate in these heavy metal removal mechanisms by involving their principal functional groups.

5.1.2 Experiments involving the removal of metal ions by the CH/HAp/CF composites (commercial & Bovine-derived) from the single-metal ion type solutions

The chitosan/HAp/Coir fibre (CH/HAp/CF) composite (a three-component composite system) was synthesised by adding coir fibre (CF) to the CH/HAp composite. The spectroscopic and microscopic characterization of the CH/HAp/CF composites was

described in Chapter 3. The CH/HAp/CF composites were the first of the three-component composite systems in this study to investigate the effect of adding a third component to the CH/HAp composite (2 component system). Other researchers have not reported previous work into this three-component composite.

This section presented the results recorded for the CH/HAp/CF composites for their heavy metal ion removal ability by following the general experimental methods described in Chapter 4. The specific methods used in each batch experiment are, however, described in their respective sections below.

The following describes the results of using this composite system in single-metal ion type water systems for the removal of metals as described earlier in the CH/HAp composites system (section 5.1.1). The adsorption behaviour of metal ions on the CH/HAp/CF composite systems and kinetics comparisons of this system with that of the control composite (CH/HAp) will be made with the data collated from Atomic Absorption Spectroscopy (AAS) measurements conducted on this three-component composite system and in the control composite system (described earlier in section 5.1.1).

The following section describes the effect of different experimental parameters in batch experiments for heavy metal ion removal from solutions containing only one dissolved metal salt present (i.e., Pb^{2+}, Cd^{2+}, Cu^{2+} or "Cr" as chromate ions).

5.1.2.1 Effect of adsorbent dose on metal ions removal by the CH/HAp/CF composites

Experimental: A similar dose of 0.01 g to 0.05 g (as used earlier in control composites for the removal of metal ions, section 5.1.1.1) of the CH/HAp/CF composites was added to the metal ions solutions at 25 ppm (for Cd^{2+} & Cu^{2+}) and 50 ppm (for Pb^{2+} and chromate anions) to measure the effect of adsorbent dose on the adsorption of these metal ions on and their removal (%) by the CH/HAp/CF composite systems. The initial solution pH was 4.5-7.0. The removal (%) and adsorption capacity "q_e" (mg g^{-1}) of the CH/HAp/CF composites were calculated using equations 4-1 and 4-2, respectively, given in Chapter 4. The solutions were stirred with an adsorbent for two hours before measuring the final concentrations (C_e) by AAS.

Results: Table 5-8 presents the metal ions adsorption capacity "q_e" (mg g^{-1}) and removal efficiency (%) as measured by Atomic Absorption Spectroscopy and calculated using equations 4-1 and 4-2 (section 4.2.7) for the CH/HAp/CF composites system with

different adsorbent doses ranging between 0.01g to 0.05 g (results are also presented in *Figures 4-33 to 4-34, in Appendix 4)*

Table 5-8 shows a similar trend of the gradual decrease in adsorption capacity (mg g^{-1}) and a gradual increase in removal efficiency (%) with increasing the adsorbent dose from 0.01 g to 0.05 g, as observed earlier for metal ion adsorption on the CH/HAp composites (see section 5.1.1.1). These trends could be attributed to similar reasons as described in earlier sections of similar batch experiments. The CH/bHAp/CF composite showed a better removal of metal ions at the equilibrium time (after 2 h) than the CH/cHAp/CF composite under the same conditions.

Table 5-8: The effect of the adsorbent dose on the removal efficiency (%) and adsorption capacity (mg g^{-1}) of the CH/HAp/CF composites for the adsorption of metal ions from single-metal ion type solutions

The effect of the adsorbent dose on removal (%) of metal ions using the CH/HAp/CF composites						
	Dose (g)	0.01	0.02	0.03	0.04	0.05
CH/cHAp/CF	Cd^{2+}	32.14	58.35	74.12	83.93	91.64
	Pb^{2+}	59.50	90.51	95.84	97.00	98.02
	Cu^{2+}	29.67	52.81	73.77	87.15	94.11
	Cr (as chromate ions)	25.87	26.53	27.08	27.62	28.22
CH/bHAp/CF	Cd^{2+}	34.03	60.54	78.84	89.98	94.59
	Pb^{2+}	70.28	96.31	97.90	97.98	98.36
	Cu^{2+}	32.26	64.17	90.69	95.04	96.27
	Cr (as chromate ions)	21.12	21.76	22.27	22.86	23.35
The effect of the adsorbent dose on the adsorption capacity (in mg g^{-1}) of the CH/HAp/CF composites with respect to the metal ions adsorbed						
CH/cHAp/CF	Cd^{2+}	16.07	14.59	12.35	10.49	9.16
	Pb^{2+}	59.50	45.25	31.95	24.25	19.60
	Cu^{2+}	14.83	13.20	12.29	10.89	9.41
	Cr (as chromate ions)	25.87	13.27	9.03	6.90	5.64
CH/bHAp/CF	Cd^{2+}	17.01	15.14	13.14	11.25	9.46
	Pb^{2+}	70.28	48.15	32.63	24.50	19.67
	Cu^{2+}	16.13	16.04	15.12	11.88	9.63
	Cr (as chromate ions)	21.12	10.88	7.42	5.71	4.67

The maximum adsorption "q_e" in mg g^{-1} of Cd^{2+} using the CH/HAp/CF composites was 16-17 mg g^{-1} for a 0.01 g adsorbent dose. At equilibrium, the % removal of Cd^{2+} and Cu^{2+} ranged from 91-96%. In comparison, the % removal of Pb^{2+} was > 98% for a 0.05 g dose of the CH/HAp/CF composites showing a better removal of Pb^{2+} than the other two metal cations studied, which agrees with the observations recorded earlier for the CH/HAp composite system.

Moreover, the Pb^{2+} removal (%) is higher for the CH/bHAp/CF composite (about 20% more) than the CH/cHAp/CF composite at a lower adsorbent dose (0.01g). The removal efficiency of Pb^{2+} plateaued for doses $\geq$ 0.03 g for both the composites. Hence, the optimum dose for realizing the maximum removal (%) was 0.03 g, which achieved more than 98% Pb^{2+} removal for the CH/HAp/CF composites. The higher removal efficiencies for Pb^{2+} were attained on the CH/bHAp/CF composite at 0.01 g to 0.04 g of adsorbent doses and attributed to its relatively higher surface area than CH/cHAp/CF. Both the composites performed equally well in Pb^{2+} removal (%) when the dose was 0.05 g which was attributed to the excess of adsorption sites available at the higher dose (0.05 g) for adsorption of available metal ions.

The different removal efficiency percentage shown by the CH/cHAp/CF composite for cation adsorption relative to the CH/bHAp/CF composite could be due to their specific surface area (estimated using Mastersizer analysis as described in section 5.1.1 and results included in appendix 3, Figure 3C & 3D). The estimated specific surface area of the CH/bHAp/CF composite was found to be higher (39.13 m^2 kg^{-1}) than that of the CH/cHAp/CF composite (28.83 m^2 kg^{-1}), consequently showing a better removal efficiency. However, as forewarned earlier, the Mastersizer estimation of the specific surface area is approximate due to several factors such as the heterogeneity of composites and the dissolution or detachment of components (such as CF dust) making up the composites. Similarly, the difference in the removal efficiency of the two composites could only be due to the heterogeneity of the sample particles. The CH/HAp/CF composite could not be ground well due to the presence of the coir fibre. This limitation of processing may have resulted in a range of particle sizes (and ultimately a range of values for the specific surface area) in the adsorbent dose exposed to the metal ion solutions so that it may cause variations in the removal efficiencies.

It has been mentioned in Chapter 1 that the addition of HAp could enhance the removal ability of the coir fibre-based composites if the fibres were the sole component of the adsorbent. The ability of the CH/HAp/CF composite to adsorb Cd^{2+} ions from solution was compared with the Cd^{2+} adsorption ability of natural CF as discussed in a literature study[520]. The composite removal efficiency recorded in the present study was found to be higher than the raw coir fibre (literature study[520]), as the reported maximum adsorption of Cd^{2+} on natural CF[520] was relatively low (0.096 mg g^{-1}) when it was used in adsorbent

doses of 0 to 5 g. However, in the present study, the adsorption of Cd^{2+} on the CH/HAp/CF composites was 16-17 mg g^{-1} for the same adsorbent dose, so it was significantly enhanced. The maximum removal efficiency of 84 % was reported for the raw coir fibre in the mentioned literature study, while the present study showed >90% adsorption of Cd^{2+} ions. Further, raw lignocellulosic fibres such as bagasse, coconut fibre, kenaf bast and spruce showed maximum adsorption values for Cu^{2+} ranging from 0.03 to 0.61 mg g^{-1} at an initial concentration of 10 ppm and an adsorbent dose of 0.5 g. The addition of HAp into raw fibre to form the composites (as CH/HAp/CF in the present study) could efficiently remove the Cu^{2+} ions, which is evident by the present study's findings (see Table 5-8). This better removal (%) could be attributed to the presence of hydroxyapatite in CH/HAp/CF composites, which could enable an ion exchange between Ca^{2+} and metal cations [128] in the CH/HAp/CF composites to remove metal cations.

Apart from the ion-exchange mechanism on the part of HAp of the CH/HAp/CF composites, the literature studies on lignocellulosic fibre (such as coir fibre) and hydroxyapatite-based adsorbents also have cited several mechanisms for explaining cations (e.g. Pb^{2+} & Cd^{2+}) uptake on these adsorbents[352,483,484,521]. The chitosan and CF are carbonaceous materials containing the ligand atom containing functional groups, which could be mainly involved in the metal-ligand complexation. However, the spectroscopic characterisation of these composites (section 3.4.2) indicated the dominance of HAp in this composite system. Additionally, the literature reported HAp could perform more efficiently than chitosan and CF, which remove metal by ion-exchange mechanism (see section 1.5.1.4). So, the ion-exchange mechanism could be considered to be the leading mechanism for the removal of Pb^{2+} ions in this experiment. Overall, the constitutional functional groups of CH/HAp/CF composites (FTIR analysis of CH/HAp/CF composites, Table 3-2, chapter 3) act as binding sites for metal ions removal by these removal mechanisms[352,483,484].

Table 5-8 also summarises the effect of adsorbent doses for chromate ion adsorption and removal on the CH/cHAp/CF and the CH/bHAp/CF composites. A gradual increase in removal efficiency was noted and was attributed expectedly to the availability of more adsorbent surface area for the uptake of chromate ions. However, it was noted that the maximum removal (%) was less than 30% for both the composites in solutions containing the maximum adsorbent dose of 0.05 g. Contrary to this, a similar (0.05 g) doses, the

composites were found to achieve at least >80% removal of the cations from those solutions (see earlier discussion on this). This observation of relatively low chromate ion removal (%) relative to cation removal (i.e., Cu^{2+}, Pb^{2+} and Cd^{2+}) on the CH/HAp/CF composites agrees with the observations recorded earlier for chromate ion removal by the control composite system (see section 5.1.1.1).

The removal efficiency (%) of CH/HAp/CF composites with respect to chromate ion increased by only 2-3% with an increase in adsorbent dose from 0.01 g to 0.05 g. The main reason why chromate removal by this composite system was so low could be due to the chemical speciation of the chromate metal ion in solution, which has been discussed in detail in the section on the CH/HAp composites. As described earlier in section 5.1.1, chromium (VI) is usually found in aquatic solution[522] in the form of $HCrO_4^-$ and $Cr_2O_7^{2-}$ at pH > 4.0, which makes its adsorption difficult on negatively charged active sites of the CH/HAp/CF composites, such as $-OH^-$, $-COO^-$, and $-PO_4^{3-}$. The acidic conditions (pH <5.0) usually promote the removal of Cr as chromate ions by adsorption or reduction in the presence of reducing agents such as nitrogenous compounds present in chitosan, as described earlier in section 1.6.2.

Moreover, the protonation of NH_2 groups (to form NH_3^+) and HAp disintegrated surface functional groups (HPO_4Ca^+ and OH_2^+) could also participate in CrO_4^{2-} ion removal via electrostatic attractions (as described in equation 5-4) at low pH (<5.0) range[523] and by opening up the surface. In the pH range of this batch experiment (4.0-6.0), the CH/HAp/CF composites could remove chromate ions using both mentioned mechanisms (electrostatic interactions and reduction of chromate ions to Cr (III)). The CH/cHAp/CF composite was found to be more efficient than the CH/bHAp/CF composite in removing chromate ions, which aligns with the observations recorded earlier for the removal of chromate ions using the CH/HAp (control) composites (section 5.1.1.1) and could be attributed to the similar reason as described earlier relating to the higher solubility of the CH/cHAp/CF composite relative to the CH/bHAp/CF composite which may facilitate adsorption/exchange of chromate anions. The dissolution of cHAp (as described in a literature study[524]) in cHAp-based composites (like CH/cHAp and CH/cHAp/CF) can provide the disintegrated and more accessible surface PO^- groups which are protonated at acidic pH <4.0 to form POH groups at the adsorbent surface. This could result in the formation of metal complexes with chromate anions, as described by Kousalya et al.[502].

Relatively better adsorption of chromate ions observed on the CH/cHAp/CF composites relative to the CH/bHAp/CF composites is aligned with the observations recorded earlier for chromate adsorption on the CH/HAp (control) composites.

5.1.2.2 Effect of solution pH on metal ions removal by the CH/HAp/CF composites

Experimental: In this experiment, the effect of pH on metal ion adsorption on the CH/HAp/CF composites was examined via AAS measurements using different experimental conditions for different metal ions.

Like the control composite systems, only a restricted pH range from 4.0 -5.8 was used for the Pb^{2+} adsorption because of the already mentioned (section 5.1.1.2) risk of precipitation of Pb^{2+} ion as $Pb(OH)_2$ at pH > 5.5. The solution concentration of Pb^{2+} was initially 20 ppm, and the adsorbent dose of the CH/HAp/CF composites sample was 0.01 g. The effect of pH on Cu^{2+} ion and Cd^{2+} ion removal by the CH/HAp/CF composites was studied at pH ranges 4 - 6.5 and 4.0-8.0, respectively. The initial Cu^{2+} and Cd^{2+} ion concentration in solutions exposed to adsorbent was 25 ppm (for both), and the adsorbent dose was 0.05 g for Cu^{2+} and 0.01 g for Cd^{2+}. A narrow pH range for Cu^{2+} adsorption was selected due to its risk of precipitation and forming copper hydroxide[488], which is usually reported to occur in the pH range 7-12. The influence of pH on the adsorption of chromate ion on the CH/HAp/CF composites was studied over the pH range 4.0-8.5 using the solution with an initial chromate ion concentration of 5.0 ppm, which was exposed to constant adsorbent dose samples of 0.01 g.

Results: Table 5-9 *(Figure 4-37 to 4-40, Appendix 4)* demonstrates a similar trend for the effect of pH on Cd^{2+}, Pb^{2+} and Cu^{2+} adsorption as described earlier in the control composites (section 5.1.1.2).

For instance, the maximum adsorption values (15.20 mg g^{-1} and 21.87 mg g^{-1} of Cd^{2+} for the CH/cHAp/CF composite and CH/bHAp/CF, respectively) were recorded at pH 7.0. Adsorption of Pb^{2+} ions was at a maximum at pH 4.0 and 5.0, decreased slightly at >5.0 and increased again when solution pH was > 5.6, while the Cu^{2+} ion adsorption was not greatly affected by the changing of pH in the solution from 4.0 to 6.5 in both the composites.

Table 5-9: The effect of the solution pH on the adsorption capacity (in mg g^{-1}) of the CH/HAp/CF composites for the adsorption of metal ions from solutions containing only one type of metal ion

	pH	**4.0**	**5.0**	**6.0**	**7.0**	**8.0**
Cd^{2+}	CH/cHAp/CF	7.68	13.79	15.01	15.21	14.91
	CH/bHAp/CF	19.04	20.73	21.28	21.87	21.66
	pH	**4.5**	**5.0**	**5.5**	**6.0**	**6.5**
Pb^{2+}	CH/cHAp/CF	36.04	36.01	33.70	34.04	36.75
	CH/bHAp/CF	38.21	38.12	35.85	37.25	37.65
	pH	**4**	**5**	**5.5**	**6**	**6.5**
Cu^{2+}	CH/cHAp/CF	9.34	9.33	9.31	9.48	9.48
	CH/bHAp/CF	9.61	9.64	9.57	9.60	9.61
	pH	**4.5-5**	**5-5.5**	**6-6.5**	**7-7.5**	**8-8.5**
Cr as chromate ions	CH/cHAp/CF	0.81	0.77	0.70	0.45	0.42
	CH/bHAp/CF	0.59	0.57	0.52	0.36	0.33

As described in the control composites systems (section 5.1.1.2), the charges on functional groups (binding sites of adsorbents) are affected by the change in the pH of the metal ion solution and control the adsorption of the metal ions on the adsorbents. A literature study dealing with a carbon/hydroxyapatite composite system reported the ionization of the functional groups on the composite at pH > 2.5, which provided negatively charged hydroxyl and phosphates groups on the carbon-based/hydroxyapatite composite for binding metal ions. Another study reported the deprotonation of carboxylic groups ($-COO^-$) at pH > 4.0 on agricultural-based adsorbent surfaces[525-527]. The principal binding sites (functional groups) of the CH/HAp part of the CH/HAp/CF composites, including the hydroxyl, amino, phosphates groups and additionally the carbonyl groups of the CF, could be protonated at lower (acidic) pH and could result in a decrease in the adsorption of metal cations at lower pH values[233,495].

Contrary to this, the lower concentration of protons that would have competed with cations at a higher (less acidic to neutral) pH range resulted in more adsorption of these ions on binding sites of the CH/HAp/CF composites[528,529] (such as $-NH_2$, -C=O, $-PO_4^{3-}$ and -OH groups). The literature study[498] indicated that a pH > 6.3 is ideal due to the existence of more negative charges at this pH on metal adsorption groups (-OH) on adsorbents (such as chitosan and HAp) which attract cations for adsorption[498]. Further, the literature studies, including Cd^{2+} adsorption on CF[530], carboxymethyl chitosan/HAp composite[531] and CF-based composites[532], reported an optimum pH range of 5-7 for optimal Cd^{2+} adsorption on such composite systems. Based on literature reports dealing

with similar adsorption systems of CF and chitosan[530,531] and as indicated in the results of this study (Table 5-9), a pH range of 5-7 was considered to be optimum for Cd^{2+} adsorption.

In contrast to Cd^{2+} ions, a decrease in Pb^{2+} adsorption over the pH range of 5.0 <pH <5.5 could be due to a relative decrease[533] in free Pb^{2+} ions to adsorb on binding sites, as a literature study reported a decline in Pb^{2+} species in solution at pH > 5.0. An increase in Pb^{2+} removal at pH greater than 5.6 could be attributed to Pb^{2+} conversion into lead hydroxyl species such as $Pb(OH)^{+}$, $Pb_3(OH)_4^{2+}$, $Pb(OH)_2$ etc., as milkiness in the Pb^{2+} solution was observed in the present study when pH rose above 5.5. The presence of hydrolysed lead species in solution[486] such as $Pb(OH)^{+}$, $Pb_3(OH)_4^{2+}$ and $Pb(OH)_2$ (aq) has been reported to increase continually at pH > 6.0. Pb^{2+} as the dominant chemical species present in solution[533] under pH 5.0, is available for adsorption on the negatively charged ionic species by electrostatic interactions. Hence a pH range of 4.0 to 5.0 indicated better adsorption of Pb^{2+} cations on the CH/HAp/CF composites due to the presence of negatively charged active sites (phosphates, hydroxyl and carboxylic groups) as supported by the literature[467,525,526].

The optimum pH range for Cu^{2+} adsorption on CH/HAp/CF composites was hence taken as 4-6. The literature also reported that pH 4.0-6.0 was an optimum pH range for removing Cu^{2+} from solution on lignocellulosic fibre-based adsorbents[534,535].

In contrast with the cationic species, Table 5-9 also presents the AAS data showing the effect of initial solution pH in chromate (an anionic species) solutions exposed to 0.01 g of adsorbent doses of the CH/HAp/CF composites on chromate ion adsorption on the composites. Overall, the observations recorded for the effect of the pH on the chromate ion adsorption on the CH/HAp/CF composites align with the observation recorded earlier for the removal of the chromate ions on the CH/HAp (control) composites 5.1.1.2 indicating that the acidic/low pH favours chromate ion adsorption on such composite system as evident from *Figure 4-40* (*Appendix 4*). Similar reasons described earlier (section 5.1.1.2) for the better adsorption of the chromate ions in the acidic conditions could be considered for this system as well, particularly on the CH/HAp part of the 3 component composites. Additionally, the functional groups of the CF become protonated under acidic conditions to provide the binding sites for the adsorption of the chromate anions. The trend of better chromate ion adsorption on low pH values (<5.0) agrees with

other published studies for the adsorption of chromate ions on coir fibre, activated carbons or chitosan-based composite systems[310,501,536]. A continuous decrease in chromate ion adsorption[213] was reported on coconut fibre/pith and activated carbons of coconut shells for a pH range of 2.0-10.0.

5.1.2.3 Effect of the initial metal ion concentration on metal ions removal by the CH/HAp/CF composites

Experimental: Initial Cd^{2+} concentration was varied between 5 ppm and 25 ppm for a constant adsorbent dose of 0.01g. In contrast, the initial solution pH was kept at 6-6.5 for evaluating the effect of initial sorbate concentration in the solution on metal ion removal. The effect of initial Pb^{2+} ion concentration on the removal and adsorption of Pb^{2+} on the CH/HAp/CF composites was recorded for a range of concentrations from 10 ppm to 50 ppm. In comparison, similar recordings for Cu^{2+} adsorption were done by exposing a constant amount of adsorbent (0.01 g) to Cu^{2+} solutions of different initial concentrations between 5 ppm and 25 ppm Cu^{2+} at an initial solution pH 4.5-5.0. Similarly, this effect on chromate ion adsorption and removal (%) using CH/HAp/CF composites was measured by changing the chromate ion concentration from 10 ppm to 50 ppm, at an initial adsorbent dose of 0.01 g and pH 5.0-6.5.

Further, the data recorded using AAS in these experiments were used to study the adsorption mechanism (in an upcoming section) by fitting the same adsorption models (Langmuir and Freundlich) as applied earlier in the control composites by using the non-linear regression method (see appendix 1, section 1.3) as used for the metal ion adsorption data recorded for the control composites. An additional method of the SNE (*Appendix 1.3B*) was applied to the Cd^{2+} and Pb^{2+} ion adsorption modelling as done for the control composites.

Results: Table 5-10 shows the effect of the initial metal ion concentration on metal ion adsorption studied on the CH/HAp/CF composites and also presented in *Figures 4-41 to 4-44* (*Appendix 4*). A similar trend (as observed earlier in the control composites) of a gradual decrease in removal efficiency and increased adsorption capacity, with increasing metal ion concentration from 5 ppm to 25 ppm, was observed. Moreover, these trends could be attributed to similar reasons as mentioned earlier in the control composites section. This trend also agrees with the literature studies, which reported a similar

tendency for the effect of initial metal ion concentration in solution on metal ion adsorption[119,537-539].

Table 5-10: The effect of the initial metal ion concentration on removal (%) and the adsorption capacity (in mg g^{-1}) of different metal ions adsorbed on the CH/HAp/CF composites from a single-metal ion type solution system

The removal (%) of metal ions using the CH/HAp/CF composites						
	Metal ion concentrations (ppm)	5	10	15	20	25
Cd^{2+}	CH/cHAp/CF	69.07	62.55	50.60	39.28	32.49
	CH/bHAp/CF	86.71	71.63	61.36	47.59	39.59
Pb^{2+}	Metal ion concentrations (ppm)	10	20	30	40	50
	CH/cHAp/CF	90.04	89.91	83.84	70.36	56.85
	CH/bHAp/CF	93.26	94.51	94.65	90.22	75.51
Cu^{2+}	Metal ion concentrations (ppm)	5	10	15	20	25
	CH/cHAp/CF	61.38	46.17	38.70	32.36	26.91
	CH/bHAp/CF	74.27	67.92	52.37	39.94	32.36
Cr as chromate ions	Metal ion concentrations (ppm)	10	20	30	40	50
	CH/cHAp/CF	28.55	24.33	20.23	20.08	17.84
	CH/bHAp/CF	20.00	19.28	18.96	18.24	15.60
The adsorption capacity (in mg g^{-1}) of the CH/HAp/CF composites or different metal ions						
	Metal ion concentrations (ppm)	5	10	15	20	25
Cd^{2+}	CH/cHAp/CF	6.91	12.51	15.18	15.71	16.24
	CH/bHAp/CF	8.67	14.33	18.41	19.03	19.79
Pb^{2+}	Metal ion concentrations (ppm)	10	20	30	40	50
	CH/cHAp/CF	18.01	35.96	50.30	56.28	56.85
	CH/bHAp/CF	18.65	37.80	56.79	72.17	75.51
Cu^{2+}	Metal ion concentrations (ppm)	5	10	15	20	25
	CH/cHAp/CF	6.14	9.23	11.61	12.94	13.45
	CH/bHAp/CF	7.43	13.58	15.71	15.98	16.18
Cr as chromate ions	Metal ion concentrations (ppm)	10	20	30	40	50
	CH/cHAp/CF	5.71	9.73	12.14	16.07	17.84
	CH/bHAp/CF	4.00	7.71	11.37	14.59	15.60

The maximum adsorption of Cd^{2+} ions ranged from 16.24 mg g^{-1} to 19.79 mg g-1 for the CH/HAp/CF composites. The maximum adsorption of Cu^{2+} (at an initial ion concentration of 25 ppm) was 13.45 mg g^{-1} and 16.18 mg g^{-1} on the CH/cHAp/CF composite and the CH/bHAp/CF composite, respectively. The maximum adsorption of Pb^{2+} was recorded at 50 ppm, which was 56.85 mg $g^{-1}$and 75.51 mg g^{-1} on the

CH/cHAp/CF composite and the CH/bHAp/CF composites, respectively. At the same time, the highest removal (%) >90% was recorded at 10 ppm initial Pb^{2+} concentration for both the composites.

It was revealed that the CH/bHAp/CF composite exhibited a better removal efficiency relative to the CH/cHAp/CF composite (Table 5-10). The difference between the removal efficiency of the two composites for similar metal ion concentrations could again be attributed to the high specific surface area of the CH/bHAp/CF composite relative to that of the CH/cHAp/CF composite. The higher surface area could assist the CH/bHAp/CF composite in metal removal mechanisms such as ion exchange, metal-complexation, or electrostatic interactions by providing active sites. Another reason for this could be the availability of more HAp in CH/bHAp composites than CH/cHAp composites, as indicated by the TGA analysis of the CH/HAp/CF composites. The higher availability of the HAp constant in the CH/bHAp/CF than CH/cHAp/CF could have also participated in its better removal efficiency. A third reason could simply be the heterogeneity of the particles in the sample (dose) exposed to the metal ions solutions, which could affect the removal efficiency by offering more available surface area for the adsorption of the metal ions.

Along with the ion-exchange possibility of Ca^{2+} (from HAp) with these metal cations in solution, as a possible metal adsorption mechanism occurring on the CH/HAp/CF composites, the literature studies also state that Cd^{2+} adsorption on CF[530] itself, on carboxymethyl chitosan/HAp composite[531] and other CF-based composites[532] utilise COO^- (from lignocellulosic and cellulosic components) as one of the fundamental functional groups to remove metal ions via metal-ligand complexation[530,531]. So, the mechanisms which could be considered for the removal of the metal cations using the CH/HAp/CF composites include the ion-exchange (mainly on the part of HAp) and metal-ligand complexation involving the electron-donating ligand atoms such as N and O, present in the functional groups (such as amino- hydroxyl and carboxyl) of the other composite components (chitosan and CF) of the system. Similarly, the literature describes Pb^{2+} adsorption on lignocellulosic[540,541], biopolymeric, and hydroxyapatite-based composites[352,483,484] as complex processes involving several metal-binding ligands (amino, hydroxyl and carboxyl groups) to chelate metal ions. Several mechanisms simultaneously assist Pb^{2+} removal from solution on such complex adsorption systems

[352,483,484]. In the present study, adsorption models were fitted to the experimental data to ascertain the best-fit model for describing the adsorption of Pb^{2+} on the CH/HAp/CF composites, as shown in the following section.

An irregular trend of difference in removal efficiencies (%) was observed in the case of the metal cation adsorption on both the CH/HAp/CF composites (see Table 5-10). These irregular results seen in the removal efficiencies shown by the two composites (i.e. the CH/cHAp/CF and the CH/bHAp/CF composites) could be attributed to the highly heterogeneous nature of the composites, which are made up of different sizes and types of particle such as coir fibre dust, homogenised chitosan/HAp matrices, a matrix of chitosan and HAp filled with coir fibre dust etc.

In Table 5-10, the maximum adsorption of 15-18 mg g^{-1} for both the composites was measured at 50 ppm concentration of chromate ions in solution. The maximum removal (%) of chromate ions was measured at 10 ppm concentration and ranged between 20 to 28% for both the composites. The CH/cHAp/CF composite was relatively more efficient at removing chromate ions than the CH/bHAp/CF composite by showing better adsorption and removal of chromate ions for all concentrations. This finding aligns with the observation recorded in earlier batch experiments of the CH/HAp/CF composites and agrees with the observations recorded for chromate adsorption on the control composites. To understand the removal mechanism and estimate the maximum adsorption capacity of this composites system, the AAS data collected in this experiment was further analysed using adsorption models as has been done in other systems.

5.1.2.4 Adsorption modelling of the CH/HAp/CF composites for the adsorption of metal ions

Experimental: The adsorption data presented in the above batch experiment was gathered to study the adsorption mechanism occurring on the CH/HAp/CF composites using adsorption isotherms. The experimental results of cation adsorption on CH/HAp/CF composites were tested against non-linear Langmuir and Freundlich isotherms *(Figures 4-45 to 4-50, Appendix 4)*, while linearised models were used for the chromate adsorption modelling *(Figures 4-51 and 4-52, Appendix 4)*. Each isotherm parameter was calculated in Microsoft Excel using the non-linear regression method employed in earlier section 5.1 (control composites).

Results: The best-fitted model was then decided from the comparison of the R^2 values from two fitted models. The calculated parameters of the adsorption models are given in Table 5-11.

Table 5-11: Adsorption isotherm parameters for metal ions (Cd^{2+}, Pb^{2+} and Cu^{2+} and chromate ions) adsorption on the CH/HAp/CF composites

Adsorption models		**Langmuir**				**Freundlich**		
Metal ions	Composites	q_{max} (mg g^{-1})	K_L	R^2	R_L	1/n	K_F (mg g^{-1})	R^2
Cd^{2+}	CH/cHAp/CF	19.57	0.38	0.96	0.62	0.32	7.06	0.85
	CH/bHAp/CF	20.66	1.04	0.98	0.50	0.25	10.48	0.93
Pb^{2+}	CH/cHAp/CF	66.10	0.47	0.95	0.68	0.26	39.42	0.81
	CH/bHAp/CF	89.85	0.72	0.89	0.60	0.29	27.73	0.72
Cu^{2+}	CH/cHAp/CF	15.95	0.29	0.99	0.16	2.93	5.20	0.98
	CH/bHAp/CF	18.55	0.60	0.94	0.09	4.32	9.02	0.79
Chromate ions	CH/cHAp/CF	29.41	0.03	0.99	0.42	1.59	0.66	0.99
	CH/bHAp/CF	72.46	0.01	1.00	0.76	0.71	0.85	0.99

The comparison of R^2 values obtained after fitting the non-linear Langmuir and Freundlich models to data revealed that the Langmuir isotherm model was the best-fitted model for explaining the adsorption of all four metal ions studied on the CH/HAp/CF composites with R^2 at least > 0.94 indicating the goodness of fit. The fitting of the Langmuir isotherm model to the experimental data for metal ion adsorption on the CH/HAp/CF composites agrees with the modelling done for these metal ion adsorptions on the CH/HAp (control composites) and also is in accord with similar systems described earlier in the literature (Table 1-8).

The Langmuir isotherm model fitted to the metal ion adsorption data for both the composites (i.e. the CH/cHAp/CF and CH/bHAp/CF composites) suggested a monolayer adsorption model for metal ions on a homogeneous adsorbent surface[494]. Using the Langmuir model, the calculated q_{max} (in mg g^{-1}) of Cd^{2+} was 19.57 mg g^{-1} and 20.66 mg g^{-1} on the CH/cHAp/CF and CH/bHAp/CF composites, respectively. The maximum adsorption capacity (q_{max} mg g^{-1}) estimated for Pb^{2+} adsorption on the CH/cHAp/CF composite and the CH/bHAp/CF composite were 66.097 mg g^{-1} and 89.85 mg g^{-1}, respectively, and Cu^{2+} adsorption was 15.95 mg g^{-1} and 18.55 mg g^{-1}. The value of K_L (Langmuir constant associated with the affinity of sorbate towards adsorbent) is relatively higher for the CH/bHAp/CF composite than for the CH/cHAp/CF composite (see Table 5-11). As described earlier in Chapter 1(section 1.10.1), the K_L relates the free adsorption energy and affinity for spontaneous adsorption of sorbate on the adsorbent surface as

mentioned in literature[542]. The higher value of K_L for the CH/bHAp/CF composite represents a better affinity exhibited by cations (due to higher free adsorption energy) towards the CH/bHAp/CF composite than for the CH/cHAp/CF composite. The values of the dimensionless factor R_L (calculated using equation 5-6) for metal ion adsorption on CH/HAp/CF composites given in Table 5-11 also indicated a favourable adsorption process as $0 < R_L < 1$.

The literature supports the fitting of the Langmuir on these systems, assuming a homogenous surface (Langmuir assumption) on these composites when observed as macroscopic levels. Further, the fitting of the Langmuir on similar heterogeneous-appearing systems also supports this model fitting to describe the Cd^{2+} adsorption.

In a published study[543], an adsorbent system (similar to CF) of lignocellulosic mass (from a camphor tree) reported that Cd^{2+} adsorption was modelled to be Langmuirian in nature. It calculated a q_{max} value of 10.99 mg g^{-1} as the maximum adsorption capacity. It suggested that surface complexation of metal ions, forming a metal-ligand complex with a functional group such as carbonyl as the primary adsorption mechanism[543] for uptake of Cd^{2+}. Another study[306] reported the Langmuir isotherm as the best-fitted model to describe the Cd^{2+} ion adsorption on coir fibre itself. It estimated a value of 5.29 mg g^{-1} for the maximum adsorption capacity for Cd^{2+} adsorption[306]. These two literature studies[543,306] agree with the findings of the present study, as Langmuirian behaviour was found to be the best-fitted model for describing Cd^{2+} adsorption on coir fibre-based adsorbents. In another literature study[544], the estimated adsorption capacity of CF for Pb^{2+} was 48.84 mg g^{-1} (at pH 4.5) calculated using the Langmuir isotherm model[544]. Similarly, the maximum adsorption capacity (mg g^{-1}) of raw coir fibre and alkali-treated coir fibre for Cu^{2+} to be 2.77 mg g^{-1} and 9.43 mg g^{-1}, respectively[545].

In contrast, the estimated maximum adsorption capacity q_{max} (mg g^{-1}) of CH/HAp/CF composites for these metal ions adsorption is higher (Table 5-11) than the estimated value calculated using the Langmuir isotherm model for CF in the mentioned literature studies (mentioned above), which confirms the hypothesis of more efficient metal cation adsorption occurring on the CH/HAp/CF composites system (present study) than raw CF (literature), and very likely attributed to the presence of HAp in the CH/HAp/CF composites, which helps to increase the adsorption capacities of the CH/HAp/CF

composites by providing an additional metal removal mechanism (ion-exchange as mentioned in chapter 1, (section 1.5.1.4).

Additionally, the q_{max} of Pb^{2+} ions (Table 5-11) is higher than the q_{max} estimated for the Cd^{2+} ions (Table 5-11) on the CH/HAp/CF composites. It indicated that the CH/HAp/CF is more efficient at removing the Pb^{2+} ions than the Cd^{2+} ions. The better removal of the Pb^{2+} ions than Cd^{2+} ions could be due to better removal of Pb^{2+} on the HAp part of the composite due to physiochemical characters of the $Pb^{2+,}$ which favours its adsorption on these composites than other cations as described earlier in section 5.1.1. This better adsorption of Pb^{2+} than Cd^{2+} on the CH/HAp/CF composites observed in a single metal ion type system would be explored further in a later section (competitive adsorption system (containing two metal ion types) for the CH/HAp/CF composites) to confirm the findings of the literature and the CH/HAp (control) composites of this study.

As mentioned above and in the control composites sections, the linearised models were used for the chromate adsorption modelling using the composites systems studied. The following Table presents the linearized Langmuir and Freundlich equation calculated using linear fitting of Langmuir and Freundlich isotherms on Microsoft Excel for chromate ion adsorption on the CH/HAp/CF composites. The equations generated from these fits using Microsoft Excel are given as follows:

Table 5-12: The linearized equations calculated for chromate ion adsorption on the CH/HAp/CF composites using linearized Langmuir and Freundlich isotherms

Composites	Linearized Langmuir Equation	Linearized Freundlich Equation
CH/cHAp/CF	y = 1.0176x+ 0.034 (R^2= 0.9936)	y = 0.6558x + 0.462 (R^2= 0.9978)
CH/bHAp/CF	y = 1.8822x+ 0.0138 (R^2= 0.9978)	y = 0.8519x - 0.346 (R^2= 0.986)

Hence using the above equations, the Langmuir and Freundlich adsorption isotherm parameters were calculated as described earlier in section 5.1.1.4.

The calculated parameters for the systems tested and derived from both the adsorption models are thus given in Table 5-11. The comparison of R^2 values of both adsorption models reveals that both the Freundlich and Langmuir adsorption isotherms were found to fit the data and suggested that the adsorption of chromate ion was occurring on a surface of heterogeneous nature. Though the Langmuir model R^2 values are relatively higher than

the Freundlich (Table 5-11) for CH/HAp/CF composites, the Freundlich model also shows a good fit with R^2 values of >0.98 being obtained from fits to data.

The maximum adsorption capacity (mg g^{-1}) of the CH/cHAp/CF composite and the CH/bHAp/CF composite for chromate ion adsorption, as estimated by the Langmuir isotherm model, is 29.41 mg g^{-1} and 72.46 mg g^{-1}, respectively, which is showing a different trend from the experimental values of chromate ion adsorption on CH/HAp/CF composites. Experimental values of adsorption (mg g^{-1}) show higher chromate ion adsorption on the CH/cHAp/CF composite than CH/bHAp/CF. The dimensionless factor R_L of Langmuir isotherm also showed favourable adsorption of chromate ions on both the composites as $0 < R_L < 1$.

The value of the Freundlich isotherm parameter "1/n" lies between 0 and 1, indicating favourable adsorption of chromate ions on both the composites. The 1/n factor of Freundlich isotherm is also used to describe the heterogeneity of the adsorption process in literature[546,547].

If the value of 1/n is higher for one adsorbent than the other, it means the adsorption is occurring on a more heterogeneous surface[547]. For chromate ion adsorption on the CH/HAp/CF composites, the value of 1/n is higher for the CH/bHAp/CF composite than for the CH/cHAp/CF, implying that the chromate ion adsorption is occurring on a more heterogeneous surface of the CH/bHAp/CF composite than CH/cHAp/CF. The value of K_F (Freundlich constant), which is used to estimate adsorption capacity (mg g^{-1})[347], is higher for the CH/cHAp/CF composite than for the CH/bHAp/CF composite, which agrees with the experimental observation of this batch experiment. It means the extent of adsorption is higher on CH/cHAp/CF composite than CH/bHAp/CF.

Based on the calculated parameters for the Langmuir and Freundlich isotherms, the Freundlich isotherm lies closer to the experimental observations of chromate ion adsorption on the CH/HAp/CF composites. It could be used to describe the adsorption of chromate ions in this system.

Parab et al. reported[232] the Langmuir isotherm model as the best-fitted model to describe the Cr(VI) adsorption on coir pith[232]. Using the Langmuir isotherm model, they estimated a maximum adsorption capacity (mg g^{-1}) of 11.56 mg g^{-1}. In the present study, the estimated value of chromate ion adsorption on the CH/HAp/CF composites ranges from 29-72 mg g^{-1} composite, which is higher than the estimated value of chromate ion

adsorption on raw coir pith, indicating that the coconut fibre materials adsorption capacity for chromate ion adsorption could be improved by making a composite with HAp, as is evident from the batch experiments mentioned above for chromate ion adsorption on the CH/HAp/CF composites.

5.1.2.5 Comparison of the maximum adsorption capacities of the CH/HAp/CF composites and CH/HAp (control composites) for metal ion adsorption as estimated by the Langmuir isotherm model

The comparison of the maximum adsorption capacities (q_{max} in mg g^{-1}) of the control and CH/HAp/CF composites, estimated by Langmuir for metal ion adsorption studied, is presented in Table 5-13.

Table 5-13: Comparison of adsorption capacities (q_{max} mg g^{-1}) of the CH/HAp (control) and CH/HAp/CF composites as estimated by the Langmuir isotherm model

Composites	Cd^{2+}	Pb^{2+}	Cu^{2+}	Chromate ions
CH/cHAp	24.33	52.42	15.91	45.04
CH/bHAp	33.93	90.13	23.67	34.72
CH/cHAp/CF	19.57	66.097	15.95	29.41
CH/bHAp/CF	20.66	89.85	18.55	72.46

Cd^{2}: The maximum adsorption capacity (q_{max} mg g^{-1} of Cd^{2+}) on the CH/HAp composites (control composites) ranges from 24.33 mg g^{-1} (CH/cHAp) to 33.93 mg g^{-1}, which is higher than the estimated value of Cd^{2+} adsorption on the CH/HAp/CF composites. It indicates the reduction in estimated adsorption capacity (q_{max}) of the CH/HAp composites after the addition of CF. There is a possibility that coir fibre blocks the HAp sites on the composites as a possible reason for the decrease in removal efficiency.

Pb^{2+}: The estimated maximum adsorption capacity (q_{max} in mg g^{-1}) of Pb^{2+} on the CH/cHAp (control) is 52.42 mg $g^{-1,}$ and it increased to 66.097 mg g^{-1} on the CH/cHAp/CF. It showed an improvement in the adsorption capacity of the CH/cHAp after adding CF into it. This improved adsorption capacity of the CH/cHAp could be attributed to the availability of more adsorption sites after adding the CF. Contrary to this, the estimated adsorption of Cd^{2+} was found to decrease after the addition of the CF into the CH/cHAp composites (see Table above). The improvement in the adsorption capacity after synthesising the composite of CF with the HAp aligns with the literature findings

discussed above. The experimental adsorption capacity (mg g^{-1}) of the CH/cHAp was also found to increase after the addition of CF to form the CH/cHAp/CF composites and agrees with the findings of the adsorption modelling. The addition of CF did not affect the estimated adsorption capacity of the CH/bHAp (control) as it ranges between 89-90 mg g^{-1} for both the CH/bHAp (control) and the CH/bHAp/CF composites. It could be due to saturation of the active sites as the constant dose of 0.01 g was used to conduct this experiment. The CH/bHAp composite was more efficient at removing Pb^{2+} ions than the CH/cHAp composite. So, the additions of CF did not show any significant improvement in the adsorption ability due to the low availability of adsorption sites on the 0.01 g adsorbent dose.

Cu^{2+}: The comparison of adsorption capacity (mg g^{-1}) of the CH/cHAp/CF composite with the CH/cHAp composite (control systems) shows similar adsorption capacities for Cu^{2+}, which illustrates that there is no effect of the addition of CF into the CH/cHAp composite on the adsorption capacity toward Cu^{2+}. The addition of CF has reduced the CH/bHAp adsorption capacity for Cu^{2+} adsorption from 23.67 mg g^{-1} to 18.55 mg $g^{-1.}$ This trend aligns with the observation recorded for the Pb^{2+} ion adsorption on the CH/HAp/CF composites. This difference of adsorption capacities between the two composites (CH/bHAp and CH/bHAp/CF) could be due to the heterogeneity of the CH/bHAp/CF composite sample (having CF into it and it shows that the Langmuir model is not suitable for describing the adsorption of cations on a highly heterogeneous composite (like the CH/HAp/CF composites). The adsorption on these composites could be considered to occur in a range of behaviours that could fit in the Langmuir model (to describe the homogenous adsorption behaviour) and could be explored further using other models (such as the Sips or Temkin) to understand it better.

Chromate ions: The maximum adsorption capacity (q_{max} mg g^{-1} of chromate ions) on the CH/HAp composites (control composites) is presented in Table 5-13. It showed q_{max} of chromate ions 45.04 mg g^{-1} (CH/cHAp), higher than the estimated value of chromate adsorption on the CH/cHAp/CF composites. The addition of CF in cHAp-based composite indicates the reduction in estimated adsorption capacity (q_{max}) of the CH/cHAp composites after the addition of CF. There is a possibility that coir fibre blocks the HAp sites on the composites as a possible reason for the decrease in removal efficiency. This observation aligns with the observations recorded for the Cd^{2+} ions (see Table 5-13).

Contrary to the cHAp-based composites, the estimated maximum adsorption capacity (q_{max} in mg g^{-1}) of chromate ions on the CH/bHAp (control) is 34.72 mg $g^{-1,}$ which increased to 72.46 mg g^{-1} on the CH/bHAp/CF. It showed an improvement in the adsorption capacity of the CH/bHAp after adding CF into it. This improved adsorption capacity of the CH/bHAp could be attributed to the availability of more adsorption sites after adding the CF. However, it is not aligned with other observations recorded for the bHAp-based composite for metal ion adsorption. This anomalous behaviour could be due to the heterogeneity of the sample.

5.1.2.6 Effect of contact time on metal ions removal by the CH/HAp/CF composites

Experimental: The effect of contact time on metal ions removal (%) by the CH/HAp/CF composites was measured by varying the contact time between 1 minute and 120 minutes for measuring adsorption on a 0.05 g dose of adsorbent in 20 mL of Cd^{2+} and Cu^{2+} (25 ppm) solution and on a 0.01 g dose of adsorbent in 20 mL of Pb^{2+} (25 ppm) and chromate ion (50 ppm) solutions. Furthermore, the collected data was also used to evaluate the kinetics of metal ion adsorption on the CH/HAp/CF composites adsorbents by kinetic modelling.

Results: Table 5-14 presents the effect of contact time on metal ions removal (%) using the CH/HAp/CF composites and is presented in *Figures 4-53 to 4-56 (Appendix 4).*

Table 5-14: The effect of the contact time on the % removal of metal ions on the CH/HAp/CF composites system from a single-metal ion type solution system

Contact Time (minutes)		**1**	**2**	**3**	**4**	**5**	**10**	**15**	**30**	**60**	**120**
Cd^{2+}	CH/cHAp/CF	18.02	34.86	42.30	50.44	56.46	69.92	73.38	77.84	82.22	85.82
	CH/bHAp/CF	36.38	45.66	53.86	60.30	61.24	68.24	75.88	82.80	86.02	88.08
Pb^{2+}	CH/cHAp/CF	21.87	32.32	37.47	43.09	51.62	57.18	63.50	75.68	79.26	84.83
	CH/bHAp/CF	28.11	37.56	42.47	48.92	54.25	62.55	70.02	85.47	89.46	93.91
Cu^{2+}	CH/cHAp/CF	13.58	28.51	33.03	34.33	44.64	56.26	61.24	86.61	93.36	93.58
	CH/bHAp/CF	23.16	27.05	28.64	39.74	49.76	73.50	79.30	88.08	95.95	96.01
Chromate	CH/cHAp/CF	15.92	17.09	17.48	17.76	19.75	20.39	20.54	22.16	22.63	22.84
	CH/bHAp/CF	15.01	16.39	17.71	17.35	17.94	19.16	19.55	19.76	19.84	21.16

The Cd^{2+} adsorption was rapid in the initial 15 minutes. The adsorption increased steeply in the initial 15 minutes, achieving about 70% removal (%), as observed by the steep

slope part of the graph *(Figure 4-53, Appendix 4).* The adsorbents reached adsorption equilibrium in 120 minutes, illustrating the saturation of active sites on the adsorbent surface and achieving >80% Cd^{2+} removal on the CH/HAp/CF composites.

For Pb^{2+}, a sharp increase in removal % (more than 50%) of Pb^{2+} ions from the solution were recorded in the initial 5 minutes for both the composites tested (Table 5-14). Maximum removal efficiency for both the composites tested was calculated to be about 85-94% over the 2 hours of exposure time. The optimum time for realising the highest Pb^{2+} ion removal with the CH/HAp/CF composites was found to be 120 minutes. Similarly, both composite samples achieved about 50% removal in just five minutes and achieved equilibrium (saturation of adsorbent) in 60 minutes with more than 90% Cu^{2+} removal, as no further change in removal (%) was recorded after 60 minutes for both the composites. The overall removal efficiency (%) of both composites was similar, ranging from 93 to 96%. The rapid increase in removal efficiency of CH/HAp/CF composites over the period of 1 to 15 minutes of contact time could be attributed to the excess availability of active sites ($-NH_2$, $-OH^-$, $-COO^-$ and $-PO_4^{3-}$) at the beginning of the adsorption process, which gradually saturates and reaches equilibrium at a maximum time of 120 minutes.

The better metal ions removal (%) on the CH/bHAp/CF than the CH/cHAp/CF composite was demonstrated by the Langmuir constant K_L value (Table 5-11), which is higher for the CH/bHAp/CF composite compared to the value obtained for the CH/cHAp/CF composite. The K_L is used to describe the affinity of sorbate for adsorbent molecules[548,549], so the higher K_L value (Langmuir model) and higher removal % observed for the CH/bHAp/CF composite compared to the CH/cHAp/CF composite show a better affinity of metal ions towards the CH/bHAp/CF composite for adsorption. This better affinity of all three metal cations (Cd^{2+}, Pb^{2+} and Cu^{2+}) towards the CH/bHAp/CF composite could be attributed to the availability of relatively more adsorption sites due to the higher surface area of the CH/bHAp/CF composite.

Similar to cation adsorption, the rapid increase in chromate ion adsorption (removal %) by both the composites is attributed to the excess availability of adsorption sites at the beginning of the adsorption process. The composites reached adsorption equilibrium at 60 minutes, which specified the saturation of adsorption sites on the surface of adsorbents. No further change in removal (%) was recorded after 60 minutes for both the composites.

The low removal efficiency of both the composites (as compared to cations removal) could be due to the anionic nature of the chromate ion species present in the solution, as discussed earlier (effect of pH experiment), which limits its adsorption on negatively charged adsorption sites which dominate the surface of CH/HAp/CF composites in the pH range (5.0-6.0) of this experiment.

5.1.2.7 Kinetic modelling for metal ion adsorption on the CH/HAp/CF composites systems

Kinetic modelling of metal ion adsorption on CH/HAp/CF composites was performed with testing done for non-linear pseudo-first-order (PFO, section 1.11.1) and pseudo-second-order (PSO, section 1.11.2) kinetics. The best fit of the PFO or PSO kinetic models was decided upon by comparing the R^2 values calculated for both models and choosing the R^2 value closest to 1 calculated for each model. The kinetics models fitted to the experimental data of metal ion adsorption on the CH/HAp/CF composites are also presented in *Figures 4-57 to 4-64 (Appendix 4).*

Results: The calculated kinetic model parameters for metal ion adsorption are given in Table 5-15. The comparison of coefficient of determination values (R^2) of PFO and PSO kinetic models showed that the PSO kinetic model was the best-fitted model with an R^2 value closer to 1 than that for the PFO kinetic model for metal cation adsorption on both composite systems (Table 5-15). The calculated adsorption capacity (q_{max} in mg g^{-1}) using the PSO kinetic model was 8.77 mg g^{-1} (CH/cHAp/CF) and 8.65 mg g^{-1} (CH/bHAp/CF) for Cd^{2+} , 41.85 mg g^{-1} (CH/cHAp/CF) and 46.43 mg g^{-1} (CH/bHAp/CF) for Pb^{2+} and 10.06 mg g^{-1} (CH/cHAp/CF) and 10.41 mg g^{-1} (CH/bHAp/CF) for Cu^{2+}.

The best fit of the PSO kinetic model to the experimental data for metal cation adsorption on the CH/HAp/CF composites indicated that the rate-limiting step for these metal cation adsorption on CH/HAp/CF composites was chemisorption on the surface[550].

Table 5-15: The parameters calculated for metal ion adsorption on the CH/HAp/CF composites based on each kinetic model fitted.

Metal ions	Composite systems	PFO			PSO		
		k_1 (min^{-1})	q_e (mg g^{-1})	R^2	k_2 (g mg^{-1} min^{-1})	q_e (mg g^{-1})	R^2
Cd^{2+}	CH/cHAp/CF	0.249	7.990	0.980	0.037	8.772	0.999
	CH/bHAp/CF	0.382	8.002	0.853	0.065	8.650	0.998
Pb^{2+}	CH/cHAp/CF	0.217	37.825	0.910	0.007	41.859	0.998
	CH/bHAp/CF	0.218	42.102	0.875	0.006	46.433	0.996
Cu^{2+}	CH/cHAp/CF	0.115	8.980	0.945	0.014	10.063	0.996
	CH/bHAp/CF	0.147	9.320	0.975	0.017	10.418	0.996
Chromate	CH/cHAp/CF	1.118	20.612	0.447	0.086	21.918	0.998
	CH/bHAp/CF	1.313	19.072	0.566	0.124	20.043	0.999

The chemisorption of metal cations on the CH/HAp/CF composites could occur through the functional groups of chitosan, HAp, and CF. As mentioned earlier, the electron-donating groups of chitosan ($-NH_2$) and the COO^- groups of CF could form metal complexes[319,551], which could assist the chemisorption of metal cations on the CH/HAp/CF composite. Additionally, the HAp could be providing the adsorption ability (by introducing the ion-exchange mechanism in CH/HAp/CF composites) given CF on its own is more weakly adsorbing of metal cations.

This finding is in good agreement with the adsorption literature, which has shown PSO kinetics to apply for metal ion adsorption on the composites made from chitosan, hydroxyapatite, and lignocellulosic fibres[83,111,368,483]. It also aligns with the kinetic modelling of metal ions on the CH/HAp (control) composites (see section 5.1.1.6).

For chromate ion adsorption modelling *(Figure 4-51 and 4-52)*, the comparison of the coefficient of determination values (R^2) from the PFO and PSO kinetic models showed that the PSO kinetic model is the best-fitted model with a higher R^2 (>0.99) than that calculated for the PFO kinetic model for chromate ion adsorption on both composite systems. The calculated adsorption capacity (q_e in mg g^{-1}) of chromate ions by the PSO kinetic model was 20.61 mg g^{-1} (CH/cHAp/CF) and 19.07 mg g^{-1} (CH/bHAp/CF). The fitting of the PSO kinetic model to the data relating top chromate ion adsorption on the CH/HAp/CF composites. It confirms that the chemisorption mechanism was the rate-limiting step for chromate ion adsorption using this composite. The findings of this batch experiment align with the literature studies, which also reported the fitting of the PSO kinetic model on the kinetics data of the chromate ion adsorption, using the lignocellulosic fibre and coir pith based-composites as adsorbents[232,523].

5.1.3 Experiments involving the removal of metal ions by the CH/HAp/SCGs composites (commercial & Bovine-derived) from the single-metal ion type system

The chitosan/HAp/Spent coffee grounds (CH/HAp/SCGs) composite (a three-component composite system) was synthesised by adding spent coffee grounds (SCGs) to the CH/HAp composite. Like the control composites (section 5.1.1) and three-component composite systems (discussed earlier in section 5.1.2), the spectroscopic and microscopic characterisation of the CH/HAp/SCGs composites was done and comprehensively described in chapter 3 (in section 3.4.3).

The methods used in each batch experiment to remove metal ions using the CH/HAp/SCGs composites are described in their respective sections below. The following describes the results of using this composite system to remove Cd^{2+}, Pb^{2+}, Cu^{2+} and chromate ions from various model solutions and their adsorption and kinetic modelling (using the same methods described for the earlier composite systems of this study) to understand better the adsorption mechanism undergone by each metal ion and the kinetics of the adsorption process in this composite system.

5.1.3.1 Effect of adsorbent dose on metal ions removal by the CH/HAp/SCGS composites

Experimental: The metal ion adsorption and removal (%) were measured using 0.01g to 0.05 g doses of the CH/HAp/SCGs composites for an initial metal ion concentration of 50 ppm (for Cd^{2+}, Pb^{2+} and chromate ions solutions) and 25 ppm (for Cu^{2+}). The initial solution pH ranged from 4.5-6.0.

Results: Table 5-16 (*Figure 4-65- to 4-68, Appendix 4*) presents the AAS results for metal ion (Cd^{2+}, Pb^{2+}, $Cu^{2+}$and chromate ions removal efficiency (%) and adsorption capacity "q_e" (mg g^{-1}) for the CH/HAp/SCGs composite system with different adsorbent doses (0.01g to 0.05 g). An obvious trend of gradual increase in removal efficiency (%) and decrease in the adsorption capacity (mg g^{-1}) of CH/HAp/SCGs composites was observed with an increase in the adsorbent dose and attributed to similar reasons discussed in detail in earlier sections (see “effect of adsorbent dose” batch experiment results in earlier sections 5.1.1.1 & 5.1.2.1).

The maximum removal of Cd^{2+} and Pb^{2+} was recorded at 0.05 g of adsorbent dose, i.e., 66-78 % (Cd^{2+}) and > 97% (Pb^{2+}) for a 0.05 g dose of the CH/HAp/SCGs composites. Similarly, the removal% values for Cu^{2+} ions range between 18.25-23.44 % recorded at the 0.01 g dose and 81.29-94.77% recorded at the 0.05 g dose for both the CH/HAp/SCGs composites tested. The systems demonstrated a 60-71% increase in the removal efficiency when the adsorbent dose was increased from 0.01 to 0.05 g. These observations agree with those made in the case of studies involving the metal ion adsorption systems on the CH/HAp (control) composites, which indicated that the removal efficiency could be enhanced by simply increasing the adsorbent dose.

The comparison of Pb^{2+} and Cd^{2+} ions adsorption for a sorbent range of 0.01 g to 0.05 g of the CH/HAp/SCGs composites indicated the removal ability of the CH/HAp/SCGs composites is higher for Pb^{2+} ions than Cd^{2+} ions. This trend confirms the findings of earlier composite systems studied for Cd^{2+} and Pb^{2+} adsorption (in sections 5.1.1 and 5.1.2), showing better adsorption of Pb^{2+} ions and could be attributed to already explained reasons related to the physicochemical characters of Pb^{2+} which allow for its relatively higher adsorption than observed for Cd^{2+} on the HAp-based composite systems.

Table 5-16: The effect of the adsorbent dose on the removal efficiency (%) and adsorption capacity (mg g^{-1}) of the CH/HAp/SCGs composites for the adsorption of the metal ions in the single-metal ion type solution systems

The effect of the adsorbent dose on removal (%) of metal ions using the CH/HAp/SCGs composites						
Dose (g)		0.01	0.02	0.03	0.04	0.05
CH/cHAp/SCGs	Cd^{2+}	17.12	32.64	47.98	59.05	66.86
	Pb^{2+}	34.93	60.01	89.78	96.21	97.97
	Cu^{2+}	18.25	34.05	49.14	65.36	81.29
	Cr (as chromate ions)	32.22	34.00	35.39	35.38	35.72
CH/bHAp/SCGs	Cd^{2+}	18.18	34.81	49.24	63.37	77.98
	Pb^{2+}	45.78	66.33	94.38	96.73	97.99
	Cu^{2+}	23.44	40.30	58.95	76.50	94.77
	Cr (as chromate ions)	32.17	33.53	34.41	39.34	39.63
The effect of the adsorbent dose on the adsorption capacity (in mg g^{-1}) of the CH/HAp/SCGs composites with respect to the metal ions adsorbed						
CH/cHAp/SCGs	Cd^{2+}	17.12	16.32	15.55	14.76	13.37
	Pb^{2+}	34.61	30.47	29.87	24.06	19.58
	Cu^{2+}	9.13	8.51	8.19	8.17	8.13
	Cr (as chromate ions)	16.11	8.50	5.90	4.42	3.57
CH/bHAp/SCGs	Cd^{2+}	18.18	17.41	16.59	15.84	15.41
	Pb^{2+}	42.43	34.09	31.29	24.15	19.59
	Cu^{2+}	11.72	10.07	9.82	9.56	9.48
	Cr (as chromate ions)	16.09	8.38	5.74	4.92	3.96

The maximum adsorption of Cd^{2+} was 17.12 mg g^{-1} and 18.18 mg g^{-1} for the CH/cHAp/SCGs and the CH/bHAp/SCGs composites, respectively, recorded at an adsorbent dose of 0.01 g. Overall, both the composites showed similar adsorption capacities (mg g^{-1}) for Cd^{2+} as the maximum difference between the adsorption capacities of the two composites is 1-2 mg g^{-1} at all adsorbent doses studied from 0.01 g to 0.05 g. In contrast, better adsorption ability of the CH/bHAp/SCGs for Pb^{2+} than the CH/cHAp/SCGs was recorded, which agrees with the effect of adsorbent dose on Pb^{2+} adsorption on the CH/bHAp composite systems. It is associated with the higher removal efficiencies of bHAp-based composites for Pb^{2+} ions due to the relatively higher surface area of these composites than cHAp-based composites.

Generally, all three bHAp-based composites (see earlier sections 5.1.1 & 5.1.2) showed a better removal efficiency for cations than the cHAp-based composites. It could be deduced from these observations that the presence of bHAp plays a role in the better adsorption ability of composites than cHAp. This better adsorption ability of these composites could be attributed to the relatively higher surface area of bHAp-based composites as observed in earlier systems.

The constitutional functional groups of CH/HAp/SCGs composites (FTIR analysis of CH/HAp/SCGs composites, Table 3-3, Chapter 3) act as binding sites for metal cations removal by ion exchange, metal-complexation, and electrostatic interactions[352,483,484]. The HAp might be the most dominantly adsorbing component of CH/HAp/SCGs, which could participate in cations removal in several ways, as described in detail in earlier sections (section 1.5.4).

AAS data for chromate ion adsorption on the CH/HAp/SCGs composites is presented in Table 5-15 (and in *Figure 4-67 to 4-68, Appendix 4*), which provides a summary of the effect of adsorbent doses for chromate ion adsorption and removal on the CH/cHAp/SCGs and the CH/bHAp/SCGs composites. A gradual increase in removal efficiency was noted (and aligned with the observations recorded for cation removal) and was attributed expectedly to the availability of more adsorbent surface area for the uptake of chromate ions. However, it was noted that the maximum removal (%) was less than 40% for both the composites in solutions containing the maximum adsorbent dose of 0.05 g. In contrast to this observation, when the same composites were exposed to solutions containing Cd^{2+}, Pb^{2+} and Cu^{2+} ions. At a similar (0.05 g) dose, the composites were found

to achieve at least >80% removal of the cations from those solutions (see earlier discussion on this). This observation of relatively low chromate ion removal (%) relative to cation removal (i.e., Cu^{2+}, Pb^{2+} and Cd^{2+}) on the CH/HAp/SCGs composites agrees with the observations recorded earlier for chromate ion removal by the control composite system (section 5.1.1) and the CH/HAp/CF composite system (5.1.2). However, compared to the control composites, the removal efficiency of CH/HAp/SCGs is better (Table 5-15) for the adsorption of chromate anions than the CH/HAp composites (control) (Table 5-1) as the maximum removal of chromate anion at 0.01 g to 0.05 g of CH/HAp composites ranged from 17-29%, while it is 32-29% for the same dose of CH/HAp/SCGs. This better adsorption of chromate anions on CH/HAp/SCGs than CH/HAp (control) composites could be attributed to the presence of SCGs providing suitable adsorption sites for the removal of chromate anions. These adsorption (binding) sites could be the polyphenolic groups of tannins found in the SCGs and the carboxyl groups found in the lignocellulosic portion of SCGs (Chapter 1, section 1.5.4 (Table 1-4)).

The removal efficiency (%) of CH/HAp/SCGs composites with respect to chromate ion increased by 3-7%, increasing the adsorbent dose from 0.01 g to 0.05 g. The CH/cHAp/SCGs composite and the CH/bHAp/SCGs composite showed comparable adsorption of chromate anions (mg g^{-1}) chromate, ranging from 16.08-16.11 mg g^{-1} at an adsorbent dose of 0.01 g.

5.1.3.2 Effect of solution pH on metal ions removal by the CH/HAp/SCGs composites

Experimental: The effect of solution pH on metal ion adsorption (mg g^{-1}) on the CH/HAp/SCGs composites was recorded by using an initial metal ion concentration of 50 ppm (for Cd^{2+} and Cu^{2+}) at 0.05 g of adsorbent dose. The initial metal ion concentrations of Pb^{2+} and chromate ion solutions were 20 ppm and 35 ppm, respectively, which were exposed to 0.01 g of adsorbent dose for the measurements of the effect of pH. The pH was altered between 4.0 and 8.0 (for Cd^{2+} ions), between 4.0 -5.8 for $Pb^{2+,}$ between 4.0-6.5 for Cu^{2+} and 4.0-9.5 for chromate ion solution. A restricted pH range was used for Pb^{2+} and Cu^{2+} due to the precipitation risk of these metals, as mentioned earlier in the results and discussion involving adsorption on the control composites).

Results: Table 5-17 and *Figures 4-69 to 4-72, appendix 4*, the AAS data demonstrate the change in adsorption capacity (mg g^{-1}) of the CH/HAp/SCGs composites for metal ion

adsorption with changing the solution pH. A similar trend in cations (Cd^{2+}, Pb^{2+} and Cu^{2+}) adsorption was recorded earlier for the CH/HAp (control) composites and base-three component composites.

About 2 mg g^{-1} increase in adsorption capacity of CH/HAp/SCGs composites was recorded for Cd^{2+} ion adsorption when the pH of the solution was varied from 4.0 to 5.0. It slightly decreased after 5.0. No prominent changes in the adsorption capacity of the composites were recorded by varying the pH of the solution from 6.0 to 8.0. Similarly, the Pb^{2+} adsorption was a maximum at pH 5.0, decreased slightly at pH >5.0 and increased again when solution pH was >5.6. The Cu^{2+} ion adsorption was not greatly affected by the changing of pH in the solution from 4.0 to 6.5 in both the composites. It was found that at a pH of 5.0-6.0, the Cu^{2+} ion removal was observed to be at its maximum with an adsorption capacity of about 9.16 and 9.51 mg g^{-1} for CH/cHAp/SCGs and CH/bHAp/SCGs, respectively. The trends could be explained by similar reasons as discussed in detail in earlier sections (see sections 5.1.1.2 & 0).

Table 5-17: The effect of the solution pH on the adsorption capacity (in mg g^{-1}) of the CH/HAp/SCGs composites for the adsorption of metal ions from solutions containing only one type of metal ion

	pH	**4.0**	**5.0**	**6.0**	**7.0**	**8.0**
Cd^{2+}	CH/cHAp/SCGs	12.68	13.19	12.44	12.62	12.71
	CH/bHAp/SCGs	13.22	15.34	14.41	14.56	15.04
	pH	**4.5**	**5.0**	**5.5**	**6.0**	**6.5**
Pb^{2+}	CH/cHAp/SCGs	36.99	41.28	38.53	40.97	42.32
	CH/bHAp/SCGs	41.32	42.94	41.17	42.67	42.71
	pH	4.0	5.0	5.5	6.0	6.5
Cu^{2+}	CH/cHAp/SCGs	9.10	9.16	9.15	9.15	9.09
	CH/bHAp/SCGs	9.50	9.51	9.51	9.51	9.31
	pH	**4.5-5**	**5-5.5**	**6-6.5**	**7-7.5**	**8-8.5**
Cr as chromate ions	CH/cHAp/SCGs	18.3	17.45	15.3	9.518	8.264
	CH/bHAp/SCGs	18.4	18.538	15.4	10.1	9.328

As discussed in detail in control composites and the base-three component composites (CH/HAp/CF composite systems), the charges on functional groups (binding sites of adsorbents) are affected by the change in the pH of the metal ions solution. The functional groups which could be potential binding sites for cation adsorption of the CH/HAp/SCGs composites include the hydroxyl, amino, carbonyl and phosphates groups as presented in FTIR Spectra of the CH/cHAp/SCGs (Table 3-3, Chapter 3). So, the lower adsorption

measured at lower pH (4.0) could be attributed to hydrogen ion competition and protonation of the mentioned active sites on the chitosan/HAp/SCGs composite. The control composite system (CH/HAp) and the CH/HAp/CF composites showed an increasing cation adsorption trend when the solution pH was >4.0. Similarly, the CH/HAp/SCGs composite system was also found to perform efficiently in pH higher than 4.0. The literature studies that employed SCGs as a bio adsorbent reported pH > 5.0 as an optimum pH for metal ion removal using the SCGs as an adsorbent for metal cations[552,553].

The literature discussed above and in earlier sections (referred to the batch experiments of the "effect of solution pH on cation adsorption" in sections 5.1.1.2 & 5.1.2.2) indicates that a pH range of > 4.0 is favourable for the availability of functional groups on the surface of chitosan and HAp part of composites. Similarly, the availability of binding/adsorption sites on carbonaceous-part of adsorbents (such as chitosan, coir fibre and SCGs) for metal cation adsorption affects the surface charges on functional groups[554] by controlling the protonation and deprotonation of the active sites of the adsorbents in the solution. For instance, the deprotonation of carboxylic groups (COO^-) found in carbonaceous materials (such as in SCGs) occurred at pH > 4.0 to provide adsorption sites for metal cation adsorption[525-527]. Moreover, the excess of metal ions in the solution at pH 4.0-5.0 further enhances the adsorption of cations on these composites, as supported by the literature[467,525,526]. So, in line with the CH/HAp (control) composites and the CH/HAp/CF composites, the pH range of 4.0-5.0 was considered optimum for cation adsorption on the CH/HAp/SCGs composites.

Table 5-17 also presents the AAS data showing the effect of initial solution pH in chromate solutions exposed to 0.01 g of adsorbent doses of the CH/HAp/SCGs composites on chromate ion adsorption on the CH/HAp/SCGs composites. Overall, the observations indicate that the acidic/low pH favours chromate ion adsorption on such composite systems and can be attributed to the factors discussed earlier, such as the speciation of chromate as $HCrO_4^-$ and CrO_4^{2-} at pH <5.0[485] to favour its interaction with protonated amino groups (NH_3^+) on the chitosan and positively charged species on HAp surface (see 5.1.1.1 & 5.1.1.2) by electrostatic interactions. Additionally, a report on chromate adsorption on SCGs[555] states that the decrease in removal of chromate ions with increasing pH is due to the deprotonation of active sites (hydroxyl and carbonyl groups)

at pH >5.3 and abundance of negative ions in solution (e.g. OH^- and COO^-) which may create competition for these anions adsorption[502,555].

The trend of better chromate ion adsorption at low pH (<5.0) agrees with other published studies for the adsorption of chromate ions on coir fibre, activated carbons or chitosan-based composite systems and SCGs based composite systems[310,501,536,555].

5.1.3.3 Effect of the initial metal ion concentration on metal ion removal by the CH/HAp/SCGs composites

Experimental: Initial metal ion concentration was varied between 10 ppm and 50 ppm (for Cd^{2+} and Pb^{2+} and chromate ions) and between 5 ppm and 25 ppm (for Cu^{2+}) for a constant adsorbent dose of 0.01g, while the initial solution pH was 4.5-5.5 for evaluating the effect of initial sorbate concentration of the solution on metal removal. Further, the data recorded using AAS in this experiment were used to study the adsorption mechanism by fitting adsorption models (non-linear Langmuir and Freundlich for cations and linearised adsorption models for chromate ions, discussed in the upcoming section) by using the same methods as have already been described for the control composite systems.

Results: Table 5-18 shows the AAS data, presenting the effect of the initial metal ion concentration on Cd^{2+} adsorption on the CH/HAp/SCGs composites. The results are also exhibited in Figures *4-73 to 4-76 (Appendix 4).*

There was a gradual decrease in removal efficiency of the CH/HAp/SCGs composites with increased metal ion concentration observed. At the same time, the adsorption capacity (q_e in mg g^{-1}) of the composites was noted to increase with increasing the metal ion concentration in solution when exposed to a constant adsorbent dose of 0.01 g.

Relatively better adsorption of cations (Cd^{2+}, Cu^{2+}, Pb^{2+}) on the CH/bHAp/SCGs composites agrees with the observations recorded earlier for the bHAp-based composites systems. This observation further strengthens the better removal efficiency of bHAp-based composites in this study. It could be attributed to the availability of the higher surface area in the CH/bHAp/SCGs composites than the CH/cHAp/SCGs composites resulting in a good performance of bHAp-based composite in the metal ions removal mechanisms. The CH/HAp/SCGs composites were extremely heterogeneous as their grain sizes (average) varied from 20 m^2/kg to 78 m^2/kg, as recorded using the Mastersizer particle size analyser (*Appendix 3, Figure G & H*). This could be attributed to the

heterogeneous nature of the components (like the SCGs) that constituted the composites. It could also have an impact on the adsorption of the metal ions and can cause irregular trends recorded for the removal of the metal ions by the CH/HAp/SCGs composites.

Table 5-18: The effect of the initial metal ion concentration on the adsorption of different metal ions on the CH/HAp/SCGs composites in a single-metal ion type solution system

The removal (%) of metal ions using the CH/HAp/SCGs composites						
	Metal ion concentrations (ppm)	10.0	20.0	30.0	40.0	50.0
Cd^{2+}	CH/cHAp/SCGs	40.48	34.21	28.16	22.82	18.87
	CH/bHAp/SCGs	44.82	37.55	29.60	24.36	20.03
Pb^{2+}	Metal ion concentrations (ppm)	10.0	20.0	30.0	40.0	50.0
	CH/cHAp/SCGs	78.51	57.84	45.71	38.71	33.59
	CH/bHAp/SCGs	79.79	64.60	58.26	49.67	41.87
Cu^{2+}	Metal ion concentrations (ppm)	5.0	10.0	15.0	20.0	25.0
	CH/cHAp/SCGs	40.30	31.36	24.12	20.14	16.30
	CH/bHAp/SCGs	57.93	42.69	35.09	29.71	25.11
Cr as chromate ions	Metal ion concentrations (ppm)	10.0	20.0	30.0	40.0	50.0
	CH/cHAp/SCGs	56.62	50.54	44.51	39.49	37.46
	CH/bHAp/SCGs	54.60	51.53	46.00	39.56	36.76
The adsorption capacity (in mg g^{-1}) of the CH/HAp/SCGs composites for different metal ions						
	Metal ion concentrations (ppm)	10.0	20.0	30.0	40.0	50.0
Cd^{2+}	CH/cHAp/SCGs	8.10	13.68	16.90	18.26	18.87
	CH/bHAp/SCGs	8.96	15.02	17.76	19.49	20.03
Pb^{2+}	Metal ion concentrations (ppm)	10.0	20.0	30.0	40.0	50.0
	CH/cHAp/SCGs	15.70	23.14	27.43	30.97	33.59
	CH/bHAp/SCGs	15.96	25.84	34.96	39.73	41.87
Cu^{2+}	Metal ion concentrations (ppm)	5.0	10.0	15.0	20.0	25.0
	CH/cHAp/SCGs	4.03	6.27	7.24	8.06	8.15
	CH/bHAp/SCGs	5.79	8.54	10.53	11.89	12.55
Cr as chromate ions	Metal ion concentrations (ppm)	10.0	20.0	30.0	40.0	50.0
	CH/cHAp/SCGs	5.66	10.11	13.35	15.80	18.73
	CH/bHAp/SCGs	5.46	10.31	13.80	15.83	18.38

The maximum adsorption of Pb^{2+} was recorded at 50 pm, which was 33.58 mg g^{-1} and 41.87 mg g^{-1} on the CH/cHAp/SCGs and CH/bHAp/SCGs composites, respectively. The highest removal (%) ≈ 80 %, was recorded at 10 ppm for both the composites. The Pb^{2+} adsorption is higher (about double) on the CH/HAp/SCGs composites than Cd^{2+}, as evident from the comparison of the removal (%) values of Pb^{2+} and Cd^{2+} ions by adsorption on the CH/HAp/SCGs composites (Table 5-18), when a 0.01 g adsorbent dose of the composites is exposed to 10 ppm solution of Pb^{2+} or Cd^{2+}. It again implies the better adsorption of Pb^{2+} ions than Cd^{2+} ions on these composite systems due to the already

mentioned chemical characteristics of Pb^{2+} ions, which enable it to better adsorb on the HAp-part of the composites by ion-exchange mechanisms (with Ca^{2+} ions) and electrostatic attractions (with negatively charged phosphates and hydroxyl groups).

Several mechanisms simultaneously assist these cations removal from solution on such complex adsorption systems, as discussed previously in earlier sections of this study.

To understand the adsorption behaviour of cations on the CH/HAp/SCGs composites system, the batch experiment data of this experiment was evaluated using non-linear adsorption isotherm models for Langmuir and Freundlich type adsorption (as described in earlier sections of this study) and discussed in the upcoming section.

Similar to cation removal using the CH/HAp/SCGs composites, a continuous increase in adsorption capacity (mg g^{-1}) of both the composites for chromate adsorption with increasing metal ion concentration from 5 ppm to 25 ppm is attributed to the availability of more metal ions to sorb on a fixed number of active sites of 0.01 g of the adsorbent at all concentrations. In comparison, a continuous decrease in removal efficiency (%) corresponds to the availability of more metal ions to sorb on a limited number of active sites to remove metal ions. The maximum adsorption ≈18 mg g^{-1} for both the composites was measured at 25 ppm concentration of chromate ions in solution. The maximum removal (%) of chromate ions was measured at 5 ppm concentration and ranged between 54 to 56% for both the composites. Both the composites showed comparable removal efficiencies at all the ion concentrations studied in this batch experiment. The maximum difference between the removal efficiencies of the two composites is less than 1%. To understand the removal mechanism and estimate the maximum adsorption capacity (q_{max} mg g^{-1}) of this composites system, the AAS data collected in this experiment was further analysed using adsorption models as has been done in other systems.

5.1.3.4 Adsorption modelling of the CH/HAp/SCGs composites for the adsorption of metal ions

Experimental: The experimental results of metal ion adsorption on the CH/HAp/SCGs composites were tested against non-linear Langmuir and Freundlich isotherms as described earlier (section 5.1.1.4) and presented in *Figures 4-77 to 4-84 (Appendix 4).*

Results: The calculated isotherm parameters for two adsorption models for metal ion adsorption on all the CH/HAp/SCGs composites are given in Table 5-19.

Table 5-19: Adsorption isotherm parameters for metal ions (Cd^{2+}, Pb^{2+} and $Cu^{2+}$and chromate) adsorption on the CH/HAp/SCGs composites

Metal ions	Adsorption Isotherms	Langmuir			Freundlich			
	Parameters	q_{max} (mg g^{-1})	K_L	R^2	R_L	1/n	K_F (mg g^{-1})	R^2
Cd^{2+}	CH/cHAp/SCGs	24.62	0.09	0.99	0.21	0.39	4.75	0.93
	CH/bHAp/SCGs	25.46	0.11	0.99	0.19	0.36	5.65	0.93
Pb^{2+}	CH/cHAp/SCGs	34.69	0.31	0.93	0.09	0.28	12.75	1.00
	CH/bHAp/SCGs	49.09	0.19	0.98	0.15	0.35	13.37	0.97
Cu^{2+}	CH/cHAp/SCGs	9.99	0.24	0.99	0.17	0.33	3.11	0.95
	CH/bHAp/SCGs	14.57	0.29	1.00	0.16	0.35	4.63	0.99
Chromate	CH/cHAp/SCGs	27.17	0.12	1.00	0.35	0.59	3.70	0.99
	CH/bHAp/SCGs	31.34	0.09	1.00	0.40	0.61	3.57	0.97

The comparison of R^2 values of non-linear Langmuir and Freundlich models revealed that the Langmuir isotherm model was the best-fitted model for explaining the adsorption of Cd^{2+} and Cu^{2+} on the CH/HAp/SCGs composite with $R^2 > 0.98$. The Langmuir isotherm model fitted to these cation adsorption data for the CH/HAp/SCGs composites suggested a monolayer adsorption model for cations on a homogeneous adsorbent surface[494]. However, the surface of these composites is highly heterogeneous, so the data could be analysed further by using another adsorption model such as the Sips isotherm, which is used to describe the adsorption behaviour on heterogeneous surfaces.

In contrast, the Freundlich isotherm model better fit the Pb^{2+} adsorption data on the CH/cHAp/SCGs composites, with the goodness of fit R^2 value closer to unity than the Langmuir isotherm model ($R^2 \geq 0.93$). The Langmuir and Freundlich are equally fit for describing adsorption on the CH/bHAp/SCGs composites, with R^2 values ranging from 0.972-0.973. Similarly, the Freundlich adsorption isotherm is also showing a good fitting with R^2 values from 0.94-0.99 being obtained (for Cu^{2+} adsorption) and >0.90 for Cd^{2+} adsorption. These findings indicate a complex adsorption mechanism involved in metal ion adsorption on CH/HAp/SCGs as the surface morphology of these composites did not show the homogenised surface to provide the adsorption sites. So, the Langmuir model could not alone describe the adsorption behaviour. The cation adsorption could be considered to follow the range of behaviours while being adsorbed on these composites. The adsorption of these metal ions on the CH/HAp/SCGs composites could be explored further to confirm the removal mechanism of the composites using more complex

adsorption models (such as Sips), which deal with the heterogeneous adsorption mechanisms.

The maximum adsorption capacity (q_{max} mg g^{-1}) in relation to Cu^{2+} adsorption on the composites was 9.98 mg g^{-1} and 14.57 mg g^{-1} (calculated using the Langmuir model) for the CH/cHAp/SCGs and CH/bHAp/SCGs composites, respectively. Similarly, q_{max} (mg g^{-1}) of Cd^{2+} was 24.62 mg g^{-1} and 25.46 mg g^{-1} on the CH/cHAp/SCGs and the CH/bHAp/SCGs composites, respectively, while the maximum adsorption capacity (q_{max} mg g^{-1}) was estimated using the Langmuir model for Pb^{2+} adsorption on the CH/cHAp/SCGs composite and the CH/bHAp/SCGs composite was 34.68 mg g^{-1} and 49.09 mg g^{-1}, respectively. The higher Pb^{2+} adsorption (q_{max}) than Cd^{2+} on the CH/HAp/SCGs composites confirms the observations of earlier composites systems discussed in earlier sections (5.1.1.4 &5.1.2.4), which also presented better adsorption capacity for Pb^{2+} than Cd^{2+} when these composites were exposed to single-metal ion type ion solutions of Pb^{2+} or Cd^{2+}.

The values of the dimensionless factor R_L (calculated using equation 5-5) for metal ion adsorption on the CH/HAp/SCGs composites given in Table 5-19 indicated a favourable adsorption process as $0 < R_L < 1$.

Several literature studies reported the fitting of Langmuir to describe the adsorption behaviour of cation on spent coffee grounds (SCGs). For instance, Patterer et al.[552] estimated the maximum adsorption (4.48 mg g^{-1}) of Cd^{2+} on spent coffee grounds using the non-linear Langmuir isotherm model, which is 6 times less than the estimated value in the present study. Another study[556] reported maximum adsorption of 15.65 mg g^{-1} of Cd^{2+} estimated using Langmuir isotherm when a 100 ppm solution was exposed to 3 to 24 g of adsorbent dose. In contrast to these literature studies, the present study presents higher maximum adsorption (q_{max}) of the CH/HAp/SCGs composite (Table 5-19). It indicated that the adsorption capacity of SCGs to adsorb metal ions could be enhanced by synthesising its composites with other efficient adsorbents such as HAp.

Apart from the removal mechanisms (discussed earlier in section 5.1.1) on the CH/HAp part of these composites, the metal complexation was reported as one of the prominent mechanisms involved in metal cations removal using polyphenolic groups (from tannin) of SCGs[557,558] (reactions are not explained in articles). The negatively charged carboxyl and hydroxyl groups of SCGs could also participate in electrostatic interactions to adsorb

positively charged cations[265]. Additionally, the presence of hydroxyapatite components in the CH/HAp/SCGs composites could enhance the removal efficiency of these bio-adsorbents by providing the sites for an effective ion-exchange mechanism as described in earlier sections.

As described above, linearized Langmuir and Freundlich isotherms were used in the adsorption modelling of chromate ion adsorption on CH/HAp/SCGs composites by the method described earlier in the CH/HAp (control) composite system (section 5.1.1.4). The results of these calculations are presented in Table 5-19 (see above).

Table 5-20 shows the linearized Langmuir and Freundlich equation calculated with linear fitting of the Langmuir and Freundlich isotherms using Microsoft Excel for chromate ion adsorption on the CH/HAp/SCGs composites. The equations generated from these fits are given as follows:

Table 5-20: The linearized equations calculated for chromate ion adsorption on the CH/HAp/SCGs composites using linearised Langmuir and Freundlich isotherms

Composites	Linearised Langmuir Equation	Linearised Freundlich Equation
CH/cHAp/SCGs	$y = 0.3042x + 0.0368$ ($R^2 = 0.9987$)	$y = 0.594x + 1.3092$ ($R^2 = 0.9933$)
CH/bHAp/SCGs	$y = 0.339x + 0.0319$ ($R^2 = 0.9963$)	$y = 0.6124x + 1.2722$ ($R^2 = 0.974$)

Hence using the above equations, the Langmuir and Freundlich isotherms parameters were calculated by the method described earlier in the CH/HAp composites (Section 5.1.1.4)

The comparison of R^2 values of both adsorption models reveals that both the Freundlich and Langmuir adsorption isotherms were found to fit the data and suggested that the adsorption of chromate ions a range of behaviours, including homogeneous and heterogeneous surfaces. Though the Langmuir model R^2 values are relatively higher than Freundlich (Table 5-19) for CH/HAp/SCGs composites and the Freundlich model also shows a good fit with R^2 values of >0.97 being obtained from fits to data. Keeping in view the complex nature of CH/HAp/SCGs, which exhibited highly heterogeneous surfaces under the SEM images (Figure 3-19 & 3-20) and also exhibited heterogeneous-type surface characteristics at the macroscopic level (visual characteristics), the data could be explored by more complex adsorption models such as three-factor adsorption models (e.g., the Sips model).

The maximum adsorption capacity (mg g^{-1}) of the CH/cHAp/SCGs composite and the CH/bHAp/SCGs composite for chromate ion adsorption, as estimated by the Langmuir isotherm model, is 27.17 mg g^{-1} and 31.34 mg g^{-1}, respectively, which is lying close to the experimental values of chromate ion adsorption on the CH/HAp/SCGs composites. The dimensionless factor R_L of Langmuir isotherm also showed favourable adsorption of chromate ions on both the composites as $0 < R_L < 1$.

The Freundlich isotherm parameter "1/n" value lies between 0 and 1, indicating favourable adsorption of chromate ions on both the composites. As described earlier (in Chapter 1), the 1/n factor of the Freundlich isotherm is also used to describe the heterogeneity of the adsorption process in literature[546,547]. If the value of 1/n is higher for one adsorbent than the other, it means the adsorption is occurring on a more heterogeneous surface[547]. For chromate ion adsorption on the CH/HAp/SCGs composites, the value of 1/n is similar for both the CH/HAp/SCGs composites (≈0.6), implying that the chromate ion adsorption is occurring on a similar heterogeneous surface of the CH/HAp/SCGs composites.

Loulidi et al. reported[555] the Langmuir isotherm model as the best-fitted model to describe the Cr(VI) adsorption on spent coffee grounds (SCGs)[232]. They estimated a maximum adsorption capacity (mg g^{-1}) of 42.9 mg g^{-1}, using the Langmuir isotherm model, at an adsorbent dose of 2.5 g exposed to 100 ppm chromate ions solution. In the present study, the estimated value of chromate ion adsorption on the CH/HAp/SCGs composites ranges from 29-31 mg g^{-1} for 0.01 g of adsorbent dose of composite exposed to 5 ppm-25 ppm chromate ions solution. The lower adsorption capacity of the CH/HAp/SCGs for chromate ions than the estimated value of chromate ion adsorption on raw SCGs in the mentioned literature study could be attributed to the higher adsorbent dose of adsorbent (2.5 g) employed in the literature study, as it has been discussed earlier that the adsorption capacity is dependent upon the sorbate molecules providing the binding sites for the removal of the metal ions. Another study[264] reported 10.2 mg g^{-1} as the maximum adsorption capacity of SCGs for the chromate ions, estimated using the Langmuir adsorption isotherm, using 0.1g of SCGs. In contrast, in the present study, the estimated maximum adsorption capacity of the CH/HAp/SCGs is higher for the chromate ions, using ten times less adsorbent dose (0.01 g) of adsorbent. It indicated that the addition of HAp could enhance the adsorption capacity for chromate removal from aqueous solutions

when the SCGs are used to form a composite with HAp (as shown by the CH/HAp/SCGs composites).

Several studies[308,559] reported the Freundlich isotherm model as the best-fitted model to describe the chromate adsorption on spent coffee grinds based adsorption systems, indicating a heterogeneous nature of adsorption for chromate ions on these adsorbents. In the present study, the Freundlich isotherm shows a suitable fitting (R^2=0.97-0.99). Considering the findings of the literature studies and the nature of the CH/HAp/SCGs composites, the Freundlich isotherm model could be regarded as a more suitable model than the Langmuir isotherm model to demonstrate the nature of chromate ion adsorption on this heterogeneous composite system. However, the empirical nature of the Freundlich model does not support its applicability. So, other models dealing with heterogeneous adsorption could be used to study the adsorption of the chromate ions on the CH/HAp/SCGs composites.

5.1.3.5 Comparison of the maximum adsorption capacities of the CH/HAp/SCGs composites and CH/HAp (control composites) for metal ion adsorption as estimated by the Langmuir isotherm model

The comparison of the maximum adsorption capacities (q_{max} in mg g^{-1}) of the control and CH/HAp/CF composites, estimated by Langmuir for metal ions adsorption studied, is presented in Table 5-21.

Table 5-21: Comparison of adsorption capacities (q_{max} mg g^{-1}) of the CH/HAp (control) and CH/HAp/SCGs composites as estimated by the Langmuir isotherm model

Composites	Cd^{2+}	Pb^{2+}	Cu^{2+}	Chromate ions
CH/cHAp	24.33	52.42	15.91	45.04
CH/bHAp	33.93	90.13	23.67	34.72
CH/cHAp/SCGs	24.62	34.69	9.99	27.17
CH/bHAp/SCGs	25.46	49.09	14.57	31.34

Table 5-21 illustrated the estimated adsorption capacity (in mg g^{-1}) of the CH/HAp/SCGs for metal ions adsorption was lower than the control composites systems, which could be attributed to the blockage of the adsorption sites on the HAp-part of the composites in particular leading to a reduction in the adsorption ability of the composites.

5.1.3.6 Effect of contact time on metal ions removal by the CH/HAp/SCGs composites

Experimental: The effect of contact time on metal ions removal (%) studied by the CH/HAp/SCGs composites was measured using different experimental conditions for each metal ion by varying the contact time between 1 minute and 120 minutes. A 0.05 g dose of adsorbent was used for Cd^{2+} and Pb^{2+} (50 ppm) and Cu^{2+} (50 ppm) adsorption in a single-metal ion type solution system. In comparison, 0.01 g of the dose was exposed to 25 ppm chromate solution to measure the effect of time on the chromate adsorption on the CH/HAp/SCGs composites.

Results: Table 5-22 (*Figures 4-85 to 4-88, Appendix 4*) presents the AAS data recorded for the effect of contact time on metal ion removal (%) using the CH/HAp/SCGs composites. A similar trend of rapid metal ion adsorption in the initial 1-30 minutes was observed and aligns with observations recorded earlier for control composites. The rapid increase in removal efficiency over the period of 1 to 30 minutes contact time could be attributed to the excess availability of active sites ($-NH_2$, -OH, $-COO^-$ and $-PO_4^{3-}$) at the beginning of the adsorption process, which gradually saturates and reaches equilibrium at 120 minutes.

Table 5-22: The effect of the contact time on the adsorption (% removal) of metal ions on the CH/HAp/SCGs composites system from a single metal ion type solution system

Contact Time (minutes)		1	2	3	4	5	10	15	30	60	120
Cd^{2+}	CH/cHAp/SCGs	10.60	14.84	20.01	24.46	26.40	32.93	41.13	54.76	60.12	67.87
	CH/bHAp/SCGs	19.53	24.48	26.49	36.06	38.69	42.16	45.08	58.58	65.04	77.99
Pb^{2+}	CH/cHAp/SCGs	24.34	28.45	33.90	34.06	42.09	57.47	66.37	85.34	97.58	97.59
	CH/bHAp/SCGs	15.71	25.33	28.95	31.37	39.23	50.47	71.64	95.89	97.81	97.99
Cu^{2+}	CH/cHAp/SCGs	7.02	9.53	13.01	16.51	17.57	32.15	42.58	59.15	64.04	81.18
	CH/bHAp/SCGs	6.43	13.53	18.4	19.19	23.74	35.09	43.04	68.06	76.29	89.73
Chromate	CH/cHAp/SCGs	18.67	20.83	21.32	22.55	22.74	23.70	36.11	36.25	36.36	36.40
	CH/bHAp/SCGs	13.89	19.78	19.89	22.03	22.10	23.28	36.3	36.64	36.65	36.56

The adsorbents reached adsorption equilibrium in 120 minutes, illustrating the saturation of active sites on the adsorbent surface and achieving 67% and 97% cations (Cd^{2+}, Pb^{2+} and Cu^{2+}) removal for the CH/HAp/SCGs composite. Relatively better removal of the CH/bHAp/SCGs than CH/cHAp/SCGs aligns with the observations recorded in earlier batch experiments conducted using the CH/HAp/SCGs composites for the removal of cations (see above).

For the chromate ions, the composites achieved maximum removal % (≈36%) within 15 minutes of contact time with the solution. This was also the adsorption equilibrium time for the CH/HAp/SCGs composites for chromate ion adsorption, as no further change in the removal (%) was recorded after 15 minutes. The rapid saturation of the binding sites on the adsorbent surface is attributed to the high affinity of chromate anions for the surface adsorption sites. The high affinity of chromate ion could be due to the availability of excess binding sites on the adsorbent surface for chromate anion adsorption. The relatively lower removal efficiency (only 36 %) of both the composites (as compared to cations removal, Table 5-22) could be due to the anionic nature of the chromate ion species present in the solution, which limits its adsorption on negatively charged adsorption sites which would dominate the surface of CH/HAp/SCGs composites in the pH range (5.0-6.0) of this experiment.

5.1.3.7 Kinetic modelling for metal ions (Cd^{2+}, Pb^{2+}, Cu^{2+} and chromate ions) adsorption on the CH/HAp/SCGs composite systems

Kinetic modelling of metal ion adsorption on the CH/HAp/SCGs composites was performed with testing done for non-linear pseudo-first-order (PFO) and pseudo-second-order (PSO) kinetics using the non-linear regression method as described earlier in the control composites section (for detail see appendix 1.3).

Results: The calculated kinetic model parameters for metal ion adsorption are given in Table 5-23. The comparison of coefficient of determination values (R^2) of PFO and PSO kinetic models showed that the PSO kinetic model is the best-fitted model with greater R^2 than PFO kinetic model for metal ion adsorption onto both composite systems. The PSO kinetic model fitting the experimental data of metal ion adsorption on the CH/HAp/SCGs composites indicating the rate-limiting step for metal ions on these composites is chemisorption[550]. These observations are in line with the findings of the control composites, illustrating the chemisorption is a rate-limiting step of the metal adsorption on these HAp-based composites. The finding is in good agreement with the adsorption literature, which has shown the PSO kinetics to apply for metal cations (such as Cd^{2+} and Pb^{2+}) adsorption on the composites made from chitosan hydroxyapatite, and lignocellulosic fibres[83,111,368,483].

Table 5-23: The parameters calculated for metal ion adsorption on the CH/HAp/SCGs composites based on each kinetic model fitted.

Metal ions	Kinetics Model	PFO			PSO		
	Parameters	k_1 (min^{-1})	q_e (mg g^{-1})	R^2	k_2 (g $mg^{-1}min^{-1}$)	q_e (mg g^{-1})	R^2
Cd^{2+}	CH/cHAp/SCGs	0.08	12.99	0.96	0.01	14.65	1
	CH/bHAp/SCGs	0.33	17.69	0.81	0.01	15.13	0.99
Pb^{2+}	CH/cHAp/SCGs	0.11	18.56	0.93	0.01	20.78	0.99
	CH/bHAp/SCGs	0.09	19.61	0.97	0.01	22.19	0.99
Cu^{2+}	CH/cHAp/SCGs	0.01	17.5	0.92	0	27.52	0.97
	CH/bHAp/SCGs	0.01	16.65	0.93	0	23.67	0.97
Chromate	CH/cHAp/SCGs	0.35	16.84	0.56	0.03	18.06	0.98
	CH/bHAp/SCGs	0.27	17.36	0.75	0.02	18.74	0.99

The chemisorption of metal ions on the CH/HAp/SCGs composites could occur through the functional groups of chitosan, HAp, and SCGs as described earlier in the batch experiment "the effect of adsorbent dose" above. Metal chelation by the electron-donating groups of chitosan ($-NH_2$), polyphenolic groups of SCGs and hydroxyl groups of all three components of CH/HAp/SCGs composites could be involved in the chemisorption of metal ions on these composites[319,557]. Additionally, another mechanism such as ion exchange between Ca^{2+} (of HAp) and cations, surface adsorption via electrostatic interactions between positively charged metal cations and negatively charged species ($-OH^-$, $-PO_4^{3-}$, COO^-) on the surface of the CH/HAp/SCGs composites, simultaneously could be involved in metal removal using such complex composite systems.

The calculated adsorption capacity (q_e in mg g^{-1}) calculated by the PSO kinetic model was 14.65 mg g^{-1} (CH/cHAp/SCGs) and 15.13 mg g^{-1} (CH/bHAp/SCGs) for Cd^{2+} , 20.78 mg g^{-1} and 22.19 mg g^{-1} for Pb^{2+} and 27.51 mg g^{-1} (CH/cHAp/SCGs) and 23.67 mg g^{-1} (CH/bHAp/SCGs) for Cu^{2+}.

The comparison of the coefficient of determination values (R^2) from the PFO and PSO kinetic models showed that the PSO kinetic model is the best-fitted model with a higher R^2 (>0.98) than that calculated for the PFO kinetic model for chromate ion adsorption on both composite systems. The calculated adsorption capacity (q_{max} in mg g^{-1}) of chromate ions (related to the adsorbent dose) by the PSO kinetic model was ≈18 mg g^{-1} for both the CH/HAp/SCGs composites. The fitting of the PSO kinetic model to the data relating the chromate ion adsorption on the CH/HAp/SCGs composites confirms that the chemisorption mechanism was the rate-limiting step for chromate ion adsorption using this composite.

5.1.4 Experiments involving the removal of metal ions by the CH/HAp/zeolite composites (commercial & bovine-derived) from the single-metal ion type solution system

The chitosan/HAp/zeolite (CH/HAp/zeolite) composite (a three-component component composite system) was synthesised by adding zeolite (mordenite) to the CH/HAp composite. Like the control composites and the three-component composite systems discussed in earlier sections (5.1.1-5.1.3), the spectroscopic and microscopic characterisation of the CH/HAp/Zeolite composites was done and comprehensively described in chapter 3 (section 3.4.4)

In the three-component composite systems discussed earlier in this study, hydroxyapatite was the dominant component, as evident by the characterisation of the composite systems in Chapter 3. The HAp part contributed about 40-50% of the composites' total mass (as estimated by the TGA analysis) in CH/HAp, CH/HAp/CF, and CH/HAp/SCGs composites. The remaining part (50-60%) of the total mass of composites was assumed to be made up of an inorganic component (that was HAp) in these composites. For instance, in the CH/HAp/CF and CH/HAp/SCGs composite systems, it was assumed by the TGA analysis of these composites (see sections 3.4.14, 3.4.2.4 &3.4.3.4) that about 40 % of the mass percentage were made up of one inorganic component (HAp). The remaining 60% was made up of the other two constituents (Chitosan and CF and Chitosan and SCGs in their respective composites).

In contrast, in the CH/HAp/Zeolite composites, the inorganic constituents (HAp and zeolite) were making more than 60% of the mass of the composites. Both of these constituents are well-known for their ion-exchange potential to remove metal ions from the solution. Based on the composition of these composites, it could be assumed that these composites would perform differently as those composites (studied in earlier sections) were made up of only one constituent (HAp) with ion-exchange potential. At the same time, this composite system has two components (HAp and zeolite), where the additional component (zeolite) also has ion-exchange potential of its own. Hence, a better removal ability from these composites relative to those studied earlier could be expected.

Different experimental parameters in batch experiments were studied for heavy metal ions removal using CH/HAp/zeolite from solutions containing only one dissolved metal

salt present (Pb^{2+}, Cd^{2+}, Cu^{2+} and Cr as chromate ions) and discussed in the following section.

5.1.4.1 Effect of adsorbent dose on metal ions removal by the CH/HAp/zeolite composites

Experimental: The metal ion adsorption and removal (%) were measured at 0.01g to 0.05 g of the CH/HAp/zeolite dose for an initial metal ion concentration of 50 ppm (for Cd^{2+}, Pb^{2+} and chromate ions) and 25 ppm (for Cu^{2+}) and initial solution pH 4.5-7.0.

Results: The results are presented in Table 5-24 (*Figures 4-97 to 4-100, Appendix 4*). A prominent trend of gradual increase in removal efficiency (%) and decrease in the adsorption capacity (mg g^{-1}) of CH/HAp/zeolite composites was observed with an increase in the adsorbent dose. It signifies that the removal efficiency of the adsorbent is essentially dependent upon the adsorbent dose of the adsorbents, as it provides the binding sites/adsorption sites for the removal of the adsorbates. The maximum removal of metal cations was recorded at 0.05 g of adsorbent dose, i.e., about 84-86 % (Cd^{2+}), ≈ 93% (Cu^{2+}) and > 97 % (Pb^{2+}) for both the composites. In contrast, the maximum adsorption was recorded at an adsorbent dose of 0.01 g (see Table 5-24).

The CH/bHAp/zeolite composite showed relatively better adsorption of Cd^{2+} ions with a maximum adsorption capacity of 25.80 mg g^{-1} at 0.01 g of adsorbent dose. The CH/cHAp/zeolite achieved 20.10 mg g^{-1} adsorption of $Cd^{2+}$for an equal dose of adsorbent, which aligns with the observations recorded in the composite systems studied earlier in the present study, where the bHAp-based composites showed a better removal efficiency for cations (Cd^{2+}, Pb^{2+} and Cu^{2+}) than cHAp-based composites. It could be deduced from these observations that the presence of bHAp plays a role in the better adsorption ability of composites than cHAp, as observed in all the composites systems of this study.

Table 5-24: The effect of the adsorbent dose on the removal efficiency (%) and adsorption capacity (mg g^{-1}) of the CH/HAp/zeolite composites for the adsorption of the metal ions in the single-metal ion type solution systems

The effect of the adsorbent dose on removal (%) of metal ions using the CH/HAp/zeolite composites						
	Dose	0.01	0.02	0.03	0.04	0.05
CH/cHAp/zeolite	Cd^{2+}	20.10	39.89	56.34	69.95	84.63
	Pb^{2+}	54.21	94.24	94.61	97.47	97.97
	Cu^{2+}	31.00	61.02	79.56	88.85	93.29
	Cr (as chromate ions)	13.31	15.54	17.22	18.89	19.81
CH/bHAp/zeolite	Cd^{2+}	25.80	46.62	63.70	77.53	86.92
	Pb^{2+}	67.23	94.51	96.32	97.96	98.07
	Cu^{2+}	33.99	64.08	82.43	92.37	93.87
	Cr (as chromate ions)	13.25	14.71	15.85	16.94	18.12
The effect of the adsorbent dose on the adsorption capacity (in mg g^{-1}) of the CH/HAp/zeolite composites with respect to the metal ions adsorbed						
CH/cHAp/zeolite	Cd^{2+}	20.10	19.95	18.78	17.49	16.93
	Pb^{2+}	54.21	47.12	31.54	24.37	19.59
	Cu^{2+}	15.50	15.25	13.26	11.11	9.33
	Cr (as chromate ions)	6.65	3.88	2.87	2.36	1.98
CH/bHAp/Zeolite	Cd^{2+}	25.80	23.31	21.23	19.38	17.38
	Pb^{2+}	67.23	47.26	32.11	24.49	19.61
	Cu^{2+}	17.00	16.02	13.74	11.55	9.39
	Cr (as chromate ions)	6.63	3.68	2.64	2.12	1.81

Alternatively, this slight difference in the adsorption abilities of the CH/cHAp/zeolite and CH/bHAp/zeolite composites could be due to the heterogeneity of the adsorbent dose (sample) exposed to the Cd^{2+} ions solution, as the grain size is a significant factor to affect the available specific surface area for the effective adsorption of adsorbate molecules.

Keeping in view the overall observations of the present study for the better removal ability of bHAp-based composites for removing the metal cations, the better adsorption of the CH/bHAp/zeolite could be attributed to the bHAp part of the composite. The maximum adsorption (mg g^{-1}) of the CH/HAp/zeolite composites recorded experimentally for Cd^{2+} ions removal is higher than all the composite systems studied in earlier sections (see earlier sections for reference), which indicates a positive effect of the presence of zeolite with HAp in these composites. This could be attributed to the ion exchange between the Cd^{2+} and cations of zeolite and HAp.

Similar to Cd^{2+} adsorption, the CH/bHAp/zeolite showed better adsorption for Pb^{2+} than CH/cHAp/zeolite at a lower adsorbent dose (0.01 g); however, it becomes comparable at 0.02-0.05 g of the adsorbent dose ranging between 87-98%, indicating an equal tendency of both the composites for Pb^{2+} adsorption at the relatively higher dose (0.05 g) of

adsorbent. Similarly, both the composite showed an equal tendency for the adsorption of Cu^{2+} ions, as demonstrated in Table 5-24 (see above).

The adsorption ability of the CH/HAp/zeolites for Pb^{2+} adsorption is about three times higher (i.e., 54-67 mg g^{-1} for Pb^{2+} ions) than recorded earlier for the Cd^{2+} adsorption (20-25 mg g^{-1}) for the same adsorbent dose of the composites. It illustrates the preference for Pb^{2+} adsorption on the available binding sites of the CH/HAp/zeolite composites. It agrees with the observations recorded in earlier sections, which also exhibited the better adsorption of Pb^{2+} ions than the Cd^{2+} ions.

The ion exchange could be considered the fundamental mechanism (due to HAp and zeolites) for the adsorption of metal cations using the CH/HAp/zeolite composites. The Pb^{2+} ions are better removed than Cd^{2+} by the ion-exchange mechanism due to their supporting physiochemical characters (such as electronegativity and ionic radius). So, the higher adsorption of Pb^{2+} ion on the CH/HAp/zeolites than the Cd^{2+} adsorption could be attributed to their better adsorption by the ion-exchange mechanism on the binding sites of the CH/HAp/zeolites, particularly on the HAp and zeolites parts.

The HAp-part, as an important component of the CH/HAp/zeolite composites, can participate in cations removal in several ways, including the ion exchange between Ca^{2+} and cations, metal-complexation by hydroxyl groups, electrostatic interactions between phosphates and positively charged cations.

AAS data for chromate ion adsorption on the CH/HAp/zeolite composites is presented in Table 5-24, showing a similar trend for the effect of adsorbent doses on chromate ion adsorption removal on the CH/HAp/zeolite composites as recorded in cation adsorption (above) and in earlier composite systems, illustrating a gradual increase in removal efficiency and decrease in adsorption capacity (mg g^{-1}) with increasing of the adsorbent dose. The maximum removal (%) was extremely low (< 20%) for both the composites, which is also lower than the removal efficiency (%) of the CH/HAp/zeolite composite for the cations removal (see above) and the maximum adsorption capacity of the CH/HAp/zeolite for the chromate ion adsorption was about 6 mg g^{-1} recorded at 0.01 g of adsorbent dose.

The adsorption of chromate ions on the CH/HAp/zeolite composite is lower than chromate adsorption on the CH/HAp (control) composites (see section 5.1.1.1). It demonstrates that the addition of zeolite into the CH/HAp (control) composites decreases

the removal efficiency of the CH/HAp composites for chromate ions adsorption. Contrary to this, in the earlier sections of the CH/HAp/zeolite composites systems, the addition of the zeolite into the CH/HAp composites exhibited a better removal efficiency for Cd^{2+}, Pb^{2+} and Cu^{2+} ions (see sections above). It is important to note that zeolite is well-known for its ion-exchange abilities, so the addition of the zeolite could be considered to improve the removal of cations (e.g., Cd^{2+}, $Pb^{2+}$and Cu^{2+}) using the ion exchange mechanism by the metal cations present in the structure of the zeolites. In contrast, chromate anions could not easily be removed by this ion-exchange mechanism by zeolites. Instead, the addition of zeolite could affect the chromate ion adsorption on the chitosan and HAp by blocking the binding sites available by involving other possible mechanisms described earlier (in Chapter 1, section1.6) for the adsorption of the chromate anions such as the electrostatic interactions and metal chelation (section) to remove chromate ions, resulting in a decrease in adsorption ability of the CH/HAp/zeolite composites.

The recordings mentioned above for the chromate removal on the CH/HAp/zeolite composites align with the findings of the earlier discussed composite systems, showing lower adsorption of chromate (anions) than the cations (Cd^{2+}, Pb^{2+} and Cu^{2+}), similarly, In the CH/HAp/zeolite composites system, the maximum adsorbent dose of 0.05 g showed relatively less adsorption ability for the chromate ions (ranging between 15-35%) than cations, e.g. Pb^{2+}, Cd^{2+} and Cu^{2+}(ranging between 80-99%).

5.1.4.2 Effect of solution pH on metal ions removal by the CH/HAp/zeolite composites

Experimental: The effect of solution pH on metal ion adsorption (mg g^{-1}) on the CH/HAp/zeolite was recorded by using solutions of different concentrations for different metals. For instance, the pH was altered between 4.0 and 8.0 for the solution of Cd^{2+} (50 ppm), which was exposed to 0.05 g of the CH/HAp/zeolite composites and kept on stirring (using a magnetic stirrer) for two hours before the analysis of final concentrations C_e (mg g^{-1}) by AAS. Similarly, the effect of pH on Pb^{2+} adsorption on the CH/HAp/zeolite composites was examined via AAS measurements in only a pH range from 4.0 -5.8 using a Pb^{2+} ion solution of 50 ppm exposed to 0.01 g of the CH/HAp/zeolite composites. Moreover, the effect of pH on Cu^{2+} ion removal by the CH/HAp/zeolite composites was studied in a narrow pH range of 4- 6.5 as selected for earlier composite systems. The initial Cu^{2+} ion concentration in solutions exposed to adsorbent was 25 ppm, and the

adsorbent dose was 0.05 g. The influence of pH on the adsorption of chromate ion on the CH/HAp/zeolite composites was studied over the pH range 4.0-8.0 using a solution with an initial chromate ion concentration of 35.0 ppm was exposed to constant adsorbent dose samples of 0.01 g.

Results: Table 5-25 shows the AAS data that changes the adsorption capacity (mg g^{-1}) of the CH/HAp/zeolite composites for metal ions adsorption with changing the solution pH. A similar change in metal ion adsorption was recorded, as noted earlier, for the CH/HAp (control) composites and three-component composites (discussed in earlier sections). This could be attributed to the reasons discussed in detail in earlier sections of this study.

Cd^{2+} adsorption was favoured at pH >5.0, which agrees with the observations recorded for the earlier composite systems. Based on the recordings of this batch experiment and the literature observations recorded for the similar composite[560,561], the pH 5.0-7.0 was considered optimum for Cd^{2+} adsorption using the CH/HAp/zeolite composites. Similarly, the adsorption of Pb^{2+} was maximum at pH 5.0, decreased slightly at >5.0 and increased again when solution pH was >5.6. The decrease in Pb^{2+} adsorption at a pH range of 5.0 <pH <5.5 to adsorb on binding sites of the composites was considered a primary reason for this Pb^{2+} decline[533], as mentioned earlier, and an increase in Pb^{2+} removal at pH greater than 5.6 was attributed to precipitation of Pb to convert into hydroxyl species of lead such as $Pb(OH)^{+}$, $Pb_3(OH)_4^{2-}$ or $Pb(OH)_2$ as milkiness in the Pb^{2+} solution was consistently observed in all the batch experiments conducted in this pH range (>5.5) in all the composite systems of this study.

Further, the AAS results (Table 5-25) showed the effect of pH on Cu^{2+} adsorption. A similar trend of "no effect on the Cu^{2+} ion adsorption by the changing of pH in the solution" from 4.0 to 6.5 in both the composites was observed as recorded in all earlier studied composite systems.

The observations for the effect of solution pH on chromate ion adsorption on the CH/HAp/zeolite composites indicate that the acidic/low pH favours chromate ion adsorption on such composite system as evident from Table 5-25, and attributed to the earlier discussed factors (in earlier sections) such as the speciation of chromate[485] as $HCrO_4^-$ and CrO_4^{2-} at pH <5.0 to favour its interaction with protonated amino groups (NH_3^+) on the chitosan and positively charged species on HAp surface (see equations 5-

4) by electrostatic interactions. The trend of better chromate ion adsorption at lower pH values (<5.0) agrees with other published studies for the adsorption of chromate ions on zeolite, chitosan/HAp composite systems and zeolite-based composite systesm[562,563].

Table 5-25: The effect of the solution pH on the adsorption capacity (in mg g^{-1}) of the CH/HAp/zeolite composites for the adsorption of metal ions from solutions containing only one type of metal ion

	pH	**4.0**	**5.0**	**6.0**	**7.0**	**8.0**
Cd^{2+}	CH/cHAp/zeolite	16.28	17.02	17.27	17.26	16.92
	CH/bHAp/zeolite	17.00	17.23	17.88	18.16	17.08
	pH	4.5	5.0	5.5	6.0	6.5
Pb^{2+}	CH/cHAp/zeolite	51.72	55.36	53.27	59.83	70.10
	CH/bHAp/zeolite	62.05	74.03	70.40	73.85	76.03
	pH	**4**	**5**	**5.5**	**6**	**6.5**
Cu^{2+}	CH/cHAp/zeolite	9.5	9.5	9.4	9.4	9.43
	CH/bHAp/zeolite	9.57	9.5	9.4	9.47	9.46
	pH	**4.5-5**	**5-5.5**	**6-6.5**	**7-7.5**	**8-8.5**
Cr as chromate ions	CH/cHAp/zeolite	1.37	1.32	0.99	0.70	0.64
	CH/bHAp/zeolite	1.50	1.48	1.40	1.07	0.94

5.1.4.3 Effect of the initial metal ion concentration on metal ions removal by the CH/HAp/zeolite composites

Experimental: For Cd^{2+} and Pb^{2+} ions adsorption on the CH/HAp/zeolite composites, the initial metal ion concentration was varied between 10 ppm and 50 ppm for a constant adsorbent dose of 0.01g, while the initial solution pH was 4.5-5.5 for evaluating the effect of initial adsorbate concentration of the solution on metal removal.

The effect of initial metal ion concentration on Cu^{2+} adsorption and chromate ions was studied by exposing a constant amount of adsorbent (0.01 g) to metal ion solutions of different initial concentrations between 5 ppm and 25 ppm at an initial solution pH of 4.5-6.5.

Further, the data recorded using AAS in this experiment were used to study the adsorption mechanism by fitting adsorption models (non-linear Langmuir and Freundlich adsorption models for cations and linear adsorption model for chromate ions, discussed in the upcoming section) by using the same regression method, as already been used for other composite systems.

Results: Table 5-26 (*Figures 4-105 to 4-108, Appendix 4*) shows the AAS data, presenting the effect of the initial metal ion concentration on metal ion adsorption on the CH/HAp/Zeolite composites. The metal ion adsorption on the CH/HAp/zeolite composites exhibited a similar trend of increasing adsorption capacity and decreasing removal efficiency (%) with an increase in initial metal ion concentration (from 10 ppm to 50 ppm for Cd^{2+} and Pb^{2+} and 5 ppm to 25 ppm for Cu^{2+} and chromate ions) as recorded in earlier sections of metal adsorption on all the synthesised composite systems in the present study.

The maximum removal (%) of Cd^{2+} was 32.14% (CH/cHAp/zeolite) and 37.3 % for the CH/bHAp/zeolite) recorded at an initial concentration of 10 ppm of Cd^{2+}. At the same time, the maximum adsorption capacity (q_e mg g^{-1}) was noted at 50 ppm of Cd^{2+} solution (19.6 mg g^{-1} and 22.2 mg g^{-1} on the CH/cHAp/zeolite and the CH/bHAp/zeolite composite, respectively). The maximum adsorption of Cu^{2+} (at an initial ion concentration of 25 ppm) was 15.28 mg g^{-1} and 16.73 mg g^{-1} on the CH/cHAp/zeolite composite and the CH/bHAp/zeolite composite, respectively. Similarly, the maximum adsorption of Pb^{2+} was recorded at 50 ppm, which was 57.01 mg $g^{-1}$and 72.26 mg g^{-1} on the CH/cHAp/zeolite composite and the CH/bHAp/zeolite composites, respectively. The highest removal (%) ≈ 84-89 %, was recorded at 10 ppm for both the composites.

It has been discussed in earlier sections (see above) that several mechanisms simultaneously assist cations removal from solutions on such adsorption systems. However, a similar trend of higher Pb^{2+} adsorption on the CH/HAp/zeolite composites than Cd^{2+} was recorded as evident from the comparison of removal (%) of Pb^{2+} and Cd^{2+} on CH/HAp/zeolite composites (see Table 5-26). This study aligns with the observations recorded, showing better Pb^{2+}ion adsorption than Cd^{2+} ion adsorption on the CH/HAp-based composite systems in the present study and also agrees with the similar trend in the literature studies. The better adsorption of Pb^{2+} than Cd^{2+} on such composite systems is attributed to the chemical characteristics of $Pb^{2+,}$ as mentioned in earlier sections and is discussed in detail in upcoming sections (section 5.2.2).

Table 5-26: The effect of the initial metal ion concentration on removal (%) and the adsorption capacity (in mg g^{-1}) of different metal ions adsorbed on the CH/HAp/zeolite composites from a single-metal ion type solution system

The removal (%) of metal ions using the CH/HAp/zeolite composites						
	Metal ion concentrations (ppm)	10.0	20.0	30.0	40.0	50.0
Cd^{2+}	CH/cHAp/zeolite	32.15	29.04	27.77	23.58	19.67
	CH/bHAp/zeolite	37.30	32.45	29.37	25.88	22.21
Pb^{2+}	Metal ion concentrations (ppm)	10.0	20.0	30.0	40.0	50.0
	CH/cHAp/zeolite	84.39	80.39	79.79	70.68	57.10
	CH/bHAp/zeolite	89.78	85.43	84.72	82.46	72.26
Cu^{2+}	Metal ion concentrations (ppm)	5.0	10.0	15.0	20.0	25.0
	CH/cHAp/zeolite	67.90	61.23	45.90	37.78	30.56
	CH/bHAp/zeolite	68.32	67.19	55.57	42.18	33.46
Cr as chromate ions	Metal ion concentrations (ppm)	5.0	10.0	15.0	20.0	25.0
	CH/cHAp/zeolite	20.87	18.41	14.49	11.31	10.33
	CH/bHAp/zeolite	20.98	18.76667	14.18	10.89	10.07
The adsorption capacity (in mg g^{-1}) of the CH/HAp/zeolite composites or different metal ions						
	Metal ion concentrations (ppm)	10.0	20.0	30.0	40.0	50.0
Cd^{2+}	CH/cHAp/zeolite	6.43	11.61	16.66	18.86	19.67
	CH/bHAp/zeolite	7.46	12.98	17.62	20.71	22.21
Pb^{2+}	Metal ion concentrations (ppm)	10.0	20.0	30.0	40.0	50.0
	CH/cHAp/zeolite	16.88	32.15	47.88	56.54	57.10
	CH/bHAp/zeolite	17.96	34.17	50.83	65.97	72.26
Cu^{2+}	Metal ion concentrations (ppm)	5.0	10.0	15.0	20.0	25.0
	CH/cHAp/zeolite	6.79	12.25	13.77	15.11	15.28
	CH/bHAp/zeolite	6.83	13.44	16.67	16.87	16.73
Cr as chromate ions	Metal ion concentrations (ppm)	5.0	10.0	15.0	20.0	25.0
	CH/cHAp/zeolite	2.09	3.68	4.35	4.52	5.16
	CH/bHAp/zeolite	2.10	3.75	4.25	4.36	5.04

Relatively better adsorption of cation (Cd^{2+}, Pb^{2+}, Cu^{2+}) on the CH/bHAp/zeolite composite could be attributed to the bHAp part of the composite, keeping in view the observations recorded earlier for the bHAp-based composites system, which showed better removal than cHAp-based composite in this study. The availability of more binding sites on the CH/bHAp/zeolite composite than on the CH/cHAp/zeolite composite could be considered the fundamental reason for its higher removal efficiency. And the larger specific surface area of CH/bHAp/zeolite could be the foundation for providing more binding sites to perform in metal removal mechanisms such as ion exchange and metal-ligand complexation.

Similar to the adsorption behaviour of cations on the CH/HAp/zeolite composites, a continuous increase in adsorption capacity (mg g^{-1}) of both the composites was recorded

(Table 5-26) with increasing chromate ion concentration from 5 ppm to 25 ppm, which is attributed to the availability of more metal ions to sorb on a fixed number of active sites of 0.01 g of the adsorbent at all concentrations and a continuous decrease in removal efficiency (%) corresponds to the availability of more metal ions to sorb on a limited number of active sites to remove metal ions. The maximum adsorption ≈5 mg g^{-1} for both the composites was measured at a 25 ppm concentration of chromate ions in solution. The maximum removal (%) of chromate ions was measured at a 5 ppm concentration of about 20% for both the composites. Both the composites showed comparable removal efficiencies at all the ion concentrations studied in this batch experiment. The maximum difference between the removal efficiencies of the two composites is less than 1%.

To understand the removal mechanism and estimate the maximum adsorption capacity (q_{max} mg g^{-1}) of this composites system, the AAS data collected in this experiment was further analysed using non-linearised and linearised adsorption models (Langmuir and Freundlich) as has been done for chromate ion and cation adsorption modelling in other systems of this study.

5.1.4.4 Adsorption modelling of the CH/HAp/zeolite composites for the adsorption of metal ions

Experimental: The experimental results of cation adsorption on the CH/HAp/zeolite composites were tested against non-linear Langmuir and Freundlich isotherms as described earlier (section 5.1.1.4, 5.1.2.4 & 5.1.3.4). The chromate adsorption modelling was done using the linear adsorption models using the method described earlier in control composites. The best-fitted model was then decided from the comparison of the R^2 values from two fitted models.

Results: The calculated isotherm parameters for two adsorption models for metal ions adsorption on the CH/HAp/zeolite composites are given in Table 5-27, and models fitted to the experimental data are presented in *Figures 4-109 to 1-116 (Appendix 4).*

The calculated isotherm parameters for two adsorption models for metal ions (all four studied) adsorption on the CH/HAp/zeolite composites are given in Table 5-27. The comparison of R^2 values of non-linear Langmuir and Freundlich models revealed that the Langmuir isotherm model was the best-fitted model for explaining the adsorption of metal ions on the CH/HAp/zeolite composite with R^2 of Langmuir adsorption model is higher

than the R^2 of Freundlich model. Both Langmuir and Freundlich showed good fitting for some composite systems. For instance, the Freundlich adsorption isotherm is showing good fitting for Cd^{2+} adsorption on the CH/HAp/Zeolite composite with R^2 value > 0.94, Pb^{2+} adsorption on the CH/bHAp/zeolite with R^2 > 0.91, and the chromate ion adsorption on the CH/HAp/zeolite composites R^2 ranging between 0.91-0.94.

Table 5-27: Adsorption isotherm parameters for metal ions (Cd^{2+}, Pb^{2+} and $Cu^{2+}$and chromate) adsorption on the CH/HAp/zeolite composites

Metal ions	Adsorption Isotherms	Langmuir			Freundlich			
	Parameters	q_{max} (mg g^{-1})	K_L	R^2	R_L	1/n	q_{max} (mg g^{-1})	R^2
Cd^{2+}	CH/cHAp/zeolite	33.22	0.04	0.98	0.38	0.56	2.66	0.94
	CH/bHAp/zeolite	37.04	0.04	1.00	0.39	0.56	3.05	0.98
Pb^{2+}	CH/cHAp/zeolite	72.49	0.24	0.95	0.16	0.36	20.72	0.84
	CH/bHAp/zeolite	100.47	0.21	0.97	0.25	0.46	23.25	0.91
Cu^{2+}	CH/cHAp/zeolite	17.56	0.47	0.97	0.11	0.28	7.37	0.87
	CH/bHAp/zeolite	20.11	0.47	0.90	0.11	0.27	8.51	0.74
Chromate ions	CH/cHAp/zeolite	7.71	0.10	0.98	0.32	0.50	1.14	0.94
	CH/bHAp/zeolite	7.27	0.11	0.97	0.30	0.47	1.21	0.91

The Langmuir isotherm model fitted to metal ion adsorption data for the CH/HAp/zeolite composites suggested a monolayer adsorption model for metal ions on a homogeneous adsorbent surface[494]. However, the SEM analysis exhibited a highly heterogeneous surface of the CH/HAp/zeolite composites with deposited particles, so the data could be analysed further by using other adsorption models such as the Sips isotherm used to describe the adsorption behaviour on heterogeneous surfaces. (Plots for the Sips model fitted to the experimental data are given in *Appendix 4 (Figure 4-117 to 4-119).*

Using the Langmuir model, the calculated q_{max} (mg g^{-1}) of Cd^{2+} was 33.21 mg g^{-1} and 37.04 mg g^{-1} on the CH/cHAp/zeolite and the CH/bHAp/zeolite composites, respectively. Similarly, the maximum adsorption of Cu^{2+} (at an initial ion concentration of 25 ppm) was 15.28 mg g^{-1} and 16.73 mg g^{-1} on the CH/cHAp/zeolite composite and the CH/bHAp/zeolite composite, respectively. At the same time, the CH/HAp/zeolite composites exhibited a higher adsorption tendency for Pb^{2+} than Cd^{2+} and Cu^{2+} ions both, with maximum adsorption (q_{max} mg g^{-1}) of 57.01 mg $g^{-1}$and 72.26 mg g^{-1} on the CH/cHAp/zeolite composite and the CH/bHAp/zeolite composites, respectively. This observation aligns with the observations recorded, showing the greater degree of Pb^{2+}ion adsorption than Cd^{2+} ion adsorption on the CH/HAp-based composite systems in the present study and also agrees with the similar trend in the literature studies. The better

adsorption of Pb^{2+} than Cd^{2+} on such composite systems is attributed to the chemical characters of $Pb^{2+,}$ as mentioned in earlier sections. The values of the dimensionless factor R_L for metal ions adsorption on the CH/HAp/zeolite composites given in Table 5-27 indicated a favourable adsorption process as $0 < R_L < 1$.

Several literature studies reported the fitting of the Langmuir isotherm model to describe the adsorption behaviour of metal cations (e.g., Cd^{2+}) on natural zeolites. For instance, a study[560] estimated the maximum adsorption (25.9 mg g^{-1}) of Cd^{2+} on natural zeolites using the Langmuir isotherm model, which is less than the estimated value of a maximum adsorption capacity of CH/HAp/zeolite composites for Cd^{2+} adsorption in the present study (Table 5-27). Another study[564] recorded 13.4 mg g^{-1} as the maximum adsorption capacity (q_{max}) of natural zeolites when the Cd^{2+} ion solution (1-10 mmol L^{-1}) was exposed to 1.0 g of adsorbent dose of natural zeolites. The estimated maximum adsorption capacity of natural zeolites[564] was found to be less (approximately half) than estimated in the present study for the Cd^{2+} ion adsorption on the CH/HAp/zeolite composites. These observations of the literature studies and the present study indicated that better adsorption of the heavy metals could be achieved by making composites of natural zeolites with the HAp.

The literature studies reported the ion exchange with metal cations (found in the of sodium, calcium and magnesium zeolites) as a principal mechanism for removing metal cations (such as Cd^{2+}, Pb^{2+}) ions from the aqueous solution using the natural zeolites. The metal removal could be enhanced by HAp addition which could assist in the ion-exchange mechanism (by Ca^{2+} ions) in the composites of HAp and zeolites. Additionally, chitosan can also participate in other metal ion removing mechanisms discussed in earlier composite systems, such as the metal-chelation by $-NH_2$ and -OH groups, to make it a promising material for the heavy metal removal from the aqueous solutions.

Along with adsorption model parameters for the cation adsorption modelling, Table 5-27 also shows the parameters of linearized Langmuir and Freundlich isotherm calculated for the chromate ion adsorption data recorded for the CH/HAp/zeolite composites. The equations generated for chromate adsorption modelling from the linearised models fitted using Microsoft Excel are given as follows.

Table 5-28: The linearised equations calculated for chromate ion adsorption on the CH/HAp/zeolite composites using linearised Langmuir and Freundlich isotherms

Composites	Linearised Langmuir Equation	Linearised Freundlich Equation
CH/cHAp/zeolite	$y = 1.3488x + 0.1296$ ($R^2 = 0.9833$)	$y = 0.594x + 1.3092$ ($R^2 = 0.9933$)
CH/bHAp/zeolite	$y = 1.2968x + 0.1375$ ($R^2 = 0.9709$)	$y = 0.6124x + 1.2722$ ($R^2 = 0.974$)

The Langmuir and Freundlich isotherms parameters were calculated using the above equations by the method described earlier in the CH/HAp (control) composites.

The calculated parameters for the systems tested and derived from both the adsorption models are thus given in Table 5-27. Comparing R^2 values of both adsorption models reveals that the Langmuir adsorption isotherms were the best fit to describe the adsorption of chromate ions on the CH/HAp/zeolites and indicates the adsorption is occurring on a homogeneous surface in a monolayer manner.

The maximum adsorption capacity (mg g^{-1}) of the CH/cHAp/zeolite composite and the CH/bHAp/zeolite composite for chromate ion adsorption, as estimated by the linearized Langmuir isotherm model, is 7.71 mg g^{-1} and 7.27 mg g^{-1}, respectively, which is lying close to the experimental values of chromate ion adsorption on the CH/HAp/zeolite composites. The dimensionless factor R_L of Langmuir isotherm also showed favourable adsorption of chromate ion on both the composites as $0 < R_L < 1$.

The fitting of Langmuir to describe the chromate ion adsorption on the CH/HAp/zeolite composites is in line with the observation recorded in the adsorption modelling of other metal ion adsorption in this system (see the earlier section of the CH/HAp/zeolite composites). It illustrates that the adsorption on the CH/HAp/zeolite composites occurs on a homogeneous surface. This observation aligns with the adsorption modelling done in the literature studies to describe the chromate ion adsorption on similar adsorbents (see Table 1-8).

5.1.4.5 Comparison of maximum adsorption capacities of the CH/HAp/zeolite and the CH/HAp (control composites) for metal ion adsorption as estimated by the Langmuir isotherm model

The adsorption modelling of the CH/HAp/zeolite composites confirms the findings of control composites which also exhibited the Langmuir as the best-fitted model to describe

metal ion adsorption. The comparison of maximum adsorption capacities (q_{max} mg g^{-1}) of control and the CH/HAp/zeolite composites, estimated by the Langmuir model for metal ion adsorption, is presented in Table 5-29.

Table 5-29: Comparison of adsorption capacities (q_{max} mg g^{-1}) of the CH/HAp (control) and CH/HAp/zeolite composites as estimated by Langmuir isotherm model

Composites	Cd^{2+}	Pb^{2+}	Cu^{2+}	Chromate ions
CH/cHAp	24.33	52.42	15.91	45.04
CH/bHAp	33.93	90.13	23.67	34.72
CH/cHAp/zeolite	33.22	72.49	17.56	7.71
CH/bHAp/zeolite	37.04	100.47	20.11	7.27

Table 5-29 indicates the increase in the q_{max} of the CH/HAp composites (control) for the adsorption of Cd^{2+} and Pb^{2+} after adding zeolites into CH/HAp to synthesise the CH/bHAp/zeolite composites. It could be attributed to the availability of more active sites, particularly the ion-exchanging sites for removing these ions from the aqueous solution exposed to the CH/HAp/zeolite composites. The adsorption capacity of Cu^{2+} is comparable, which is not aligned with the trends recorded for the other two cations, and this unusual trend of Cu^{2+} could be associated with other experimental factors such as the heterogeneity of the sample (grain size etc.), affecting the adsorption ability of the composites.

Expectedly, the adsorption capacity (q_{max}) of the CH/HAp (control) composites decreased for the chromate ion adsorption after the addition of zeolite into the composites, which is attributed to the availability of fewer adsorption sites for the adsorption of chromate ions, as the ion-exchange (particularly with cations) is considered the dominating mechanisms for HAp and zeolite, which does not favour the adsorption of chromate ions on this composite system.

5.1.4.6 Effect of contact time on metal ion removal by the CH/HAp/zeolite composites

Experimental: The effect of contact time on metal ion removal (%) by the CH/HAp/zeolite composites was measured by varying the contact time between 1 minute and 120 minutes. The adsorption was measured on a 0.05 g dose of adsorbent in 20 mL of solution using an initial metal concentration of 50 ppm (of Cd^{2+} and Pb^{2+}) and 25 ppm (of Cu^{2+}). Similarly, the effect of contact time on chromate ion removal (%) on the

CH/HAp/zeolite composites was recorded for a solution with an initial chromate ion concentration of 25 ppm exposed to 0.01 g of composite adsorbent.

Results: Table 5-30 presents the AAS data recorded for the effect of contact time on metal ions removal (%) using the CH/HAp/zeolite composites. A similar trend of rapid metal ion adsorption in the initial 1-30 minutes was observed, as recorded earlier for the CH/HAp (control) composites and attributed to the very obvious reason of excess adsorption sites at the beginning of the adsorption process.

Table 5-30: The effect of the contact time on the adsorption of metal ions on the CH/HAp/zeolite composites system from a single metal ion type solution system

Contact Time (minutes)		**1**	**2**	**3**	**4**	**5**	**10**	**15**	**30**	**60**	**120**
Cd^{2+}	CH/cHAp/zeolite	20.96	26.60	32.26	36.76	39.34	48.43	55.32	67.82	74.46	86.39
	CH/bHAp/zeolite	30.47	36.18	40.00	42.65	44.34	55.96	60.22	76.03	78.89	87.62
Pb^{2+}	CH/cHAp/zeolite	41.19	57.09	61.06	72.31	75.64	91.06	92.75	93.25	93.32	93.32
	CH/bHAp/zeolite	43.38	60.85	69.84	75.18	80.36	90.89	92.74	95.12	97.30	97.31
Cu^{2+}	CH/cHAp/zeolite	15.09	25.62	35.62	37.68	39.58	53.24	67.92	76.72	92.78	93.24
	CH/bHAp/zeolite	22.65	32.47	40.83	42.69	52.32	67.42	67.89	92.50	93.14	94.83
Chromate	CH/cHAp/zeolite	10.12	10.39	12.24	13.64	14.14	14.33	14.83	18.92	19.48	19.52
	CH/bHAp/zeolite	13.12	13.70	13.86	15.02	16.16	16.62	17.10	17.20	18.36	19.20

The adsorbents reached adsorption equilibrium in 60 minutes for Cd^{2+} adsorption, illustrating the saturation of active sites on the adsorbent surface and achieving 85% and 87% Cd^{2+} removal for the CH/cHAp/zeolite and the CH/bHAp/zeolite composites, respectively. Similarly, maximum removal efficiency for both the composites tested was calculated to be about 93-97% for Pb^{2+} adsorption over the 2 hours of exposure time. The optimum time for realising the highest Pb^{2+} ion removal with the CH/HAp/zeolite composites was found to be 60 minutes, as no prominent change in the removal efficiency was recorded after 60 minutes. Both the composites showed comparable removal (%) of Cd^{2+} and Pb^{2+} at 0.01-0.05 g of adsorbent dose, which agrees with the observations recorded above for "the effect of adsorbent dose" on metal cation adsorption on the CH/HAp/zeolite composites (Table 5-24). The similar adsorption capacities of the CH/HAp/zeolite composites are attributed to the availability of excess adsorption sites at 0.05 g of adsorbent (optimum) dose.

Both composite samples achieved about 40- 50% removal in just 5 minutes and reached equilibrium (saturation of adsorbent) in 60 minutes with more than 92% Cu^{2+} removal, as no further change in removal (%) was recorded after 120 minutes for both the composites. The rapid increase (similar to kinetics data observations of Cd^{2+} and Pb^{2+} in this composite system) in removal efficiency over 1 to 15 minutes of contact time, indicating about 67% removal, could be attributed to the excess availability of active sites (NH_2, OH^-, and PO_4^{3-} and cationic species of zeolites) at the beginning of the adsorption process, which gradually saturates and reaches equilibrium at 60 minutes.

Similar to the kinetics observations of cation adsorption on the CH/HAp/zeolite composites, Table 5-30 shows that both the composites achieved maximum removal % for the chromate ions (≈20%) in solution within 120 minutes of contact time with the solution. This was also the adsorption equilibrium time for the CH/HAp/zeolite composites for the chromate ion adsorption. The rapid saturation of the binding sites on the adsorbent surface occurred in 5 minutes, where the composites achieved about 14-15 % removal, and additional 5% removal was achieved in the next 105 minutes. The rapid adsorption in 5 minutes is attributed to the fast affinity of chromate anions and the surface adsorption sites. The fast affinity of chromate anions could be due to the availability of excess binding sites on the adsorbent surface for chromate anion adsorption. The relatively lower removal efficiency (only 20 %) of both the composites (as compared to cation removal) could be due to the anionic nature of the chromate ion species present in the solution, as it has been recorded in all the batch experiments of this study, which were conducted for chromate ion adsorption on the CH/HAp (control composites) and other three-component composite systems. The anionic nature of chromate ions could limit its adsorption on negatively charged adsorption sites which probably dominate the surface of CH/HAp/zeolite composites in the pH range (5.0-6.0) of this experiment.

5.1.4.7 Kinetic modelling for metal ion (Cd^{2+}, Pb^{2+}, Cu^{2+} and chromate ions) adsorption on the CH/HAp/zeolite composite systems

Experimental: Kinetic modelling of metal ion adsorption on the CH/HAp/zeolite composites was performed with testing done for non-linear pseudo-first-order (PFO) and pseudo-second-order (PSO) kinetics using the non-linear regression method as described earlier in the control composites section (for detail see appendix 1.3A).

Results: Table 5-31 shows the calculated parameters of kinetic models fitted to the experimental data of metal ion adsorption on the CH/HAp/zeolite composites.

The comparison of coefficient of determination values (R^2) of PFO and PSO kinetic models showed that the PSO kinetic model is the best-fitted model with a greater R^2 value noted than that for the PFO kinetic model for metal ion adsorption on both composite systems.

Table 5-31: The parameters calculated for metal ion adsorption on the CH/HAp/zeolite composites based on each kinetic model fitted.

Metal ions	Kinetics Model	PFO			PSO		
	Parameters	**k_1 (min^{-1})**	**q_e (mg g^{-1})**	**R^2**	**k_2 (g mg^{-1} min^{-1})**	**q_e (mg g^{-1})**	**R^2**
Cd^{2+}	CH/cHAp/zeolite	0.13	15.83	0.90	0.01	17.39	1.00
	CH/bHAp/zeolite	0.18	16.76	0.83	0.01	17.62	0.99
Pb^{2+}	CH/cHAp/zeolite	0.43	18.39	0.94	0.04	19.56	1.00
	CH/bHAp/zeolite	0.48	18.74	0.95	0.04	19.95	1.00
Cu^{2+}	CH/cHAp/zeolite	0.12	8.71	0.94	0.02	9.80	1.00
	CH/bHAp/zeolite	0.17	8.95	0.93	0.02	9.92	1.00
Chromate	CH/cHAp/zeolite	0.47	1.61	0.53	0.41	1.74	0.99
	CH/bHAp/zeolite	0.88	1.65	0.54	0.80	1.75	1.00

The PSO kinetic model fitting the experimental data of metal ion adsorption on the CH/HAp/zeolite composites, indicating the rate-limiting step for metal ions on these composites is chemisorption[550]. These observations align with the findings of control composites, illustrating that the chemisorption is a rate-limiting step of metal ion adsorption on these HAp-based composites.

The chemisorption of metal ions on the CH/HAp/zeolite composites could occur through the mechanism involving the functional groups of chitosan, HAp, and zeolite. Metal chelation by the $-NH_2$ and hydroxyl groups would be considered one of the fundamental mechanisms for chemisorption of metal cations on CH/HAp/zeolite composites, as mentioned in earlier composite systems discussed in this study. The ion exchange is not considered a chemisorption mechanism, but it is discussed as chemisorption in the broader perspective of metal adsorption processes. It has been mentioned that zeolite is the dominating component of the CH/HAp/zeolite composite systems (referred to characterisation of the composite). However, the ion exchange would be considered the fundamental mechanism involved in the adsorption of cations by these composites, mainly on the part of zeolite and HAp both.

In all other composite systems discussed earlier in this study, the HAp was considered as a dominating part of the composite systems to remove heavy metal ions as the addition of the third component (like coir fibre, SCGs) did not improve the removal efficiency of the CH/HAp (control) composites. In the CH/HAp/zeolite composites system, it was realised while characterising the CH/HAp/zeolite composites (Chapter 3, section 3.4.4) that the zeolite was dominating the HAp in the composites, as evident by the FTIR and XRD analysis of the CH/HAp/zeolites composites (see section 3.4.4). It is signified further by the findings of these batch experiments (mentioned above) that, unlike the other three-component composite systems, adding the third component (zeolite) into the CH/HAp composites improved the adsorption ability attributed to the zeolites. It has also been described in the literature review (chapter 1, section 1.5) that zeolites are well-known for ion-exchange mechanisms, so the increase in the ion-exchange ability of the CH/HAp composites after the addition of zeolites could be a reason for the improved removal efficiency of these composites.

For the chromate ion adsorption, the comparison of the coefficient of determination values (R^2) from the PFO and PSO kinetic models showed that the PSO kinetic model is the best-fitted model with a higher R^2 (>0.98) than that calculated for the PFO kinetic model for chromate ion adsorption on both composite systems. The calculated adsorption capacity (q_{max} in mg g^{-1}) of chromate ions (related to the adsorbent dose) by the PSO kinetic model was ≈1 mg g^{-1} for both the CH/HAp/zeolite composites. The fitting of the PSO kinetic model to the data relating the chromate ion adsorption on the CH/HAp/zeolite composites confirms that the chemisorption mechanism was the rate-limiting step for chromate ion adsorption using this composite. The earlier observations of this study demonstrate that the PSO kinetic model is the best-fitted model to describe the adsorption behaviours of chromate ions on such composite systems.

The relatively lower adsorption ability of the CH/HAp/zeolite than the CH/HAp (control) composites could be attributed to the relatively lower surface area of the CH/HAp/zeolite than the CH/HAp (control), or it could be due to less availability of the adsorption sites suitable for chromate anion adsorption, as it is composed of HAp and zeolites.

5.1.4.8 Intra-particle diffusion kinetic model for the metal ion adsorption on the CH/HAp/zeolite composites

It has been discussed in the literature review section of the zeolites (section 1.5.5) that the zeolites are porous materials. Keeping in view the porosity factor of the CH/HAp/zeolite composites, the kinetic data of the metal ion adsorption was further analysed using a third model called the intra-particle diffusion model described in Chapter 1 (section 1.11.3), which is applicable to porous adsorbents like zeolites.

The above-mentioned kinetics models (the PFO and PSO) do not recognise the diffusion mechanism during adsorption on a porous adsorbent surface. For this, the kinetic model (also given in chapter 1), including the square root of time, is employed to explain diffusion called the intra-particle diffusion model (IPD) and given as:

Equation 5-9

$$q_t = k_d t^{0.5} + C$$

Where q_t is the amount of adsorbed metal ions (mg g^{-1}) at the time "t", C (mg g^{-1}) is the interparticle diffusion constant equal to the intercept of the line, giving an insight into adsorption boundary thickness, k_d is intra-particle diffusion constant (mg g^{-1} $min^{-0.5}$) indicating the rate of adsorption[83].

Generally, adsorption includes more than one step[565], such as boundary diffusion, which involves the rapid transport of the sorbate molecule into the water film surrounding the adsorbent surface (Step I), followed by sorbate diffusion to the external surface of the adsorbent (step II). Then the sorbate molecules diffuse from the outer surface of the adsorbent to the intra-particle spaces (pore diffusion, step III). In some cases, the IPD kinetic model involves two steps only[566], including the rapid transport of the adsorbate from bulk to the external surface of the adsorbent (step I), followed by the pore diffusion (rate-limiting step) as it is slower than step I[356].

For the IPD kinetic model fitted to the metal ion adsorption data for CH/HAp/zeolites composites; two distinct regions were recognised, attributed to bulk diffusion (fast initial step) and intra-particle diffusion (step II) for both composite systems *(see Figures 4-132-4-135, appendix 4 for reference)* which is in line with results reported for heavy metal removal by a cellulose-based adsorbent[567].

The parameters of the IPD kinetic model were calculated from the linear equations (Table 5-32), which were obtained from fitting of the IPD kinetic model to the kinetic data of metal ion adsorption on the CH/HAp/zeolites. The linear equations obtained from fitting of the IPD model are given as follows:

Table 5-32: The IPD kinetic model equations calculated for the kinetics data of CH/HAp/zeolite composites

Metal ions	Composites	Step I	Step II
Cd^{2+}	CH/cHAp/zeolite	$y = 2.364x + 2.2131$ ($R^2 = 0.981$)	$y = 0.6944x + 10.1$ ($R^2 = 0.946$)
	CH/bHAp/zeolite	$y = 2.0906x + 4.2484$ ($R^2 = 0.989$)	$y = 0.4585x + 12.945$ ($R^2 = 0.8596$)
Pb^{2+}	CH/cHAp/zeolite	$y = 5.5493x + 2.9886$ ($R^2 = 0.974$)	$y = 0.0564x + 18.124$ ($R^2 = 0.702$)
	CH/bHAp/zeolite	$y = 5.8842x + 3.3195$ ($R^2 = 0.972$)	$y = 0.1933x + 17.483$ ($R^2 = 0.965$)
Cu^{2+}	CH/cHAp/zeolite	$y = 1.7071x + 0.1649$ ($R^2 = 0.976$)	$y = 0.2826x + 6.4809$ ($R^2 = 0.683$)
	CH/bHAp/zeolite	$y = 1.6414x + 1.0457$ ($R^2 = 0.935$)	$y = 0.0433x + 9.0003$ ($R^2 = 0.975$)
Chromate	CH/cHAp/zeolite	$y = 0.1776x + 0.8196$ ($R^2 = 0.818$)	$y = 0.0812x + 1.1215$ ($R^2 = 0.767$)
	CH/bHAp/zeolite	$y = 0.1679x + 1.0607$ ($R^2 = 0.935$)	$y = 0.0399x + 1.4615$ ($R^2 = 0.863$)

The parameters of the IPD kinetic model calculated from the linear equations (Table 5-32), obtained from fitting of the IPD kinetic model to the kinetic data of metal ion adsorption on the CH/HAp/zeolites, are given as follows:

Table 5-33: The IPD model parameters calculated for metal ion adsorption on the CH/HAp/zeolite composites calculated by using the linear equations given in Table 5-32

Metal ions	Composite systems	IPD Kinetic Model					
		Step I			Step II		
		K_d	C	R^2	K_d	C	R^2
Cd^{2+}	CH/cHAp/zeolite	2.35	2.21	0.98	0.69	10.10	0.95
	CH/bHAp/zeolite	2.09	4.25	0.99	0.46	12.95	0.86
Pb^{2+}	CH/cHAp/zeolite	5.55	2.99	0.97	0.06	18.12	0.70
	CH/bHAp/zeolite	5.88	3.19	0.97	0.19	17.48	0.97
Cu^{2+}	CH/cHAp/zeolite	1.71	0.16	0.98	0.28	6.48	0.68
	CH/bHAp/zeolite	1.64	1.05	0.94	0.04	9.00	0.98
Chromate	CH/cHAp/zeolite	0.18	0.82	0.82	0.08	1.12	0.77
	CH/bHAp/zeolite	0.17	1.06	0.94	0.04	1.46	0.86

For all the metal ions studied, the slope values of the above-mentioned linear equations (Table 5-32) are equal to the $k_{d,}$ and the boundary thickness (C) is equal to the intersection value.

A higher slope value (K_d) of the first step than the second step of the IPD model fitted (See Table 5-33) to the metal ion kinetic data for both the composites indicates the availability of excessive adsorption sites initially to adsorb metal ions fast. It also illustrates that the intra-particle diffusion is the rate-limiting step (with chemisorption) for the metal ion adsorption on the CH/HAp/zeolite composites, as is evident from the lower values of k_d at step (II), as a slow rate of diffusion indicates a rate-limiting step. A more significant intercept (C values) in the second step (intra-particle diffusion) is attributed to the boundary thickness due to the adsorption of metal ions in the boundary diffusion step[354].

However, the intra-particle diffusion is not the only mechanism involved in the metal removal, as the plots (in *Figures 4-132 to 4-135 in appendix 4*) are not linear and passing through the origin. Ion exchange and surface adsorption processes, possibly through electrostatic interactions between negatively charged functional groups (hydroxyl, phosphates), could also be involved in removing metal ions using this composite system.

Summary

The summary of the optimal experimental conditions recorded for each metal ion adsorption by using the synthesised composite systems (discussed above) in single-metal-ion type solutions is presented in Table 5-34.

Table 5-34: Summary of optimal experimental conditions recorded for metal ion adsorption on the synthesised composite system in this study, in a single metal ion type solution system

Composite adsorbents	**Optimal experimental conditions were recorded for the metal ion adsorption on the synthesised composites in single-metal ion type solutions**				
	Metal ions	**Adsorbent Dose (g)**	**pH**	**Contact time**	**q_e (mg g^{-1}) recorded at 0.01 g adsorbent dose**
CH/cHAp	Cd^{2+}	0.05	5.0-7.0	60	15.88
	Pb^{2+}	0.03	4.0-5.0	60	49.56
	Cu^{2+}	0.05	4.0-6.0	60	13.42
	Chromate ions	0.05	4.0-5.0	60	21

CH/bHAp	Cd^{2+}	0.05	5.0-7.0	60	19.72
	Pb^{2+}	0.03	4.0-5.0	60	87.99
	Cu^{2+}	0.05	4.0-6.0	60	17.34
	Chromate ions	0.05	4.0-5.0	60	17
CH/cHAp/CF	Cd^{2+}	0.05	5.0-7.0	120	16.06
	Pb^{2+}	0.03	4.0-5.0	120	59.49
	Cu^{2+}	0.05	4.0-6.0	120	14.83
	Chromate ions	0.05	4.0-5.0	30	25.87
CH/bHAp/CF	Cd^{2+}	0.05	5.0-7.0	120	17.01
	Pb^{2+}	0.03	4.0-5.0	120	70.27
	Cu^{2+}	0.05	4.0-6.0	120	16.13
	Chromate ions	0.05	4.0-5.0	60	21.12
CH/cHAp/SCGs	Cd^{2+}	0.05	7.0-8.0	90	17.12
	Pb^{2+}	0.04	5	60	34.6
	Cu^{2+}	0.05	5	120	9.12
	Chromate ions	0.04	4.0-5.0	15	16.11
CH/bHAp/SCGs	Cd^{2+}	0.05	7.0-8.0	90	18.18
	Pb^{2+}	0.04	5	60	42.43
	Cu^{2+}	0.05	5	60	11.71
	Chromate ions	0.04	4.0-5.0	15	16.08
CH/cHAp/zeolite	Cd^{2+}	0.05	5.0-7.0	60	20.09
	Pb^{2+}	0.04	5	60	54.21
	Cu^{2+}	0.05	5	60	15.49
	Chromate ions	0.04	4.0-5.0	60	13.3
CH/bHAp/zeolite	Cd^{2+}	0.05	5.0-7.0	90	25.79
	Pb^{2+}	0.04	5	60	67.22
	Cu^{2+}	0.05	5	60	16.99
	Chromate ions	0.04	4.0-5.0	60	13.25

This section demonstrates the comparison of the adsorption capacities (q_{max}) of the synthesised composite systems for the removal of metal ions in single-metal ion type systems.

There were four composite systems studied to remove the metal ions using the solutions containing the single metal ion type. The non-linear Langmuir isotherm model was used to estimate the maximum adsorption capacity (q_{max} in mg g^{-1}) of these adsorbents for each metal ion studied and presented in Table 5-35.

Table 5-35: Comparison of the maximum adsorption capacity (q_{max}) of the synthesised composites in this study to remove metal ions as calculated by using the Langmuir adsorption isotherm model

Metal ions removed	Composite systems	CH/HAp	CH/HAp/CF	CH/HAp/SCGs	CH/HAp/zeolite
Cd^{2+}	cHAp-based	24.33	19.57	24.62	33.21
	bHAp-based	33.93	20.66	25.46	37.04
Pb^{2+}	cHAp-based	52.42	66.09	34.68	72.49
	bHAp-based	90.03	89.85	49.09	100.47
Cu^{2+}	cHAp-based	15.91	15.95	9.98	17.56
	bHAp-based	23.67	18.55	14.57	20.11
Chromate	cHAp-based	45.04	29.41	27.17	7.71
	bHAp-based	34.72	72.46	31.34	7.27

Table 5-35 demonstrated that the estimated adsorption of Cd^{2+} ions was the highest for the CH/HAp/Zeolite composites, which could be due to the presence of zeolite and HAp in this composite system which can remove the metal ions using the ion-exchange mechanism. The CH/HAp and CH/HAp/SCGs exhibit comparable removal for the Cd^{2+} ions, followed by the CH/HAp/CF composites. Overall, the addition of the zeolite exhibited an improvement in the removal efficiency of the CH/HAp (control) composites. The bHAp-based composites (in all four composite systems) were found to be better at adsorbing Cd^{2+} ions than the cHAp composites, which aligns with the experimental observations of these composite systems.

The CH/HAp/zeolite composites showed the highest value of the estimated maximum adsorption for Pb^{2+} ions, which confirms the trend recorded for the Cd^{2+} ion (see above). After the CH/HAp/zeolite composites, the CH/HAp (control) composites showed the maximum adsorption capacity for Pb^{2+} ions, followed by the CH/HAp/CF and

CH/HAp/SCGs composites. The bHAp-based composites (in all our composite systems) were found to be better at adsorbing the Pb^{2+} ion (as recorded for the Cd^{2+} ions) than the cHAp composites, which agrees with the experimental observations of these composite systems recorded for the removal of Pb^{2+} ions.

Generally, the bHAp-based composites exhibit a better adsorption capacity (q_{max}) than the cHAp-based composites for the Cu^{2+} ion adsorption, which agrees with the observations of this study.

The chromate ion adsorption (q_{max}) was the lowest for the CH/HAp/zeolite composites, which provides support to the higher ion-exchange ability of binding sites of this composite system with respect to cation adsorption, resulting in lower adsorption observed for chromate anions. The highest value of the q_{max} was recorded for the CH/bHAp/CF composite, which is supported by several literature studies which showed that the coir-based composites were a favourable adsorbent for the removal of chromate anions. The irregular trends recorded for the estimated q_{max} of the chromate ions on these composites could be due to many factors, such as the heterogeneity of the samples (grain sizes) or the applicability of the adsorption models on these systems. A comprehensive data analysis using different adsorption models could be done to confirm the findings recorded for these systems. Overall, the bHAp-based composites (except CH/bHAp) showed better adsorption of chromate ions than the cHAp-based composites.

5.2 Experiments involving the removal of metal ions by the composite adsorbents from solutions containing two metal ion types (competitive adsorption)

The results obtained from the optimal conditions deduced for Pb^{2+} and Cd^{2+} removal by the composite adsorbents (when exposed to solutions of the *single metal ion systems* (as discussed in earlier section 5.1) were used to evaluate the adsorption of these metals from solutions containing both dissolved Pb^{2+} and Cd^{2+} ions where there will be competition for the surface adsorption sites on the composites by the two metal ions present in solution. The competitive Pb^{2+} and Cd^{2+} adsorption experiments on the CH/HAp (control) and three-component composites as a function of (contact) time were conducted at two adsorbent doses, 0.01 g and 0.05 g and the contact time varied from 15 minutes to 180 minutes. The removal efficiency was calculated using equation 4-1 (see earlier). The

adsorption capacity q_t (mg g^{-1}) as a function of time was calculated using the following equation (5-10):

Equation 5-10:

$$q_t = \frac{(C_0 - C_t)V}{m}$$

In the above equation, C_0 and C_t denote the metal ion concentrations in the liquid phase (mg L^{-1}) at contact times "0" and "t", respectively. V is the volume of the solution in litres (L), m (in g) represents the mass of adsorbent, and q_t is the amount of sorbate adsorbed to the solid phase (i.e., the adsorption capacity) in mg g^{-1} at the time "t" ranging from 15 minutes to 180 minutes.

In terms of kinetic models, the PSO model was fitted to the data in order to estimate the maximum adsorption parameters, including q_e (mg g^{-1}) and k_2 (g mg^{-1} min^{-1}) for these systems as the PSO kinetic model was always found to be the best-fit model for describing the kinetics of adsorption in the single metal ion adsorption systems both in this study and in similar studies reported in the literature[518,550].

Hence the next section describes the results for:

1. Competitive adsorption of Cd^{2+} and Pb^{2+} on the composite adsorbents in systems where two metal ion types have been dissolved on two doses of adsorbent used (0.01 g, Figure 5-1 and 0.05 g, Figure 5-2)
2. The kinetic modelling for Cd^{2+} and Pb^{2+} competitive adsorption from a solution containing both metal ions dissolved, and comparison of the kinetic model parameters as calculated ***for the single metal ion systems and for those where two metal ion types were dissolved in solution and exposed to different adsorbent doses*** (0.01 g, Table 5-36 and 0.05 g, Table 5-37)
3. Detailed results collected for this experimental set-up (two-metal ion type solution systems) are presented in Appendix 5.

5.2.1 Comparison of the removal efficiencies of the synthesised composites for the removal of Pb^{2+} and Cd^{2+} ions in two-metal ion type systems (competitive adsorption system)

This section demonstrates the removal of Pb^{2+} and Cd^{2+} ions in a solution containing two-metal ion types. Figure 5-1 illustrates the removal % of the composites for the Cd^{2+} and Pb^{2+} ions recorded by AAS at 0.01 g of adsorbent dose in competitive adsorption systems. The Pb^{2+} ion removal is higher than Cd^{2+} ion on all the composite systems studied (see Figure 5-1), confirming the findings noted earlier in the single-metal ion type solution systems. Similarly, the bHAp-based composite exhibited a higher removal for both the cations than the cHAp-based composites, which also aligned with the observations of the single-metal in type systems discussed in detail in earlier sections.

The data was recorded for adsorption on 0.01 g of the adsorbent dose, showing the highest removal of the Pb^{2+} ions on the CH/HAp/zeolite composites, which agrees with the Pb^{2+} ion adsorption observations recorded in the single-metal ion type solution systems (see above 5.1.4). In contrast, Cd^{2+} ions were removed to the highest extent by adsorption on the CH/HAp/CF composites, followed by the CH/HAp/SCGs, CH/HAp/zeolite and CH/HAp composites. Overall, the three-component composites systems showed better removal of Pb^{2+} and Cd^{2+} ions than the CH/HAp (control) composites in two-metal ion type solution, which contradicts the results recorded in single-metal ion type solutions, where the removal efficiency of the control two-component composites was better than observed for the three-component composites.

The difference between the removal efficiencies in the two systems (single and two-metal ion type) could be attributed to the irregularities in the sample conditions (sizes and specific surface areas). Alternatively, the addition of the third component could have a synergistic effect on the adsorption capacities of the composite in competitive adsorption systems (like two-metal ion type systems).

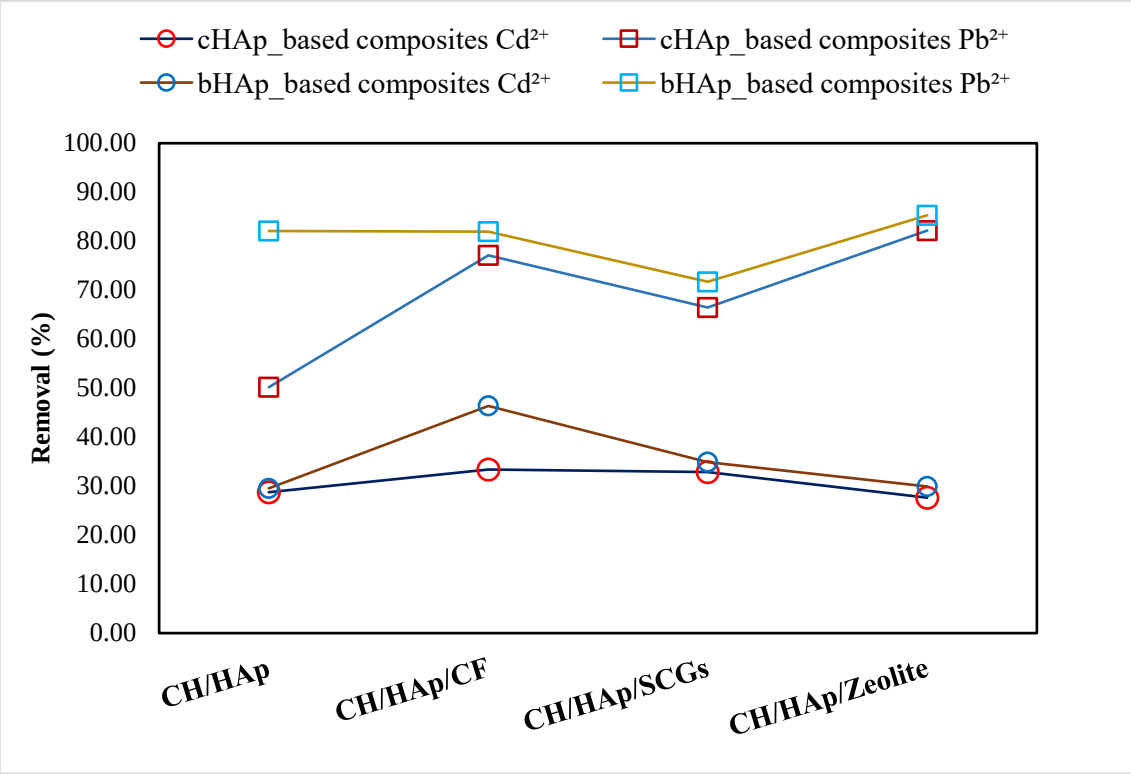

Figure 5-1: Comparison of the removal efficiencies of the synthesised composites for the competitive removal of Pb^{2+} and Cd^{2+} by adsorption (in solutions containing two metal ion types) when using 0.01 g of adsorbent

Figure 5-2 (for 0.05 g of adsorbent dose) exhibited the highest adsorption of Pb^{2+} and Cd^{2+} ions on the CH/HAp/Zeolite composites, followed by the CH/HAp/SCGs, which agrees with the observations recorded for the single-metal ion type solution system. The three-component composite systems were more efficient at removing the Cd^{2+} and Pb^{2+} ions than the CH/HAp (control) composites, showing a better removal (%) than the control composites in this two-metal ion type solution, which agrees with the observations recorded when using a low dose (0.01 g) of the adsorbents (Figure 5-1).

These findings are different from the observation recorded in the single-metal ion type solution system. The results recorded in the competitive adsorption systems (Figure 5-1 and 5-2) demonstrate that the performance of the CH/HAp (control) composites could be enhanced by adding a third component when they are used as metal ion removal substrates in competitive adsorption system scenarios. Due to the limited data collected in this study, it is felt that these three component composites would be good systems to study further by using different experimental conditions and set ups to explore their future applicability in complex water treatment systems.

Overall, cHAp-based and bHAp-based composites showed comparable removal efficiencies when 0.05 g of the adsorbent dose was used for the removal of Cd^{2+} and Pb^{2+} ions. It could be attributed to the higher adsorbent dose (0.05 g) used in experiments, which would have provided the adsorption sites for maximum removal of these metal cations from the solutions containing both Cd^{2+} and Pb^{2+} ions. The adsorbent dose was one of the most important factors to attain the maximum adsorption of the metal ions on the composite.

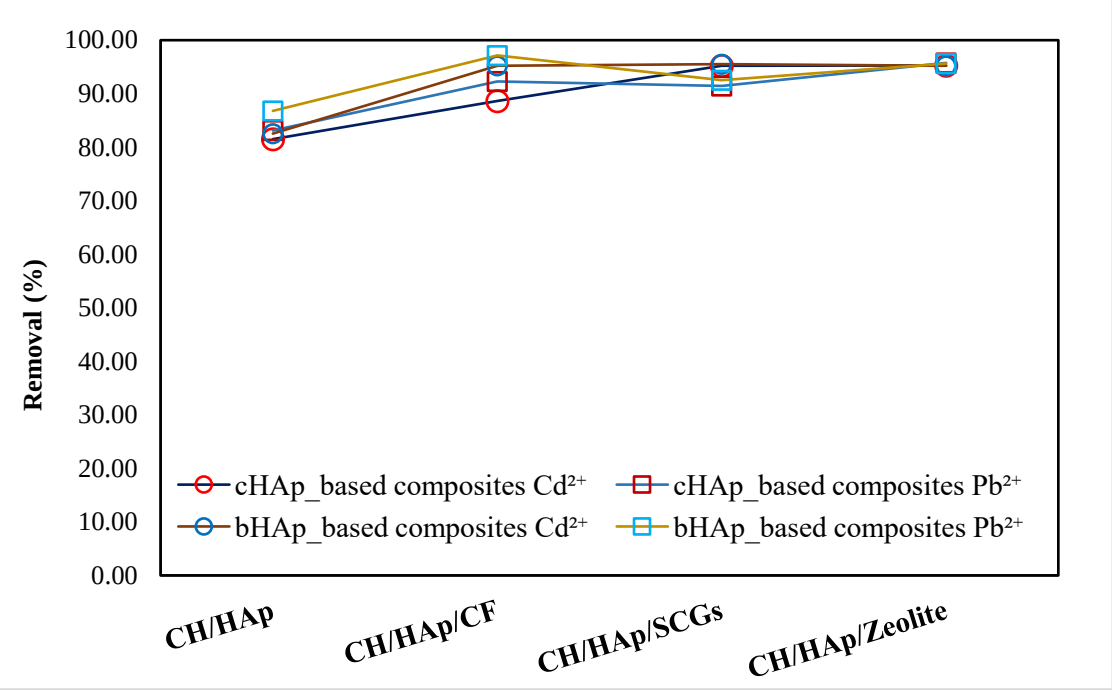

Figure 5-2: Comparison of the removal efficiencies of the synthesised composites for the removal of Pb^{2+} and Cd^{2+} in competitive adsorption system (in solutions containing two metal ion types) at 0.05 g of adsorbent dose

5.2.2 Preferential adsorption of Pb^{2+} in competitive adsorption systems from solutions containing both Cd^{2+} and Pb^{2+} by using the composite adsorbents of this study

Overall, the better removal of Pb^{2+} than Cd^{2+} was recorded for all the composite systems using both adsorbent doses (0.01 g and 0.05 g). The results are presented (in detail) in appendix 5 for reference, which agrees with the observations recorded in the single-metal ion type solution systems (as discussed in earlier sections above).

The improved uptake of Pb^{2+} relative to other cations such as Cu^{2+}, Cd^{2+}, Ni^{2+} in competitive adsorption systems has been reported before in literature studies for several adsorption systems such as nanohydroxyapatite[568], hydroxyapatite-biochar nanocomposite[569], carbonaceous nanofibres[570], xanthate-modified magnetic chitosan adsorbent[571] and modified chitosan/$CoFe_2O_4$ particles[572]. Explanations for this enhanced adsorption ability of Pb^{2+} can be offered as follows.

The literature studies described higher electronegativity, stronger covalent bond strength, and larger ionic radii of the Pb^{2+} ion as essential indicators for explaining why Pb^{2+} adsorbs on substrates more readily than Cd^{2+} in competitive adsorption systems from solutions containing these two metal ions[515,573]. The literature has many reports that agree that the Pb^{2+} and Cd^{2+} ions are subject to different removal mechanisms such as surface complexation and ion exchange for removal from the solution by the chitosan and the hydroxyapatite adsorbents. These mechanisms have already been explained in chapter 1. The following section discusses these two fundamental mechanisms in detail in the context of preferential adsorption of Pb^{2+} ions using the composite adsorbents employed in this study.

5.2.2.1 Metal-ligand complexation involved in preferential Pb^{2+} adsorption on the composite adsorbents

A ligand is a charged or uncharged molecular species[574], which can cause metal ion removal by forming metal-ion-ligand complexes (termed metal ion chelation). The ligand contains electron-donating atoms (e.g., N or O), while the metal cations (Pb^{2+} and Cd^{2+}) act as electron acceptors when forming the metal-ligand complexes via a covalent bond. The metal ion interactions with ligands (such as amino and hydroxyl groups) to form metal-ligand complexes are well-known mechanisms for removing heavy metal ions using biological macromolecules such as cellulose, chitin and chitosan[575]. The CH/HAp-based composite has the potential to remove Pb^{2+} and Cd^{2+} ions using this mechanism by involving the $-NH_2$ groups and $-OH^-$ groups detected to be present in the CH/HAp-based composite system can form metal-ligand complexes while removing metal ions. When the solution pH is low (acidic), it leads to protonation of the $-NH_2$ groups to produce positively charged NH_3^+ groups, which could compromise the metal-complexation mechanism.

The tendency of Pb^{2+} to form metal complexes with ligands including N and O atoms (e.g., amino and hydroxyl groups) is thermodynamically more favourable than it is for Cd^{2+} according to a classification discussing the metal-ligand complex formation and stability constant (K_{ML}). Metals will tend to make more stable metal-ligand complexes if the stability constant is higher[576]. According to this classification, so-called Class B metals are preferentially complexed with ligands in the following order S > N > O, with Pb^{2+} having a greater tendency to form the chelation complexes[574,576] than Cd^{2+}. Hence Pb^{2+} is taken up to a larger extent than Cd^{2+} on these CH/HAp-based composites.

5.2.2.2 Ion-exchange mechanisms involved in the preferential Pb^{2+} adsorption on the composite adsorbents

Suzuki et al.[128,577] provided the experimental evidence for higher Pb^{2+} adsorption on synthetic HAp compared to Cd^{2+} ion under the same experimental conditions. They showed in their work that an ion-exchange mechanism was responsible for removing Pb^{2+} and Cd^{2+} when HAp was employed as an adsorbent to remove these metal ions[128,577]. Ions with a more significant electronegativity value may exchange more favourably with Ca^{2+} ions in HAp. Ions with radii in the range of 0.9-1.3 Å were readily exchanged for Ca^{2+} ions in HAp. The metal ions with a higher electronegativity value and ionic radius in this range favoured the ion-exchange process with Ca^{2+}. Literature states that Pb^{2+} ions have higher electronegativity[578,579] (2.33) than Cd^{2+} (1.69) and larger ionic radii (Pb^{2+} has an ionic radius of 0.118 nm, so falling in the range given by Suzuki et al.[128]) compared to Cd^{2+} ion (0.097 nm) hence this would explain why more Pb^{2+} than Cd^{2+} would be attracted more strongly towards negatively charged adsorption sites of composites and to ion exchange with Ca^{2+} ions on hydroxyapatite. Hence literature provides strong support for why there is higher Pb^{2+} adsorption than Cd^{2+}, especially on HAp-based adsorption systems such as the CH/HAp-based composites discussed in the present study.

5.2.3 Kinetic modelling of competitive Pb^{2+} and Cd^{2+} ion adsorption on the composite adsorbents and comparison of kinetic model parameters calculated for adsorption from solutions containing either one or two metal ion types

As has normally been the case in previous experiments and model fitting exercises in this study, the pseudo-second-order model (PSO) was the best-fitted model to describe the adsorption of Pb^{2+} and Cd^{2+} in the single metal system. The fitting of PSO was done on kinetic data of competitive adsorption of Pb^{2+} and Cd^{2+} for all the synthesised composite adsorbents of the present study (*see Figures 5-5 and Figure 5-6 appendix 5*). The comparison of the calculated parameters of PSO for data pertaining to adsorption from solutions containing either one or two metal ion types is given in Table 5-36 (0.01 g) and Table 5-37 (0.05 g) to show the estimated adsorption of Pb^{2+} and Cd^{2+} in two systems using the composite adsorbents discussed in this study.

Table 5-36: The calculated parameters from the fitted non-linear PSO kinetic model for competitive Pb^{2+} and Cd^{2+} adsorption (two-metal ion type solution system) and single metal ion adsorption on 0.01 g of the composite adsorbents

Composite adsorbents	PSO	Single-metal ion type solution system			Two-metal ion type solution system		
		q_e (mg g^{-1})	k_2 (g mg^{-1} min^{-1})	R^2	q_e (mg g^{-1})	k_2 (g mg^{-1} min^{-1})	R^2
CH/cHAp	Cd^{2+}	15.930	0.139	0.999	15.507	0.003	0.998
	Pb^{2+}	48.173	0.013	0.999	27.305	0.001	0.977
CH/bHAp	Cd^{2+}	19.070	0.039	0.999	15.749	0.009	0.999
	Pb^{2+}	49.518	0.014	0.999	45.042	0.001	0.997
CH/cHAp/CF	Cd^{2+}	19.274	0.010	0.993	15.664	0.013	0.996
	Pb^{2+}	46.912	0.003	0.998	34.995	0.002	0.978
CH/bHAp/CF	Cd^{2+}	23.646	0.002	0.991	23.195	0.003	0.994
	Pb^{2+}	49.797	0.003	0.999	43.384	0.002	0.998
CH/cHAp/SCGs	Cd^{2+}	26.090	0.012	0.999	18.856	0.003	0.993
	Pb^{2+}	47.790	0.025	0.999	38.430	0.001	0.997
CH/bHAp/SCGs	Cd^{2+}	25.820	0.048	0.999	18.800	0.006	0.999
	Pb^{2+}	48.086	0.016	0.999	41.850	0.001	0.999
CH/cHAp/zeolite	Cd^{2+}	20.890	0.003	1.000	15.560	0.005	0.991
	Pb^{2+}	48.390	0.006	0.998	48.390	0.006	0.998
CH/bHAp/zeolite	Cd^{2+}	22.789	0.005	0.999	16.090	0.006	0.998
	Pb^{2+}	48.954	0.006	0.999	48.010	0.007	1.000

The PSO is fitted well with $R^2 > 0.97$ to describe the kinetics of adsorption of these cations on the CH/HAp-based composites and confirms that chemisorption is the rate-limiting step for removing Pb^{2+} and Cd^{2+} in the competitive adsorption system. The competitive adsorption of Pb^{2+} is preferred over Cd^{2+} adsorption on both types of composites (cHAp-based and bHAp-based composites) (see Table 5-36 & 5-37). This is because the estimated q_e (in mg g^{-1}) of Pb^{2+} ranges from 27-48 mg g^{-1} while it ranges from 15.50-23.19 mg g^{-1} for Cd^{2+}, for all the composites studied (Table 5-37).

It reiterates the preference of the CH/HAp-based composites discussed in this study to adsorb Pb^{2+}ions. Similarly, the estimated q_e values (for both Pb^{2+} and Cd^{2+} ions) using PSO are higher in the single metal ion system than in systems where two metal ions are co-dissolved in solution, signifying the previously discussed antagonistic effect of competitive adsorption of metal cations on the available adsorption sites (see Table 5-36 for reference).

Table 5-37: The calculated parameters from the fitted non-linear PSO kinetic model for competitive Pb^{2+} and Cd^{2+} adsorption (two-metal ion type system) and single metal ion adsorption on 0.05 g of composite adsorbents

Composite adsorbents	PSO	Single-metal ion type solution system			Two-metal ion type solution system		
		q_e (mg g^{-1})	k_2 (g mg^{-1} min^{-1})	R^2	q_e (mg g^{-1})	k_2 (g mg^{-1} min^{-1})	R^2
CH/cHAp	Cd^{2+}	7.505	0.037	0.997	8.464	0.005	0.995
	Pb^{2+}	9.625	0.080	0.999	8.450	0.030	0.999
CH/bHAp	Cd^{2+}	9.808	0.127	0.999	8.450	0.015	0.999
	Pb^{2+}	10.172	0.041	0.999	8.590	0.181	0.999
CH/cHAp/CF	Cd^{2+}	11.804	0.002	0.998	9.176	0.008	0.998
	Pb^{2+}	9.969	0.025	1.000	9.107	0.060	1.000
CH/bHAp/CF	Cd^{2+}	12.163	0.002	0.992	9.928	0.018	1.000
	Pb^{2+}	9.946	0.036	0.999	9.623	0.036	1.000
CH/cHAp/SCGs	Cd^{2+}	9.868	0.035	0.999	9.637	0.011	0.998
	Pb^{2+}	9.890	0.047	0.999	9.970	0.007	0.999
CH/bHAp/SCGs	Cd^{2+}	9.850	0.053	0.999	9.849	0.017	1.000
	Pb^{2+}	9.690	0.083	0.999	10.087	0.007	1.000
CH/cHAp/zeolite	Cd^{2+}	9.728	0.008	1.000	9.760	0.024	0.999
	Pb^{2+}	9.262	0.050	0.999	9.483	0.042	1.000
CH/bHAp/zeolite	Cd^{2+}	9.881	0.008	0.999	9.770	0.024	0.999
	Pb^{2+}	9.546	0.038	1.000	9.515	0.045	1.000

Table 5-37 (above) presents the calculated parameters for the fitting of the PSO kinetic model to contact time data on the competitive adsorption of Pb^{2+} and Cd^{2+} on the CH/HAp-based composites (of the present study) using 0.05 g of adsorbent dose. The PSO model was also a good fit for this data, with $R^2 > 0.99$. In contrast to the 0.01 g adsorption system (for adsorption from a solution containing two metal ion types), the 0.05 g adsorbent dose shows similar adsorption capacities in relation to Pb^{2+} and Cd^{2+} adsorption from both solutions with single metal ion and two metal ion types. (see Table 5-36). The difference between the q_e (mg g^{-1}) values was found to be *ca.* 1 mg g^{-1} or less between systems. The similar adsorption abilities of both types of composites (cHAp-based composites and bHAp-based composites) when exposed to the single metal ion and two metal ion type (competitive) systems for Cd^{2+} and Pb^{2+} can be attributed to the availability of excess adsorption sites from the use of the higher adsorbent dose (0.05 g vs 0.01 g).

5.3 An industrial input stream sample containing three heavy metals for testing the adsorption performance of the composite adsorbents

Experimental: After studying the adsorption behaviour of the two-component (control) and three-component composites (discussed in earlier sections) in solutions containing either one or two metal ion types, it was desired to test the performance of the composites by exposing them to an industrial type of solution consisting of three co-dissolved heavy metal species of relevance to the wood treatment industry. The sample supplied was not a sample of wastewater from the company but an ***input stream*** (i.e., before it was exposed to the wood). This nevertheless was regarded as a suitable mimic for an industrial wastewater sample except that the concentrations of heavy metals present were higher than they would have been due to non-exposure of the solution to the wood. The other aspect of the sample was that it contained a metal that had not previously been tested in the solutions containing either one or two metal ion types (as it was not available as an element for analysis by AAS). This was arsenic (as the arsenate ion).

The industrial input stream sample solution supplied was not in a suitable state to be exposed directly to the composite materials. Particulate matter was present from the industrial holding tanks they originated from. Also, the pH of the media was too acidic (pH < 2), meaning that it would have dissolved the HAp in the composites studied. The

input sample was dark orange suggesting “Cr” in the sample was present as a dichromate ion (i.e. $Cr_2O_7^{2-}(aq)$), which is known to exist at very acidic pH[580]. The fundamental purpose of this experiment was an evaluation of the removal efficiency of the composites when exposed to such a solution, so the initial metal ions concentration (before exposure to the composites) and final metal ion concentration (after exposing the water to the synthesised composites, needed to be evaluated.

5.3.1 Pre-treatment and dilution of water for analysis and metal removal treatment

Before the metal removal experimentation using the adsorbent, a pre-analysis of the industrial input stream water sample was done using ICP-MS. For the analysis, the actual (dark orange) sample was diluted by 2000X (the dilution factor) using double distilled water. After the dilution, the colour of the water changed from dark orange to light yellow, while the pH increased to values between 4 and 5. Dichromate is likely converted to chromate ion under these conditions, given the colour change that was observed.

The sub-sample (from the 2000X diluted water sample) was taken for analysis by ICP-MS in a 100 mL volumetric flask and filtered twice using a syringe filter (0.45 micron). The two replicates were taken in falcon tubes (15 mL) for ICP-MS analysis before metal ion removal experimentation to obtain a reliable pre-characterisation of the industrial water sample. The results generated by ICP-MS analysis were in ppb units, which were converted subsequently into ppm values. These were then multiplied by the dilution factor (2000X) to get the actual concentrations of arsenate ions, copper and chromate ions in the industrial input water samples.

For instance, the arsenic concentration in ICP-MS analysis was given as 831.7 ppb. To get an actual concentration of arsenic in the industrial input stream sample, it was multiplied by the dilution factor “2000”, so the calculated value (actual) for arsenic concentration was 1663,400 ppb. Then this value was converted to ppm unit by dividing it by 1000. In this way, the calculation was also done for the other two metal ions (chromium as chromate ion and copper (cupric) ion).

The calculations gave the following values for chromium, arsenic and copper ions concentrations:

Arsenic (as arsenate) 1663.4 ppm

Copper (as Cu^{2+}) 999.8 ppm

Chromium (as chromate) 1621 ppm

Isotopic concentrations of Cu and Cr elements (for different isotopes) were measured by ICP-MS in the industrial water sample (Table 6.2B in appendix 6). Generally, the concentrations of abundant isotopes of the metals in nature are selected to represent the metal ion concentrations (C_i (ppm) in later experimentation. For instance, ^{63}Cu is the most abundant isotope of copper[581], with an isotopic ratio of 68.94% and is usually taken into account to evaluate the removal efficiency of synthesised composites with respect to cupric ions. However, a number of mass interferences (resulting from the use of Argon or other components) occurring in ICP-MS must also be considered in order to choose the most suitable isotope to analyse for representing an accurate value of the metal ion concentrations (i.e. which is not so affected by or subject to the mass interferences). Usually, at least two different isotopes are measured using the ICP-MS, and if the difference between the concentrations of the two is very high, then it is assumed to be caused by a possible interference. However, in industrial input stream samples, several cations and anions were present in very low concentrations, which could be assumed to be negligible for causing any interferences. The other interferences which would always be present include the Ar, O, H and N due to the argon plasma, water, and nitric acid. For this, the quality control samples of known concentrations were used in the analysis. Additionally, the results were recorded for at least two isotopes of the metals of interest (Cu^{2+}, chromate), which showed comparable concentrations in ppm. The primary purpose was to evaluate the removal efficiency of the composite materials, so the ^{63}Cu and ^{53}Cr concentrations were selected to calculate the removal efficiencies of the composites in this study.

Experimental:

Industrial water sample preparation: For the batch experiments involving metal removal using the composite adsorbents (discussed in the present study), the industrial input stream sample was diluted by a factor of 1000.

Batch experiment: The kinetics of metal ion adsorption (of the three above mentioned metals Cu^{2+}, chromate and arsenate ion)) on the composites was studied using **two adsorbent doses, 0.01 g and 0.1 g**.

Targeted metals: Due to technical issues with the AAS instrument, it was decided to use ICP-MS to monitor the change of ion concentrations in the industrial input stream sample after exposure to the CH/HAp composites. The metals targeted were *copper*, *chromium (chromate ion), and arsenic (arsenate ion)*. Given the ICP-MS technique can simultaneously monitor many metal ion concentrations, it was also decided to measure the concentrations of *calcium (present as Ca^{2+}) and phosphorus (present as phosphate)* to explore if the ion-exchange mechanism was occurring as reported for hydroxyapatite-containing composite matrices when adsorbing heavy metal ions. This would not have been easy to do using AAS due to matrix interference issues and the need to use other reagents to prevent this from occurring. Also, P is not amenable to AAS measurement.

5.3.2 Results and discussion for experiments involving metal ion removal from the industrial type of input stream sample by the composites synthesised and discussed in the present study

This section concludes the observations recorded for the Cu^{2+}, chromate and arsenate ions on the synthesised composites exposed to the industrial input stream solutions.

5.3.2.1 Removal of Cu^{2+} ions on the synthesised composite systems exposed to an industrial input stream water sample

In Figure 5-3, the removal efficiencies of the composite adsorbents (of the present study) recorded using the ICP-MS to remove the Cu^{2+} ions are demonstrated using 0.01 g of an adsorbent dose. The Cu^{2+} ion adsorption was the highest on the CH/HAp/zeolite composites, followed by the CH/HAp/SCGs, CH/HAp/CF and CH/HAp composites. The observation of the highest removal of the Cu^{2+} ion (a cation) by the CH/HAp/zeolite composites agrees with the observations recorded for the other cations in the single-metal ion type solution system, which was attributed to the more ion-exchange ability of this composite system (the CH/HAp/zeolite) due to the presence of the HAp and zeolite than other composite systems.

The lower removal of the Cu^{2+} ions on the CH/HAp (control) composites compared to that recorded on three-component composite systems illustrated the positive effect of third-component addition into the CH/HAp (control) composites, and this observation is aligned with the observations recorded for the CH/HAp/CF and CH/HAp/zeolite

composite systems, in the two-metal ion type solution systems, where these composite systems (CH/HAp/CF and CH/HAp/zeolite) performed well in term of removal efficiencies compared to the CH/HAp (control) composite, for the removal of Pb^{2+} and Cd^{2+} in a competitive adsorption system (see section 5.2). It was concluded from these observations that the addition of the third component (like CF and zeolite) in the CH/HAp (control) composites could enhance its removal ability and utility for cation removal in complex systems, as evidenced by the observations recorded in the two-metal ion type (section 5-2) and "industrial input stream" sample systems.

The bHAp-based composites showed a relatively better removal efficiency for Cu^{2+} than observed for cHAp-based composites (Figure 5-3), which agrees with the observations of the single metal ion type system where the bHAp-based composite systems showed a better removal (%) for Cu^{2+} cHAp-based composites (see Cu^{2+} removal in single metal ion type system). This better removal ability of the bHAp-based composites was observed for all metal cations studies (Pb^{2+}, Cu^{2+} and Cd^{2+}) and attributed to its higher surface area compared to the cHAp-based composites by providing more binding sites. Additionally, the presence of more HAp in bHAp-based composites (deduced from TGA analysis of the composites) was also considered as a possible reason for this better performance.

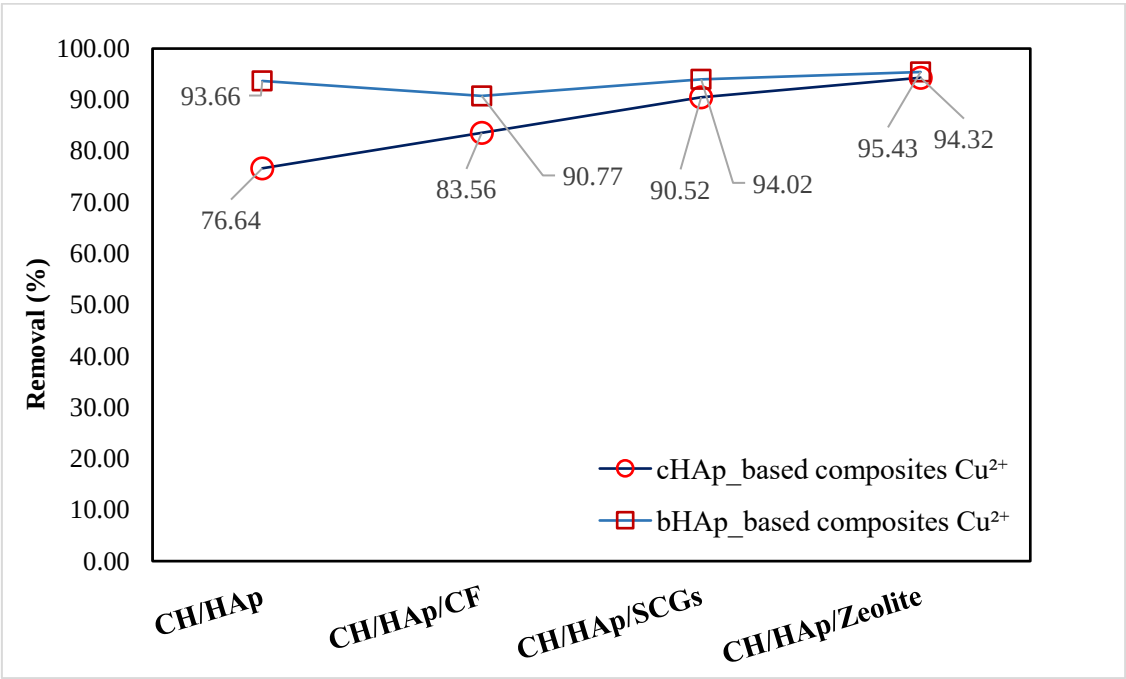

Figure 5-3: Comparison of the removal efficiencies of the synthesised composites for the removal of Cu^{2+} in industrial input stream sample when using 0.01 g of adsorbent dose

Figure 5-4 (see below) shows the removal efficiencies recorded by ICP-MS when using 0.1 g of adsorbent exposed to the industrial input stream water samples. All the composites show comparable removal efficiencies ranging between 98-99% (Figure 5-4). In earlier observations using the lower adsorbent dose (0.01 g), different trends of removal efficiencies for the synthesised composite were observed for the removal of the metal ions. However, all the composites showed an optimal removal of 97% or more for the Cu^{2+} ions. Similar observations "in terms of removal efficiencies" for all the composite systems to remove the metal ions (Figure 5-4) showed the positive effect of the adsorbent dose on the removal ability of the composites for metal cation removal. Based on this observation, it could be concluded that the maximum adsorption of the metal ions in each system could be achieved by simply increasing the adsorbent dose, which provides the surface area and adsorption sites for the removal of the metal ions.

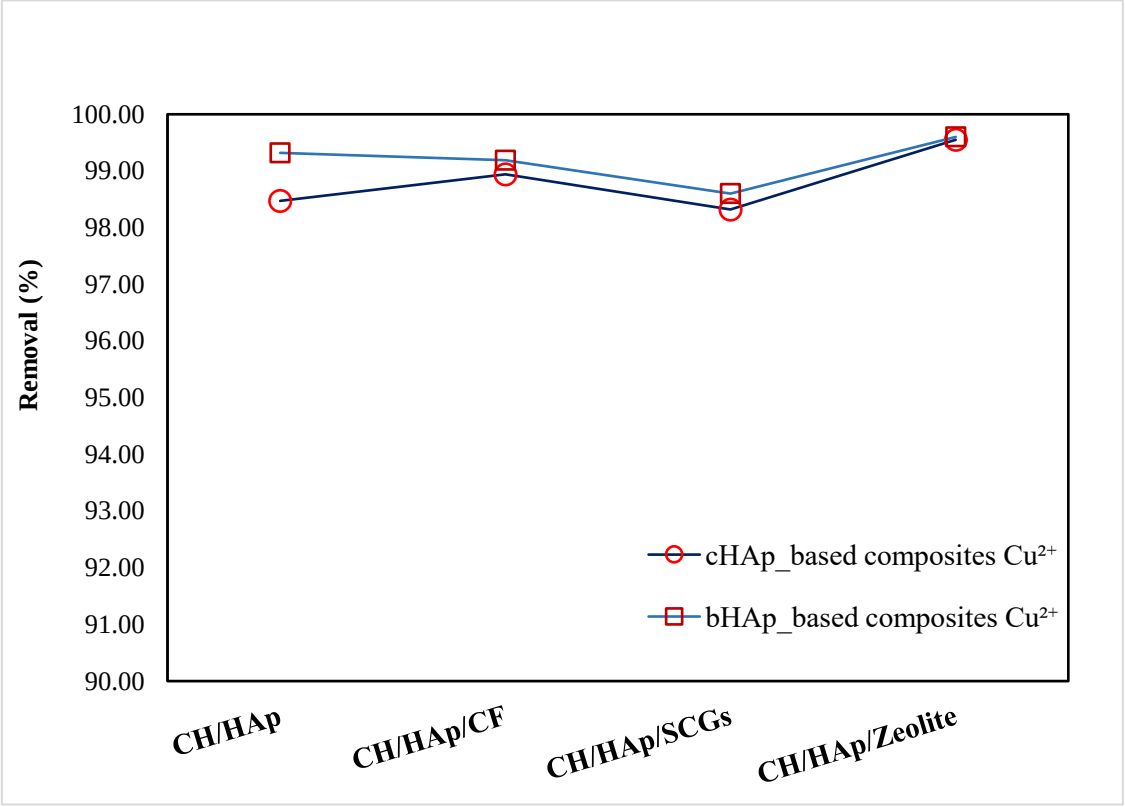

Figure 5-4: Comparison of the removal efficiencies of the synthesised composites for the removal of Cu^{2+} ions from an industrial input stream sample using 0.1 g of adsorbent

5.3.2.2 Removal of chromate ions on the synthesised composite systems exposed to an industrial input stream water sample

Figures 5-5 & 5-6 present the ICP-MS data recorded for different composite systems studied, which were exposed to industrial input stream solutions. Figures illustrate the results recorded using two adsorbent doses at 0.01 g (Figure 5-5) and 0.1 g (Figure 5-6) for chromate ion adsorption.

The maximum adsorption of the chromate ion recorded on the CH/HAp (control) composites ranged between 32-35%, while the lowest removal was recorded on the CH/HAp/zeolite composites and was 11-14%. The removal of chromate ions on all the composites ranged between 11-32%, which is lower than the removal of Cu^{2+} (Figure 5-3) on these composites, which ranged between 73-95% using a similar dose of adsorbents under similar experimental conditions. The more efficient removal of cationic species (Cu^{2+}) relative to the anionic species (e.g., chromate ion) agrees with the earlier behaviour observed when chromate ion adsorption from single metal ion solutions was studied. These tended to show removal % values of > 80% for Cd^{2+}, Cu^{2+} and Pb^{2+} but only 20-30% maximum for chromate ion.

The highest removal of chromate ions on the CH/HAp (control) composites could be explained by the greater partial dissolution of HAp in this two-component composite system. More dissolution could lead to more availability of integrated surface groups on the CH/HAp (control) composites. These integrated functional groups of HAp could assist in the adsorption of chromate ions. In contrast, the addition of the third component can hinder this mechanism by blocking the adsorption sites on the HAp-part of the composites. The lowest removal of the chromate ions on the CH/HAp/zeolites could be due to a relatively lower availability of the adsorption sites as most of the binding sites of this composite system could be involved in the ion-exchange mechanism for the removal of cations from the solution.

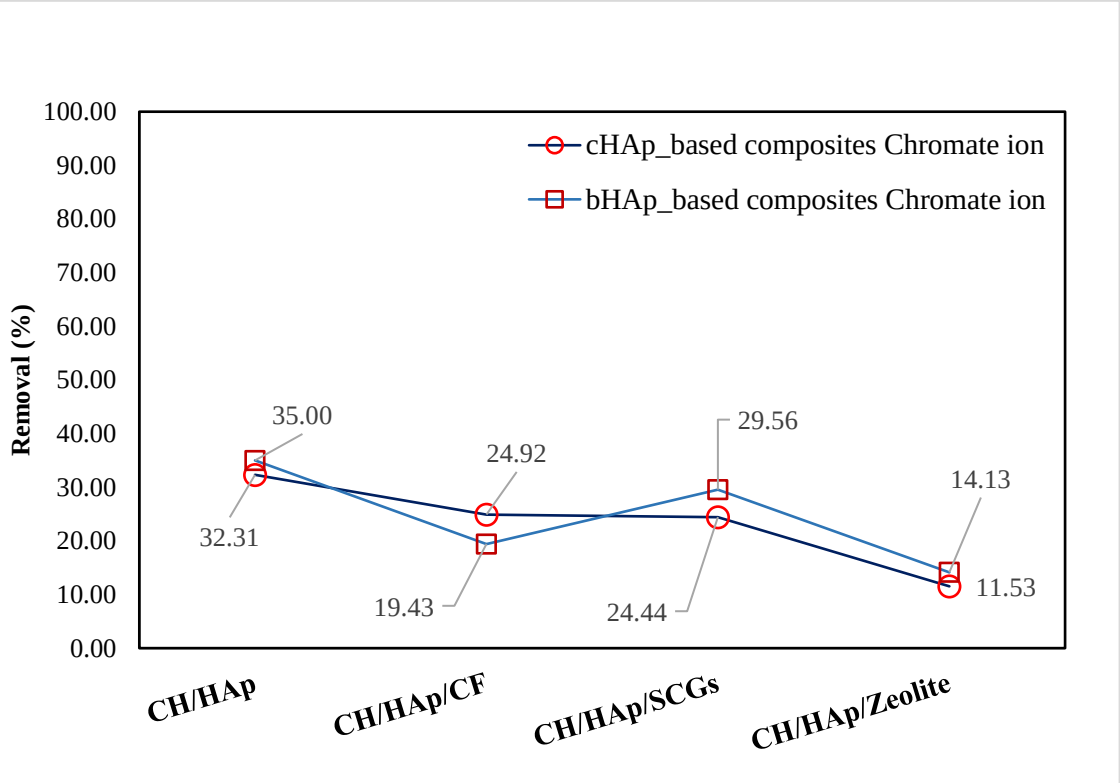

Figure 5-5: Comparison of the removal efficiencies of the synthesised composites for the removal of chromate ions from an industrial input stream sample using 0.01 g of adsorbent

Similar trends, as described for chromate ion removal using 0.01 g of the adsorbent, were recorded using 0.1 g of the adsorbents (Figure 5-6) and could be explained by using similar reasoning as described above.

The removal of chromate ions on all the composites was recorded to be higher using 0.1 g (Figure 5-6) of adsorbent than it was when using 0.01 g of adsorbent (Figure 5-5). Removal % was the highest for the CH/HAp composites ranging between 39-40%, while the lowest removal % was recorded for the CH/HAp/zeolite varying between 19 to 22%. The better adsorption recorded for the higher dose (0.1 g) compared to the lower adsorbent dose (0.01g) could be attributed to the relatively higher surface area offered by the use of the higher adsorbent dose (0.1 g) of the composite.

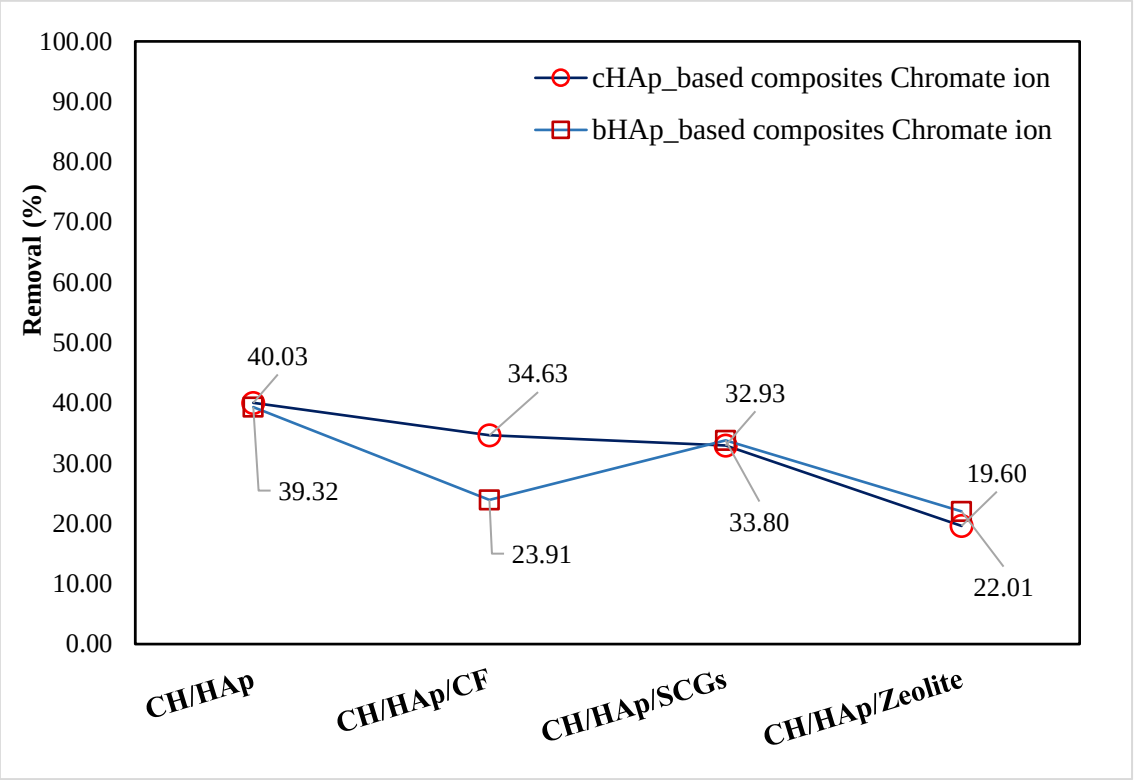

Figure 5-6: Comparison of the removal efficiencies of the synthesised composites for the removal of chromate ions in industrial input stream sample using 0.1 g of adsorbent dose

5.3.2.3 Removal of arsenate ions on the synthesised composite systems exposed to an industrial input stream water sample

Figure 5-7 & Figure 5-8 present the summary of the removal efficiencies recorded for the arsenate removal using the ICP-MS on different adsorbent systems at two doses, 0.01 g and 0.1 g, respectively.

In general, the removal of arsenate ion was higher (by 3-4%) on the bHAp-based composites (Figure 5-7) than on the cHAp-based composites. It could be attributed to the higher component of HAp present in the bHAp-based composites, providing relatively higher adsorption sites for arsenate removal by the ion-exchange mechanism (explained in an upcoming section).

The arsenate removal was higher than chromate removal (%) on the three-component composites (see Figure 5-5 & 5-7 for reference); in contrast, the chromate removal % was higher than arsenate removal % values on the CH/HAp (control) composites.

The higher adsorption of chromate ions on the CH/HAp composite than on the three-component composite systems could be explained in terms of the dissolution of HAp in these composites systems. The higher adsorption ability of two-component composite systems (the CH/HAp composites) could be associated with the relatively higher dissolution of HAp to provide these surface groups. In contrast, the three-component composites could be assumed to dissolve less than the control composites (as demonstrated by the lower adsorption of chromate ion on these systems), which could be attributed to the presence of the third composite. Alternatively, the presence of third components (like CF, SCGs and zeolite) could also cause the blockage of surface functional groups, resulting in a decrease in the removal of chromate ions.

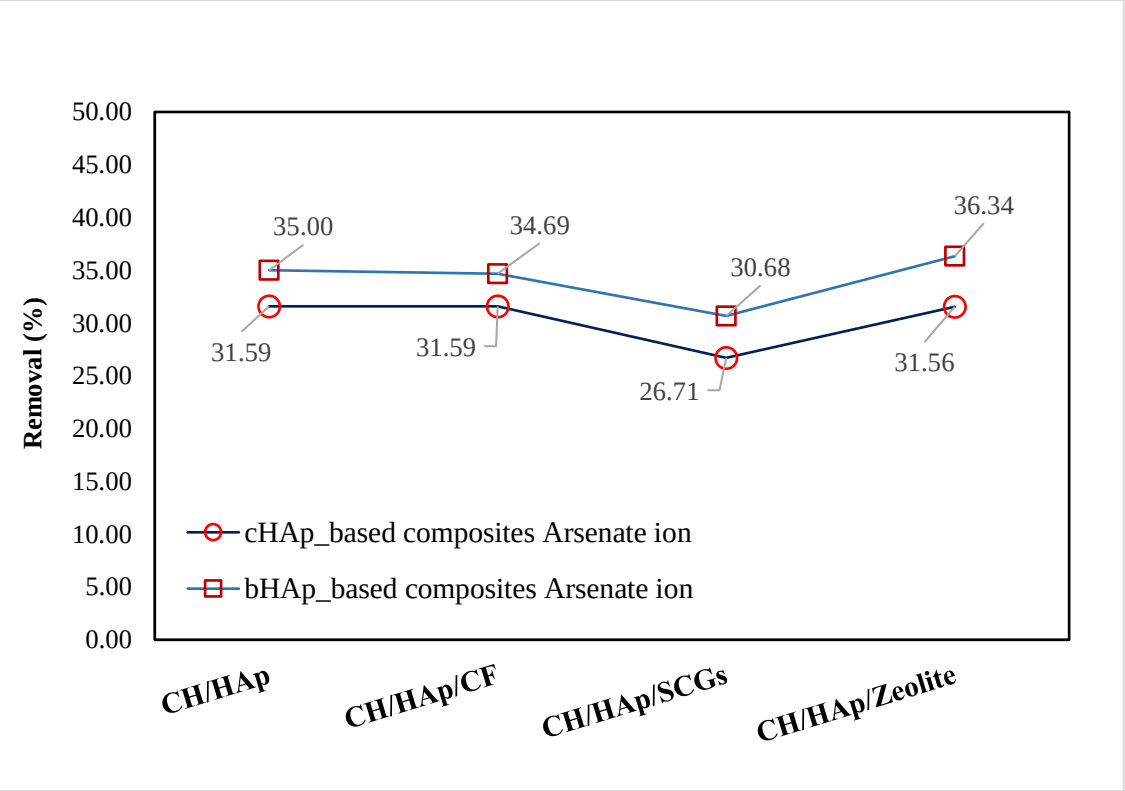

Figure 5-7: Comparison of the removal efficiencies of the synthesised composites for the removal of arsenate ions from the industrial input stream sample using 0.01 g of adsorbent dose

Figure 5-8 shows the removal efficiency of the composite adsorbents recorded using 0.1 g of the adsorbent. The arsenate removal is following a similar trend as recorded when using 0.01 g of adsorbent (Figure 5-7) and could be attributed to the ion-exchange mechanism, assisting better the adsorption of arsenate ion on the CH/HAp/Zeolite composites.

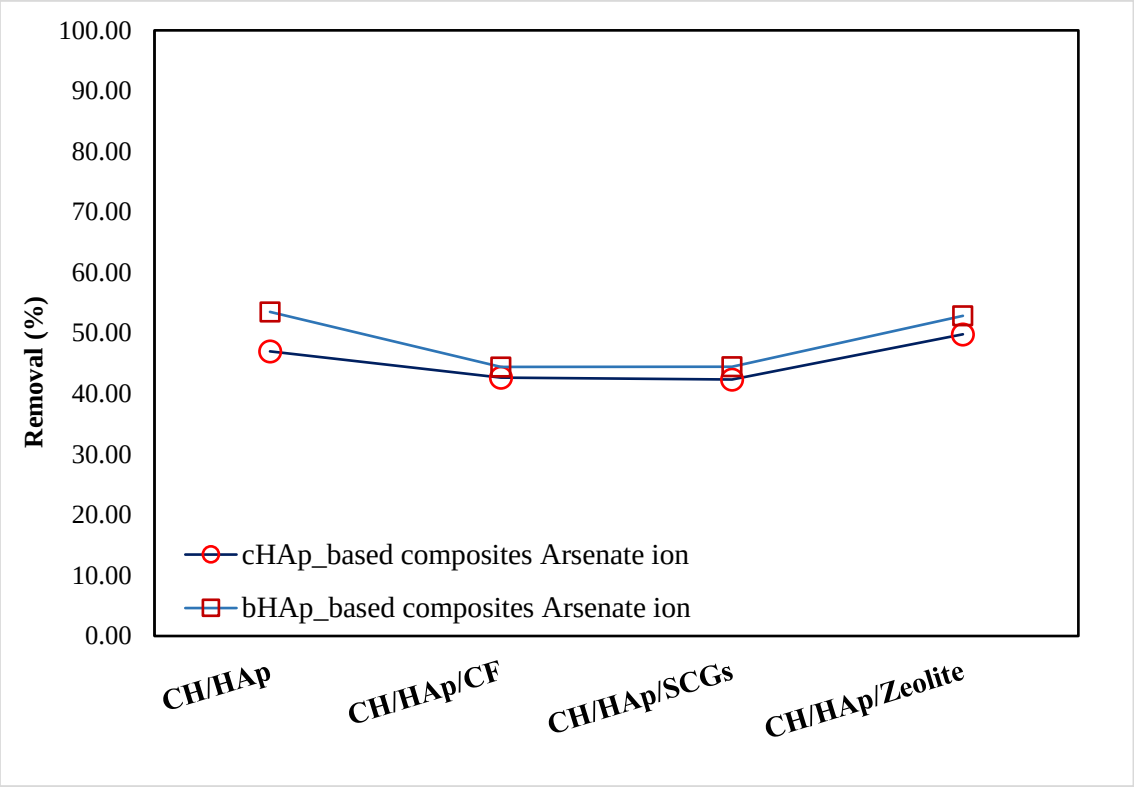

Figure 5-8: Comparison of the removal efficiencies of the synthesised composites for the removal of arsenate ions in industrial input stream sample using 0.1 g of adsorbent.

5.3.2.4 Comparison of chromate ion and arsenate ion removal by the CH/HAp composites from the industrial input stream solutions

In general, arsenate ion removal is better than that of chromate ion from industrial input stream samples when using a higher dose of adsorbent (0.1 g), as discussed above. The mechanism of chromate ion removal involves electrostatic interactions between the anion and positively charged protonated active sites and metal complex formation involving the electron-donating groups on the composite material (as discussed in section 5.1.1.1).

In contrast, the literature does report the possibility of ion exchange for arsenate ion when hydroxyapatite is used to remove arsenic as arsenate ion. Arsenic is predominantly present as arsenate [As(V)] in the industrial water sample (present study), which is a commonly encountered arsenic species that is chemically stable under aerobic conditions[582]. Chen et al.[91] explained that the ion-exchange mechanism for arsenate ion removal on bone char is as follows, which involves the exchange of hydroxyl ions:

$$Ca_{10}(PO_4)_6(OH)_2 + HAsO_4^{2-} \longrightarrow Ca_{10}(PO_4)_6(HAsO_4) + 2OH^- \quad 5\text{-}11$$

Arsenate ($HAsO_4^{2-}$) and phosphate (HPO_4^{2-}) have chemical similarities[129], which means that arsenate could exchange for phosphate on a hydroxyapatite surface. Liu et al.[130] proposed a mechanism of ion-exchange between arsenate and phosphate ion species for removal of arsenic using synthetic hydroxyapatite as given in the following equation:

("≡" denotes a surface) $\equiv HAP\text{-}PO_4^{3-} + AsO_4^{3-} \longrightarrow \equiv HAP\text{-}AsO_4^{3-} + PO_4^{3-}$ 5-12

To confirm if the ion exchange mechanism shown above is occurring, the elemental phosphorus concentration was monitored by ICP-MS before and after exposure of the industrial input stream solution to the CH/HAp composites. The results of this experiment are discussed in the next section.

5.3.2.5 Investigation (by ICP-MS) of the ion-exchange mechanism for cation and anion removal by the CH/HAp composites when exposed to the industrial input stream solutions

5.3.2.5.1 Increase in concentration of Ca^{2+} ions in solution when the CH/HAp composites were exposed to the industrial input stream solutions

Table 5-38 shows the Ca^{2+} ion concentration analysed using ICP-MS in the industrial input stream solution after exposure to 0.01 g and 0.1 g doses of the CH/HAp-based composites.

In Table 5-38, results recorded for industrial input stream solutions at 180 minutes of exposure with the composite systems are presented. For both the composite systems tested, with the industrial type of industrial input stream solution, the concentration of Ca^{2+} ions increased gradually throughout the contact time experiment (15 minutes to 180 minutes, *see Figures 6-9 to 6-12, Appendix 6*). This was taken to mean that ion exchange occurred on the HAp part of the composite between HAp lattice Ca^{2+} and the metal cations present in solution (i.e., Cu^{2+}, Cd^{2+}, and Pb^{2+} etc.)

When using low adsorbent doses (0.01 g), cHAp-based composite systems showed a total 68.72 % to≈112% (Table 5-38) increase in the concentration of Ca^{2+} (plots showing the detailed presentation of each system are given *in appendix 6).* Similarly, an increase of 163.56% to ≈ 144% in Ca^{2+} concentration was observed for the bHAp-based composite,

which indicated that the bHAp-sourced composite demonstrated a better cation exchangeability than that of the commercially sourced HAp. This agreed overall with the better cation removal efficiency of the bHAp- based composites as observed in the experiments conducted in the single metal ion type, two metal ion type and "industrial" input stream water samples. It is possible that the higher surface area of the bHAp-based composite may also be assisting to improve adsorption outcomes for cation uptake relative to the cHAp-based composite system. Alternatively, it could be attributed to the higher content of HAp in the bHAp-based composites, as revealed by the TGA analysis of these composites.

When using a higher dose of adsorbent (0.1 g, Table 5-38), the bHAp-based composites showed a relatively higher increase (%) in Ca^{2+} ions concentration than that observed for the cHAp-based composites and could be attributed to higher ion-exchange between the cations and bHAp-based composites.

Apart from ion exchange between Ca^{2+} of HAp and cations, the increase in the concentration of Ca^{2+} ions were very high in all the solutions exposed to these composites systems, and it could be additionally due to the partial dissolution of these composites to release Ca^{2+} ions in solution.

Table 5-38: The percentage increase in the concentration of Ca^{2+} ions analysed by ICP-MS in an industrial input stream sample during its exposure to 0.01 g and 0.1 g of the composite adsorbents of the present study

Composite adsorbents	cHAp-based composites		bHAp-based composites	
	0.01 g	0.1 g	0.01 g	0.1 g
CH/HAp	68.73	138.86	163.56	172.15
CH/HAp/CF	157.72	202.35	200.33	399.74
CH/HAp/SCGs	178.90	185.74	197.99	181.57
CH/HAp/Zeolites	112.78	194.10	144.21	202.81

5.3.2.5.2 Increase in concentration of phosphorus (P) in solution during the metal removal experimentation

As intimated earlier, the phosphate ions in the hydroxyapatite lattice could be a potential site for ion exchange for metal anions such as arsenate, as presented in equations 5-12. To confirm experimentally whether this ion exchange mechanism had occurred between phosphate anion and other anionic chemical species in the industrial input stream solution

(e.g., arsenate anion), the elemental phosphorus concentration was also monitored simultaneously by ICP-MS in adsorption experiments and the results shown in Table 5-10.

In Table 5-39, a continuous increase in P concentration was observed (presumably as mostly phosphate ion) for both composite systems tested with the industrial input stream solution and presented in *Appendix 6 (Figures 6-13 to 6-16).*

In Table 5-39, the results are presented for the composite systems exposed to the industrial input stream sample, and P concentration was recorded after 180 minutes of exposure time. Using 0.01 g of composite, the cHAp-based composite systems showed an increase in phosphorus concentration ranging between ≈376.15 (the lowest recorded for the CH/HAp/SCGs) and 706.93 % (the highest for the CH/HAp/zeolite) composites. This observation agrees with those recorded earlier for arsenate removal using 0.01 g of adsorbent dose (Figure 5-7), showing the lowest removal of arsenate on the CH/HAp/SCGs and the highest by using the CH/HAp/zeolite of all the composites studied. From this observation, it could be assumed that the exchange between arsenate and phosphate ions is a possible mechanism for the removal of arsenate using these composite systems. The percentage increase in P concentration was found to be relatively higher for the CH/cHAp compared to the CH/bHAp based composite, which could be attributed to the dissolution of HAp, which was reasoned to be higher in the cHAp-based system than in the bHAp-based composite system.

Table 5-39: The percentage increase in the concentration of elemental P analysed by ICP-MS in an industrial input stream sample during its exposure to 0.01 g and 0.1 g of the composite adsorbents of the present study

Composite adsorbents	cHAp-based composites		bHAp-based composites	
	0.01 g	0.1 g	0.01 g	0.1 g
CH/HAp	504.72	454.319	457.02	109.08
CH/HAp/CF	524.09	329.52	571.29	233.08
CH/HAp/SCGs	376.15	458.51	407.14	509.77
CH/HAp/Zeolites	706.93	199.25	671.95	138.32

For the 0.1 g dose of the composites, the cHAp-based composite showed a higher relative increase in phosphorus (≈454% to 199.25%) relative to the bHAp-based composite(≈109% to 233 %), except the CH/HAp/SCGs composite, which exhibited an unusual increase in

the P concentration at 0.1 g of adsorbent dose which could be due to phosphate release from coffee grounds as well (see EDX analysis of SCGs, Figure 2-19).

The higher phosphorus concentration in solutions exposed to the cHAp-based composite could be due to the higher solubility of the cHAp in these composites compared to the bHAp in bHAp-based composites. The large increase in % of P in the solution could also mean that the phosphate detected could have come from the partial dissolution of composites in the solution. The same possibility was mentioned earlier for the Ca^{2+} concentration; hence it is probable that not only has ion exchange occurred but also some dissolution of the composites themselves, albeit with the uptake of Cu^{2+} arsenate and chromate ion from solution into the composites.

This observation of higher dissolution of cHAp-based composite could be supported by the results of chromate removal using these composites in the single metal system where the cHAp-based composite (such as the CH/cHAp) was found to remove chromate ion more efficiently than the CH/bHAp composite, which could be due to the better adsorption properties of CH/cHAp for chromate ions relative to CH/bHAp resulting from the cHAp's greater relative solubility in aqueous solutions, attributed to the higher solubility of cHAp. The electrostatic interactions are one of the dominating mechanisms for the removal of the chromate (as described above). The integrated surface functional groups of HAp could adsorb the chromate ions by electrostatic interactions. For this, the $\equiv PO^-$ groups of the HAp were reported to participate in chromate adsorption, as, after the dissolution of the cHAp, these groups were reported to dominate the surface of the HAp. These groups are protonated in slightly acidic conditions to produce ≡POH groups, resulting in adsorption of the adsorbate (such as chromate) from the aqueous solutions[524]. In the present study, the pH of the solution was 4.0-5.0, which could cause the protonation of $\equiv PO^-$ functional groups to produce ≡ POH species and ultimately providing adsorption sites for chromate anions. This is evident by better chromate adsorption in single metal ion type and industrial input stream water removal systems where the chromate was removed more efficaciously using CH/cHAp than CH/bHAp.

Another possibility could be the higher percentage of carbonate in the cHAp samples, which exchange out for chromate better, but this possible interpretation could not be supported by any literature evidence. However, it was assumed that the higher HAp content in the bHAp-based composite (as demonstrated in TGA analysis) could be due to

the lower carbonate content in this particular HAp phase relative to the cHAp (commercial HAp). So, the presence of the carbonates in cHAp, and ion-exchange between carbonates and chromates could be considered as a mechanism for better chromate ions removal by these systems and could be interesting to explore in future studies.

Contrary to this, the arsenate removal was reported[130] to occur by an ion-exchange mechanism involving phosphates. The arsenate removal (%) was relatively higher for the bHAp-based composites than the cHAp-based composites, which could be attributed to the relatively higher content of HAp in these composite systems, as mentioned above providing higher adsorption sites for the ion-exchange removal of arsenate by the phosphate groups.

From the observation of single metal ion type and industrial input stream system exposure experiments, the CH/cHAp (control) composite was found to be more efficient at removing chromate ions than the CH/bHAp composite. A higher concentration of P was detected in solutions exposed to CH/cHAp. These two findings could be attributed to the relatively higher solubility of CH/cHAp composites (due to cHAp) providing more adsorption sites (≡ POH) for chromates and could be the reason for the higher phosphorus concentration in solution. The relatively better removal of arsenate ion from solution (at both adsorbent doses of 0.01 g and 0.1 g) could only be attributed to the ion-exchangeability of CH/bHAp, including phosphates of the crystal lattice as presented in equation 5-11.

In contrast, in the three-component systems, there was no regular trend for the chromate ion adsorption and phosphorus concentration in the solution exposed to these systems. The arsenate ion removal appeared more efficient when using the bHAp-based composites than the cHAp-based composites, which can be attributed to the higher content of HAp in these systems, a fact also supported by TGA analysis of these composite systems.

5.4 Summary

The batch experiments to evaluate the metal ion removal efficiency of the synthesised composite systems were conducted in three different removal systems, including a single metal ion type, two metal ion types and three metal ion type removal systems.

In single metal ion type removal systems, Cd^{2+}, Pb^{2+}, Cu^{2+} and Cr (as chromate ions) model solutions were used, and the effect of experimental parameters such as dose, initial metal ion concentration, time and pH on removal efficiency of the composite adsorbents was studied. In all the systems studied, a continuous increase in removal efficiency and a decrease in the adsorbent capacity of the composite adsorbents were recorded when the adsorbent dose was gradually increased. On the contrary, a continuous increase in the adsorbent capacity of the composite adsorbents and a decrease in removal efficiency were recorded when the initial concentration of metal ions in the solution was increased gradually. A pH range of 5.0- 7.0 was recorded as an optimum pH for removing Cd^{2+}, a range between 4.5-5.5 for Pb^{2+} and Cu^{2+}. The removal of Cr (as chromate ions) was favoured in an acidic pH range <5.0. Cation (Cd^{2+}, Pb^{2+}, Cu^{2+}) removal % was recorded to be higher than anion (as chromate ions) removal for all the composite adsorbents. In terms of cation adsorption, all the composites showed a preferential removal efficiency for the Pb^{2+} than for the other two cations (Cd^{2+} and Cu^{2+}). The bHAp-based composite adsorbents showed a relatively higher removal % for cations than the cHAp-based composites.

In contrast, the cHAp-based composites showed a higher removal efficiency for Cr (as chromate ions) than the bHAp-based composites. A maximum time of 120 minutes was considered optimum to achieve equilibrium for the adsorption of metal ions using the composite adsorbents. The addition of a third component (CF, SCGs and zeolite) into the two-component composite systems (control composites) exhibited an improvement in the removal efficiency of the composite adsorbents for the removal of cations.

In adsorption modelling, most of the adsorption systems were found to fit Langmuir adsorption behaviour. The Langmuir model showed a better fit than the Freundlich model when the adsorption data of metal ion adsorption using the composite adsorbents was analysed using the adsorption models (Langmuir and Freundlich). The pseudo-second-order kinetic model fitted the kinetic data for metal ion adsorption better than the pseudo-first-order kinetics model did.

In two metal ion type removal systems, two experimental parameters (adsorption dose and time) were used to study the removal efficiency of the composite adsorbents in a relatively complex removal system. In line with a single metal ion type removal system, a positive effect of adsorbent dose on the adsorption of metal ions was recorded while the

adsorbents achieved equilibrium in 120 minutes. All the systems showed good fitting for to pseudo-second-order kinetic model, which illustrated that the chemisorption was the rate-limiting step for the adsorption of metal ions on the adsorbents studied. A comparison of the estimated adsorption capacities of the composites in single-metal ion type and two-metal ion type removal systems showed lower adsorption in the two-metal ions type removal systems relative to the single metal ion type removal systems. It illustrated the antagonistic effect of having two metal ion types in solution, which leads to a competition of the ions with each other for the available adsorption sites. The three-component composite systems showed a better removal % than the two-component composite systems (control composites), which further illustrated that adding a third component (like CF, SCGs and Zeolite) improved the adsorption ability of the composite adsorbents. The adsorbents were also tested in a more complex, real-life industrial-type system containing three metal ions (Cu^{2+}, Cr (as chromate ions) and As (as arsenate ions). The results illustrated that the Cu^{2+} (a cation) removal % was higher than the other two ions (anions) using the composite adsorbents. In contrast, the removal of As (as arsenate ions) was higher than the Cr (as chromate ions). The bHAp-based composite adsorbents showed higher Cu^{2+} and arsenate ions adsorption than the cHAp-based composites. The three-component composite systems showed a higher removal of metal ions than the two-component composite systems, which illustrated the positive effect of adding a third component into the control composites.

The three-metal ion type removal systems were analysed to monitor the calcium and phosphorus ions concentration. A continuous increase in the concentration of both Ca and P ions was recorded, which indicated the occurrence of an ion-exchange mechanism during the removal of cations (Cu^{2+}) and As (arsenate). However, the increase in the concentration of Ca and P was very high, which could be additionally due to the dissolution of the composites themselves when these were exposed to aqueous solutions in the industrial input stream sample containing the three metal ion types.

Chapter 6

Conclusions, Limitations and Future Research

This research focused on the design and testing of some economically viable materials that could be used to remove ions of some of the major heavy metals causing severe environmental damage due to excessive intrusion into water bodies, including Cd^{2+}, Pb^{2+}, Cu^{2+}, Cr (as chromate ions) and arsenic (as arsenate anions).

Among the existing treatment methods for wastewater treatment, particularly for heavy metal ion removal, adsorption was selected as the most efficient, environmentally sustainable, economically feasible, and simple method. For this, low-cost materials such as locally available zeolite and industrial and agricultural by-products, including HAp, chitosan, coir fibre, and SCGs, which are customarily discarded into the environment, were selected as potential materials to remove heavy metal ions from the aqueous solutions. These by-products are produced in enormous amounts and offer a low-cost option for synthesising the adsorbents with a high potential to remove metal ions. These candidate materials were used to make composite adsorbents with hydroxyapatite. Based on the literature findings, it was hypothesised that the addition of HAp could help enhance the removal efficiency of the selected candidate materials. Two different composite systems were synthesised based on two different sources of HAp, including commercially sourced and bovine-sourced HAp, to make a comparison between the removal abilities of cHAp-based and bHAp-based composite adsorbents. The composites were synthesised using the chemical precipitation method. The composites included the two-component composite systems, such as chitosan and hydroxyapatite, which were used as the control composites to compare the removal efficiencies with the novel three-component composite systems developed in this study. These novel three-component composite systems were developed by adding a third component (viz., CF. SCGs and Zeolite) into the two-component composite systems (control composites) to evaluate the effect of the third component on the removal efficiency of the control composites for the adsorption of the metal ions.

6.1 Characterisation of the candidate materials used to synthesise the composite adsorbents

Before employing the composite systems, the candidate materials were characterised using spectroscopic and microscopic techniques, including SEM, EDX, FTIR, XRD, and TGA. The selected raw materials were well-studied and well-reported in the literature studies, so the characterisation results were compared with the observation reported in the literature studies. The purpose of the characterisation of raw materials was to make a foundation for the characterisation of the composite adsorbents and confirm the successful incorporation of the candidate materials into the composites.

SEM micrographs of chitosan showed flake-like morphology, while the coir fibre and SCGs showed a tubular-like structure with central holes and cavities, respectively. The zeolite powder exhibited needle-like particles with a patchy surface. The SEM micrographs of cHAp and bHAp showed different morphologies. For cHAp, aggregates of irregular particles with a rough surface were recorded, while the bHAp showed interconnected spherical particles and pores. The porosity originating from the interconnected particles was attributed to the synthesis method (thermal calcination). The EDX analysis of the chosen biopolymeric materials such as chitosan and lignocellulosic materials like coir fibre and spent coffee grounds exhibited carbon and oxygen as the major elemental components. The principal element of the hydroxyapatites included Ca, P, and O. The Mg was found to be due to the biogenic source of the bovine-derived HAp (bHAp). The Ca:P ratio calculated by elemental percentages of the hydroxyapatite was 1.67-1.8 (for cHAp) and 1.80-1.84 (for bHAp). The EDX analysis of zeolite showed Al, Si and O as principal elements and some cations (Na^+ and K^+). The materials exhibited all constitutional functional groups while being evaluated using the FTIR. These functional groups provide the binding sites for the adsorption of the heavy metal ions by employing several adsorption mechanisms. The major functional groups of these materials included hydroxyl, amino, carboxyl, alkanes and phosphates. Additionally, the presence of carbonate was also recorded by IR absorption peaks in the HAp.

The diffractograms of selected candidate materials (XRD) were compared with the reference patterns of the pure materials (from the XRD database) to identify the characteristic peaks in XRD analysis. The bHAp showed relatively higher crystallinity than cHAp. The chitosan, coir fibre and SCGs were shown to be poorly crystalline phases

from the featuring of one or two broad peaks in the XRD diffractograms. The TGA analysis showed the complete combustion of chitosan and coir fibre in a temperature range of <700 °C. The SCGs left a greyish powder after heating up to 1000° C, which was attributed to the inorganic content of SCGs (ash). The bHAp showed relatively less weight loss than cHAp, which was interpreted as indicative of the more crystalline (calcined) nature of bHAp.

In general, all three characterisation techniques (EDX, FTIR and p-XRD) reinforced the observation that c-HAp was less crystalline. However, these techniques also indicated the bHAp had been formed by a higher temperature thermal calcination process which gave the more highly crystalline materials observed in the case of bHAp.

6.2 Synthesis and characterisation of the low-cost composite materials

The study's first aim was to synthesise the composite materials using the chosen candidate materials and their characterisation, which was achieved by forming two-component and three-component composite systems. The characterisation of the composites was done by the same microscopic and spectroscopic techniques as used for the candidate materials.

In SEM analysis of the control composites, CH/cHAp exhibited a homogenised surface while the CH/bHAp was relatively heterogeneous, showing fine particles deposition at the surface attributed to the deposition of the nano-bHAp crystal or the composite matrix itself. Overall, both the composite exhibited similar morphological characteristics as particles of irregular shapes. The EDX analysis presented the Ca, P, C and O as the major constitutional elements coming from the chitosan and HAp. The presence of bovine sourced HAp in CH/bHAp was confirmed by the Mg peak in the micrograph. The FTIR spectrum of the composites exhibited fewer peaks than the candidate materials (chitosan and HAp) after the formation of the composites, showing the poorly crystalline nature of the materials. Overall, both the composites showed similar morphological and spectroscopic characters, which was attributed to the re-precipitation of the materials during the synthesis of the composites, which could be a reason for similar HAp deposition in the composites. The differences between the two composite systems were recorded in the TGA and XRD analyses. The XRD diffractogram of the CH/bHAp showed some additional peaks compared to the diffractogram of the CH/cHAp composites, which might be due to the higher crystallinity of the bHAp.

Similarly, the residual mass in TGA analysis for the CH/bHAp is higher than CH/cHAp. The white coloured powder residue was identified as HAp. It revealed that a relatively higher mass of pure HAp is incorporated into the CH/bHAp composites because bHAp has higher purity than cHAp.

In the three-component composite systems, SEM analysis showed that CH/HAp/CF and CH/HAp/SCGs composites exhibited highly amorphous and irregular surfaces. The deposition of finely powdered particles of coir fibre dust and spent coffee grounds were visible in their respective composites in SEM micrographs. The carbon content was high due to their constitutional components (coir fibre and SCGs, and chitosan), while the presence of the HAp was evident from the Ca and P peaks. The Mg was present in the bHAp-based composites to confirm its source. Similarly, the FTIR and XRD analysis showed similar results for the cHAp and bHAp based composites. Like the control composites, the TGA analysis exhibited a higher weight loss (%) for cHAp-based composites (CH/cHAp/CF and CH/cHAp/SCGs) than the bHAp-based composites (CH/bHAp/CF and CH/bHAp/SCGs). It confirmed the higher thermal stability of the bHAp relative to the cHAp used in the composites.

6.3 Application of synthesised composite systems for the removal of metal ion solutions

The second aim of the study was to employ the synthesised composites in aqueous systems to evaluate their efficiency at removing heavy metal ions by adsorption from various solutions. The synthesised composites were applied in three different systems and showed good removal efficiency for heavy metal ion cations. The characterisation of the materials (FTIR analysis) exhibited that the hydroxyl, carboxyl and phosphates groups are the dominating functional groups of the composites, which provide the adsorption sites for the metal ions and favour the adsorption of cations on these composite adsorbents. Moreover, the presence of HAp also favours the ion exchange between the cations and Ca^{2+} ions, which could also enhance the overall removal ability of the composites for the adsorption of cations. It showed that the selection of materials based upon their chemical composition (functional groups) is an important indicator while synthesising the composite adsorbents for the application of metal ions removal.

The adsorbent dose positively affected the removal efficiency of the composites for the removal of metal ions (both cations and anions), which was assigned to the availability of more adsorption sites per g of adsorbent to adsorb the metal ions available in the metal ion solutions, exposed to these composites. It demonstrated the importance of the adsorbent dose while applying the adsorbents into the water treatment systems. It illustrated that the higher removal efficiency could be achieved by simply enhancing the adsorbent dose of adsorbents.

A solution pH > 4.0 was found to be favourable for the adsorption of cations (Cd^{2+}, Pb^{2+}, Cu^{2+}), while the adsorbents showed better adsorption of anions (chromate ions) at slightly acidic pH < 5.0. The pH of the solution is an important parameter as it controls the overall charges on the surface of the composites and controls the speciation of metal ions. The results revealed that if the adsorbents carry a positive charge in acidic conditions, they favour removing anions in the acidic pH ranges. In the present study, the protonation of some functional groups (such as amino and hydroxyl groups) in the acidic pH range was considered as a favourable characteristic for the removal of anions (such as chromate ions) from relatively low (< 5.0) pH solutions. In contrast, a slight increase in pH from the acidic range favours the adsorption of cations due to deprotonation of the functional groups, which ultimately provide adsorption sites for the adsorption of cations.

The contact time of approximately two hours was recorded as optimum for attaining an adsorption equilibrium in regard to the adsorption of metal ions on the adsorbents studied. The findings were in agreement in all three systems showing > 70% removal efficiency for the removal of cations using the two-component systems and >80% removal of cations when using the three-component composite systems. The chemical characterisation of the composite adsorbents justifies preferential removal of cations over anions when using the synthesised composites as all of the materials contain functional groups (such as amino, hydroxyl and carboxyl), which predominantly provide binding sites for the cations. Additionally, the presence of hydroxyapatite further enhanced the cation removal ability of the composite adsorbents by providing adsorption sites (i.e., Ca^{2+} in the HAp lattice) for the exchange of cations.

All the composite systems studied showed the preferential adsorption of Pb^{2+} ions from both the single-metal ion and the two-metal ion type solution systems. This was attributed to the physicochemical character of Pb^{2+} with preferential removal of Pb^{2+} being

attributed to its higher electronegativity value (relative to the other two metal cations studied) and values of the respective ionic radii. The higher electronegativity value enhances its metal-ligand complexation ability when the metal ions undergo adsorption on the amino and hydroxyl groups. The ionic radii play a role in the metal ion-exchange mechanism. The ionic radii of Ca^{2+} and Pb^{2+} make a more feasible exchange between these two cations relative to the other cations studied. It illustrated that the physicochemical characteristics are also very important to consider when designing composite adsorbents and using them to adsorb metal ions.

The industrial input stream solutions sample exposed to adsorbents showed better adsorption of cations (e.g., Cu^{2+} ions) than anions (chromate and arsenate), in agreement with observations recorded for the corresponding single-metal ion type solution systems. The bHAp-based composites showed a better adsorption ability for the arsenate ions than the cHAp-based composites, which was attributed to the higher ion-exchange-ability of bHAp-based composites (between arsenate and phosphates) and this was due to the higher level of HAp incorporated into these composites compared to the cHAp-based composites. The highest adsorption of arsenate and the lowest adsorption of chromate ions was recorded for the CH/HAp/Zeolite composites, which was also expected to occur due to the ion-exchange mechanism involved in the removal of metal cations and anions by this composite system.

Overall, the composites performed better (in terms of removal ability) in the two-metal ion type and the industrial input stream solution sample systems compared to the single-metal ion type systems for the adsorption of metal ions. It showed that the applicability of the CH/HAp (control) composites could be enhanced in complex systems (like two metal or multi-metal systems) by adding the third component (e.g., CF, SCGs and Zeolite). Similarly, the adsorption of cations could be maximised by adding a zeolitic material which could help to enhance the overall ion-exchange ability of the composites.

An increase in calcium and phosphorus (elemental) concentrations were monitored in the solutions exposed to the composites. The increase in Ca^{2+} ions was attributed to ion exchange between cations and Ca^{2+} of HAp. Similarly, an increase in P was attributed to ion exchange between P and As. However, for an extremely large increase in the concentrations of Ca^{2+} and P, it was reasoned that the dissolution of the composites was also occurring along with ion exchange processes.

6.3.1 *Adsorption modelling for the adsorption of the metal ions from single-metal ion systems using the synthesised composite*

Based on the literature review carried out for the adsorption of the metal ions on similar systems studied in this research, two non-linear adsorption models were selected for the adsorption modelling of the metal ion adsorption behaviour on these composites. These models included the Langmuir and the Freundlich isotherms. These are the most reported models in the literature for describing the adsorption mechanism of the metal ions using a variety of adsorbents. The non-linear regression method was used to fit these models on the experimental data of the metal ion adsorption recorded for the adsorbent systems of this study. Table 6-1 summarises the "coefficient of determination" (R^2) recorded for these models fitted to the experimental adsorption data of the metal ions recorded for the adsorption of these metals on the composites systems.

It is evident from Table 6-1 the adsorption behaviour of the metal ions is different in different systems. Similarly, each composite system interacts with each metal ion in a different way. For instance, the Langmuir model is the best-fitted model for Cd^{2+} adsorption on the CH/HAp composites, while the Pb^{2+} and chromate ion adsorption data is best described by the Freundlich isotherm model (see the value of R^2 above). Moreover, Cu^{2+} ion adsorption follows the Langmuir isotherm when modelling adsorption on the CH/cHAp composites. In contrast, the Freundlich isotherm model is the best-fitted model for Cu^{2+} adsorption on the CH/bHAp composite system. It illustrated that the metal ion could follow different adsorption behaviour when adsorption of the same metal ion occurs on different composite systems.

Table 6-1: The coefficient of determination (R^2) values recorded for the non-linear Langmuir and Freundlich isotherms fitted to the adsorption data of the metal ion adsorption on the composite systems

Composite systems	Metal ions	cHAp-based composites		bHAp-based composites	
		Langmuir	**Freundlich**	**Langmuir**	**Freundlich**
CH/HAp	Cd^{2+}	**0.996**	0.969	**0.999**	0.988
	Pb^{2+}	0.965	**0.986**	0.938	**0.983**
	Cu^{2+}	**0.973**	0.896	**0.961**	0.900
	Chromate	0.996	**1.000**	0.988	**0.995**
CH/HAp/CF	Cd^{2+}	**0.961**	0.847	**0.977**	0.925
	Pb^{2+}	**0.952**	0.810	**0.890**	0.720
	Cu^{2+}	**0.987**	0.978	**0.939**	0.793
	Chromate	**0.993**	**0.993**	**0.997**	0.986
CH/HAp/SCGs	Cd^{2+}	**0.987**	0.931	**0.993**	0.933
	Pb^{2+}	0.932	**1**	**0.975**	0.972
	Cu^{2+}	**0.994**	0.947	**0.995**	0.991
	Chromate	**0.998**	0.993	**0.996**	0.974
CH/HAp/Zeolite	Cd^{2+}	**0.975**	0.94	**0.996**	0.975
	Pb^{2+}	**0.947**	0.839	**0.97**	0.913
	Cu^{2+}	**0.968**	0.871	**0.895**	0.744
	Chromate	**0.983**	0.937	**0.971**	0.912

For most of the composite systems, the Langmuir isotherm was found to be the best-fitted model to describe the adsorption of metal ions. However, Freundlich was also a good fit for some systems. Based on the literature observations, the Langmuir could be suggested as the best-fitted model for describing the adsorption of the metal ions on these systems, as it is one of the most reliable models, as mentioned in several literature studies.

The data could be explored further by employing the other adsorption isotherm models, which are suggested for the adsorption of the metal ions on heterogeneous surfaces, such as the Sips isotherm model.

6.3.2 Kinetic modelling for the adsorption of the metal ions in single-metal ion type and two-metal ion types of systems using the synthesised composite

The non-linear pseudo-first-order and pseudo-second-order models were employed to fit the contact time data of the metal ion adsorption on the synthesised composite. The non-linear regression method was used to fit the non-linear PFO and PSO models to the experimental data.

Based on the observations recorded in all the composite systems, the pseudo-second-order kinetic model was the best-fitted model, with R^2 values being > the R2 values calculated for the PFO model. It suggested, therefore, that chemisorption was the rate-limiting step for the adsorption of the metal ions on these systems. The functional groups of the composites (as summarised in the FTIR analyses of the composites as detailed in chapter 4) were regarded as being the sites where chemisorption of the metal ions occurred and mainly involved metal-ligand complexation. Additionally, the ion exchange on the part of HAp of the composites was demonstrated as the leading agent for the removal of the metal ions by the ion exchange mechanism. In the CH/HAp/Zeolite composite systems, the zeolites also could be assumed to assist in the ion-exchange mechanism due to the presence of cations in the zeolite structure.

The single-metal ion type solution systems established that the PSO kinetic model was the best-fitted model to the experimental data of the metal ions, which was further employed in the two-metal ion types of removal systems. It showed a good fitting on the kinetics data of Cd^{2+} and Pb^{2+} ions recorded in these competitive adsorption systems. It confirmed that the chemisorption is the rate-limiting step for the adsorption of these metal ions.

6.4 Limitations of current research project and suggestions for future research

During this research, several challenges were faced, which limited the number of experimentations conducted and consequently affected the data collection, analysis, and conclusions drawn based on that data.

Experimental Limitation: One of the most important limitations was the synthesis of small quantities of composite materials. This project was based on various composite

adsorbents, and relatively smaller composites were made to manage the available time effectively. Consequently, a limited quantity of materials affected the comprehensive characterisation of materials; for example, the Brunauer-Emmett-Teller (BET) analysis could not be performed, as it requires a relatively larger quantity of materials to get optimal results. Additionally, if synthesising of a large amount of materials were possible, a column study could have been conducted to compare with the batch experiments, and it could also have been used to test the practical applicability of the materials in water treatment systems.

Instrumental limitation: The Atomic Absorption Spectrometer (AAS) was the analytical instrument that was used in this study. It was easy to access and relatively cheap as compared to other available instruments. However, Inductively Coupled Plasma Mass-Spectrometry (ICP-MS), in place of AAS, could have been used to a greater extent to analyse the samples as it provides more reliable results as it is a more sensitive instrument, is not sensitive to matrix interferences and can also do simultaneous analysis of multiple elements.

Based on the limitations mentioned above, some suggestions regarding the material characterisation and metal removal experimentation are given below, which could aid in advancing future research in this area.

The application of low-cost composite materials in water treatment systems could be enhanced in different ways. The first is to explore their chemical and physical characteristics in detail with additional methods. For instance, surface area and pore size distribution of materials could be studied using BET analysis. Secondly, physical and chemical modification before their employment in composite matrices could help to increase their effectiveness. For example, the surface area of clays (such as zeolites) could be increased by converting them into nanosized materials using physical and chemical methods. Thirdly, different proportions of raw materials could be used to make the composites. It can help to evaluate the involvement of each raw material in the metal removal mechanism. For example, the proportion of one raw material (such as HAp) could be changed by keeping the other material (e.g. chitosan) constant to make the composite.

For the metal removal experimentation, a large mass of composites could be synthesised to conduct relatively large-scale experimental studies. A bulk quantity of materials could

help to conduct comprehensive research using different experimental setups. For example, in the current study, only batch experimental systems were used, which are preferred for small-scale laboratory studies due to dealing with small quantities of materials and easy operational methods; however, this is not effective for larger volumes of water. For comprehensive research dealing with large volumes of water, a column bed design is preferred, which provides a scaled-up design to apply in industries for wastewater treatment. Therefore, a column study could be designed along with the batch experiments to compare the removal efficiencies of the materials in two different experimental setups. Moreover, different combinations of the metal ion solutions could be used to evaluate the competitive adsorption of the metal ions using the composite systems. For this, different metal ion concentrations could be used (e.g., 10 to 50 ppm). Similarly, the metal ion concentration of one metal could be varied by keeping the other metal concentration constant. It could help evaluate the effect of one metal ion on the adsorption of the other metal ion in a competitive adsorption system.

Lastly, a study by using the output stream water (industrial wastewater) could be conducted to compare the results of removal efficiency of the composite materials which were recorded for the industrial input stream water samples.

6.5 References

1. Zia, Z.; Hartland, A.; Mucalo, M. Use of low-cost biopolymers and biopolymeric composite systems for heavy metal removal from water. *International Journal of Environmental Science and Technology* **2020**, *17*, 4389-4406.
2. Fund(WWF), W. W.: Washington, DC 20037

2021.
3. Corcoran, E. *Sick water?: the central role of wastewater management in sustainable development: a rapid response assessment*; UNEP/Earthprint, 2010.
4. Vakili, M.; Rafatullah, M.; Salamatinia, B.; Abdullah, A. Z.; Ibrahim, M. H.; Tan, K. B.; Gholami, Z.; Amouzgar, P. Application of chitosan and its derivatives as adsorbents for dye removal from water and wastewater: A review. *Carbohydrate polymers* **2014**, *113*, 115-130.
5. Salem, H. S.; Chilingarian, G. V. Influence of porosity and direction of flow on tortuosity in unconsolidated porous media. *Energy Sources* **2000**, *22*, 207-213.

6. Lenntech, K. Water treatment and air purification. *Published by Rotter Dam Seweg, Netherlands* **2004**
7. Duruibe, J.; Ogwuegbu, M.; Egwurugwu, J. Heavy metal pollution and human biotoxic effects. *International Journal of Physical Sciences* **2007**, *2*, 112-118.
8. Ahmed, Q.; Bat, L.; Ali, Q. M. Heavy metal levels in Thunnus albacares (Bonnaterre, 1788) from Karachi fish harbour, Pakistan. *Pakistan Journal of Marine Sciences* **2012**, *21*, 13-21.
9. Hutton, M.; Symon, C. The quantities of cadmium, lead, mercury and arsenic entering the UK environment from human activities. *Science of the total environment* **1986**, *57*, 129-150.
10. Battarbee, R. The causes of lake acidification, with special reference to the role of acid deposition. *Phil. Trans. R. Soc. Lond. B* **1990**, *327*, 339-347.
11. Nriagu, J. O. A global assessment of natural sources of atmospheric trace metals. *Nature* **1989**, *338*, 47-49.
12. Peplow, A. T.; Jones, C.; Petyt, M. Surface vibration propagation over a layered elastic half-space with an inclusion. *Applied Acoustics* **1999**, *56*, 283-296.
13. Ogwuegbu, M.; Muhanga, W. Investigation of lead concentration in the blood of people in the Copperbelt Province of Zambia. *J Environ* **2005**, *1*, 66-75.
14. Akpor, O. B.; Ohiobor, G. O.; Olaolu, T. D. Heavy metal pollutants in wastewater effluents: sources, effects and remediation. *Advances in Bioscience and Bioengineering* **2014**, *2*, 37-43.
15. Amaral, A.; Cruz, J.; Cunha, R. T. d.; Rodrigues, A. Baseline levels of metals in volcanic soils of the Azores (Portugal). *Soil & Sediment Contamination* **2006**, *15*, 123-130.
16. Qu, X.; Alvarez, P. J.; Li, Q. Applications of nanotechnology in water and wastewater treatment. *Water research* **2013**, *47*, 3931-3946.
17. Rousseau, M.-C.; Straif, K.; Siemiatycki, J. IARC carcinogen update. *Environmental health perspectives* **2005**, *113*, A580.
18. George, C. M.; Sima, L.; Arias, M.; Mihalic, J.; Cabrera, L. Z.; Danz, D.; Checkley, W.; Gilman, R. H. Arsenic exposure in drinking water: an unrecognized health threat in Peru. *Bulletin of the World Health Organization* **2014**, *92*, 565-572.

19. Tolins, M.; Ruchirawat, M.; Landrigan, P. The developmental neurotoxicity of arsenic: cognitive and behavioral consequences of early life exposure. *Annals of global health* **2014**, *80*, 303-314.
20. Tyler, C. R.; Allan, A. M. The effects of arsenic exposure on neurological and cognitive dysfunction in human and rodent studies: a review. *Current environmental health reports* **2014**, *1*, 132-147.
21. Robinson, B.; Kim, N.; Marchetti, M.; Moni, C.; Schroeter, L.; van den Dijssel, C.; Milne, G.; Clothier, B. Arsenic hyperaccumulation by aquatic macrophytes in the Taupo Volcanic Zone, New Zealand. *Environmental and Experimental Botany* **2006**, *58*, 206-215.
22. Smedley, P.; Kinniburgh, D. A review of the source, behaviour and distribution of arsenic in natural waters. *Applied geochemistry* **2002**, *17*, 517-568.
23. Bolan, N. S.; Thiagarajan, S. Retention and plant availability of chromium in soils as affected by lime and organic matter amendments. *Soil Research* **2001**, *39*, 1091-1103.
24. Nriagu, J. O.; Pacyna, J. M. Quantitative assessment of worldwide contamination of air, water and soils by trace metals. *nature* **1988**, *333*, 134-139.
25. Eisler, R. Arsenic hazards to humans, plants, and animals from gold mining. *Reviews of environmental contamination and toxicology* **2004**, 133-165.
26. Kumar, P. S.; Ramakrishnan, K.; Kirupha, S. D.; Sivanesan, S. Thermodynamic and kinetic studies of cadmium adsorption from aqueous solution onto rice husk. *Brazilian Journal of Chemical Engineering* **2010**, *27*, 347-355.
27. Madala, S.; Nadavala, S. K.; Vudagandla, S.; Boddu, V. M.; Abburi, K. Equilibrium, kinetics and thermodynamics of Cadmium (II) biosorption on to composite chitosan biosorbent. *Arabian Journal of Chemistry* **2013**
28. Taylor, M.; Kim, N.; Hill, R.; Chapman, R. A review of soil quality indicators and five key issues after 12 yr soil quality monitoring in the Waikato region. *Soil Use and Management* **2010**, *26*, 212-224.
29. Kim, N. *Cadmium accumulation in Waikato soils*; Environment Waikato Regional Council, 2008.

30. Taylor, M.; Gibb, R.; Willoughby, J.; Hewitt, A.; Arnold, G. Soil maps of cadmium in New Zealand (Prepared for Ministry of Agriculture and Forestry). *Hamilton, New Zealand: Landcare Research* **2007**
31. Clark, C.; Rampal, K.; Thuppil, V.; Chen, C.; Clark, R.; Roda, S. The lead content of currently available new residential paint in several Asian countries. *Environmental Research* **2006**, *102*, 9-12.
32. Barbosa Jr, F.; Tanus-Santos, J. E.; Gerlach, R. F.; Parsons, P. J. A critical review of biomarkers used for monitoring human exposure to lead: advantages, limitations, and future needs. *Environmental health perspectives* **2005**, *113*, 1669.
33. Todd, G.; Wohlers, D.; Citra, M. Agency for toxic substances and disease registry. *Atlanta, GA* **2003**
34. Wright, J. P.; Dietrich, K. N.; Ris, M. D.; Hornung, R. W.; Wessel, S. D.; Lanphear, B. P.; Ho, M.; Rae, M. N. Association of prenatal and childhood blood lead concentrations with criminal arrests in early adulthood. *PLoS Medicine* **2008**, *5*, e101.
35. Needleman, H. L.; McFarland, C.; Ness, R. B.; Fienberg, S. E.; Tobin, M. J. Bone lead levels in adjudicated delinquents: a case control study. *Neurotoxicology and teratology* **2002**, *24*, 711-717.
36. Sachs, H. K. Bone lead levels and delinquent behavior. *JAMA* **1996**, *275*, 1725-1726.
37. Braun, J. M.; Kahn, R. S.; Froehlich, T.; Auinger, P.; Lanphear, B. P. Exposures to environmental toxicants and attention deficit hyperactivity disorder in US children. *Environmental health perspectives* **2006**, *114*, 1904.
38. Barnowski, C.; Jakubowski, N.; Stuewer, D.; Broekaert, J. A. Speciation of chromium by direct coupling of ion exchange chromatography with inductively coupled plasma mass spectrometry. *Journal of Analytical Atomic Spectrometry* **1997**, *12*, 1155-1161.
39. Beghetto, V.; Agostinis, L.; Taffarello, R.; Samiolo, R. Innovative Active Cross-Linking Agents for Sustainable Leather Manufacturing. In *Sustainable Design and Manufacturing 2016*; Springer, 2016; pp 149-155.
40. Wuana, R. A.; Okieimen, F. E. Heavy Metals in Contaminated Soils: A Review of Sources, Chemistry, Risks and Best Available Strategies for Remediation. *ISRN Ecology* **2011**, *2011*, 402647.

41. Rehman, M.; Liu, L.; Wang, Q.; Saleem, M. H.; Bashir, S.; Ullah, S.; Peng, D. Copper environmental toxicology, recent advances, and future outlook: A review. *Environmental Science and Pollution Research* **2019**, *26*, 18003-18016.
42. Fraga, C. G. Relevance, essentiality and toxicity of trace elements in human health. *Molecular Aspects of Medicine* **2005**, *26*, 235-244.
43. Singh, O.; Labana, S.; Pandey, G.; Budhiraja, R.; Jain, R. Phytoremediation: an overview of metallic ion decontamination from soil. *Applied microbiology and biotechnology* **2003**, *61*, 405-412.
44. Shrivastava, A. A review on copper pollution and its removal from water bodies by pollution control technologies. *Indian Journal of Environmental Protection* **2009**, *29*, 552-560.
45. Connor, R.; Renata, A.; Ortigara, C.; Koncagül, E.; Uhlenbrook, S.; Lamizana-Diallo, B. M.; Zadeh, S. M.; Qadir, M.; Kjellén, M.; Sjödin, J. The United Nations World Water Development Report 2017. Wastewater: The Untapped Resource. *The United Nations World Water Development Report* **2017**
46. Gunatilake, S. Methods of removing heavy metals from industrial wastewater. *Methods* **2015**, *1*, 14.
47. Feng, D.; Aldrich, C.; Tan, H. Treatment of acid mine water by use of heavy metal precipitation and ion exchange. *Minerals Engineering* **2000**, *13*, 623-642.
48. Akpor, O.; Muchie, M. Remediation of heavy metals in drinking water and wastewater treatment systems: processes and applications. *International Journal of Physical Sciences* **2010**, *5*, 1807-1817.
49. Sud, D.; Mahajan, G.; Kaur, M. Agricultural waste material as potential adsorbent for sequestering heavy metal ions from aqueous solutions–A review. *Bioresource technology* **2008**, *99*, 6017-6027.
50. Adamson, A. Kineics of gas phase reactions. In *A textbook of physical chemistry*

Elsevier, 2012.
51. Ruthven, D. M. *Principles of adsorption and adsorption processes*; John Wiley & Sons, 1984.
52. Wang, J.; Guo, X. Adsorption isotherm models: Classification, physical meaning, application and solving method. *Chemosphere* **2020**, *258*, 127279.

53. Sahoo, T. R.; Prelot, B. Adsorption processes for the removal of contaminants from wastewater: the perspective role of nanomaterials and nanotechnology. In *Nanomaterials for the Detection and Removal of Wastewater Pollutants*; Elsevier, 2020; pp 161-222.
54. Zhang, H.; Wang, J.; Zhou, B.; Zhou, Y.; Dai, Z.; Zhou, Q.; Chriestie, P.; Luo, Y. Enhanced adsorption of oxytetracycline to weathered microplastic polystyrene: kinetics, isotherms and influencing factors. *Environmental Pollution* **2018**, *243*, 1550-1557.
55. Agboola, O. D.; Benson, N. U. Physisorption and Chemisorption Mechanisms Influencing Micro (Nano) Plastics-Organic Chemical Contaminants Interactions: A Review. *FRONTIERS IN ENVIRONMENTAL SCIENCE* **2021**, *9*
56. Bonilla-Petriciolet, A.; Mendoza-Castillo, D. I.; Reynel-Ávila, H. E. *Adsorption processes for water treatment and purification*; Springer, 2017.
57. Durst, R. Chemically modified electrodes: recommended terminology and definitions (IUPAC Recommendations 1997). *Pure and applied chemistry* **1997**, *69*, 1317-1324.
58. Zhang, W.; Zhuang, L.; Yuan, Y.; Tong, L.; Tsang, D. C. Enhancement of phenanthrene adsorption on a clayey soil and clay minerals by coexisting lead or cadmium. *Chemosphere* **2011**, *83*, 302-310.
59. Worch, E. *Adsorption technology in water treatment: fundamentals, processes, and modeling*; Walter de Gruyter, 2012.
60. Jagtoyen, M.; Derbyshire, F. Activated carbons from yellow poplar and white oak by H3PO4 activation. *Carbon* **1998**, *36*, 1085-1097.
61. Nahil, M. A.; Williams, P. T. Pore characteristics of activated carbons from the phosphoric acid chemical activation of cotton stalks. *Biomass and Bioenergy* **2012**, *37*, 142-149.
62. Aliabadi, M.; Irani, M.; Ismaeili, J.; Najafzadeh, S. Design and evaluation of chitosan/hydroxyapatite composite nanofiber membrane for the removal of heavy metal ions from aqueous solution. *Journal of the Taiwan Institute of Chemical Engineers* **2014**, *45*, 518-526.

63. Rajiv Gandhi, M.; Kousalya, G. N.; Meenakshi, S. Removal of copper(II) using chitin/chitosan nano-hydroxyapatite composite. *International Journal of Biological Macromolecules* **2011**, *48*, 119-124.
64. Efome, J. E.; Rana, D.; Matsuura, T.; Lan, C. Q. Effects of operating parameters and coexisting ions on the efficiency of heavy metal ions removal by nano-fibrous metal-organic framework membrane filtration process. *Science of The Total Environment* **2019**, *674*, 355-362.
65. Kelly, A. The nature of composite materials. *Scientific American* **1967**, *217*, 160-179.
66. Berghezan, A. Non-ferrous materials. *Nucleus* **1966**, *8*, 5-11.
67. Van, S. Philips Research Reports. **1972**
68. Ghaedi, M.; Mosallanejad, N. Removal of heavy metal ions from polluted waters by using of low cost adsorbents. *Journal of Chemical Health Risks* **2013**, *3*
69. Upadhyay, U.; Sreedhar, I.; Singh, S. A.; Patel, C. M.; Anitha, K. L. Recent advances in heavy metal removal by chitosan based adsorbents. *Carbohydrate Polymers* **2021**, *251*, 117000.
70. Negm, N. A.; Ali, H. E. Modification of heavy metal uptake efficiency by modified chitosan/anionic surfactant systems. *Engineering in Life Sciences* **2010**, *10*, 218-224.
71. Guibal, E. Interactions of metal ions with chitosan-based sorbents: a review. *Separation and purification technology* **2004**, *38*, 43-74.
72. Rahmi; Lelifajri; Julinawati; Shabrina. Preparation of chitosan composite film reinforced with cellulose isolated from oil palm empty fruit bunch and application in cadmium ions removal from aqueous solutions. *Carbohydrate Polymers* **2017**, *170*, 226-233.
73. Sun, X.; Peng, B.; Ji, Y.; Chen, J.; Li, D. Chitosan (chitin)/cellulose composite biosorbents prepared using ionic liquid for heavy metal ions adsorption. *AIChE journal* **2009**, *55*, 2062-2069.
74. HPS, A. K.; Saurabh, C. K.; Adnan, A.; Fazita, M. N.; Syakir, M.; Davoudpour, Y.; Rafatullah, M.; Abdullah, C.; Haafiz, M.; Dungani, R. A review on chitosan-cellulose blends and nanocellulose reinforced chitosan biocomposites: Properties and their applications. *Carbohydrate polymers* **2016**, *150*, 216-226.

75. Laszlo, J. A.; Dintzis, F. R. Crop resides as lon-exchange materials. Treatment of soybean hull and sugar beet fiber (pulp) with epichlorohydrin to improve cation-exchange capacity and physical stability. *Journal of Applied Polymer Science* **1994**, *52*, 531-538.

76. Kalita, S. J.; Bhardwaj, A.; Bhatt, H. A. Nanocrystalline calcium phosphate ceramics in biomedical engineering. *Materials Science and Engineering: C* **2007**, *27*, 441-449.

77. Krestou, A.; Xenidis, A.; Panias, D. Mechanism of aqueous uranium (VI) uptake by hydroxyapatite. *Minerals Engineering* **2004**, *17*, 373-381.

78. Ma, Q. Y.; Traina, S. J.; Logan, T. J.; Ryan, J. A. Effects of aqueous Al, Cd, Cu, Fe (II), Ni, and Zn on Pb immobilization by hydroxyapatite. *Environmental Science & Technology* **1994**, *28*, 1219-1228.

79. Mousa, S.; Hanna, A. Synthesis of nano-crystalline hydroxyapatite and ammonium sulfate from phosphogypsum waste. *Materials Research Bulletin* **2013**, *48*, 823-828.

80. Sneddon, I.; Orueetxebarria, M.; Hodson, M.; Schofield, P.; Valsami-Jones, E. Use of bone meal amendments to immobilise Pb, Zn and Cd in soil: a leaching column study. *Environmental Pollution* **2006**, *144*, 816-825.

81. Hasan, S. H.; Ranjan, D.; Talat, M. Water hyacinth biomass (WHB) for the biosorption of hexavalent chromium: optimization of process parameters. *BioResources* **2010**, *5*, 563-575.

82. Mohammad, A. M.; Eldin, T. A. S.; Hassan, M. A.; El-Anadouli, B. E. Efficient treatment of lead-containing wastewater by hydroxyapatite/chitosan nanostructures. *Arabian Journal of Chemistry* **2015**

83. Mousa, S.; Ammar, N.; Ibrahim, H. Removal of lead ions using hydroxyapatite nano-material prepared from phosphogypsum waste. *Journal of Saudi Chemical Society* **2016**, *20*, 357-365.

84. Mobasherpour, I.; Salahi, E.; Pazouki, M. Comparative of the removal of Pb 2+, Cd 2+ and Ni 2+ by nano crystallite hydroxyapatite from aqueous solutions: Adsorption isotherm study. *Arabian Journal of Chemistry* **2012**, *5*, 439-446.

85. Pham Minh, D.; Tran, N. D.; Nzihou, A.; Sharrock, P. One-step synthesis of calcium hydroxyapatite from calcium carbonate and orthophosphoric acid under moderate conditions. *Industrial & Engineering Chemistry Research* **2013**, *52*, 1439-1447.
86. Minh, D. P.; Tran, N. D.; Nzihou, A.; Sharrock, P. Hydroxyapatite gel for the improved removal of Pb 2+ ions from aqueous solution. *Chemical engineering journal* **2013**, *232*, 128-138.
87. Kader, A. A.; Aly, A.; Girgis, B. Bone char decolorisation efficiency. A laboratory study over four consecutive cycles. *International Sugar Journal (Worldwide Sugar Edition)(United Kingdom)* **1996**
88. Moreno, J. C.; Gómez, R.; Giraldo, L. Removal of Mn, Fe, Ni and Cu ions from wastewater using cow bone charcoal. *Materials* **2010**, *3*, 452-466.
89. Ghrab, S.; Benzina, M.; Lambert, S. D. Copper Adsorption from Wasterwater Using Bone Charcoal. *Advances in Materials Physics and Chemistry* **2017**, *7*, 139.
90. de Souza, S. V.; Pinto, C. T.; Junqueira, R. G. In-house method validation: application in arsenic analysis. *Journal of Food Composition and Analysis* **2007**, *20*, 241-247.
91. Chen, Y.-N.; Chai, L.-Y.; Shu, Y.-D. Study of arsenic (V) adsorption on bone char from aqueous solution. *Journal of Hazardous Materials* **2008**, *160*, 168-172.
92. Pattanayak, J.; Mondal, K.; Mathew, S.; Lalvani, S. A parametric evaluation of the removal of As (V) and As (III) by carbon-based adsorbents. *Carbon* **2000**, *38*, 589-596.
93. Garg, U. K.; Kaur, M.; Garg, V.; Sud, D. Removal of hexavalent chromium from aqueous solution by agricultural waste biomass. *Journal of Hazardous materials* **2007**, *140*, 60-68.
94. Chen, S.-B.; Zhu, Y.-G.; Ma, Y.-B.; McKay, G. Effect of bone char application on Pb bioavailability in a Pb-contaminated soil. *Environmental Pollution* **2006**, *139*, 433-439.
95. Bazargan-Lari, R.; Zafarani, H. R.; Bahrololoom, M. E.; Nemati, A. Removal of Cu(II) ions from aqueous solutions by low-cost natural hydroxyapatite/chitosan composite: Equilibrium, kinetic and thermodynamic studies. *Journal of the Taiwan Institute of Chemical Engineers* **2014**, *45*, 1642-1648.

96. Chen, F.; Wang, Z.-C.; Lin, C.-J. Preparation and characterization of nano-sized hydroxyapatite particles and hydroxyapatite/chitosan nano-composite for use in biomedical materials. *Materials letters* **2002**, *57*, 858-861.

97. Sundaram, C. S.; Viswanathan, N.; Meenakshi, S. Uptake of fluoride by nano-hydroxyapatite/chitosan, a bioinorganic composite. *Bioresource technology* **2008**, *99*, 8226-8230.

98. Kramer, E. R.; Morey, A. M.; Staruch, M.; Suib, S. L.; Jain, M.; Budnick, J. I.; Wei, M. Synthesis and characterization of iron-substituted hydroxyapatite via a simple ion-exchange procedure. *Journal of Materials Science* **2013**, *48*, 665-673.

99. Crini, G. Recent developments in polysaccharide-based materials used as adsorbents in wastewater treatment. *Progress in polymer science* **2005**, *30*, 38-70.

100. Barakat, M. New trends in removing heavy metals from industrial wastewater. *Arabian Journal of Chemistry* **2011**, *4*, 361-377.

101. Saber-Samandari, S.; Saber-Samandari, S.; Nezafati, N.; Yahya, K. Efficient removal of lead (II) ions and methylene blue from aqueous solution using chitosan/Fe-hydroxyapatite nanocomposite beads. *Journal of environmental management* **2014**, *146*, 481-490.

102. Saber-Samandari, S.; Gazi, M.; Yilmaz, E. UV-induced synthesis of chitosan-g-polyacrylamide semi-IPN superabsorbent hydrogels. *Polymer bulletin* **2012**, *68*, 1623-1639.

103. Guvendiren, M.; Lu, H. D.; Burdick, J. A. Shear-thinning hydrogels for biomedical applications. *Soft matter* **2012**, *8*, 260-272.

104. Saber-Samandari, S.; Saber-Samandari, S.; Gazi, M. Cellulose-graft-polyacrylamide/hydroxyapatite composite hydrogel with possible application in removal of Cu (II) ions. *Reactive and Functional Polymers* **2013**, *73*, 1523-1530.

105. McGrellis, S.; Serafini, J.-N.; JeanJean, J.; Pastol, J.-L.; Fedoroff, M. Influence of the sorption protocol on the uptake of cadmium ions in calcium hydroxyapatite. *Separation and Purification technology* **2001**, *24*, 129-138.

106. Fuller, C.; Bargar, J.; Davis, J.; Piana, M. Mechanisms of uranium interactions with hydroxyapatite: Implications for groundwater remediation. *Environmental Science & Technology* **2002**, *36*, 158-165.

107. Ghrab, S.; Benzina, M.; Lambert, S. D. Copper Adsorption from Wasterwater Using Bone Charcoal. *Advances in Materials Physics and Chemistry* **2017**, *7*, 139-147.
108. Mobasherpour, I.; Salahi, E.; Pazouki, M. Comparative of the removal of Pb2+, Cd2+ and Ni2+ by nano crystallite hydroxyapatite from aqueous solutions: Adsorption isotherm study. *Arabian Journal of Chemistry* **2012**, *5*, 439-446.
109. Minh, D. P.; Tran, N. D.; Nzihou, A.; Sharrock, P. Hydroxyapatite gel for the improved removal of Pb2+ ions from aqueous solution. *Chemical engineering journal* **2013**, *232*, 128-138.
110. del Rıo, J. G.; Morando, P.; Cicerone, D. Natural materials for treatment of industrial effluents: comparative study of the retention of Cd, Zn and Co by calcite and hydroxyapatite. Part I: batch experiments. *Journal of Environmental Management* **2004**, *71*, 169-177.
111. Hamad, A. A.; Hassouna, M. S.; Shalaby, T. I.; Elkady, M. F.; Abd Elkawi, M. A.; Hamad, H. A. Electrospun cellulose acetate nanofiber incorporated with hydroxyapatite for removal of heavy metals. *International Journal of Biological Macromolecules* **2020**, *151*, 1299-1313.
112. Vahdat, A.; Ghasemi, B.; Yousefpour, M. Synthesis of hydroxyapatite and hydroxyapatite/Fe3O4 nanocomposite for removal of heavy metals. *Environmental Nanotechnology, Monitoring & Management* **2019**, *12*, 100233.
113. Elkady, M.; Shokry, H.; Hamad, H. Microwave-assisted synthesis of magnetic hydroxyapatite for removal of heavy metals from groundwater. *Chemical Engineering & Technology* **2018**, *41*, 553-562.
114. Hernández-Cocoletzi, H.; Salinas, R. A.; Águila-Almanza, E.; Rubio-Rosas, E.; Chai, W. S.; Chew, K. W.; Mariscal-Hernández, C.; Show, P. L. Natural hydroxyapatite from fishbone waste for the rapid adsorption of heavy metals of aqueous effluent. *Environmental Technology & Innovation* **2020**, *20*, 101109.
115. Avram, A.; Frentiu, T.; Horovitz, O.; Mocanu, A.; Goga, F.; Tomoaia-Cotisel, M. Hydroxyapatite for removal of heavy metals from wastewater. *Studia Ubb Chemia* **2017**, *4*, 93-104.
116. Zhou, C.; Wang, X.; Wang, Y.; Song, X.; Fang, D.; Ge, S. The sorption of single- and multi-heavy metals in aqueous solution using enhanced nano-hydroxyapatite

assisted with ultrasonic. *Journal of Environmental Chemical Engineering* **2021**, *9*, 105240.

117. Iconaru, S. L.; Motelica-Heino, M.; Guegan, R.; Beuran, M.; Costescu, A.; Predoi, D. Adsorption of Pb (II) ions onto hydroxyapatite nanopowders in aqueous solutions. *Materials* **2018**, *11*, 2204.
118. Li, L.; Iqbal, J.; Zhu, Y.; Zhang, P.; Chen, W.; Bhatnagar, A.; Du, Y. Chitosan/Ag-hydroxyapatite nanocomposite beads as a potential adsorbent for the efficient removal of toxic aquatic pollutants. *International journal of biological macromolecules* **2018**, *120*, 1752-1759.
119. Zhu, X.-h.; Li, J.; Luo, J.-h.; Jin, Y.; Zheng, D. Removal of cadmium (II) from aqueous solution by a new adsorbent of fluor-hydroxyapatite composites. *Journal of the Taiwan Institute of Chemical Engineers* **2017**, *70*, 200-208.
120. Pătescu, R.; Busuioc, L. T.; Nechifor, G.; Simonescu, C. M.; Deleanu, C. Applicability of chitosan/hydroxyapatite composites for adsorptive removal of lead, copper, zinc and nickel from synthetic aqueous solutions. *UPB Sci. Bull., Ser. B* **2017**, *79*, 119-134.
121. Hokkanen, S.; Bhatnagar, A.; Srivastava, V.; Suorsa, V.; Sillanpää, M. Removal of Cd2+, Ni2+ and PO43− from aqueous solution by hydroxyapatite-bentonite clay-nanocellulose composite. *International Journal of Biological Macromolecules* **2018**, *118*, 903-912.
122. Liu, G.; Li, Z.; Xu, L.; Xu, X.; Huang, Q.; Zeng, Y.; Wen, M. The dynamics and adsorption of Cd (II) onto hydroxyapatite attapulgite composites from aqueous solution. *Journal of Sol-Gel Science and Technology* **2018**, *87*, 269-284.
123. Corami, A.; Mignardi, S.; Ferrini, V. Cadmium removal from single-and multi-metal (Cd+ Pb+ Zn+ Cu) solutions by sorption on hydroxyapatite. *Journal of Colloid and Interface Science* **2008**, *317*, 402-408.
124. Ma, Q. Y.; Traina, S. J.; Logan, T. J.; Ryan, J. A. In situ lead immobilization by apatite. *Environmental Science & Technology* **1993**, *27*, 1803-1810.
125. Leyva, A. G.; Marrero, J.; Smichowski, P.; Cicerone, D. Sorption of antimony onto hydroxyapatite. *Environmental science & technology* **2001**, *35*, 3669-3675.
126. Wang, Y.; Chen, T.; Yeh, K.; Shue, M. Stabilization of an elevated heavy metal contaminated site. *Journal of Hazardous Materials* **2001**, *88*, 63-74.

127. Vega, E.; Pedregosa, J.; Narda, G. Interaction of oxovanadium (IV) with crystalline calcium hydroxyapatite: surface mechanism with no structural modification. *Journal of Physics and Chemistry of Solids* **1999**, *60*, 759-766.
128. Suzuki, T.; Hatsushika, T.; Hayakawa, Y. Synthetic hydroxyapatites employed as inorganic cation-exchangers. *Journal of the Chemical Society, Faraday Transactions 1: Physical Chemistry in Condensed Phases* **1981**, *77*, 1059-1062.
129. Yang, H.-C.; Fu, H.-L.; Lin, Y.-F.; Rosen, B. P. Pathways of arsenic uptake and efflux. *Current topics in membranes* **2012**, *69*, 325-358.
130. Liu, G.; Talley, J. W.; Na, C.; Larson, S. L.; Wolfe, L. G. Copper doping improves hydroxyapatite sorption for arsenate in simulated groundwaters. *Environmental science & technology* **2010**, *44*, 1366-1372.
131. Terry, P. A.; Dolan, D.; Maccoux, M. J.; Meyer, M. Removal of Phosphates and Chromates in a Multi-ion System. *Global Journal of Research In Engineering* **2014**
132. Hokkanen, S.; Bhatnagar, A.; Repo, E.; Lou, S.; Sillanpää, M. Calcium hydroxyapatite microfibrillated cellulose composite as a potential adsorbent for the removal of Cr (VI) from aqueous solution. *Chemical Engineering Journal* **2016**, *283*, 445-452.
133. Shen, J.; Kaur, I.; Baktash, M. M.; He, Z.; Ni, Y. A combined process of activated carbon adsorption, ion exchange resin treatment and membrane concentration for recovery of dissolved organics in pre-hydrolysis liquor of the kraft-based dissolving pulp production process. *Bioresource technology* **2013**, *127*, 59-65.
134. Arbia, W.; Arbia, L.; Adour, L.; Amrane, A. Chitin extraction from crustacean shells using biological methods–a review. *Food Technology and Biotechnology* **2013**, *51*, 12-25.
135. Younes, I.; Rinaudo, M. Chitin and chitosan preparation from marine sources. Structure, properties and applications. *Marine drugs* **2015**, *13*, 1133-1174.
136. Sen, D. *Advances in fish processing technology*; Allied Publishers, 2005.
137. Kurita, K. Controlled functionalization of the polysaccharide chitin. *Progress in Polymer science* **2001**, *26*, 1921-1971.
138. Rinaudo, M. Chitin and chitosan: properties and applications. *Progress in polymer science* **2006**, *31*, 603-632.

139. Crini, G.; Badot, P.-M. Application of chitosan, a natural aminopolysaccharide, for dye removal from aqueous solutions by adsorption processes using batch studies: a review of recent literature. *Progress in polymer science* **2008**, *33*, 399-447.
140. Mourya, V.; Inamdar, N. N. Chitosan-modifications and applications: opportunities galore. *Reactive and Functional polymers* **2008**, *68*, 1013-1051.
141. Pillai, C.; Paul, W.; Sharma, C. P. Chitin and chitosan polymers: Chemistry, solubility and fiber formation. *Progress in polymer science* **2009**, *34*, 641-678.
142. Yusof, N. L. B. M.; Wee, A.; Lim, L. Y.; Khor, E. Flexible chitin films as potential wound-dressing materials: Wound model studies. *Journal of biomedical materials research Part A* **2003**, *66*, 224-232.
143. Madhumathi, K.; Binulal, N.; Nagahama, H.; Tamura, H.; Shalumon, K.; Selvamurugan, N.; Nair, S.; Jayakumar, R. Preparation and characterization of novel β-chitin–hydroxyapatite composite membranes for tissue engineering applications. *International journal of biological macromolecules* **2009**, *44*, 1-5.
144. Azuma, K.; Izumi, R.; Osaki, T.; Ifuku, S.; Morimoto, M.; Saimoto, H.; Minami, S.; Okamoto, Y. Chitin, chitosan, and its derivatives for wound healing: old and new materials. *Journal of functional biomaterials* **2015**, *6*, 104-142.
145. Yusof, N. L. B. M.; Lim, L. Y.; Khor, E. Preparation and characterization of chitin beads as a wound dressing precursor. *Journal of Biomedical Materials Research Part A* **2001**, *54*, 59-68.
146. Gerente, C.; Lee, V.; Cloirec, P. L.; McKay, G. Application of chitosan for the removal of metals from wastewaters by adsorption—mechanisms and models review. *Critical reviews in environmental science and technology* **2007**, *37*, 41-127.
147. Guibal, E.; Van Vooren, M.; Dempsey, B. A.; Roussy, J. A review of the use of chitosan for the removal of particulate and dissolved contaminants. *Separation science and technology* **2006**, *41*, 2487-2514.
148. Cardenas, G.; Orlando, P.; Edelio, T. Synthesis and applications of chitosan mercaptanes as heavy metal retention agent. *International Journal of Biological Macromolecules* **2001**, *28*, 167-174.

149. Mcafee, B. J.; Gould, W. D.; Nadeau, J. C.; da Costa, A. C. Biosorption of metal ions using chitosan, chitin, and biomass of Rhizopus oryzae. *Separation Science and technology* **2001**, *36*, 3207-3222.

150. Carvalho, L. H. d.; Canedo, E.; Neto, S. F.; de Lima, A. B.; Silva, C. Moisture transport process in vegetable fiber composites: theory and analysis for technological applications. In *Industrial and technological applications of transport in porous materials*; Springer, 2013; pp 37-62.

151. Wu, F.-C.; Tseng, R.-L.; Juang, R.-S. A review and experimental verification of using chitosan and its derivatives as adsorbents for selected heavy metals. *Journal of Environmental Management* **2010**, *91*, 798-806.

152. Varma, A.; Deshpande, S.; Kennedy, J. Metal complexation by chitosan and its derivatives: a review. *Carbohydrate Polymers* **2004**, *55*, 77-93.

153. Ngah, W. W.; Teong, L.; Hanafiah, M. Adsorption of dyes and heavy metal ions by chitosan composites: A review. *Carbohydrate polymers* **2011**, *83*, 1446-1456.

154. Miretzky, P.; Cirelli, A. F. Hg (II) removal from water by chitosan and chitosan derivatives: a review. *Journal of hazardous materials* **2009**, *167*, 10-23.

155. Liu, B.; Lv, X.; Meng, X.; Yu, G.; Wang, D. Removal of Pb (II) from aqueous solution using dithiocarbamate modified chitosan beads with Pb (II) as imprinted ions. *Chemical engineering journal* **2013**, *220*, 412-419.

156. Lee, H. C.; Jeong, Y. G.; Min, B. G.; Lyoo, W. S.; Lee, S. C. Preparation and acid dye adsorption behavior of polyurethane/chitosan composite foams. *Fibers and Polymers* **2009**, *10*, 636-642.

157. Liu, J.; Wang, Q.; Wang, A. Synthesis and characterization of chitosan-g-poly (acrylic acid)/sodium humate superabsorbent. *Carbohydrate Polymers* **2007**, *70*, 166-173.

158. Ngah, W. S. W.; Ariff, N. F. M.; Hanafiah, M. A. K. M. Preparation, characterization, and environmental application of crosslinked chitosan-coated bentonite for tartrazine adsorption from aqueous solutions. *Water, air, and soil pollution* **2010**, *206*, 225-236.

159. Chang, M.-Y.; Juang, R.-S. Adsorption of tannic acid, humic acid, and dyes from water using the composite of chitosan and activated clay. *Journal of Colloid and Interface Science* **2004**, *278*, 18-25.

160. Zhu, H.; Jiang, R.; Xiao, L.; Zeng, G. Preparation, characterization, adsorption kinetics and thermodynamics of novel magnetic chitosan enwrapping nanosized γ-Fe 2 O 3 and multi-walled carbon nanotubes with enhanced adsorption properties for methyl orange. *Bioresource technology* **2010**, *101*, 5063-5069.
161. Kalyani, S.; Priya, J. A.; Rao, P. S.; Krishnaiah, A. Removal of copper and nickel from aqueous solutions using chitosan coated on perlite as biosorbent. *Separation science and technology* **2005**, *40*, 1483-1495.
162. Hasan, M.; Ahmad, A.; Hameed, B. Adsorption of reactive dye onto cross-linked chitosan/oil palm ash composite beads. *Chemical Engineering Journal* **2008**, *136*, 164-172.
163. Uddin, M. K. A review on the adsorption of heavy metals by clay minerals, with special focus on the past decade. *Chemical Engineering Journal* **2017**, *308*, 438-462.
164. Hasan, S.; Krishnaiah, A.; Ghosh, T. K.; Viswanath, D. S.; Boddu, V. M.; Smith, E. D. Adsorption of chromium (VI) on chitosan-coated perlite. *Separation science and technology* **2003**, *38*, 3775-3793.
165. Hasan, S.; Krishnaiah, A.; Ghosh, T. K.; Viswanath, D. S.; Boddu, V. M.; Smith, E. D. Adsorption of divalent cadmium (Cd (II)) from aqueous solutions onto chitosan-coated perlite beads. *Industrial & engineering chemistry research* **2006**, *45*, 5066-5077.
166. Swayampakula, K.; Boddu, V. M.; Nadavala, S. K.; Abburi, K. Competitive adsorption of Cu (II), Co (II) and Ni (II) from their binary and tertiary aqueous solutions using chitosan-coated perlite beads as biosorbent. *Journal of Hazardous Materials* **2009**, *170*, 680-689.
167. Fan, D.; Zhu, X.; Xu, M.; Yan, J. Adsorption properties of chromium (VI) by chitosan coated montmorillonite. *Journal of Biological Sciences* **2006**, *6*, 941-945.
168. YANG, Y.-q.; CHEN, H.-j. Study on the Intercalation Organobentonite and its Adsorption [J]. *Journal of Xinyang Normal University (Natural Science Edition)* **2007**, *3*, 023.
169. Copello, G.; Varela, F.; Vivot, R. M.; Díaz, L. Immobilized chitosan as biosorbent for the removal of Cd (II), Cr (III) and Cr (VI) from aqueous solutions. *Bioresource technology* **2008**, *99*, 6538-6544.

170. Boddu, V. M.; Abburi, K.; Randolph, A. J.; Smith, E. D. Removal of copper (II) and nickel (II) ions from aqueous solutions by a composite chitosan biosorbent. *Separation science and technology* **2008**, *43*, 1365-1381.

171. George, M.; Abraham, T. E. Polyionic hydrocolloids for the intestinal delivery of protein drugs: alginate and chitosan—a review. *Journal of controlled release* **2006**, *114*, 1-14.

172. Gombotz, W. R.; Wee, S. F. Protein release from alginate matrices. *Advanced drug delivery reviews* **2012**, *64*, 194-205.

173. Ngah, W. W.; Fatinathan, S. Adsorption of Cu (II) ions in aqueous solution using chitosan beads, chitosan–GLA beads and chitosan–alginate beads. *Chemical Engineering Journal* **2008**, *143*, 62-72.

174. Mututuvari, T. M.; Tran, C. D. Synergistic adsorption of heavy metal ions and organic pollutants by supramolecular polysaccharide composite materials from cellulose, chitosan and crown ether. *Journal of hazardous materials* **2014**, *264*, 449-459.

175. Tran, C. D.; Duri, S.; Delneri, A.; Franko, M. Chitosan-cellulose composite materials: preparation, characterization and application for removal of microcystin. *Journal of hazardous materials* **2013**, *252*, 355-366.

176. Rico, M.; Rodríguez-Llamazares, S.; Barral, L.; Bouza, R.; Montero, B. Processing and characterization of polyols plasticized-starch reinforced with microcrystalline cellulose. *Carbohydrate polymers* **2016**, *149*, 83-93.

177. Qu, R.; Sun, C.; Wang, M.; Ji, C.; Xu, Q.; Zhang, Y.; Wang, C.; Chen, H.; Yin, P. Adsorption of Au (III) from aqueous solution using cotton fiber/chitosan composite adsorbents. *Hydrometallurgy* **2009**, *100*, 65-71.

178. Liimatainen, H.; Visanko, M.; Sirviö, J. A.; Hormi, O. E.; Niinimaki, J. Enhancement of the nanofibrillation of wood cellulose through sequential periodate–chlorite oxidation. *Biomacromolecules* **2012**, *13*, 1592-1597.

179. Rahmi, L.; Julinawati, S. Preparation of chitosan composite film reinforced with cellulose isolated from oil palm empty fruit bunch and application in cadmium ions removal from aqueous solutions. *Carbohydrate Polymers* **2017**, *170*, 226-233.

180. Mohan, D.; Singh, K. P.; Singh, V. K. Trivalent chromium removal from wastewater using low cost activated carbon derived from agricultural waste material and activated carbon fabric cloth. *Journal of hazardous materials* **2006**, *135*, 280-295.
181. Jin, X.; Li, K.; Ning, P.; Bao, S.; Tang, L. Removal of Cu (II) ions from aqueous solution by magnetic chitosan-tripolyphosphate modified silica-coated adsorbent: characterization and mechanisms. *Water, Air, & Soil Pollution* **2017**, *228*, 302.
182. Ge, H.; Hua, T.; Chen, X. Selective adsorption of lead on grafted and crosslinked chitosan nanoparticles prepared by using Pb2+ as template. *Journal of hazardous materials* **2016**, *308*, 225-232.
183. Reddy, N. S.; Rao, K. Polymeric hydrogels: recent advances in toxic metal ion removal and anticancer drug delivery applications. *Indian J. Adv. Chem. Sci* **2016**, *4*
184. Sargın, İ.; Kaya, M.; Arslan, G.; Baran, T.; Ceter, T. Preparation and characterisation of biodegradable pollen–chitosan microcapsules and its application in heavy metal removal. *Bioresource technology* **2015**, *177*, 1-7.
185. Liu, T.; Yang, X.; Wang, Z.-L.; Yan, X. Enhanced chitosan beads-supported Fe0-nanoparticles for removal of heavy metals from electroplating wastewater in permeable reactive barriers. *Water research* **2013**, *47*, 6691-6700.
186. Kwok, K. C.; Koong, L. F.; Chen, G.; McKay, G. Mechanism of arsenic removal using chitosan and nanochitosan. *Journal of colloid and interface science* **2014**, *416*, 1-10.
187. Su, F.; Zhou, H.; Zhang, Y.; Wang, G. Three-dimensional honeycomb-like structured zero-valent iron/chitosan composite foams for effective removal of inorganic arsenic in water. *Journal of colloid and interface science* **2016**, *478*, 421-429.
188. Qi, H.; Jiang, X.; Zhou, D.; Zhu, B.; Qin, L.; Ma, C.; Ong, Y.; Murata, Y. Removal of heavy metals in aqueous solution using Antarctic krill chitosan/hydroxyapatite composite. *Fibers and polymers* **2013**, *14*, 1134-1140.
189. Kusrini, E.; Sofyan, N.; Nurjaya, D. M.; Santoso, S.; Tristantini, D. Removal of heavy metals from aqueous solution by hydroxyapatite/chitosan composite. Presented at Advanced Materials Research; Place,Trans Tech Publ; Vol. 789, p 176-179.

190. Bazargan-Lari, R.; Zafarani, H. R.; Bahrololoom, M. E.; Nemati, A. Removal of Cu (II) ions from aqueous solutions by low-cost natural hydroxyapatite/chitosan composite: Equilibrium, kinetic and thermodynamic studies. *Journal of the Taiwan Institute of Chemical Engineers* **2014**, *45*, 1642-1648.
191. Park, S.; Gomez-Flores, A.; Chung, Y. S.; Kim, H. Removal of cadmium and lead from aqueous solution by hydroxyapatite/chitosan hybrid fibrous sorbent: kinetics and equilibrium studies. *Journal of Chemistry* **2015**, *2015*
192. Mohammad, A. M.; Eldin, T. A. S.; Hassan, M. A.; El-Anadouli, B. E. Efficient treatment of lead-containing wastewater by hydroxyapatite/chitosan nanostructures. *Arabian Journal of Chemistry* **2017**, *10*, 683-690.
193. Rakati, K. K.; Mirzaei, M.; Maghsoodi, S.; Shahbazi, A. Preparation and characterization of poly aniline modified chitosan embedded with ZnO-Fe3O4 for Cu (II) removal from aqueous solution. *International journal of biological macromolecules* **2019**, *130*, 1025-1045.
194. Vijayalakshmi, K.; Gomathi, T.; Latha, S.; Hajeeth, T.; Sudha, P. Removal of copper (II) from aqueous solution using nanochitosan/sodium alginate/microcrystalline cellulose beads. *International journal of biological macromolecules* **2016**, *82*, 440-452.
195. Zhua, X.; Tanga, Y.-b.; Chena, F.-y.; Shia, Y.; Wanga, X.-g. Synthesis of magnetic rectorite/humic acid/chitosan composite for removal of heavy metal ions from water. *DESALINATION AND WATER TREATMENT* **2019**, *163*, 155-165.
196. Kuczajowska-Zadrożna, M.; Filipkowska, U.; Jóźwiak, T. Adsorption of Cu (II) and Cd (II) from aqueous solutions by chitosan immobilized in alginate beads. *Journal of Environmental Chemical Engineering* **2020**, 103878.
197. Tang, S.; Yang, J.; Lin, L.; Peng, K.; Chen, Y.; Jin, S.; Yao, W. Construction of Physically Crosslinked Chitosan/Sodium Alginate/Calcium Ion Double-Network Hydrogel and Its Application to Heavy Metal Ions Removal. *Chemical Engineering Journal* **2020**, 124728.
198. Zhang, M.; Zhang, Z.; Peng, Y.; Feng, L.; Li, X.; Zhao, C.; Zheng, H. Novel cationic polymer modified magnetic chitosan beads for efficient adsorption of heavy metals and dyes over a wide pH range. *International Journal of Biological Macromolecules* **2020**

199. Liu, J.; Chen, Y.; Han, T.; Cheng, M.; Zhang, W.; Long, J.; Fu, X. A biomimetic SiO2@ chitosan composite as highly-efficient adsorbent for removing heavy metal ions in drinking water. *Chemosphere* **2019**, *214*, 738-742.

200. El-Reash, Y. A. Magnetic chitosan modified with cysteine-glutaraldehyde as adsorbent for removal of heavy metals from water. *Journal of Environmental Chemical Engineering* **2016**, *4*, 3835-3847.

201. Li, D.; Tian, X.; Wang, Z.; Guan, Z.; Li, X.; Qiao, H.; Ke, H.; Luo, L.; Wei, Q. Multifunctional adsorbent based on metal-organic framework modified bacterial cellulose/chitosan composite aerogel for high efficient removal of heavy metal ion and organic pollutant. *Chemical Engineering Journal* **2020**, *383*, 123127.

202. Kumar, J.; Arland, S.; Gour, P. Mercury removal from simulated waste water by chitosan nano composite embedded with leaf extract of Brassica Gongylodes. *Materials Today: Proceedings* **2020**

203. Wittmar, A. S.; Klug, J.; Ulbricht, M. Cellulose/chitosan porous spheres prepared from 1-butyl-3-methylimidazolium acetate/dimethylformamide solutions for Cu2+ adsorption. *Carbohydrate Polymers* **2020**, 116135.

204. Zia, Q.; Tabassum, M.; Lu, Z.; Khawar, M. T.; Song, J.; Gong, H.; Meng, J.; Li, Z.; Li, J. Porous poly (L–lactic acid)/chitosan nanofibres for copper ion adsorption. *Carbohydrate polymers* **2020**, *227*, 115343.

205. Swarnalatha, K.; Ayoob, S. Adsorption studies on coir pith for heavy metal removal. *International Journal of Sustainable Engineering* **2016**, *9*, 259-265.

206. Van Dam, J. Coir processing technologies. *Technical paper* **2002**

207. Van Dam, J. Coir processing technologies: improvement of drying, softening, bleaching and dyeing coir fibre/yarn and printing coir floor coverings. *Technical paper/Common Fund for Commodities (Netherlands)* **2002**

208. Rout, P. P.; Arulmozhiselvan, K. Investigating the suitability of pressmud and coir pith for use as soilless substrate by SEM, XRF, UV-VIS and FTIR spectroscopy techniques. *nature* **2019**, *10*, 11.

209. Wambua, P.; Ivens, J.; Verpoest, I. Natural fibres: can they replace glass in fibre reinforced plastics? *composites science and technology* **2003**, *63*, 1259-1264.

210. Haque, M. M.; Hasan, M.; Islam, M. S.; Ali, M. E. Physico-mechanical properties of chemically treated palm and coir fiber reinforced polypropylene composites. *Bioresource Technology* **2009**, *100*, 4903-4906.
211. Lee, B.-G.; Rowell, R. M. Removal of heavy metal ions from aqueous solutions using lignocellulosic fibers. *Journal of natural fibers* **2004**, *1*, 97-108.
212. Namasivayam, C.; Sureshkumar, M. Removal of chromium (VI) from water and wastewater using surfactant modified coconut coir pith as a biosorbent. *Bioresource technology* **2008**, *99*, 2218-2225.
213. Suksabye, P.; Thiravetyan, P.; Nakbanpote, W.; Chayabutra, S. Chromium removal from electroplating wastewater by coir pith. *Journal of Hazardous Materials* **2007**, *141*, 637-644.
214. Shen, Y.-S.; Wang, S.-L.; Huang, S.-T.; Tzou, Y.-M.; Huang, J.-H. Biosorption of Cr (VI) by coconut coir: spectroscopic investigation on the reaction mechanism of Cr (VI) with lignocellulosic material. *Journal of hazardous materials* **2010**, *179*, 160-165.
215. Quek, S.; Al-Duri, B.; Wase, D.; Forster, C. Coir as a biosorbent of copper and lead. *Process Safety and Environmental Protection* **1998**, *76*, 50-54.
216. Parab, H.; Joshi, S.; Shenoy, N.; Lali, A.; Sarma, U.; Sudersanan, M. Determination of kinetic and equilibrium parameters of the batch adsorption of Co (II), Cr (III) and Ni (II) onto coir pith. *Process Biochemistry* **2006**, *41*, 609-615.
217. Buczek, B. Preparation of active carbon by additional activation with potassium hydroxide and characterization of their properties. *Advances in Materials Science and Engineering* **2016**, *2016*
218. Ahmadpour, A.; Do, D. The preparation of active carbons from coal by chemical and physical activation. *Carbon* **1996**, *34*, 471-479.
219. Johnson, E. Goodbye to carbon neutral: Getting biomass footprints right. *Environmental impact assessment review* **2009**, *29*, 165-168.
220. Santhy, K.; Selvapathy, P. Removal of reactive dyes from wastewater by adsorption on coir pith activated carbon. *Bioresource Technology* **2006**, *97*, 1329-1336.
221. Mohan, D.; Singh, K. P.; Singh, V. K. Trivalent chromium removal from wastewater using low cost activated carbon derived from agricultural waste material and

activated carbon fabric cloth. *Journal of Hazardous Materials* **2006**, *135*, 280-295.

222. Namasivayam, C.; Kadirvelu, K. Activated carbons prepared from coir pith by physical and chemical activation methods. *Bioresource Technology* **1997**, *62*, 123-127.

223. Kadirvelu, K.; Namasivayam, C. Activated carbon from coconut coirpith as metal adsorbent: adsorption of Cd (II) from aqueous solution. *Advances in Environmental Research* **2003**, *7*, 471-478.

224. Kadirvelu, K.; Thamaraiselvi, K.; Namasivayam, C. Adsorption of nickel (II) from aqueous solution onto activated carbon prepared from coirpith. *Separation and purification Technology* **2001**, *24*, 497-505.

225. Ewecharoen, A.; Thiravetyan, P.; Nakbanpote, W. Comparison of nickel adsorption from electroplating rinse water by coir pith and modified coir pith. *Chemical Engineering Journal* **2008**, *137*, 181-188.

226. Reddad, Z.; Gerente, C.; Andres, Y.; Le Cloirec, P. Adsorption of several metal ions onto a low-cost biosorbent: kinetic and equilibrium studies. *Environmental science & technology* **2002**, *36*, 2067-2073.

227. Amuda, M.; Olaniyan, T.; Amadi, J.; Subair, O. CORROSION CHARACTERISTICS OF REBAR AND FIBRE REINFORCED CONCRETES IN SELECTED ENVIRONMENTS. *UNILAG Journal of Medicine, Science and Technology* **2017**, *4*, 15.

228. Kadirvelu, K.; Kavipriya, M.; Karthika, C.; Radhika, M.; Vennilamani, N.; Pattabhi, S. Utilization of various agricultural wastes for activated carbon preparation and application for the removal of dyes and metal ions from aqueous solutions. *Bioresource technology* **2003**, *87*, 129-132.

229. Shen, Y.-S.; Wang, S.-L.; Huang, S.-T.; Tzou, Y.-M.; Huang, J.-H. Biosorption of Cr (VI) by coconut coir: spectroscopic investigation on the reaction mechanism of Cr (VI) with lignocellulosic material. *Journal of hazardous materials* **2010**, *179*, 160-165.

230. Johari, K.; Saman, N.; Song, S. T.; Chin, C. S.; Kong, H.; Mat, H. Adsorption enhancement of elemental mercury by various surface modified coconut husk as

eco-friendly low-cost adsorbents. *International Biodeterioration & Biodegradation* **2016**, *109*, 45-52.

231. Santhy, K.; Selvapathy, P. Removal of heavy metals from wastewater by adsorption on coir pith activated carbon. *Separation Science and Technology* **2004**, *39*, 3331-3351.
232. Parab, H.; Joshi, S.; Shenoy, N.; Lali, A.; Sarma, U. S.; Sudersanan, M. Determination of kinetic and equilibrium parameters of the batch adsorption of Co(II), Cr(III) and Ni(II) onto coir pith. *Process Biochemistry* **2006**, *41*, 609-615.
233. Shukla, S. R.; Pai, R. S.; Shendarkar, A. D. Adsorption of Ni(II), Zn(II) and Fe(II) on modified coir fibres. *Separation and Purification Technology* **2006**, *47*, 141-147.
234. Ratan, S.; Singh, I.; Sarkar, J.; Naik, R. The removal of nickel from waste water by modified coconut coir pith. *Chem. Sci. J* **2016**, *7*, 1-6.
235. Parab, H.; Joshi, S.; Shenoy, N.; Lali, A.; Sarma, U. S.; Sudersanan, M. Esterified coir pith as an adsorbent for the removal of Co(II) from aqueous solution. *Bioresource Technology* **2008**, *99*, 2083-2086.
236. Parab, H.; Joshi, S.; Shenoy, N.; Lali, A.; Sarma, U.; Sudersanan, M. Esterified coir pith as an adsorbent for the removal of Co (II) from aqueous solution. *Bioresource technology* **2008**, *99*, 2083-2086.
237. Crossley, O. P.; Thorpe, R. B.; Peus, D.; Lee, J. Phosphorus recovery from process waste water made by the hydrothermal carbonisation of spent coffee grounds. *Bioresource technology* **2020**, *301*, 122664.
238. Scully, D. S.; Jaiswal, A. K.; Abu-Ghannam, N. An investigation into spent coffee waste as a renewable source of bioactive compounds and industrially important sugars. *Bioengineering* **2016**, *3*, 33.
239. Nguyen, H. C.; Nguyen, M. L.; Wang, F.-M.; Juan, H.-Y.; Su, C.-H. Biodiesel production by direct transesterification of wet spent coffee grounds using switchable solvent as a catalyst and solvent. *Bioresource Technology* **2020**, *296*, 122334.
240. Campos-Vega, R.; Loarca-Piña, G.; Vergara-Castañeda, H. A.; Oomah, B. D. Spent coffee grounds: A review on current research and future prospects. *Trends in Food Science & Technology* **2015**, *45*, 24-36.

241. Cruz, R.; Cardoso, M. M.; Fernandes, L.; Oliveira, M.; Mendes, E.; Baptista, P.; Morais, S.; Casal, S. Espresso coffee residues: a valuable source of unextracted compounds. *Journal of agricultural and food chemistry* **2012**, *60*, 7777-7784.

242. Cameron, A.; O'Malley, S. Coffee ground recovery program summary report. *Planet Ark: Sydney, Australia* **2016**

243. Sousa, L. M.; Ferreira, M. Spent coffee grounds as a renewable source of energy: An analysis of bulk powder flowability. *Particuology* **2019**, *43*, 92-100.

244. CAIT, W. 2.0 (2013) Climate Analysis Indicators Tool: WRI's Climate Data Explorer. *Washington, DC: World Resources Institute. Available at cait2. wri. org*

245. Hegnsholt, E.; Unnikrishnan, S.; Pollmann-Larsen, M.; Askelsdottir, B.; Gerard, M. Tackling the 1.6-billion-ton food loss and waste crisis. *The Boston Consulting Group, Food Nation, State of Green* **2018**

246. Mussatto, S. I.; Carneiro, L. M.; Silva, J. P.; Roberto, I. C.; Teixeira, J. A. A study on chemical constituents and sugars extraction from spent coffee grounds. *Carbohydrate polymers* **2011**, *83*, 368-374.

247. Simões, J.; Madureira, P.; Nunes, F. M.; do Rosário Domingues, M.; Vilanova, M.; Coimbra, M. A. Immunostimulatory properties of coffee mannans. *Molecular nutrition & food research* **2009**, *53*, 1036-1043.

248. Sampaio, A.; Dragone, G.; Vilanova, M.; Oliveira, J. M.; Teixeira, J. A.; Mussatto, S. I. Production, chemical characterization, and sensory profile of a novel spirit elaborated from spent coffee ground. *LWT-Food Science and Technology* **2013**, *54*, 557-563.

249. Belitz, H.-D.; Grosch, W.; Schieberle, P. Food Cemistry. Springer, 2009.

250. Andrade, K. S.; Gonçalvez, R. T.; Maraschin, M.; Ribeiro-do-Valle, R. M.; Martínez, J.; Ferreira, S. R. Supercritical fluid extraction from spent coffee grounds and coffee husks: antioxidant activity and effect of operational variables on extract composition. *Talanta* **2012**, *88*, 544-552.

251. Ramalakshmi, K.; Rao, L. J. M.; Takano-Ishikawa, Y.; Goto, M. Bioactivities of low-grade green coffee and spent coffee in different in vitro model systems. *Food Chemistry* **2009**, *115*, 79-85.

252. Murthy, P. S.; Naidu, M. M. Recovery of phenolic antioxidants and functional compounds from coffee industry by-products. *Food and Bioprocess Technology* **2012**, *5*, 897-903.

253. Murthy, P. S.; Naidu, M. M. Sustainable management of coffee industry by-products and value addition—A review. *Resources, Conservation and recycling* **2012**, *66*, 45-58.

254. Freitas, S. P.; Monteiro, P. L.; Lago, R. C. A. Extração do óleo da borra de café solúvel com etanol comercial. **2000**

255. Jenkins, R. W.; Stageman, N. E.; Fortune, C. M.; Chuck, C. J. Effect of the type of bean, processing, and geographical location on the biodiesel produced from waste coffee grounds. *Energy & Fuels* **2014**, *28*, 1166-1174.

256. Oestreich-Janzen, S. H. Chemistry of coffee. **2019**

257. Mussatto, S. I.; Ballesteros, L. F.; Martins, S.; Teixeira, J. A. Extraction of antioxidant phenolic compounds from spent coffee grounds. *Separation and Purification Technology* **2011**, *83*, 173-179.

258. Panusa, A.; Zuorro, A.; Lavecchia, R.; Marrosu, G.; Petrucci, R. Recovery of natural antioxidants from spent coffee grounds. *Journal of agricultural and food chemistry* **2013**, *61*, 4162-4168.

259. Zhang, X.; Zhang, Y.; Ngo, H. H.; Guo, W.; Wen, H.; Zhang, D.; Li, C.; Qi, L. Characterization and sulfonamide antibiotics adsorption capacity of spent coffee grounds based biochar and hydrochar. *Science of The Total Environment* **2020**, *716*, 137015.

260. Kua, T.-A.; Arulrajah, A.; Horpibulsuk, S.; Du, Y.-J.; Suksiripattanapong, C. Engineering and environmental evaluation of spent coffee grounds stabilized with industrial by-products as a road subgrade material. *Clean technologies and environmental policy* **2017**, *19*, 63-75.

261. Kraus, T. E.; Dahlgren, R. A.; Zasoski, R. J. Tannins in nutrient dynamics of forest ecosystems-a review. *Plant and soil* **2003**, *256*, 41-66.

262. Rosson, E.; Garbo, F.; Marangoni, G.; Bertani, R.; Lavagnolo, M. C.; Moretti, E.; Talon, A.; Mozzon, M.; Sgarbossa, P. Activated Carbon from Spent Coffee Grounds: A Good Competitor of Commercial Carbons for Water Decontamination. *Applied Sciences* **2020**, *10*, 5598.

263. Santos, C.; Fonseca, J.; Aires, A.; Coutinho, J.; Trindade, H. Effect of different rates of spent coffee grounds (SCG) on composting process, gaseous emissions and quality of end-product. *Waste management* **2017**, *59*, 37-47.

264. Fiol, N.; Escudero, C.; Villaescusa, I. Re-use of exhausted ground coffee waste for Cr (VI) sorption. *Separation Science and Technology* **2008**, *43*, 582-596.

265. Boonamnuayvitaya, V.; Chaiya, C.; Tanthapanichakoon, W.; Jarudilokkul, S. Removal of heavy metals by adsorbent prepared from pyrolyzed coffee residues and clay. *Separation and Purification Technology* **2004**, *35*, 11-22.

266. Minamisawa, M.; Minamisawa, H.; Yoshida, S.; Takai, N. Adsorption behavior of heavy metals on biomaterials. *Journal of agricultural and food chemistry* **2004**, *52*, 5606-5611.

267. Alvarez, N. M. M.; Pastrana, J. M.; Lagos, Y.; Lozada, J. J. Evaluation of mercury (Hg2+) adsorption capacity using exhausted coffee waste. *Sustainable Chemistry and Pharmacy* **2018**, *10*, 60-70.

268. Davila-Guzman, N. E.; Cerino-Córdova, F. d. J.; Loredo-Cancino, M.; Rangel-Mendez, J. R.; Gómez-González, R.; Soto-Regalado, E. Studies of adsorption of heavy metals onto spent coffee ground: equilibrium, regeneration, and dynamic performance in a fixed-bed column. *International Journal of Chemical Engineering* **2016**, *2016*

269. Kyzas, G. Z. Commercial Coffee Wastes as Materials for Adsorption of Heavy Metals from Aqueous Solutions. *Materials* **2012**, *5*, 1826-1840.

270. Babu, A. N.; Reddy, D. S.; Kumar, G. S.; Ravindhranath, K.; Mohan, G. K. Removal of lead and fluoride from contaminated water using exhausted coffee grounds based bio-sorbent. *Journal of environmental management* **2018**, *218*, 602-612.

271. Kim, M.-S.; Min, H.-G.; Koo, N.; Park, J.; Lee, S.-H.; Bak, G.-I.; Kim, J.-G. The effectiveness of spent coffee grounds and its biochar on the amelioration of heavy metals-contaminated water and soil using chemical and biological assessments. *Journal of Environmental Management* **2014**, *146*, 124-130.

272. Edathil, A. A.; Shittu, I.; Zain, J. H.; Banat, F.; Haija, M. A. Novel magnetic coffee waste nanocomposite as effective bioadsorbent for Pb (II) removal from aqueous solutions. *Journal of Environmental Chemical Engineering* **2018**, *6*, 2390-2400.

273. Dávila-Guzmán, N. E.; de Jesús Cerino-Córdova, F.; Soto-Regalado, E.; Rangel-Mendez, J. R.; Díaz-Flores, P. E.; Garza-Gonzalez, M. T.; Loredo-Medrano, J. A. Copper Biosorption by Spent Coffee Ground: Equilibrium, Kinetics, and Mechanism. *CLEAN – Soil, Air, Water* **2013**, *41*, 557-564.

274. Chavan, A. A.; Pinto, J.; Liakos, I.; Bayer, I. S.; Lauciello, S.; Athanassiou, A.; Fragouli, D. Spent Coffee Bioelastomeric Composite Foams for the Removal of Pb2+and Hg2+from Water. *ACS Sustainable Chemistry & Engineering* **2016**, *4*, 5495-5502.

275. Wu, C.-H.; Kuo, C.-Y.; Guan, S.-S. Adsorption of heavy metals from aqueous solutions by waste coffee residues: kinetics, equilibrium, and thermodynamics. *Desalination and Water Treatment* **2015**, *57*, 5056-5064.

276. Armbruster, T.; Gunter, M. E. Crystal structures of natural zeolites. *Reviews in mineralogy and geochemistry* **2001**, *45*, 1-67.

277. Brathwaite, B.; Hill, D. Zeolite deposits in the Central North Island Taupo Volcanic Zone of New Zealand.

278. Braithwaite, R. Geological and mineralogical characterization of zeolites in lacustrine tuffs, Ngakuru, Taupo Volcanic Zone, New Zealand. *Clays and Clay Minerals* **2003**, *51*, 589-598.

279. Dessalegne, M.; Zewge, F.; Diaz, I. Aluminum hydroxide supported on zeolites for fluoride removal from drinking water. *Journal of Chemical Technology & Biotechnology* **2017**, *92*, 605-613.

280. Haidouti, C. Inactivation of mercury in contaminated soils using natural zeolites. *Science of the Total Environment* **1997**, *208*, 105-109.

281. Panayotova, M. Kinetics and thermodynamics of copper ions removal from wastewater by use of zeolite. *Waste Management* **2001**, *21*, 671-676.

282. Hokkanen, S.; Repo, E.; Sillanpää, M. Removal of heavy metals from aqueous solutions by succinic anhydride modified mercerized nanocellulose. *Chemical engineering journal* **2013**, *223*, 40-47.

283. Carland, R.; Aplan, F. Improving the ion-exchange capacity and elution of Cu+ 2 from natural sedimentary zeolites. *Minerals and Metallurgical Processing* **1995**, *12*, 210-218.

284. Colella, C. Use of Italian chabazite and phillipsite for the removal of heavy metals from wastewaters: a review. *Natural zeolite'93,(DW Ming and FA Mumpton, eds.), int. comm. natural zeolites* **1995**

285. Halimoon, N.; Yin, R. G. S. Removal of heavy metals from textile wastewater using zeolite. *Environment Asia* **2010**, *3*, 124-130.

286. Zhang, Y.; Li, Y.; Li, J.; Sheng, G.; Zhang, Y.; Zheng, X. Enhanced Cr (VI) removal by using the mixture of pillared bentonite and zero-valent iron. *Chemical Engineering Journal* **2012**, *185*, 243-249.

287. Fiúza, A.; Silva, A.; Carvalho, G.; António, V.; Delerue-Matos, C. Heterogeneous kinetics of the reduction of chromium (VI) by elemental iron. *Journal of hazardous materials* **2010**, *175*, 1042-1047.

288. Katsou, E.; Malamis, S.; Haralambous, K. J.; Loizidou, M. Use of ultrafiltration membranes and aluminosilicate minerals for nickel removal from industrial wastewater. *Journal of Membrane Science* **2010**, *360*, 234-249.

289. Thanos, A. G.; Katsou, E.; Malamis, S.; Drakopoulos, V.; Paschalakis, P.; Pavlatou, E. A.; Haralambous, K. J. Cr (VI) removal from aqueous solutions using aluminosilicate minerals in their Pb-exchanged forms. *Applied Clay Science* **2017**, *147*, 54-62.

290. Faghihian, H.; Bowman, R. S. Adsorption of chromate by clinoptilolite exchanged with various metal cations. *Water research* **2005**, *39*, 1099-1104.

291. Zendehdel, M.; Shoshtari-Yeganeh, B.; Cruciani, G. Removal of heavy metals and bacteria from aqueous solution by novel hydroxyapatite/zeolite nanocomposite, preparation, and characterization. *Journal of the Iranian Chemical Society* **2016**, *13*, 1915-1930.

292. Zhang, S.; Lv, T.; Mu, Y.; Zheng, J.; Meng, C. High adsorption of Cd (II) by modification of synthetic zeolites Y, A and mordenite with thiourea. *Chinese Journal of Chemical Engineering* **2020**, *28*, 3117-3125.

293. Belova, T. P. Adsorption of heavy metal ions (Cu2+, Ni2+, Co2+ and Fe2+) from aqueous solutions by natural zeolite. *Heliyon* **2019**, *5*, e02320.

294. Pitcher, S. K.; Slade, R. C. T.; Ward, N. I. Heavy metal removal from motorway stormwater using zeolites. *Science of The Total Environment* **2004**, *334-335*, 161-166.

295. Dimas Rivera, G. L.; Martínez Hernández, A.; Pérez Cabello, A. F.; Rivas Barragán, E. L.; Liñán Montes, A.; Flores Escamilla, G. A.; Sandoval Rangel, L.; Suarez Vazquez, S. I.; De Haro Del Río, D. A. Removal of chromate anions and immobilization using surfactant-modified zeolites. *Journal of Water Process Engineering* **2021**, *39*, 101717.

296. Álvarez-Ayuso, E.; García-Sánchez, A.; Querol, X. Purification of metal electroplating waste waters using zeolites. *Water Research* **2003**, *37*, 4855-4862.

297. Wang, X.; Shao, D.; Hou, G.; Wang, X.; Alsaedi, A.; Ahmad, B. Uptake of Pb(II) and U(VI) ions from aqueous solutions by the ZSM-5 zeolite. *Journal of Molecular Liquids* **2015**, *207*, 338-342.

298. Hernández-Montoya, V.; Pérez-Cruz, M. A.; Mendoza-Castillo, D. I.; Moreno-Virgen, M. R.; Bonilla-Petriciolet, A. Competitive adsorption of dyes and heavy metals on zeolitic structures. *Journal of Environmental Management* **2013**, *116*, 213-221.

299. Bosso, S. T.; Enzweiler, J. Evaluation of heavy metal removal from aqueous solution onto scolecite. *Water Research* **2002**, *36*, 4795-4800.

300. Suazo-Hernández, J.; Sepúlveda, P.; Manquián-Cerda, K.; Ramírez-Tagle, R.; Rubio, M. A.; Bolan, N.; Sarkar, B.; Arancibia-Miranda, N. Synthesis and characterization of zeolite-based composites functionalized with nanoscale zero-valent iron for removing arsenic in the presence of selenium from water. *Journal of Hazardous Materials* **2019**, *373*, 810-819.

301. Anari-Anaraki, M.; Nezamzadeh-Ejhieh, A. Modification of an Iranian clinoptilolite nano-particles by hexadecyltrimethyl ammonium cationic surfactant and dithizone for removal of Pb(II) from aqueous solution. *Journal of Colloid and Interface Science* **2015**, *440*, 272-281.

302. Pandey, S.; Fosso-Kankeu, E.; Spiro, M. J.; Waanders, F.; Kumar, N.; Ray, S. S.; Kim, J.; Kang, M. Equilibrium, kinetic, and thermodynamic studies of lead ion adsorption from mine wastewater onto MoS2-clinoptilolite composite. *Materials Today Chemistry* **2020**, *18*, 100376.

303. Kragović, M.; Daković, A.; Marković, M.; Krstić, J.; Gatta, G. D.; Rotiroti, N. Characterization of lead sorption by the natural and Fe(III)-modified zeolite. *Applied Surface Science* **2013**, *283*, 764-774.

304. Vinod, V. T. P.; Sashidhar, R. B.; Sreedhar, B.; Rama Rao, B.; Nageswara Rao, T.; Abraham, J. T. Interaction of Pb2+ and Cd2+ with gum kondagogu (Cochlospermum gossypium): A natural carbohydrate polymer with biosorbent properties. *Carbohydrate Polymers* **2009**, *78*, 894-901.

305. Adeniyi, A. G.; Onifade, D. V.; Ighalo, J. O.; Adeoye, A. S. A review of coir fiber reinforced polymer composites. *Composites Part B: Engineering* **2019**, *176*, 107305.

306. Gondhalekar, S. C.; Singh, S. A.; Shukla, S. R. Removal of Cd (II) ions by oxidized coconut coir. *Journal of Natural Fibers* **2019**, *16*, 37-48.

307. Verma, D.; Gope, P. The use of coir/coconut fibers as reinforcements in composites. In *Biofiber Reinforcements in Composite Materials*; Elsevier, 2015; pp 285-319.

308. Cherdchoo, W.; Nithettham, S.; Charoenpanich, J. Removal of Cr(VI) from synthetic wastewater by adsorption onto coffee ground and mixed waste tea. *Chemosphere* **2019**, *221*, 758-767.

309. Gonzalez, M. H.; Araújo, G. C. L.; Pelizaro, C. B.; Menezes, E. A.; Lemos, S. G.; de Sousa, G. B.; Nogueira, A. R. A. Coconut coir as biosorbent for Cr(VI) removal from laboratory wastewater. *Journal of Hazardous Materials* **2008**, *159*, 252-256.

310. Guo, D.-M.; An, Q.-D.; Xiao, Z.-Y.; Zhai, S.-R.; Yang, D.-J. Efficient removal of Pb (II), Cr (VI) and organic dyes by polydopamine modified chitosan aerogels. *Carbohydrate polymers* **2018**, *202*, 306-314.

311. Sağ, Y.; Aktay, Y. Kinetic studies on sorption of Cr(VI) and Cu(II) ions by chitin, chitosan and Rhizopus arrhizus. *Biochemical Engineering Journal* **2002**, *12*, 143-153.

312. Subedi, N.; Lähde, A.; Abu-Danso, E.; Iqbal, J.; Bhatnagar, A. A comparative study of magnetic chitosan (Chi@Fe3O4) and graphene oxide modified magnetic chitosan (Chi@Fe3O4GO) nanocomposites for efficient removal of Cr(VI) from water. *International Journal of Biological Macromolecules* **2019**, *137*, 948-959.

313. Aaseth, J.; Skaug, M. A.; Cao, Y.; Andersen, O. Chelation in metal intoxication—Principles and paradigms. *Journal of Trace Elements in Medicine and Biology* **2015**, *31*, 260-266.

314. Flora, S. J.; Pachauri, V. Chelation in metal intoxication. *International journal of environmental research and public health* **2010**, *7*, 2745-2788.

315. Chen, Z.; Zhang, C.; Tan, Y.; Zhou, T.; Ma, H.; Wan, C.; Lin, Y.; Li, K. Chitosan-functionalized gold nanoparticles for colorimetric detection of mercury ions based on chelation-induced aggregation. *Microchimica Acta* **2015**, *182*, 611-616.

316. Hassan, R. M. Prospective and comparative Novel technique for evaluation the affinity of alginate for binding the alkaline-earth metal ions during formation the coordination biopolymer hydrogel complexes. *International Journal of Biological Macromolecules* **2020**, *165*, 1022-1028.

317. Phan, D.-N.; Khan, M. Q.; Nguyen, N.-T.; Phan, T.-T.; Ullah, A.; Khatri, M.; Kien, N. N.; Kim, I.-S. A review on the fabrication of several carbohydrate polymers into nanofibrous structures using electrospinning for removal of metal ions and dyes. *Carbohydrate Polymers* **2020**, 117175.

318. Myung, O. P.; Kwanghee, K. P. Mechanism of metal ion binding to chitosan in solution. Cooperative inter-and intramolecular chelations. *Bulletin of the Korean Chemical Society* **1984**, *5*, 108-112.

319. Gamage, A.; Shahidi, F. Use of chitosan for the removal of metal ion contaminants and proteins from water. *Food Chemistry* **2007**, *104*, 989-996.

320. Suen, R.-B.; Lin, S.-C.; Hsu, W.-H. Hydroxyapatite-based immobilized metal affinity adsorbents for protein purification. *Journal of chromatography A* **2004**, *1048*, 31-39.

321. Ofomaja, A. E.; Naidoo, E. B.; Pholosi, A. Intraparticle diffusion of Cr (VI) through biomass and magnetite coated biomass: A comparative kinetic and diffusion study. *South African Journal of Chemical Engineering* **2020**, *32*, 39-55.

322. Sen, M.; Dastidar, M. G. Chromium removal using various biosorbents. *Journal of Environmental Health Science & Engineering* **2010**, *7*, 182-190.

323. Namasivayam, C.; Sureshkumar, M. V. Removal of chromium(VI) from water and wastewater using surfactant modified coconut coir pith as a biosorbent. *Bioresource Technology* **2008**, *99*, 2218-2225.

324. Lee, C.-K.; Kim, H.-S.; Kwon, J.-H. The removal of heavy metals using hydroxyapatite. *Environmental Engineering Research* **2005**, *10*, 205-212.

325. Michalev, T.; Petrov, I. The Removal of Heavy Metal Ions by Synthetic Zeolites: A Review. *Proceedings, University of Ruse* **2012**, *51*, 79-84.

326. Alvarez-Ayuso, E.; Garcıa-Sánchez, A.; Querol, X. Purification of metal electroplating waste waters using zeolites. *Water research* **2003**, *37*, 4855-4862.
327. Zamzow, M.; Eichbaum, B.; Sandgren, K.; Shanks, D. Removal of heavy metals and other cations from wastewater using zeolites. *Separation science and technology* **1990**, *25*, 1555-1569.
328. Abdel-Raouf, M.; Abdul-Raheim, A. Removal of Heavy Metals from Industrial Waste Water by Biomass-Based Materials: A Review. *J Pollut Eff Cont* **2017**, *5*, 180.
329. Lim, A. P.; Aris, A. Z. A review on economically adsorbents on heavy metals removal in water and wastewater. *Reviews in Environmental Science and Bio/Technology* **2014**, *13*, 163-181.
330. Yan, N.; Chen, X. Don't waste seafood waste: Turning cast-off shells into nitrogen-rich chemicals would benefit economies and the environment. *Nature* **2015**, *524*, 155-158.
331. Netravali, A. Advanced Natural Fibers, Plastics and Composites Recent Advances. Kluwer Academic Publishers, New York, 2004.
332. Pei, Q.; Zhang, Y.; Shenoy, V. A molecular dynamics study of the mechanical properties of hydrogen functionalized graphene. *Carbon* **2010**, *48*, 898-904.
333. Ayawei, N.; Ebelegi, A. N.; Wankasi, D. Modelling and interpretation of adsorption isotherms. *Journal of chemistry* **2017**, *2017*
334. Silva, T. L.; Ronix, A.; Pezoti, O.; Souza, L. S.; Leandro, P. K. T.; Bedin, K. C.; Beltrame, K. K.; Cazetta, A. L.; Almeida, V. C. Mesoporous activated carbon from industrial laundry sewage sludge: Adsorption studies of reactive dye Remazol Brilliant Blue R. *Chemical Engineering Journal* **2016**, *303*, 467-476.
335. Sahu, O.; Singh, N. Significance of bioadsorption process on textile industry wastewater. In *The Impact and Prospects of Green Chemistry for Textile Technology*; Elsevier, 2019; pp 367-416.
336. Aremu, J. O. Target separation of arsenic from contaminated raw waterThesis, The University of Waikato, 2020.
337. Guo, X.; Wang, J. Comparison of linearization methods for modeling the Langmuir adsorption isotherm. *Journal of Molecular Liquids* **2019**, *296*, 111850.

338. Inyinbor, A. A.; Adekola, F. A.; Olatunji, G. A. Kinetics, isotherms and thermodynamic modeling of liquid phase adsorption of Rhodamine B dye onto Raphia hookerie fruit epicarp. *Water Resources and Industry* **2016**, *15*, 14-27.

339. Guo, X.; Wang, J. The phenomenological mass transfer kinetics model for Sr2+ sorption onto spheroids primary microplastics. *Environmental Pollution* **2019**, *250*, 737-745.

340. Kong, S.; Huang, X.; Li, K.; Song, X. Adsorption/desorption isotherms of CH4 and C2H6 on typical shale samples. *Fuel* **2019**, *255*, 115632.

341. Mondal, S.; Majumder, S. K. Honeycomb-like porous activated carbon for efficient copper (II) adsorption synthesized from natural source: Kinetic study and equilibrium isotherm analysis. *Journal of Environmental Chemical Engineering* **2019**, *7*, 103236.

342. Sparks, D. L. 5 - Sorption Phenomena on Soils. In *Environmental Soil Chemistry (Second Edition)*; D. L. Sparks, Ed.; Academic Press: Burlington, 2003; pp 133-186.

343. Khan, A. R.; Riazi, M. R.; Al-Roomi, Y. A. A thermodynamic model for liquid adsorption isotherms. *Separation and Purification Technology* **2000**, *18*, 237-250.

344. Nakahara, O. Reconsideration of theoretical basis of Freundlich adsorption isotherm equation: II. Approximative derivation. *Soil science and plant nutrition* **1996**, *42*, 51-61.

345. Murai, S.; Imajo, S.; Takasu, Y.; Takahashi, K.; Hattori, K. Removal of phthalic acid esters from aqueous solution by inclusion and adsorption on β-cyclodextrin. *Environmental science & technology* **1998**, *32*, 782-787.

346. Saruchi; Kumar, V. Adsorption kinetics and isotherms for the removal of rhodamine B dye and Pb+2 ions from aqueous solutions by a hybrid ion-exchanger. *Arabian Journal of Chemistry* **2019**, *12*, 316-329.

347. Dada, A.; Olalekan, A.; Olatunya, A.; Dada, O. Langmuir, Freundlich, Temkin and Dubinin–Radushkevich isotherms studies of equilibrium sorption of Zn2+ unto phosphoric acid modified rice husk. *IOSR Journal of Applied Chemistry* **2012**, *3*, 38-45.

348. Lim, L. B.; Priyantha, N.; Tennakoon, D.; Chieng, H. I.; Dahri, M. K.; Suklueng, M. Breadnut peel as a highly effective low-cost biosorbent for methylene blue:

equilibrium, thermodynamic and kinetic studies. *Arabian Journal of Chemistry* **2017**, *10*, S3216-S3228.

349. Apopei, D. F.; Dinu, M. V.; Trochimczuk, A. W.; Dragan, E. S. Sorption isotherms of heavy metal ions onto semi-interpenetrating polymer network cryogels based on polyacrylamide and anionically modified potato starch. *Industrial & engineering chemistry research* **2012**, *51*, 10462-10471.
350. Reddy, D. H. K.; Lee, S.-M. Magnetic biochar composite: facile synthesis, characterization, and application for heavy metal removal. *Colloids and Surfaces A: Physicochemical and Engineering Aspects* **2014**, *454*, 96-103.
351. Deniz, F.; Karabulut, A. Biosorption of heavy metal ions by chemically modified biomass of coastal seaweed community: studies on phycoremediation system modeling and design. *Ecological Engineering* **2017**, *106*, 101-108.
352. Ramesh, S. T.; Rameshbabu, N.; Gandhimathi, R.; Srikanth Kumar, M.; Nidheesh, P. V. Adsorptive removal of Pb(II) from aqueous solution using nano-sized hydroxyapatite. *Applied Water Science* **2012**, *3*, 105-113.
353. Ho, Y.-S.; McKay, G. Pseudo-second order model for sorption processes. *Process biochemistry* **1999**, *34*, 451-465.
354. Wu, F.-C.; Tseng, R.-L.; Juang, R.-S. Initial behavior of intraparticle diffusion model used in the description of adsorption kinetics. *Chemical Engineering Journal* **2009**, *153*, 1-8.
355. Ghaedi, A. M.; Panahimehr, M.; Nejad, A. R. S.; Hosseini, S. J.; Vafaei, A.; Baneshi, M. M. Factorial experimental design for the optimization of highly selective adsorption removal of lead and copper ions using metal organic framework MOF-2 (Cd). *Journal of Molecular Liquids* **2018**, *272*, 15-26.
356. Biswas, S.; Sharma, S.; Siddiqi, H.; Meikap, B. C.; Sen, T. K.; Khiadani, M. Semifluidized Bed Adsorption Column Studies for Simultaneous Removal of Aqueous Phase Pb 2+ and Cd 2+ by Composite Adsorbents: an Experimental and Mass Transfer Dynamic Model–Based Approach. *Water, Air, & Soil Pollution* **2021**, *232*, 1-17.
357. Jiang, S.; Yu, T.; Xia, R.; Wang, X.; Gao, M. Realization of super high adsorption capability of 2D δ-MnO2 /GO through intra-particle diffusion. *Materials Chemistry and Physics* **2019**, *232*, 374-381.

358. Li, G.; Zhao, Z.; Liu, J.; Jiang, G. Effective heavy metal removal from aqueous systems by thiol functionalized magnetic mesoporous silica. *Journal of hazardous materials* **2011**, *192*, 277-283.

359. Valderrama, C.; Gamisans, X.; De las Heras, X.; Farran, A.; Cortina, J. Sorption kinetics of polycyclic aromatic hydrocarbons removal using granular activated carbon: intraparticle diffusion coefficients. *Journal of hazardous materials* **2008**, *157*, 386-396.

360. Qu, R.; Sun, C.; Ma, F.; Zhang, Y.; Ji, C.; Xu, Q.; Wang, C.; Chen, H. Removal and recovery of Hg(II) from aqueous solution using chitosan-coated cotton fibers. *Journal of Hazardous Materials* **2009**, *167*, 717-727.

361. Zhang, G.; Qu, R.; Sun, C.; Ji, C.; Chen, H.; Wang, C.; Niu, Y. Adsorption for metal ions of chitosan coated cotton fiber. *Journal of Applied Polymer Science* **2008**, *110*, 2321-2327.

362. Boddu, V. M.; Abburi, K.; Talbott, J. L.; Smith, E. D.; Haasch, R. Removal of arsenic (III) and arsenic (V) from aqueous medium using chitosan-coated biosorbent. *Water Research* **2008**, *42*, 633-642.

363. Boddu, V. M.; Abburi, K.; Talbott, J. L.; Smith, E. D. Removal of hexavalent chromium from wastewater using a new composite chitosan biosorbent. *Environmental science & technology* **2003**, *37*, 4449-4456.

364. Ngah, W. S. W.; Fatinathan, S. Adsorption of Cu(II) ions in aqueous solution using chitosan beads, chitosan–GLA beads and chitosan–alginate beads. *Chemical Engineering Journal* **2008**, *143*, 62-72.

365. Pavithra, S.; Thandapani, G.; S, S.; P.N, S.; Alkhamis, H. H.; Alrefaei, A. F.; Almutairi, M. H. Batch adsorption studies on surface tailored chitosan/orange peel hydrogel composite for the removal of Cr(VI) and Cu(II) ions from synthetic wastewater. *Chemosphere* **2021**, *271*, 129415.

366. Ye, X.; Shang, S.; Zhao, Y.; Cui, S.; Zhong, Y.; Huang, L. Ultra-efficient adsorption of copper ions in chitosan–montmorillonite composite aerogel at wastewater treatment. *Cellulose* **2021**, *28*, 7201-7212.

367. Bambaeero, A.; Bazargan-Lari, R. Simultaneous removal of copper and zinc ions by low cost natural snail shell/hydroxyapatite/chitosan composite. *Chinese Journal of Chemical Engineering* **2021**, *33*, 221-230.

368. Zhang, C.-J.; Hu, M.; Ke, Q.-F.; Guo, C.-X.; Guo, Y.-J.; Guo, Y.-P. Nacre-inspired hydroxyapatite/chitosan layered composites effectively remove lead ions in continuous-flow wastewater. *Journal of hazardous materials* **2020**, *386*, 121999.

369. Naseer, A.; Hamid, A.; Ghauri, M.; Nasrullah, A.; Iqbal, J.; Shah, N. S.; Rafiq, S.; Irfan, M.; Muhammad, N. Lignin/alginate/hydroxyapatite composite beads for the efficient removal of copper and nickel ions from aqueous solutions. *Desalination and Water Treatment* **2020**, *184*, 199.

370. Liaw, B.-S.; Chang, T.-T.; Chang, H.-K.; Liu, W.-K.; Chen, P.-Y. Fish scale-extracted hydroxyapatite/chitosan composite scaffolds fabricated by freeze casting—An innovative strategy for water treatment. *Journal of hazardous materials* **2020**, *382*, 121082.

371. Fang, X.; Zhu, S.; Ma, J.; Wang, F.; Xu, H.; Xia, M. The facile synthesis of zoledronate functionalized hydroxyapatite amorphous hybrid nanobiomaterial and its excellent removal performance on Pb2+ and Cu2+. *Journal of Hazardous Materials* **2020**, *392*, 122291.

372. Islam, M.; Mishra, P. C.; Patel, R. Arsenate removal from aqueous solution by cellulose-carbonated hydroxyapatite nanocomposites. *Journal of Hazardous Materials* **2011**, *189*, 755-763.

373. Hokkanen, S.; Bhatnagar, A.; Repo, E.; Lou, S.; Sillanpää, M. Calcium hydroxyapatite microfibrillated cellulose composite as a potential adsorbent for the removal of Cr(VI) from aqueous solution. *Chemical Engineering Journal* **2016**, *283*, 445-452.

374. Jayaweera, H. D. A. C.; Siriwardane, I.; de Silva, K. M. N.; de Silva, R. M. Synthesis of multifunctional activated carbon nanocomposite comprising biocompatible flake nano hydroxyapatite and natural turmeric extract for the removal of bacteria and lead ions from aqueous solution. *Chemistry Central Journal* **2018**, *12*, 18.

375. Zhang, Z.; Wang, X.; Wang, H.; Zhao, J. Removal of Pb(II) from aqueous solution using hydroxyapatite/calcium silicate hydrate (HAP/C-S-H) composite adsorbent prepared by a phosphate recovery process. *Chemical Engineering Journal* **2018**, *344*, 53-61.

376. Choi, S.; Jeong, Y. The removal of heavy metals in aqueous solution by hydroxyapatite/cellulose composite. *Fibers and Polymers* **2008**, *9*, 267-270.

377. Salah, T. A.; Mohammad, A. M.; Hassan, M. A.; El-Anadouli, B. E. Development of nano-hydroxyapatite/chitosan composite for cadmium ions removal in wastewater treatment. *Journal of the Taiwan Institute of Chemical Engineers* **2014**, *45*, 1571-1577.

378. Jang, S. H.; Min, B. G.; Jeong, Y. G.; Lyoo, W. S.; Lee, S. C. Removal of lead ions in aqueous solution by hydroxyapatite/polyurethane composite foams. *Journal of Hazardous Materials* **2008**, *152*, 1285-1292.

379. Jang, S. H.; Jeong, Y. G.; Min, B. G.; Lyoo, W. S.; Lee, S. C. Preparation and lead ion removal property of hydroxyapatite/polyacrylamide composite hydrogels. *Journal of Hazardous Materials* **2008**, *159*, 294-299.

380. Gupta, N.; Kushwaha, A. K.; Chattopadhyaya, M. C. Adsorptive removal of Pb2+, Co2+ and Ni2+ by hydroxyapatite/chitosan composite from aqueous solution. *Journal of the Taiwan Institute of Chemical Engineers* **2012**, *43*, 125-131.

381. Dong, L.; Zhu, Z.; Qiu, Y.; Zhao, J. Removal of lead from aqueous solution by hydroxyapatite/magnetite composite adsorbent. *Chemical Engineering Journal* **2010**, *165*, 827-834.

382. Raghavendra, S.; Swamy, S. R.; Rastogi, N.; Raghavarao, K.; Kumar, S.; Tharanathan, R. Grinding characteristics and hydration properties of coconut residue: A source of dietary fiber. *Journal of Food Engineering* **2006**, *72*, 281-286.

383. Moraes, L. G. P.; Rocha, R. S. F.; Menegazzo, L. M.; Araújo, E. B. d.; Yukimito, K.; Moraes, J. C. S. Infrared spectroscopy: a tool for determination of the degree of conversion in dental composites. *Journal of Applied Oral Science* **2008**, *16*, 145-149.

384. Hossain, M. A. Development of novel biosorbents in removing heavy metals from aqueous solutionThesis, 2013.

385. Patel, J. P.; Parsania, P. H. 3 - Characterization, testing, and reinforcing materials of biodegradable composites. In *Biodegradable and Biocompatible Polymer Composites*; N. G. Shimpi, Ed.; Woodhead Publishing, 2018; pp 55-79.

386. Vishwakarma, V.; Uthaman, S. 9 - Environmental impact of sustainable green concrete. In *Smart Nanoconcretes and Cement-Based Materials*; M. S. Liew; P. Nguyen-Tri; T. A. Nguyen and S. Kakooei, Eds.; Elsevier, 2020; pp 241-255.

387. Echlin, P.; Fiori, C.; Goldstein, J.; Joy, D. C.; Newbury, D. E. *Advanced scanning electron microscopy and X-ray microanalysis*; Springer Science & Business Media, 2013.

388. Goldstein, J. I.; Newbury, D. E.; Michael, J. R.; Ritchie, N. W.; Scott, J. H. J.; Joy, D. C. *Scanning electron microscopy and X-ray microanalysis*; Springer, 2017.

389. Lee, R. E. *Scanning electron microscopy and X-ray microanalysis*, 1993.

390. Loganathan, S.; Valapa, R. B.; Mishra, R. K.; Pugazhenthi, G.; Thomas, S. Thermogravimetric Analysis for Characterization of Nanomaterials. In *Thermal and Rheological Measurement Techniques for Nanomaterials Characterization*, 2017; pp 67-108.

391. Foo Lee, Y.; Dollimore, D. The identification of the reaction mechanism in rising temperature kinetic studies based on the shape of the DTG curve. *Thermochimica Acta* **1998**, *323*, 75-81.

392. Yang, J.; Kaliaguine, S.; Roy, C. Improved quantitative determination of elastomers in tire rubber by kinetic simulation of DTG curves. *Rubber chemistry and technology* **1993**, *66*, 213-229.

393. Eddya, M.; Tbib, B.; Khalil, E.-H. A comparison of chitosan properties after extraction from shrimp shells by diluted and concentrated acids. *Heliyon* **2020**, *6*, e03486.

394. Mende, M.; Schwarz, D.; Steinbach, C.; Boldt, R.; Schwarz, S. Simultaneous adsorption of heavy metal ions and anions from aqueous solutions on chitosan—Investigated by spectrophotometry and SEM-EDX analysis. *Colloids and Surfaces A: Physicochemical and Engineering Aspects* **2016**, *510*, 275-282.

395. Eddya, M.; Tbib, B.; El-Hami, K. A comparison of chitosan properties after extraction from shrimp shells by diluted and concentrated acids. *Heliyon* **2020**, *6*, e03486.

396. Fernandes Queiroz, M.; Melo, K. R.; Sabry, D. A.; Sassaki, G. L.; Rocha, H. A. Does the use of chitosan contribute to oxalate kidney stone formation? *Mar Drugs* **2014**, *13*, 141-158.

397. de Queiroz Antonino, R.; Lia Fook, B. R. P.; de Oliveira Lima, V. A.; de Farias Rached, R. I.; Lima, E. P. N.; da Silva Lima, R. J.; Peniche Covas, C. A.; Lia

Fook, M. V. Preparation and Characterization of Chitosan Obtained from Shells of Shrimp (Litopenaeus vannamei Boone). *Mar Drugs* **2017**, *15*

398. Di Foggia, M.; Taddei, P.; Torreggiani, A.; Dettin, M.; Tinti, A. Self-Assembling Peptides for Biomedical Applications: IR and Raman Spectroscopies for the Study of Secondary Structure. *Proteomics Research Journal* **2011**, *2*, 231.
399. Jiménez-Ocampo, R.; Valencia-Salazar, S.; Pinzón-Díaz, C. E.; Herrera-Torres, E.; Aguilar-Pérez, C. F.; Arango, J.; Ku-Vera, J. C. The role of chitosan as a possible agent for enteric methane mitigation in ruminants. *Animals* **2019**, *9*, 942.
400. Kumar, S.; Koh, J. Physiochemical, optical and biological activity of chitosan-chromone derivative for biomedical applications. *International journal of molecular sciences* **2012**, *13*, 6102-6116.
401. Ma, F.; Zhang, S.; Li, P.; Sun, B.; Xu, Y.; Tao, D.; Zhao, H.; Cui, S.; Zhu, R.; Zhang, B. Investigation on the role of the free radicals and the controlled degradation of chitosan under solution plasma process based on radical scavengers. *Carbohydrate Polymers* **2020**, 117567.
402. Delezuk, J.; Pavinatto, A.; Campana-Filho, S. Effects of chitosan characteristics on its thermal stability. *Braz J Therm Anal* **2014**, *6*, 36-39.
403. Wanjun, T.; Cunxin, W.; Donghua, C. Kinetic studies on the pyrolysis of chitin and chitosan. *Polymer Degradation and Stability* **2005**, *87*, 389-394.
404. Mezahi, F.; Oudadesse, H.; Harabi, A.; Lucas-Girot, A.; Le Gal, Y.; Chaair, H.; Cathelineau, G. Dissolution kinetic and structural behaviour of natural hydroxyapatite vs. thermal treatment: comparison to synthetic hydroxyapatite. *Journal of Thermal Analysis and Calorimetry* **2009**, *95*, 21-29.
405. Rahavi, S. S.; Ghaderi, O.; Monshi, A.; Fathi, M. H. A comparative study on physicochemical properties of hydroxyapatite powders derived from natural and synthetic sources. *Russian Journal of Non-Ferrous Metals* **2017**, *58*, 276-286.
406. Abifarin, J.; Obada, D.; Dauda, E.; Dodoo-Arhin, D. Experimental data on the characterization of hydroxyapatite synthesized from biowastes. *Data in brief* **2019**, *26*, 104485.
407. Akindoyo, J. O.; Ghazali, S.; Beg, M. D.; Jeyaratnam, N. Characterization and elemental quantification of natural hydroxyapatite produced from cow bone. *Chemical Engineering & Technology* **2019**, *42*, 1805-1815.

408. Miculescu, F.; Luță, C.; Constantinescu, A. E.; Maidaniuc, A.; Mocanu, A.-C.; Miculescu, M.; Voicu, Ș. I.; Ciocan, L. T. Considerations and Influencing Parameters in EDS Microanalysis of Biogenic Hydroxyapatite. *Journal of Functional Biomaterials* **2020**, *11*, 82.

409. Londoño-Restrepo, S. M.; Ramirez-Gutierrez, C. F.; del Real, A.; Rubio-Rosas, E.; Rodriguez-García, M. E. Study of bovine hydroxyapatite obtained by calcination at low heating rates and cooled in furnace air. *Journal of Materials Science* **2016**, *51*, 4431-4441.

410. Mostafa, N. Y. Characterization, thermal stability and sintering of hydroxyapatite powders prepared by different routes. *Materials Chemistry and Physics* **2005**, *94*, 333-341.

411. Giraldo-Betancur, A. L.; Espinosa-Arbelaez, D. G.; Real-López, A. d.; Millan-Malo, B. M.; Rivera-Muñoz, E. M.; Gutierrez-Cortez, E.; Pineda-Gomez, P.; Jimenez-Sandoval, S.; Rodriguez-García, M. E. Comparison of physicochemical properties of bio and commercial hydroxyapatite. *Current Applied Physics* **2013**, *13*, 1383-1390.

412. Ooi, C. Y.; Hamdi, M.; Ramesh, S. Properties of hydroxyapatite produced by annealing of bovine bone. *Ceramics International* **2007**, *33*, 1171-1177.

413. Joschek, S.; Nies, B.; Krotz, R.; Göpferich, A. Chemical and physicochemical characterization of porous hydroxyapatite ceramics made of natural bone. *Biomaterials* **2000**, *21*, 1645-1658.

414. Niakan, A.; Ramesh, S.; Ganesan, P.; Tan, C. Y.; Purbolaksono, J.; Chandran, H.; Ramesh, S.; Teng, W. D. Sintering behaviour of natural porous hydroxyapatite derived from bovine bone. *Ceramics International* **2015**, *41*, 3024-3029.

415. Manalu, J.; Soegijono, B.; Indrani, D. J. Characterization of hydroxyapatite derived from bovine bone. *Asian Journal of Applied Sciences* **2015**, *3*

416. Ramirez-Gutierrez, C. F.; Palechor-Ocampo, A. F.; Londono-Restrepo, S. M.; Millan-Malo, B. M.; Rodriguez-Garcia, M. E. Cooling rate effects on thermal, structural, and microstructural properties of bio-hydroxyapatite obtained from bovine bone. *J Biomed Mater Res B Appl Biomater* **2016**, *104*, 339-344.

417. Ramesh, S.; Loo, Z. Z.; Tan, C. Y.; Chew, W. J. K.; Ching, Y. C.; Tarlochan, F.; Chandran, H.; Krishnasamy, S.; Bang, L. T.; Sarhan, A. A. D. Characterization of

biogenic hydroxyapatite derived from animal bones for biomedical applications. *Ceramics International* **2018**, *44*, 10525-10530.

418. Tariqa, U.; Haidera, Z.; Tufaila, K.; Hussainb, R.; Alia, J. Determination of Calcium to Phosphate Ratio in Hydroxyapatite Extracted from Bovine Bone using LIBS. *Bul Opt* **2016**, *2*, 48-53.

419. Bano, N.; Jikan, S. S.; Basri, H.; Bakar, S. A. A.; Nuhu, A. H. Natural hydroxyapatite extracted from bovine bone. *Journal of Science and Technology* **2017**, *9*

420. Figueiredo, M.; Fernando, A.; Martins, G.; Freitas, J.; Judas, F.; Figueiredo, H. Effect of the calcination temperature on the composition and microstructure of hydroxyapatite derived from human and animal bone. *Ceramics International* **2010**, *36*, 2383-2393.

421. Jaine, J. E. A Study on Supported Metal Catalysts Prepared from Colloidal PrecursorsThesis, University of Waikato, 2016.

422. Venkatesan, J.; Qian, Z. J.; Ryu, B.; Thomas, N. V.; Kim, S. K. A comparative study of thermal calcination and an alkaline hydrolysis method in the isolation of hydroxyapatite from Thunnus obesus bone. *Biomedical Materials* **2011**, *6*, 035003.

423. Gopi, D.; Shinyjoy, E.; Karthika, A.; Nithiya, S.; Kavitha, L.; Rajeswari, D.; Tang, T. Single walled carbon nanotubes reinforced mineralized hydroxyapatite composite coatings on titanium for improved biocompatible implant applications. *RSC Advances* **2015**, *5*, 36766-36778.

424. Akindoyo, J. O.; Ghazali, S.; Beg, M. D. H.; Jeyaratnam, N. Characterization and Elemental Quantification of Natural Hydroxyapatite Produced from Cow Bone. *Chemical Engineering & Technology* **2019**, *42*, 1805-1815.

425. Drouet, C. Apatite formation: why it may not work as planned, and how to conclusively identify apatite compounds. *BioMed research international* **2013**, *2013*

426. Madupalli, H.; Pavan, B.; Tecklenburg, M. M. J. Carbonate substitution in the mineral component of bone: Discriminating the structural changes, simultaneously imposed by carbonate in A and B sites of apatite. *Journal of solid state chemistry* **2017**, *255*, 27-35.

427. Baxter, J. D.; Biltz, R. M.; Pellegrino, E. D. The physical state of bone carbonate. A comparative infra-red study in several mineralized tissues. *Yale J Biol Med* **1966**, *38*, 456-470.

428. El Boujaady, H.; Mourabet, M.; El Rhilassi, A.; Bennani-Ziatni, M.; El Hamri, R.; Taitai, A. Adsorption of a textile dye on synthesized calcium deficient hydroxyapatite (CDHAp): kinetic and thermodynamic studies. *J. Mater. Environ. Sci* **2016**, *7*, 4049-4063.

429. Rincón-López, J. A.; Hermann-Muñoz, J. A.; Giraldo-Betancur, A. L.; Vizcaya-Ruiz, D.; Alvarado-Orozco, J. M.; Muñoz-Saldaña, J. Synthesis, characterization and in vitro study of synthetic and bovine-derived hydroxyapatite ceramics: a comparison. *Materials* **2018**, *11*, 333.

430. Ergun, C.; Evis, Z.; Webster, T. J.; Sahin, F. C. Synthesis and microstructural characterization of nano-size calcium phosphates with different stoichiometry. *Ceramics International* **2011**, *37*, 971-977.

431. Pu'ad, N. M.; Koshy, P.; Abdullah, H.; Idris, M.; Lee, T. Syntheses of hydroxyapatite from natural sources. *Heliyon* **2019**, *5*, e01588.

432. Murugan, R.; Ramakrishna, S.; Panduranga Rao, K. Nanoporous hydroxy-carbonate apatite scaffold made of natural bone. *Materials Letters* **2006**, *60*, 2844-2847.

433. Chakravarty, J.; Rabbi, M. F.; Chalivendra, V.; Ferreira, T.; Brigham, C. J. Mechanical and biological properties of chitin/polylactide (PLA)/hydroxyapatite (HAP) composites cast using ionic liquid solutions. *International Journal of Biological Macromolecules* **2020**, *151*, 1213-1223.

434. Tran, L. Q. N.; Minh, T. N.; Fuentes, C.; Chi, T. T.; Van Vuure, A. W.; Verpoest, I. Investigation of microstructure and tensile properties of porous natural coir fibre for use in composite materials. *Industrial Crops and Products* **2015**, *65*, 437-445.

435. Abraham, E.; Deepa, B.; Pothen, L.; Cintil, J.; Thomas, S.; John, M. J.; Anandjiwala, R.; Narine, S. Environmental friendly method for the extraction of coir fibre and isolation of nanofibre. *Carbohydrate polymers* **2013**, *92*, 1477-1483.

436. Kramera, D. G.; Rochaa, B. G.; Pereirab, M. C.; Souzab, R. S.; Alvesb, C. R.; Júniord, G. B.; Nascimentoc, J. H. O.; Quinae, M. J.; Ferreirae, L. G.; Ladchumananandasivama, R. Determination of the biosorption of Cd (II) by coconut fiber. **2014**

437. Khan, M. N.; Rehman, N.; Sharif, A.; Ahmed, E.; Farooqi, Z. H.; Din, M. I. Environmentally benign extraction of cellulose from dunchi fiber for nanocellulose fabrication. *International Journal of Biological Macromolecules* **2020**

438. Rajesh, R.; Ravichandran, Y. D.; Nambi Raj, N. A.; Senthilkumar, N. Development of a Biodegradable Composite (Hydroxyapatite-Chitosan-Coir Pith) as a Packing Material. *Polymer-Plastics Technology and Engineering* **2014**, *53*, 1105-1110.

439. Wan Ishak, W. H.; Ahmad, I.; Ramli, S.; Mohd Amin, M. C. I. Gamma irradiation-assisted synthesis of cellulose nanocrystal-reinforced gelatin hydrogels. *Nanomaterials* **2018**, *8*, 749.

440. Jagdale, P.; Ziegler, D.; Rovere, M.; Tulliani, J. M.; Tagliaferro, A. Waste coffee ground biochar: A material for humidity sensors. *Sensors* **2019**, *19*, 801.

441. Mora Alvarez, N. M.; Pastrana, J. M.; Lagos, Y.; Lozada, J. J. Evaluation of mercury (Hg2+) adsorption capacity using exhausted coffee waste. *Sustainable Chemistry and Pharmacy* **2018**, *10*, 60-70.

442. Mussatto, S. I.; Machado, E. M.; Carneiro, L. M.; Teixeira, J. A. Sugars metabolism and ethanol production by different yeast strains from coffee industry wastes hydrolysates. *Applied Energy* **2012**, *92*, 763-768.

443. Obi Reddy, K.; Shukla, M.; Uma Maheswari, C.; Varada Rajulu, A. Mechanical and physical characterization of sodium hydroxide treated Borassus fruit fibers. *Journal of Forestry Research* **2012**, *23*, 667-674.

444. Hao, L.; Wang, N.; Wang, C.; Li, G. Arsenic removal from water and river water by the combined adsorption - UF membrane process. *Chemosphere* **2018**, *202*, 768-776.

445. Ballesteros, L. F.; Teixeira, J. A.; Mussatto, S. I. Chemical, functional, and structural properties of spent coffee grounds and coffee silverskin. *Food and bioprocess technology* **2014**, *7*, 3493-3503.

446. Wei-Lung, C. Investigation of indium ions removal from aqueous solutions using spent coffee grounds. *International Journal of Physical Sciences* **2012**, *7*

447. Zarrinbakhsh, N.; Wang, T.; Rodriguez-Uribe, A.; Misra, M.; Mohanty, A. K. Characterization of wastes and coproducts from the coffee industry for composite material production. *BioResources* **2016**, *11*, 7637-7653.

448. Esquivel, P.; Jimenez, V. M. Functional properties of coffee and coffee by-products. *Food Research International* **2012**, *46*, 488-495.

449. Edathil, A. A.; Shittu, I.; Hisham Zain, J.; Banat, F.; Haija, M. A. Novel magnetic coffee waste nanocomposite as effective bioadsorbent for Pb(II) removal from aqueous solutions. *Journal of Environmental Chemical Engineering* **2018**, *6*, 2390-2400.

450. Siddiqui, H. A.; Pickering, K. L.; Mucalo, M. R. Study of biomorphic calcium deficient hydroxyapatite fibres derived from a natural Harakeke (Phormium tenax) leaf fibre template. *Bioinspiration & Biomimetics* **2020**, *16*, 016015.

451. Lethesh, K. C.; Evjen, S.; Venkatraman, V.; Shah, S. N.; Fiksdahl, A. Highly efficient cellulose dissolution by alkaline ionic liquids. *Carbohydrate Polymers* **2020**, *229*, 115594.

452. Abdul Majid, S.; Ahmad Mir, M.; Mir, J. M. Nitrate and phosphate sorption efficiency of mordenite versus zeolite-A at the convergence of experimental and density functionalized evaluation. *Journal of the Chinese Advanced Materials Society* **2018**, *6*, 691-705.

453. Sakizci, M.; KILINÇ, L. Ö. Influence of acid and heavy metal cation exchange treatments on methane adsorption properties of mordenite. *Turkish Journal of Chemistry* **2015**, *39*, 970-983.

454. Hyeon Kim, M.; Hwang, U.-C.; Nam, I.-S.; Gul Kim, Y. The characteristics of a copper-exchanged natural zeolite for NO reduction by NH3 and C3H6. *Catalysis Today* **1998**, *44*, 57-65.

455. Wahono, S. K.; Prasetyo, D. J.; Jatmiko, T. H.; Pratiwi, D.; Suwanto, A.; Hernawan; Vasilev, K. Multi-stage dealumination for characteristic engineering of mordenite-clinoptilolite natural zeolite. Presented at AIP Conference Proceedings; Place,AIP Publishing LLC; Vol. 2085, p 020044.

456. Gili, M. B. Z.; Conato, M. T. Synthesis and characterization of mordenite-type zeolites with varying Si/Al ratio. *Materials Research Express* **2018**, *6*, 015515.

457. Pe-Piper, G.; Tsolis-Katagas, P. K-rich mordenite from late Miocene rhyolitic tuffs, Island of Samos, Greece. *Clays and Clay Minerals* **1991**, *39*, 239-247.

458. Elizalde-González, M. a. P.; Mattusch, J.; Wennrich, R.; Morgenstern, P. Uptake of arsenite and arsenate by clinoptilolite-rich tuffs. *Microporous and Mesoporous Materials* **2001**, *46*, 277-286.

459. Elaiopoulos, K.; Perraki, T.; Grigoropoulou, E. Mineralogical study and porosimetry measurements of zeolites from Scaloma area, Thrace, Greece. *Microporous and Mesoporous Materials* **2008**, *112*, 441-449.

460. Elaiopoulos, K.; Perraki, T.; Grigoropoulou, E. Monitoring the effect of hydrothermal treatments on the structure of a natural zeolite through a combined XRD, FTIR, XRF, SEM and N2-porosimetry analysis. *Microporous and Mesoporous Materials* **2010**, *134*, 29-43.

461. Ostroumov, M.; Chávez, P. C. Mineralogical study of mordenite from the Sierra Madre del Sur, southwestern Mexico. *Revista Mexicana de Ciencias Geológicas* **2003**, *20*, 133-138.

462. Varela, M. B.; Ramírez, S. M.; Ereña, I.; Gener, M.; Carmona, P. Characterization and pozzolanicity of zeolitic rocks from two Cuban deposits. *Applied Clay Science* **2006**, *33*, 149-159.

463. Breck, D. W. *Zeolite molecular sieves: structure, chemistry and use*; Krieger, 1984.

464. Hu, C.; Guo, R.; Li, B.; Ma, X.; Wu, H.; Jiang, Z. Development of novel mordenite-filled chitosan–poly(acrylic acid) polyelectrolyte complex membranes for pervaporation dehydration of ethylene glycol aqueous solution. *Journal of Membrane Science* **2007**, *293*, 142-150.

465. Liu, T.-Y.; Chen, S.-Y.; Li, J.-H.; Liu, D.-M. Study on drug release behaviour of CDHA/chitosan nanocomposites—Effect of CDHA nanoparticles. *Journal of Controlled Release* **2006**, *112*, 88-95.

466. Nikpour, M. R.; Rabiee, S. M.; Jahanshahi, M. Synthesis and characterization of hydroxyapatite/chitosan nanocomposite materials for medical engineering applications. *Composites Part B: Engineering* **2012**, *43*, 1881-1886.

467. Nematidil, N.; Sadeghi, M.; Nezami, S.; Sadeghi, H. Synthesis and characterization of Schiff-base based chitosan-g-glutaraldehyde/NaMMTNPs-APTES for removal Pb2+ and Hg2+ ions. *Carbohydrate Polymers* **2019**, *222*, 114971.

468. Adamczuk, A.; Kołodyńska, D. Equilibrium, thermodynamic and kinetic studies on removal of chromium, copper, zinc and arsenic from aqueous solutions onto fly ash coated by chitosan. *Chemical Engineering Journal* **2015**, *274*, 200-212.

469. Kou, S.; Peters, L.; Mucalo, M. Chitosan: A review of sources and preparation methods. *International Journal of Biological Macromolecules* **2020**

470. Alexopoulou, M.; Mystiridou, E.; Mouzakis, D.; Zaoutsos, S.; Fatouros, D. G.; Bouropoulos, N. Preparation, characterization and in vitro assessment of ibuprofen loaded calcium phosphate/gypsum bone cements. *Crystal Research and Technology* **2016**, *51*, 41-48.

471. Zhan, Y.; Lin, J.; Li, J. Preparation and characterization of surfactant-modified hydroxyapatite/zeolite composite and its adsorption behavior toward humic acid and copper (II). *Environmental science and pollution research* **2013**, *20*, 2512-2526.

472. Kuwahara, Y.; Ohmichi, T.; Kamegawa, T.; Mori, K.; Yamashita, H. A novel synthetic route to hydroxyapatite–zeolite composite material from steel slag: investigation of synthesis mechanism and evaluation of physicochemical properties. *Journal of Materials Chemistry* **2009**, *19*, 7263-7272.

473. Iqbal, N.; Kadir, M. R. A.; Iqbal, S.; Razak, S. Izwan A.; Rafique, M. S.; Bakhsheshi-Rad, H. R.; Idris, M. H.; Khattak, M. A.; Raghavendran, H. R. B.; Abbas, A. A. Nano-hydroxyapatite reinforced zeolite ZSM composites: A comprehensive study on the structural and in vitro biological properties. *Ceramics International* **2016**, *42*, 7175-7182.

474. Sastri, V. S.; Chakrabarti, C. L.; Willis, D. E. Some aspects of “chemical” interferences in atomic-absorption spectroscopy. *Talanta* **1969**, *16*, 1093-1098.

475. Aksu, Z.; Tezer, S. Biosorption of reactive dyes on the green alga Chlorella vulgaris. *Process Biochemistry* **2005**, *40*, 1347-1361.

476. Wang, S.; Wang, N.; Yao, K.; Fan, Y.; Li, W.; Han, W.; Yin, X.; Chen, D. Characterization and interpretation of Cd (II) adsorption by different modified rice straws under contrasting conditions. *Scientific reports* **2019**, *9*, 1-13.

477. El Nemr, A. Potential of pomegranate husk carbon for Cr (VI) removal from wastewater: Kinetic and isotherm studies. *Journal of Hazardous Materials* **2009**, *161*, 132-141.

478. Mahdi, Z.; Qiming, J. Y.; El Hanandeh, A. Removal of lead (II) from aqueous solution using date seed-derived biochar: batch and column studies. *Applied Water Science* **2018**, *8*, 181.

479. Pooladi, A.; Bazargan-Lari, R. Simultaneous removal of copper and zinc ions by Chitosan/Hydroxyapatite/nano-Magnetite composite. *Journal of Materials Research and Technology* **2020**, *9*, 14841-14852.

480. Pourshadlou, S.; Mobasherpour, I.; Majidian, H.; Salahi, E.; Bidabadi, F. S.; Mei, C.-T.; Ebrahimi, M. Adsorption system for Mg2+ removal from aqueous solutions using bentonite/γ-alumina nanocomposite. *Journal of Colloid and Interface Science* **2020**

481. Callesen, I.; Keck, H.; Andersen, T. J. Particle size distribution in soils and marine sediments by laser diffraction using Malvern Mastersizer 2000—method uncertainty including the effect of hydrogen peroxide pretreatment. *Journal of Soils and Sediments* **2018**, *18*, 2500-2510.

482. Safinejad, A.; Goudarzi, N.; Chamjangali, M. A.; Bagherian, G. Effective simultaneous removal of Pb (II) and Cd (II) ions by a new magnetic zeolite prepared from stem sweep. *Materials Research Express* **2017**, *4*, 116104.

483. Gupta, N.; Kushwaha, A. K.; Chattopadhyaya, M. Adsorptive removal of Pb2+, Co2+ and Ni2+ by hydroxyapatite/chitosan composite from aqueous solution. *Journal of the Taiwan Institute of Chemical Engineers* **2012**, *43*, 125-131.

484. Wu, L.; Forsling, W.; Schindler, P. W. Surface complexation of calcium minerals in aqueous solution: 1. Surface protonation at fluorapatite—water interfaces. *Journal of Colloid and Interface Science* **1991**, *147*, 178-185.

485. Hamadi, N. K.; Chen, X. D.; Farid, M. M.; Lu, M. G. Q. Adsorption kinetics for the removal of chromium(VI) from aqueous solution by adsorbents derived from used tyres and sawdust. *Chemical Engineering Journal* **2001**, *84*, 95-105.

486. Srivastava, P.; Singh, B.; Angove, M. Competitive adsorption behavior of heavy metals on kaolinite. *Journal of Colloid and Interface Science* **2005**, *290*, 28-38.

487. Wang, X.; Wang, L.; Wang, Y.; Tan, R.; Ke, X.; Zhou, X.; Geng, J.; Hou, H.; Zhou, M. Calcium sulfate hemihydrate whiskers obtained from flue gas desulfurization gypsum and used for the adsorption removal of lead. *Crystals* **2017**, *7*, 270.

488. Huang, J.; Yuan, F.; Zeng, G.; Li, X.; Gu, Y.; Shi, L.; Liu, W.; Shi, Y. Influence of pH on heavy metal speciation and removal from wastewater using micellar-enhanced ultrafiltration. *Chemosphere* **2017**, *173*, 199-206.
489. Manzoor, K.; Ahmad, M.; Ahmad, S.; Ikram, S. Removal of Pb (II) and Cd (II) from wastewater using arginine cross-linked chitosan–carboxymethyl cellulose beads as green adsorbent. *RSC advances* **2019**, *9*, 7890-7902.
490. Dahman, Y. *Nanotechnology and functional materials for engineers*; Elsevier, 2017.
491. van Riemsdijk, W. Precipitation-dissolution reactions. In *Soil pollution and soil protection*; Int. Training Centre (PHLO), WAU, 1996; pp 127-136.
492. Kamiński, W.; Modrzejewska, Z. Application of chitosan membranes in separation of heavy metal ions. *Separation science and technology* **1997**, *32*, 2659-2668.
493. Wang, Y.; Shi, L.; Gao, L.; Wei, Q.; Cui, L.; Hu, L.; Yan, L.; Du, B. The removal of lead ions from aqueous solution by using magnetic hydroxypropyl chitosan/oxidized multiwalled carbon nanotubes composites. *Journal of Colloid and Interface Science* **2015**, *451*, 7-14.
494. Khawar, A.; Aslam, Z.; Zahir, A.; Akbar, I.; Abbas, A. Synthesis of Femur extracted hydroxyapatite reinforced nanocomposite and its application for Pb(II) ions abatement from aqueous phase. *International Journal of Biological Macromolecules* **2019**, *122*, 667-676.
495. Snoeyink, V. L.; Jenkins, D. *Water chemistry*; John Wiley & Sons, Ltd, 1980.
496. Pagnanelli, F.; Esposito, A.; Toro, L.; Veglio, F. Metal speciation and pH effect on Pb, Cu, Zn and Cd biosorption onto Sphaerotilus natans: Langmuir-type empirical model. *Water research* **2003**, *37*, 627-633.
497. Melnikov, F.; Geohagen, B. C.; Gavin, T.; LoPachin, R. M.; Anastas, P. T.; Coish, P.; Herr, D. W. Application of the hard and soft, acids and bases (HSAB) theory as a method to predict cumulative neurotoxicity. *Neurotoxicology* **2020**, *79*, 95-103.
498. Udaybhaskar, P.; Iyengar, L.; Rao, A. P. Hexavalent chromium interaction with chitosan. *Journal of Applied Polymer Science* **1990**, *39*, 739-747.
499. Oyetade, O. A.; Nyamori, V. O.; Jonnalagadda, S. B.; Martincigh, B. S. Removal of Cd2+ and Hg2+ from aqueous solutions by adsorption onto nitrogen-functionalized carbon nanotubes. *Desalin. Water Treat* **2018**, *108*, 253-267.

500. Li, R.; An, Q.-D.; Mao, B.-Q.; Xiao, Z.-Y.; Zhai, S.-R.; Shi, Z. PDA-meditated green synthesis of amino-modified, multifunctional magnetic hollow composites for Cr (VI) efficient removal. *Journal of the Taiwan Institute of Chemical Engineers* **2017**, *80*, 596-606.

501. Gong, X.; Li, W.; Wang, K.; Hu, J. Study of the adsorption of Cr (VI) by tannic acid immobilised powdered activated carbon from micro-polluted water in the presence of dissolved humic acid. *Bioresource technology* **2013**, *141*, 145-151.

502. Kousalya, G.; Gandhi, M. R.; Meenakshi, S. Removal of toxic Cr (VI) ions from aqueous solution using nano-hydroxyapatite-based chitin and chitosan hybrid composites. *Adsorption Science & Technology* **2010**, *28*, 49-64.

503. Schmuhl, R.; Krieg, H.; Keizer, K. Adsorption of Cu (II) and Cr (VI) ions by chitosan: Kinetics and equilibrium studies. *Water Sa* **2001**, *27*, 1-8.

504. Liu, Y.; Zhu, X.; Qian, F.; Zhang, S.; Chen, J. Magnetic activated carbon prepared from rice straw-derived hydrochar for triclosan removal. *RSC Advances* **2014**, *4*, 63620-63626.

505. Weber, T. W.; Chakravorti, R. K. Pore and solid diffusion models for fixed-bed adsorbers. *AIChE Journal* **1974**, *20*, 228-238.

506. Meroufel, B.; Benali, O.; Benyahia, M.; Benmoussa, Y.; Zenasni, M. Adsorptive removal of anionic dye from aqueous solutions by Algerian kaolin: Characteristics, isotherm, kinetic and thermodynamic studies. *J. Mater. Environ. Sci* **2013**, *4*, 482-491.

507. Chiban, M.; Soudani, A.; Sinan, F.; Persin, M. Single, binary and multi-component adsorption of some anions and heavy metals on environmentally friendly Carpobrotus edulis plant. *Colloids and Surfaces B: Biointerfaces* **2011**, *82*, 267-276.

508. Hall, K. R.; Eagleton, L. C.; Acrivos, A.; Vermeulen, T. Pore-and solid-diffusion kinetics in fixed-bed adsorption under constant-pattern conditions. *Industrial & Engineering Chemistry Fundamentals* **1966**, *5*, 212-223.

509. Han, X.; Zhang, Y.; Li, L.; Han, R.; Wang, G.; Wei, W. Nanosized hydroxyapatite supported on natural sepiolite: a novel adsorbent for Cd (II) removal from simulated groundwater. *Materials Research Express* **2019**, *6*, 125518.

510. Ko, D. C. K.; Cheung, C. W.; Choy, K. K. H.; Porter, J. F.; McKay, G. Sorption equilibria of metal ions on bone char. *Chemosphere* **2004**, *54*, 273-281.

511. Miyake, M.; Ishigaki, K.; Suzuki, T. Structure refinements of Pb2+ ion-exchanged apatites by X-ray powder pattern-fitting. *Journal of Solid State Chemistry* **1986**, *61*, 230-235.

512. Shashkova, I. L.; Rat'ko, A. I.; Kitikova, N. V. Removal of heavy metal ions from aqueous solutions by alkaline-earth metal phosphates. *Colloids and surfaces A: Physicochemical and engineering aspects* **1999**, *160*, 207-215.

513. Sugiyama, S.; Fukuda, N.; Matsumoto, H.; Hayashi, H.; Shigemoto, N.; Hiraga, Y.; Moffat, J. Interdependence of anion and cation exchanges in calcium hydroxyapatite: Pb2+ and Cl−. *Journal of colloid and interface science* **1999**, *220*, 324-328.

514. Chui, V.; Mok, K.; Ng, C.; Luong, B.; Ma, K. Removal and recovery of copper (II), chromium (III), and nickel (II) from solutions using crude shrimp chitin packed in small columns. *Environment international* **1996**, *22*, 463-468.

515. Li, G.; Zhang, J.; Li, Y.; Liu, J.; Yan, Z. Adsorption characteristics of Pb (II), Cd (II) and Cu (II) on carbon nanotube-hydroxyapatite. *Environmental technology* **2019**, 1-22.

516. Kavand, M.; Eslami, P.; Razeh, L. The adsorption of cadmium and lead ions from the synthesis wastewater with the activated carbon: optimization of the single and binary systems. *Journal of Water Process Engineering* **2020**, *34*, 101151.

517. Jeanjean, J.; Vincent, U.; Fedoroff, M. Structural modification of calcium hydroxyapatite induced by sorption of cadmium ions. *Journal of Solid State Chemistry* **1994**, *108*, 68-72.

518. Barka, N.; Ouzaouit, K.; Abdennouri, M.; El Makhfouk, M.; Qourzal, S.; Assabbane, A.; Ait-Ichou, Y.; Nounah, A. Kinetics and equilibrium of cadmium removal from aqueous solutions by sorption onto synthesized hydroxyapatite. *Desalination and Water Treatment* **2012**, *43*, 8-16.

519. Foroutan, R.; Peighambardoust, S. J.; Hosseini, S. S.; Akbari, A.; Ramavandi, B. Hydroxyapatite biomaterial production from chicken (femur and beak) and fishbone waste through a chemical less method for Cd2+ removal from shipbuilding wastewater. *Journal of Hazardous Materials* **2021**, *413*, 125428.

520. Hutchenson, S. Characterization of heavy metal removal from aqueous solutions using natural fiber impregnated with metallic nanoparticles. **2016**

521. de Quadros Melo, D.; Vidal, C. B.; da Silva, A. L.; Raulino, G. S. C.; de Luz, A.; da Luz, C.; Fechine, P.; Mazzeto, S.; do Nascimento, R. Removal of toxic metal ions using modified lignocellulosic fibers as eco-friendly biosorbents: Mathematical modeling and numerical simulation. *International Journal of Civil and Environmental Engineering* **2015**, *15*, 14-25.

522. Rakhunde, R.; Deshpande, L.; Juneja, H. Chemical speciation of chromium in water: a review. *Critical reviews in environmental science and technology* **2012**, *42*, 776-810.

523. Samani, M. R.; Toghraie, D. Removal of hexavalent chromium from water using polyaniline/wood sawdust/poly ethylene glycol composite: an experimental study. *Journal of Environmental Health Science and Engineering* **2019**, *17*, 53-62.

524. Nikolenko, N.; Esajenko, E. Surface properties of synthetic calcium hydroxyapatite. *Adsorption Science & Technology* **2005**, *23*, 543-553.

525. Abbar, B.; Alem, A.; Pantet, A.; Marcotte, S.; Ahfir, N.; Duriatti, D. Removal of dissolved and particulate contaminants from aqueous solution using natural flax fibres. *Academic Journal of Civil Engineering* **2017**, *35*, 656-661.

526. Zhu, Y.; Jiang, Y.; Zhu, Z.; Deng, H.; Ding, H.; Li, Y.; Zhang, L.; Lin, J. Preparation of a porous hydroxyapatite-carbon composite with the bio-template of sugarcane top stems and its use for the Pb (II) removal. *Journal of Cleaner Production* **2018**, *187*, 650-661.

527. Nemeş, L. N.; Bulgariu, L. Optimization of process parameters for heavy metals biosorption onto mustard waste biomass. *Open Chemistry* **2016**, *14*, 175-187.

528. Pino, G. H.; de Mesquita, L. M. S.; Torem, M. L.; Pinto, G. A. S. Biosorption of cadmium by green coconut shell powder. *Minerals engineering* **2006**, *19*, 380-387.

529. Amuda, O.; Giwa, A.; Bello, I. Removal of heavy metal from industrial wastewater using modified activated coconut shell carbon. *Biochemical Engineering Journal* **2007**, *36*, 174-181.

530. Kramer, D. G.; Rocha, B. G.; Pereira, M.; Souza, R. S.; Alves, C. R.; BC Junior, G.; Nascimento, J. H. O.; Quina, M. J.; Ferreira, L. G.; Ladchumananandasivam, R. Determination of the Biosorption of Cd (II) by Coconut Fiber. **2014**

531. Manatunga, D. C.; de Silva, R. M.; de Silva, K. N.; Ratnaweera, R. Natural polysaccharides leading to super adsorbent hydroxyapatite nanoparticles for the removal of heavy metals and dyes from aqueous solutions. *RSC advances* **2016**, *6*, 105618-105630.

532. Ramesh, S. T.; Gandhimathi, R.; Badabhagni, N.; Nidheesh, P. V. Removal of Cd (II) from aqueous solution by adsorption onto coir pith, an agricultural solid waste: batch experimental study. *Environmental Engineering & Management Journal (EEMJ)* **2011**, *10*

533. Shahid, M.; Dumat, C.; Aslam, M.; Pinelli, E. Assessment of lead speciation by organic ligands using speciation models. *Chemical Speciation & Bioavailability* **2012**, *24*, 248-252.

534. Boota, R.; Bhatti, H. N.; Hanif, M. A. Removal of Cu (II) and Zn (II) using lignocellulosic fiber derived from Citrus reticulata (Kinnow) waste biomass. *Separation Science and Technology* **2009**, *44*, 4000-4022.

535. Altun, T.; Pehlivan, E. Removal of copper (II) ions from aqueous solutions by walnut-, hazelnut-and almond-shells. *CLEAN–Soil, Air, Water* **2007**, *35*, 601-606.

536. Bishnoi, N. R.; Bajaj, M.; Sharma, N.; Gupta, A. Adsorption of Cr (VI) on activated rice husk carbon and activated alumina. *Bioresource technology* **2004**, *91*, 305-307.

537. Abu-Danso, E.; Peräniemi, S.; Leiviskä, T.; Kim, T.; Tripathi, K. M.; Bhatnagar, A. Synthesis of clay-cellulose biocomposite for the removal of toxic metal ions from aqueous medium. *Journal of hazardous materials* **2020**, *381*, 120871.

538. Saad, E. M.; Elshaarawy, R. F.; Mahmoud, S. A.; El-Moselhy, K. M. New Ulva lactuca Algae Based Chitosan Bio-composites for Bioremediation of Cd (II) Ions☆. *Journal of Bioresources and Bioproducts* **2021**

539. Sangeetha, K.; Vidhya, G.; Vasugi, G.; Girija, E. Lead and cadmium removal from single and binary metal ion solution by novel hydroxyapatite/alginate/gelatin nanocomposites. *Journal of environmental chemical engineering* **2018**, *6*, 1118-1126.

540. Pehlivan, E.; Altun, T.; Cetin, S.; Bhanger, M. I. Lead sorption by waste biomass of hazelnut and almond shell. *Journal of hazardous materials* **2009**, *167*, 1203-1208.

541. Brudey, T.; Largitte, L.; Jean-Marius, C.; Tant, T.; Dumesnil, P. C.; Lodewyckx, P. Adsorption of lead by chemically activated carbons from three lignocellulosic precursors. *Journal of Analytical and Applied Pyrolysis* **2016**, *120*, 450-463.

542. Liu, L.; Luo, X.-B.; Ding, L.; Luo, S.-L. Application of nanotechnology in the removal of heavy metal from water. In *Nanomaterials for the removal of pollutants and resource reutilization*; Elsevier, 2019; pp 83-147.

543. Wang, C.; Wang, H.; Gu, G.; Liu, Y. Sorption of Cd (II) ion by lignocellulose biomass from leaves of camphor tree. *Desalination and Water Treatment* **2017**, *68*, 211-219.

544. Quek, S. Y.; Al-Duri, B.; Wase, D. A. J.; Forster, C. F. Coir as a Biosorbent of Copper and Lead. *Process Safety and Environmental Protection* **1998**, *76*, 50-54.

545. Shukla, P. M.; Shukla, S. R. Biosorption of Cu (II), Pb (II), Ni (II), and Fe (II) on alkali treated coir fibers. *Separation Science and Technology* **2013**, *48*, 421-428.

546. Olalekan, A.; Dada, A.; Okewale, A. Comparative adsorption isotherm study of the removal of Pb2+ and Zn2+ onto agricultural waste. *Res J Chem Env Sci* **2013**, *1*, 22-27.

547. Goldberg, S. Equations and models describing adsorption processes in soils. *Chemical processes in soils* **2005**, *8*, 489-517.

548. Naji, L. A.; Jassam, S. H.; Yaseen, M. J.; Faisal, A. A.; Al-Ansari, N. Modification of Langmuir model for simulating initial pH and temperature effects on sorption process. *Separation Science and Technology* **2020**, *55*, 2729-2736.

549. Balarak, D.; Mostafapour, F. K.; Azarpira, H.; Joghataei, A. Langmuir, Freundlich, Temkin and Dubinin–radushkevich isotherms studies of equilibrium sorption of ampicilin unto montmorillonite nanoparticles. *Journal of Pharmaceutical Research International* **2017**, 1-9.

550. Hubbe, M. A.; Azizian, S.; Douven, S. Implications of apparent pseudo-second-order adsorption kinetics onto cellulosic materials: A review. *BioResources* **2019**, *14*, 7582-7626.

551. Carrell, H.; Glusker, J. P.; Piercy, E. A.; Stallings, W. C.; Zacharias, D. E.; Davis, R. L.; Astbury, C.; Kennard, C. H. Metal chelation versus internal hydrogen bonding of the. alpha.-hydroxy carboxylate group. *Journal of the American Chemical Society* **1987**, *109*, 8067-8071.

552. Patterer, M. S.; Bavasso, I.; Sambeth, J. E.; Medici, F. Cadmium removal from acqueous solution by adsorption on spent coffee grounds. **2017**

553. Delil, A. D.; Gülçiçek, O.; Gören, N. Optimization of adsorption for the removal of cadmium from aqueous solution using Turkish coffee grounds. *International Journal of Environmental Research* **2019**, *13*, 861-878.

554. Khawar, A.; Aslam, Z.; Zahir, A.; Akbar, I.; Abbas, A. Synthesis of Femur extracted hydroxyapatite reinforced nanocomposite and its application for Pb (II) ions abatement from aqueous phase. *International journal of biological macromolecules* **2019**, *122*, 667-676.

555. Loulidi, I.; Boukhlifi, F.; Ouchabi, M.; Amar, A.; Jabri, M.; Kali, A.; Hadey, C. Assessment of Untreated Coffee Wastes for the Removal of Chromium (VI) from Aqueous Medium. *International Journal of Chemical Engineering* **2021**, *2021*

556. Azouaou, N.; Sadaoui, Z.; Djaafri, A.; Mokaddem, H. Adsorption of cadmium from aqueous solution onto untreated coffee grounds: Equilibrium, kinetics and thermodynamics. *Journal of Hazardous Materials* **2010**, *184*, 126-134.

557. McNutt, J.; He, Q. Spent coffee grounds: A review on current utilization. *Journal of Industrial and Engineering Chemistry* **2019**, *71*, 78-88.

558. Kim, M.-S.; Kim, J.-G. Adsorption characteristics of spent coffee grounds as an alternative adsorbent for cadmium in solution. *Environments* **2020**, *7*, 24.

559. Mohan, G. K.; Babu, A. N.; Kalpana, K.; Ravindhranath, K. Removal of chromium (VI) from water using adsorbent derived from spent coffee grounds. *International Journal of Environmental Science and Technology* **2019**, *16*, 101-112.

560. Taamneh, Y.; Sharadqah, S. The removal of heavy metals from aqueous solution using natural Jordanian zeolite. *Applied Water Science* **2017**, *7*, 2021-2028.

561. Elboughdiri, N. The use of natural zeolite to remove heavy metals Cu (II), Pb (II) and Cd (II), from industrial wastewater. *Cogent Engineering* **2020**, *7*, 1782623.

562. Shyaa, A. A.; Hasan, O. A.; Abbas, A. M. Synthesis and characterization of polyaniline/zeolite nanocomposite for the removal of chromium (VI) from aqueous solution. *Journal of Saudi Chemical Society* **2015**, *19*, 101-107.

563. Adam, M. R.; Salleh, N. M.; Othman, M. H. D.; Matsuura, T.; Ali, M. H.; Puteh, M. H.; Ismail, A. F.; Rahman, M. A.; Jaafar, J. The adsorptive removal of chromium (VI) in aqueous solution by novel natural zeolite based hollow fibre ceramic membrane. *Journal of Environmental Management* **2018**, *224*, 252-262.

564. Ćurković, L.; Cerjan-Stefanović, Š.; Filipan, T. Metal ion exchange by natural and modified zeolites. *Water research* **1997**, *31*, 1379-1382.

565. Briones, R. M.; Sarmah, A. K. Detailed sorption characteristics of the anti-diabetic drug metformin and its transformation product guanylurea in agricultural soils. *Science of the Total Environment* **2018**, *630*, 1258-1268.

566. Ghasemi, M.; Ghasemi, N.; Zahedi, G.; Alwi, S.; Goodarzi, M.; Javadian, H. Kinetic and equilibrium study of Ni (II) sorption from aqueous solutions onto Peganum harmala-L. *International Journal of Environmental Science and Technology* **2014**, *11*, 1835-1844.

567. Chen, X.; Cui, J.; Xu, X.; Sun, B.; Zhang, L.; Dong, W.; Chen, C.; Sun, D. Bacterial cellulose/attapulgite magnetic composites as an efficient adsorbent for heavy metal ions and dye treatment. *Carbohydrate polymers* **2020**, *229*, 115512.

568. Chen, S.; Ma, Y.; Chen, L.; Xian, K. Adsorption of aqueous Cd2+, Pb2+, Cu2+ ions by nano-hydroxyapatite: single-and multi-metal competitive adsorption study. *Geochemical Journal* **2010**, *44*, 233-239.

569. Wang, Y.-Y.; Liu, Y.-X.; Lu, H.-H.; Yang, R.-Q.; Yang, S.-M. Competitive adsorption of Pb (II), Cu (II), and Zn (II) ions onto hydroxyapatite-biochar nanocomposite in aqueous solutions. *Journal of Solid State Chemistry* **2018**, *261*, 53-61.

570. Ding, C.; Cheng, W.; Wang, X.; Wu, Z.-Y.; Sun, Y.; Chen, C.; Wang, X.; Yu, S.-H. Competitive sorption of Pb (II), Cu (II) and Ni (II) on carbonaceous nanofibers: a spectroscopic and modeling approach. *Journal of hazardous materials* **2016**, *313*, 253-261.

571. Zhu, Y.; Hu, J.; Wang, J. Competitive adsorption of Pb (II), Cu (II) and Zn (II) onto xanthate-modified magnetic chitosan. *Journal of hazardous materials* **2012**, *221*, 155-161.

572. Fan, C.; Li, K.; Li, J.; Ying, D.; Wang, Y.; Jia, J. Comparative and competitive adsorption of Pb(II) and Cu(II) using tetraethylenepentamine modified chitosan/CoFe2O4 particles. *Journal of Hazardous Materials* **2017**, *326*, 211-220.

573. Heidari, A.; Younesi, H.; Mehraban, Z.; Heikkinen, H. Selective adsorption of Pb (II), Cd (II), and Ni (II) ions from aqueous solution using chitosan–MAA nanoparticles. *International journal of biological macromolecules* **2013**, *61*, 251-263.

574. Zhu, Y.; Hu, J.; Wang, J. Competitive adsorption of Pb(II), Cu(II) and Zn(II) onto xanthate-modified magnetic chitosan. *Journal of Hazardous Materials* **2012**, *221-222*, 155-161.

575. Sánchez, J.; Butter, B.; Rivas, B. L. BIOPOLYMERS APPLIED TO REMOVE METAL IONS THROUGH ULTRAFILTRATION. A REVIEW. *Journal of the Chilean Chemical Society* **2020**, *65*, 5004-5010.

576. Nieboer, E.; Richardson, D. H. S. The replacement of the nondescript term 'heavy metals' by a biologically and chemically significant classification of metal ions. *Environmental Pollution Series B, Chemical and Physical* **1980**, *1*, 3-26.

577. Suzuki, T.; Hatsushika, T.; Miyake, M. Synthetic hydroxyapatites as inorganic cation exchangers. Part 2. *Journal of the Chemical Society, Faraday Transactions 1: Physical Chemistry in Condensed Phases* **1982**, *78*, 3605-3611.

578. Zhang, Z.; Li, M.; Chen, W.; Zhu, S.; Liu, N.; Zhu, L. Immobilization of lead and cadmium from aqueous solution and contaminated sediment using nano-hydroxyapatite. *Environmental Pollution* **2010**, *158*, 514-519.

579. Yan, Y.; Dong, X.; Sun, X.; Sun, X.; Li, J.; Shen, J.; Han, W.; Liu, X.; Wang, L. Conversion of waste FGD gypsum into hydroxyapatite for removal of Pb2+ and Cd2+ from wastewater. *Journal of Colloid and Interface Science* **2014**, *429*, 68-76.

580. Markiewicz, B.; Komorowicz, I.; Sajnóg, A.; Belter, M.; Barałkiewicz, D. Chromium and its speciation in water samples by HPLC/ICP-MS – technique

establishing metrological traceability: A review since 2000. *Talanta* **2015**, *132*, 814-828.

581. Bertinato, J. Copper: Physiology. In *Encyclopedia of Food and Health*; B. Caballero; P. M. Finglas and F. Toldrá, Eds.; Academic Press: Oxford, 2016; pp 321-326.
582. Fowler, B. A. Arsenical Kidney Toxicity. In *Handbook of Arsenic Toxicology*; Elsevier, 2015; pp 349-361.
583. Vandenbossche, M.; Jimenez, M.; Casetta, M.; Bellayer, S.; Beaurain, A.; Bourbigot, S.; Traisnel, M. Chitosan-grafted nonwoven geotextile for heavy metals sorption in sediments. *Reactive and Functional Polymers* **2013**, *73*, 53-59.
584. Kundu, S.; Gupta, A. Arsenic adsorption onto iron oxide-coated cement (IOCC): regression analysis of equilibrium data with several isotherm models and their optimization. *Chemical Engineering Journal* **2006**, *122*, 93-106.
585. Terdputtakun, A.; Arqueropanyo, O.-a.; Sooksamiti, P.; Janhom, S.; Naksata, W. Adsorption isotherm models and error analysis for single and binary adsorption of Cd (II) and Zn (II) using leonardite as adsorbent. *Environmental Earth Sciences* **2017**, *76*, 777.
586. Chan, L. S.; Cheung, W. H.; Allen, S. J.; McKay, G. Error Analysis of Adsorption Isotherm Models for Acid Dyes onto Bamboo Derived Activated Carbon. *Chinese Journal of Chemical Engineering* **2012**, *20*, 535-542.
587. .
588. Scientific, H. Understanding and Interpreting Particle Size Distribution Calculations. 2021.

Appendix 1

1.1A: Arrhenius equation

The Arrhenius equation is used to calculate the activation energy of the reaction by using the rate constant, which an appropriate kinetic model usually calculates.

The linear form of the Arrhenius equation is given as follows:

$$\ln(k) = \ln(A) - E_a / RT$$

In the above equation:

k = the reaction rate constant

A = Pre-exponential factor (demonstrate the collision frequency between the reactant during the reaction)

E_a = Activation energy of adsorption (kJ mol^{-1})

R = Ideal gas constant (8.31 J $mol^{-1}K^{-1}$)

T = Absolute temperature (K)

When the activation energy is found to be 5-30 kJ $mol^{-1,}$ then the adsorption is described as physical adsorption, while for the chemical adsorption, the value of activation energy should be higher than 80 kJ mol^{-1} [583].

1.2 A: Error Analysis

It has been already mentioned that the experimentation involving soaking of composites in metal ion solutions to gauge removal efficiencies was done in triplicate to ascertain reproducibility error. For each optimised soaking experiment (from which AAS or ICP-MS data had been obtained), the standard error (SE) for recorded data was carried out by using the following formula in Microsoft Excel:

$$SE = \frac{\sigma}{\sqrt{n}}$$

Where "σ" is the standard deviation and "n" is the number of measurement/replications.

1.3A: Non-linear regression functions (Error Functions)

A method to overcome the limitations of the linear regression for the adsorption modelling (mentioned in section 1.6), is to use non-linearised regression functions by employing the true sorption modelling equations to fit the data to a model. It requires an assessment of the error analysis using the error functions (or non-linear regression functions) to optimise procedure[584].

Different non-linear regression functions have been used to determine the best-fit model in earlier literature by calculating the coefficient of determination (R^2) for non-linear

regression functions[338,585]. Among them, a few that have been used in this study for adsorption and kinetic modelling of experimental data are given below[336].

1. The sum of the squares of the errors (SSE):

1-A

$$SSE = \sum_{i=1}^{n} \left(q_{e,calc} - q_{e,exp}\right)_i^2$$

2. The sum of the absolute errors (SAE):

1-B

$$SAE = \sum_{i=1}^{n} \left|q_{e,calc} - q_{e,exp}\right|_i$$

3. The average relative error (ARE):

1-C

$$ARE = \frac{100}{n} \sum_{i=1}^{n} \left|\frac{q_{e,exp} - q_{e,calc}}{q_{e,exp}}\right|_i$$

4. The hybrid functional error function (HYBRID):

1-D

$$HYBRID = \frac{100}{n-p} \sum_{i=1}^{n} \left[\frac{\left(q_{e,exp} - q_{e,cal}\right)^2}{q_{e,exp}}\right]_i$$

5. Marquardt's percent standard deviation (MPSD):

1-E

$$MPSD = 100 \sqrt{\frac{1}{n-p} \sum_{i=1}^{n} \left(\frac{q_{e,exp} - q_{e,calc}}{q_{e,exp}}\right)_i^2}$$

6. Non-linear Chi-test (χ2-test): (It was used for the non-linear regression analysis of kinetics data to fit the kinetics models in the two-metal ion type solution systems).

Equation 1-F

$$\chi 2 = \frac{\Sigma\,(qe,\exp\ -\ qe,th)2}{qe,th}$$

In the above equations, $q_{e,cal}$ and $q_{e,exp}$ are the adsorbate quantities at adsorption equilibrium in mg g^{-1}. $q_{e,cal}$ is calculated by model equations equation (using the solver

add-in in Microsoft Excel) and $q_{e,exp}$ is calculated theoretically by experimental data (using equation 4-1).

"n" represents the number of points in a data set, for instance, in the present study, while "p" represents the number of the adsorption isotherm parameters calculated. For instance, for the Langmuir and Freundlich isotherm model, the number of the parameters calculated is 2.

The adsorption isotherm parameters were calculated for each of the functions using Microsoft excel solver add-in. All non-linear regression functions produce different adsorption isotherm parameters with different coefficients of determination (R^2). The best-fitted parameter set is decided by comparing the R^2 values. The error function which produces the highest (close to one) R^2 value is selected as the best-fitted modelling data for describing the adsorption isotherm for a particular adsorption data.

Non-linear regression method for adsorption isotherm model fitting: Example

Step 1: Enter experimental data values from the batch experiment as C_i, C_e and q_e. Initially, suppose the values of model parameters are close to the experimental values.

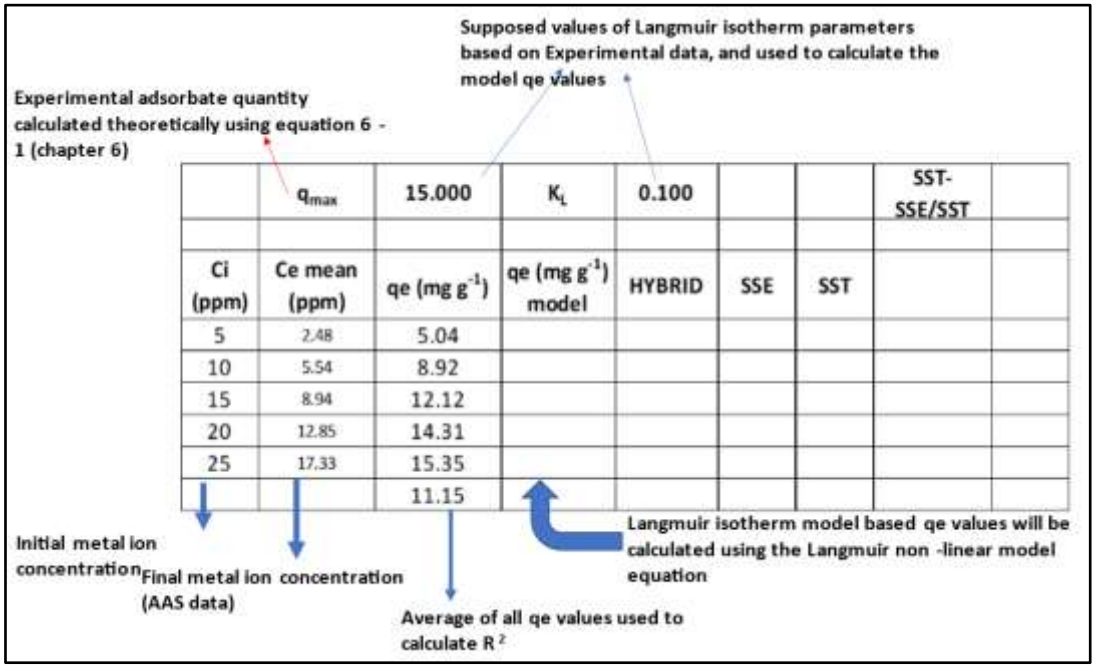

	q_{max}	15.000	K_L	0.100			SST-SSE/SST	
Ci (ppm)	Ce mean (ppm)	qe (mg g^{-1})	qe (mg g^{-1}) model	HYBRID	SSE	SST		
5	2.48	5.04						
10	5.54	8.92						
15	8.94	12.12						
20	12.85	14.31						
25	17.33	15.35						
		11.15						

Step 2: Calculate Langmuir model parameter values, using the adsorption model equation i.e. the Non-linear Langmuir model, to calculate the q_e value for the model (using the supposed parameter values)

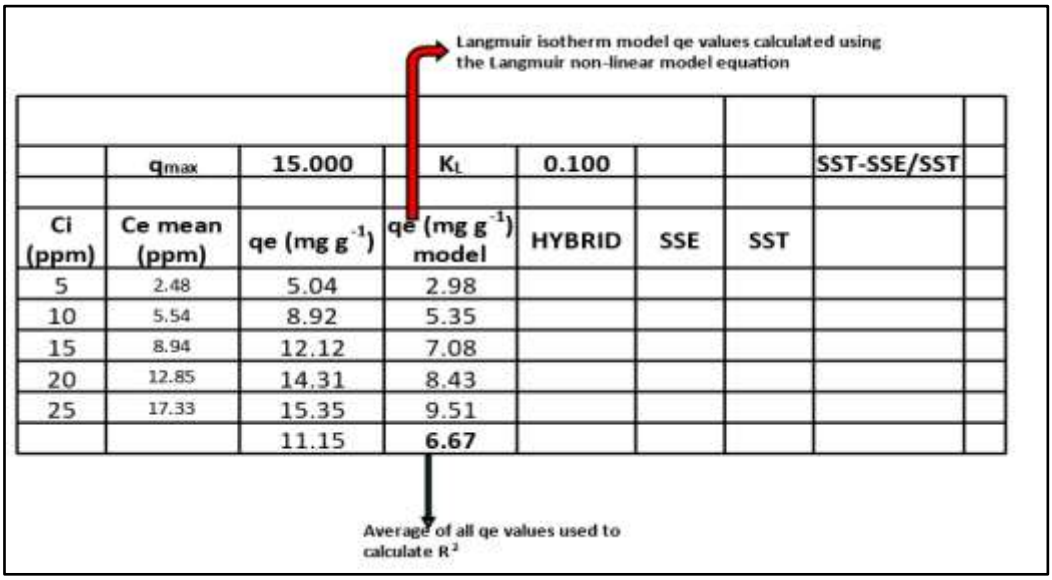

	q_{max}	15.000	K_L	0.100			SST-SSE/SST	
Ci (ppm)	Ce mean (ppm)	qe (mg g^{-1})	qe (mg g^{-1}) model	HYBRID	SSE	SST		
5	2.48	5.04	2.98					
10	5.54	8.92	5.35					
15	8.94	12.12	7.08					
20	12.85	14.31	8.43					
25	17.33	15.35	9.51					
		11.15	**6.67**					

Step 2: Calculate the error values using the error analysis functions (non-linear regression function) given above in equations 1-A to 1-D (one by one).

For instance, we use the hybrid error function to calculate the error, by using the q_{exp} values and $q_{e,cal}$ values, the Hybrid error function is given as follows :

$$HYBRID = \frac{100}{n-p} \sum_{i=1}^{n} \left[\frac{(q_{e,exp} - q_{e,cal})^2}{q_{e,exp}} \right]_i$$

In the above formula,

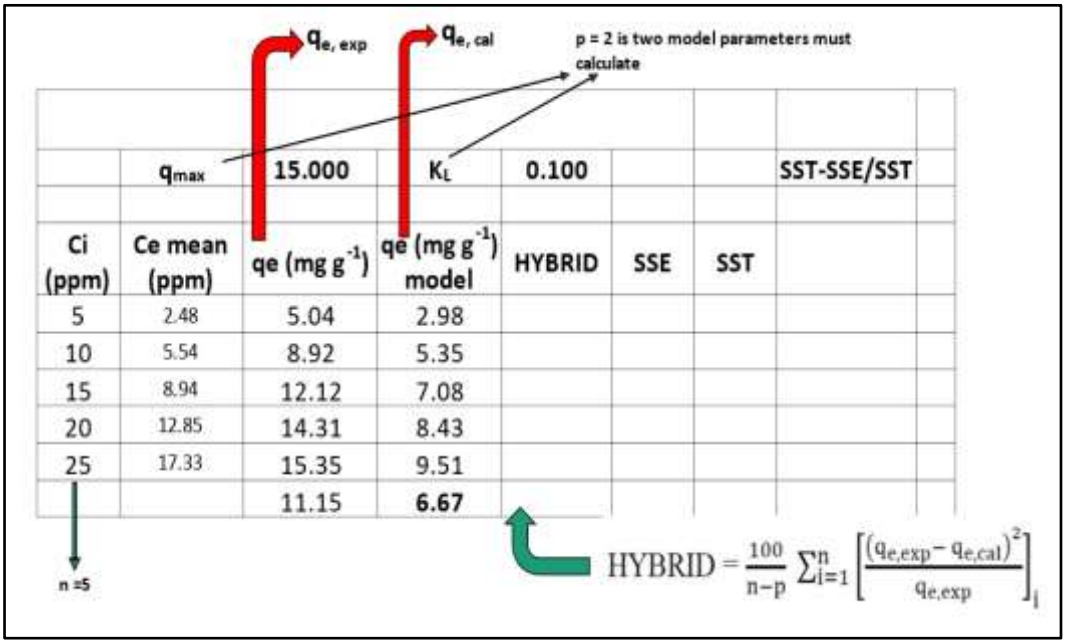

	q_{max}	15.000	K_L	0.100			SST-SSE/SST	
Ci (ppm)	Ce mean (ppm)	qe (mg g^{-1})	qe (mg g^{-1}) model	HYBRID	SSE	SST		
5	2.48	5.04	2.98					
10	5.54	8.92	5.35					
15	8.94	12.12	7.08					
20	12.85	14.31	8.43					
25	17.33	15.35	9.51					
		11.15	**6.67**					

HYBRID Error function								
	q_{max}	15.000	K_L	0.100			SST-SSE/SST	
Ci (ppm)	Ce mean (ppm)	qe (mg g^{-1})	qe (mg g^{-1}) model	HYBRID	SSE	SST		
5	2.48	5.04	2.98	0.8379				
10	5.54	8.92	5.35	1.4326				
15	8.94	12.12	7.08	2.0951				
20	12.85	14.31	8.43	2.4118				
25	17.33	15.35	9.51	2.2192				
		11.15	6.67	8.9965				
				299.8827				

Important to note that the value of error is very high for the suppose value of qmax and k_L (model parameters)

Step 2: Calculate the coefficient of determination value (R^2) using the experimental and calculated q_{max} values:

which is given as

R^2 = SST -SSE / SST

$$SST = \sum (y - \bar{y})^2$$

$$SSE = \sum (y - \hat{y})^2$$

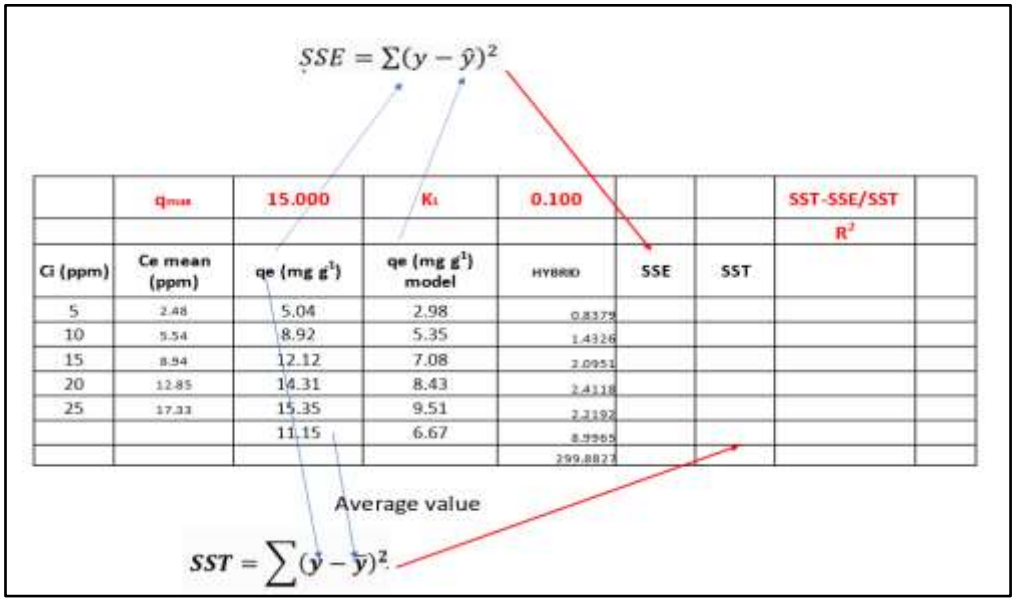

- After the calculation of SST, SSE and R^2, the following was obtained:

HYBRID Error function								
	q_{max}	15.000	K_L	0.100			SST-SSE/SST	
Ci (ppm)	Ce mean (ppm)	qe (mg g^{-1})	qe (mg g^{-1}) model	HYBRID	SSE	SST	R^2	
5	2.48	5.04	2.98	0.8379	37.33	4.220	-0.566	
10	5.54	8.92	5.35	1.4326	4.95	12.782		
15	8.94	12.12	7.08	2.0951	0.95	25.391		
20	12.85	14.31	8.43	2.4118	10.00	34.509		
25	17.33	15.35	9.51	2.2192	17.64	34.057		
		11.15	**6.67**	**8.9965**	**70.87**	**110.96**		
				299.8827				

Note the values of $q_{max,}$ K_L ,R^2 and Hybrid error values (299.88). The next step is to minimise the error value to calculate the best-fitted model values with optimised parameter values, which would also allow calculation of the maximum possible R^2 value

Step 3: Calculate the error values again using the excel solver add in, for this:

2. Click on the solver function (if not found then it needs to be added into task bar by using the (file < options< add <excel add in < go < solver-add in <ok) ,
When we click the solver add-in, it opens a drop box as follows

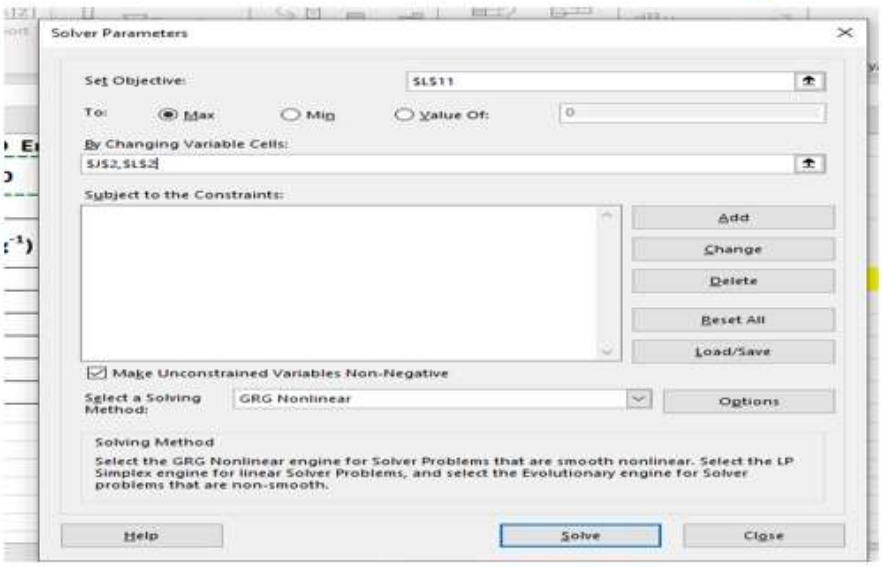

1. In set Objective tab: select the “cell” with error value calculated
2. In variable cells tab select the cells with q_{max} and K_L values
3. Select the minimise option just below the objective cell, to select the error value in the objective cell, and to minimise the error values for our calculated models values to find the best fit

For example:

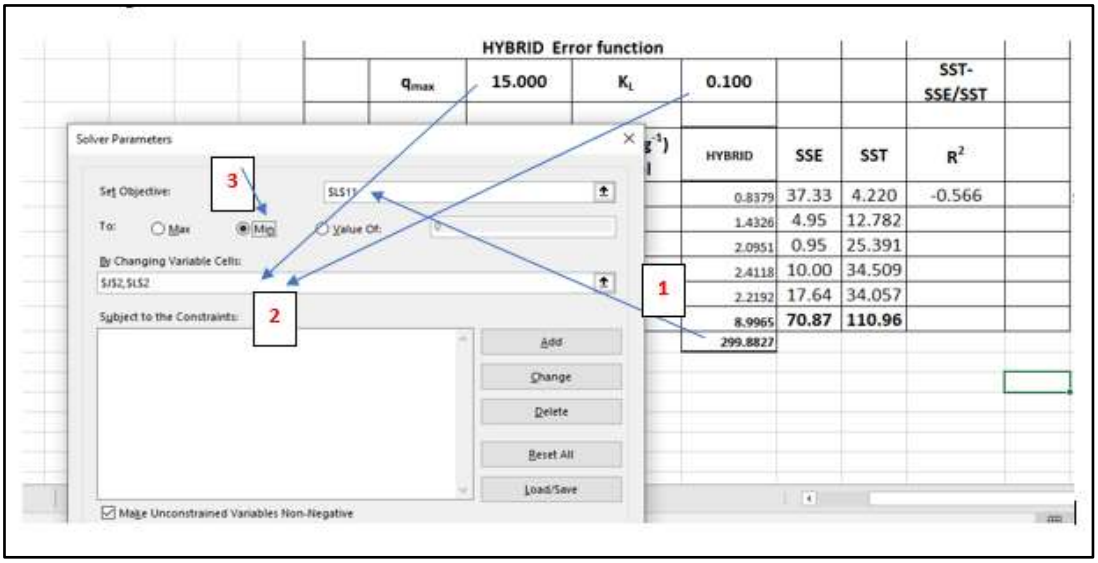

Step 4: After selecting all these options, click the solve button at the bottom of the dialog box, it will give the following dialogue box

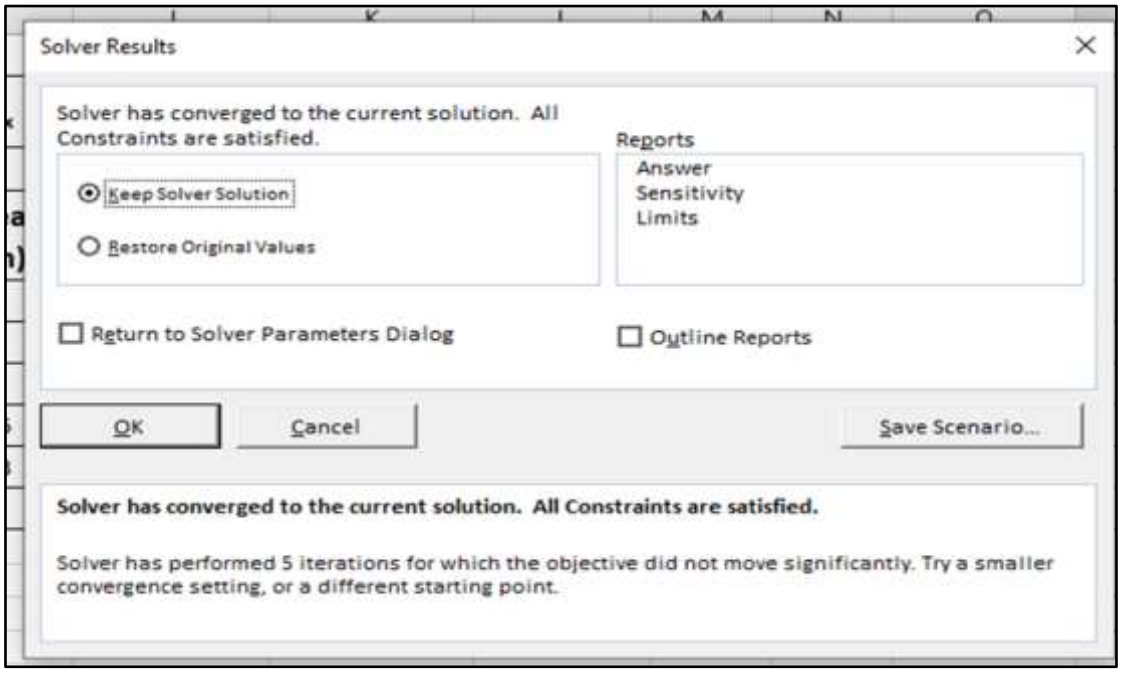

Step 5: Click OK; it will calculate the optimised values of the parameters by calculating the minimum error and maximum R^2 value. Those values correspond to the best-fit model values that can be used to plot the graph.

HYBRID Error function								
	q_{max}	24.058	K_L	0.109			SST-SSE/SST	
Ci (ppm)	Ce mean (ppm)	qe (mg g^{-1})	qe (mg g^{-1}) model	HYBRID	SSE	SST	R^2	
5	2.48	5.04	5.11	0.0010	37.33	0.005	0.996	
10	5.54	8.92	9.03	0.0014	4.95	0.013		
15	8.94	12.12	11.85	0.0060	0.95	0.073		
20	12.85	14.31	14.01	0.0062	10.00	0.088		
25	17.33	15.35	15.71	0.0085	17.64	0.130		
		11.15	**11.14**	0.0230	**70.87**	**0.31**		
				0.7683				

Compare the values of model parameters, R^2, and error values before and after using the solver add-in function. The calculated error is thee minimum value as it has reduced from 299.88 to 0.7683; similarly, the values of R^2, q_{max} and K_L have also been changed.

The same method is employed by using all the mentioned error functions (non-linear regression function in equation 1A-1E) for each model. For example, all the error functions would be used to calculate the q_{max} and K_L values of the Langmuir isotherm model, which will be different with different R^2 values. The best-fitted parameters values would be selected by comparing the R^2 values calculated for each error function. The parameter set, with maximum R^2 (close to unity), would be selected as the best-fitted set for the Langmuir to plot and fit the experimental values.

A similar method using the error function would be repeated for the Freundlich isotherm model and to plot the Freundlich model fitted to the experimental data.

Finally, the R^2 values of the Langmuir model and the Freundlich model would be compared to find out the best fit model between the two.

1.3B: The sum of normalised error (SNE)

All the non-linear regression function values make it more challenging to select the optimum parameter set for a sorption isotherm as they lie very close to each other. Hence a procedure was introduced to calculate the sum of normalised error (SNE), taking into account all the parameter sets calculated by all error functions to find out the non-biased optimised parameter set of sorption isotherm to fit the experimental data [584,586]. The following method was used as an example only for the adsorption modelling of the Cd^{2+} and Pb^{2+} ion adsorption data on the first two composite systems. While for the rest of the

systems and metal ions, only the functions mentioned above were used for the non-linear regression method to calculate the adsorption isotherm parameters.

The sum of normalised error (SNE) was calculated to standardise the adsorption modelling using the following procedure as described in the literature [584,586]:

1. Adsorption Isotherm parameters (e.g., q_{max} and K_L for the Langmuir adsorption isotherm model) were calculated by selecting one error function (from the functions mentioned above) at a time to by selecting the minimise error option on Microsoft excel-solver add-in.
2. One parameter set calculated by one error function was used to calculate the parameters sets for other error functions. It was repeated for all parameter sets calculated by all error functions to calculate all associated errors.
3. All error values for a parameter set (calculated for all error functions) were divided by the maximum value of that error function to get all normalised errors
4. Lastly, add up all normalised errors for one parameter set

Hence, the parameter set that gives the least normalised error value is selected as the optimum set of parameters to fit the experimental data best.

Appendix 2

The masses of the salts used to prepare 1 M stock solutions of metal ions in 1000 mL volume is given in the following table.

Table 2-1: Metal ion salts to prepare solutions of 1 M (1000 ppm) concentration in a 1 L volume

Metals	Molar mass of salt used	Atomic mass (amu)	Mass of metal ion salt in g /L	Volume prepared
Cd	228.36	112.411	2.0314 ($CdCl_2$. $2.5H_2O$)	1 L
	308.47		2.7441 ($Cd(NO_3)_2$. $4\ H_2O$)	1 L
Pb	331.208	207.2	1.5985 ($Pb(NO_3)_2$)	1 L
Cr	294.185	51.9961	5.6578 ($K_2Cr_2O_7$)	1 L
Cu	159.60	63.546	2.5116 ($CuSO_4$)	1L

Appendix 3

3.1A: Average particle sizes and estimated specific surface areas of the synthesised composites

Matersizer Analysis: Method

The grain (or particle) size distribution was measured using a Malvern Mastersizer 3000, which produced results in 100 logarithmically spaced size classes of particles (in volume distributions) ranging from 0.01 to 10,000 μm. The particle size distributions were given as three percentiles, namely the Dv(10), Dv(50) and Dv(90), which are interpreted below (in results interpretations). The materials were "composites" in nature, so the refractive index value was taken as 1.5 for all the composites.

The ground sample of the composites was used to make a suspension of materials in water. The suspension was added to the "measurement cell" containing water as a solvent to make a suspension (containing at least 1% weight of sample), and results were collected as an average of the three replicates.

Working principle of the instrument used in particle size measurement of the composites

The Malvern Masterszier uses a laser diffraction method (LDM) to measure the particle size distribution in terms of volume percentage. For this, a monochromatic laser beam is passed through the measurement cell containing the suspended particles of the sample. It was assumed that the particles are spherical, which would cause the scattering of the light beam, and will scatter the light at an angle that would be directly related to particle size[481,587].

Limitations of the analysis

Ground samples of the composite materials were used to analyse the average grain sizes of the materials. The materials were ground using a mortar and pestle, which gave a relatively heterogeneous sample in terms of the grain sizes. Additionally, some of the composites were extremely heterogeneous in nature due to their composition, for instance, the CH/HAp/CF and CH/HAp/SCGs, which were rendered heterogeneous in nature on account of the presence of coir fibre and spent coffee grounds in them. In comparison, some other composites were relatively less heterogeneous, for instance, the CH/HAp composites.

Additionally, the instrument measures the particle sizes on the assumption of spherical particles; it is not very accurate for the true measurement of the samples with irregular and angular shapes. The synthesised materials were not uniform in size, so this analysis was used to take an estimation of particle sizes and specific surface area of the composites.

Interpretations of results

The plot is presented as the particle sizes in micrometre (μm) at the horizontal axis and the percentage volume of the particles at the y-axis (vertical axis). The term Dv(10), Dv(50) and Dv(90) are broadly expressed to illustrate the percentage of the particle sizes. The Dv(10) indicates that 10 % of the particles are smaller than the diameter given as Dv (10). Similarly, Dv(50) illustrates that 50 percent particles are less or greater than the diameter given as Dv(50), which gives the median value of particle size of the sample[588]. And Dv(90) describes the 90% of the particles are less than the diameter (micrometre). For instance, if the sample analysis using the Mastersizer is showing the grain sizes as:

Dv(10) 100 μm

Dv(50) 250 μm

Dv(90) 200 μm

Then it would be expressed as: 10% of the grain sizes of the samples are less than 100 μm, 50 % are less than or greater than 250 μm (as it is the median value) and 90% of the grain sizes are less than 200 μm.

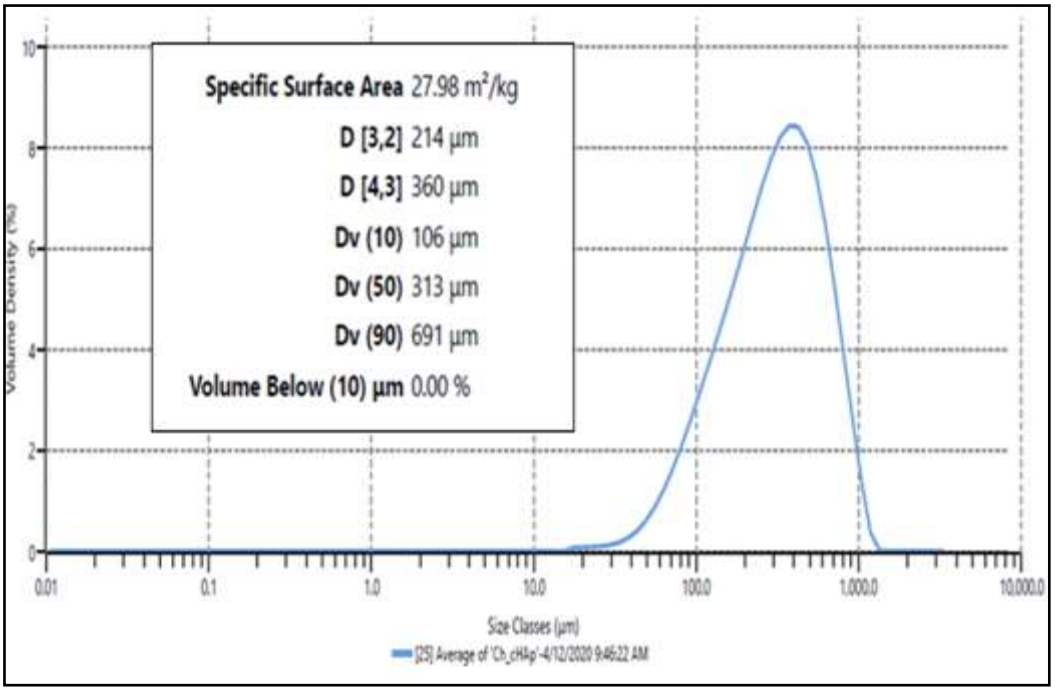

Figure 3A: The average particle size of the CH/cHAp composites and estimated specific surface area (the results are presented as an average of three replicates)

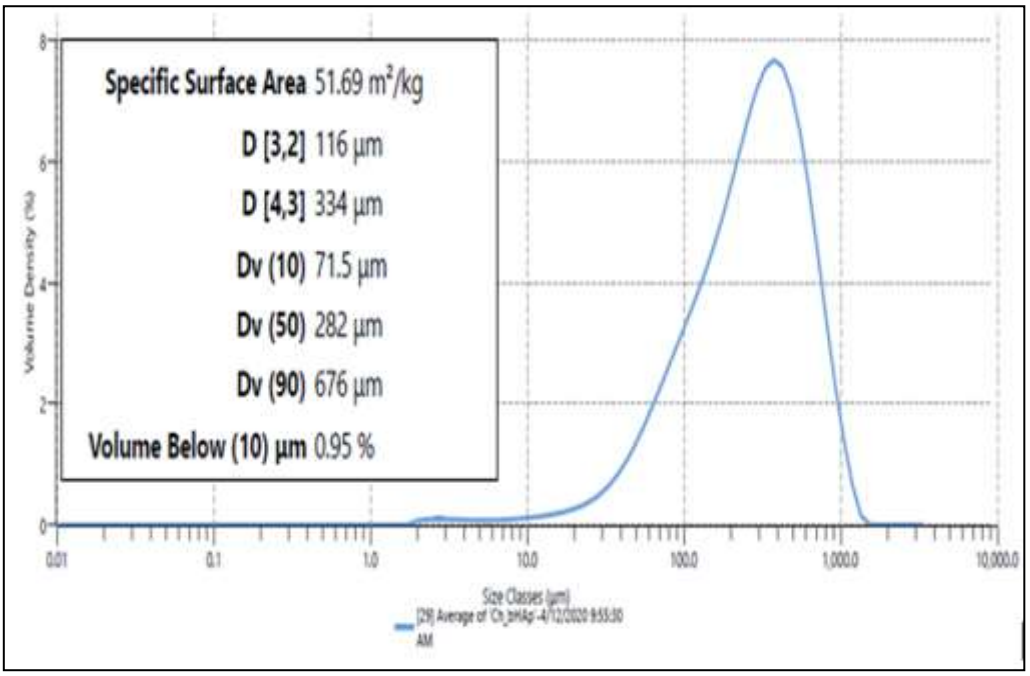

Figure 3B: The average particle size of CH/bHAp composites and estimated specific surface area (the results are presented as an average of three replicates)

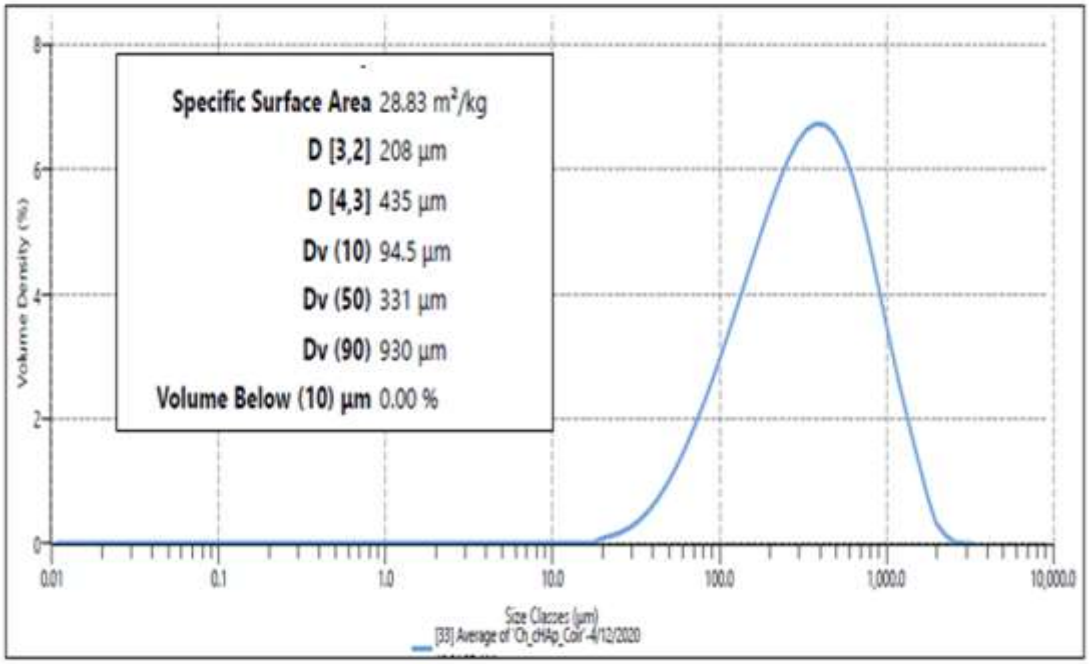

Figure 3 C: The average particle size of CH/cHAp/CF composites and estimated specific surface area (the results are presented as an average of three replicates)

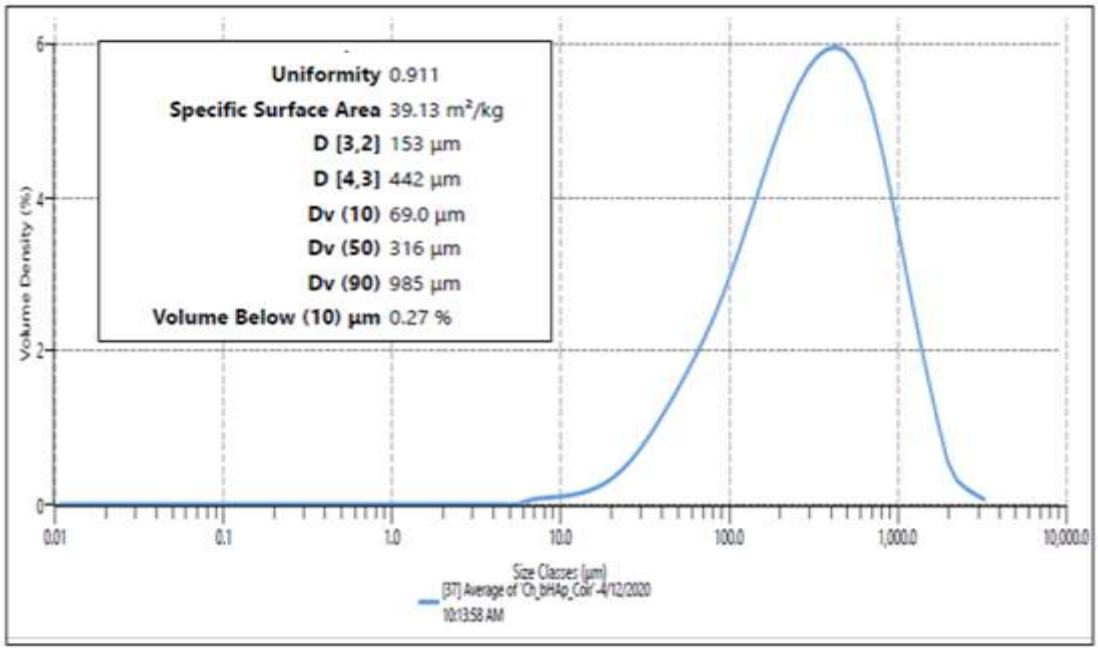

Figure 3 D: The average particle size of CH/bHAp/CF composites and estimated specific surface area (the results are presented as an average of three replicates)

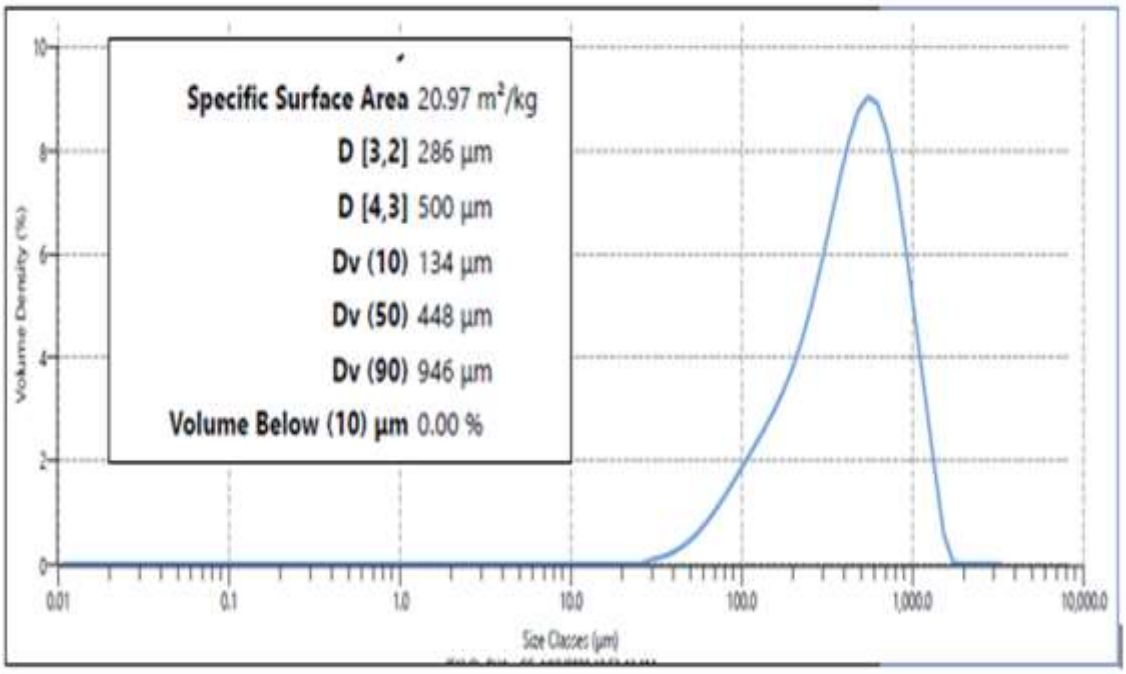

Figure 3 G: The average particle size of CH/cHAp/SCGs composites and estimated specific surface area (the results are presented as an average of three replicates)

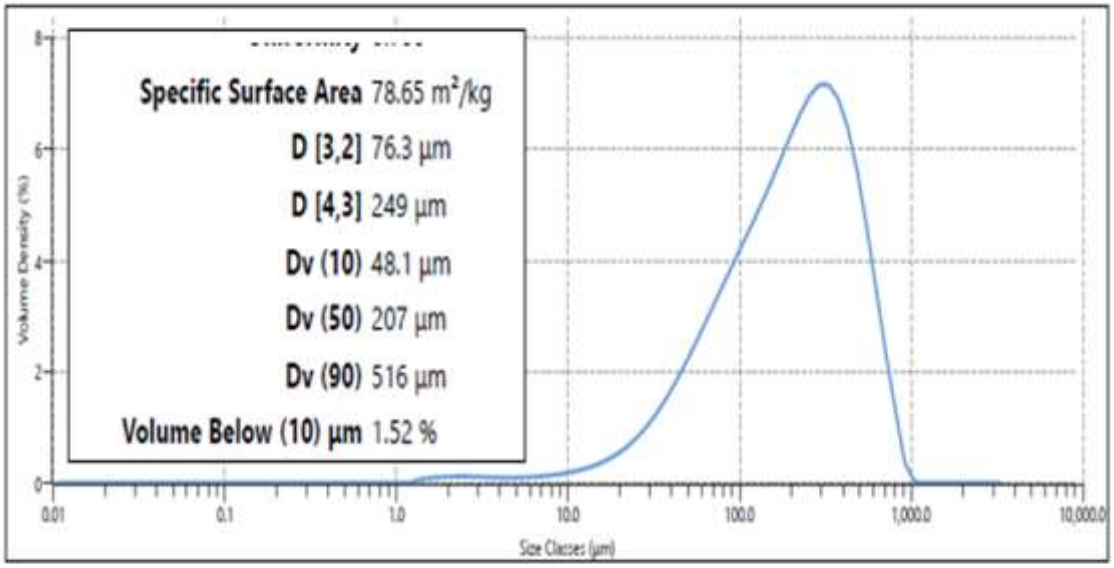

Figure 3 H: The average particle size of CH/bHAp/SCGs composites and estimated specific surface area (the results are presented as an average of three replicates

Appendix 4

The following section includes the plots for illustrating the effect of various experimental factors on the removal efficiency of the synthesised composites. The plots were drawn by using the OriginPro software. For the following plots, the scales of x-axis and y-axis were selected manually.

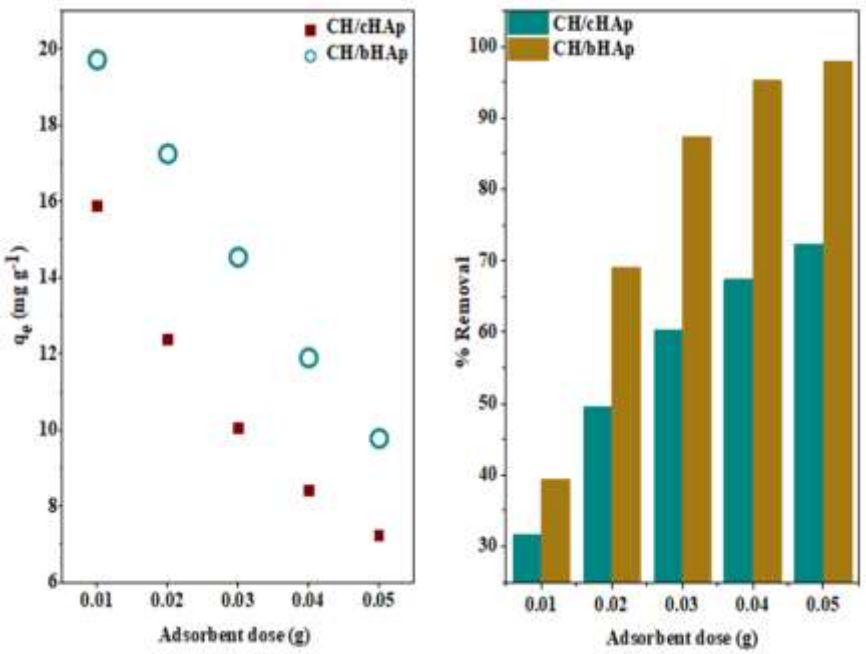

Figure 4-1: AAS results showing the effect of adsorbent dose on Cd^{2+} ion removal and adsorption of Cd^{2+} ion on the CH/HAp composites: Results are presented as the average of measurements from 3 replicates. SE = ± 0.1

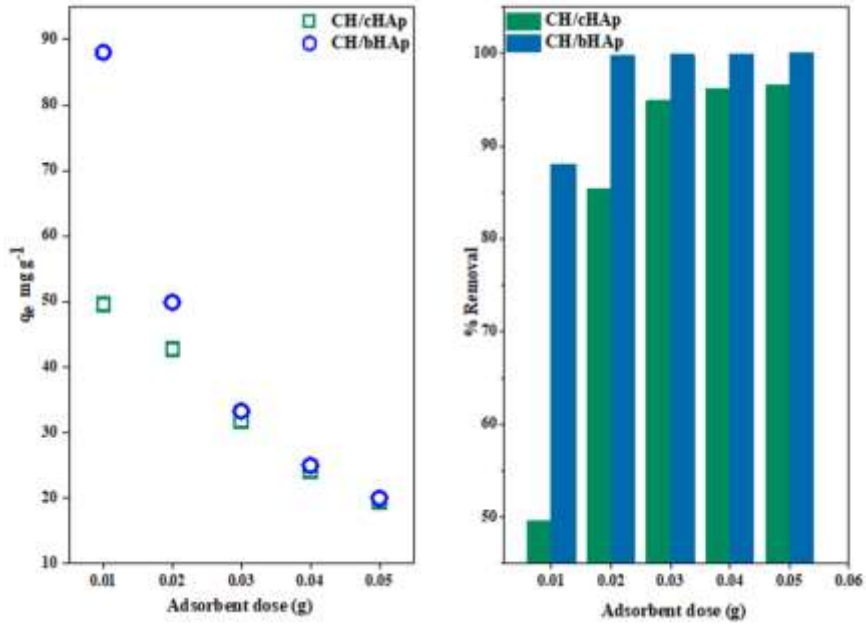

Figure 4-2: AAS results showing the effect of adsorbent dose on Pb^{2+} ion removal and adsorption of Pb^{2+} ion on the CH/HAp composites: Results are presented as the average of measurements from 3 replicates. SE = ± 0.1

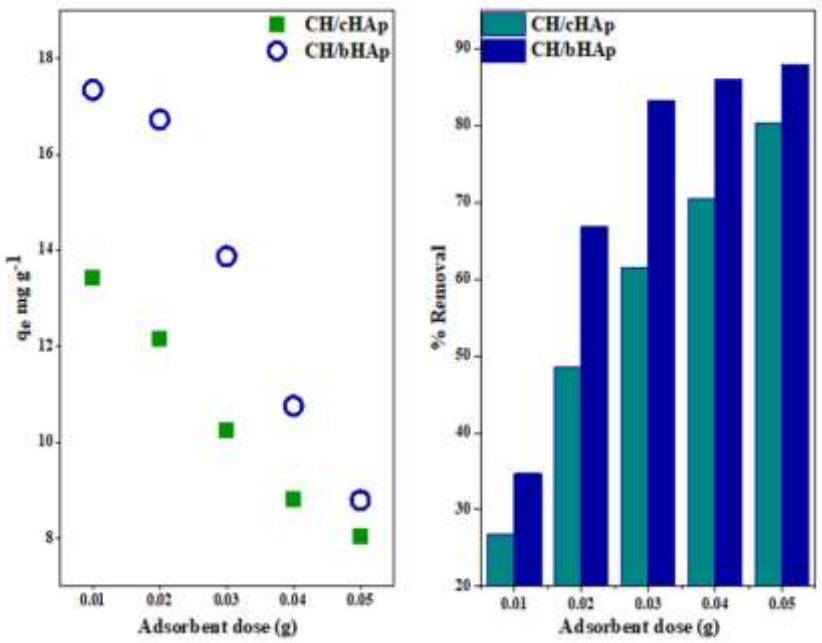

Figure 4-3: AAS results showing the effect of adsorbent dose on Cu^{2+} ion removal and adsorption of Cu^{2+} ion on the CH/HAp composites: Results are presented as the average of measurements from 3 replicates. SE = ± 0.1

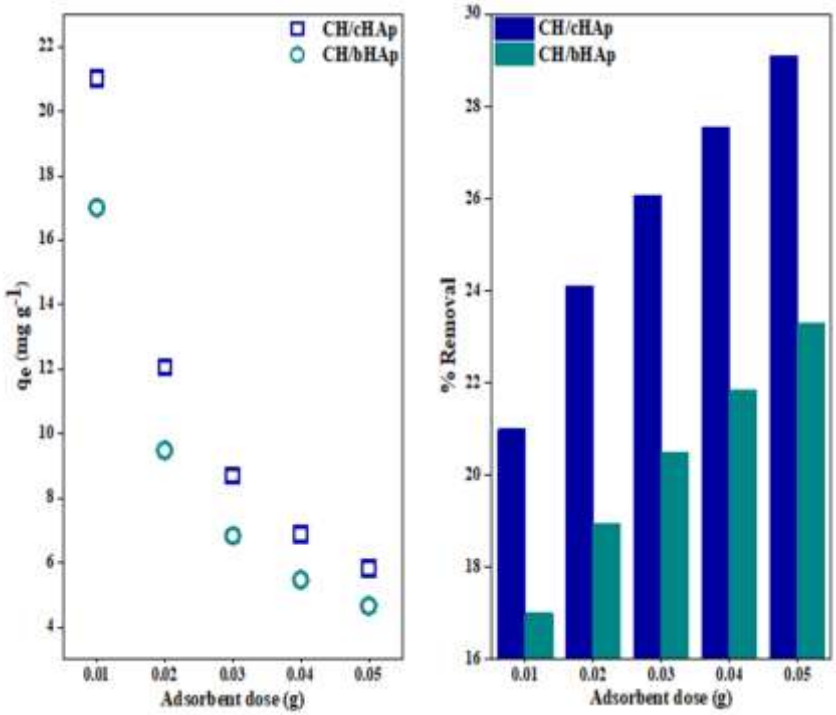

Figure 4-4: AAS results showing the effect of adsorbent dose on chromate ion removal and adsorption of chromate ion on the CH/HAp composites: Results are presented as the average of measurements from 3 replicates. SE = ± 0.1

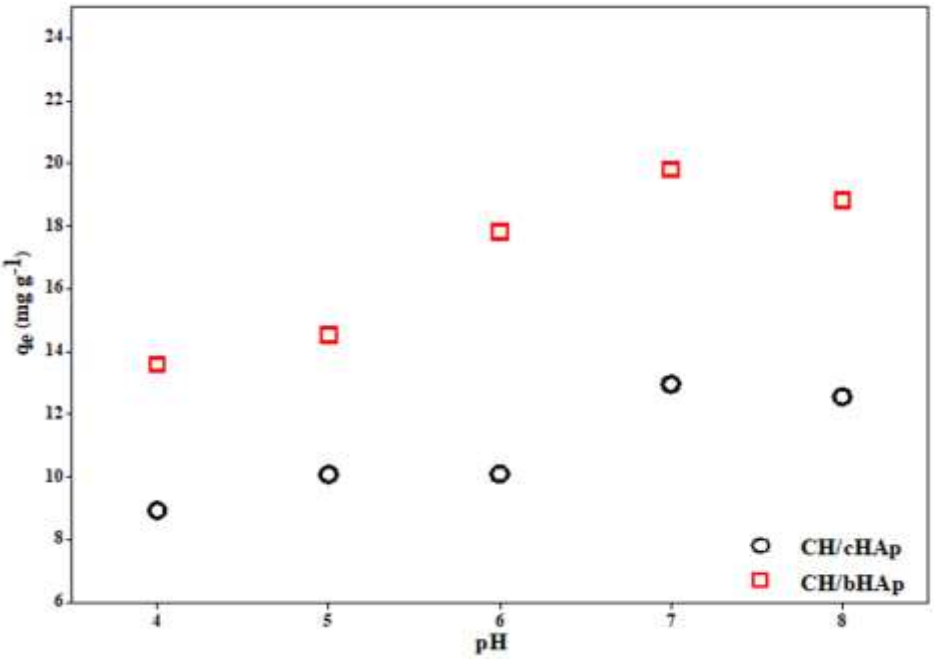

Figure 4-5: AAS data showing the effect of initial solution pH on Cd^{2+} adsorption on the CH/HAp composites. Results are reported as the average of 3 replicates. SE=±0.01

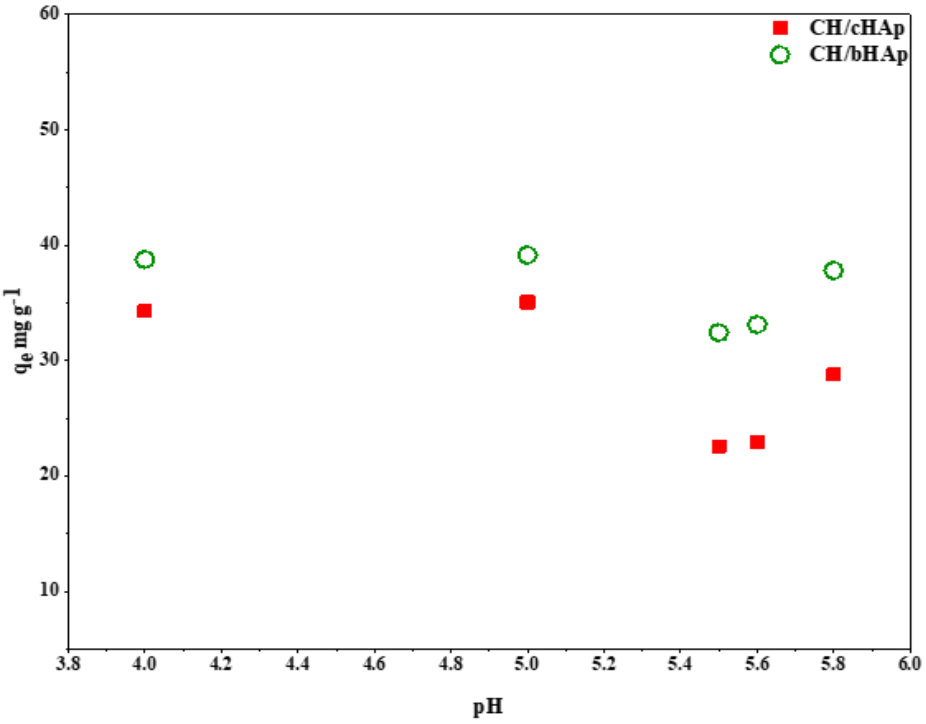

Figure 4-6: AAS data showing the effect of initial solution pH on Pb^{2+} adsorption on the CH/HAp composites. Results are reported as the average of 3 replicates. SE=±0.1

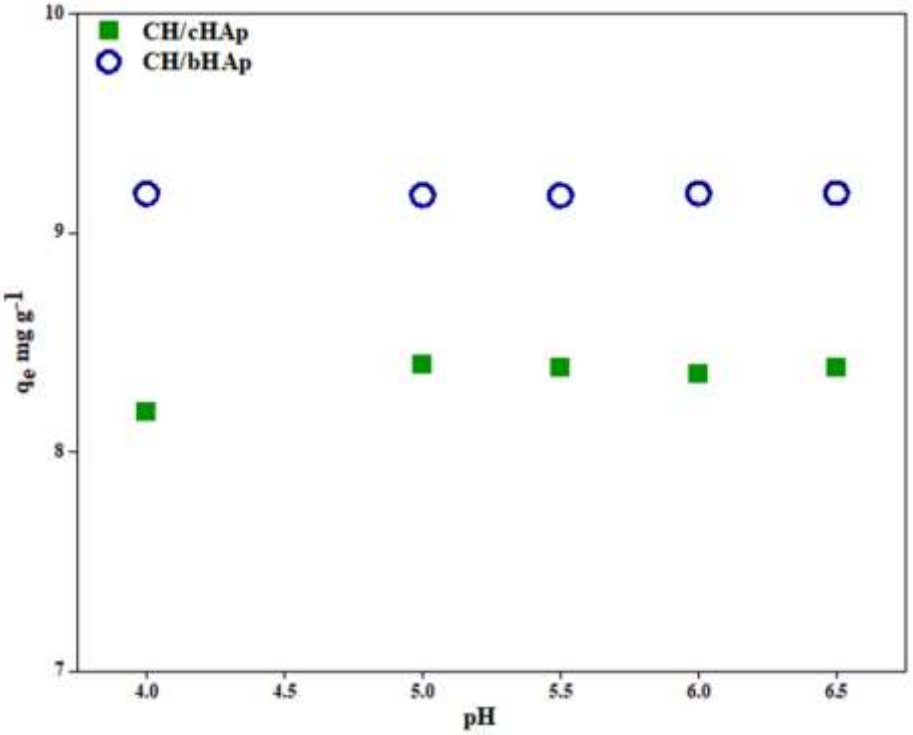

Figure 4-7: AAS data showing the effect of initial solution pH on Cu^{2+} adsorption on the CH/HAp composites. Results are reported as the average of 3 replicates. SE=±0.01

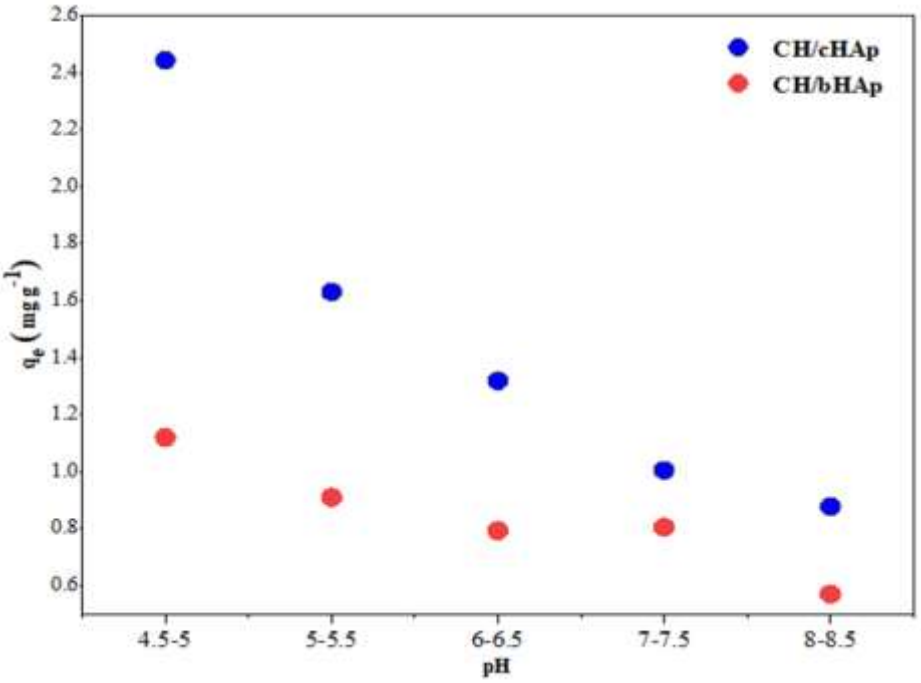

Figure 4-8: AAS data showing the effect of initial solution pH on chromate ion adsorption on the CH/HAp composites. Results are reported as the average of 3 replicates. SE=±0.01

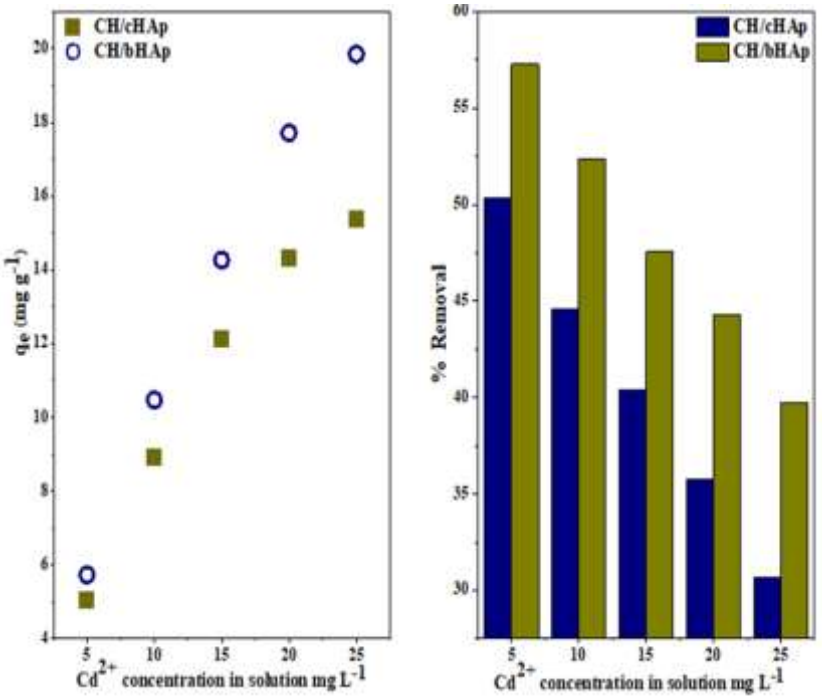

Figure 4-9: AAS data showing the effect of initial metal ion concentration on Cd^{2+} adsorption on the CH/HAp composites. Results are calculated as an average of 3 replicates. SE = ± 0.1.

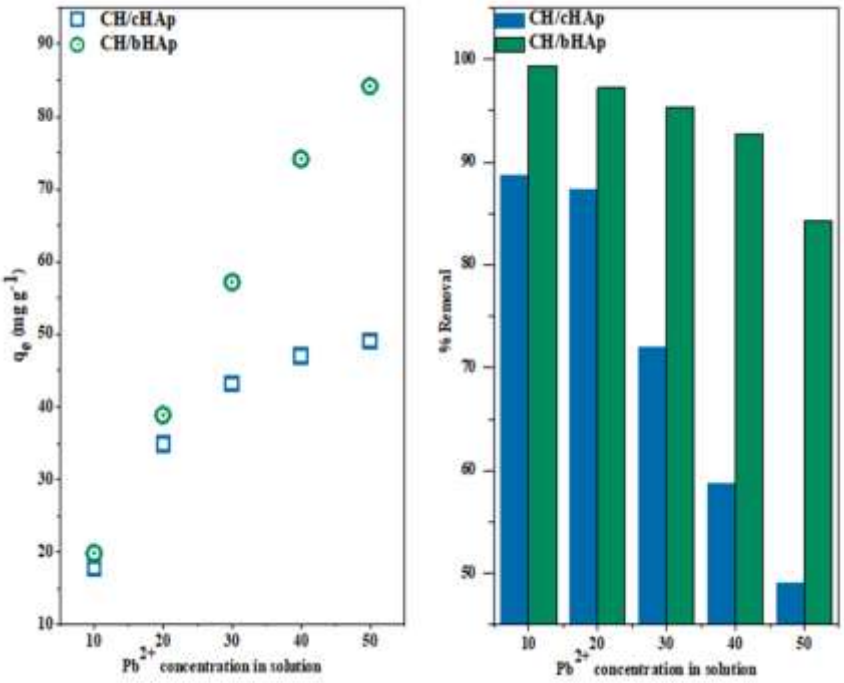

Figure 4-10: AAS data showing the effect of initial metal ion concentration on Pb^{2+} adsorption on the CH/HAp composites. Results are calculated as an average of 3 replicates. SE = ± 0.1.

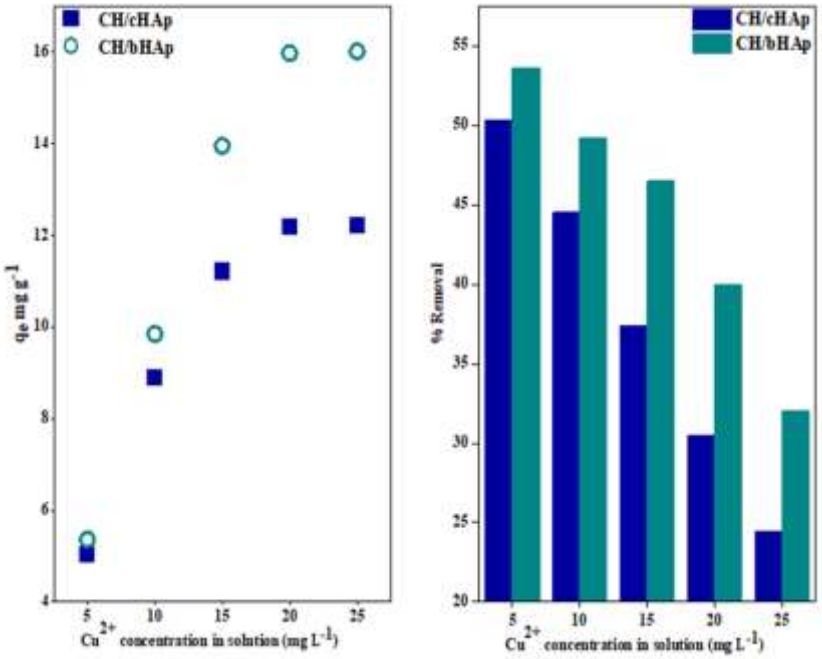

Figure 4-11: AAS data showing the effect of initial metal ion concentration on Cu^{2+} adsorption on the CH/HAp composites. Results are calculated as an average of 3 replicates. SE = ± 0.1.

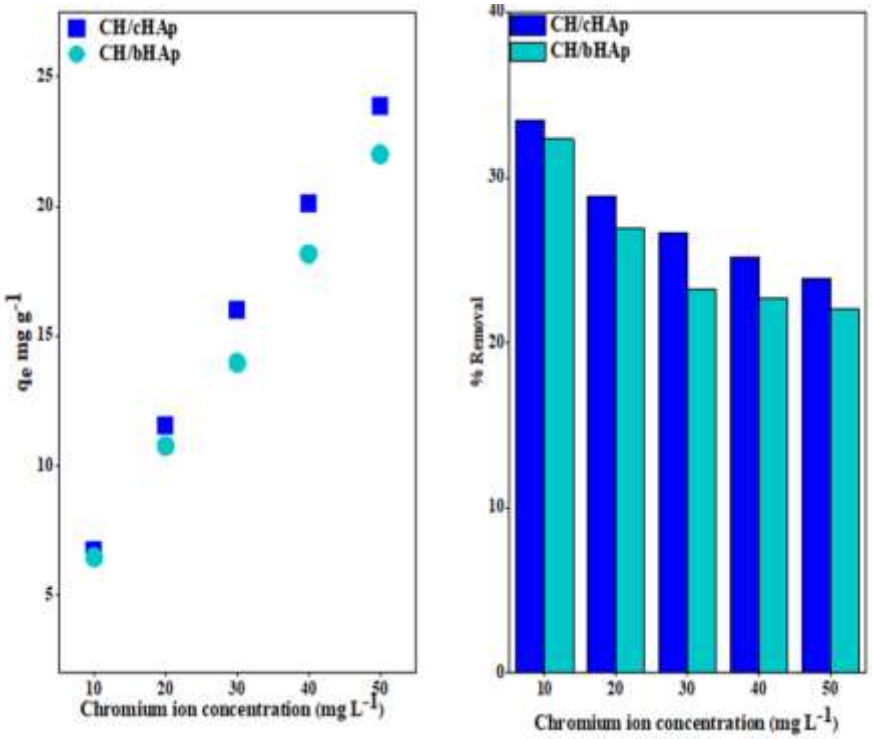

Figure 4-12: AAS data showing the effect of initial metal ion concentration on chromate ion adsorption on the CH/HAp composites. Results are calculated as an average of 3 replicates. SE = ± 0.1.

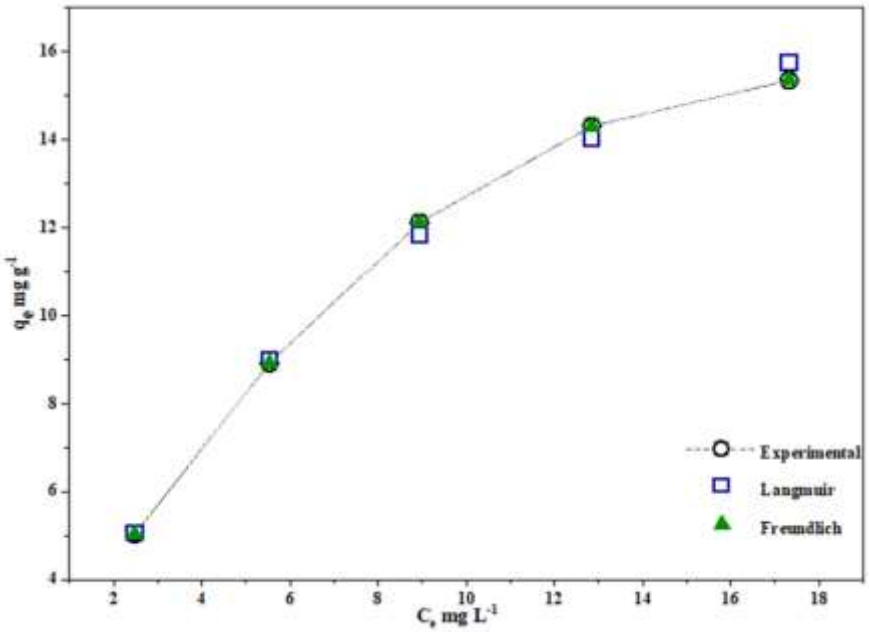

Figure 4-13: Graph showing the fitting of the non-linear Langmuir and Freundlich adsorption models to the experimental data for Cd^{2+} adsorption on the CH/cHAp composite

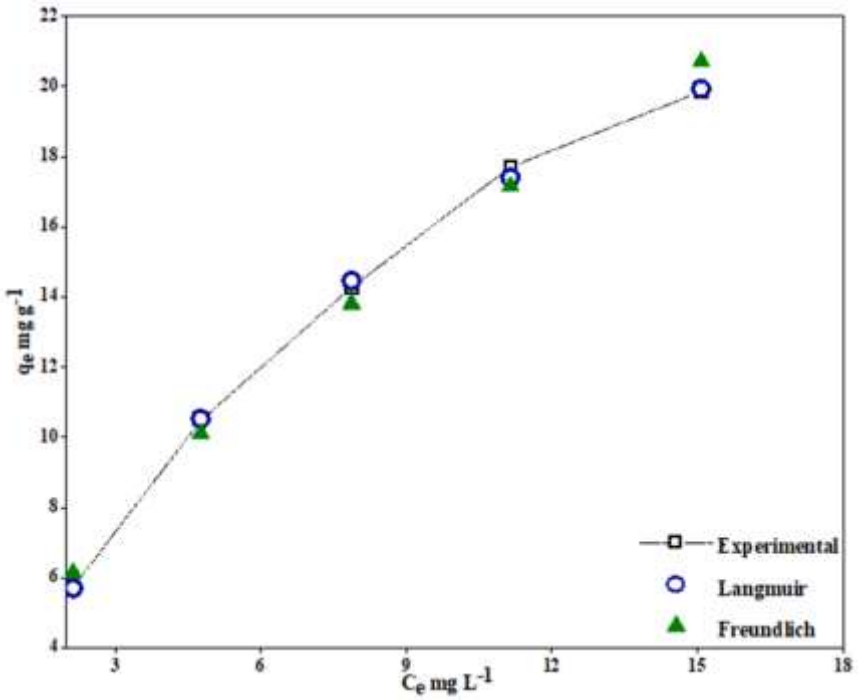

Figure 4-14: Graph showing the fitting of the non-linear Langmuir and Freundlich adsorption models to the experimental data for Cd^{2+} adsorption on the CH/bHAp composite

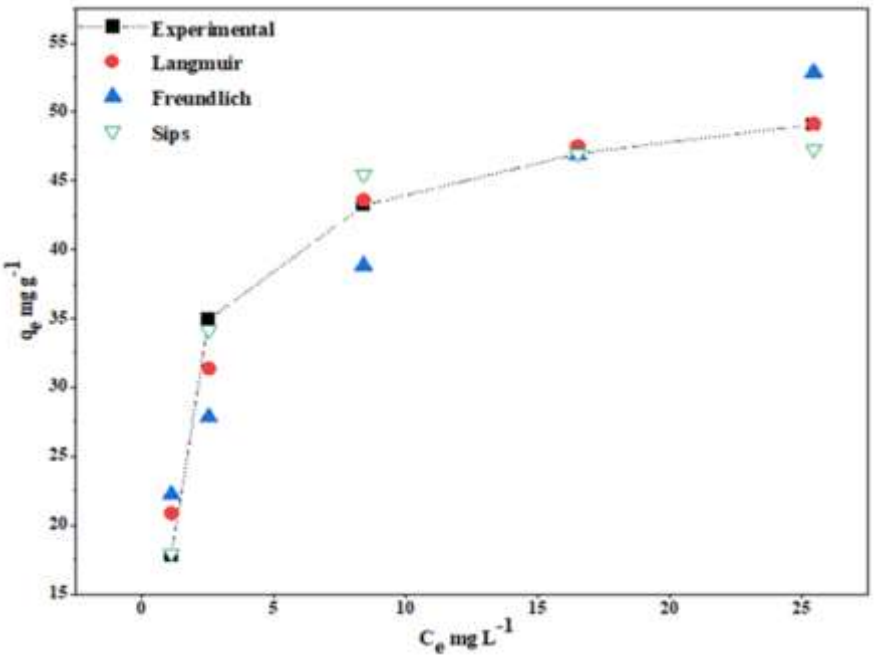

Figure 4-15: The fitting of various non-linear adsorption models to experimental data for Pb^{2+} adsorption on the CH/cHAp composites

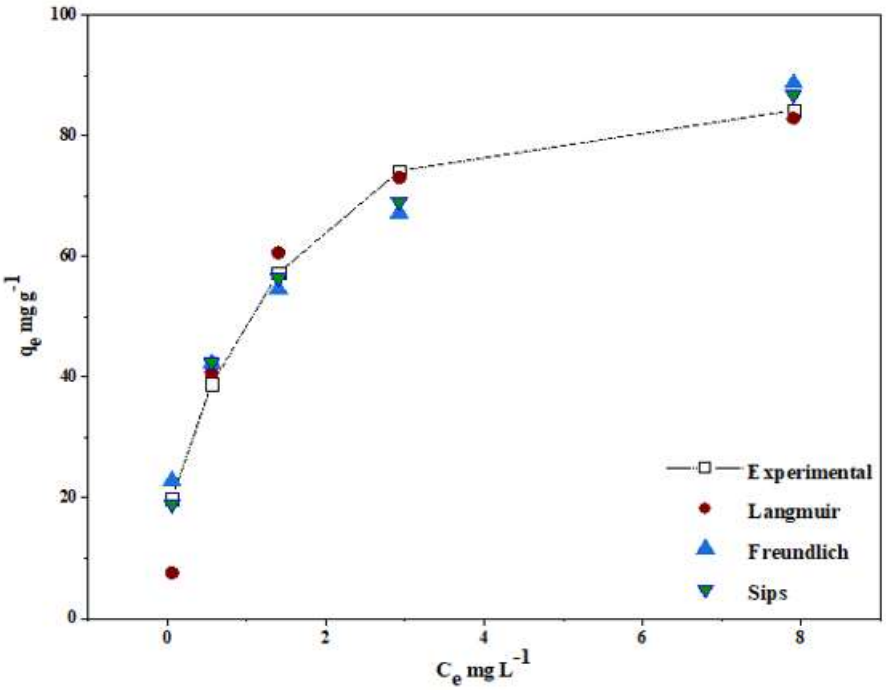

Figure 4-16: The fitting of various non-linear adsorption models to experimental data for Pb^{2+} adsorption on the CH/bHAp composites

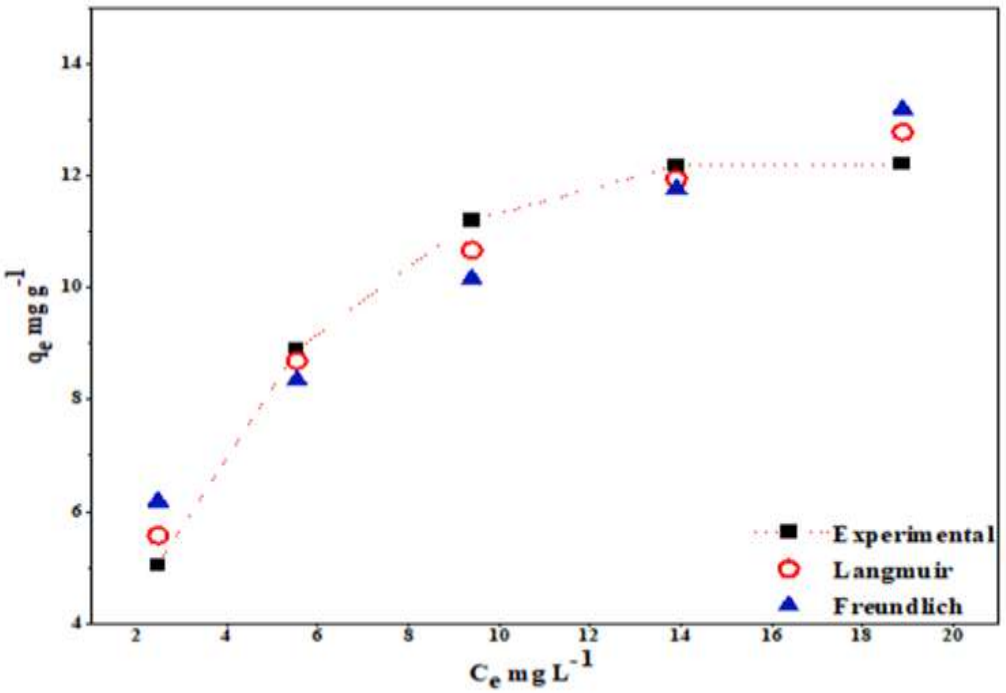

Figure 4-17: The fitting of the non-linear adsorption models to the experimental data for Cu^{2+} adsorption on the CH/cHAp composites

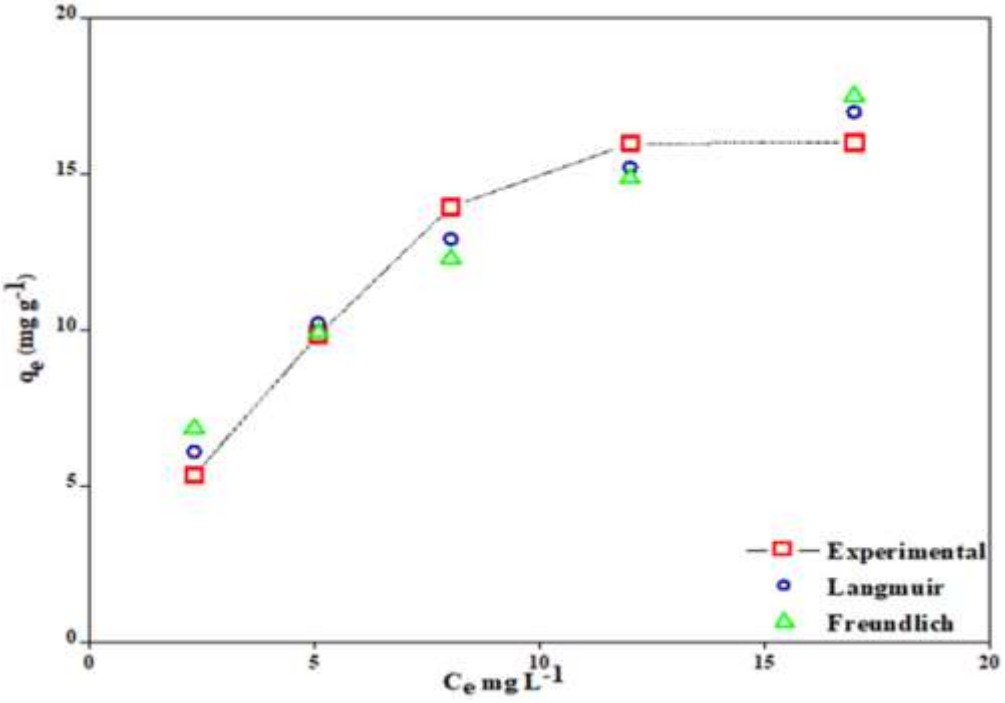

Figure 4-18: The fitting of the non-linear Langmuir and Freundlich isotherm models to the experimental data relating to Cu^{2+} adsorption on the CH/bHAp composites.

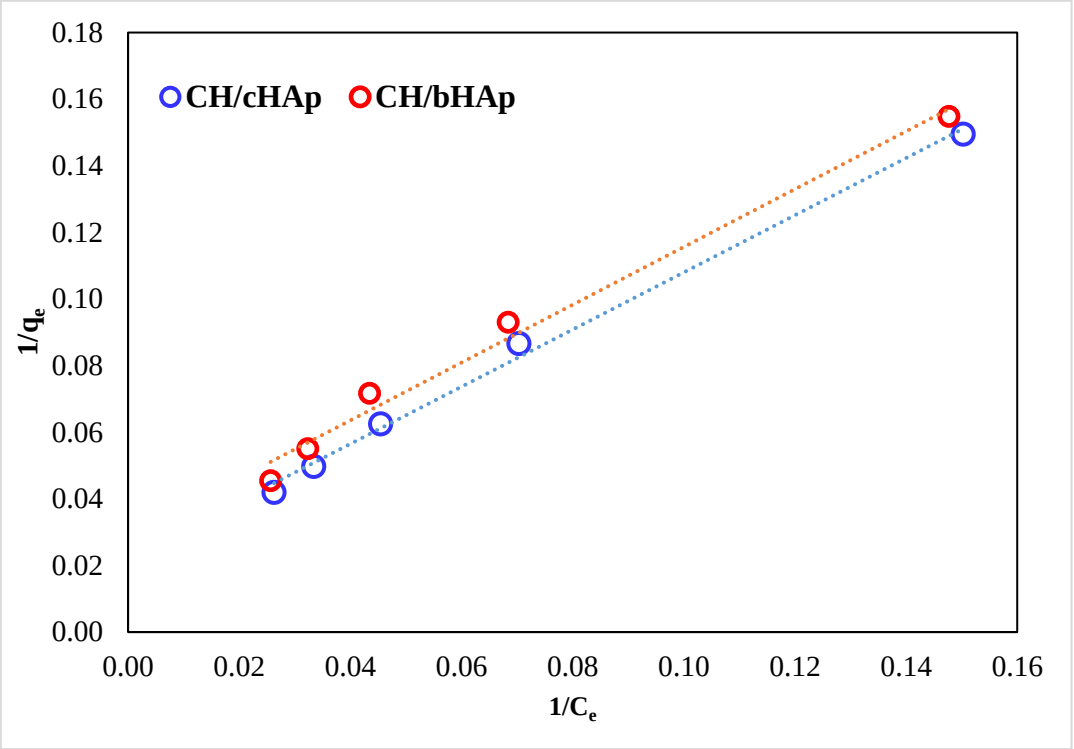

Figure 4-19: Fitting of the linearized Langmuir isotherm model to the experimental data for chromate ion adsorption on the CH/HAp composites

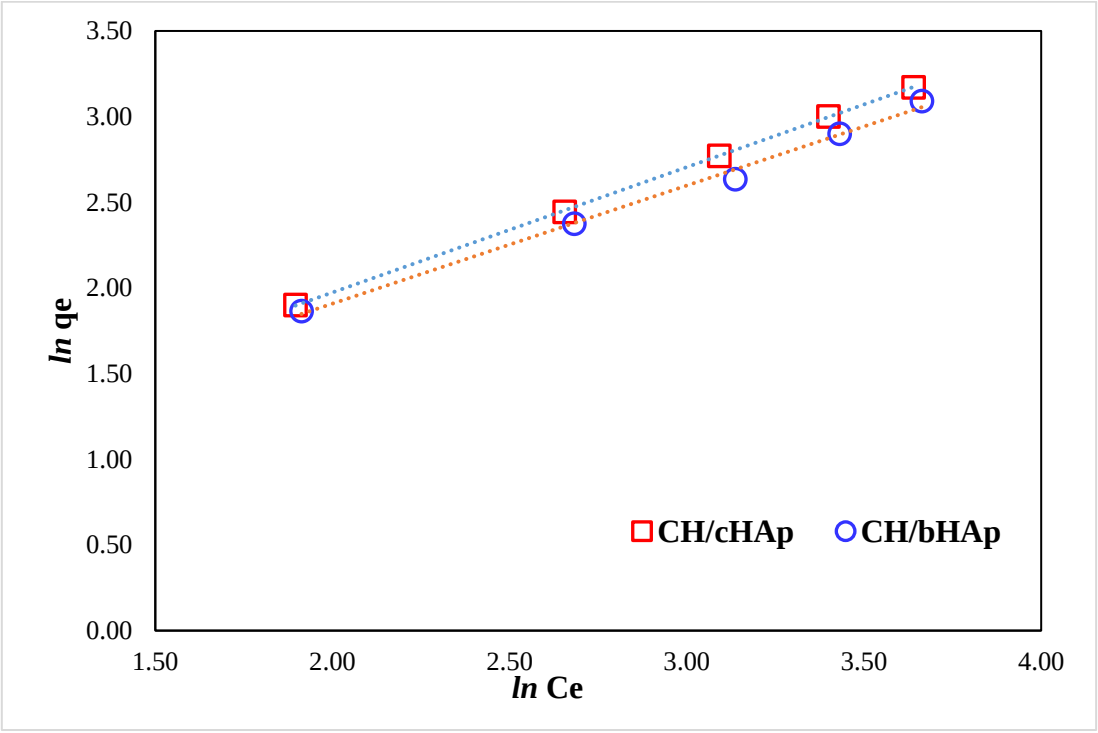

Figure 4-20: The fitting of the linearized Freundlich isotherm model to the experimental data for chromate ion adsorption on the CH/HAp composites.

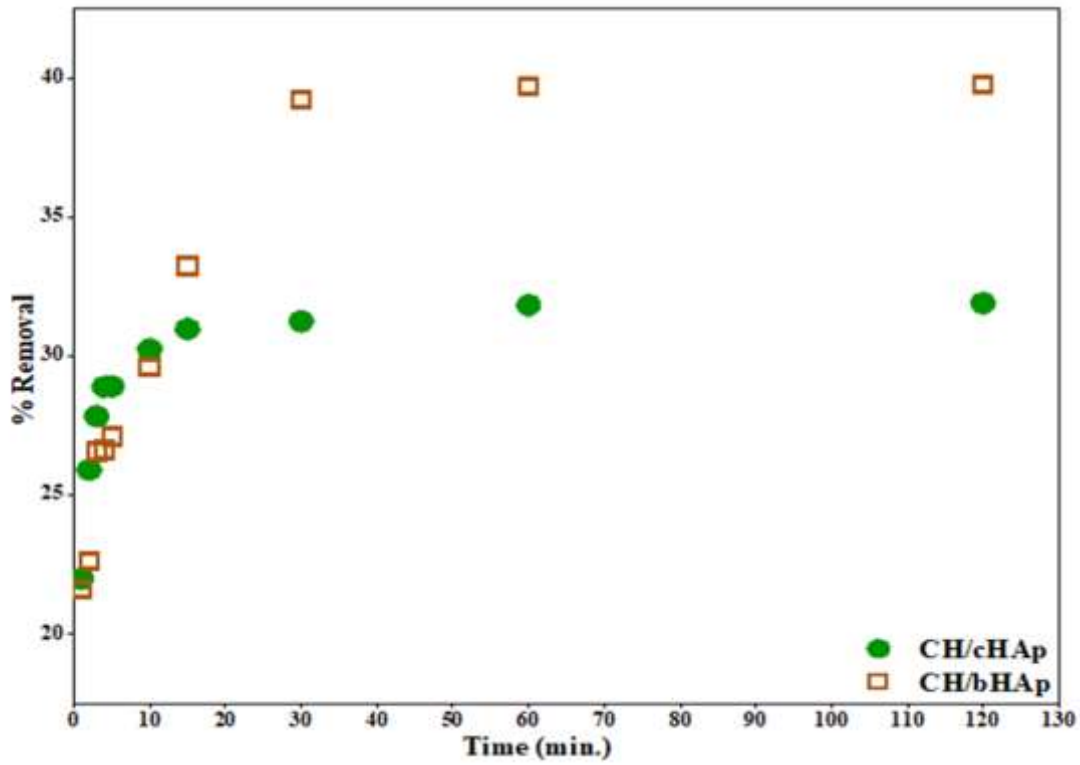

Figure 4-21: The effect of contact time on Cd^{2+} removal by the CH/HAp composites (from AAS data). Results are reported as the average of 3 replicates. SE=±0.1

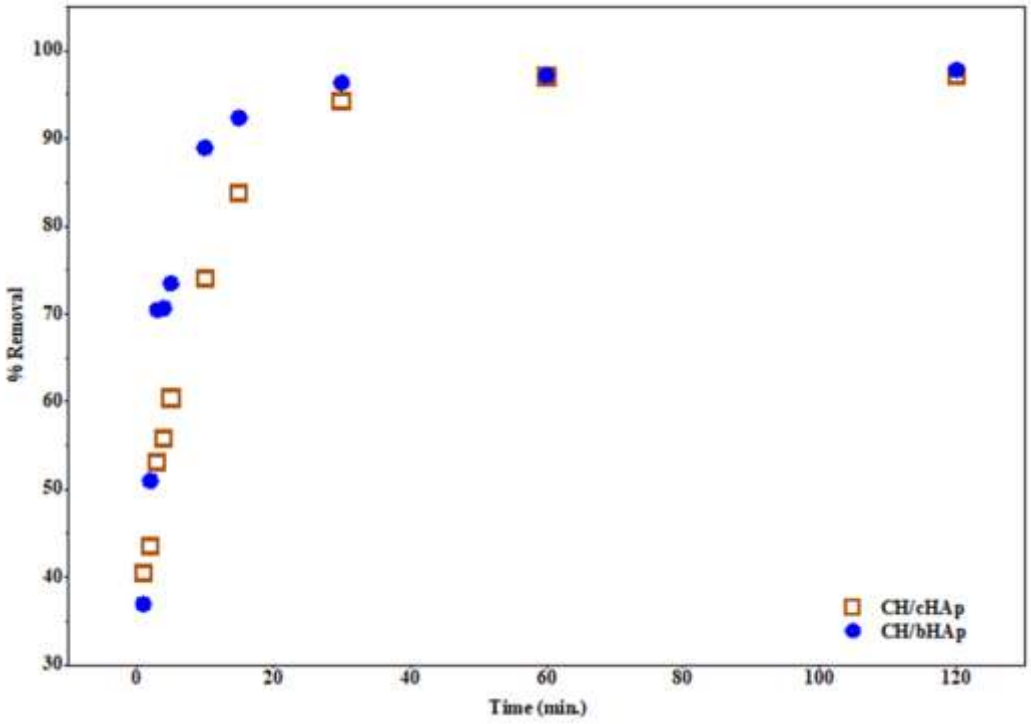

Figure 4-22: AAS data showing the effect of contact time on Pb^{2+} adsorption on the CH/HAp composites. Results are reported as the average of 3 replicates. SE = ±0.1.

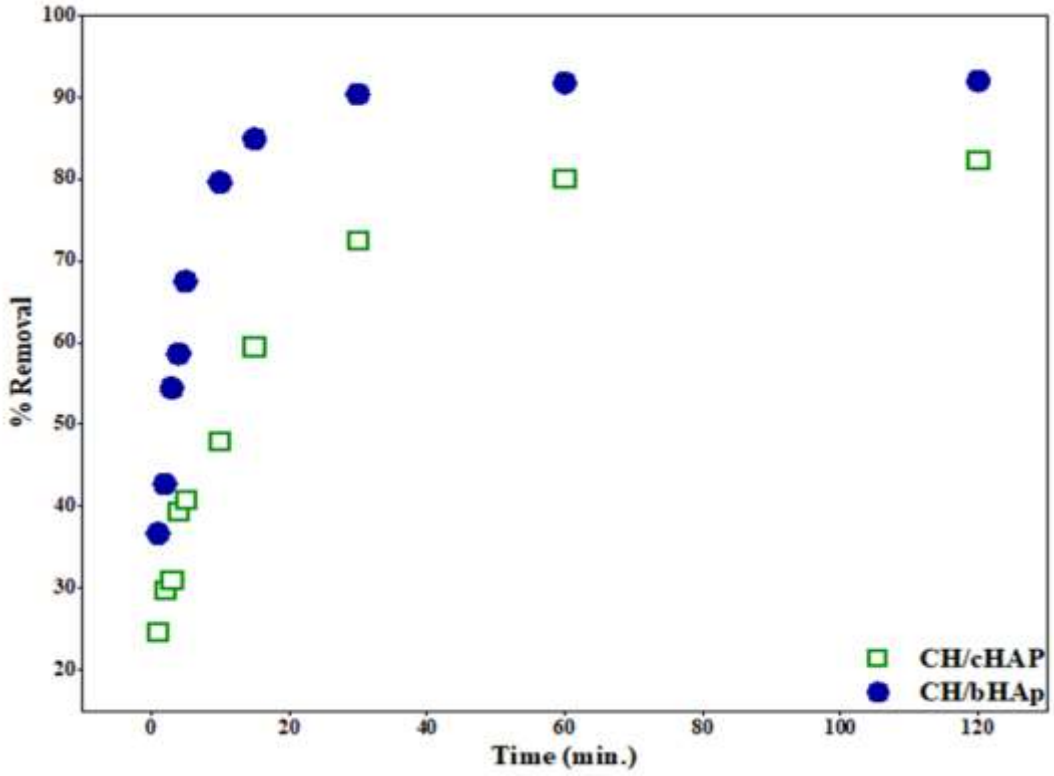

Figure 4-23: AAS data showing the effect of contact time on Cu^{2+} adsorption by the CH/HAp composites. Results are reported as the average of 3 replicates. SE = ±0.1

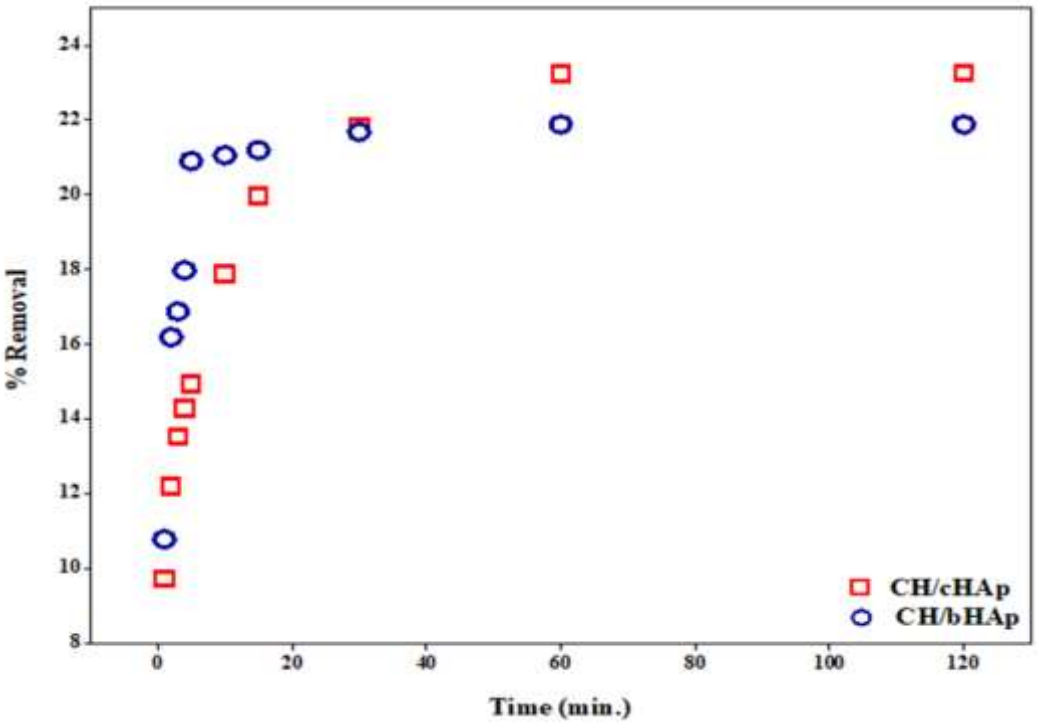

.

Figure 4-24: Effect of contact time of the composite adsorbent with the chromate ion solution on removal (%) of chromate ion from solution using the CH/HAp composites. Results are calculated as the average of 3 replicates. SE= ±0.1

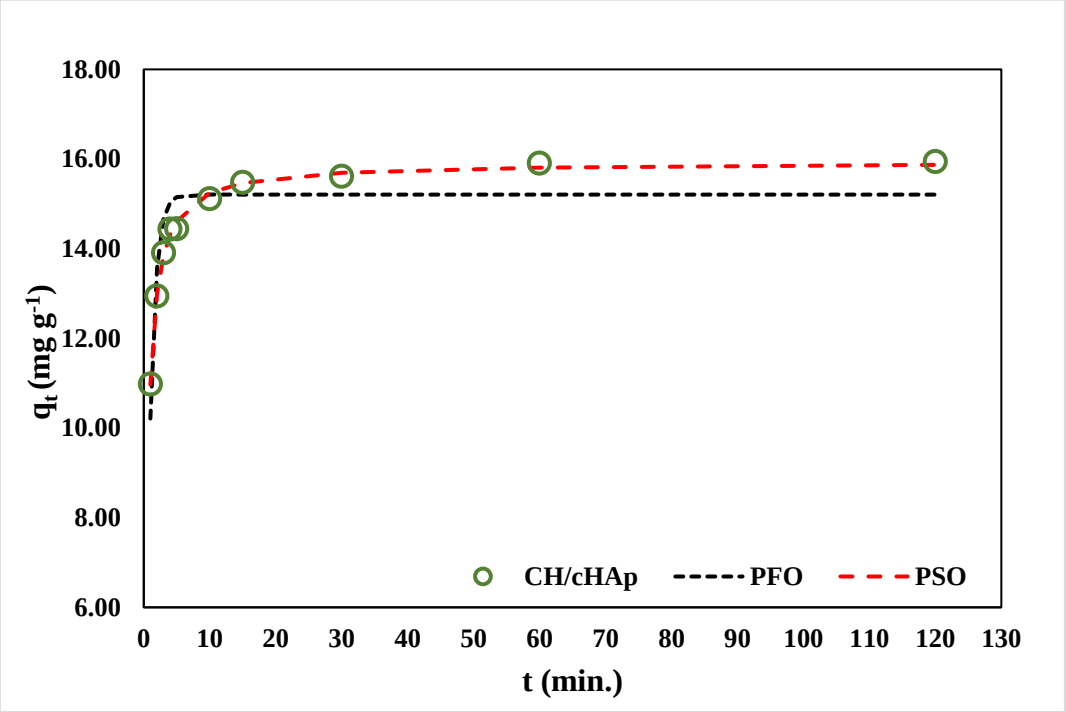

Figure 4-25: The fitting of the non-linear pseudo-first-order (PFO) and pseudo-second-order (PSO) kinetic models to the contact time experimental data for Cd^{2+} adsorption on the CH/cHAp composite

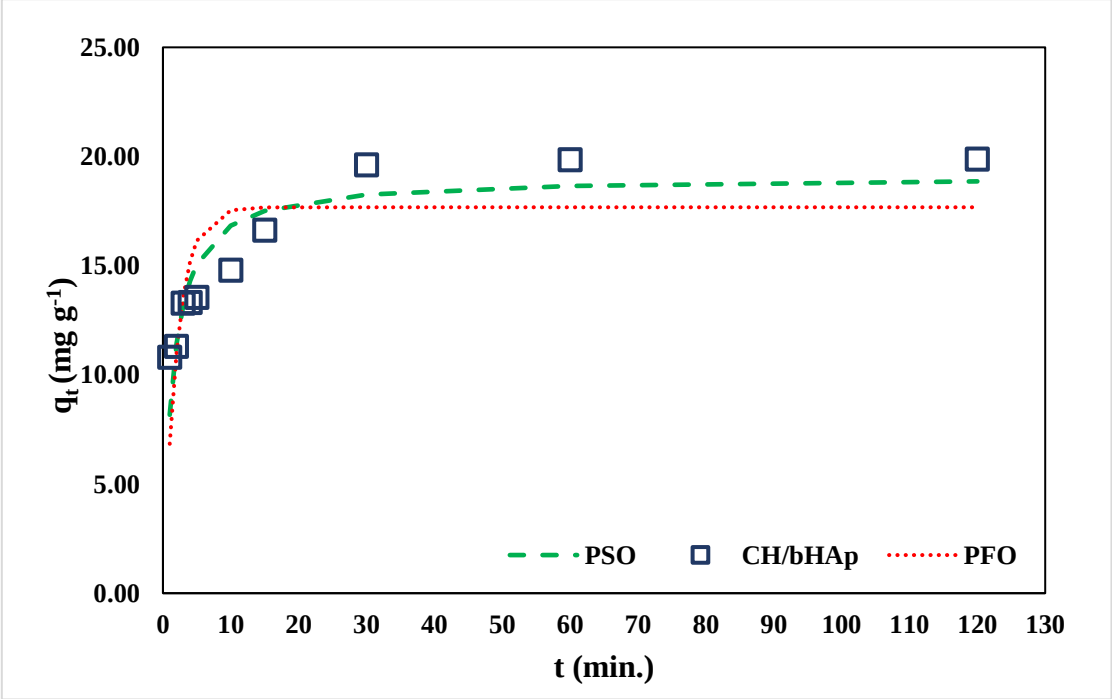

Figure 4-26: The fitting of the non-linear pseudo-first-order (PFO) and pseudo-second-order (PSO) kinetic models to the contact time experimental data for Cd^{2+} adsorption on the CH/bHAp composite

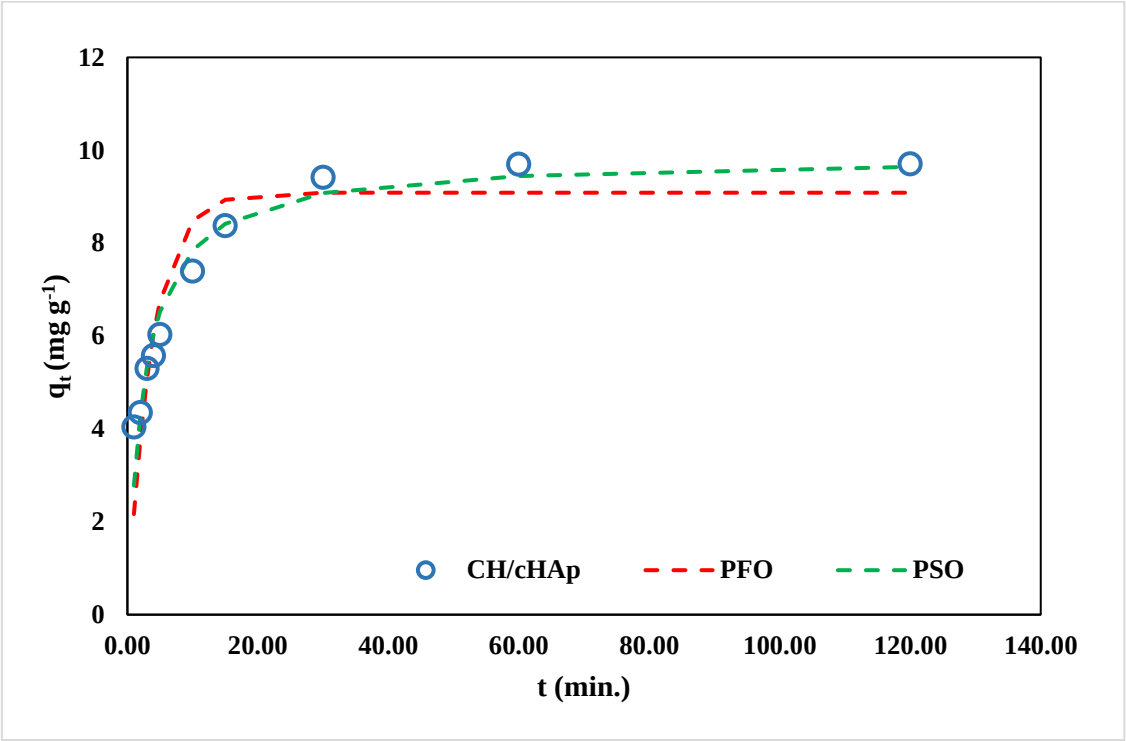

Figure 4-27: The fitting of the non-linear pseudo-first-order (PFO) and pseudo-second-order (PSO) kinetic models of the contact time experimental data for Pb^{2+} adsorption on the CH/cHAp composite

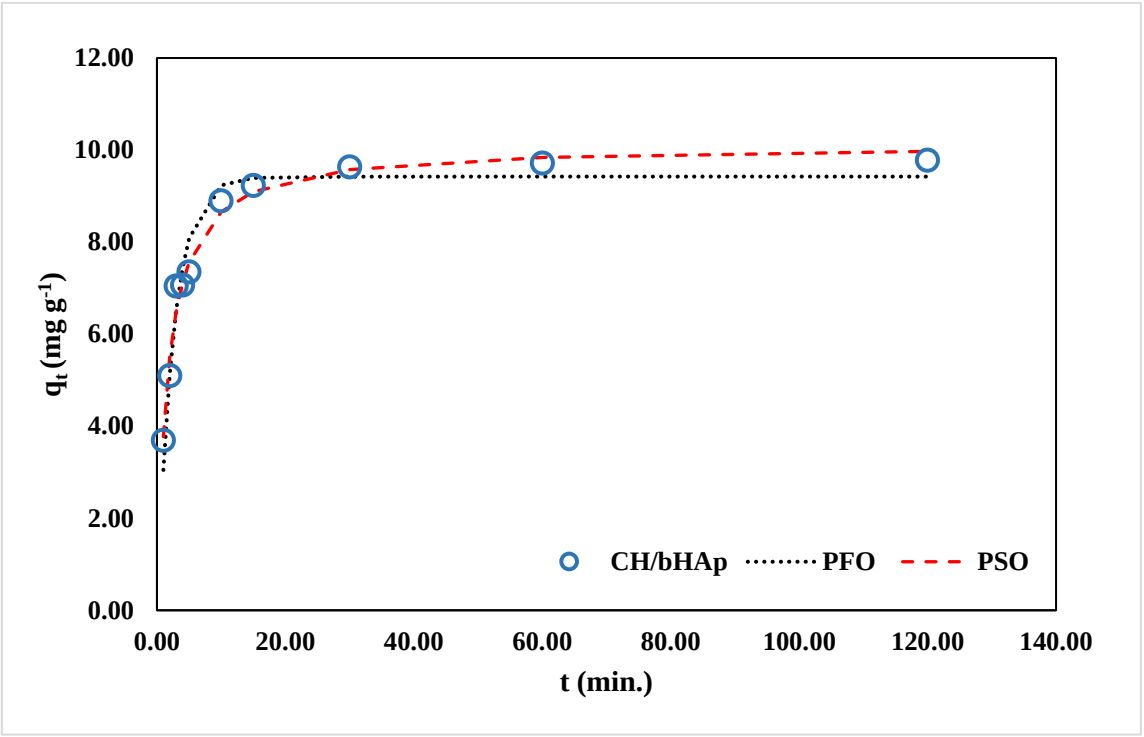

Figure 4-28: The fitting of the non-linear pseudo-first-order (PFO) and pseudo-second-order (PSO) kinetic models to the contact time experimental data for Pb^{2+} adsorption on the CH/bHAp composite

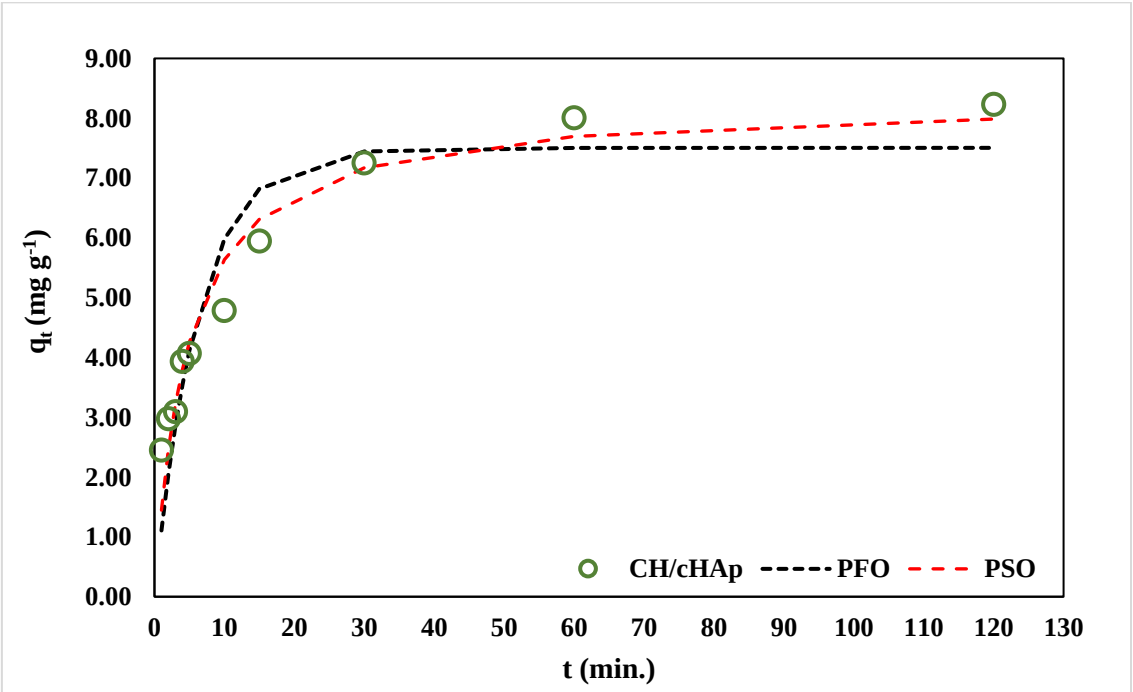

Figure4-29: The fitting of the non-linear pseudo-first-order (PFO) and pseudo-second-order (PSO) kinetic models to the contact time experimental data for Cu^{2+} adsorption on the CH/cHAp composite

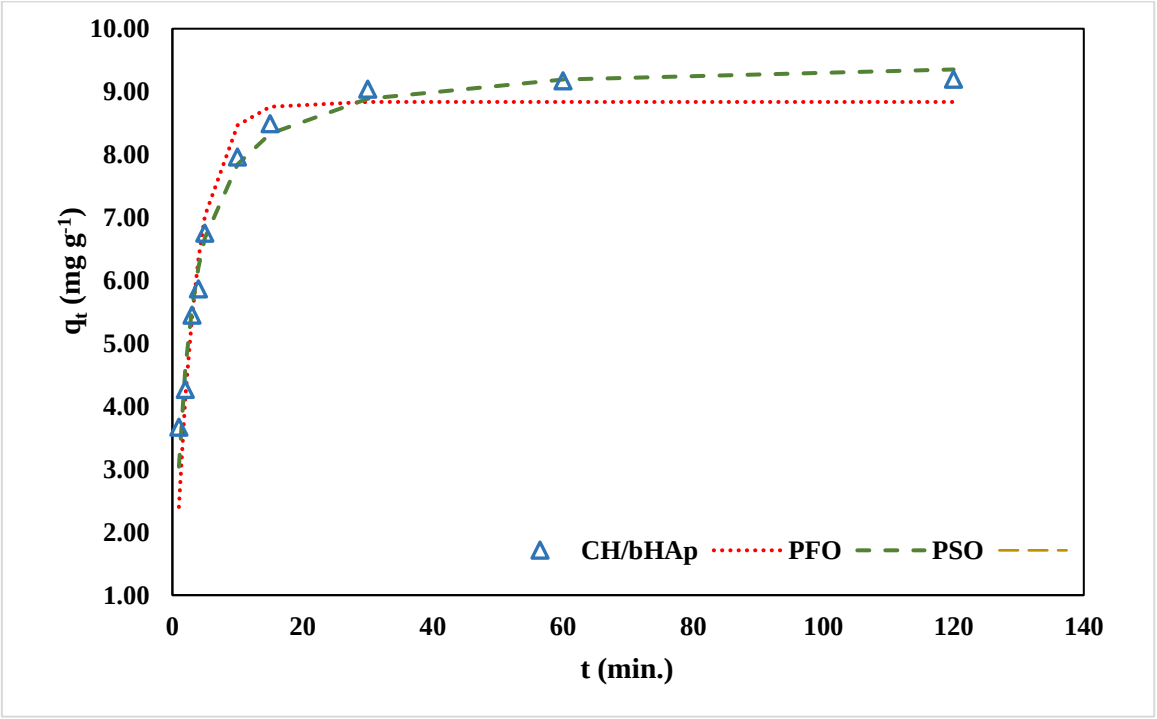

Figure 4-30: The fitting of the non-linear pseudo-first-order (PFO) and pseudo-second-order (PSO) kinetic models to the contact time experimental data for Cu^{2+} adsorption on the CH/bHAp composite

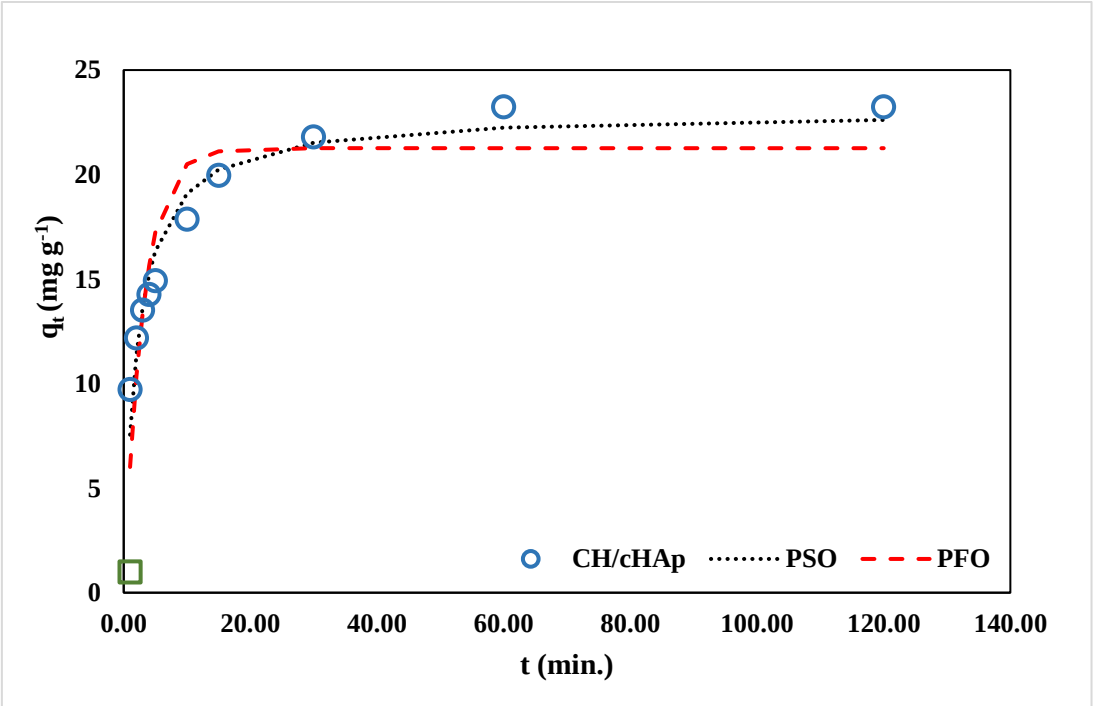

Figure 4-31: The fitting of the non-linear PFO and PSO kinetic models to the experimental contact time data for chromate ion adsorption on the CH/cHAp composites

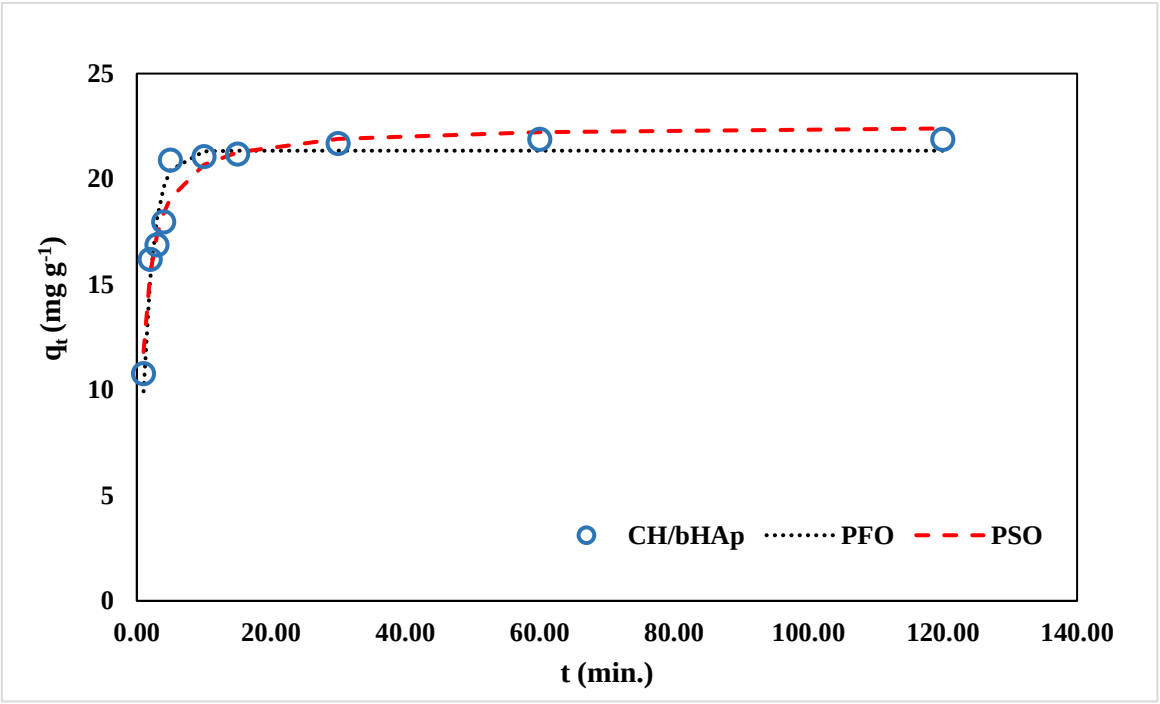

Figure 4-32: The fitting of the non-linear PFO and PSO kinetic models to the contact time experimental data for chromate ion adsorption on the CH/bHAp composites

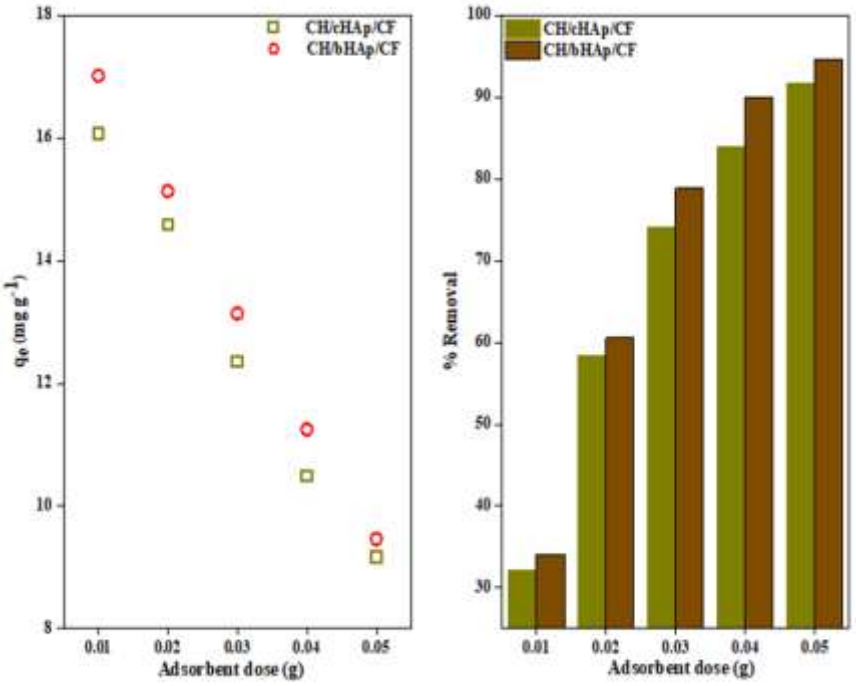

Figure 4-33: AAS data showing the effect of adsorbent dose on Cd^{2+} ion removal and adsorption of Cd^{2+} ion on CH/HAp/CF composites: Results are presented as the average of measurements from 3 replicates. SE = $\pm$ 0.1

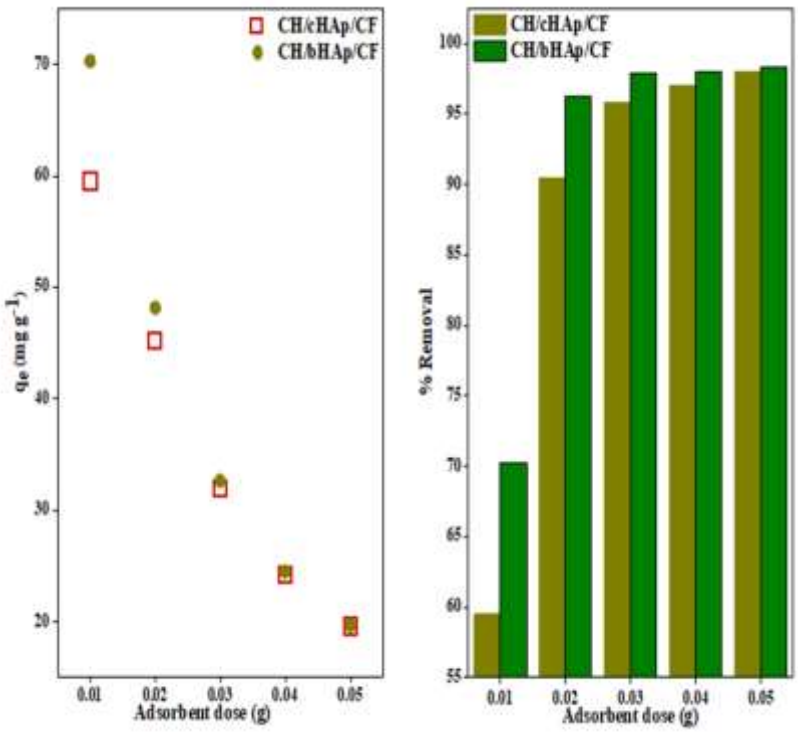

Figure 4-34: AAS data showing the effect of adsorbent dose on Pb^{2+} removal and adsorption on the CH/HAp/CF composites. The results are presented as the average of measurements of three replicates. SE = ± 0.1

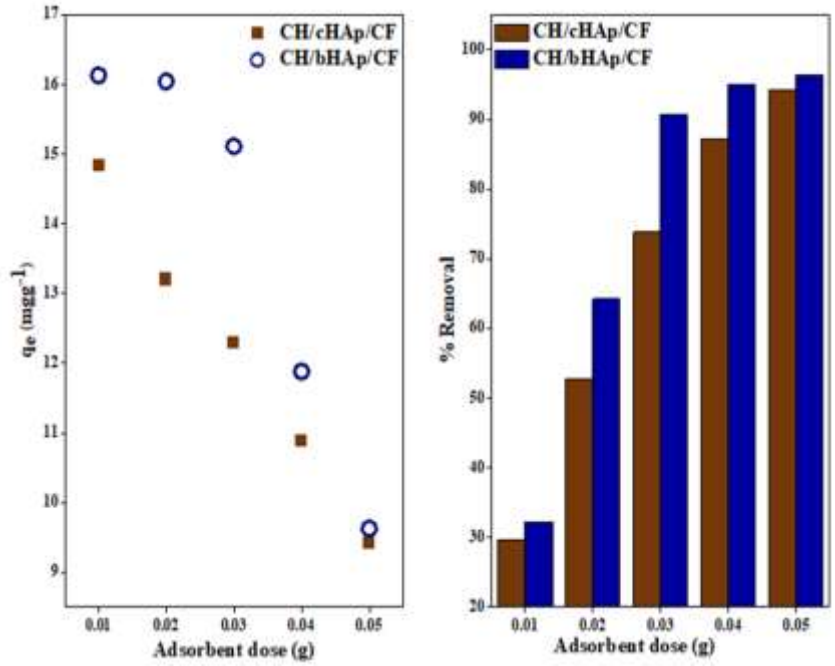

Figure 4-35: AAS data showing the effect of adsorbent dose on Cu^{2+} adsorption on the CH/HAp/CF composites. Results are presented as the average of 3 replicates. SE = ±0.1

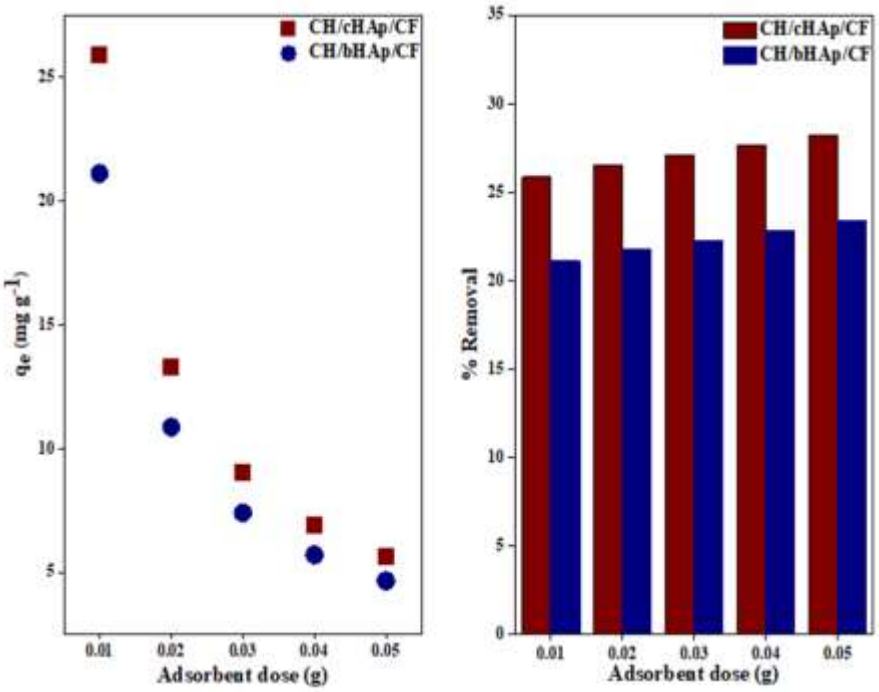

Figure 4-36: AAS data showing the effect of adsorbent dose on chromate ion removal and adsorption on the CH/HAp/CF composites. The results are presented as the average of measurements of three replicates. SE = ± 0.1

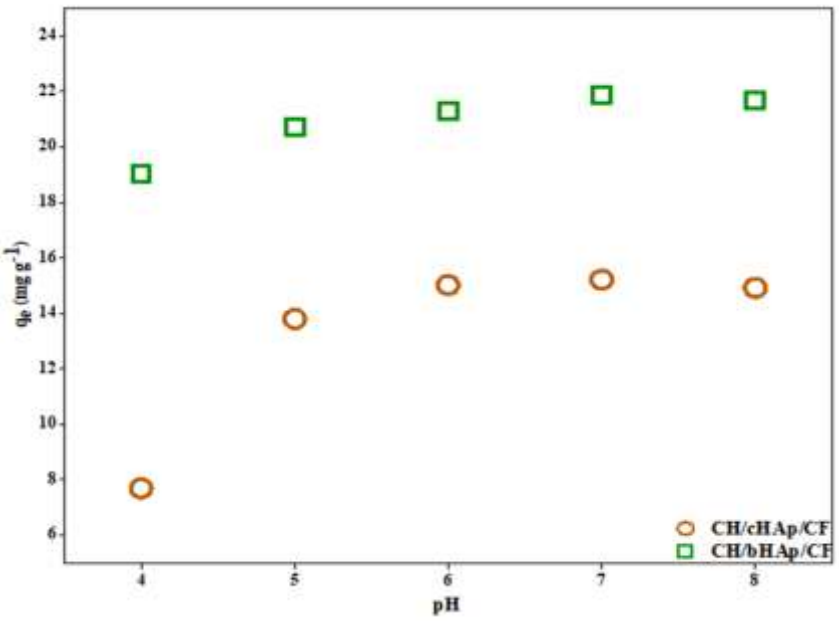

Figure 4-37: AAS data showing the effect of solution pH on Cd^{2+} removal and adsorption on the CH/HAp/CF composites. The results are presented as the average of measurements of three replicates. SE = ± 0.1

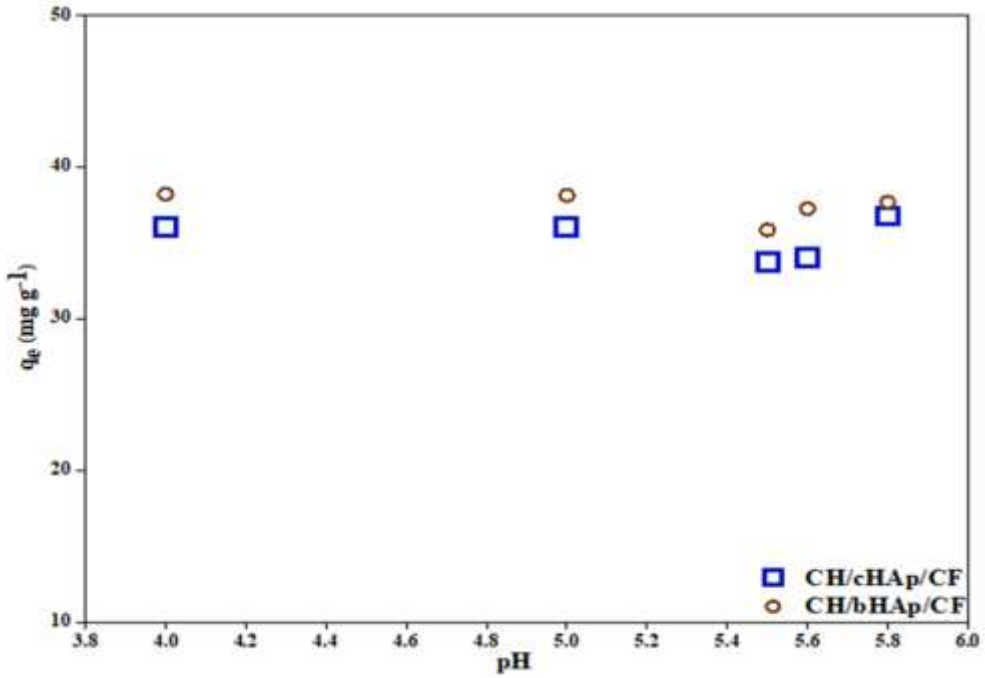

Figure4-38: AAS data showing the effect of solution pH on Pb^{2+} removal and adsorption on CH/HAp/Composites. The results are presented as the average of measurements of three replicates. SE = ± 0.1

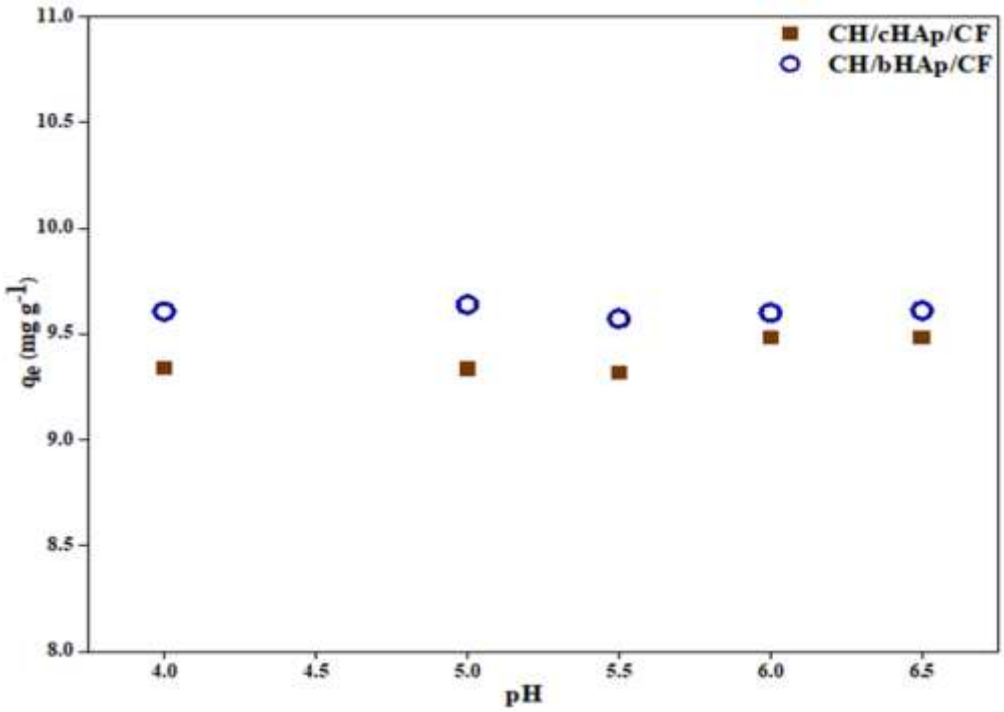

Figure 4-39: AAS data showing the effect of adsorbent dose on Cu^{2+} removal and adsorption on CH/HAp/CF composites. The results are presented as the average of measurements of three replicates. SE = ± 0.1

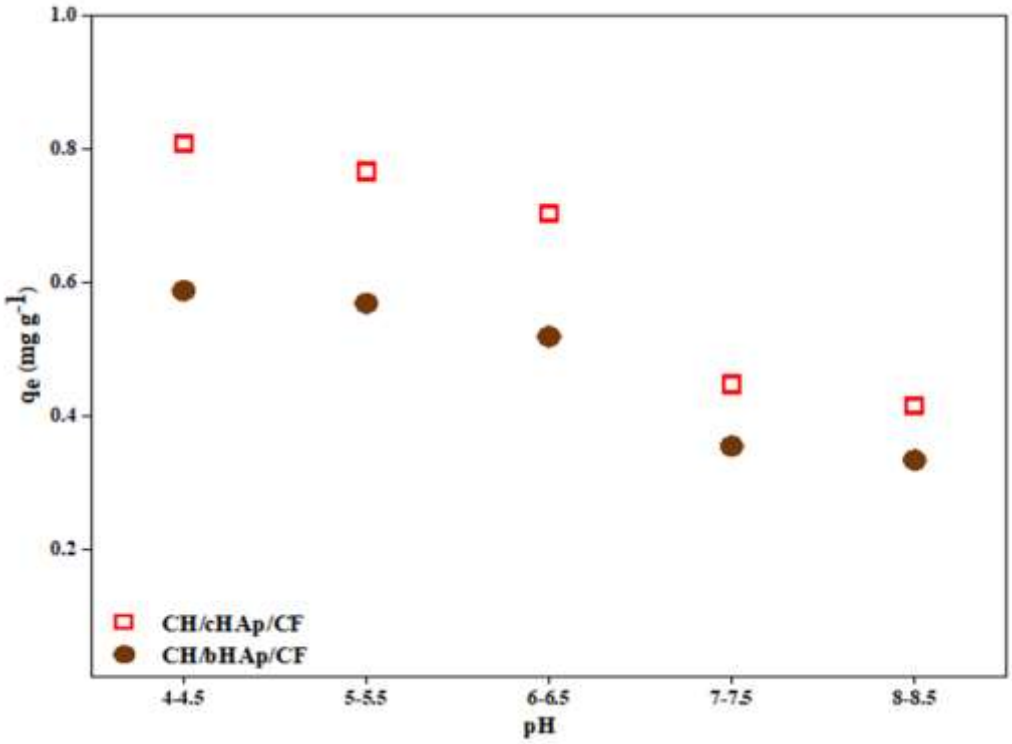

Figure 4-40: AAS data showing the effect of initial pH of the metal ion solution on chromate ion adsorption on the CH/HAp/CF composites. The results are presented as the average of measurements of three replicates. SE = ± 0.1

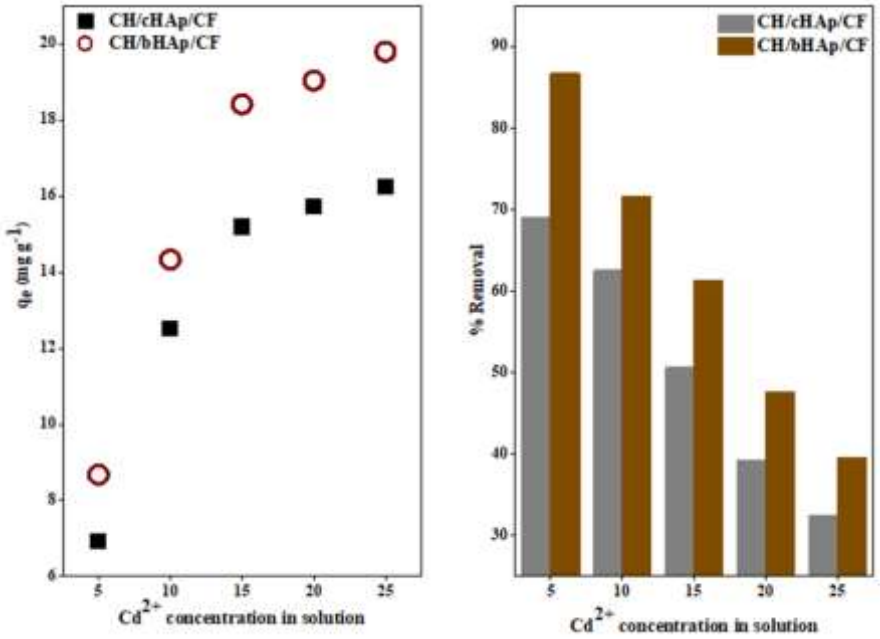

Figure 4-41: AAS data showing the effect of initial metal ion concentration on Cd^{2+} adsorption on CH/HAp/CF composites. Results are calculated as an average of 3 replicates. SE = ± 0.1.

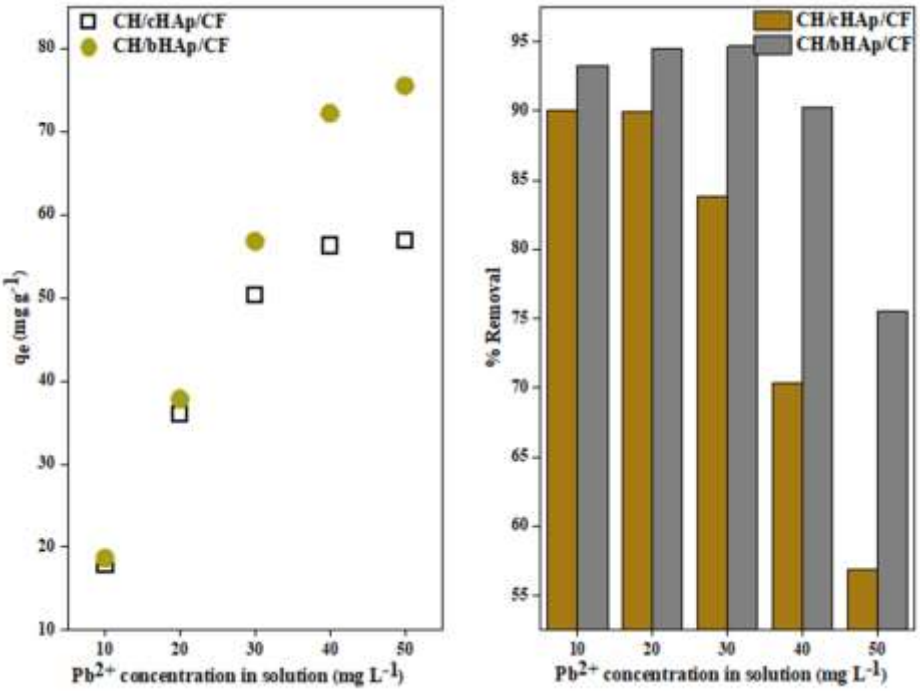

Figure 4-42: AAS data showing the effect of initial metal ion concentration on Pb^{2+} removal and adsorption on CH/HAp/CF composites. The results are presented as the average of measurements of three replicates. SE = $\pm$ 0.1

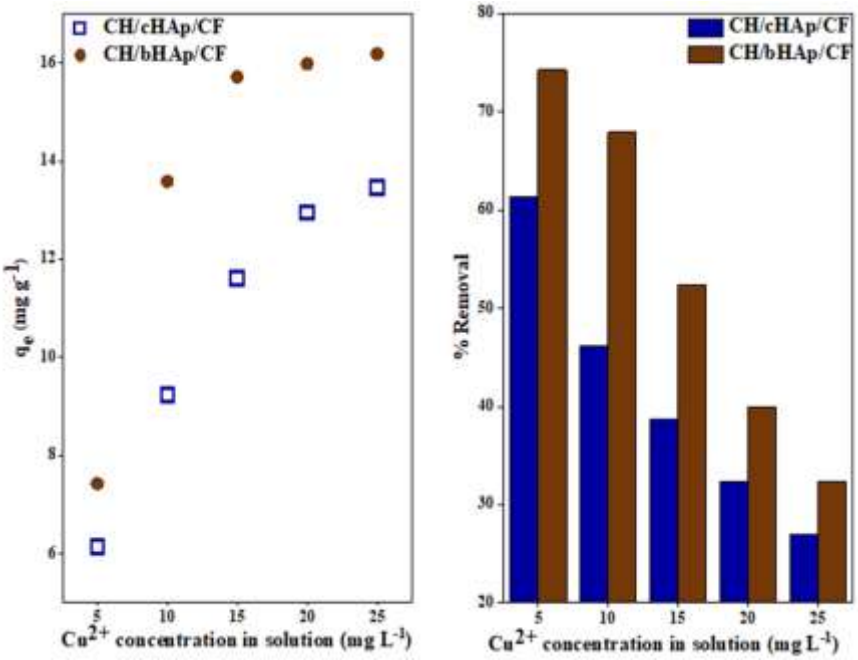

Figure 4-43: AAS data showing the effect of initial metal ion concentration on Cu^{2+} removal and adsorption on the CH/HAp/CF composites. The results are presented as the average of measurements of three replicates. SE = $\pm$ 0.1

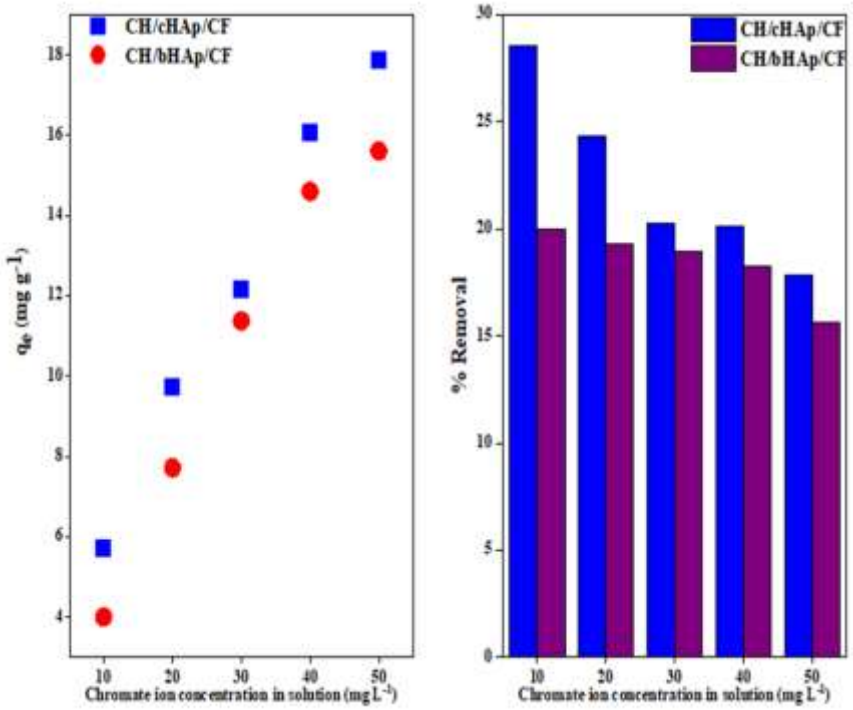

Figure 4-44: AAS data showing the effect of the initial metal ion concentration on chromate ion removal and adsorption on the CH/HAp/CF composites. The results are presented as the average of measurements of three replicates. SE = ± 0.1

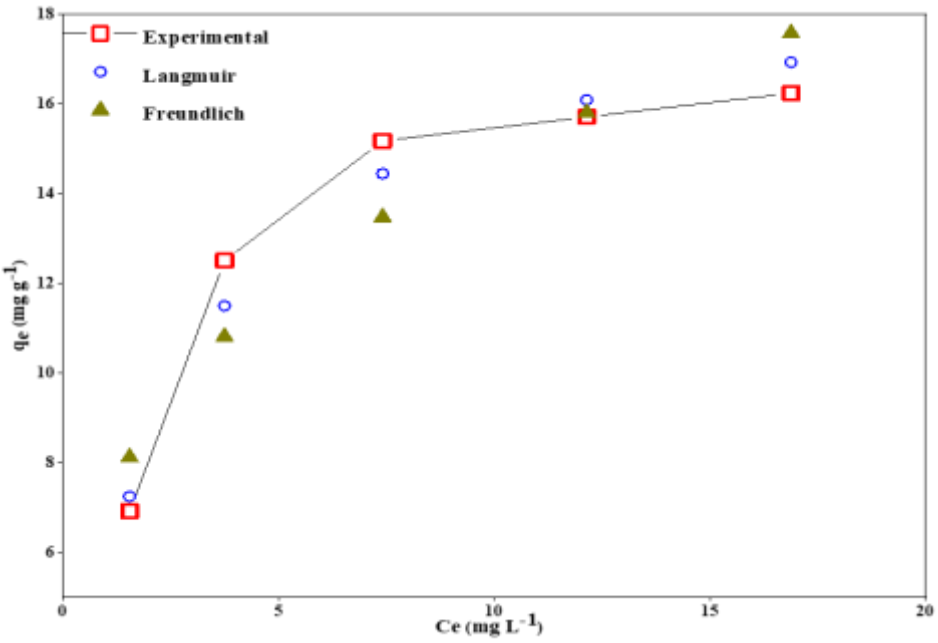

Figure 4-45: The fitting of non-linear Langmuir and Freundlich isotherm models to experimental data for Cd^{2+} adsorption on the CH/cHAp/CF composite.

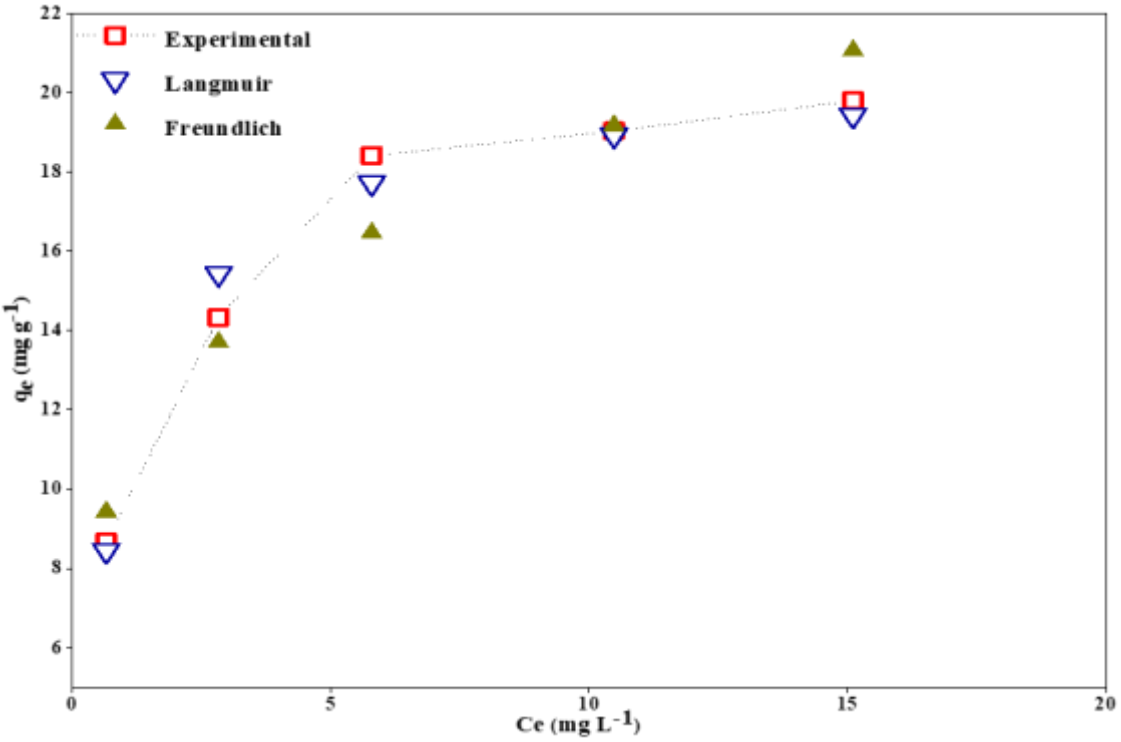

Figure 4-46: The fitting of non-linear Langmuir and Freundlich isotherm models to experimental data for Cd^{2+} adsorption on the CH/bHAp/CF composite.

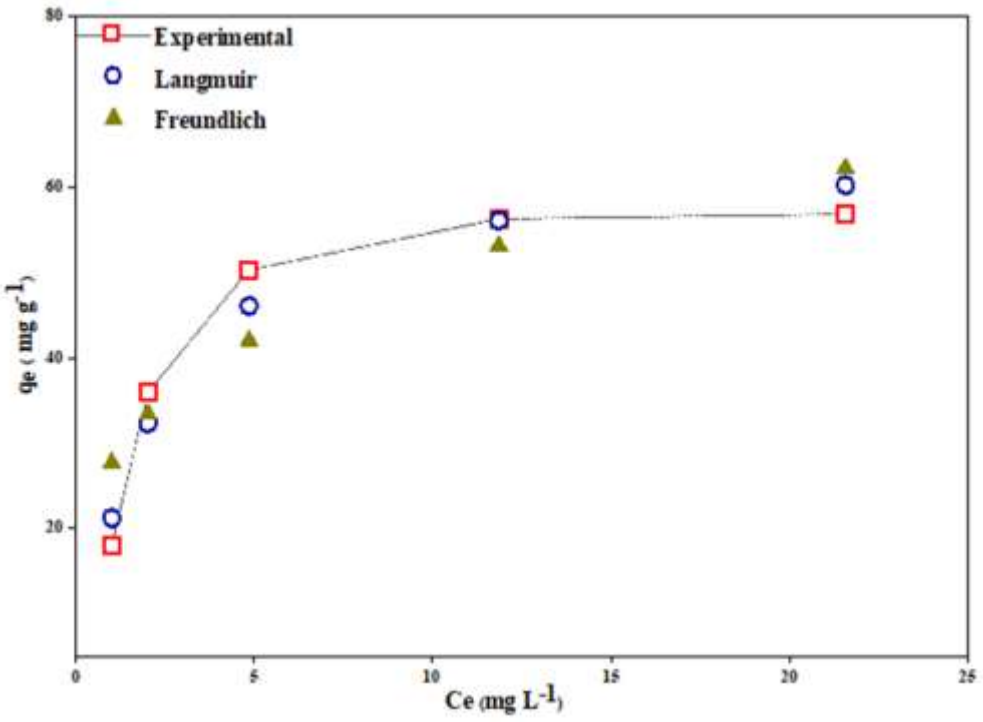

Figure 4-47: The fitting of non-linear Langmuir and Freundlich adsorption isotherms to experimental data for Pb^{2+} adsorption on the CH/cHAp/CF composite

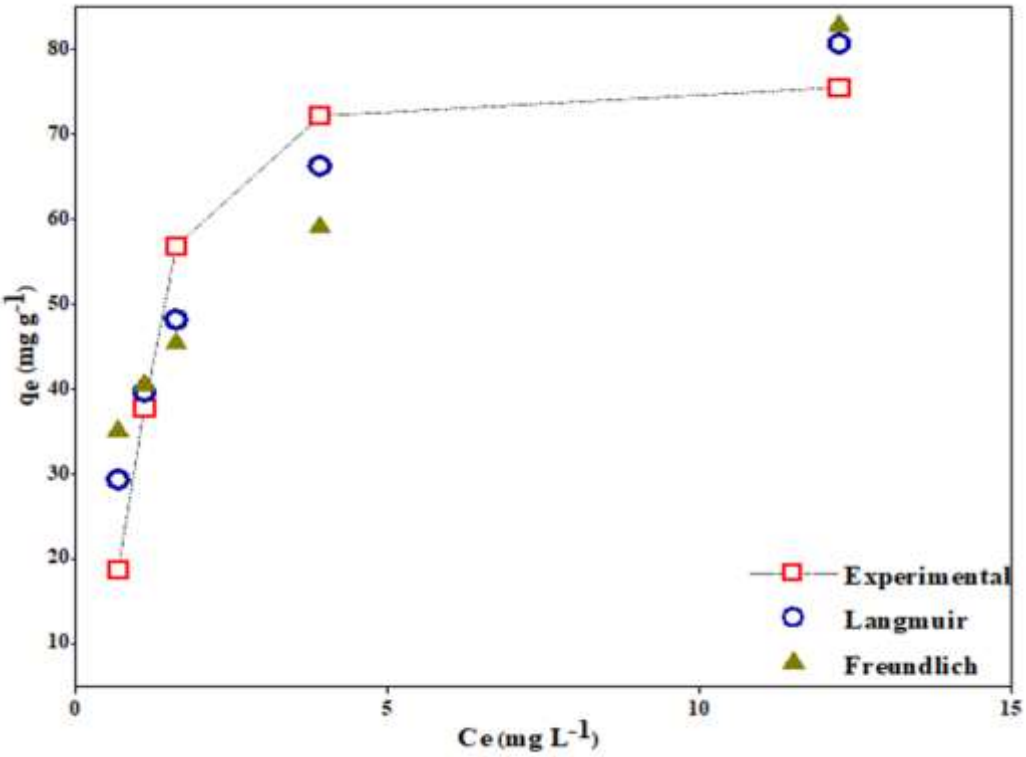

Figure 4-48: The fitting of non-linear Langmuir and Freundlich adsorption isotherms to experimental data for Pb^{2+} adsorption on the CH/bHAp/CF composite.

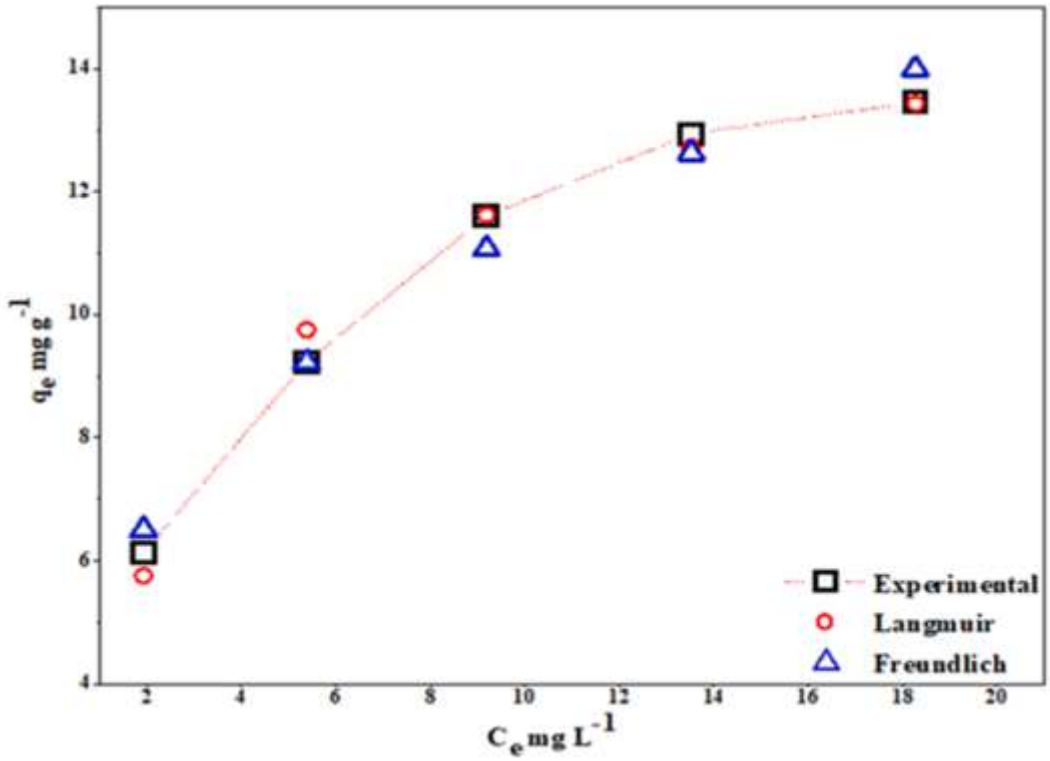

Figure 4-49: The fitting of the non-linear Langmuir and Freundlich isotherms to data for Cu^{2+} adsorption on the CH/cHAp/CF composite

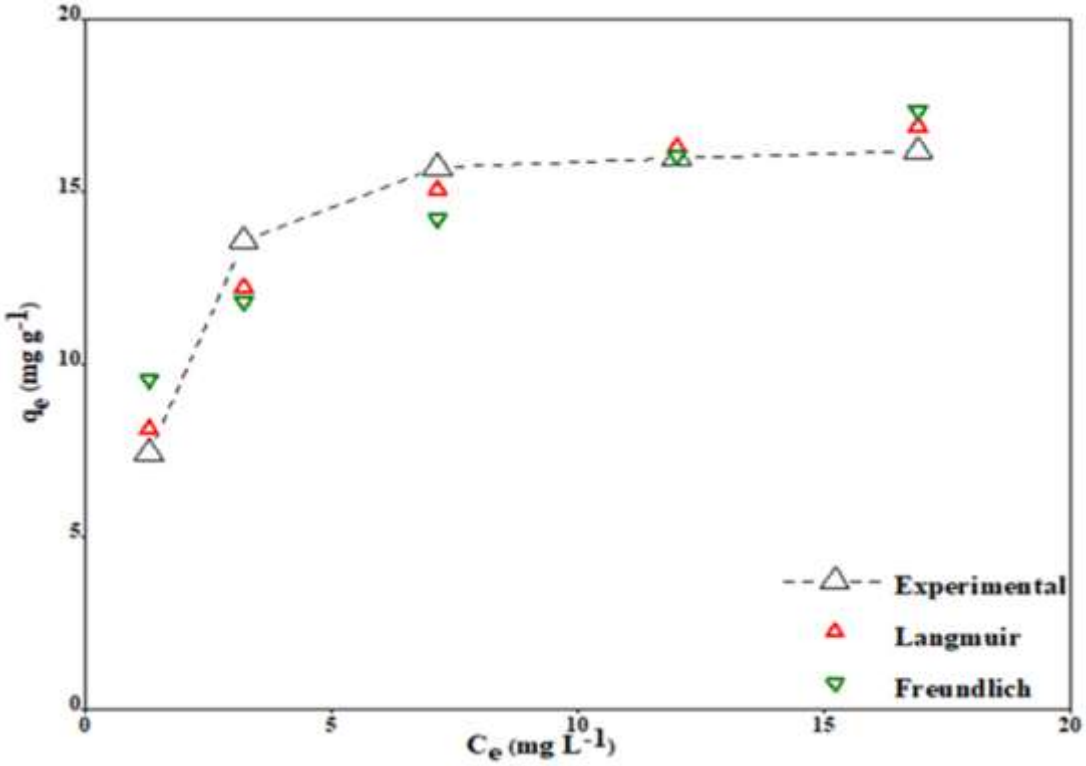

Figure 4-50: The fitting of the non-linear Langmuir and Freundlich isotherms to data for Cu^{2+} adsorption on the CH/bHAp/CF composite.

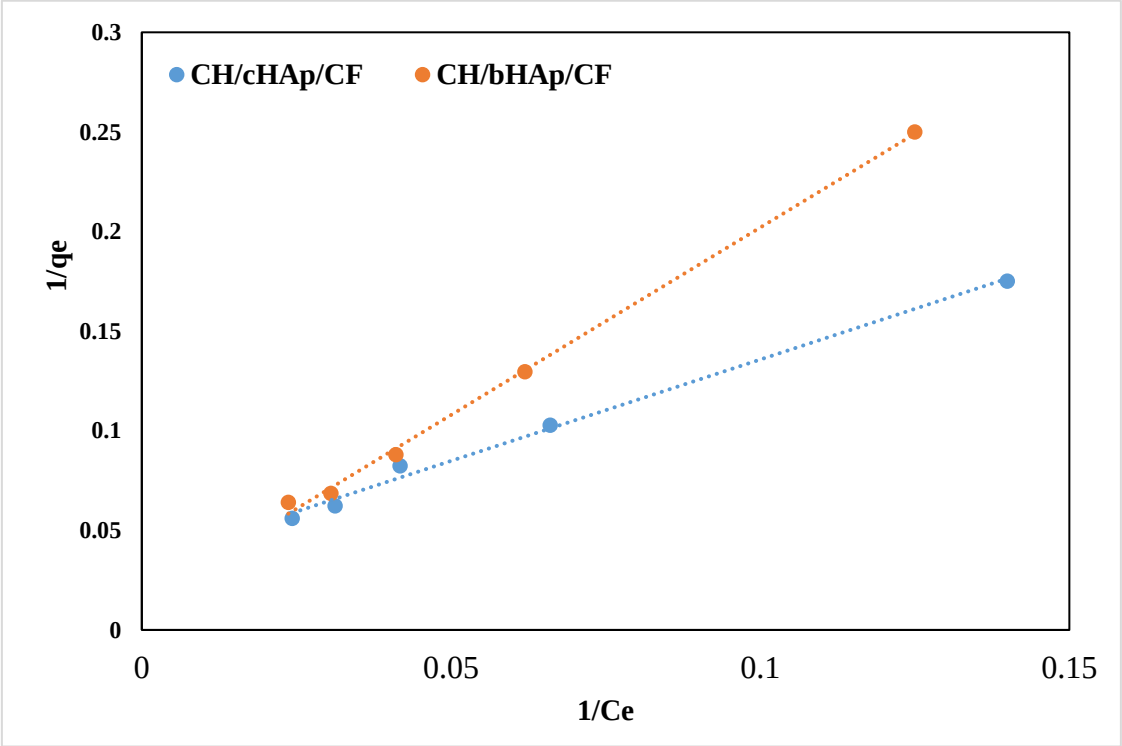

Figure 4-51: Fitting of the Linearized Langmuir isotherm model to the experimental data for chromate ion adsorption on the CH/HAp/CF composites

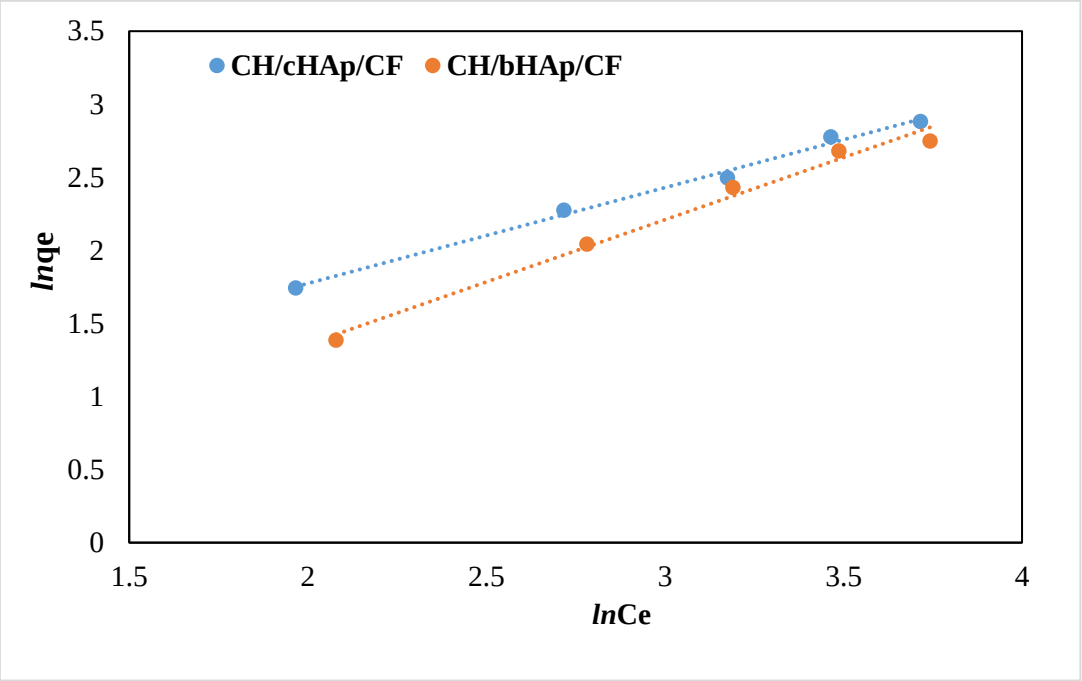

Figure 4-52: Fitting of the linearized Freundlich isotherm model to the experimental data for chromate ion adsorption on the CH/HAp/CF composites.

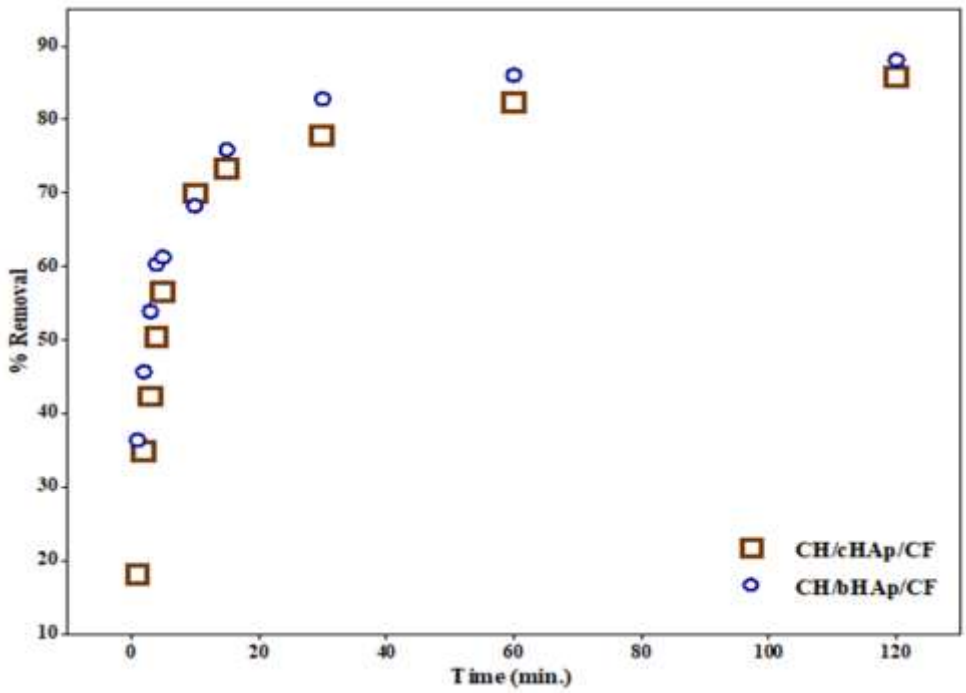

Figure 4-53: AAS data showing the effect of adsorbent dose on Cd^{2+} removal (%) using CH/HAp/CF composites. The results are presented as the average of measurements of three replicates. SE = ± 0.1

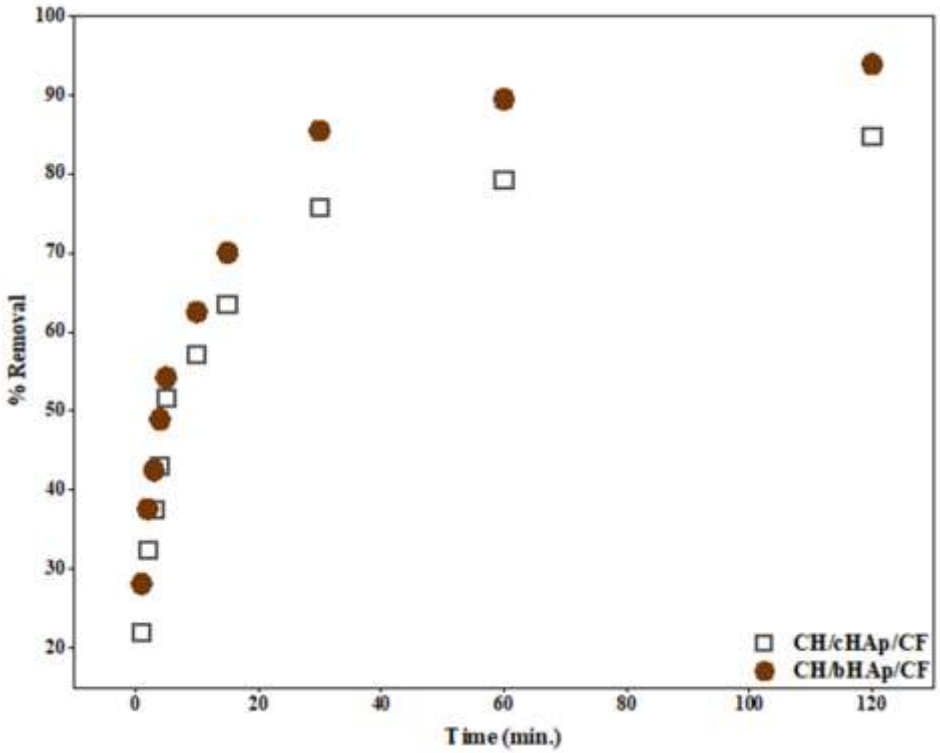

Figure4-54: AAS data showing the effect of contact time on Pb^{2+} adsorption on CH/HAp/CF composites. Results are reported as the average of 3 replicates. SE = ±0.1.

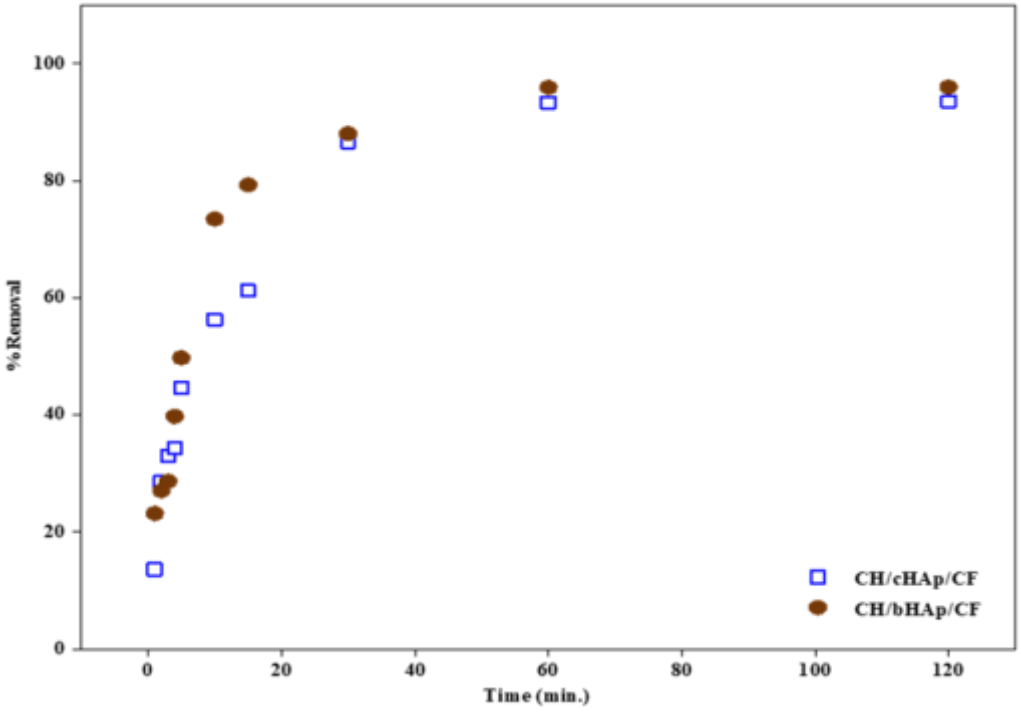

Figure 4-55: AAS data showing the effect of contact time on Cu^{2+} removal by the CH/HAp/CF composites. The results are presented as the average of measurements of three replicates. SE= ± 0.1

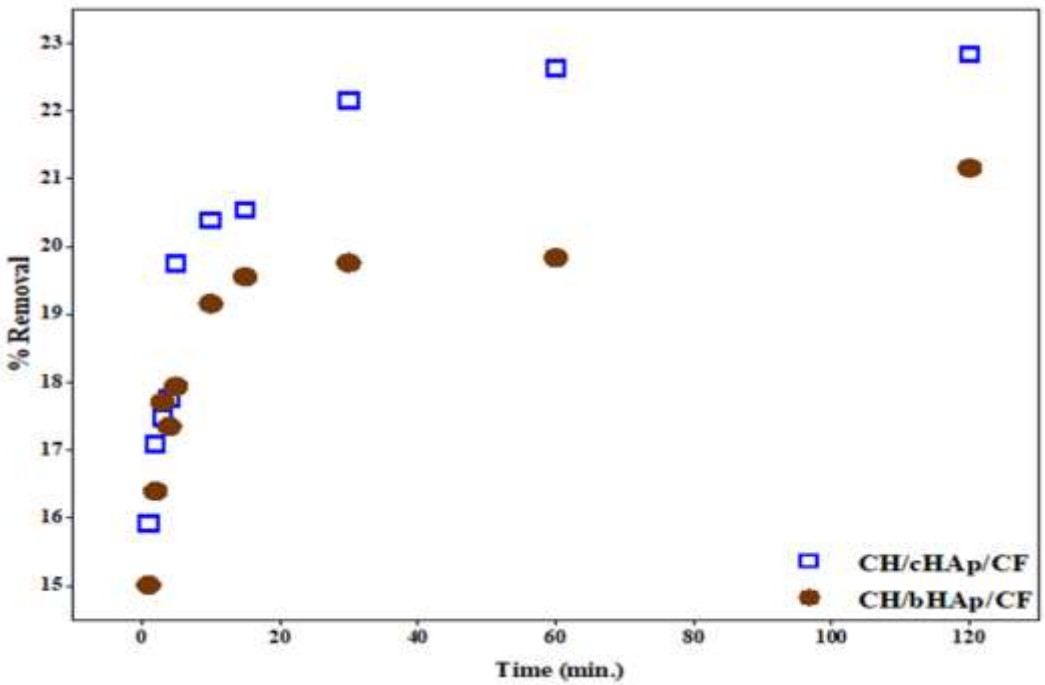

Figure 4-56: AAS data showing the effect of contact time on chromate ion removal and adsorption on the CH/HAp/CF composites. The results are presented as the average of measurements of three replicates. SE = ± 0.1

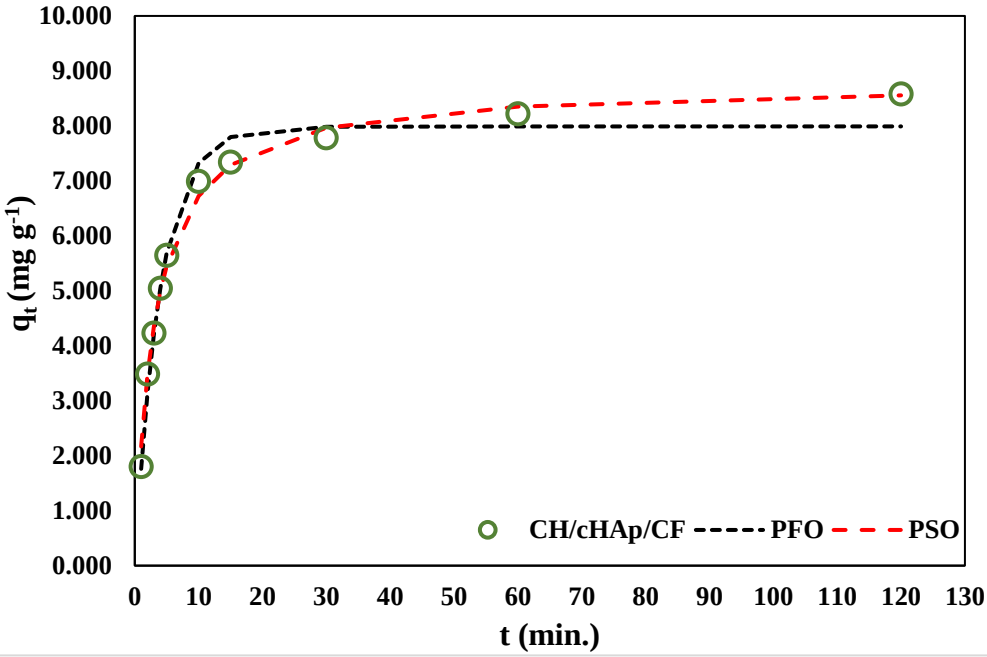

Figure 4-57: The fitting of the non-linear pseudo-first-order (PFO) and pseudo-second-order kinetic models to the contact time experimental data for Cd^{2+} adsorption on the CH/cHAp/CF composites

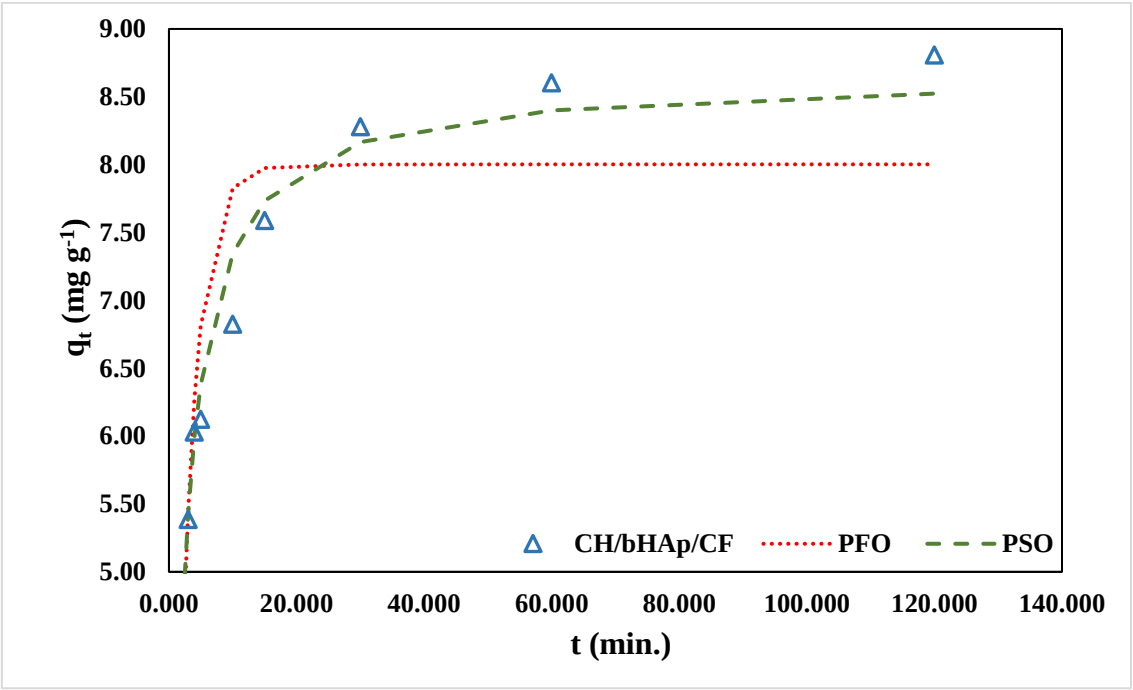

Figure 4-58: The fitting of the non-linear pseudo-first-order (PFO) and pseudo-second-order kinetic models to the contact time experimental data for Cd^{2+} adsorption on the CH/bHAp/CF composites

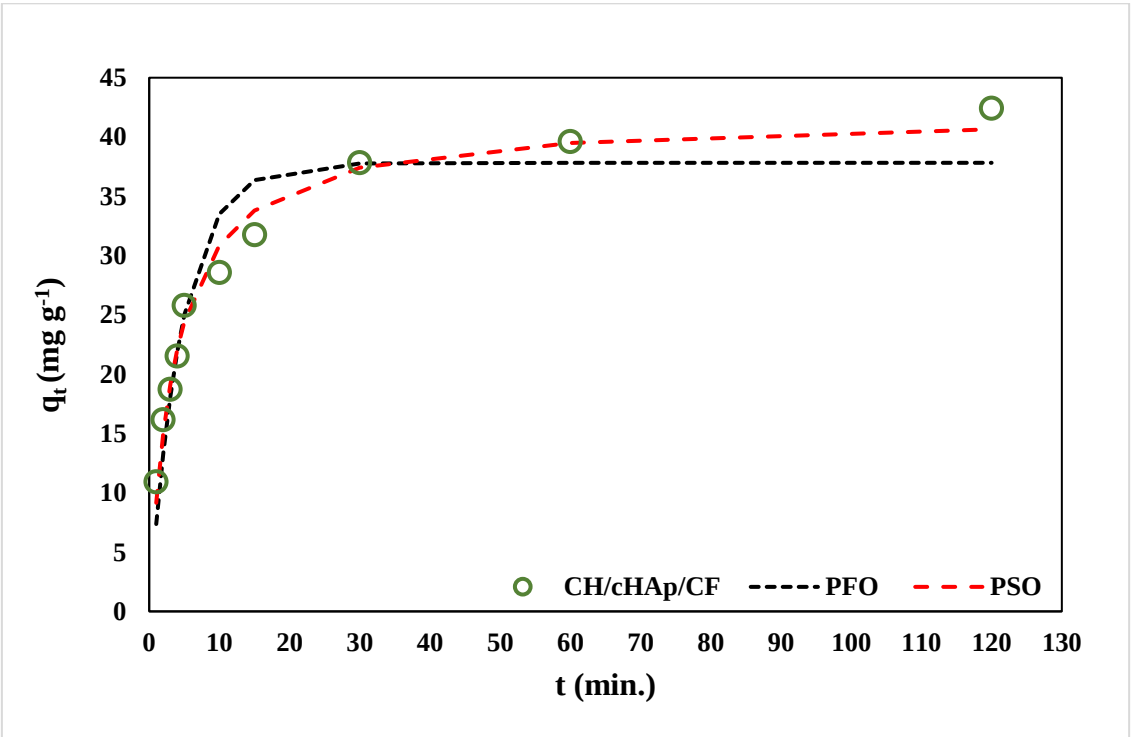

Figure 4-59: The fitting of the non-linear pseudo-first-order and pseudo-second-order kinetics models to contact time data for Pb^{2+} adsorption on the CH/cHAp/CF composite

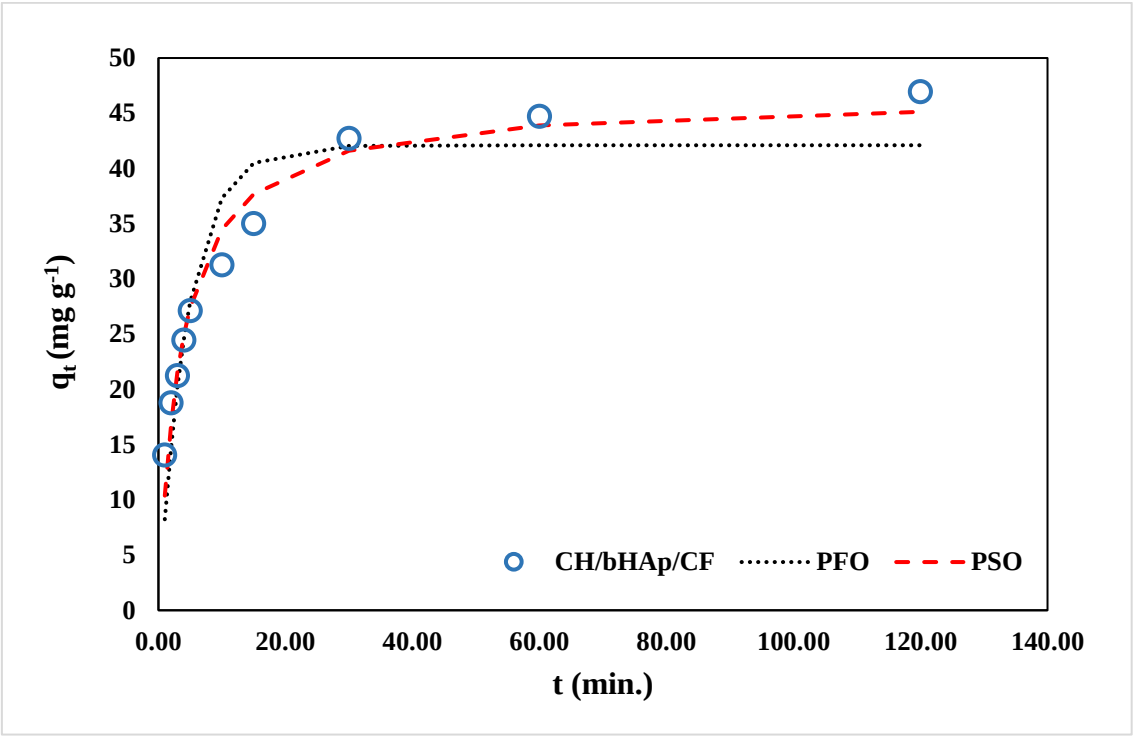

Figure 4-60: The fitting of the pseudo-first-order and pseudo-second-order kinetics models to contact time data for Pb^{2+} adsorption on the CH/bHAp/CF composite

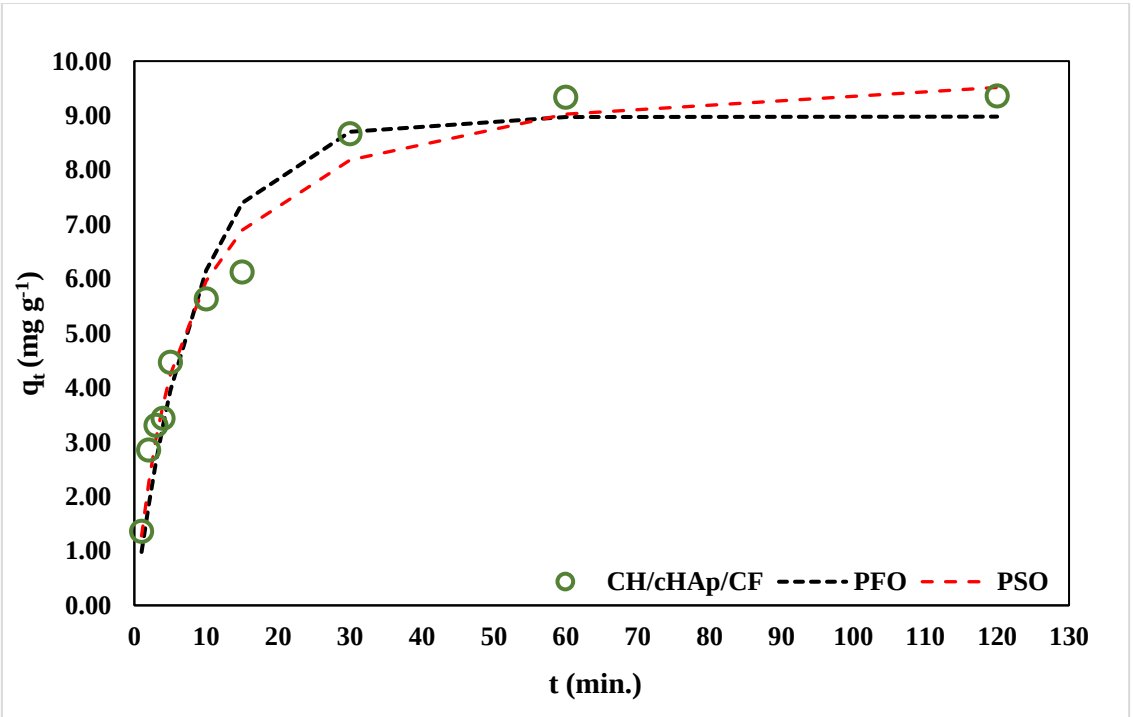

Figure 4-61: The fitting of the non-linear pseudo-first-order and pseudo-second-order kinetics models to contact experimental time data for Cu^{2+} adsorption on the CH/cHAp/CF composite

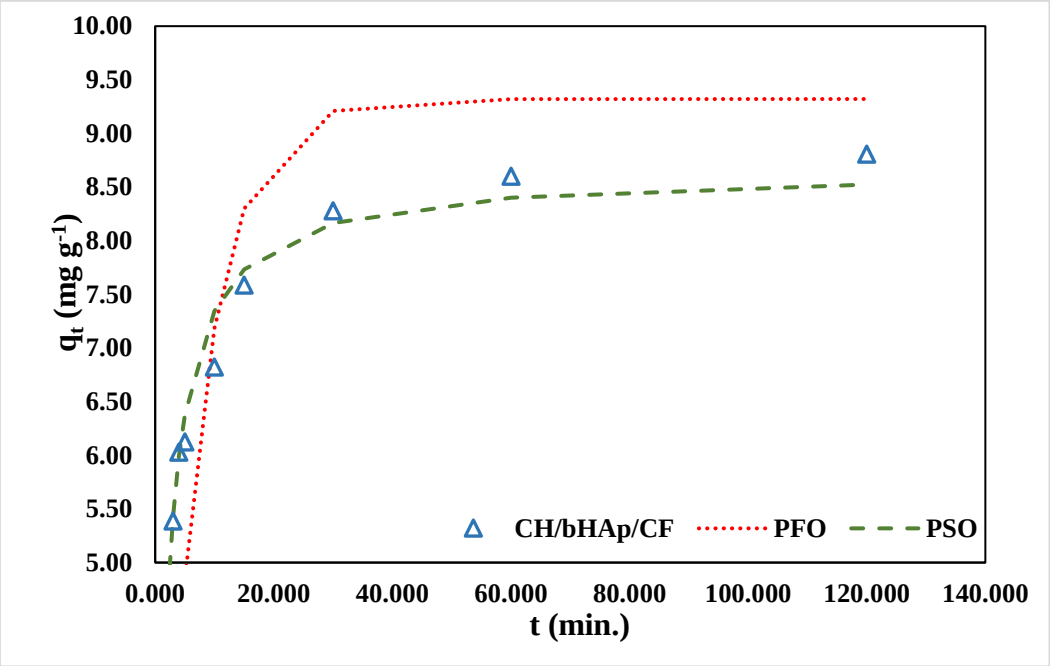

Figure 4-62: The fitting of the non-linear pseudo-first-order and pseudo-second-order kinetics models to contact time experimental data for Cu^{2+} adsorption on the CH/bHAp/CF composite

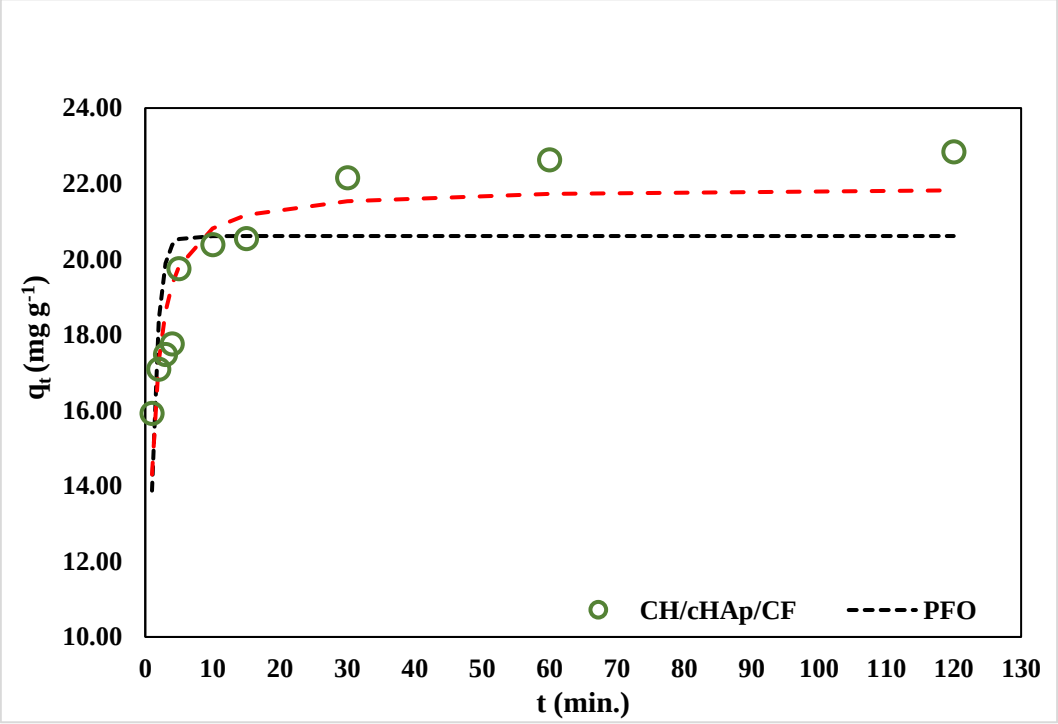

Figure 4-63: The fitting of the non-linear pseudo-first-order and pseudo-second-order kinetic models to the contact time data for chromate ion adsorption on the CH/cHAp/CF composites

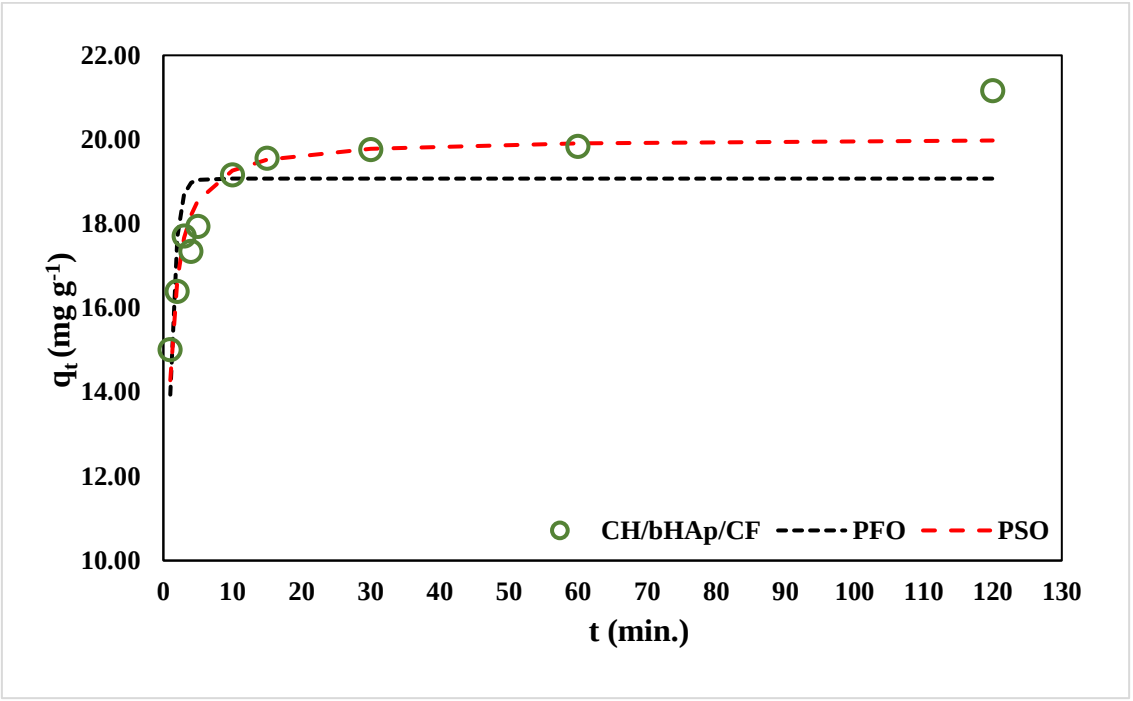

Figure 4-64: The fitting of the non-linear pseudo-first-order and pseudo-second-order kinetic models to the contact time data for chromate ion adsorption on the CH/bHAp/CF composites

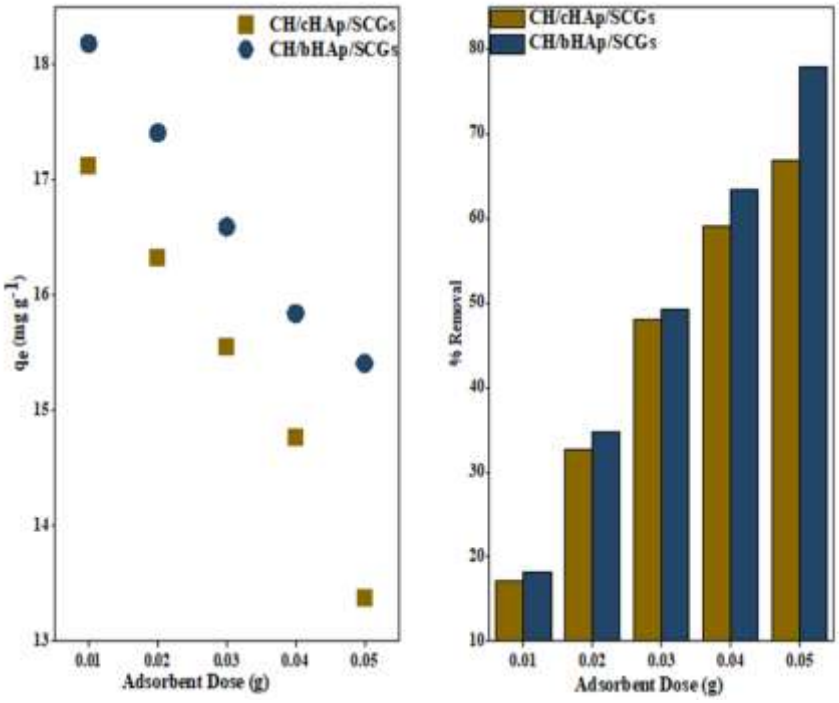

Figure 4-65: AAS data showing the effect of adsorbent dose on Cd^{2+} ion removal and adsorption of cadmium ion on the CH/HAp/SCGs composites: Results are presented as the average of measurements from 3 replicates. SE = ± 0.

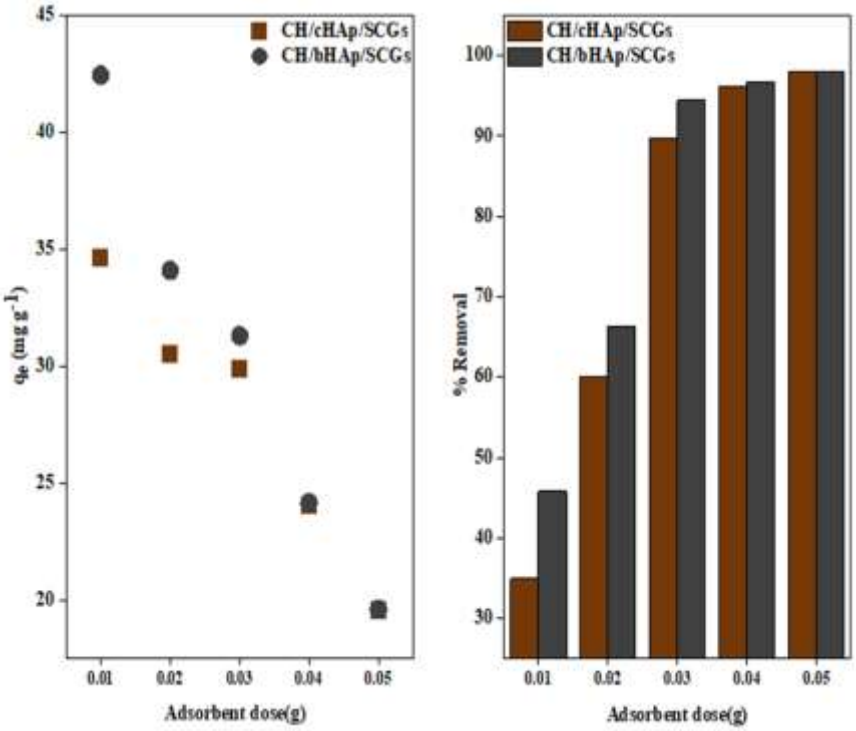

Figure 4-66: AAS data showing the effect of adsorbent dose on Pb^{2+} removal and adsorption on the CH/HAp/SCGs composites. The results are presented as the average of measurements of three replicates. SE = $\pm$ 0.2

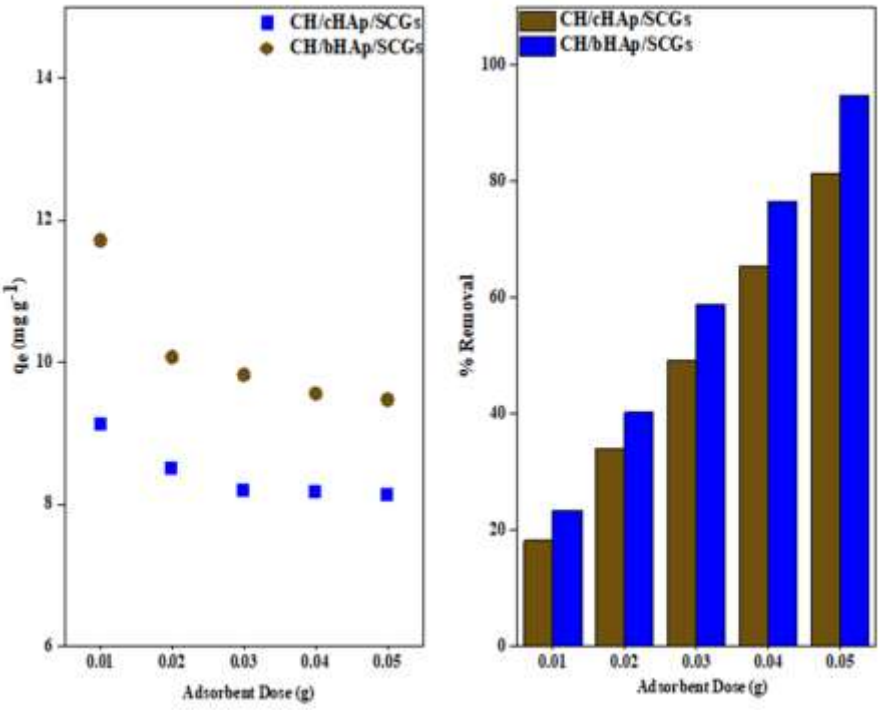

Figure 4-67: AAS data showing the effect of adsorbent dose on Cu^{2+} adsorption on the CH/HAp/SCGs composites. Results are presented as the average of 3 replicates. SE = $\pm$0.4

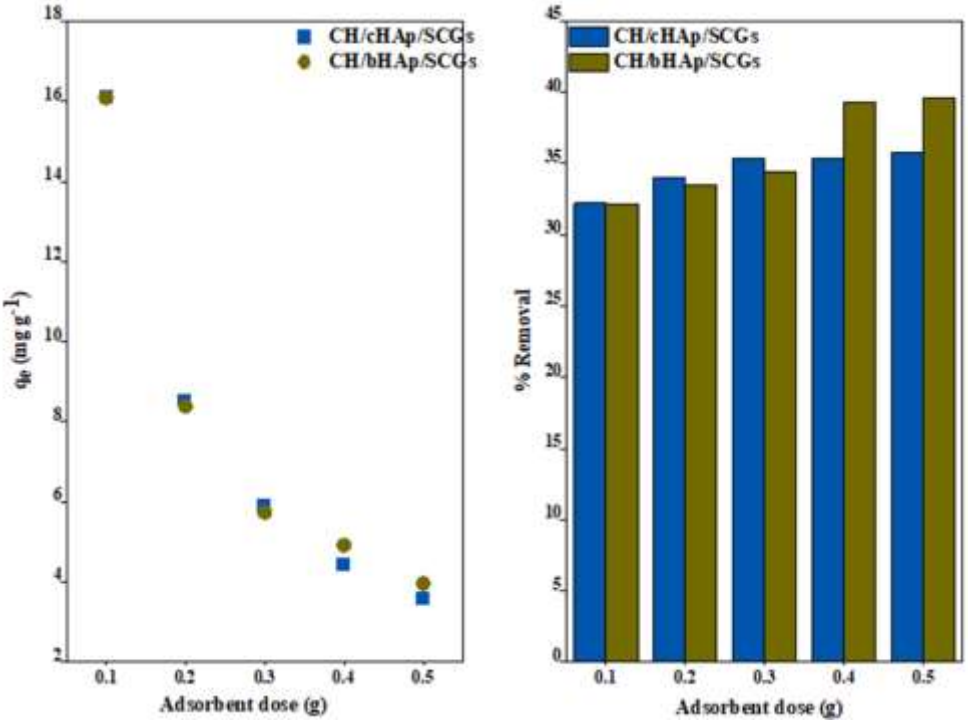

Figure 4-68: AAS data showing the effect of adsorbent dose on chromate ion removal and adsorption on the CH/HAp/SCGs composites. The results are presented as the average of measurements of three replicates. SE = ± 0.7

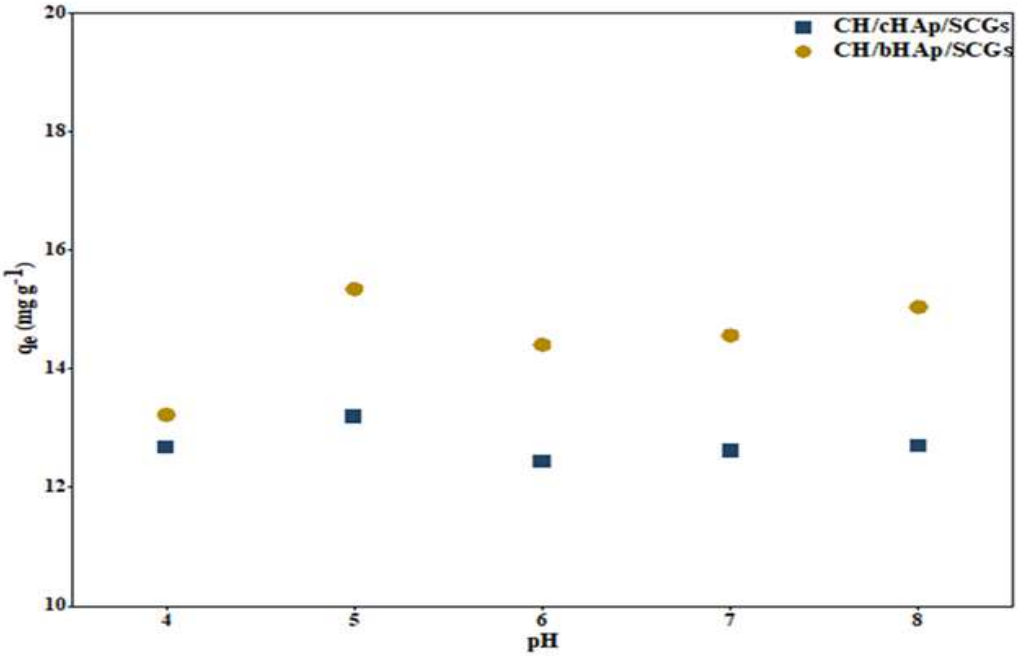

Figure 4-69: AAS data showing the effect of the solution pH on Cd^{2+} removal and adsorption on the CH/HAp/SCGs composites. The results are presented as the average of measurements of three replicates. SE = ± 0.1

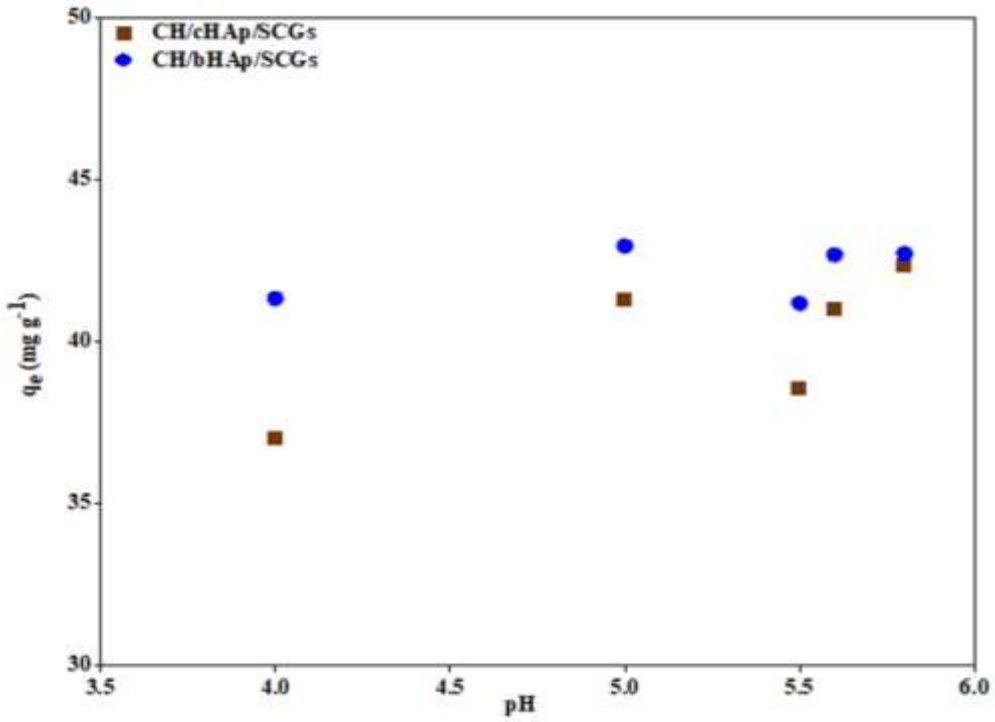

Figure 4-70: AAS data showing the effect of solution pH on Pb^{2+} adsorption on the CH/HAp/SCGs composites. The results are presented as the average of measurements of three replicates. SE = ± 0.2

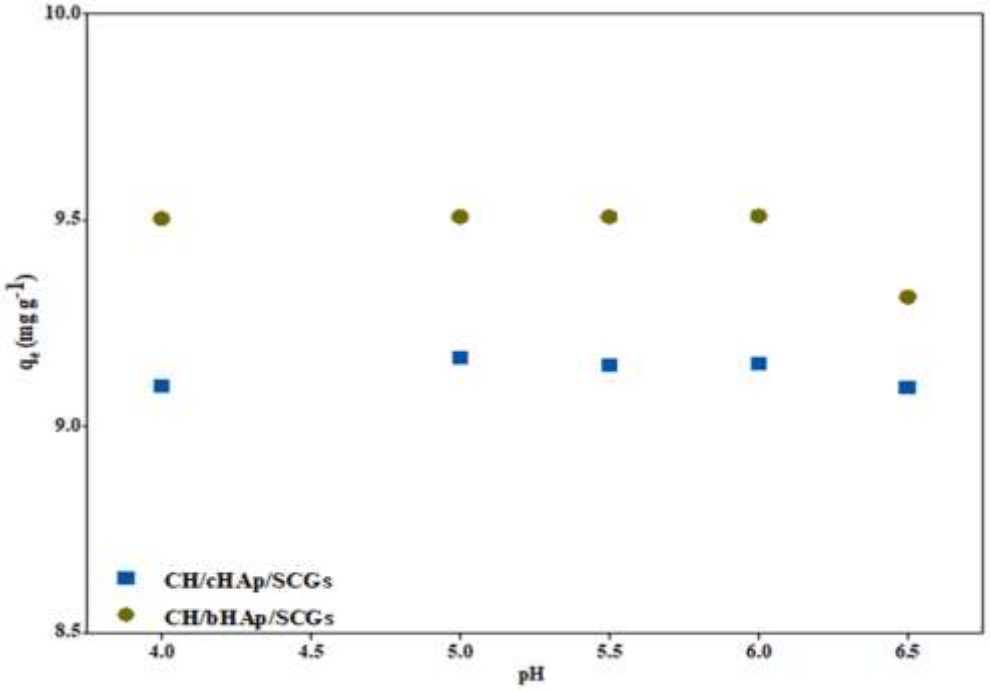

Figure 4-71: AAS data showing the effect of adsorbent dose on Cu^{2+} adsorption on the CH/HAp/SCGs composites. The results are presented as the average of measurements of three replicates. SE = ± 0.07

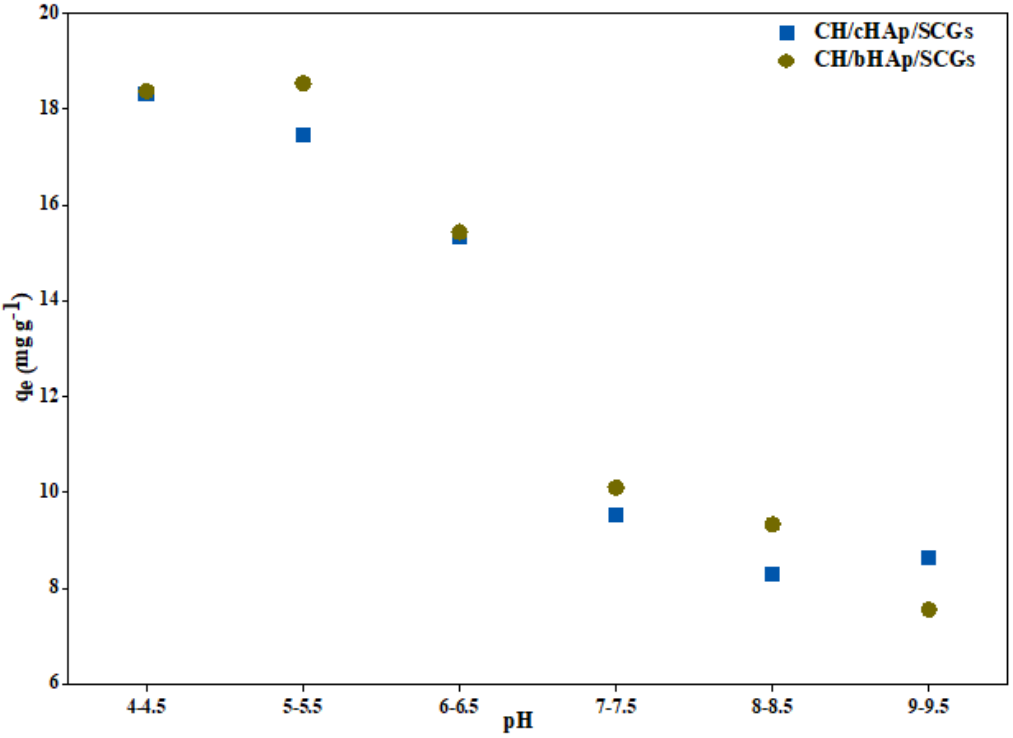

Figure 4-72: AAS data showing the effect of adsorbent dose on chromate ion removal and adsorption on the CH/HAp/SCGs composites. The results are presented as the average of measurements of three replicates. SE = ± 0.1

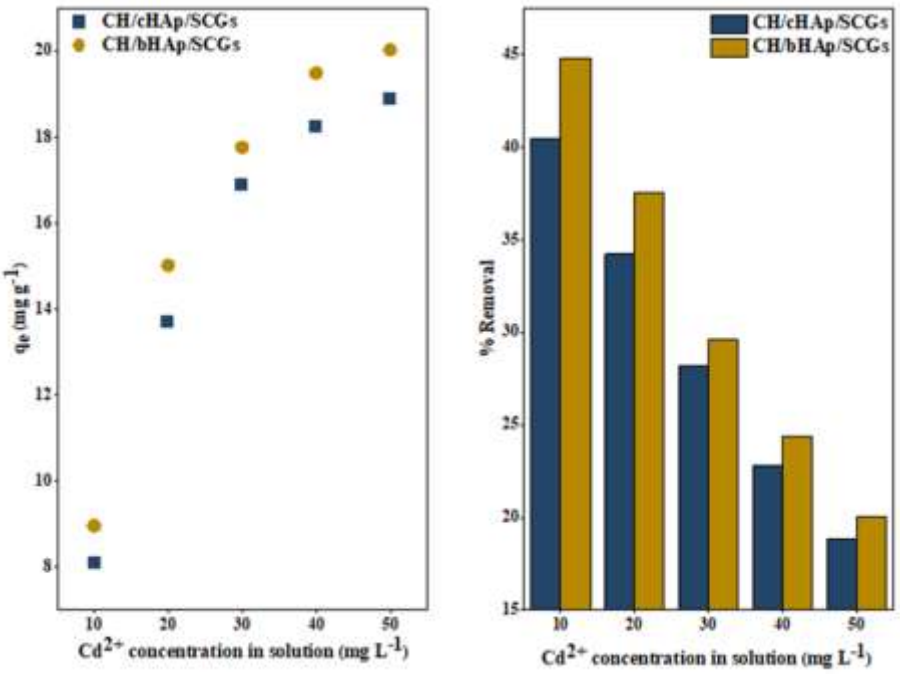

Figure 4-73: AAS data showing the effect of initial metal ion concentration on Cd^{2+} adsorption on the CH/HAp/SCGs composites. Results are calculated as an average of 3 replicates. SE = ± 0.1.

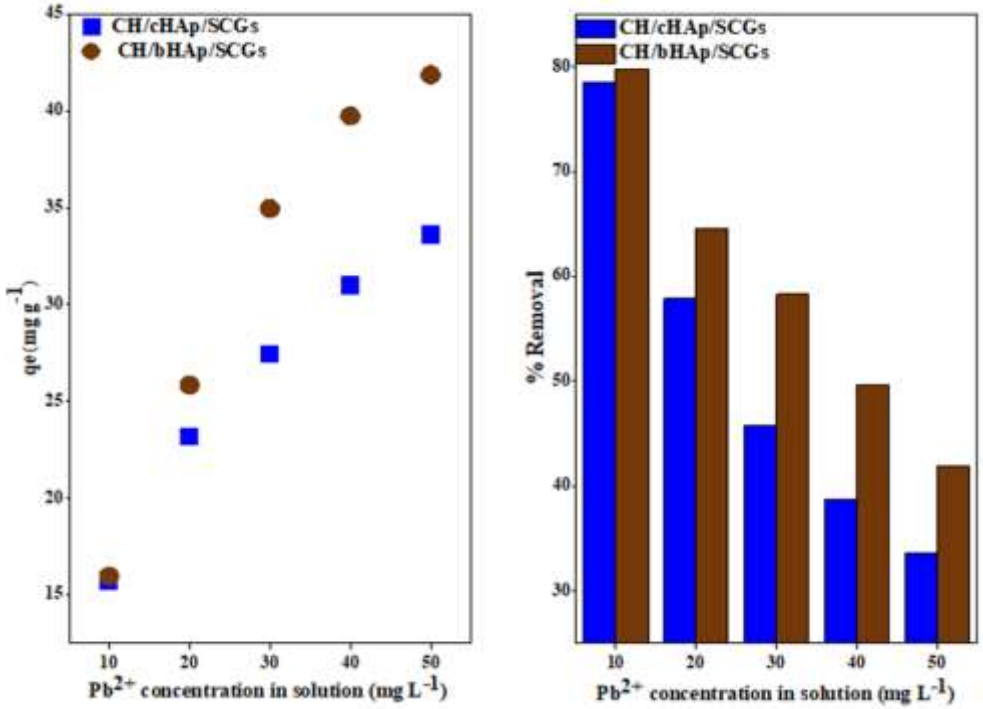

Figure 4-74: AAS data showing the effect of initial metal ion concentration on Pb^{2+} removal and adsorption on CH/HAp/SCGs composites. The results are presented as the average of measurements of three replicates. SE = ± 0.3

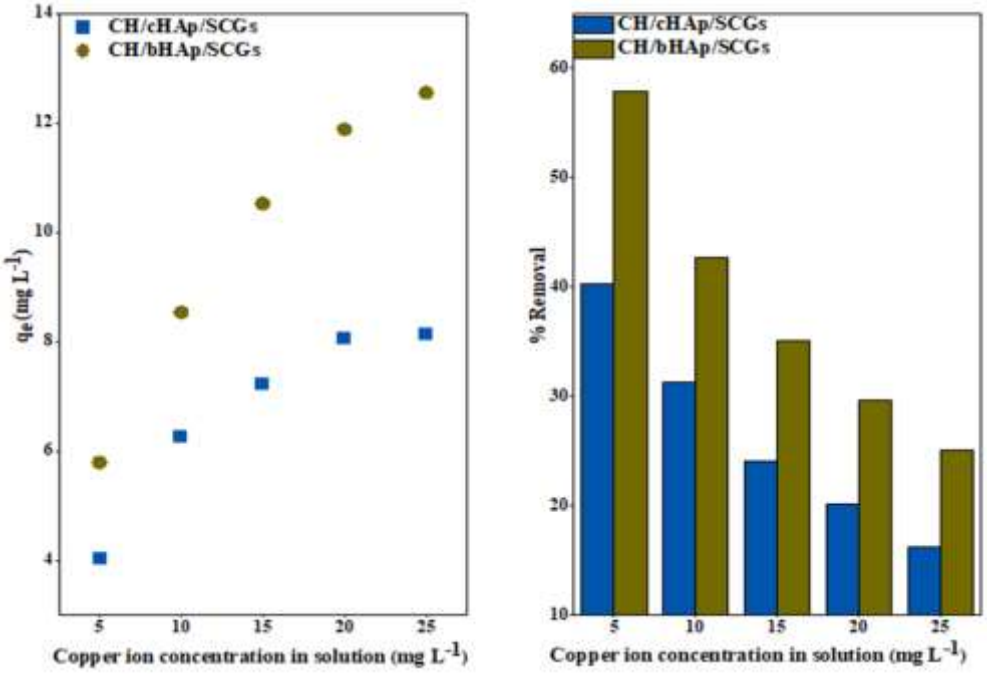

Figure 4-75 AAS data showing the effect of initial metal ion concentration on Cu^{2+} removal and adsorption on the CH/HAp/SCGs composites. The results are presented as the average of measurements of three replicates. SE = ± 0.3

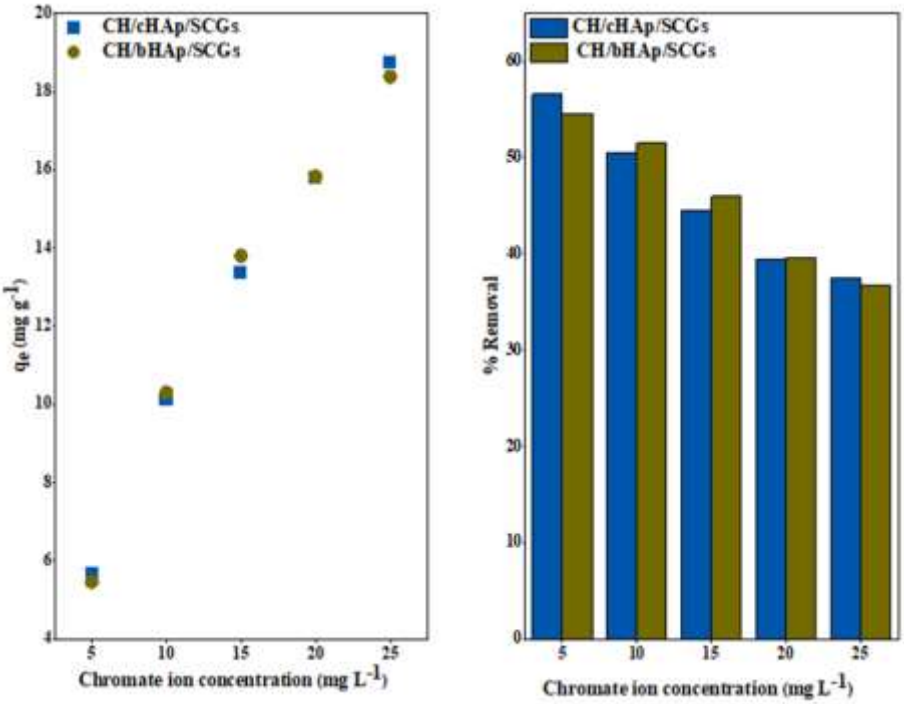

Figure 4-76: AAS data showing the effect of initial metal ion concentration on chromate ion removal and adsorption on the CH/HAp/SCGs composites. The results are presented as the average of measurements of three replicates. SE = ± 0.3

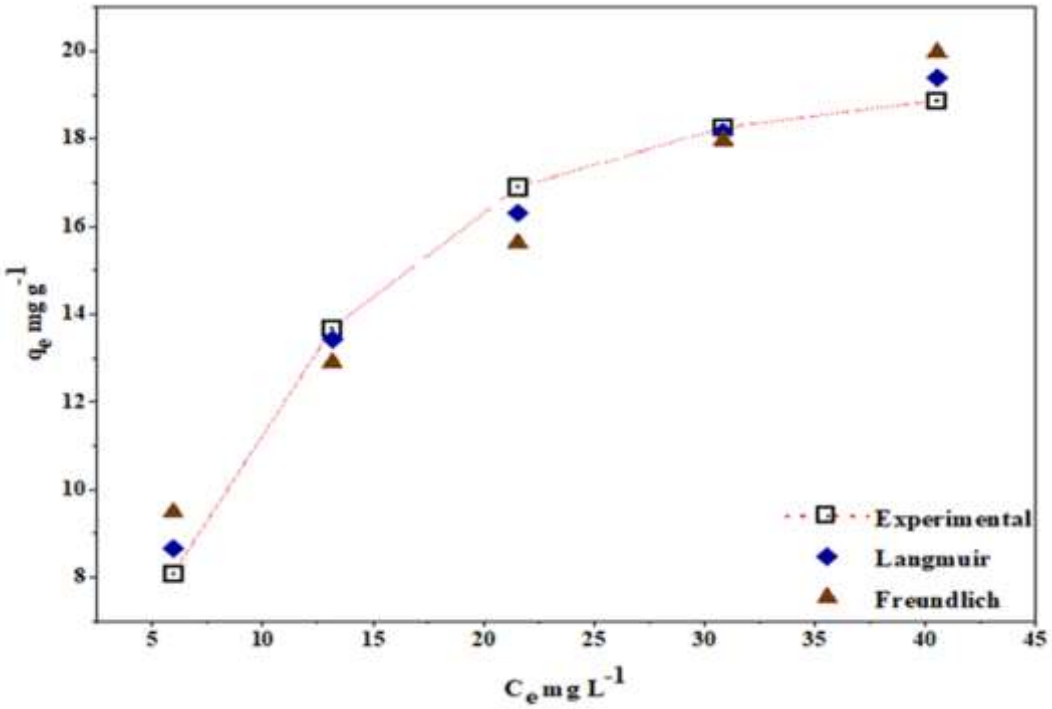

Figure 4-77: The fitting of the non-linear Langmuir and Freundlich adsorption isotherms to experimental data for Cd^{2+} adsorption on the CH/cHAp/SCGs composite

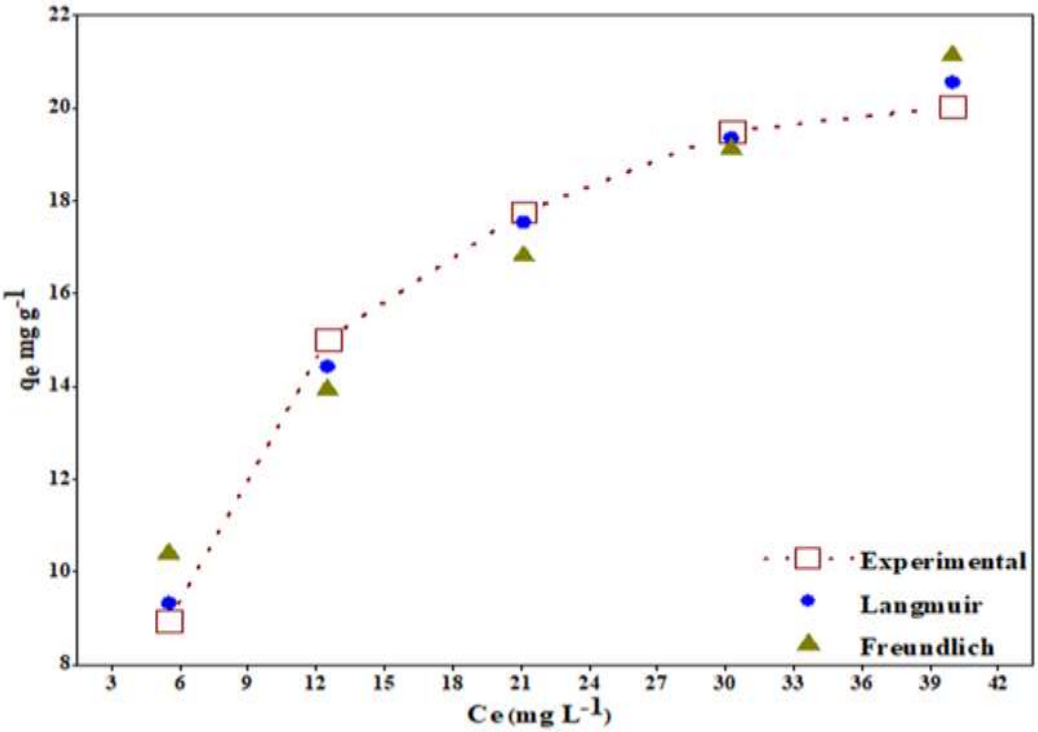

Figure 4-78: The fitting of the non-linear Langmuir and Freundlich adsorption isotherms to experimental data for Cd^{2+} adsorption on the CH/bHAp/SCGs composites

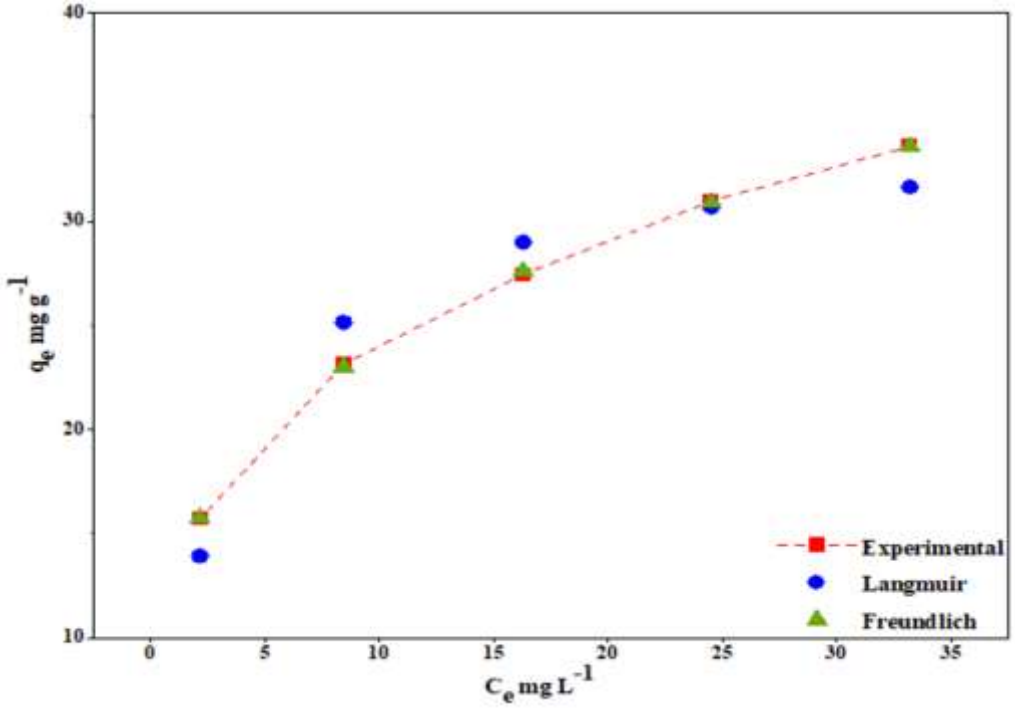

Figure 4-79: The fitting of non-linear Langmuir and Freundlich adsorption isotherms to experimental data for Pb^{2+} adsorption on the CH/cHAp/SCGs composite

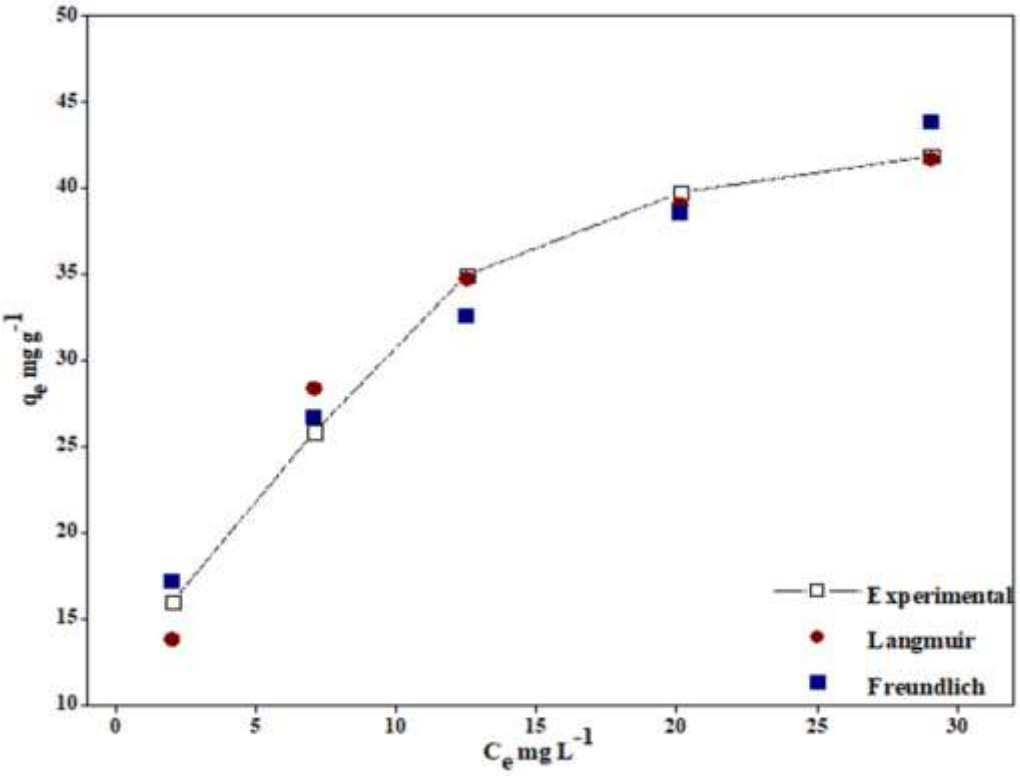

Figure 4-80: The fitting of the non-linear Langmuir and Freundlich adsorption isotherms to experimental data for Pb^{2+} adsorption on the CH/bHAp/SCGs composite

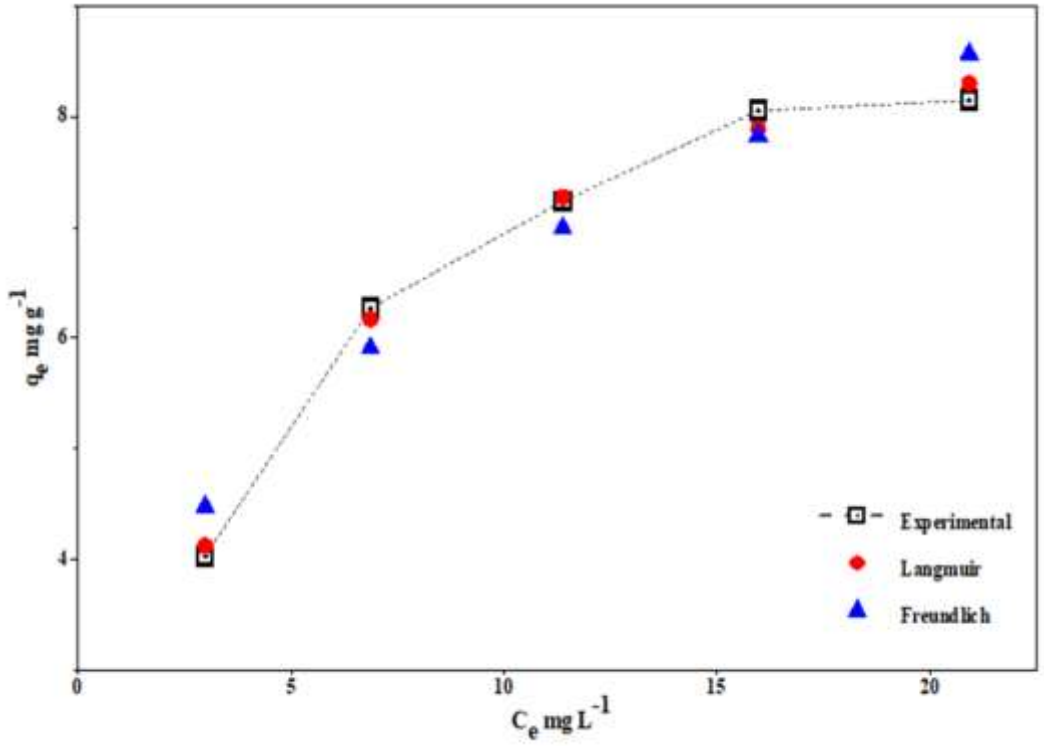

Figure 4-81: The fitting of the non-linear Langmuir and Freundlich isotherms to data for Cu^{2+} adsorption on the CH/cHAp/SCGs composite

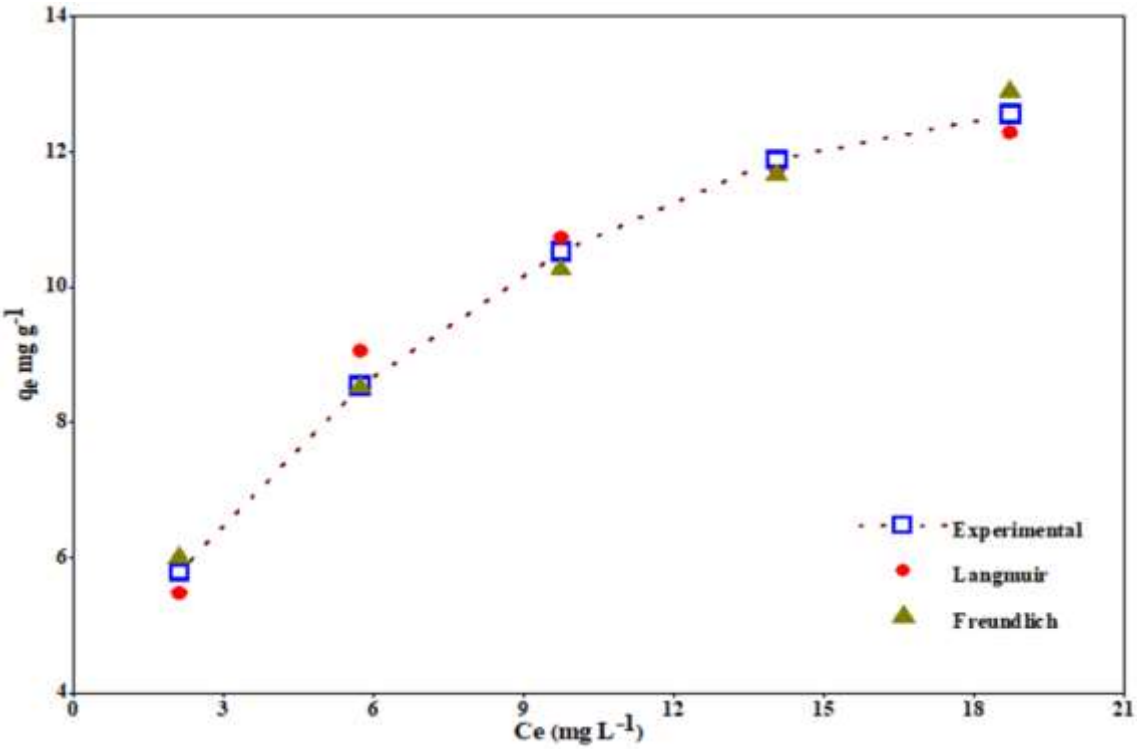

Figure 4-82: The fitted non-linear Langmuir and Freundlich isotherms for Cu^{2+} adsorption on the CH/bHAp/SCGs composite

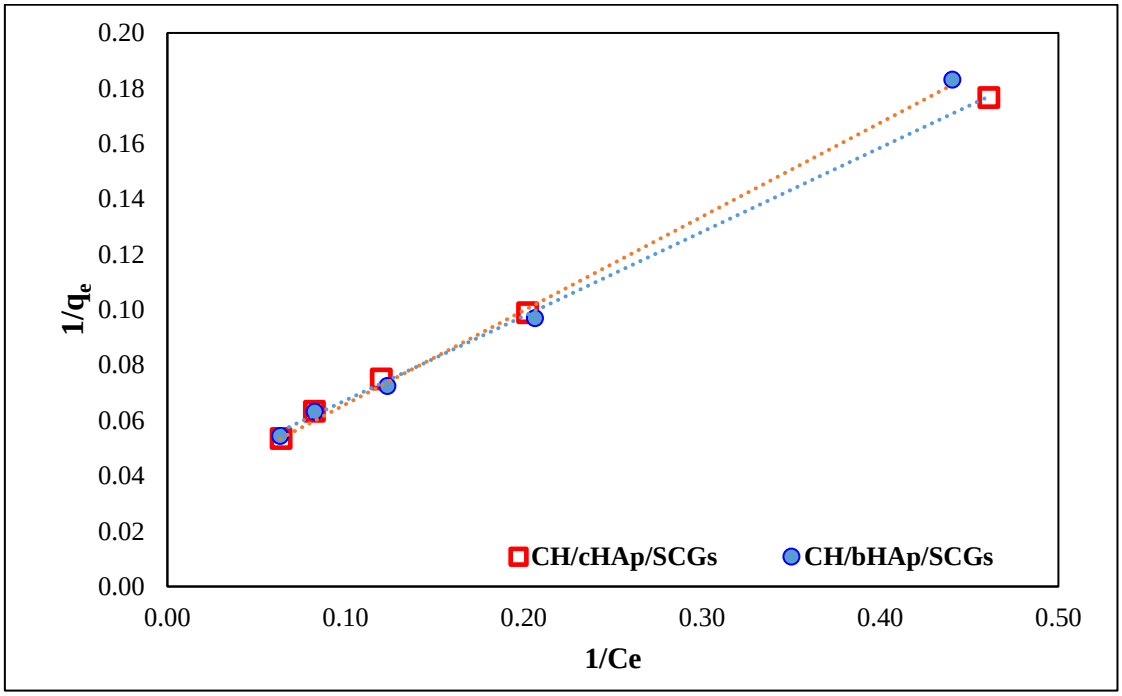

Figure 4-83: The fitting of the linearized Langmuir isotherm model to the experimental data for chromate ion adsorption on the CH/HAp/SCGs composites

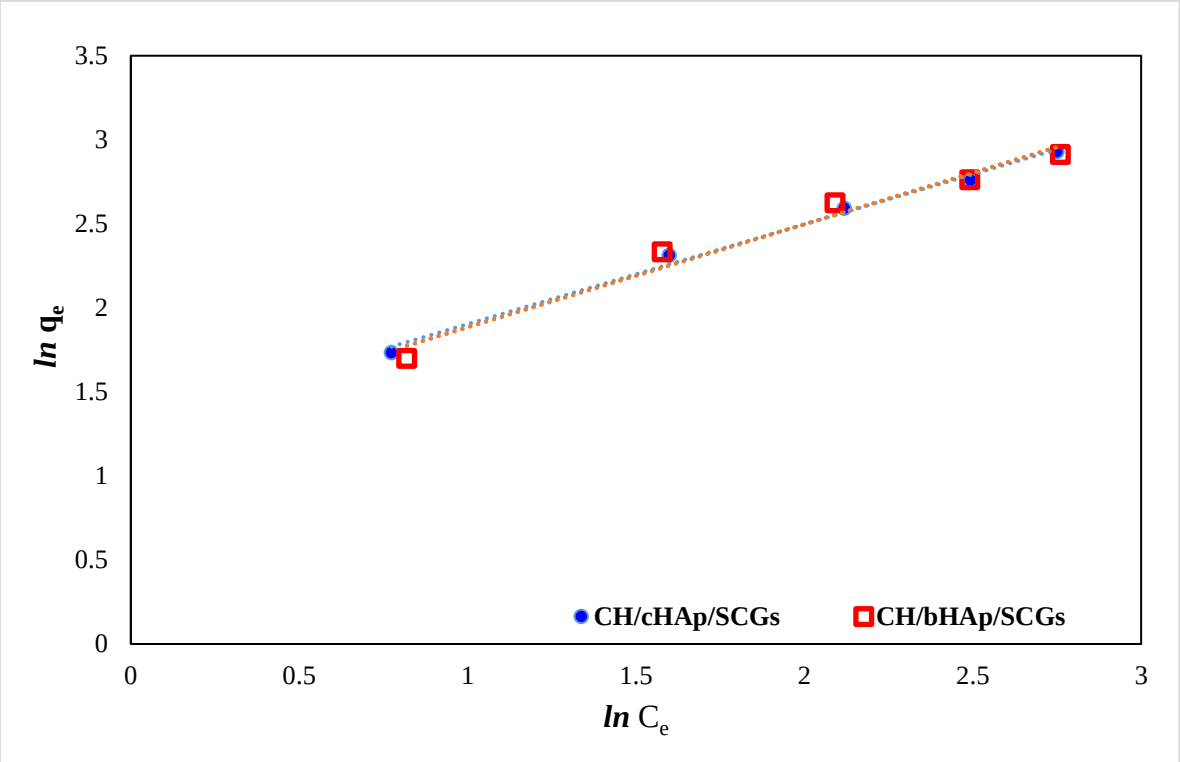

Figure 4-84: The fitting of the linearized Freundlich isotherm model to the experimental data for chromate ion adsorption on the CH/HAp/SCGs composites

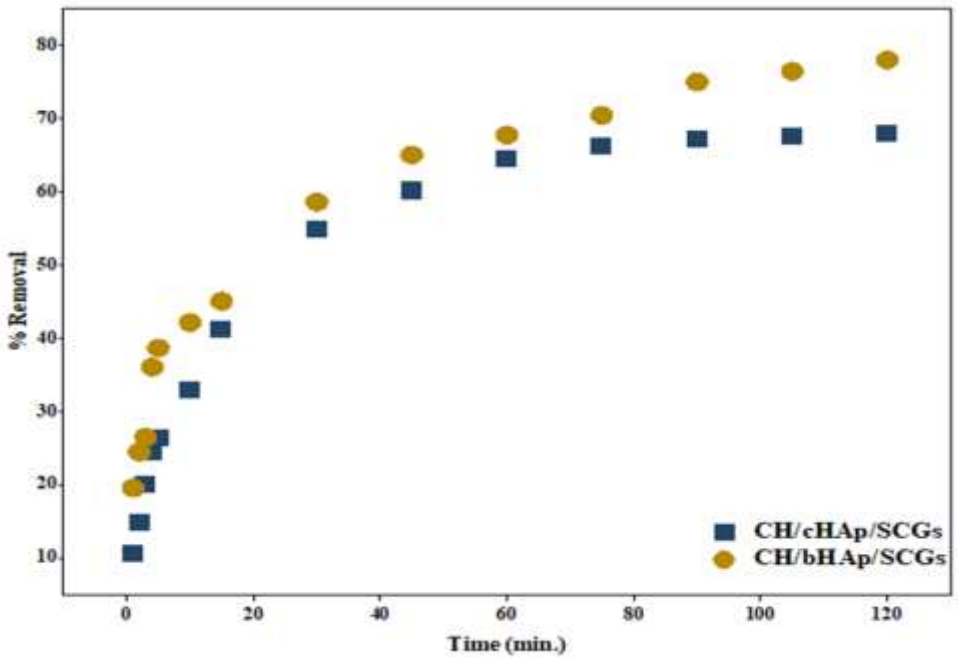

Figure 4-85: AAS data showing the effect of contact time on Cd^{2+} removal (%) by the CH/HAp /SCGs composites. The results are presented as the average of measurements of three replicates. SE = ± 0.1

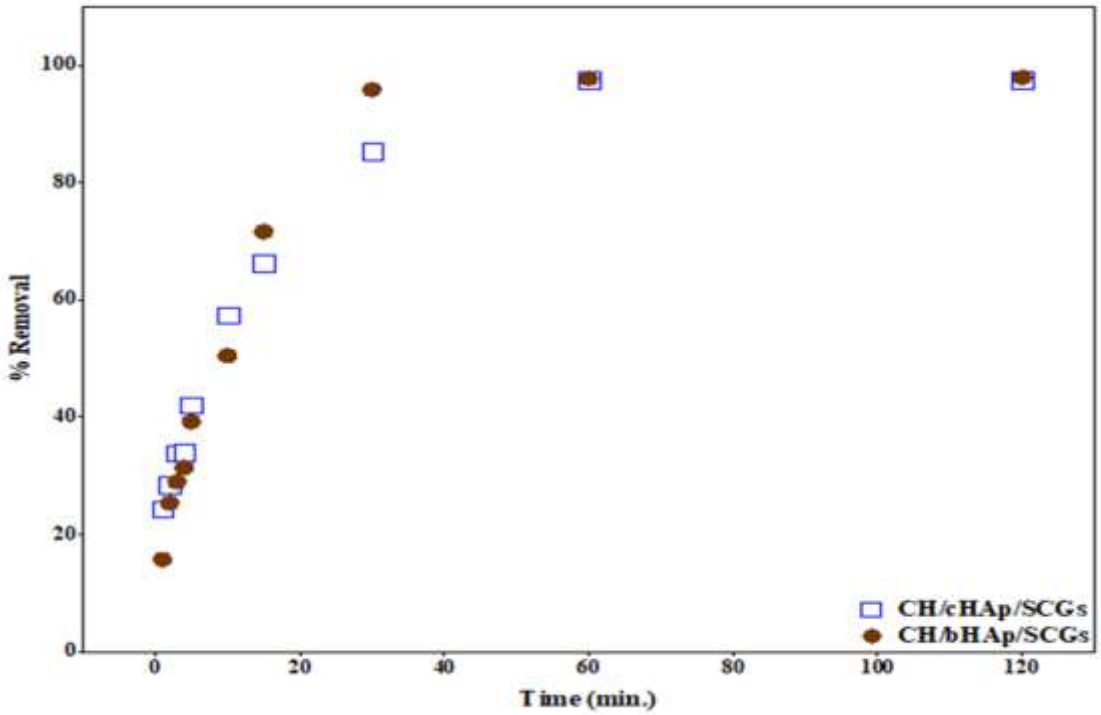

Figure 4-86: AAS data showing the effect of contact time on Pb^{2+} adsorption on the CH/HAp/SCGs composites. Results are reported as the average of 3 replicates. SE = ±0.1.

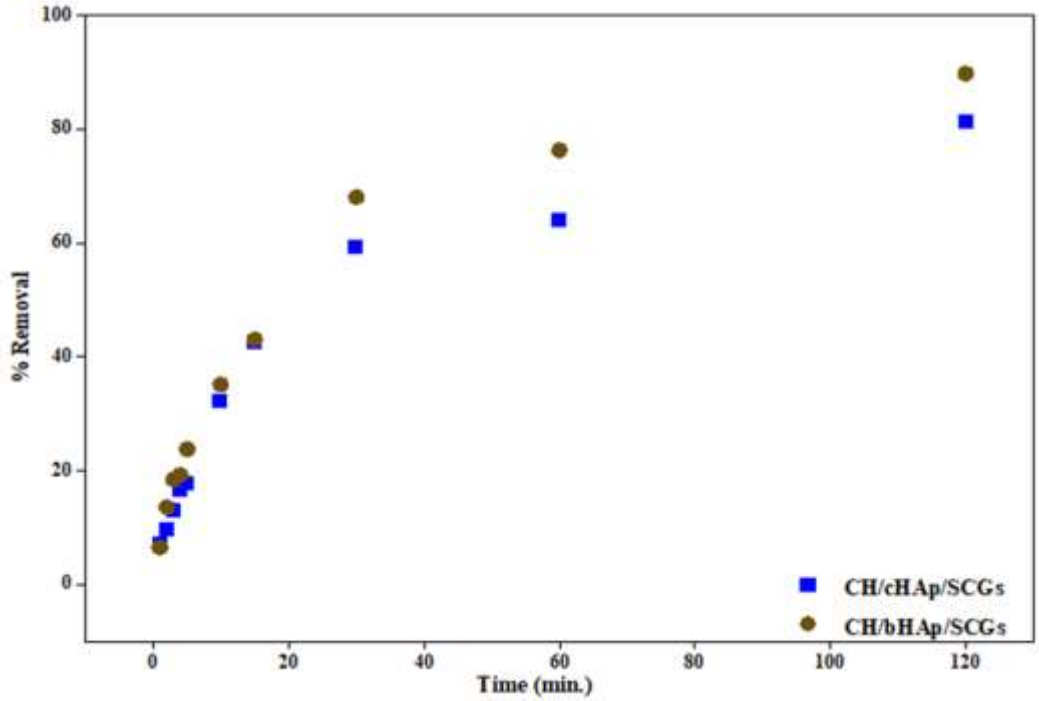

Figure 4-87: AAS data showing the effect of contact time on Cu^{2+} removal by the CH/HAp/SCGs composites. The results are presented as the average of measurements of three replicates. SE= ± 0.02

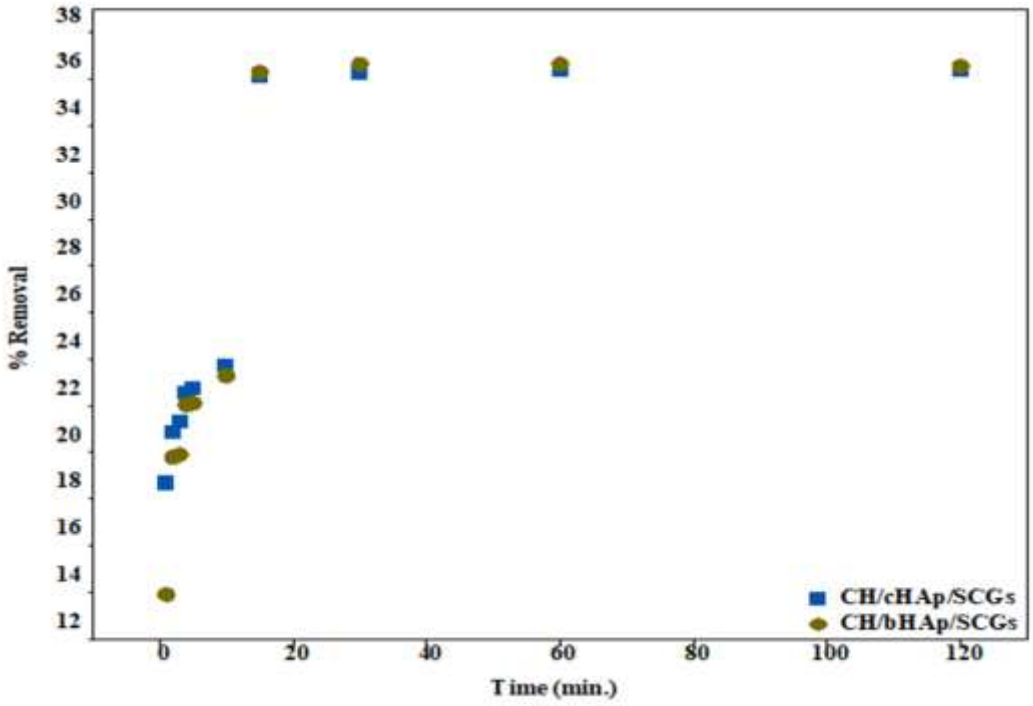

Figure 4-88: AAS data showing the effect of contact time on chromate ion removal and adsorption on the CH/HAp/SCGs composites. The results are presented as the average of measurements of three replicates. SE = ± 0.2

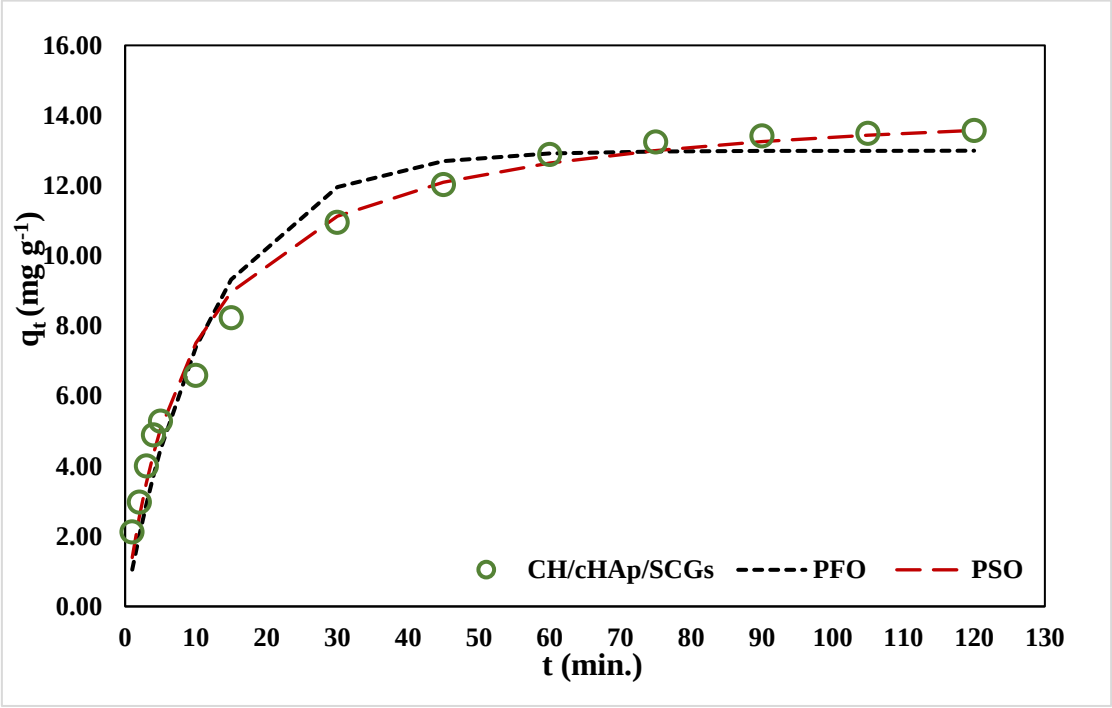

Figure 4-89: The fitting of the non-linear pseudo-first-order (PFO) and pseudo-second-order (PSO) kinetic models to the experimental data for Cd^{2+} adsorption on the CH/cHAp/SCGs composites

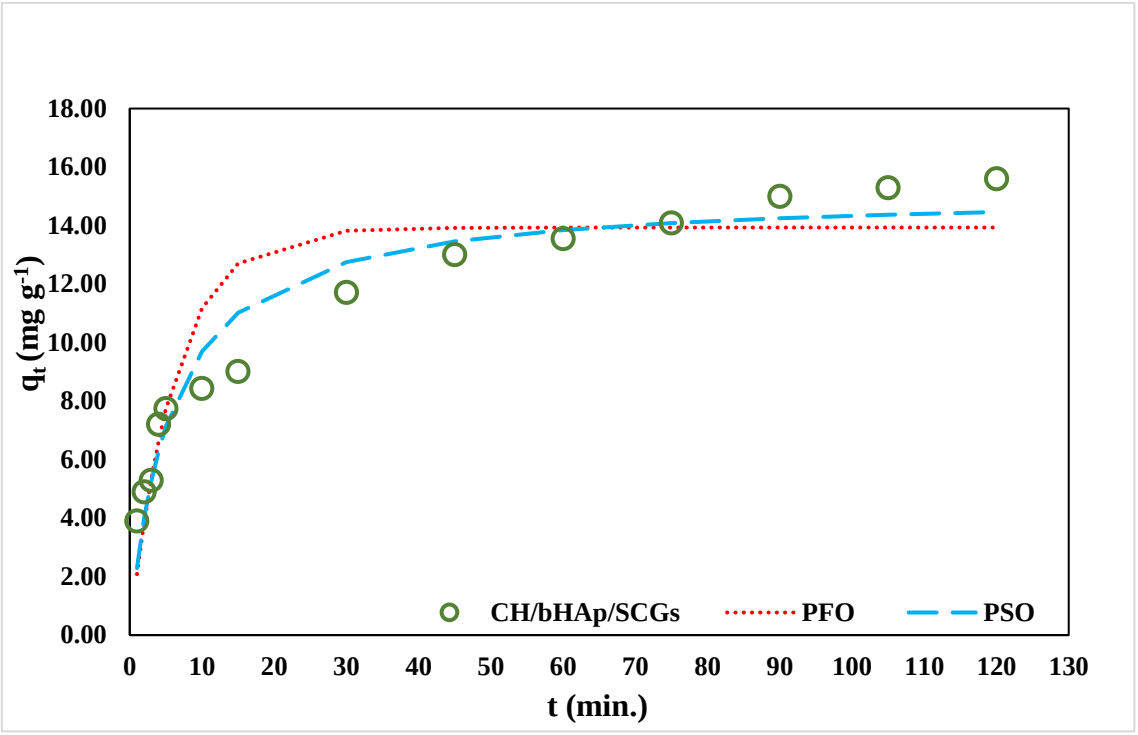

Figure 4-90: The fitting of the non-linear pseudo-first-order (PFO) and pseudo-second-order (PSO) kinetic models to the experimental data for Cd^{2+} adsorption on the CH/bHAp/SCGs composites

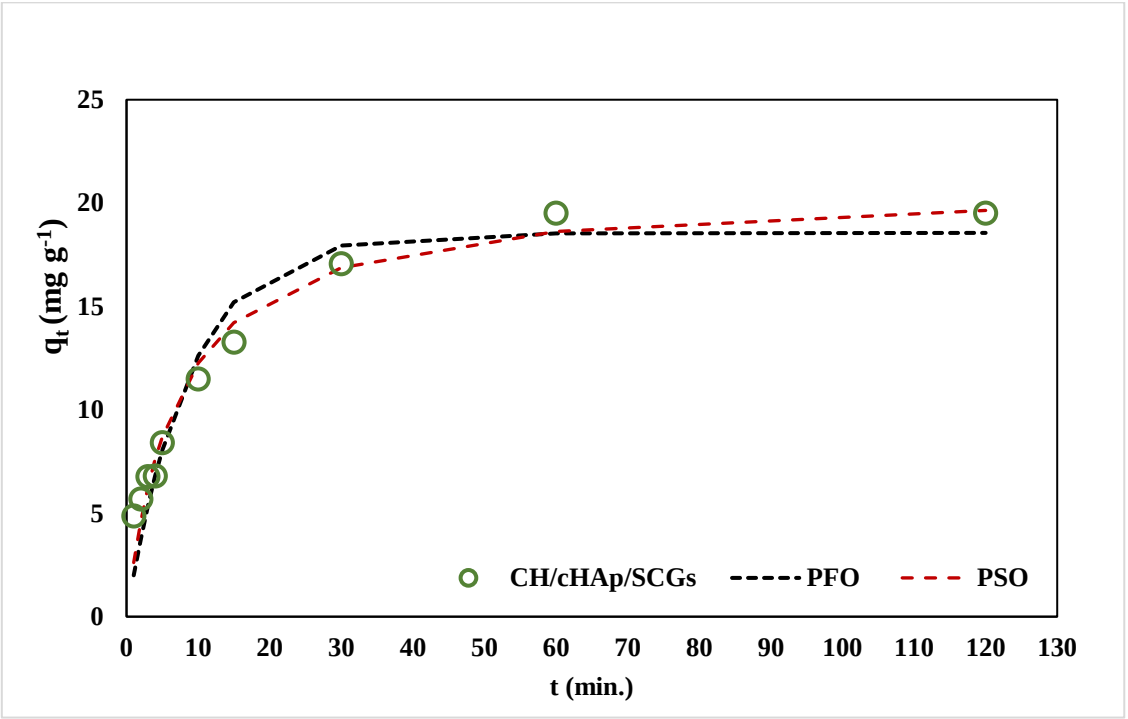

Figure 4-91: The fitting of the non-linear pseudo-first-order (PFO) and pseudo-second-order (PSO) kinetics models to the experimental data for Pb^{2+} adsorption on the CH/cHAp/SCGs composites

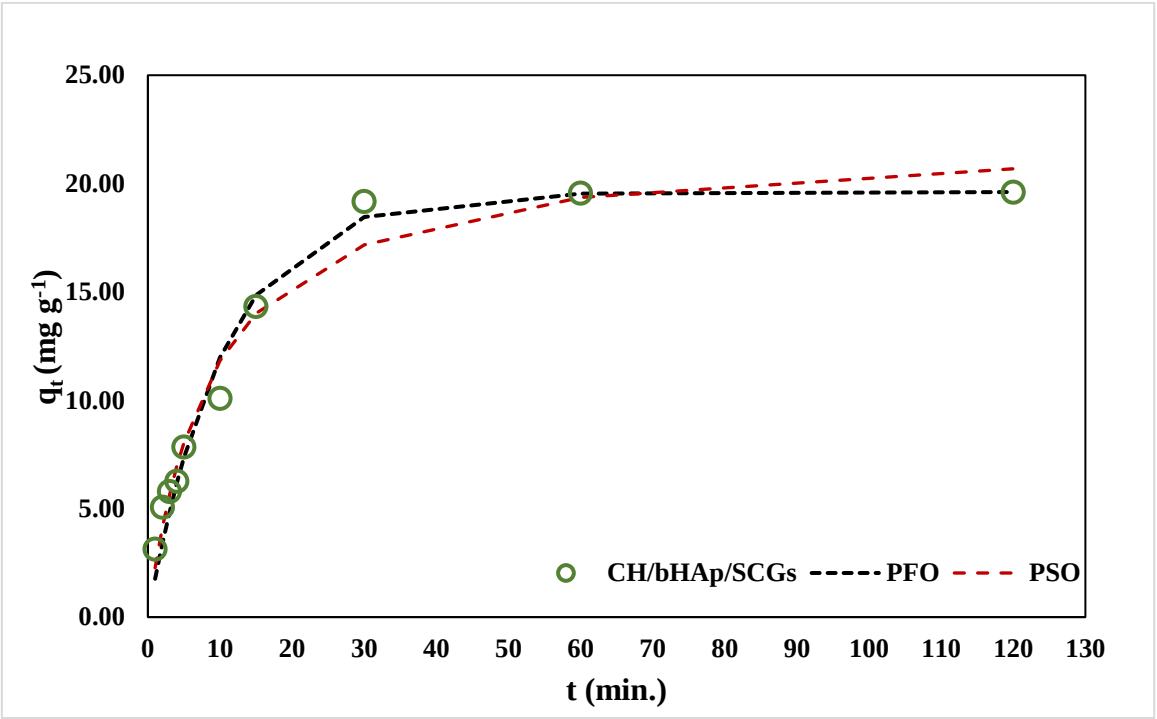

Figure 4-92: The fitting of the non-linear pseudo-first-order (PFO) and pseudo-second-order (PSO) kinetics models to the experimental data for Pb^{2+} adsorption on the CH/bHAp/SCGs composites

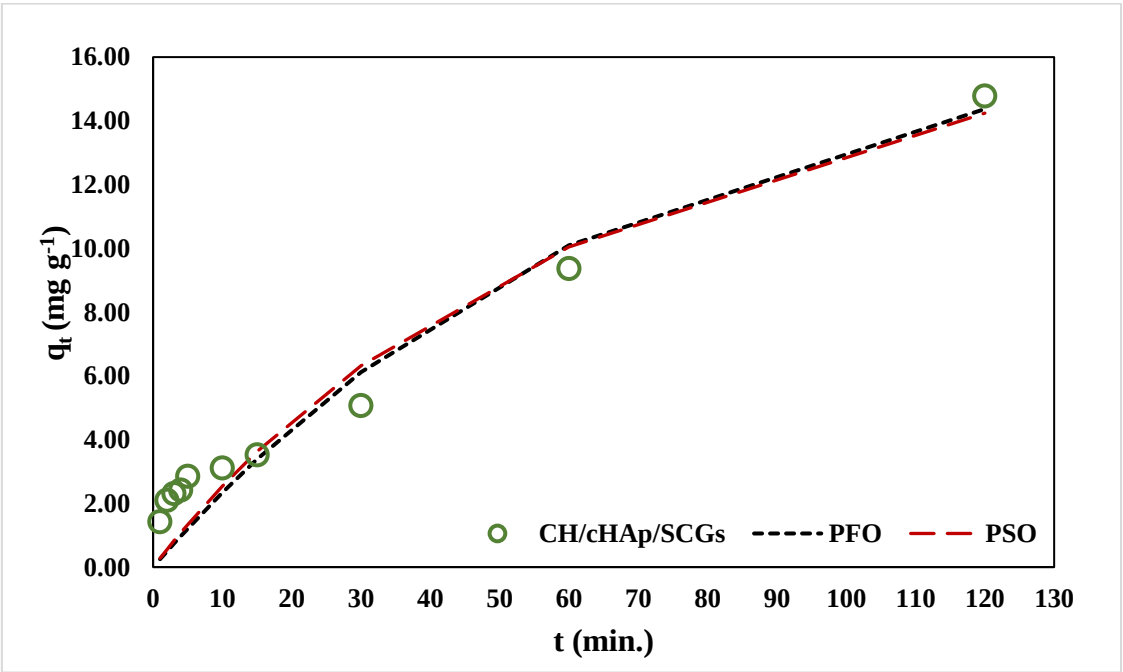

Figure 4-93: The fitting of the non-linear pseudo-first-order and pseudo-second-order kinetics models to experimental data for Cu^{2+} adsorption on the CH/cHAp/SCGs composite

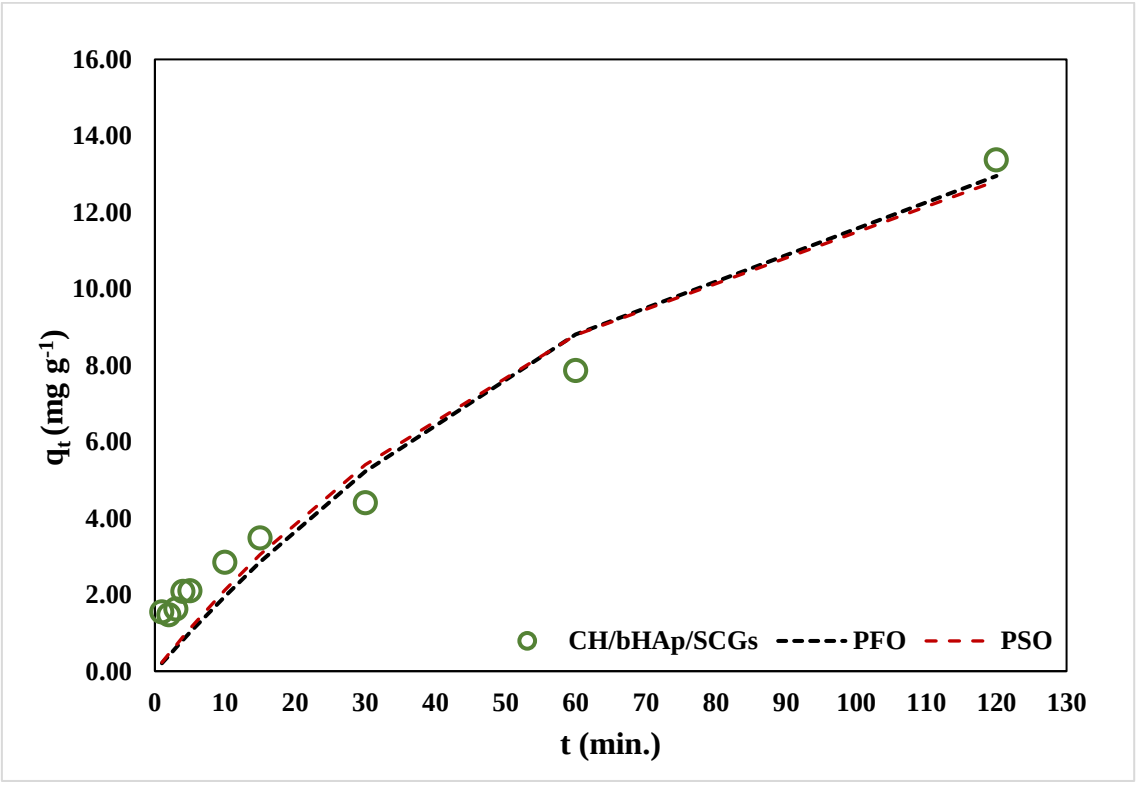

Figure 4-94: The fitting of the non-linear pseudo-first-order and pseudo-second-order kinetics models to experimental data for Cu^{2+} adsorption on the CH/bHAp/SCGs composite

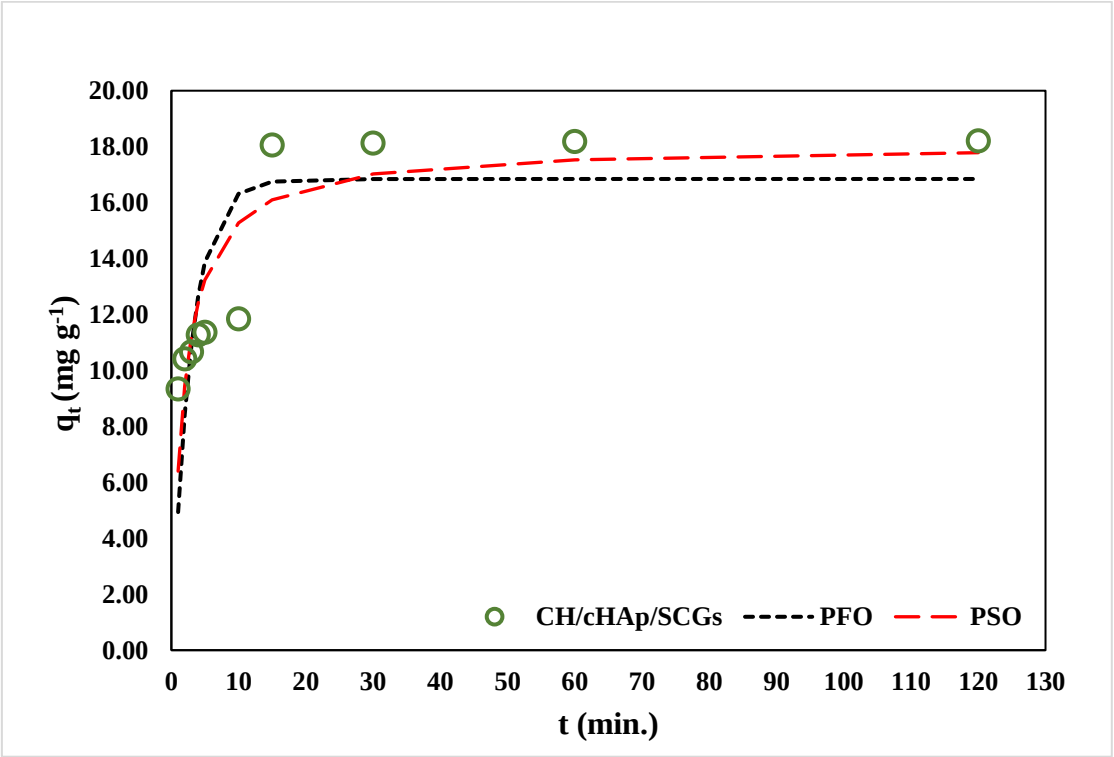

Figure 4-95: The fitting of the non-linear pseudo-first-order and pseudo-second-order kinetics model to the data for chromate ion adsorption on the CH/cHAp/SCGs composites

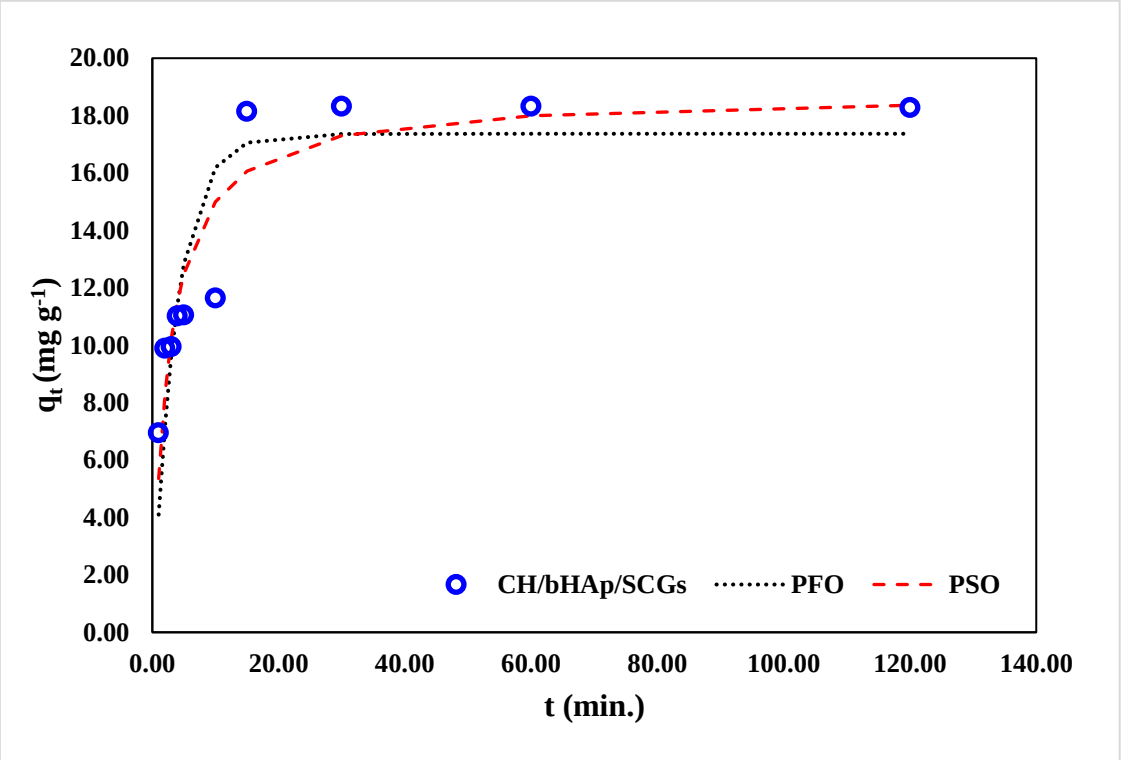

Figure 4-96: The fitting of the non-linear pseudo-first-order and pseudo-second-order kinetics model to the data for chromate ion adsorption on the CH/bHAp/SCGs composites

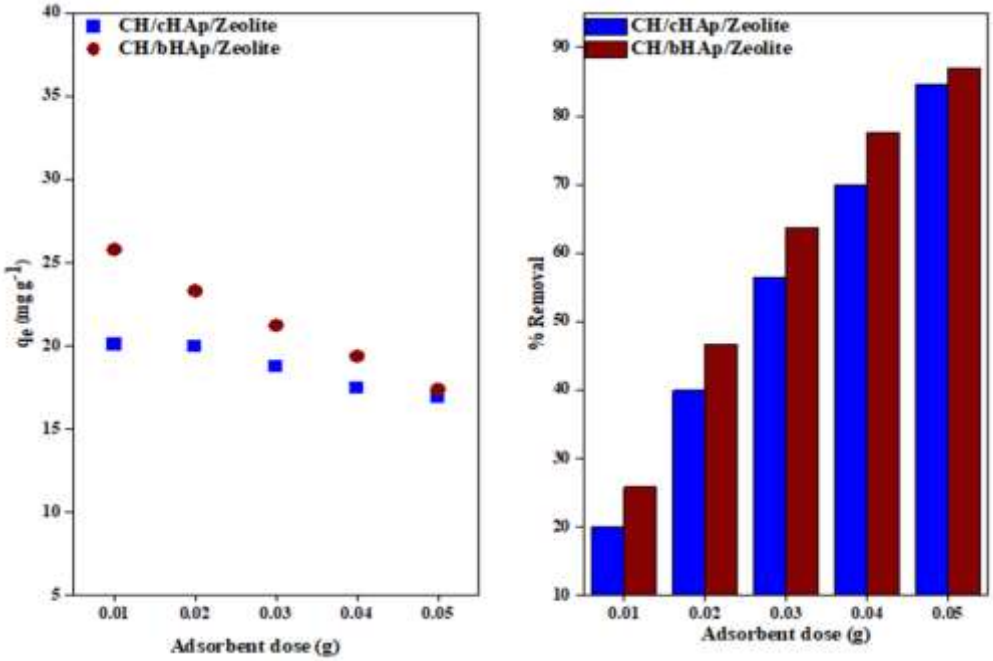

Figure 4-97: AAS data showing the effect of adsorbent dose on Cd^{2+} ion removal and adsorption of Cd2+ ion on the CH/HAp/zeolite composites: Results are presented as the average of measurements from 3 replicates. SE = ± 0.7

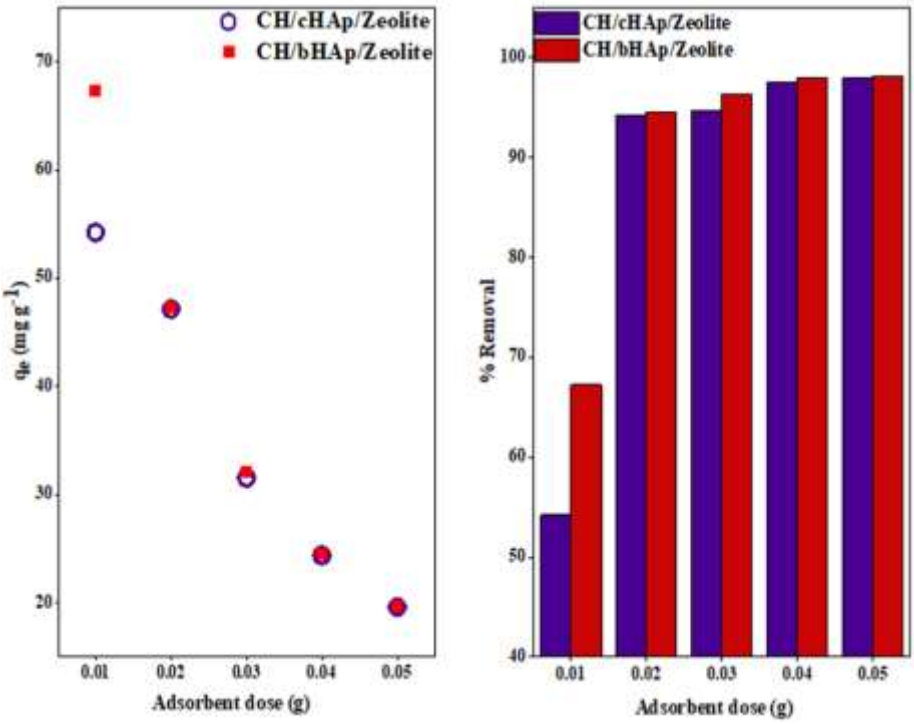

Figure 4-98: AAS data showing the effect of adsorbent dose on Pb^{2+} removal and adsorption on the CH/HAp/zeolite composites: The results are presented as the average of measurements of three replicates. SE = $\pm$ 0.4

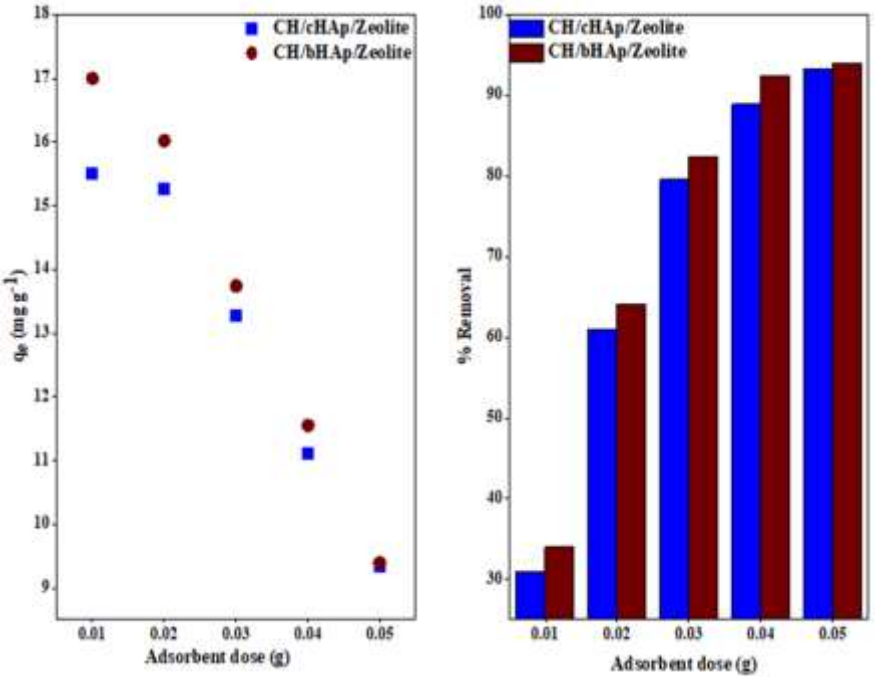

Figure 4-99: AAS data showing the effect of adsorbent dose on Cu^{2+} adsorption and removal of Cu^{2+} by the CH/HAp/zeolite composites. Results are presented as the average of 3 replicates. SE = $\pm$0.2

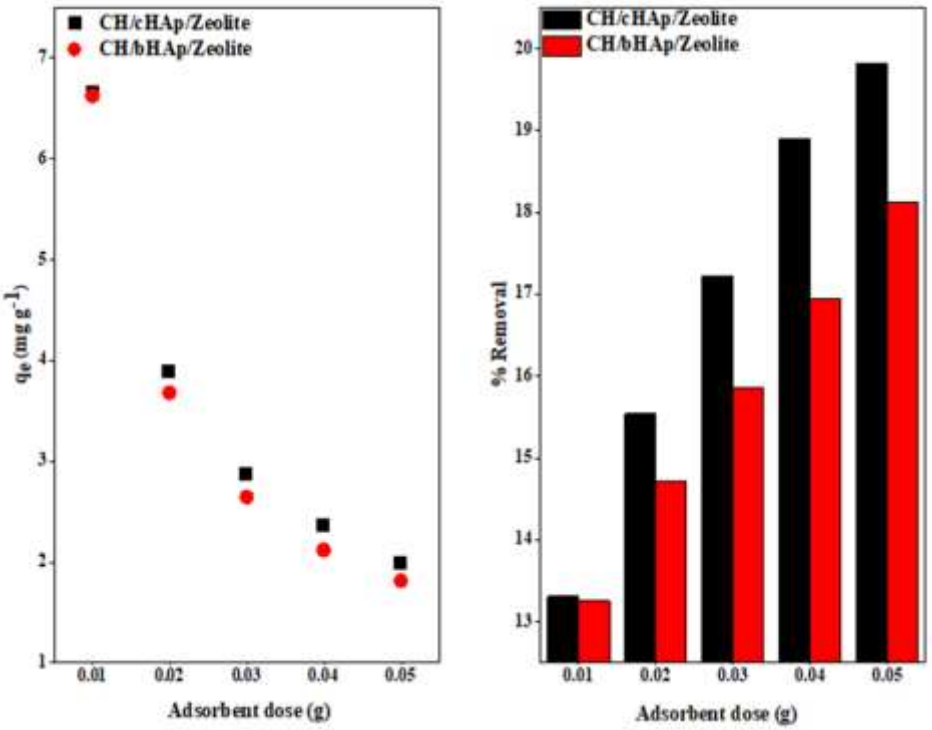

Figure 4-100: AAS data showing the effect of adsorbent dose on chromate ion removal and adsorption on the CH/HAp/zeolite composites. The results are presented as the average of measurements of three replicates. SE = ± 0.1

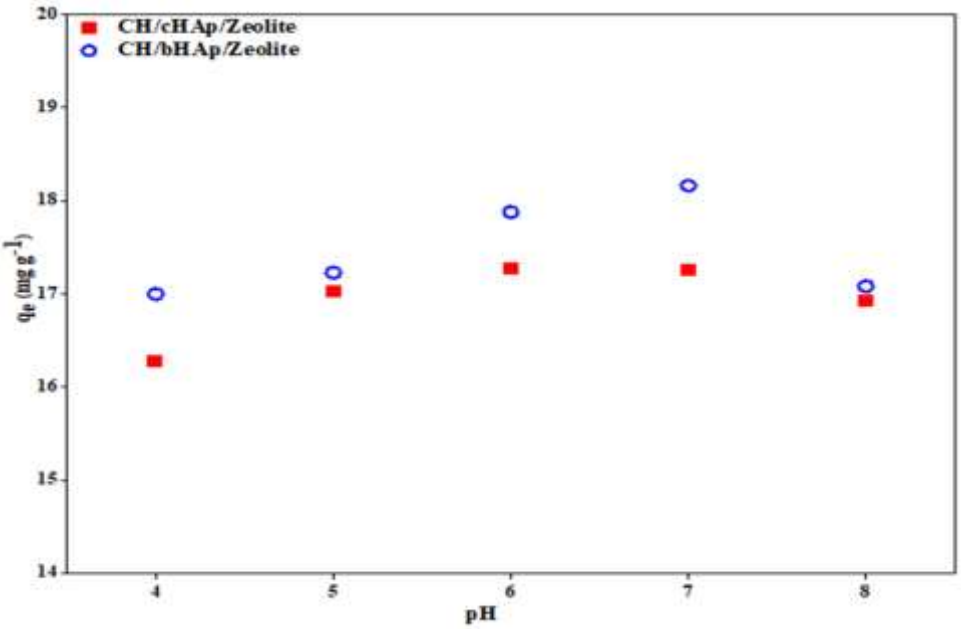

Figure 4-101: AAS data showing the effect of solution pH on Cd^{2+} adsorption on the CH/HAp/zeolite composites. The results are presented as the average of measurements of three replicates. SE = ± 0.3

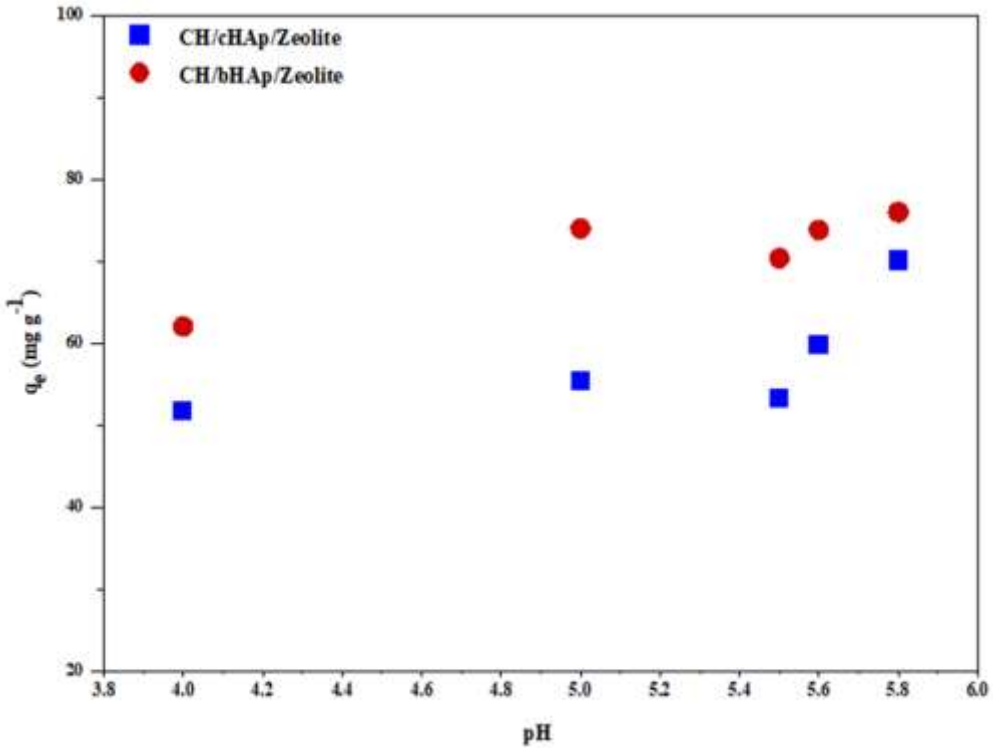

Figure 4-102: AAS data showing the effect of solution pH on Pb^{2+} adsorption on the CH/HAp/zeolite composites. The results are presented as the average of measurements of three replicates. SE = ± 0.2

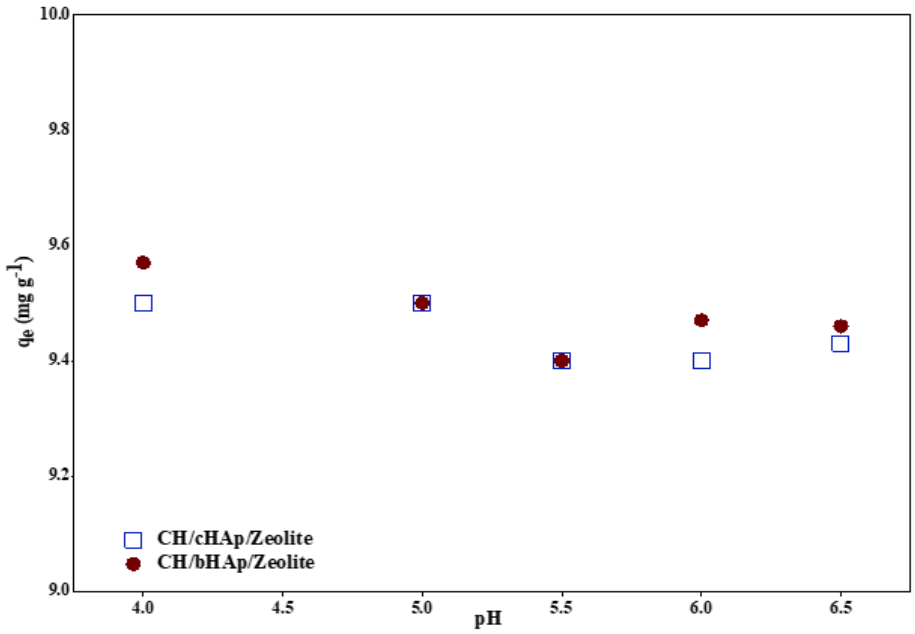

Figure 4-103 AAS data showing the effect of adsorbent dose on Cu^{2+} adsorption on the CH/HAp/zeolite composites. The results are presented as the average of measurements of three replicates. SE = ± 0.01

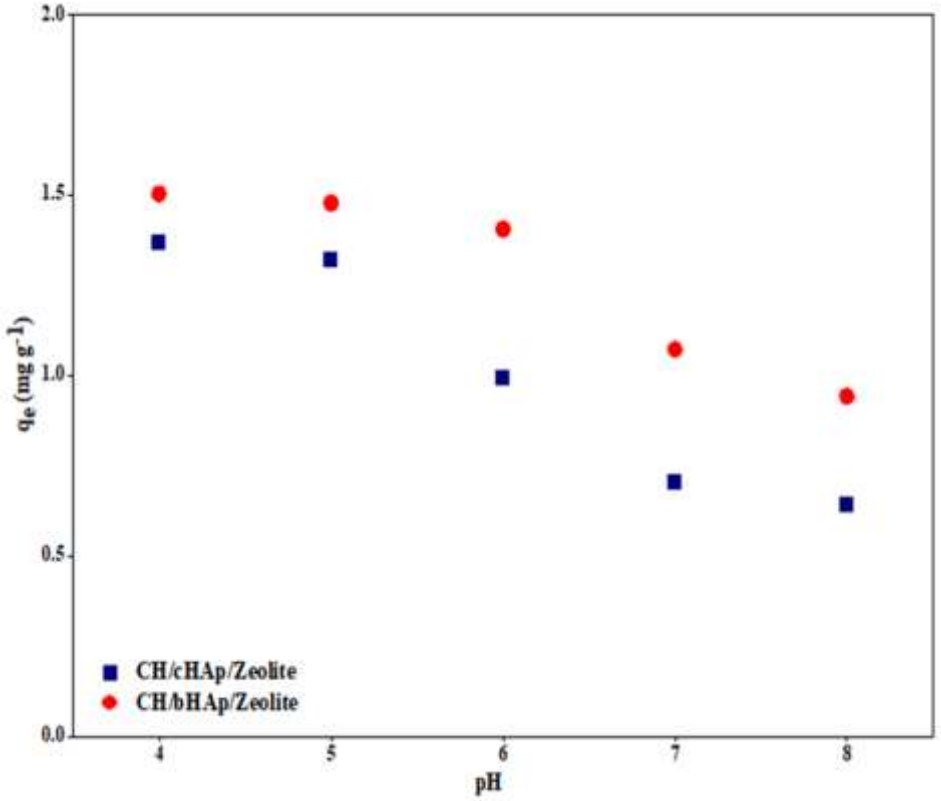

Figure 4-104: AAS data showing the effect of adsorbent dose on chromate ion removal and adsorption on the CH/HAp/zeolite composites. The results are presented as the average of measurements of three replicates. SE = ± 0.1

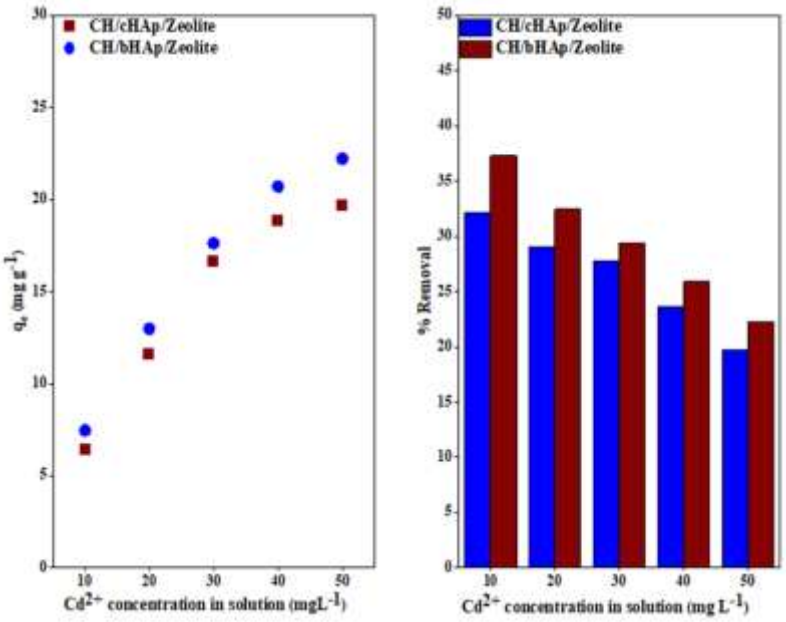

Figure 4-105: AAS data showing the effect of initial metal ion concentration on Cd^{2+} adsorption on CH/HAp/zeolite composites. Results are calculated as an average of 3 replicates. SE = ± 0.2.

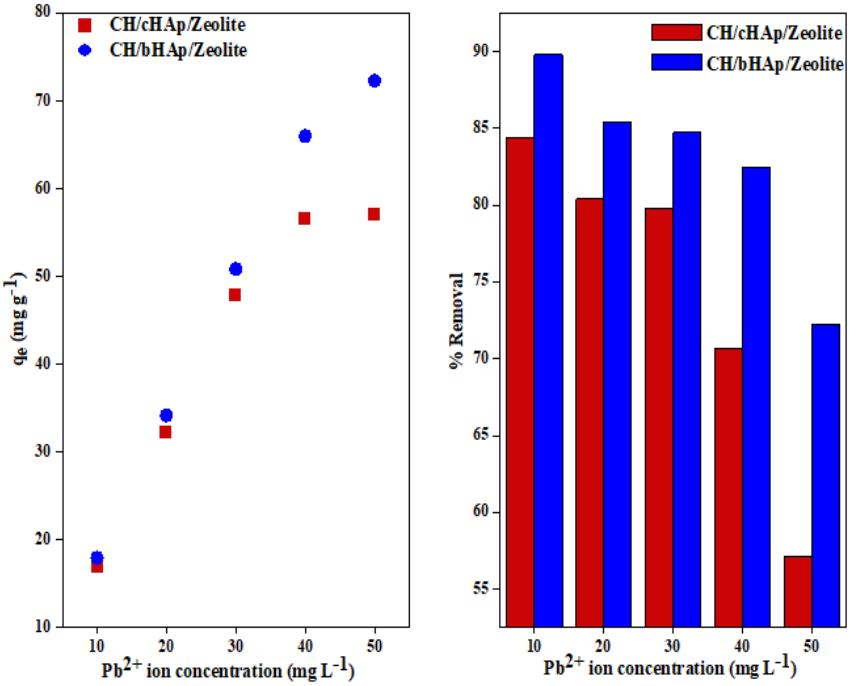

Figure 4-106: AAS data showing the effect of initial metal ions concentration on Pb^{2+} removal and adsorption on the CH/HAp/zeolite composites. The results are presented as the average of measurements of three replicates. SE = ± 0.3

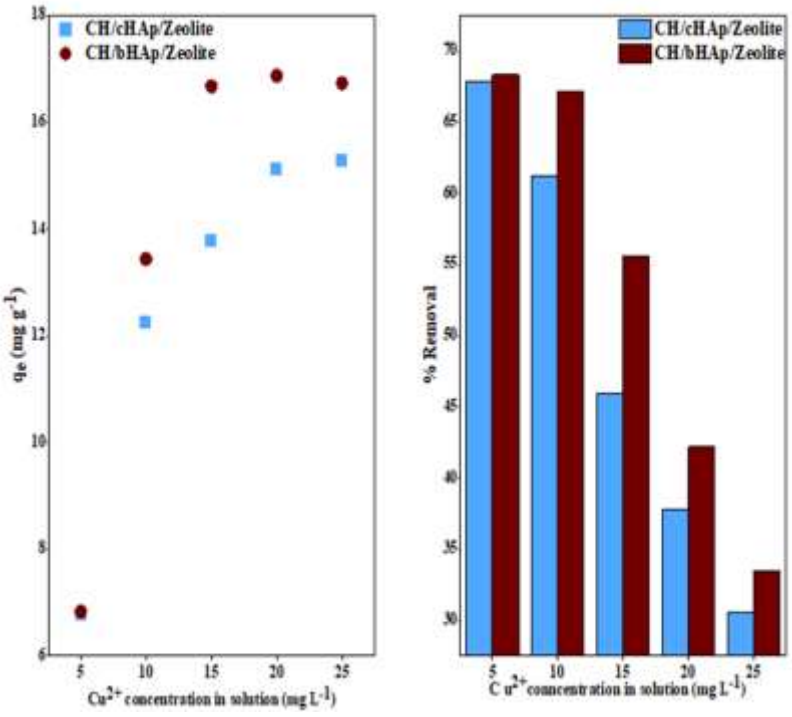

Figure 4-107: AAS data showing the effect of initial metal ion concentration on Cu^{2+} removal and adsorption on the CH/HAp/zeolite composites. The results are presented as the average of measurements of three replicates. SE = ± 0.3

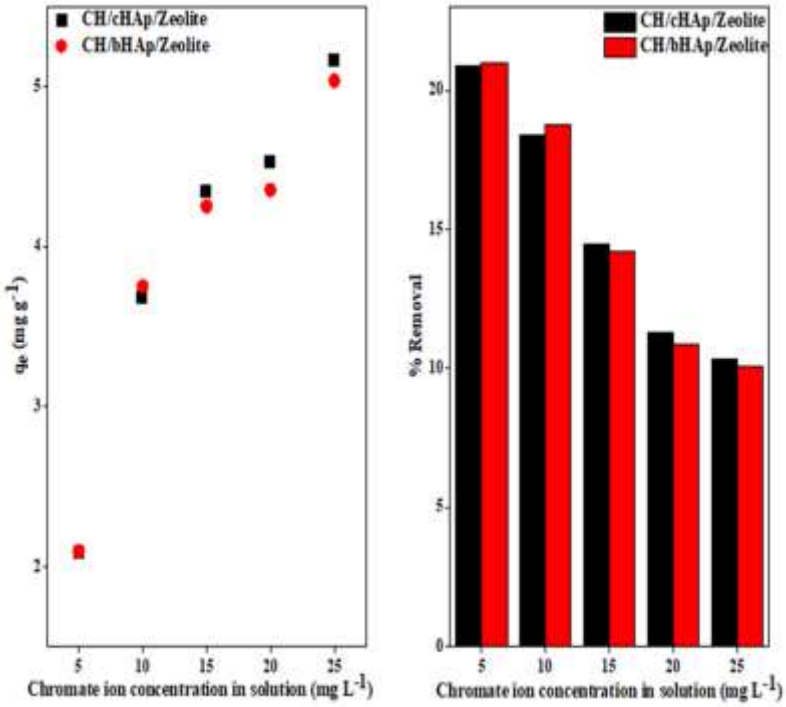

Figure 4-108: AAS data showing the effect of initial metal ion concentration on chromate ion removal and adsorption on the CH/HAp/zeolite composites. The results are presented as the average of measurements of three replicates. SE = ± 0.

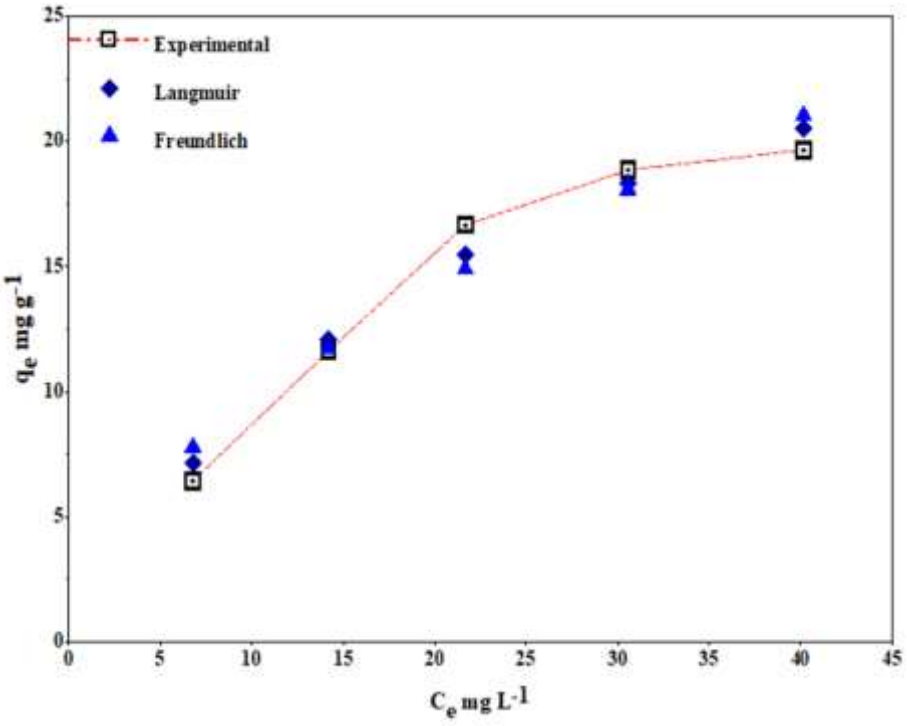

Figure4-109: The fitting of the non-linear Langmuir and Freundlich adsorption isotherms to experimental data for Cd^{2+} adsorption on the CH/cHAp/zeolite composite

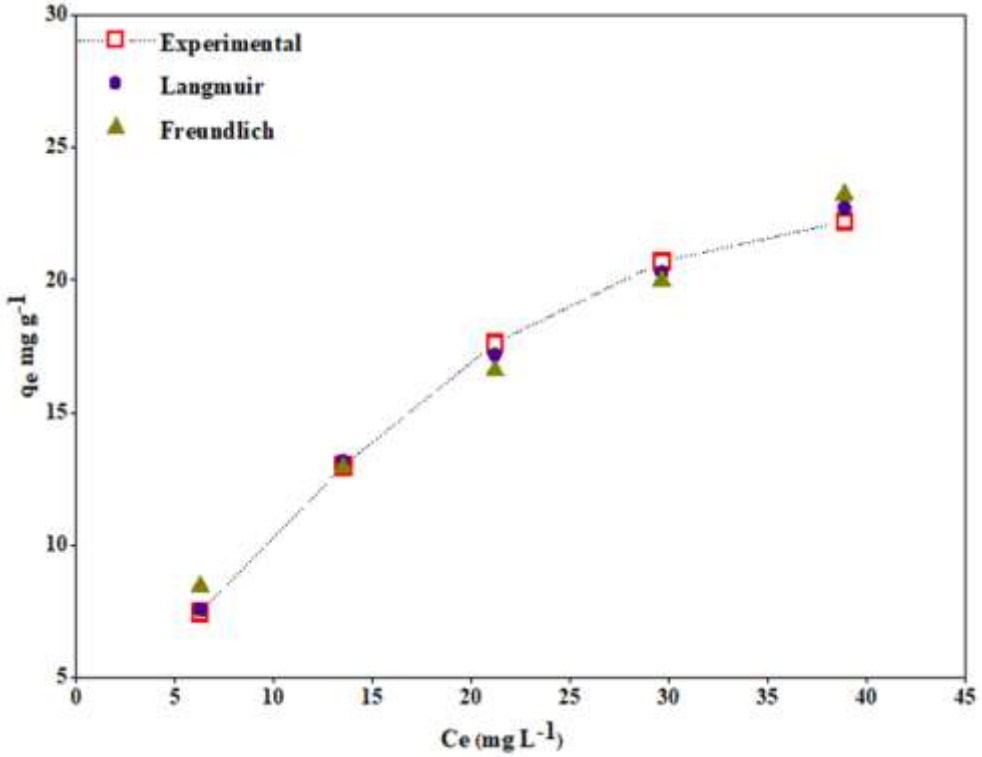

Figure 4-110: The fitting of the non-linear Langmuir and Freundlich adsorption isotherms to the experimental data for Cd^{2+} adsorption on the CH/bHAp/zeolite composite

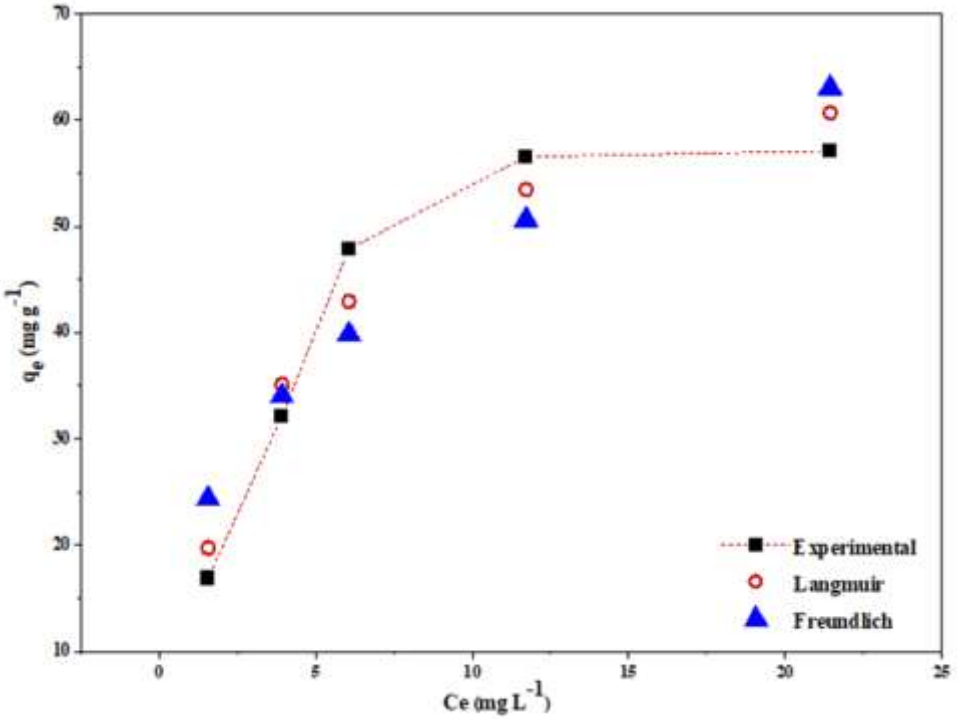

Figure 4-111: The fitting of the non-linear Langmuir and Freundlich adsorption isotherms to experimental data for Pb^{2+} adsorption on the CH/cHAp/zeolite composite

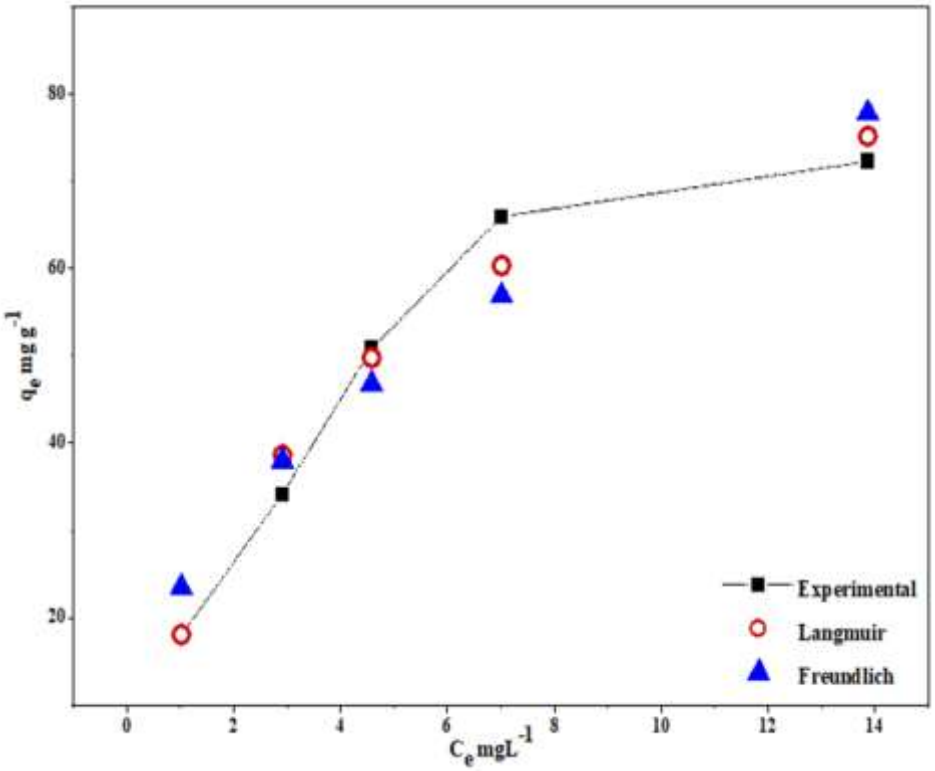

Figure 4-112: The fitting of the non-linear Langmuir and Freundlich adsorption isotherms to experimental data for Pb^{2+} adsorption on the CH/bHAp/zeolite composite

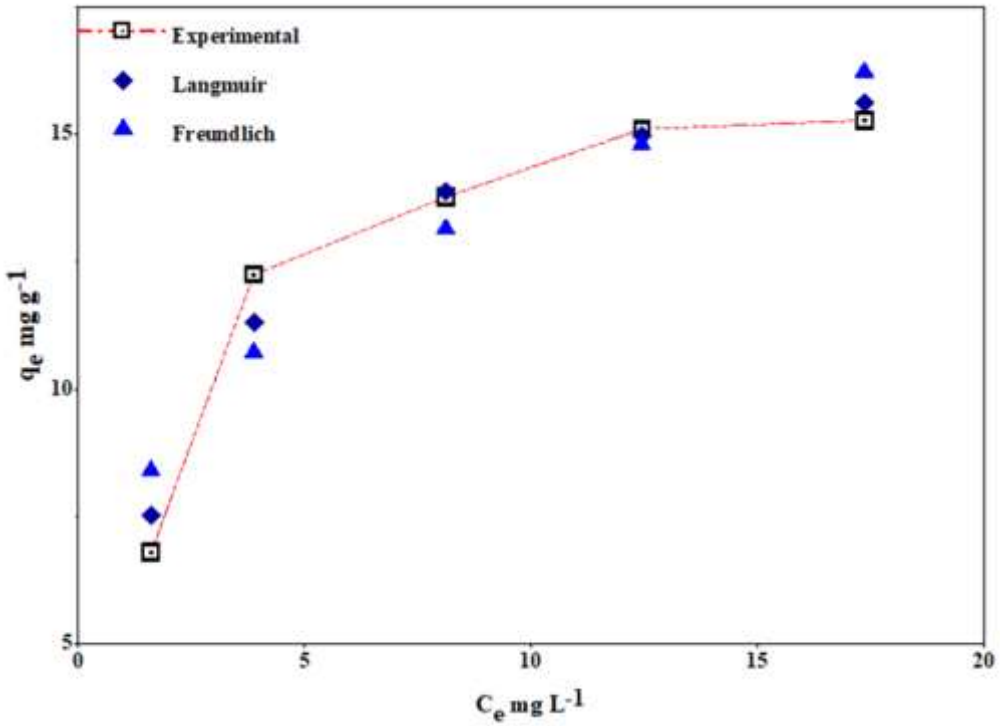

Figure 4-113: The fitting of the non-linear Langmuir and Freundlich isotherms to data for Cu^{2+} adsorption on the CH/cHAp/zeolite composite

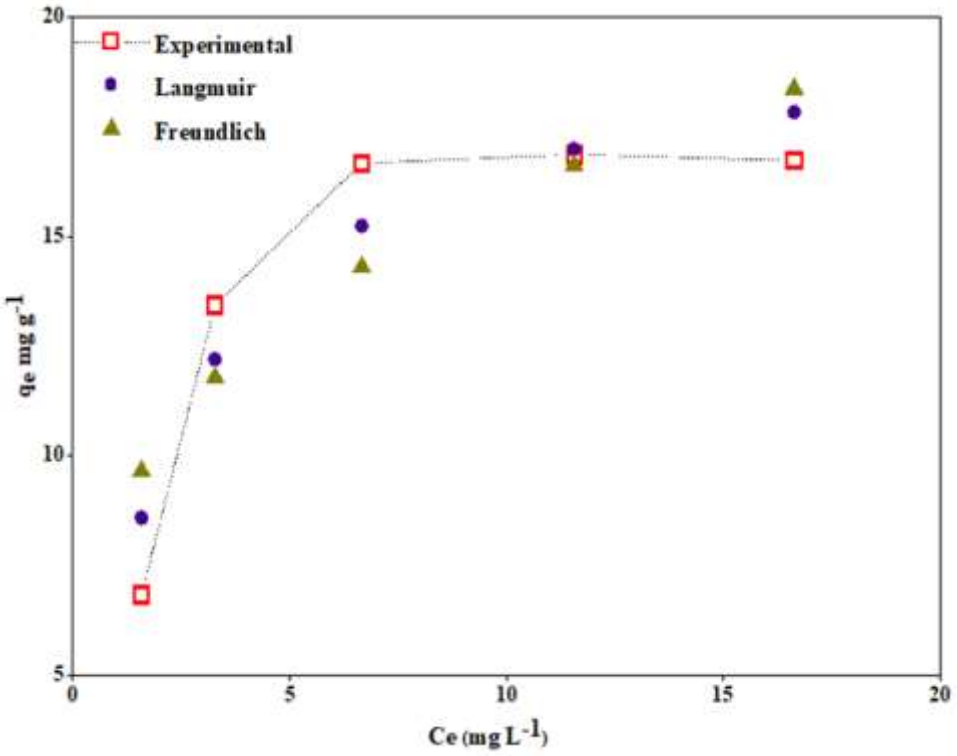

Figure 4-114: The fitting of the non-linear Langmuir and Freundlich isotherms to data for Cu^{2+} adsorption on the CH/bHAp/zeolite composite

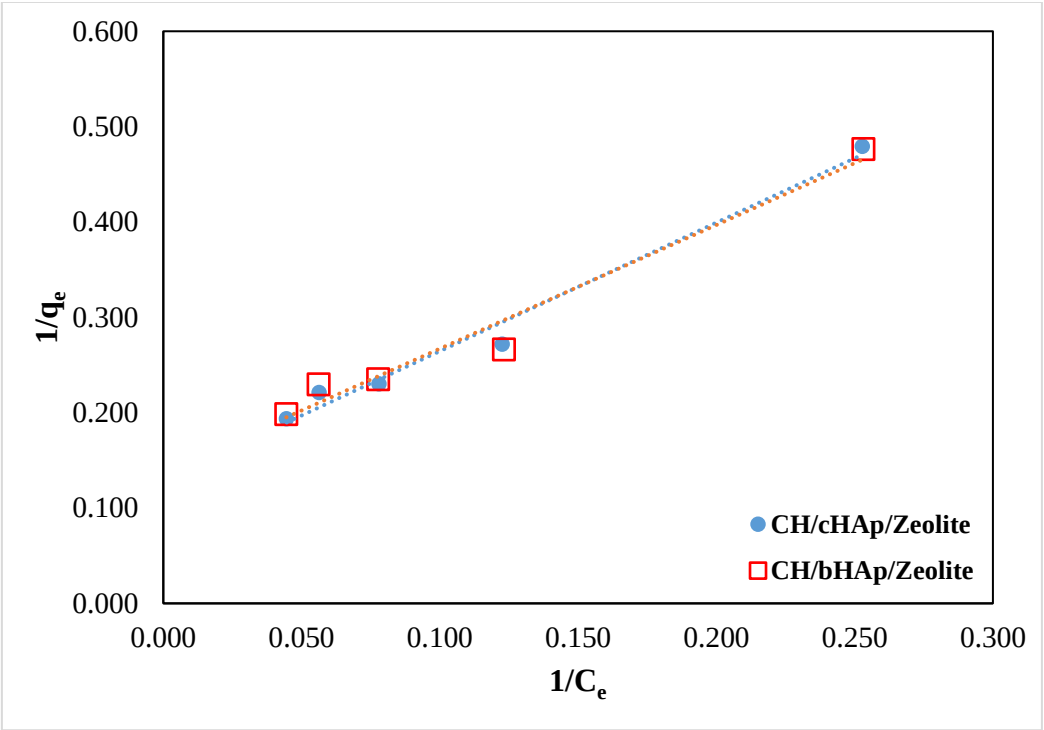

Figure 4-115: The fitting of the Linearized Langmuir isotherm model to the experimental data for chromate ion adsorption on the CH/HAp/zeolite composites

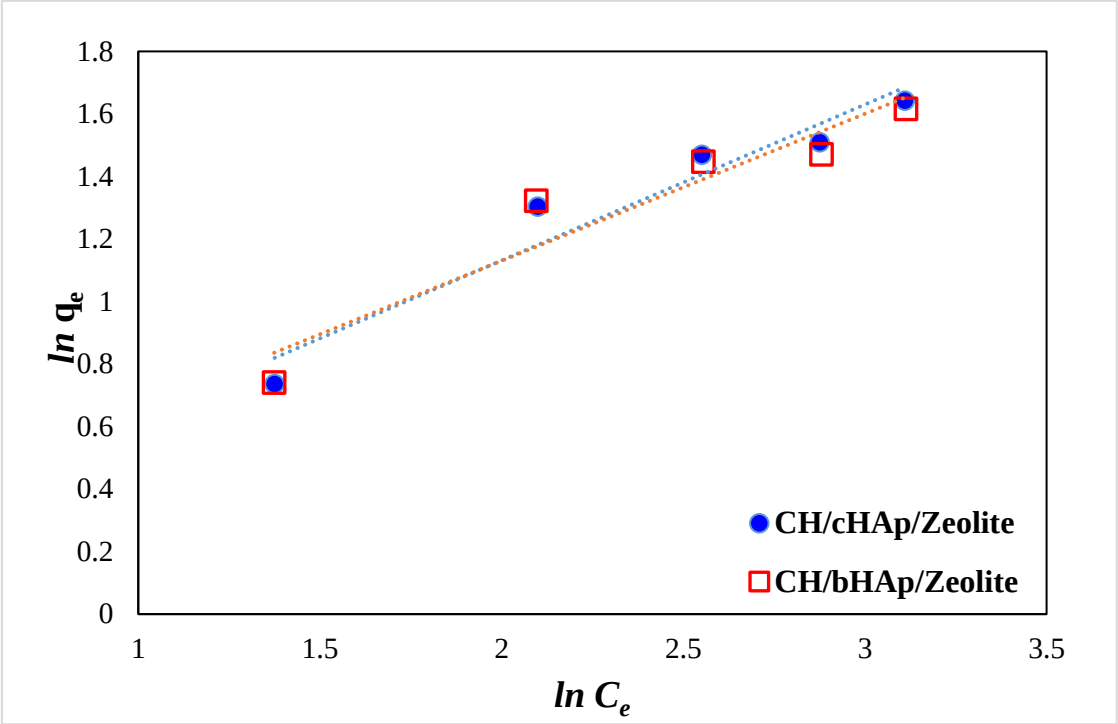

Figure 4-116: The fitting of the Linearized Freundlich isotherm model to the experimental data for chromate ion adsorption on the CH/HAp/zeolite composites

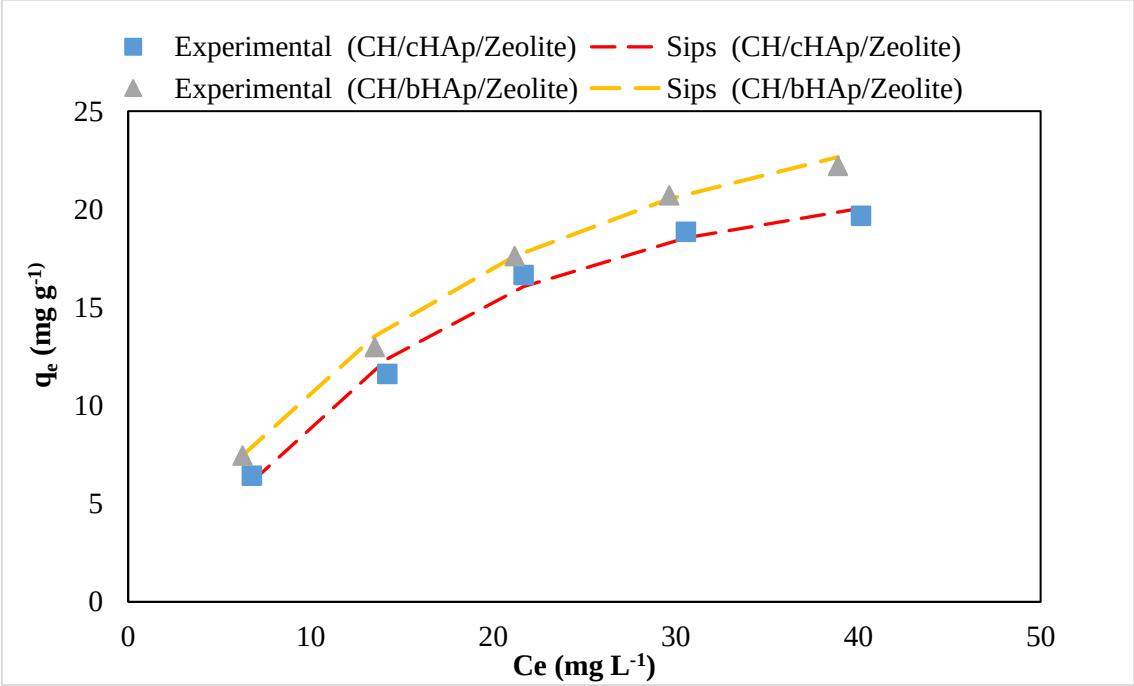

Figure 4-117: The fitting of the Sips isotherm model to the experimental data for Cd^{2+} ion adsorption on the CH/HAp/zeolite composites

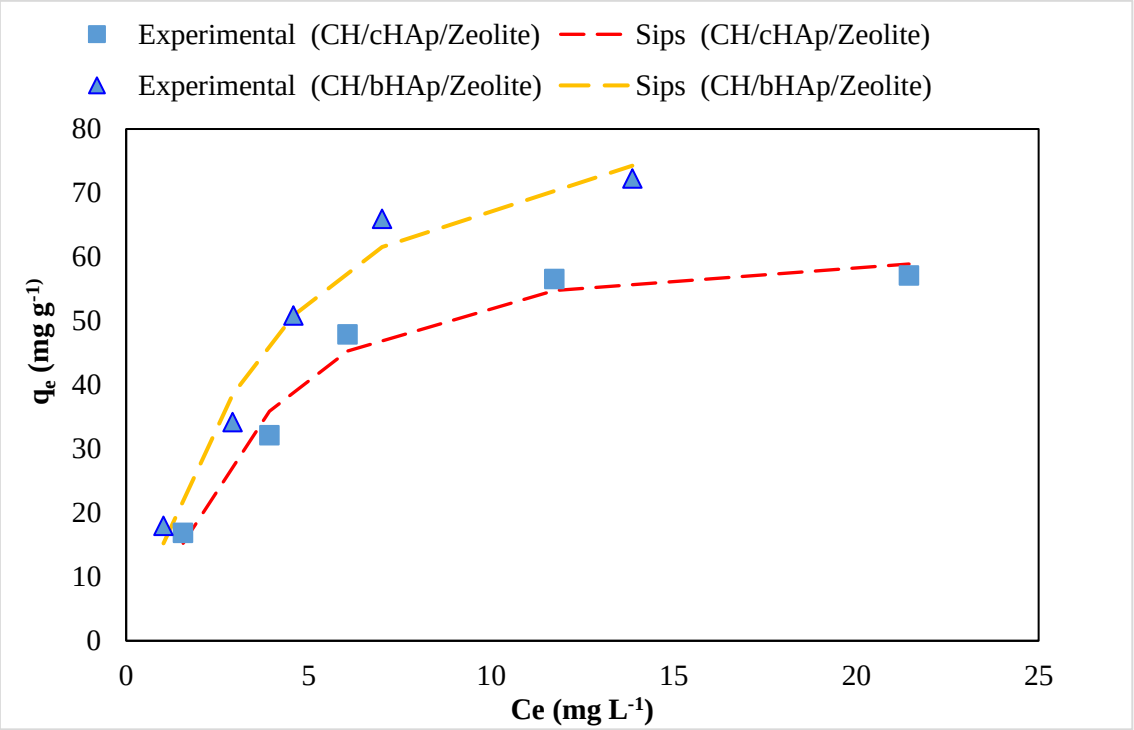

Figure 4-118: The fitting of the Sips isotherm model to the experimental data for Pb^{2+} ion adsorption on the CH/HAp/zeolite composites

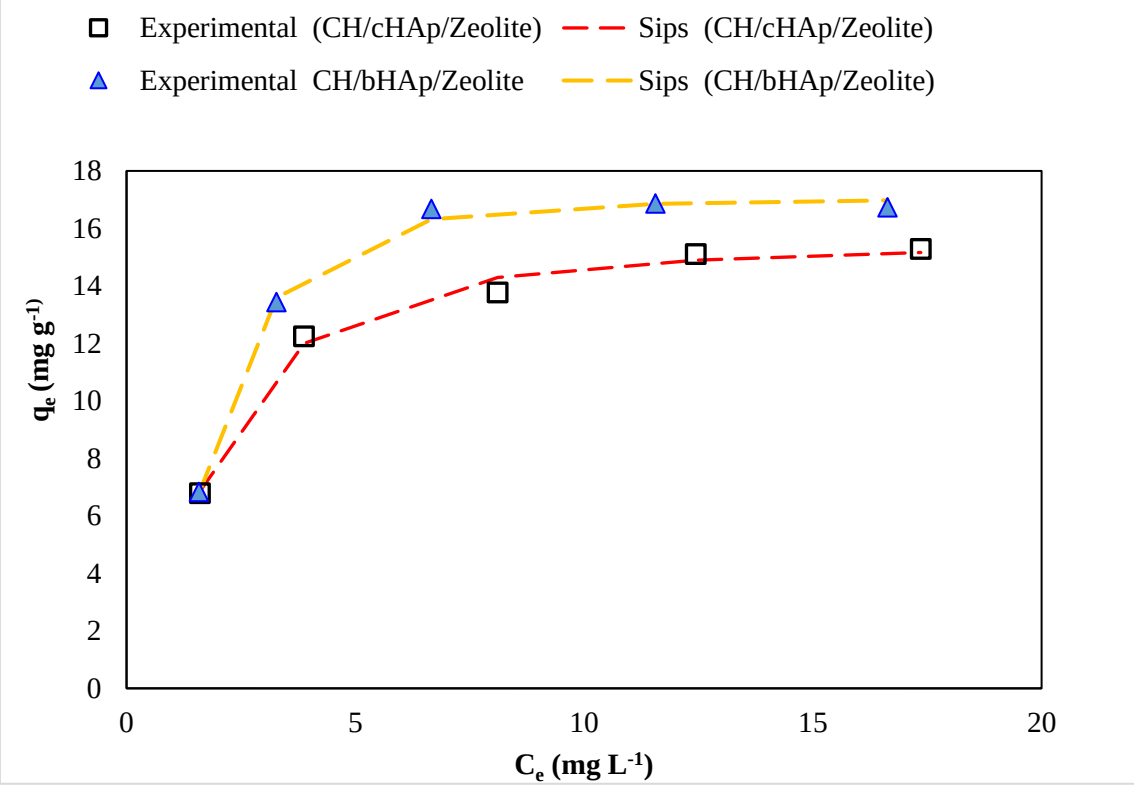

Figure 4-119: The fitting of the Sips isotherm model to the experimental data for Cu^{2+} ion adsorption on the CH/HAp/zeolite composite

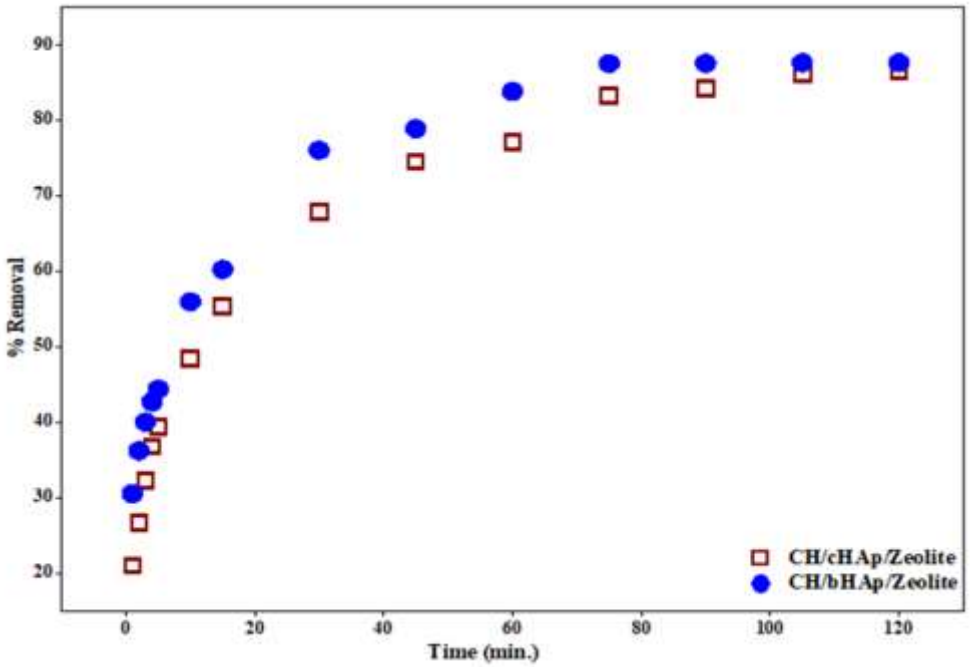

Figure 4-120: AAS data showing the effect of adsorbent dose on Cd^{2+} removal (%) using the CH/HAp/zeolite composites. The results are presented as the average of measurements of three replicates. SE = ± 0.3

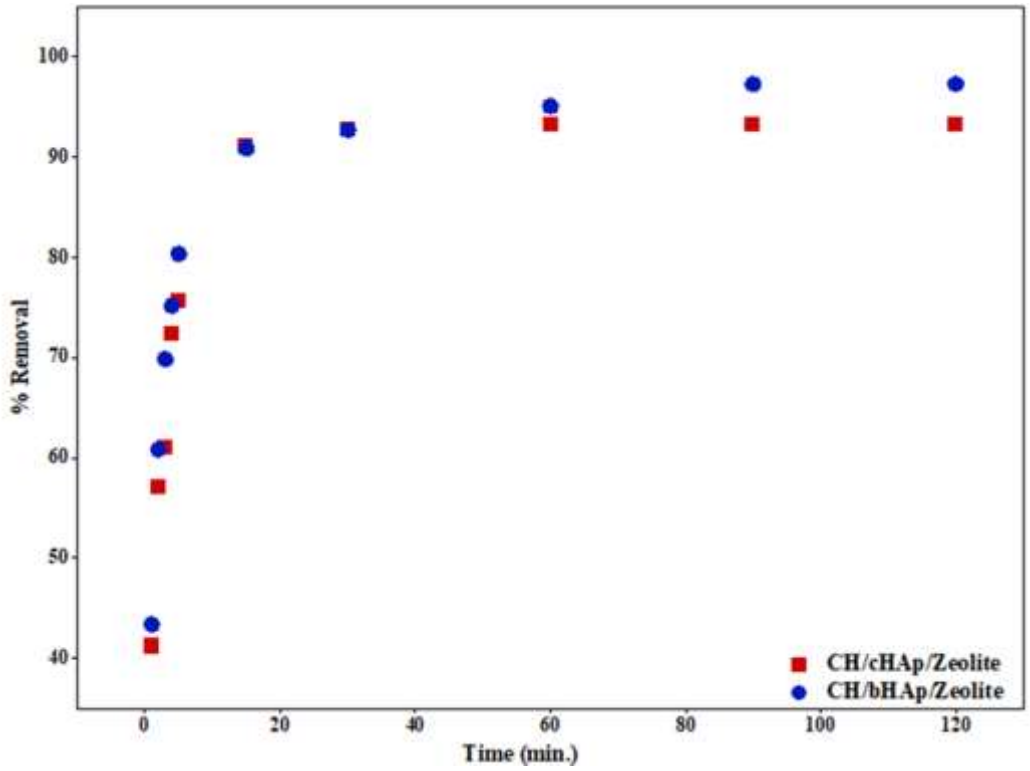

Figure 4-121: AAS data showing the effect of contact time on Pb^{2+} adsorption on the CH/HAp/zeolite composites. Results are reported as the average of 3 replicates. SE = ±0.1.

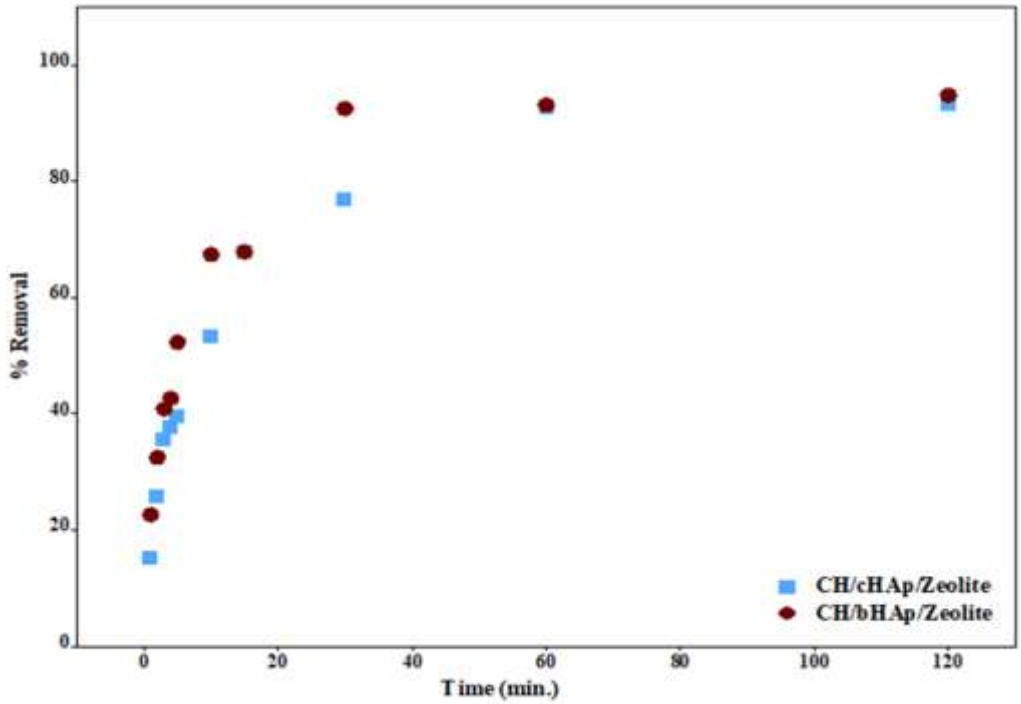

Figure 4-122: AAS data showing the effect of contact time on Cu^{2+} removal by the CH/HAp/zeolite composites. The results are presented as the average of measurements of three replicates. SE= ± 0.1

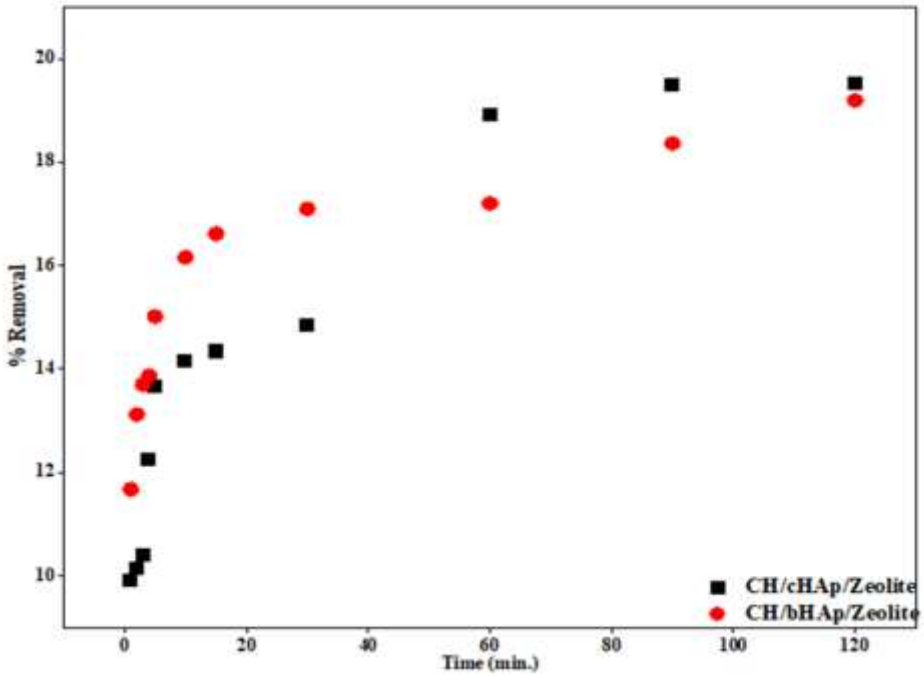

Figure 4-123: AAS data showing the effect of contact time on chromate ion removal by using the CH/HAp/zeolite composites. The results are presented as the average of measurements of three replicates. SE = ± 0.02

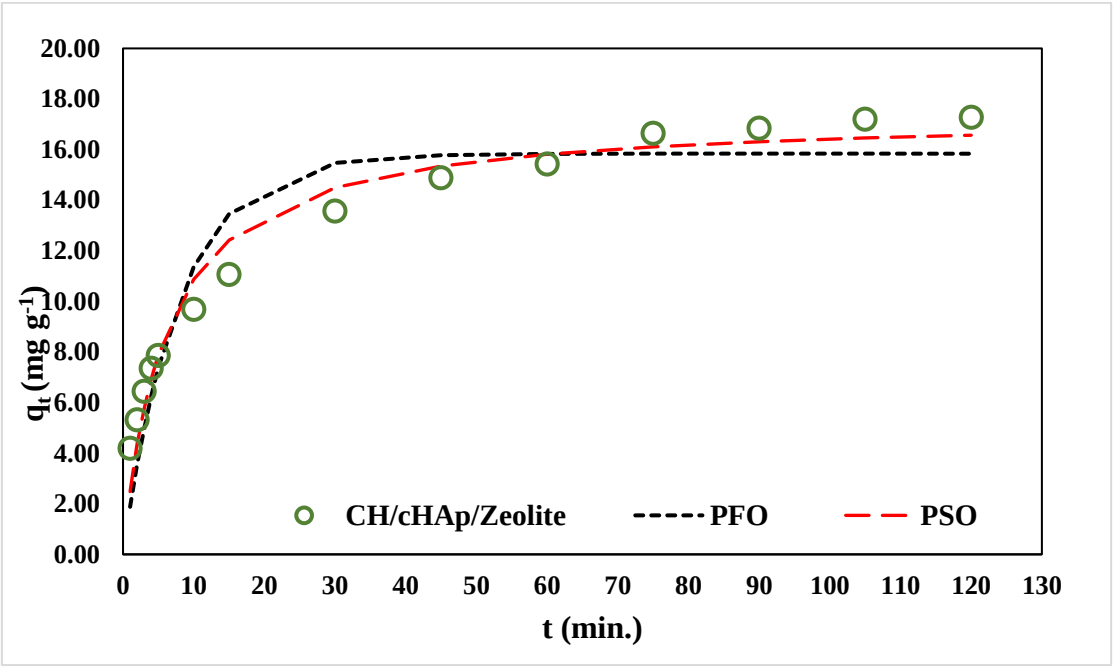

Figure4-124: The fitting of the pseudo-first-order (PFO) and pseudo-second-order (PSO) kinetic models to the experimental data for Cd^{2+} adsorption on the CH/cHAp/zeolite composites

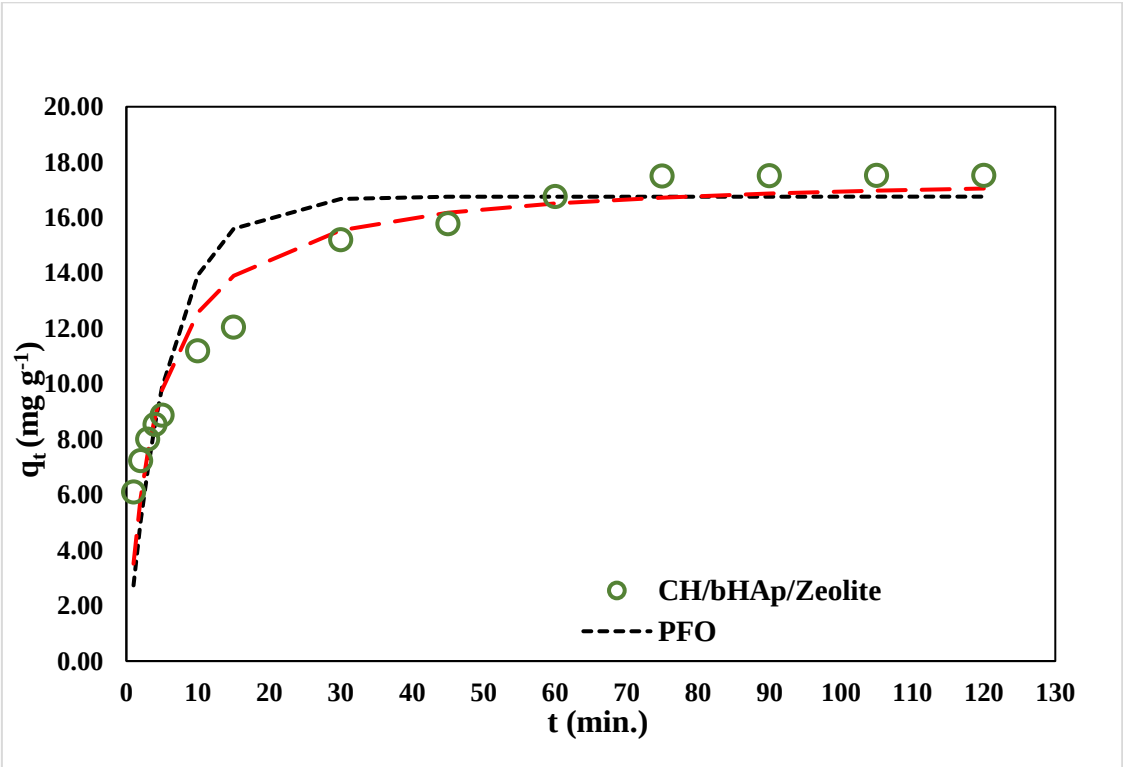

Figure 4-125: The fitting of the non-linear pseudo-first-order (PFO) and pseudo-second-order (PSO) kinetic models to the experimental data for Cd^{2+} adsorption on the CH/bHAp/zeolite composites

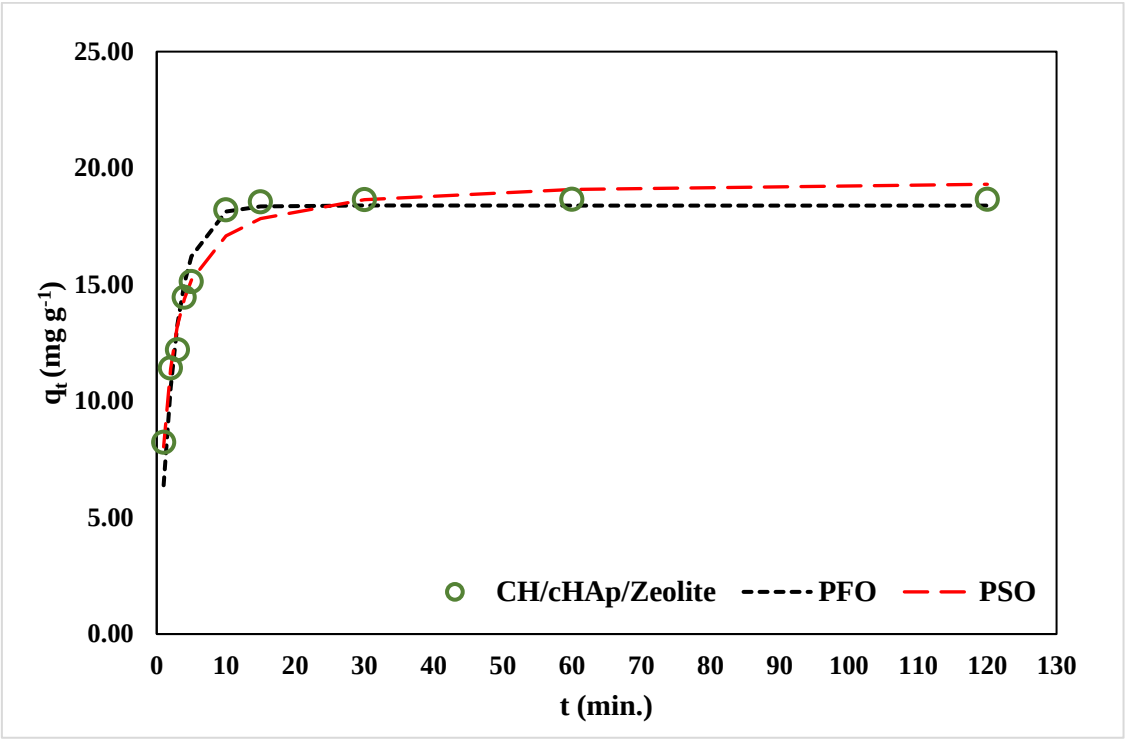

Figure 4-126: The fitting of the non-linear pseudo-first-order (PFO) and pseudo-second-order (PSO) kinetic models to the experimental data for Pb^{2+} adsorption on the CH/cHAp/zeolite composites

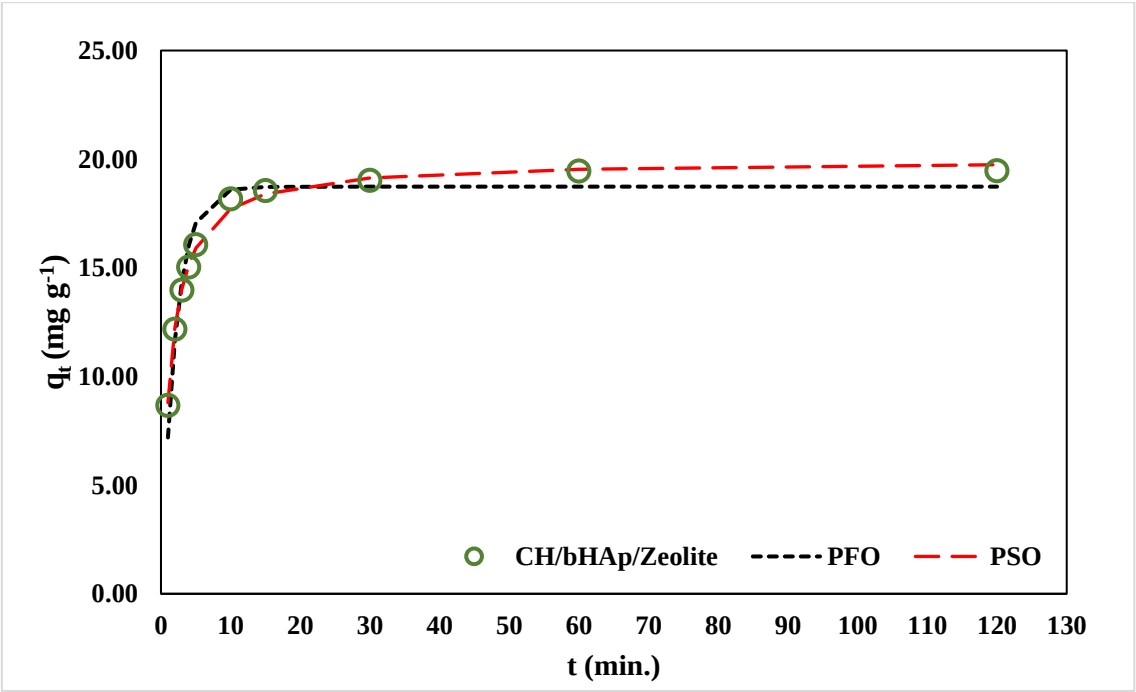

Figure 4-127: The fitting of the non-linear pseudo-first-order (PFO) and pseudo-second-order (PSO) kinetic models to the experimental data for Pb^{2+} adsorption on the CH/bHAp/zeolite composites

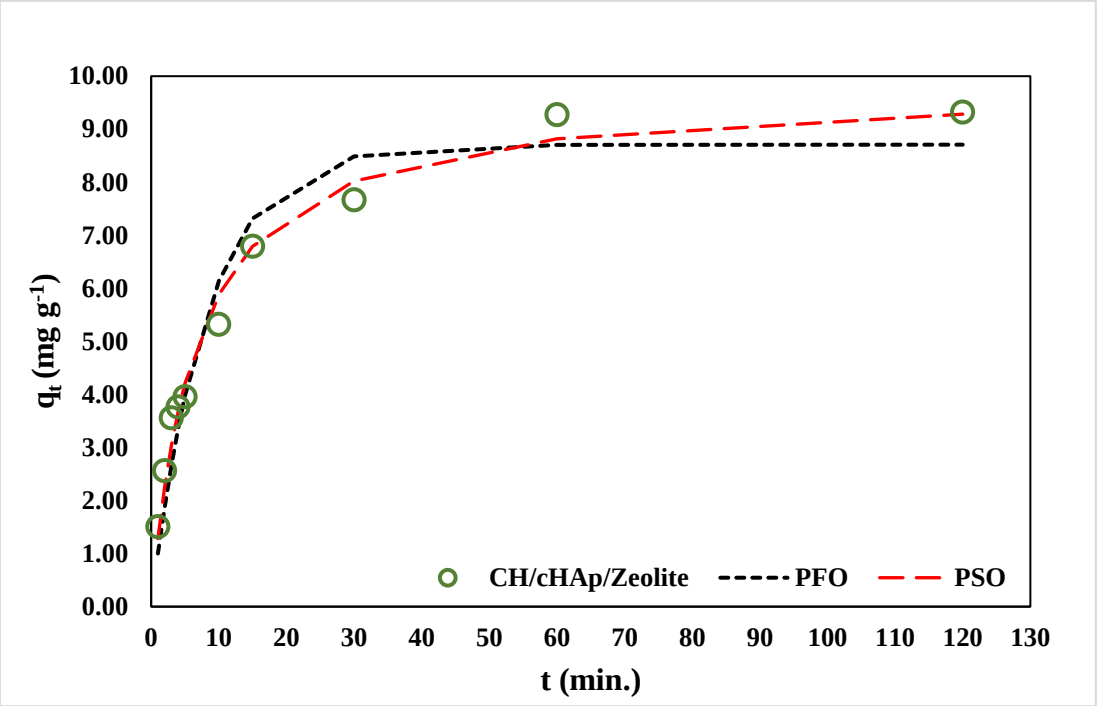

Figure 4-128: The fitting of the non-linear pseudo-first-order and pseudo-second-order kinetics models to experimental data for Cu^{2+} adsorption on the CH/cHAp/zeolite composite

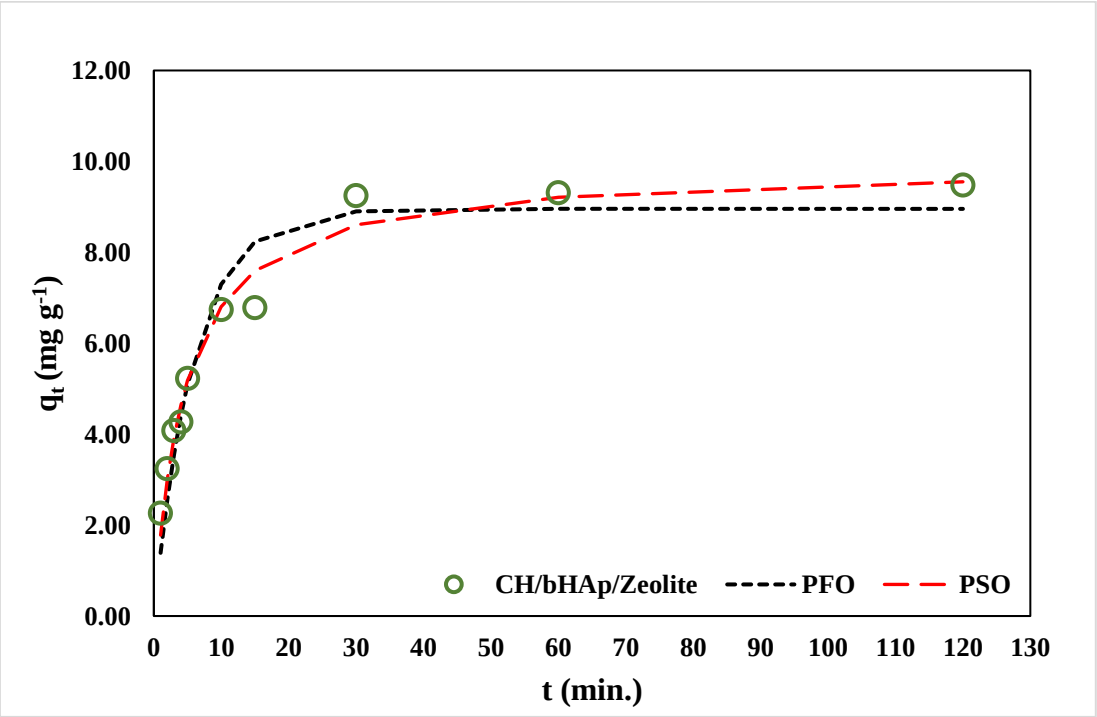

Figure 4-129: The fitting of the non-linear pseudo-first-order and pseudo-second-order kinetics models to experimental data for Cu^{2+} adsorption on the CH/bHAp/zeolite composite

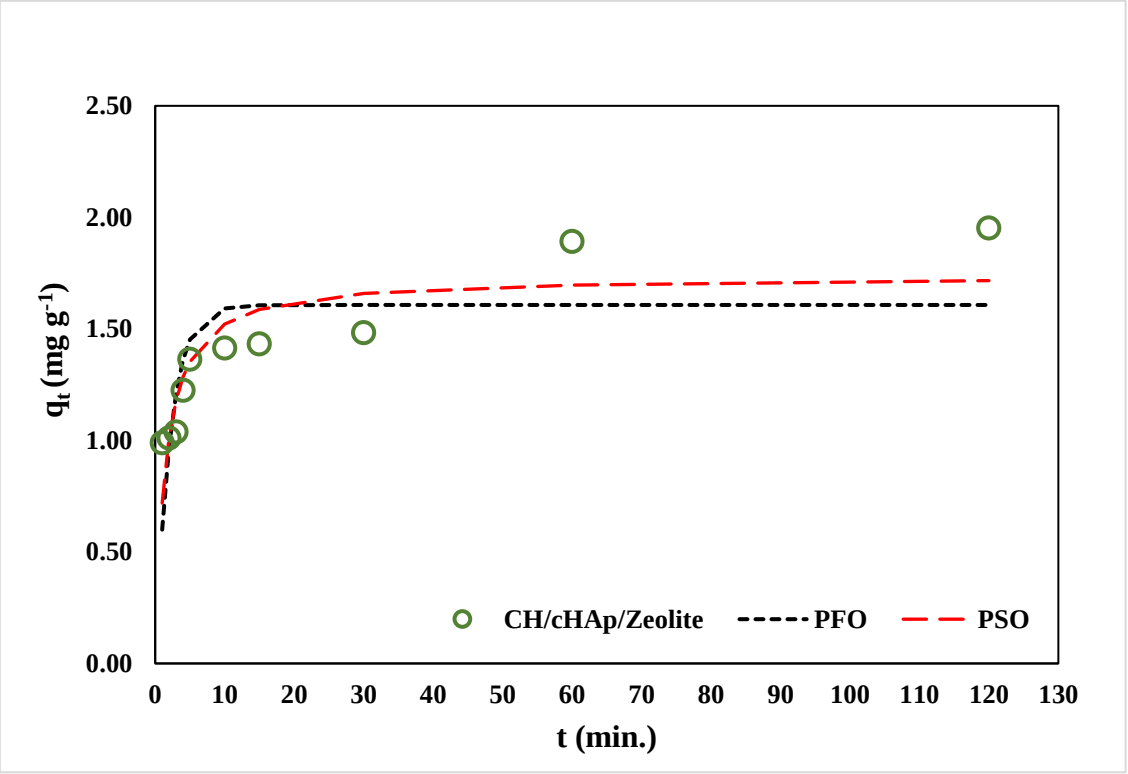

Figure 4-130: The fitting of the non-linear pseudo-first-order and pseudo-second-order kinetics model to the data for chromate ion adsorption on the CH/cHAp/zeolite composites

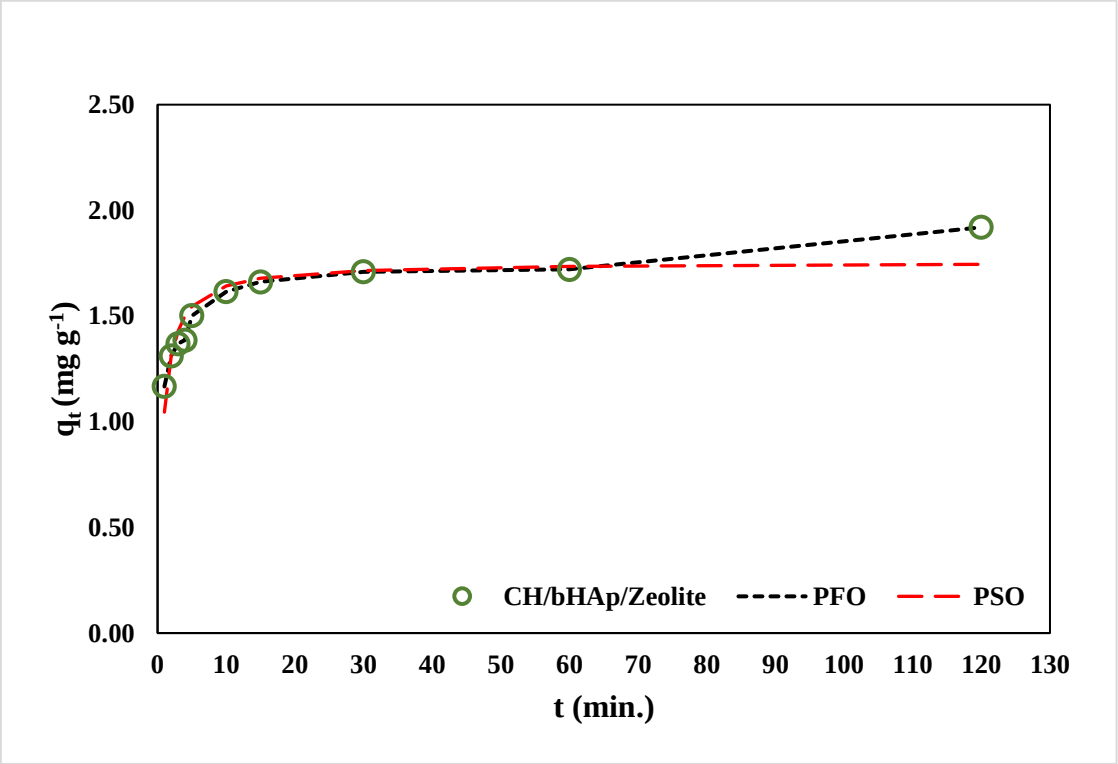

Figure 4-131: The fitting of the pseudo-first-order and pseudo-second-order kinetics model to the data for chromate ion adsorption on the CH/bHAp/zeolite composites

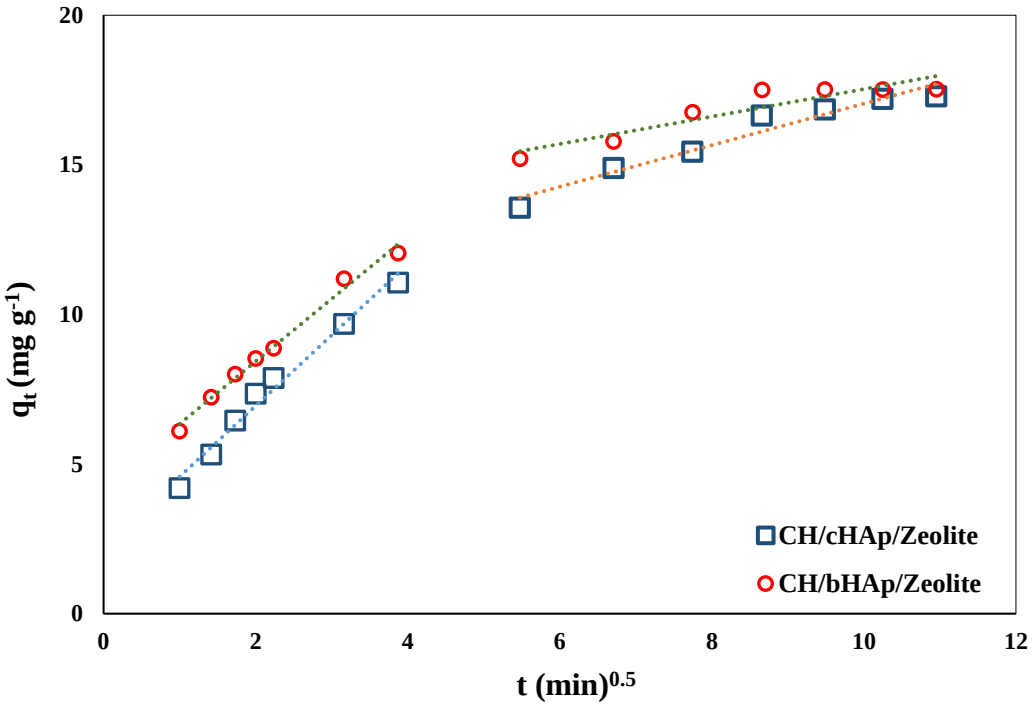

Figure 4-132: The fitting of the intra-particle diffusion model (IPD) to the experimental data for Cd^{2+} adsorption on the CH/HAp/zeolite composites

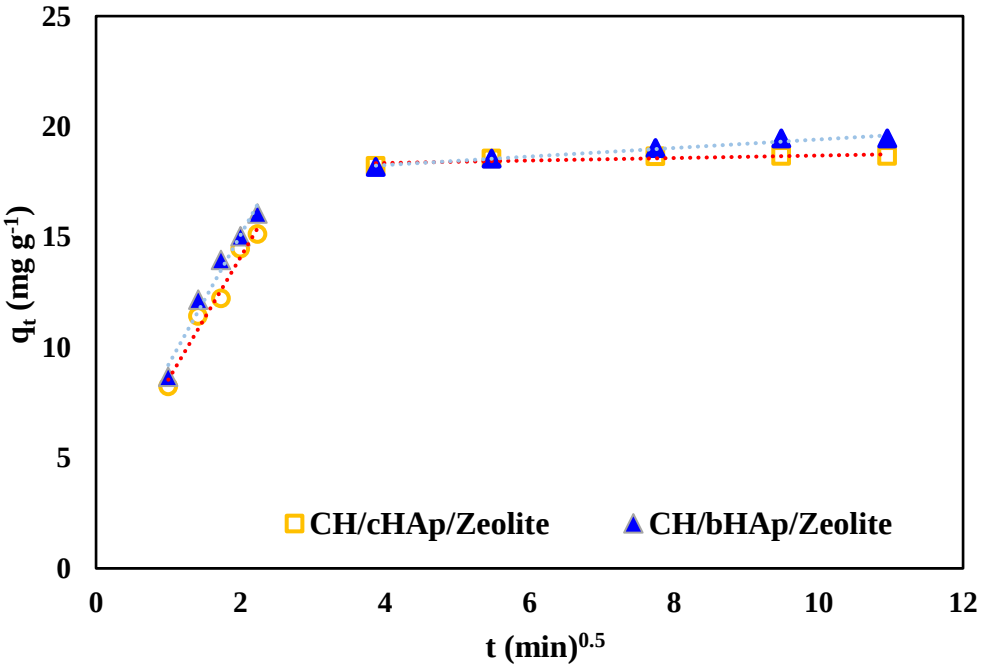

Figure4-133: The fitting of the intra-particle diffusion model (IPD) to the experimental data for Pb^{2+} adsorption kinetics data on the CH/HAp/zeolite composites

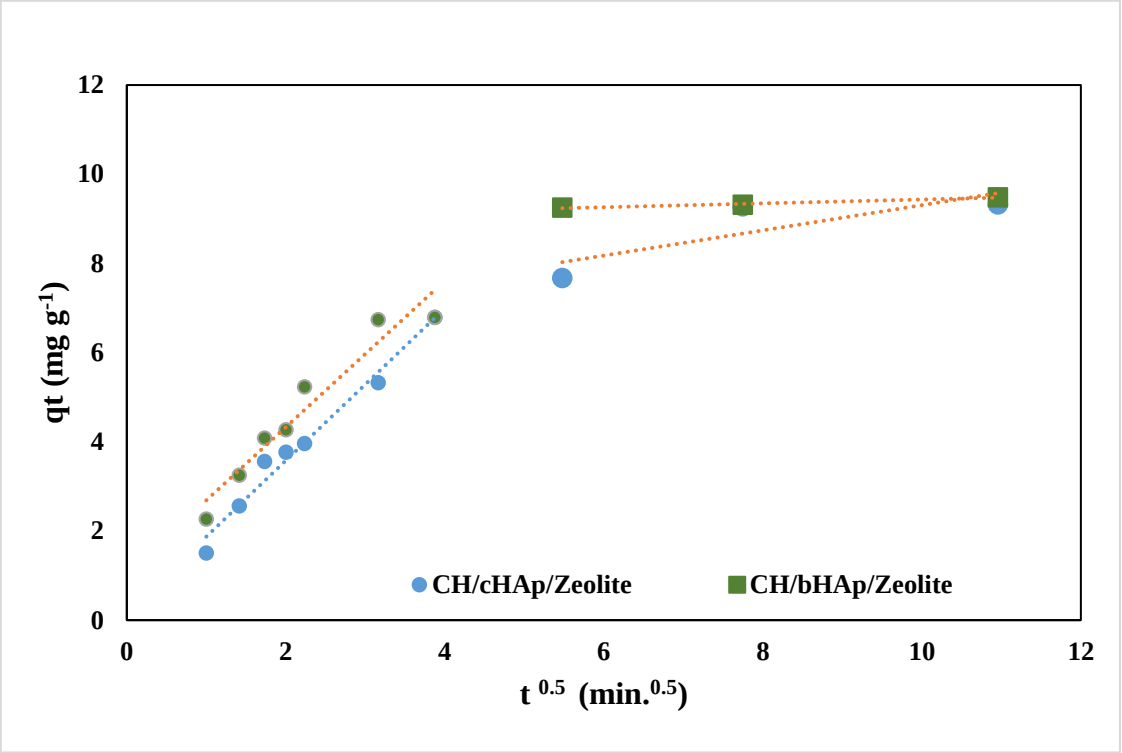

Figure 4-134: The fitting of the intra-particle diffusion model (IPD) to the experimental data for Cu^{2+} adsorption on the CH/HAp/zeolite composites

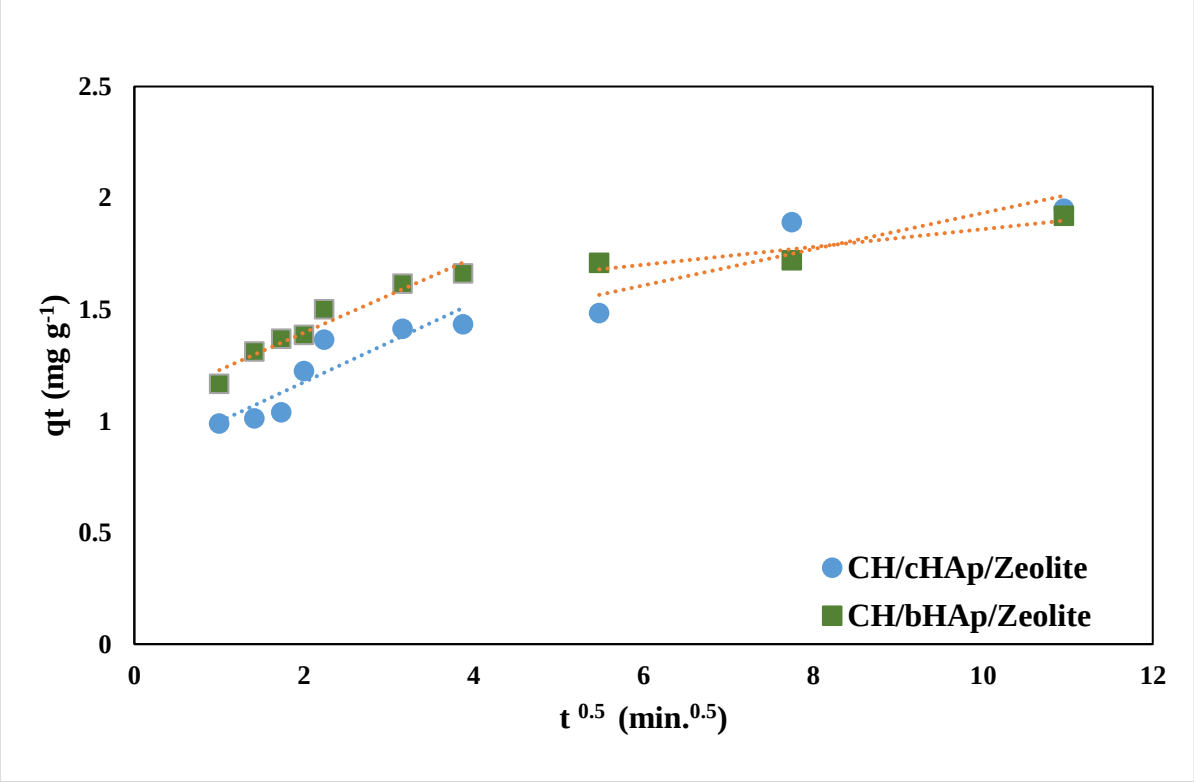

Figure 4-135: The fitting of intra-particle diffusion model (IPD) to the experimental data for chromate ion adsorption on the CH/HAp/zeolite composites

Appendix 5:

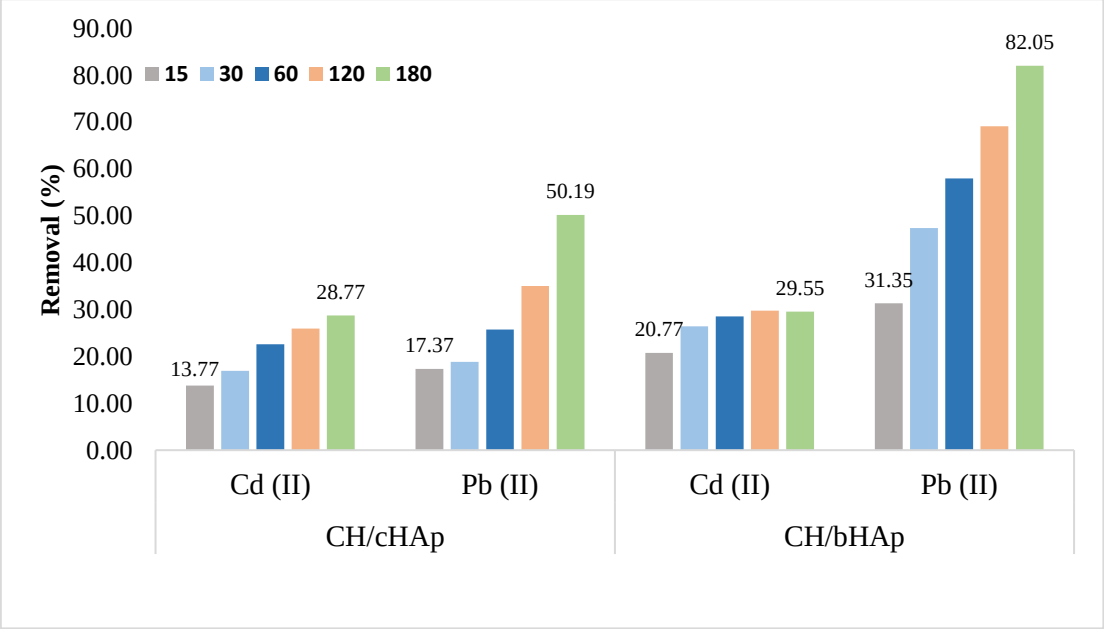

Figure 5-1: The competitive Cd^{2+} and Pb^{2+} ion removal (%) by 0.01 g doses of the CH/HAp composites at contact times ranging from 15 minutes to 180 minutes.

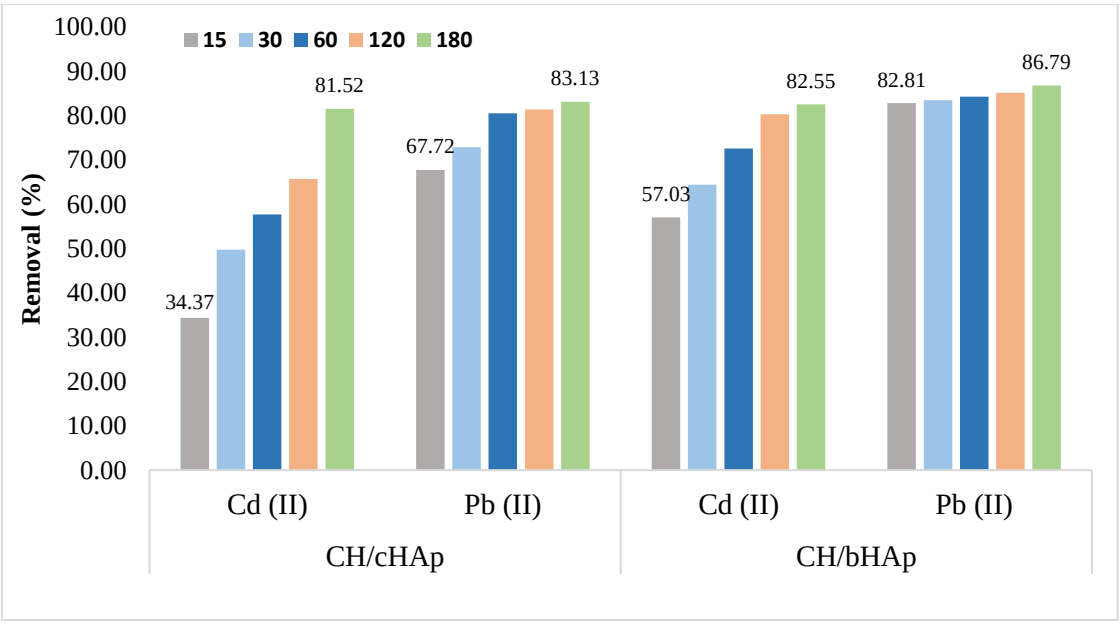

Figure 5-2: The competitive adsorption of Cd^{2+} and Pb^{2+} shown as removal (%) values at 0.01 g of the CH/HAp composites during contact times ranging from 15 minutes to 180 minutes.

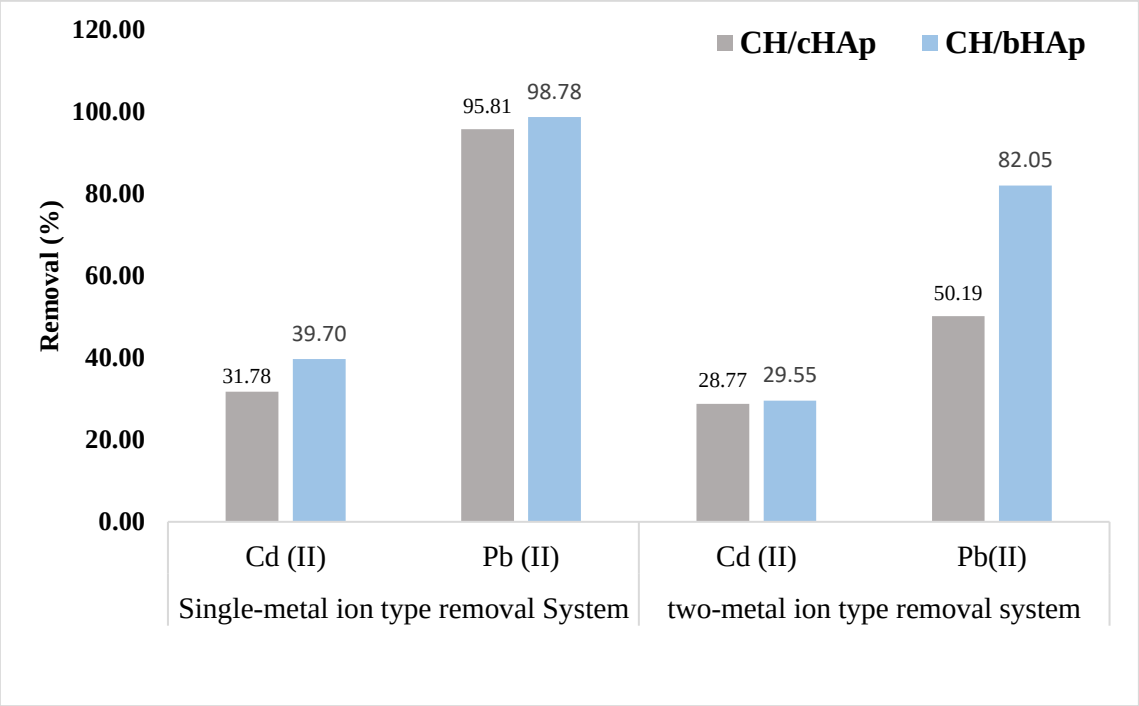

Figure 5-3: Comparison of removal data for Cd^{2+} and Pb^{2+} ions by a 0.01 g adsorbent dose of the CH/HAp composites from solutions containing either one or two metal ion types.

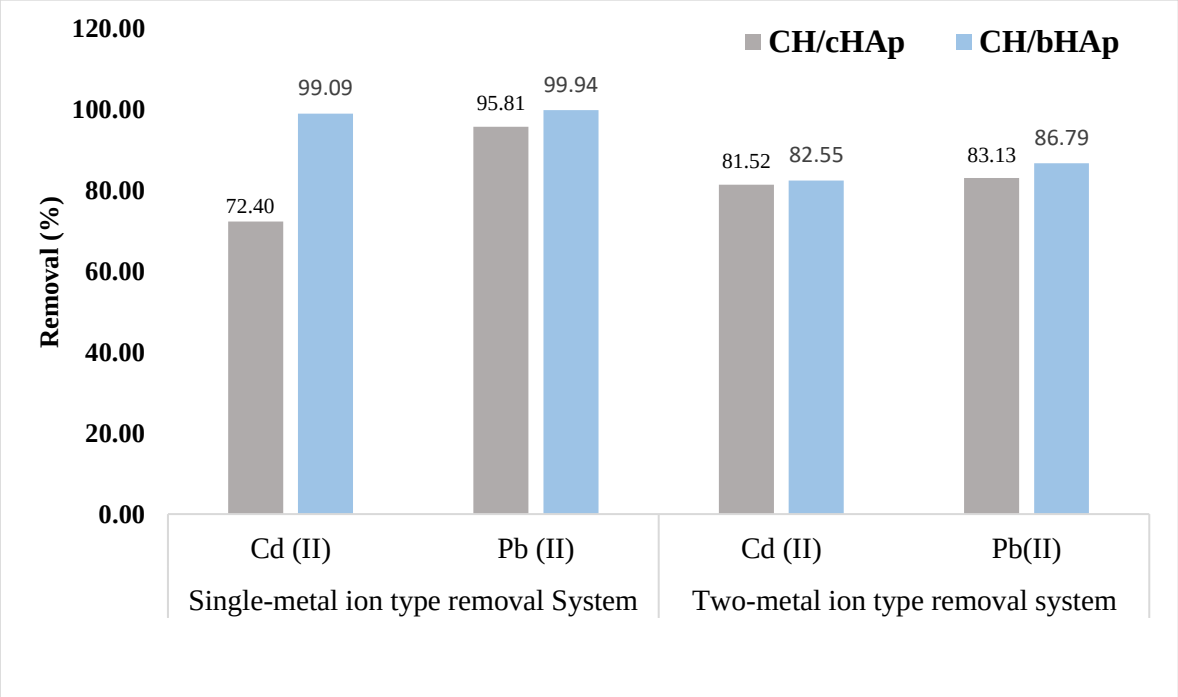

Figure 5-4: Comparison of removal data for Cd^{2+} and Pb^{2+} ions by a 0.05 g adsorbent dose of the CH/HAp composites from solutions containing either one or two metal ion types.

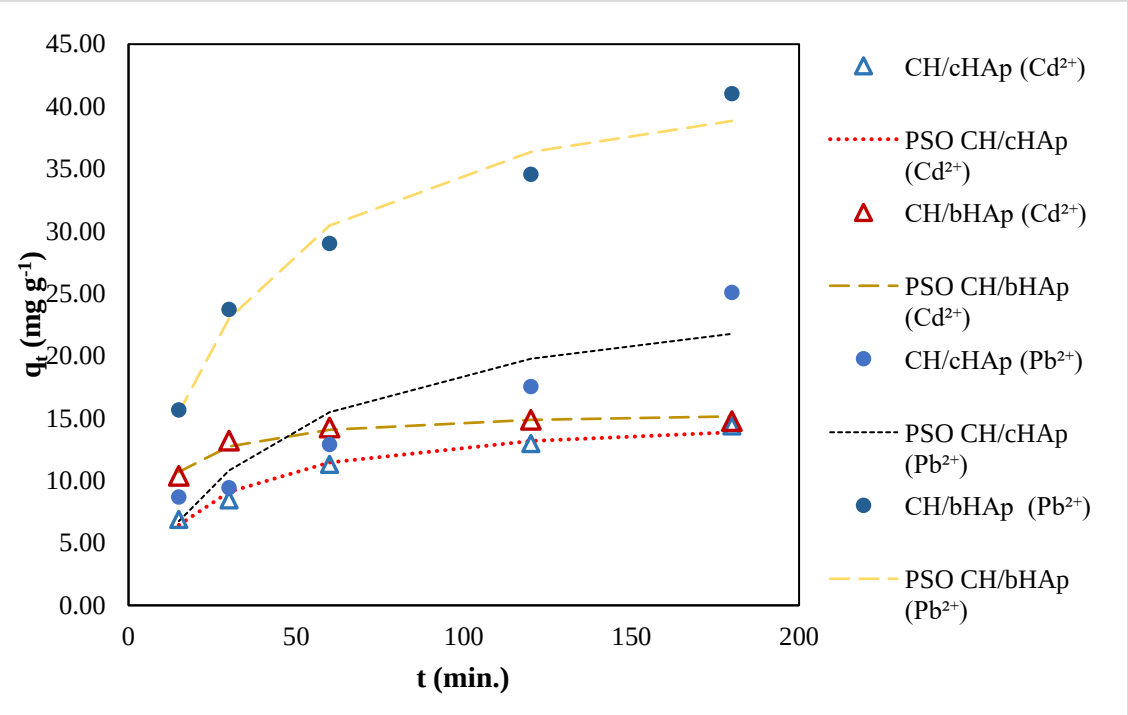

Figure 5-5: The fitting of the pseudo-second-order kinetic model to experimental (contact time) data relating to Cd^{2+} and Pb^{2+} competitive adsorption on the CH/HAp composites on an adsorbent dose of 0.01 g.

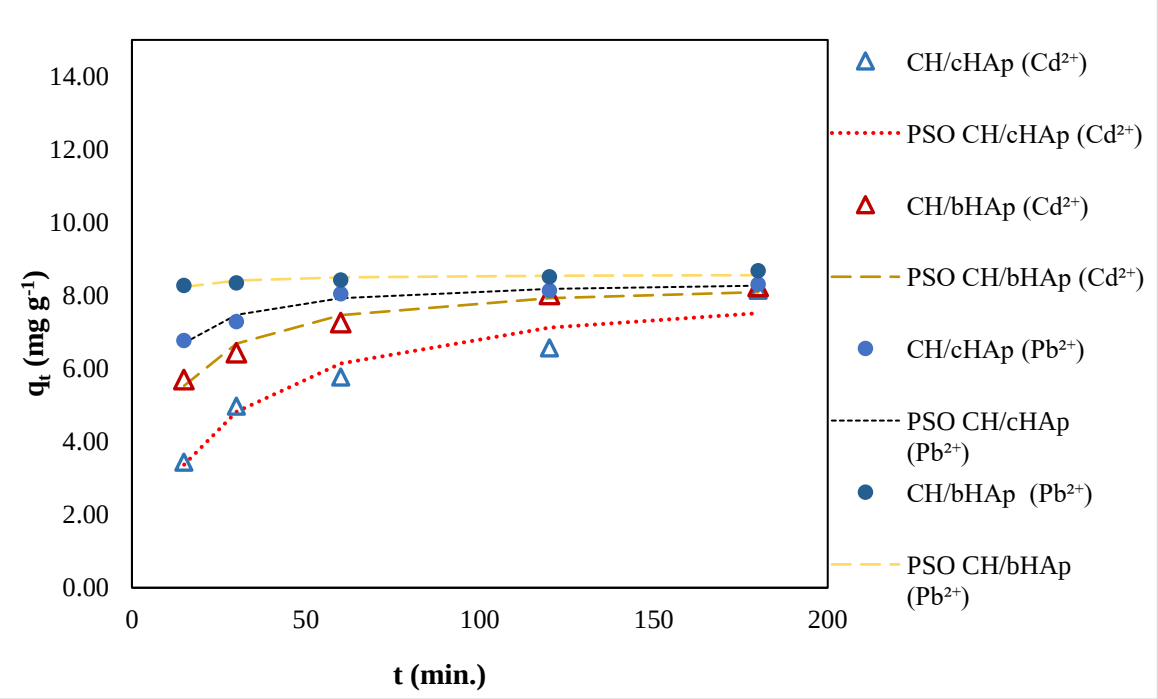

Figure 5-6: The fitting of the PSO kinetic model to the experimental contact time data for the CH/HAp composites exposed to solutions containing both Cd^{2+} and Pb^{2+} for an adsorbent dose of 0.05 g

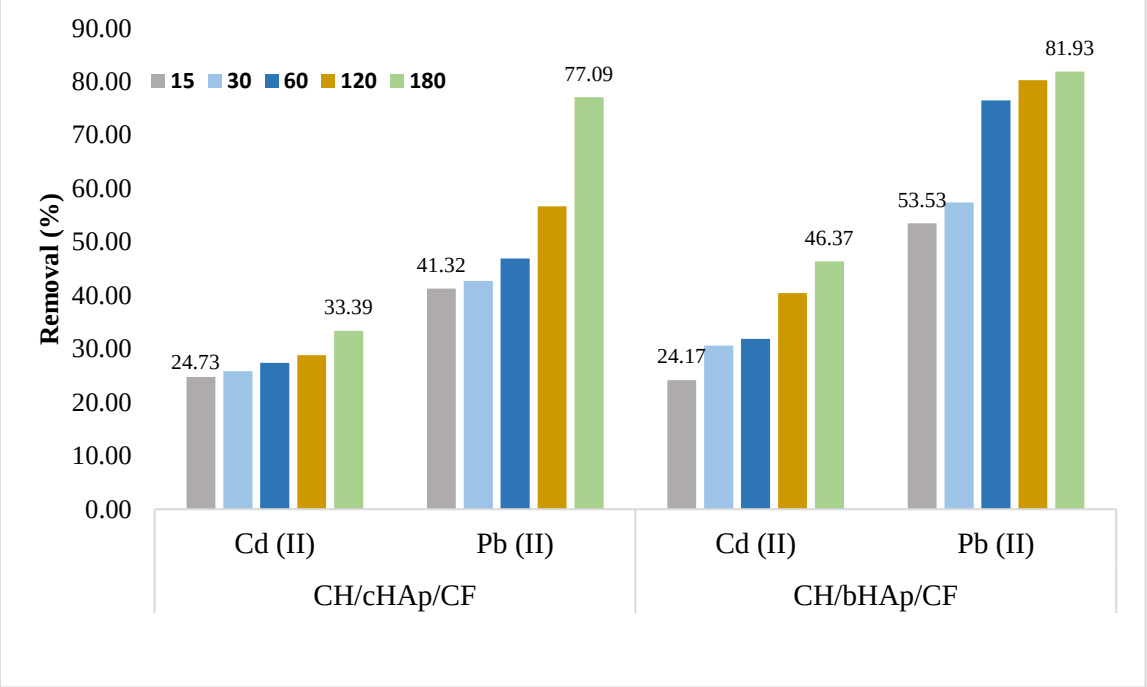

Figure 5-7: Graph showing the competitive removal (%) of Cd^{2+} and Pb^{2+} ions by 0.01 g doses of the CH/HAp/CF composites at contact times ranging from 15 minutes to 180 minutes.

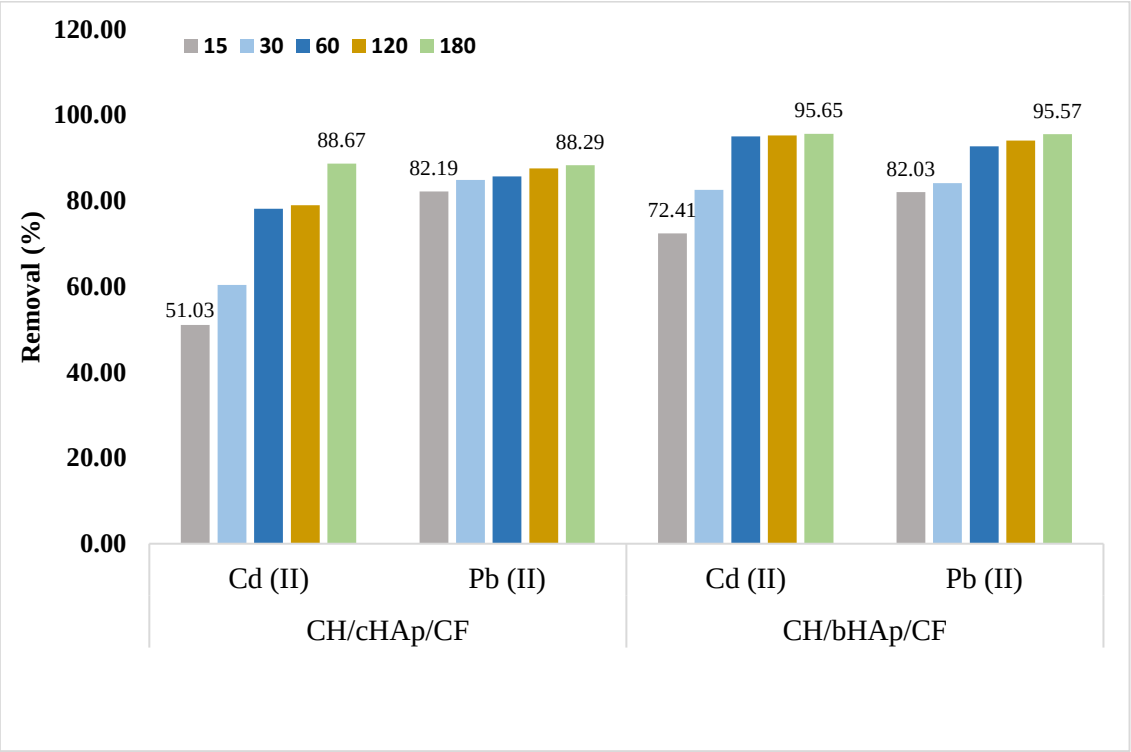

Figure 5-8: The competitive Cd^{2+} and Pb^{2+} removal (%) using 0.05 g of the CH/HAp/CF composites at contact times ranging from 15 minutes to 180 minutes.

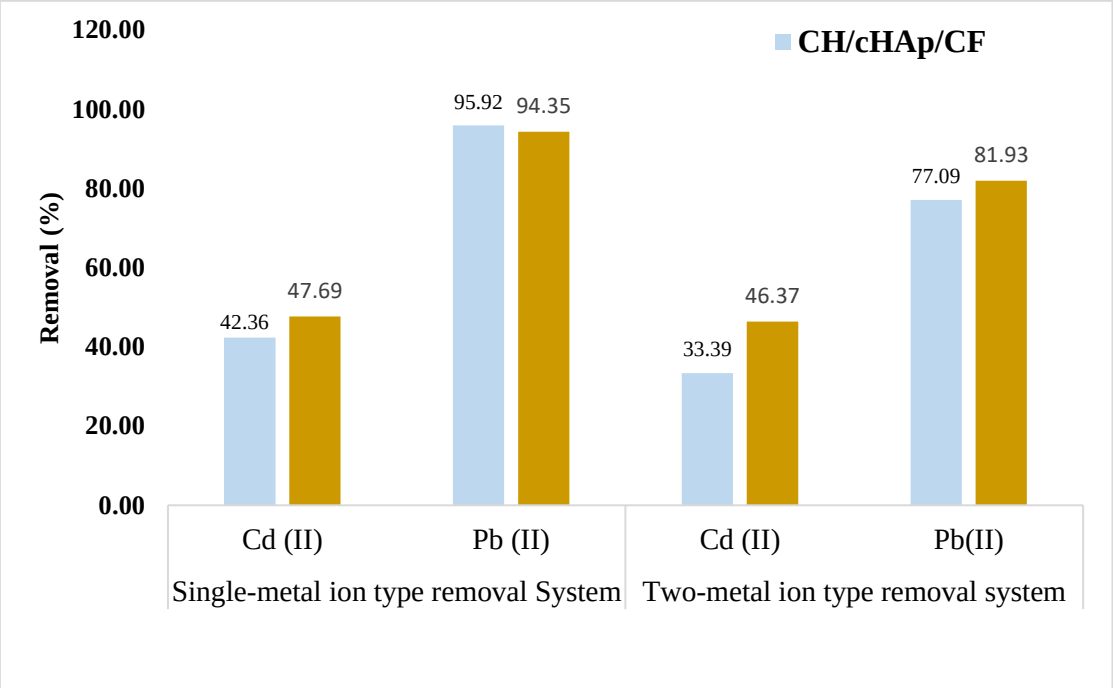

Figure 5-9: The comparison of single metal ion type and two-metal ion type systems for Cd^{2+} and Pb^{2+} adsorption on 0.01 g of adsorbent dose of CH/HAp/CF composites

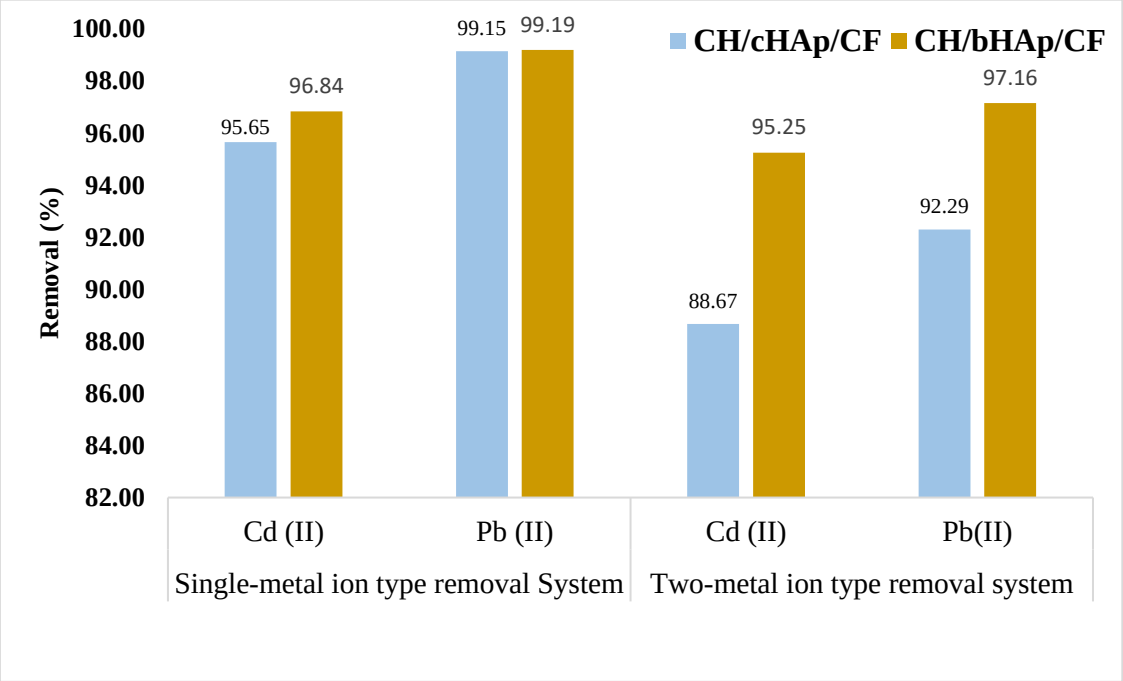

Figure 5-10: The comparison of single metal ion type and two-metal ion type systems for Cd^{2+} and Pb^{2+} adsorption on 0.05 g of adsorbent dose of CH/HAp/CF composites.

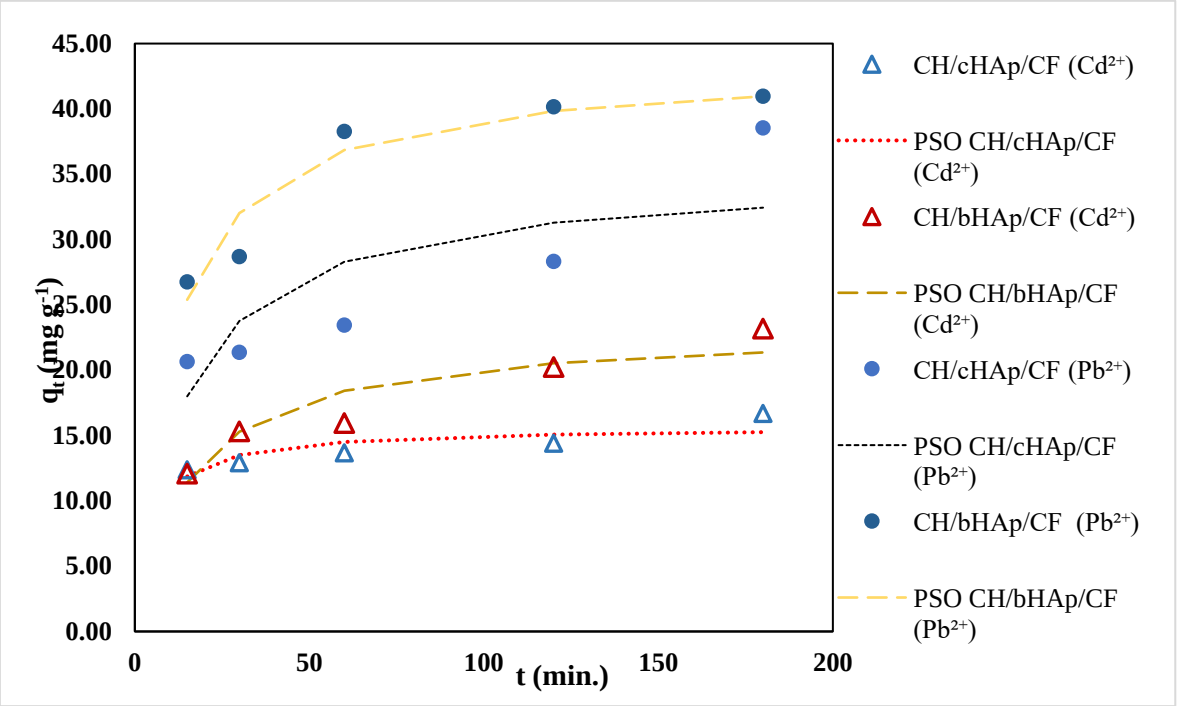

Figure 5-11: The fitting of the non-linear pseudo-second-order kinetic model to experimental (contact time) data relating to Cd^{2+} and Pb^{2+} competitive adsorption on the CH/HAp/CF composites for an adsorbent dose of 0.01 g

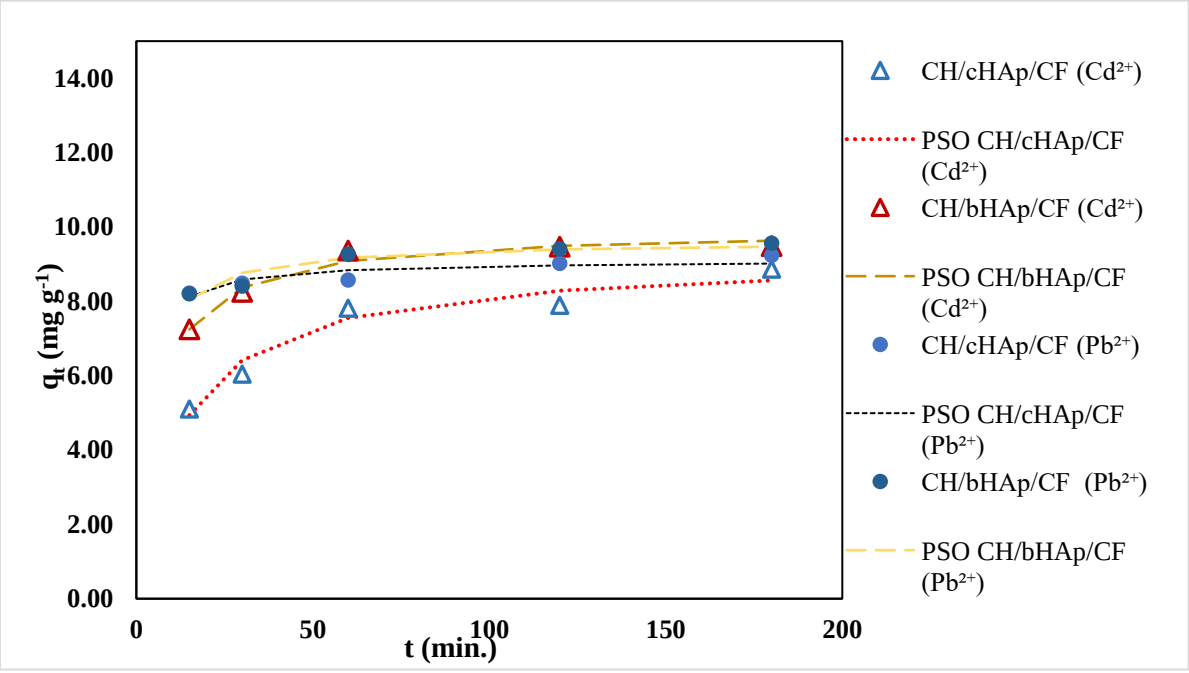

Figure 5-12: The fitting of the non-linear pseudo-second-order kinetic model to experimental (contact time) data relating to Cd^{2+} and Pb^{2+} competitive adsorption on the CH/HAp/CF composites on an adsorbent dose of 0.05 g

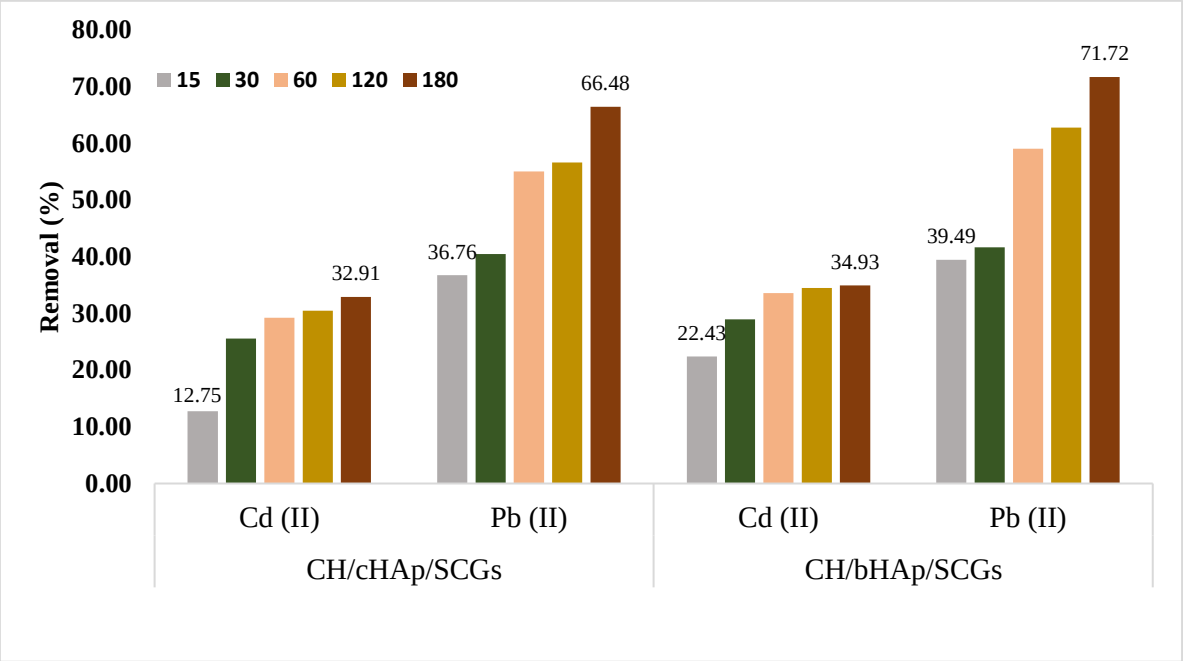

Figure 5-13: Graph showing the competitive removal (%) of Cd^{2+} and Pb^{2+} ions by 0.01 g doses of the CH/HAp/SCGs composites at contact times ranging from 15 minutes to 180 minutes.

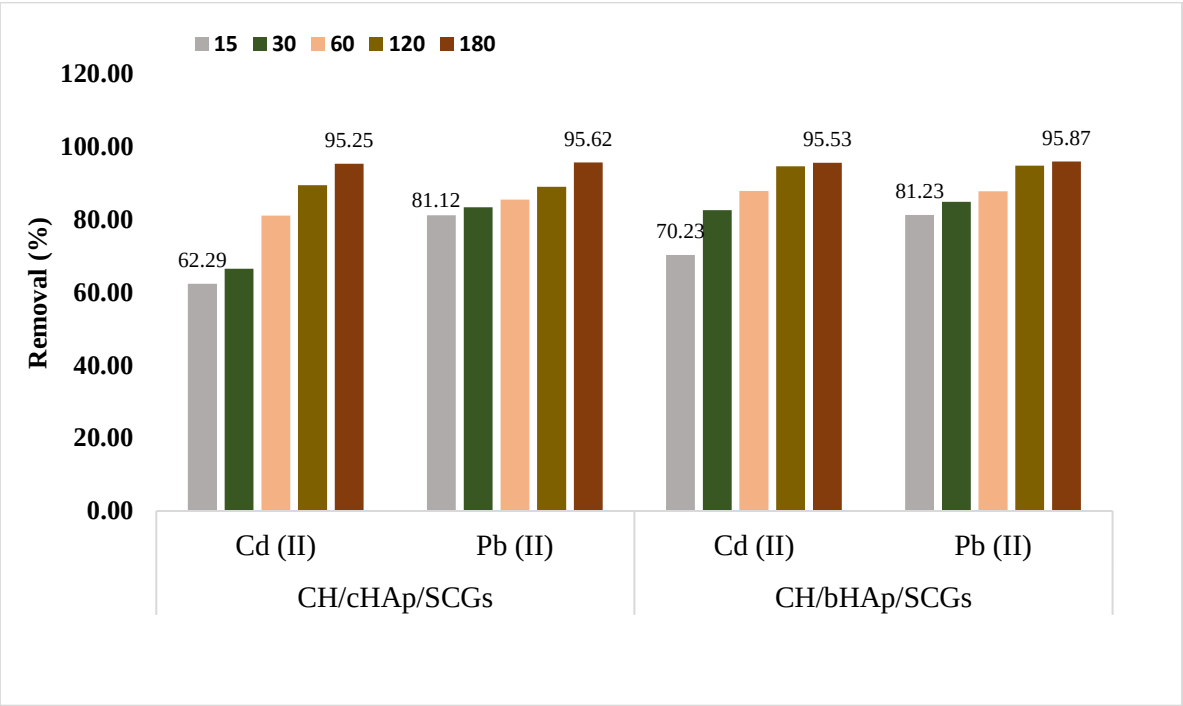

Figure 5-14: The competitive Cd^{2+} and Pb^{2+} removal (%) using 0.05 g of the CH/HAp/SCGs composites at contact times ranging from 15 minutes to 180 minutes.

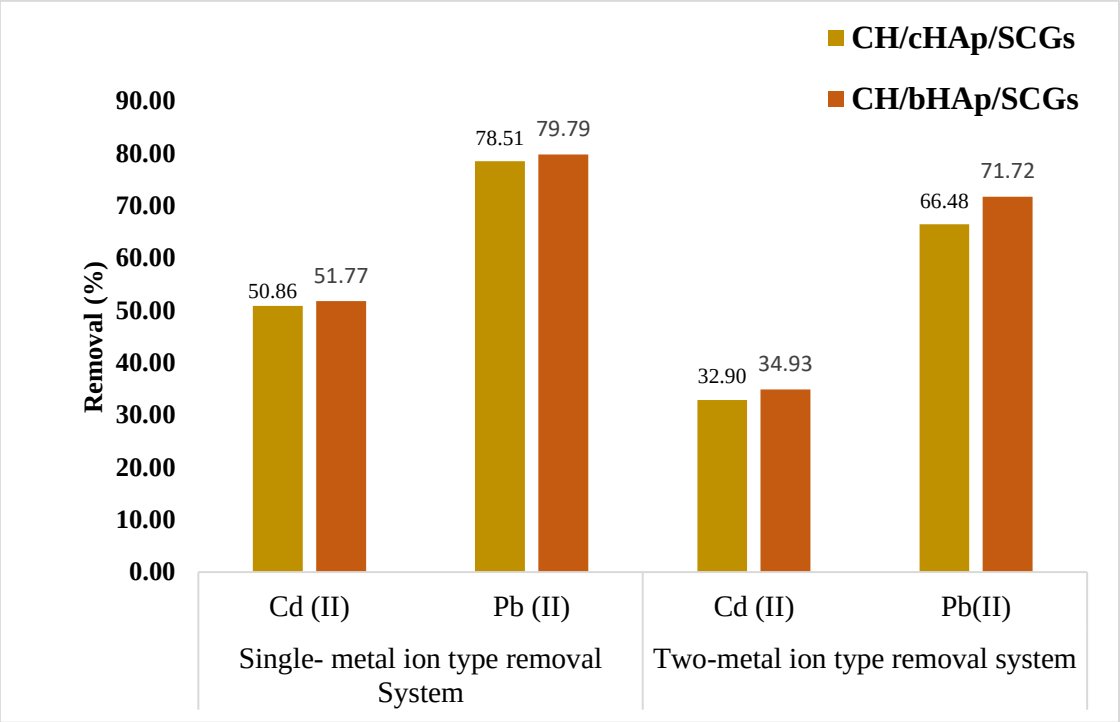

Figure 5-15: The comparison of single and two-metal ion type solution systems for Cd^{2+} and Pb^{2+} ions adsorption on 0.01 g of adsorbent dose of CH/HAp/SCGs composites

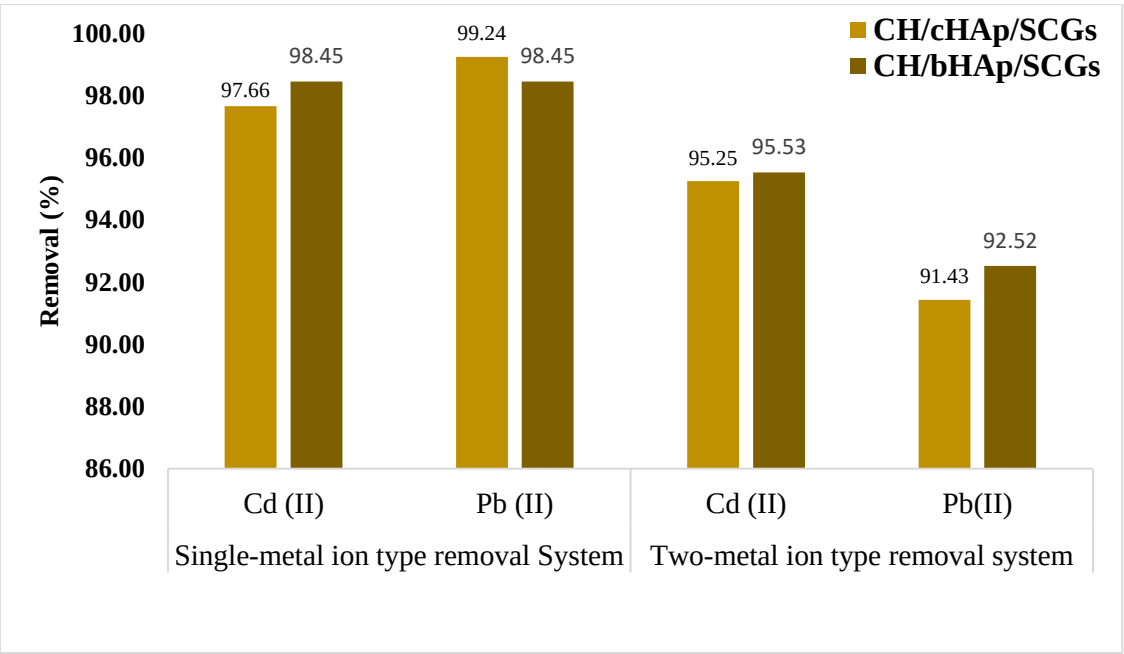

Figure 5-16: The comparison of one and two-metal ion type solution systems for Cd^{2+} and Pb^{2+} adsorption on 0.05 g of adsorbent dose of CH/HAp/SCGs composites

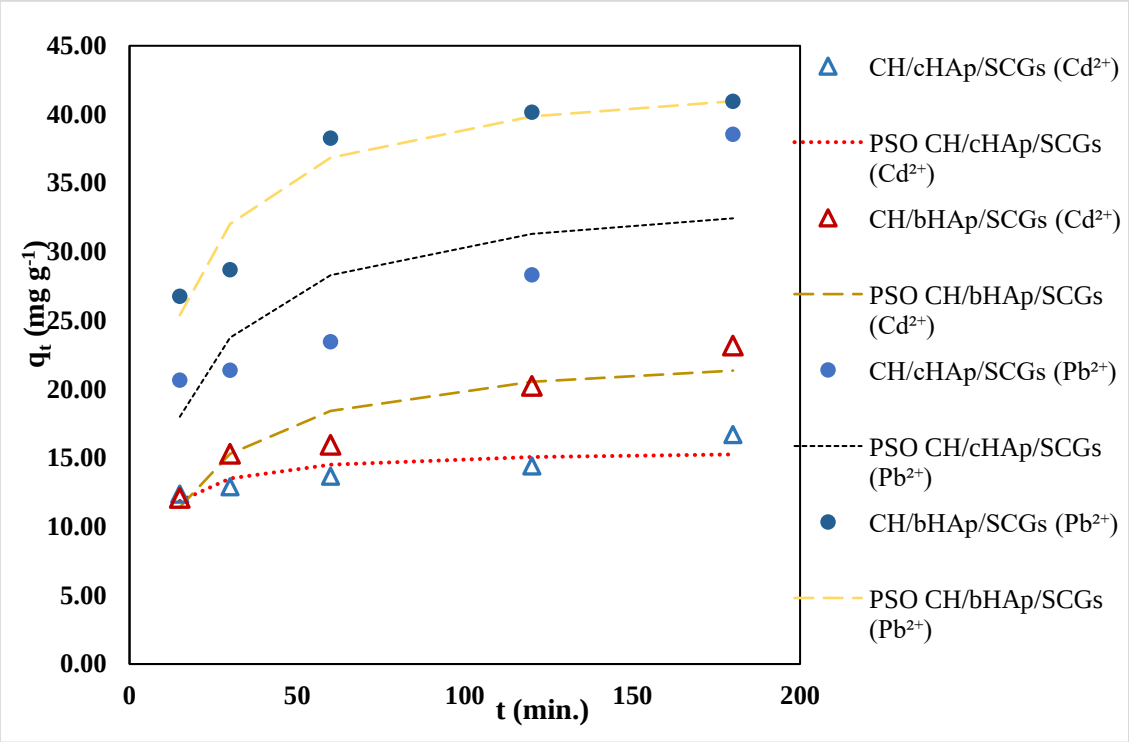

Figure 5-17: The fitting of the non-linear pseudo-second-order kinetic model to experimental (contact time) data relating to Cd^{2+} and Pb^{2+} competitive adsorption on the CH/HAp/SCGs composites for an adsorbent dose of 0.01 g

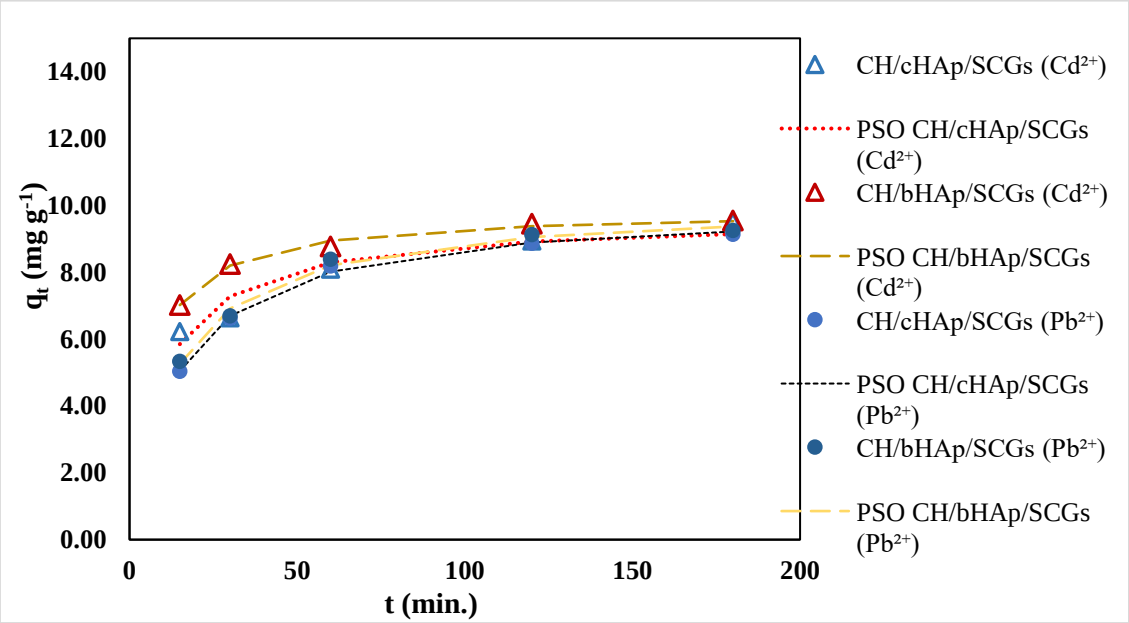

Figure 5-18: The fitting of the non-linear pseudo-second-order kinetic model to experimental (contact time) data relating to Cd^{2+} and Pb^{2+} competitive adsorption on the CH/HAp/SCGs composites on an adsorbent dose of 0.05 g

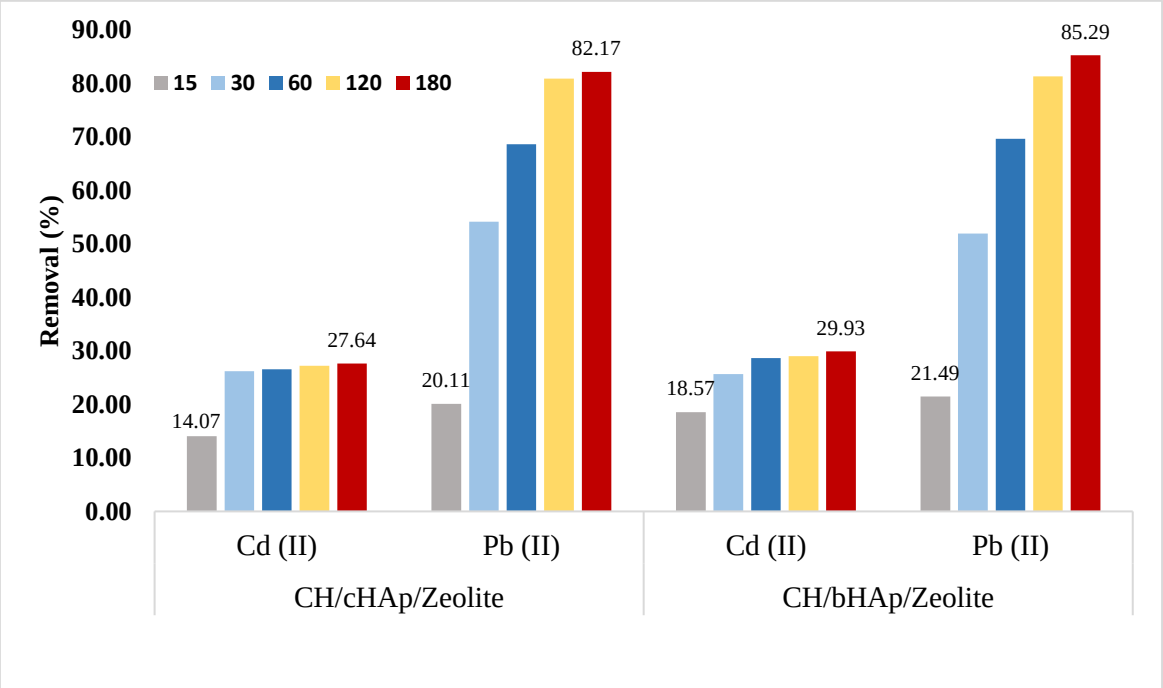

Figure 5-19: Graph showing the competitive removal (%) of Cd^{2+} and Pb^{2+} ions by 0.01 g doses of the CH/HAp/zeolite composites at contact times ranging from 15 minutes to 180 minutes.

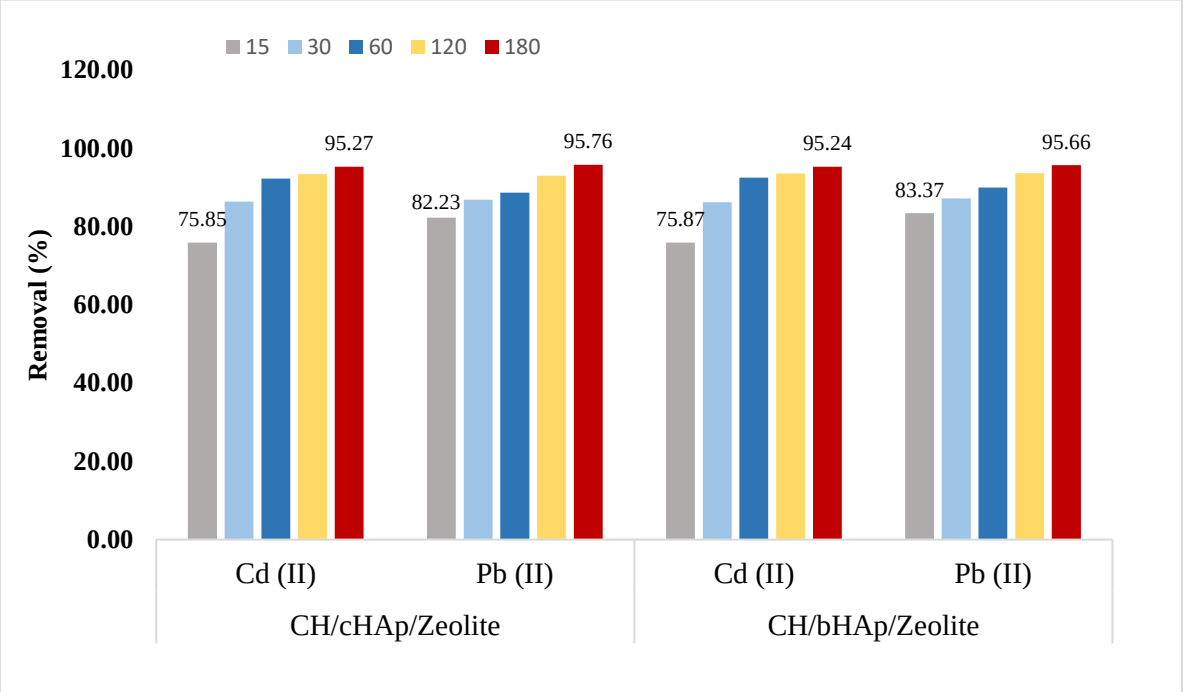

Figure 5-20: The competitive Cd^{2+} and Pb^{2+} removal (%) using 0.05 g of the CH/HAp/zeolite composites at contact times ranging from15 minutes to 180 minutes.

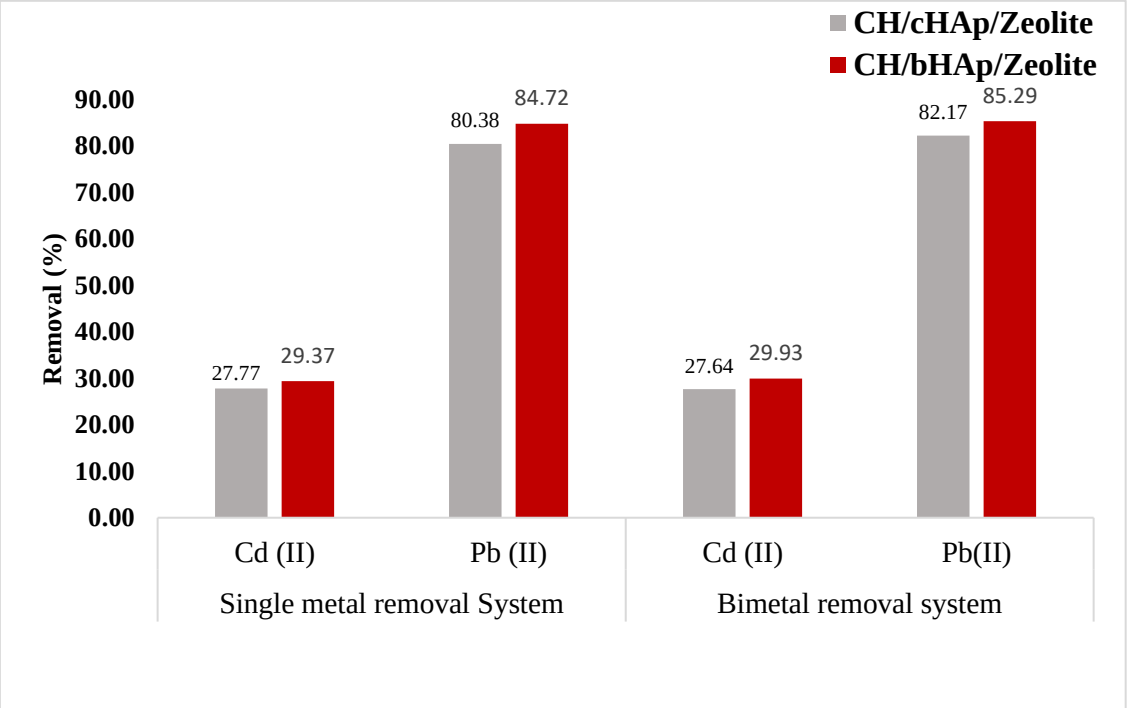

Figure 5-21: The comparison of the single and two-metal ion types removal systems for Cd^{2+} and Pb^{2+} ions adsorption on 0.01 g of adsorbent dose of CH/HAp/zeolite composites

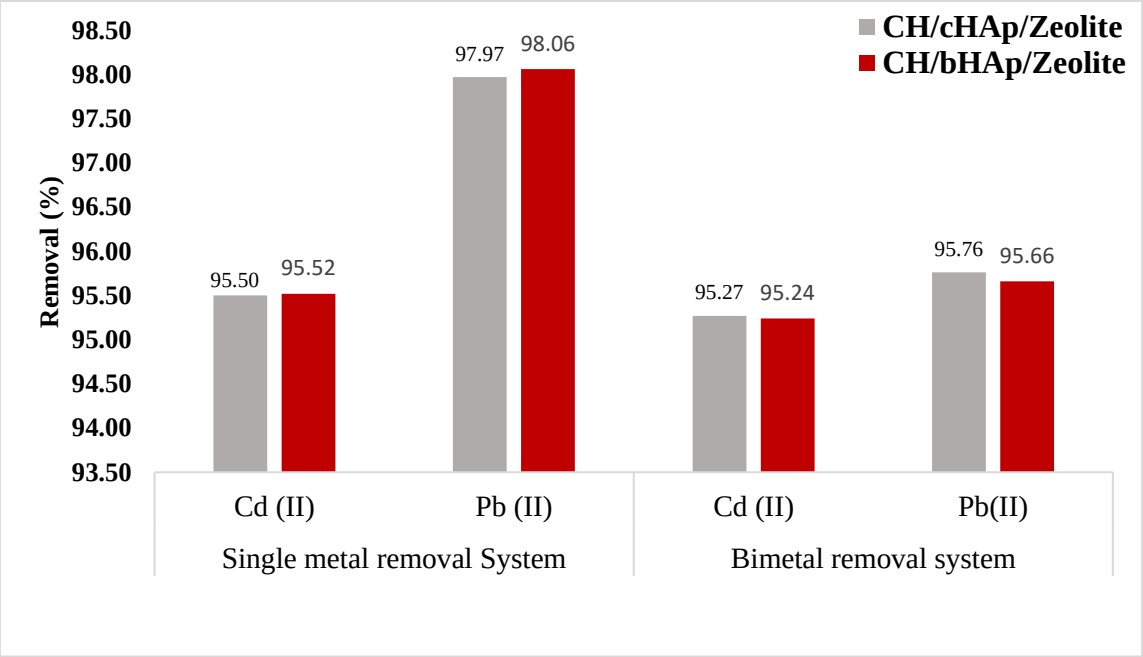

Figure 5-22: The comparison one-metal ion type and two-metal ion type solution systems for Cd^{2+} and Pb^{2+} adsorption on 0.05 g of adsorbent dose of CH/HAp/Zeolite composites

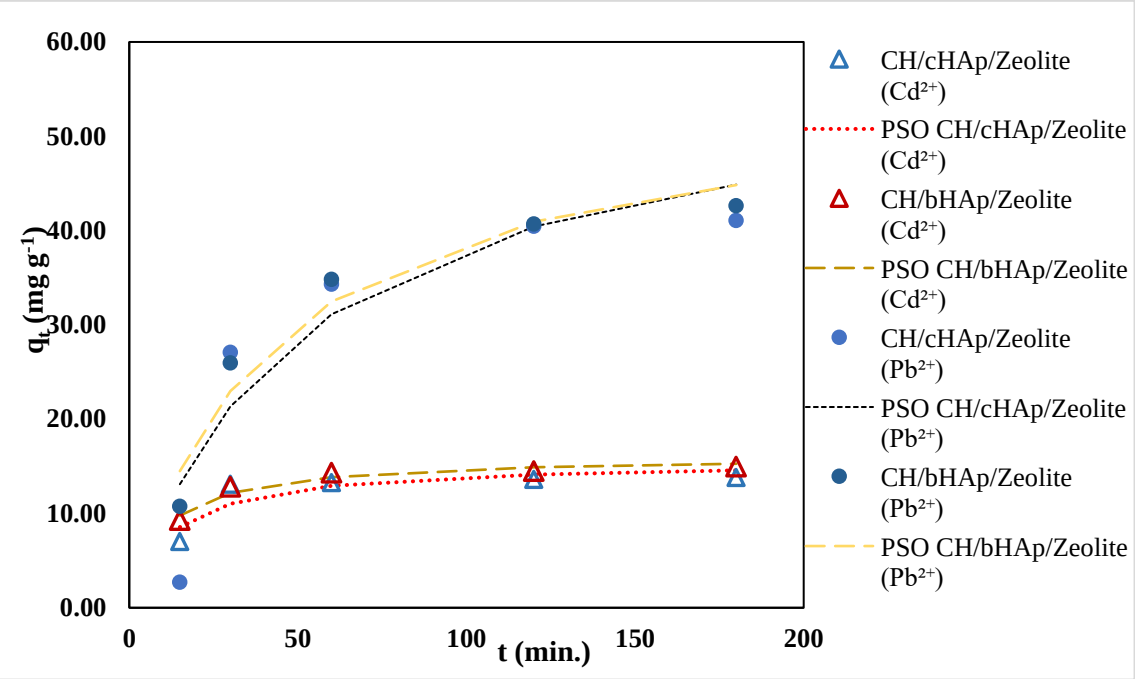

Figure 5-23: relating to Cd^{2+} and Pb^{2+} competitive adsorption on the CH/HAp/zeolite composites for an adsorbent dose of 0.01 g

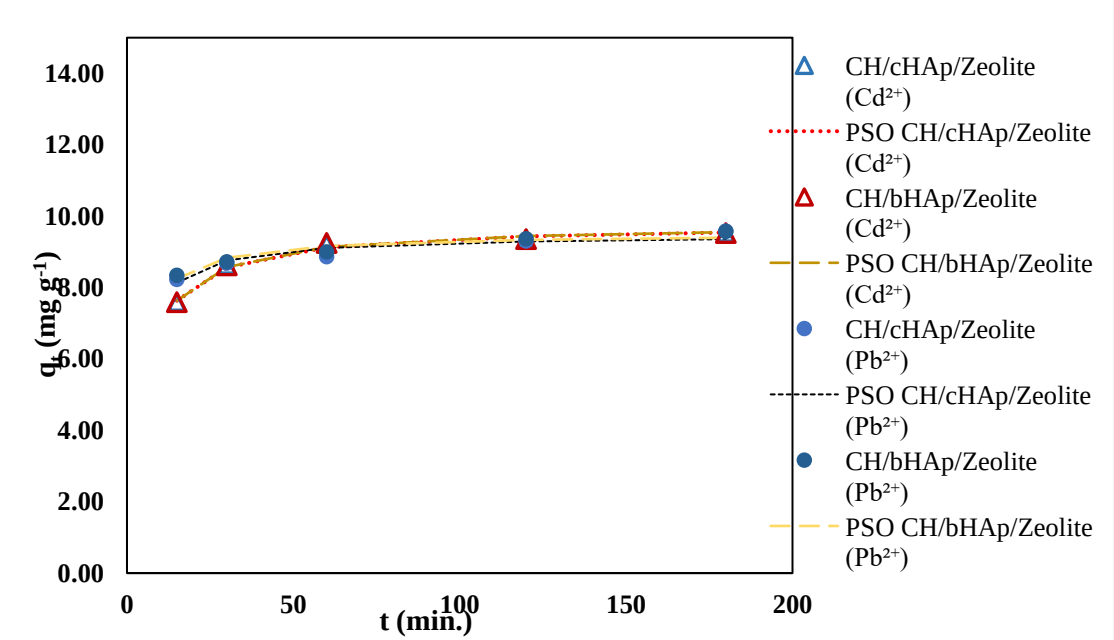

Figure 5-24: relating to Cd^{2+} and Pb^{2+} competitive adsorption on the CH/HAp/zeolite composites for an adsorbent dose of 0.05 g

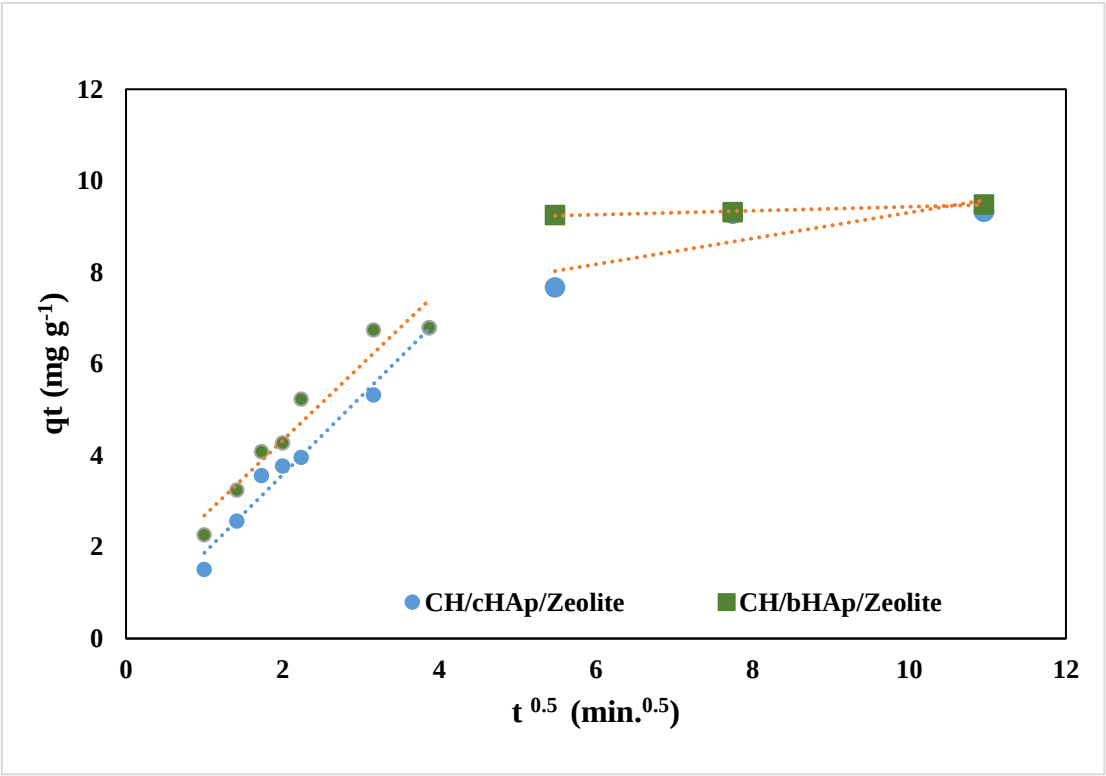

Figure 5-25 : The fitting of the intra-particle diffusion model (IPD) to the experimental data for Cu^{2+} adsorption on the CH/HAp/zeolite composites

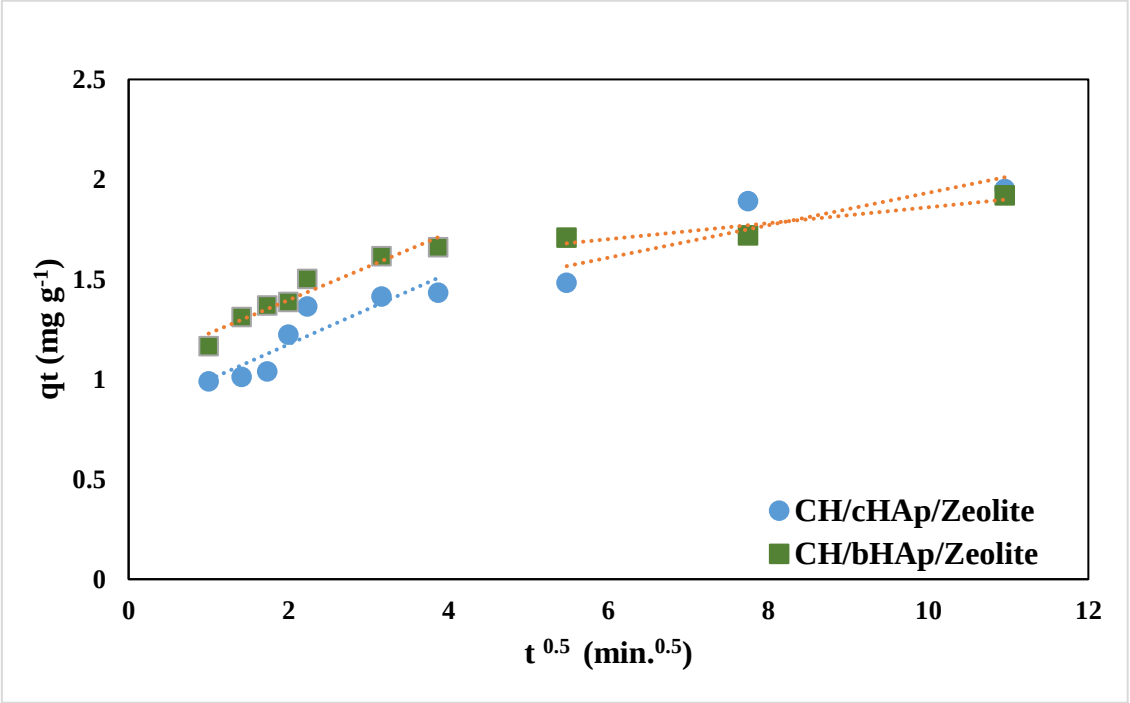

Figure 5-26: The fitting of the intra-particle diffusion model (IPD) to the experimental data for chromate ion adsorption on the CH/HAp/zeolite composites

Appendix 6:

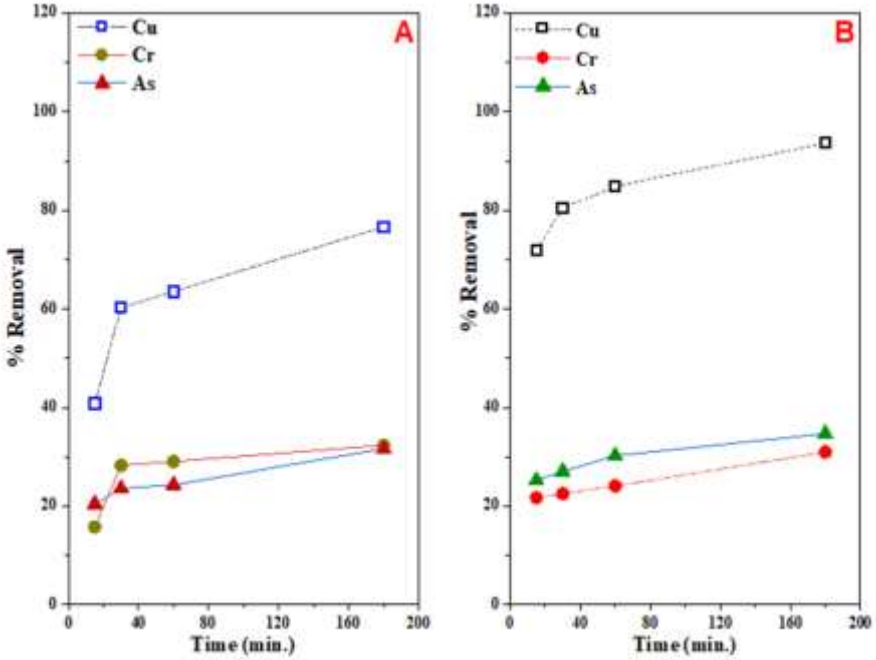

Figure 6-1: Simultaneous removal of Cu^{2+}, arsenate ion and chromate ion by the CH/HAp composites using 0.01 g adsorbent doses of (A) CH/cHAp composite and (B) CH/bHAp composites

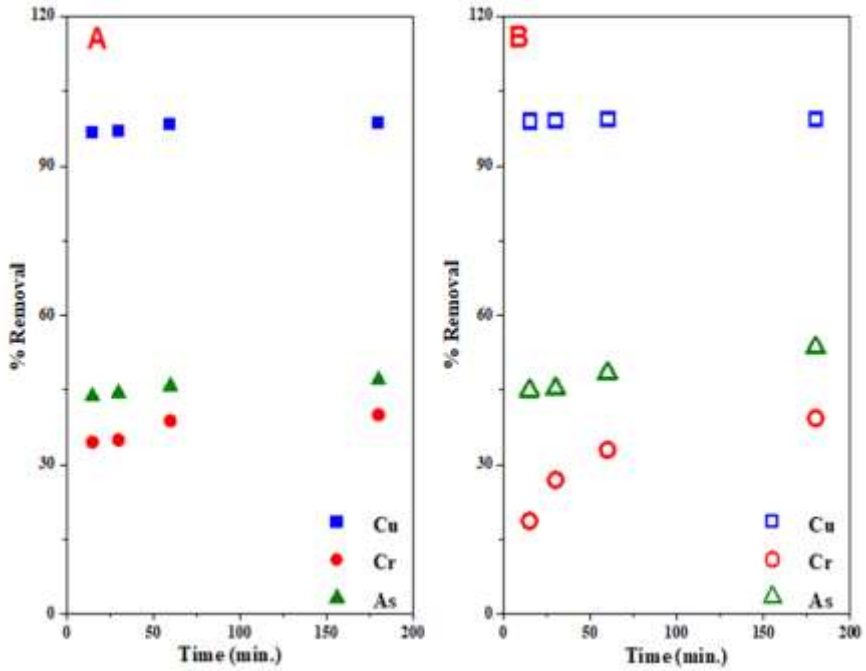

Figure 6-2: Simultaneous removal of Cu^{2+}, arsenate ion and chromate ion by the CH/HAp composites using 0.1 g adsorbent doses of (A) CH/cHAp composite and (B) CH/bHAp composites

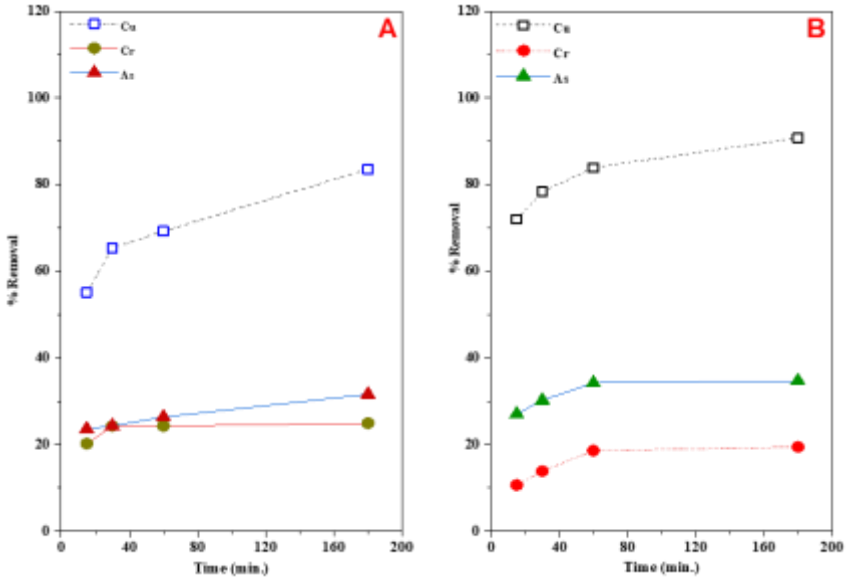

Figure 6-3: ICP-MS data showing the removal of Cu^{2+}, chromate ion and arsenate ion from an industrial input stream sample by the CH/HAp/CF composites for a 0.01 g dose of (A) CH/cHAp/CF composites and (B) CH/bHAp/CF composites (Contact time data).

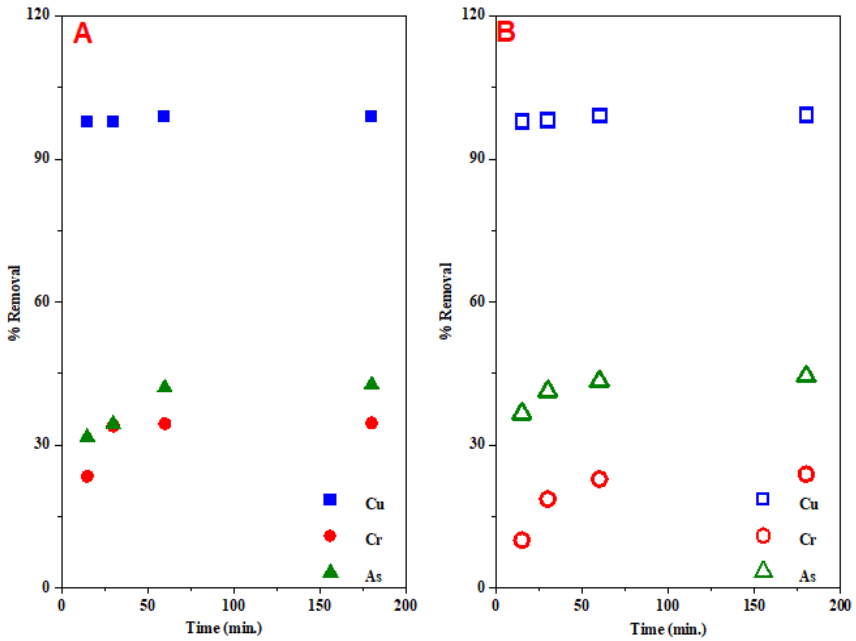

Figure 6-4: ICP-MS data showing the removal of Cu^{2+}, chromate ion and arsenate ion from an industrial input stream solution sample by the CH/HAp/CF composites for a 0.1 g dose of (A) CH/cHAp/CF and (B) CH/bHAp/CF (Contact time data).

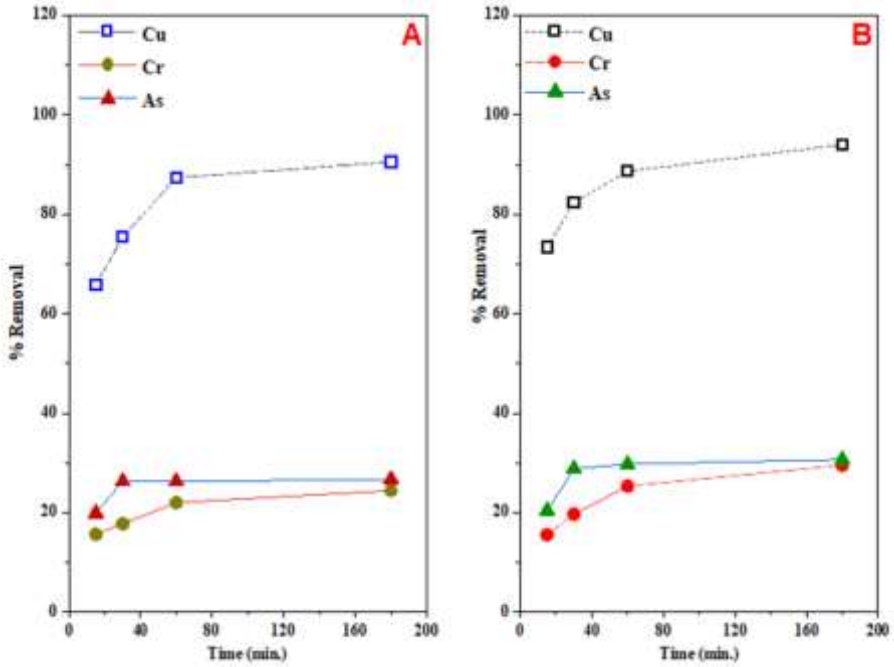

Figure 6-5: ICP-MS data for simultaneous removal of Cu^{2+}, arsenate and chromate ions by the CH/HAp/SCGs composites using 0.01 g adsorbent doses of (A) CH/cHAp/SCGs composite and (B) CH/bHAp/SCGs composites.

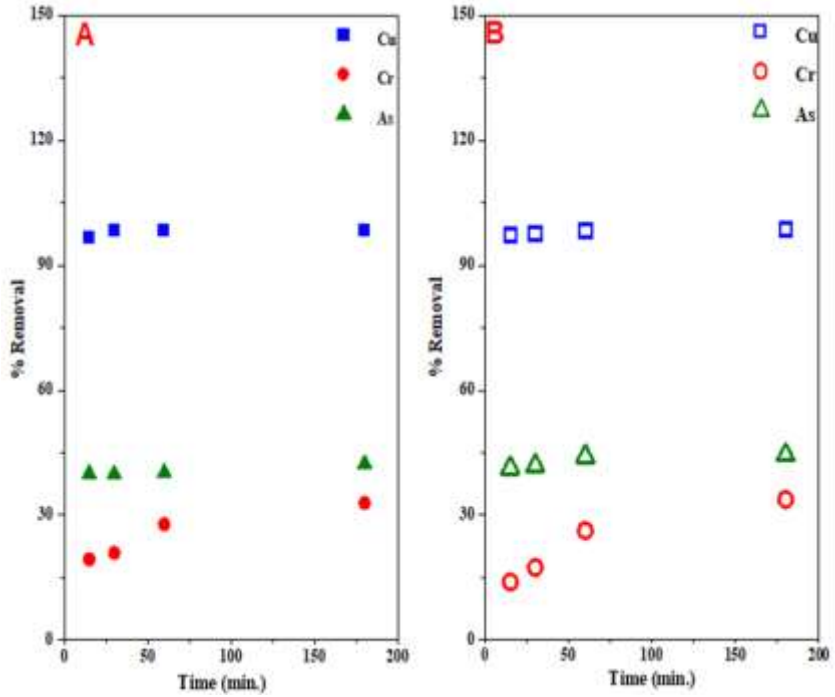

Figure 6-6: ICP-MS data showing simultaneous removal of Cu^{2+}, arsenate ion and chromate ion by the CH/HAp/SCGs composites using 0.1 g adsorbent doses of (A) CH/cHAp/SCGs composite and (B) CH/bHAp/SCGs composites.

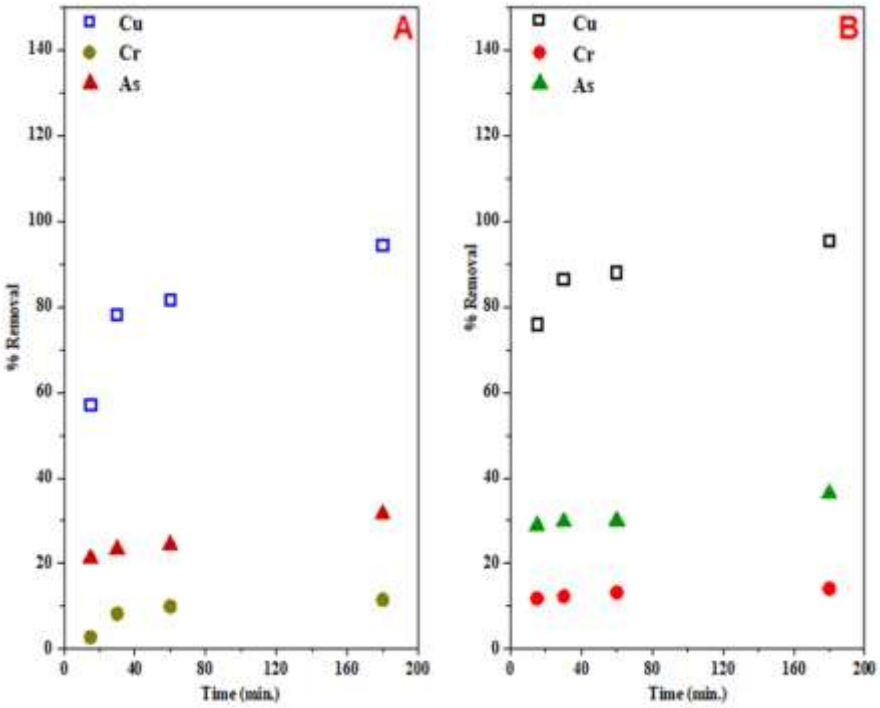

Figure 6-7: ICP-MS data for simultaneous removal of Cu^{2+}, arsenate and chromate ions by the CH/HAp/Zeolite composites using 0.01 g adsorbent doses of (A) CH/cHAp/Zeolite composite and (B) CH/bHAp/Zeolite composites.

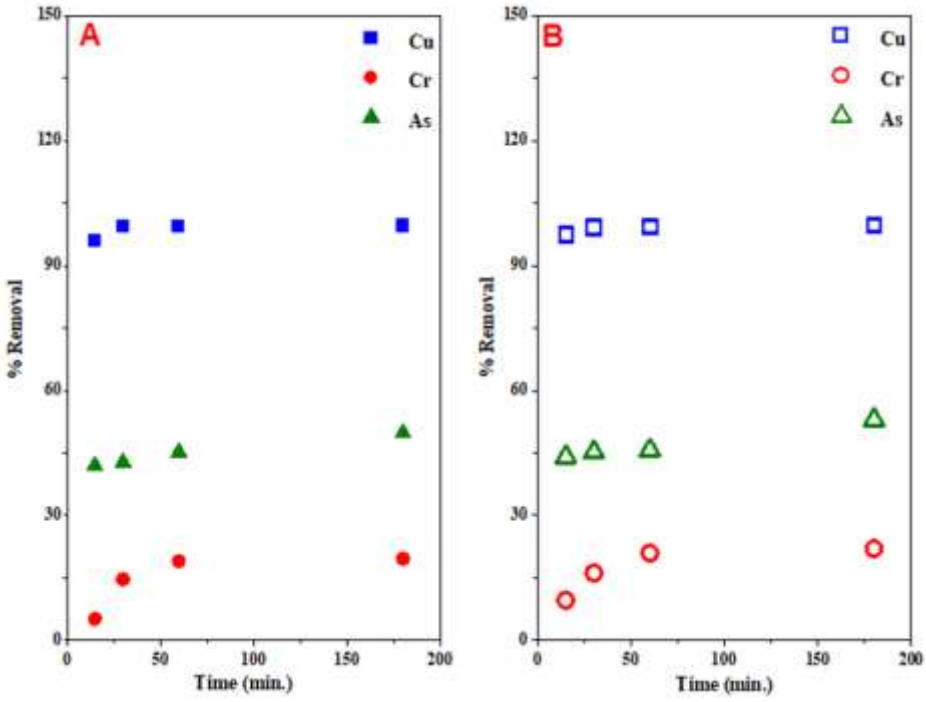

Figure 6-8: ICP-MS data showing simultaneous removal of Cu^{2+}, arsenate ion and chromate ion by the CH/HAp/Zeolite composites using 0.1 g adsorbent doses of (A) CH/cHAp/zeolite composite and (B) CH/bHAp/zeolite composites

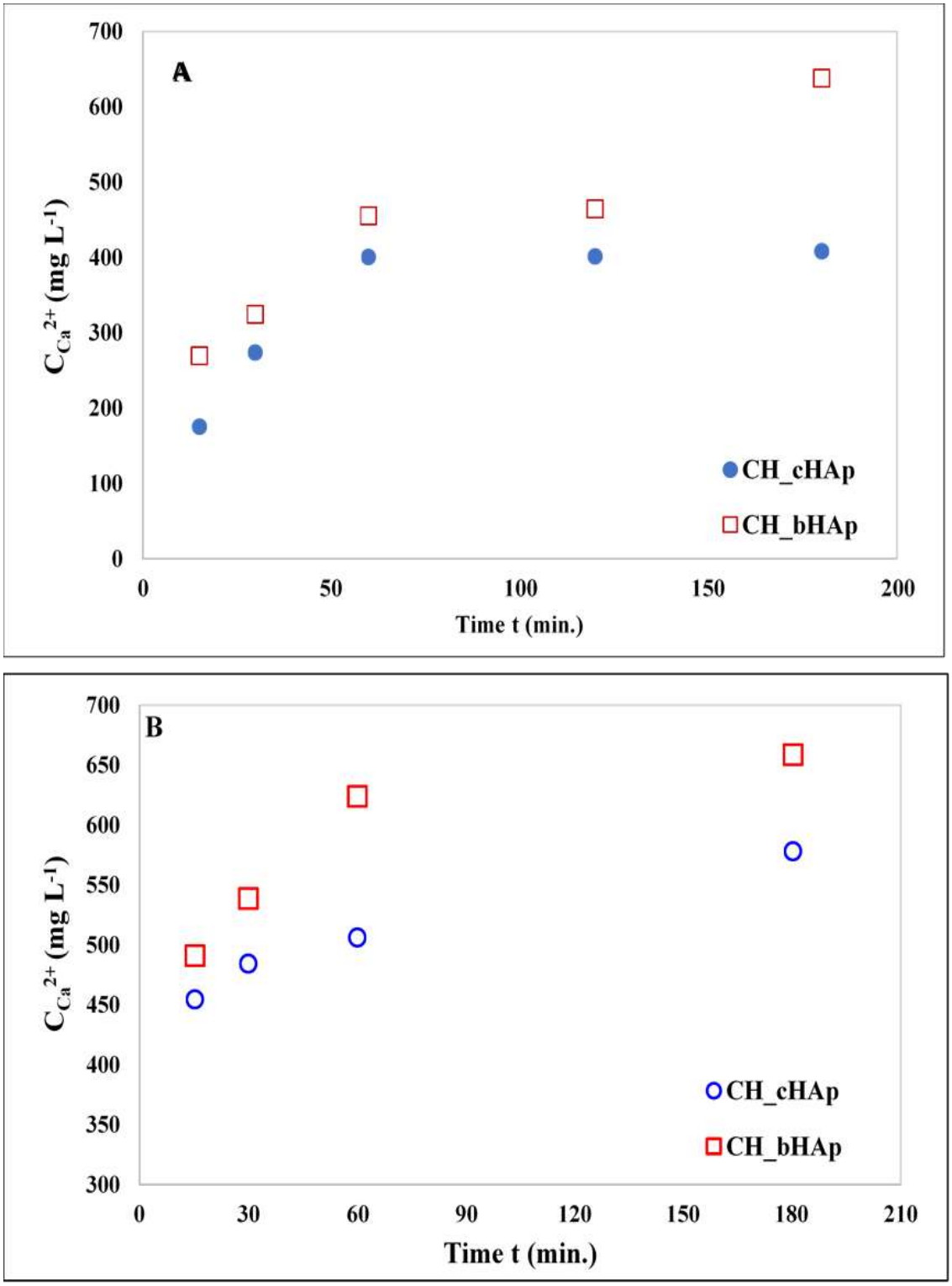

Figure 6-9: The concentration of Ca^{2+} ions analysed by ICP-MS in an industrial input stream sample during its exposure to (A) 0.01 g and (B) 0.1 g of the CH/HAp composites

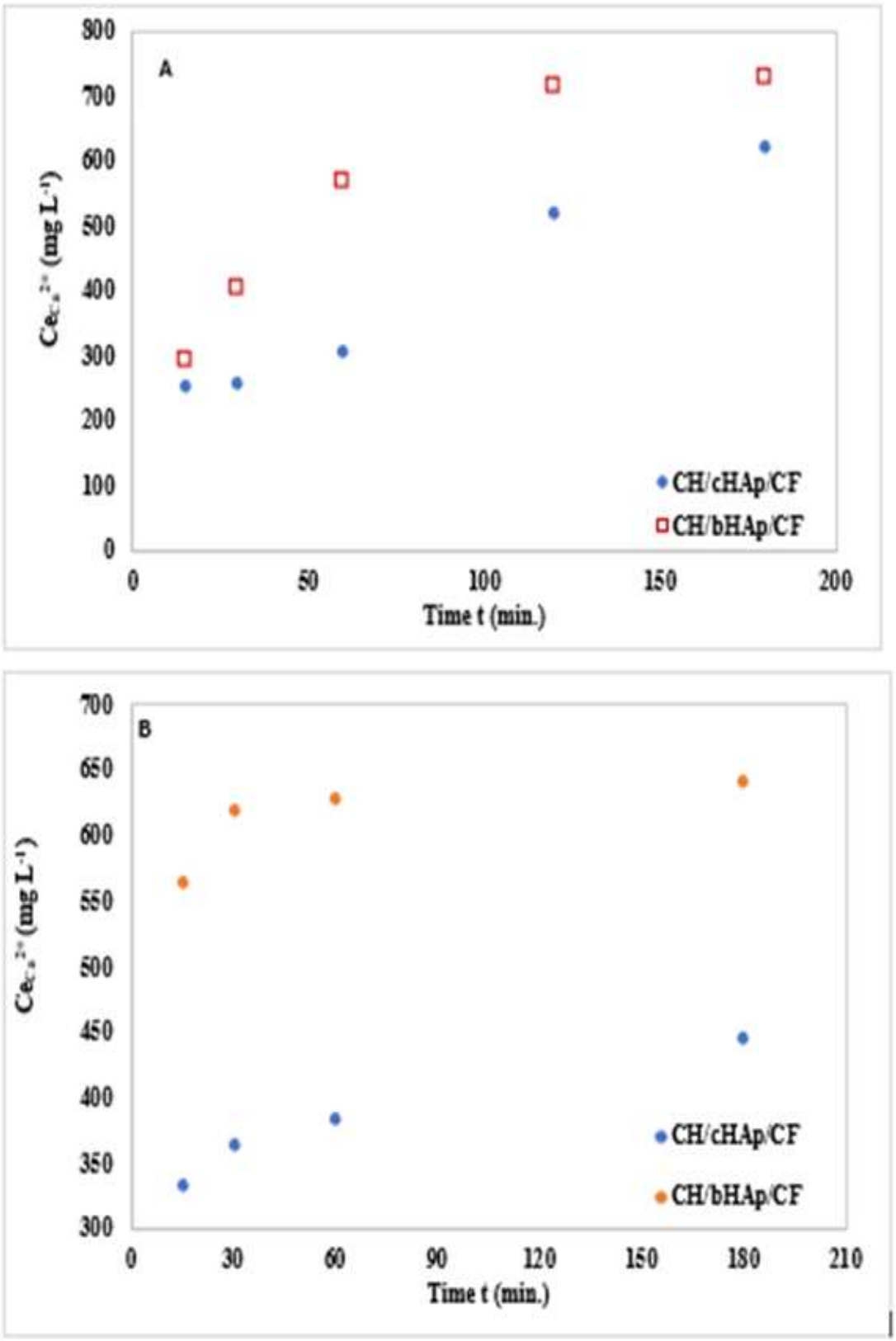

Figure 6-10: The concentration of Ca^{2+} ions analysed by ICP-MS in an industrial input stream during its exposure to (A) 0.01 g and (B) 0.1 g doses of the CH/HAp/CF composites

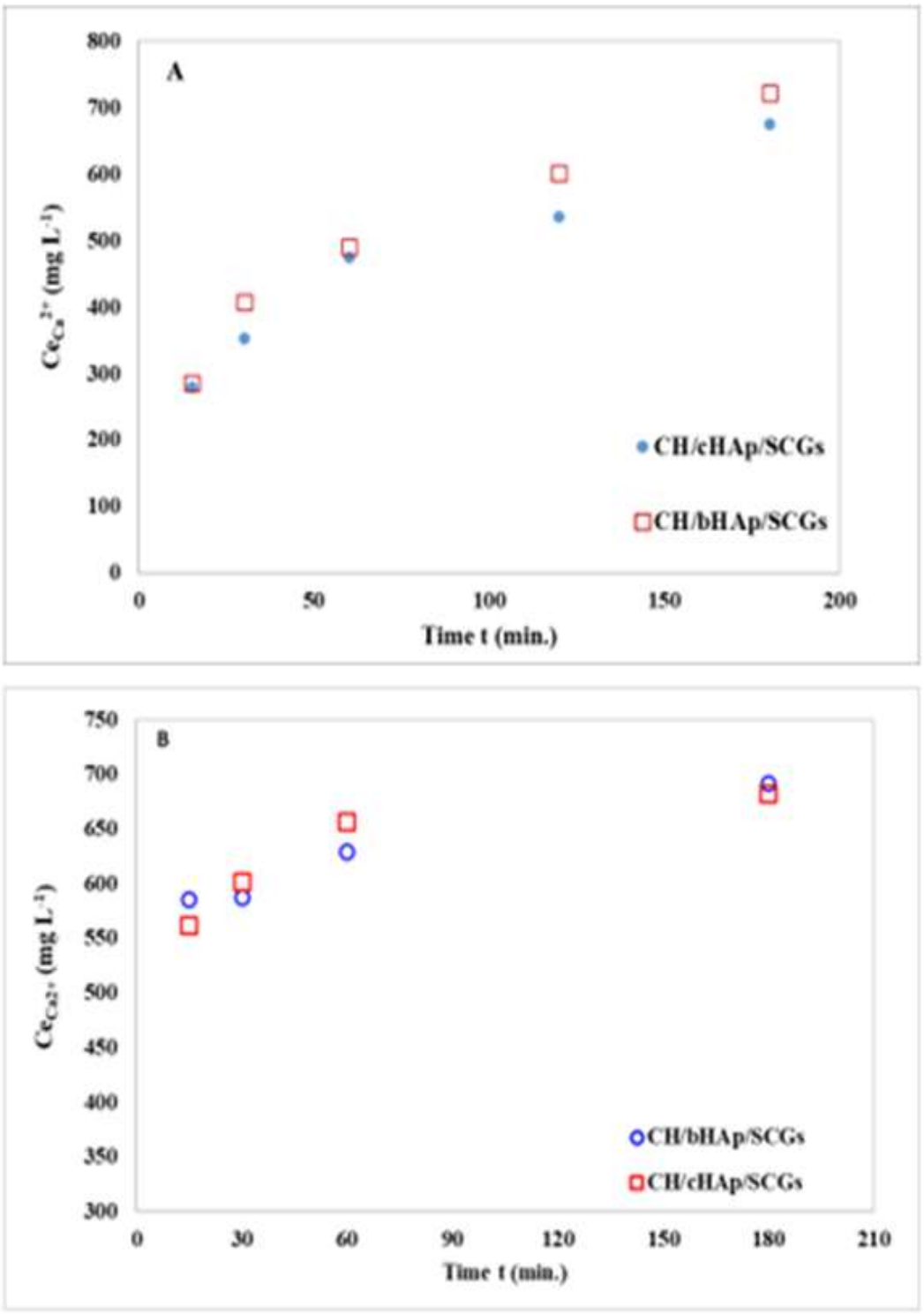

Figure 6-11: The concentration of Ca^{2+} ions analysed by ICP-MS in an industrial input stream solution during its exposure to (A) 0.01 g and (B) 0.1 g doses of the CH/HAp/SCGs composites

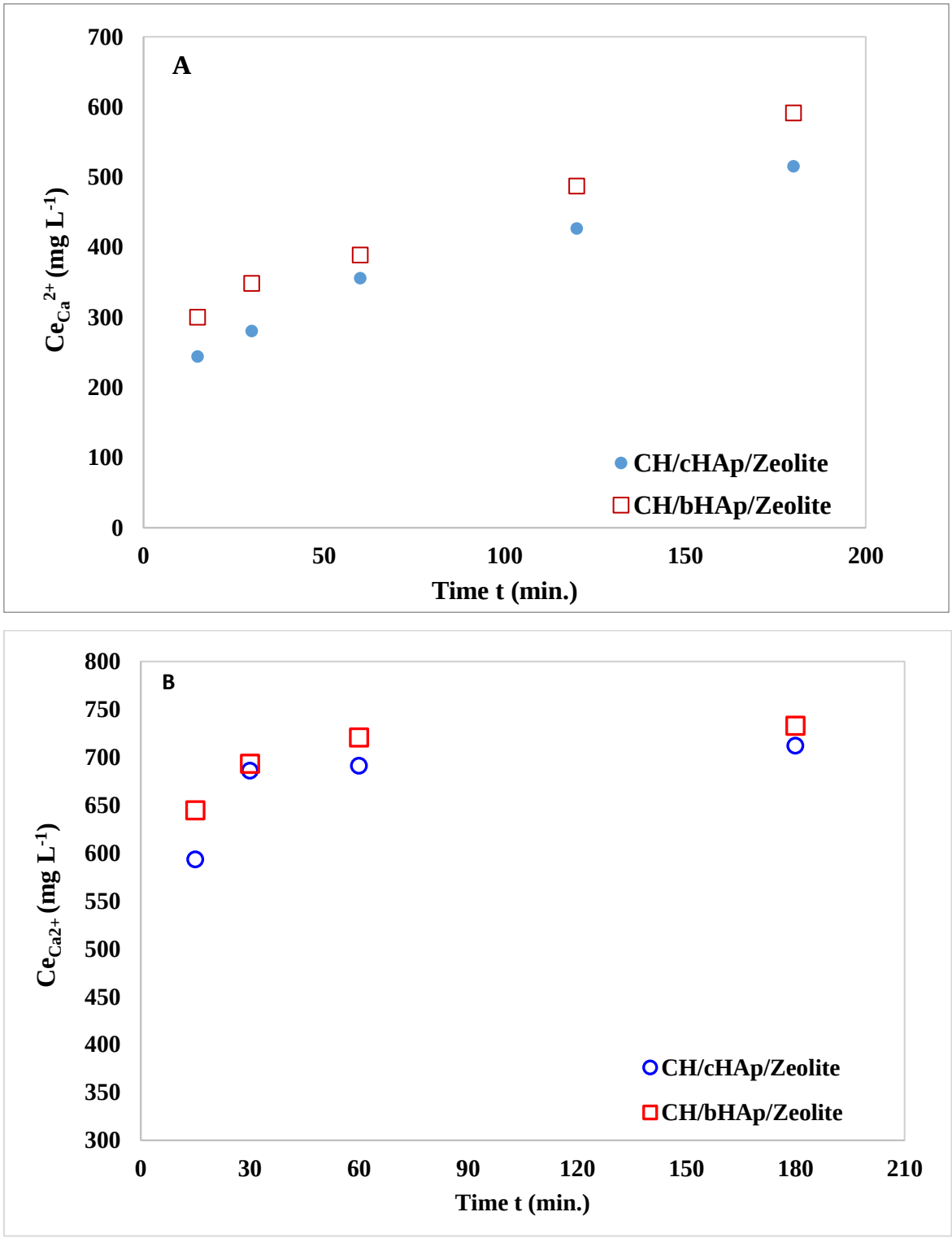

Figure 6-12: The concentration of Ca^{2+} ions analysed by ICP-MS in an industrial input stream during its exposure to (A) 0.01 g and (B) 0.1 g doses of the CH/HAp/zeolite composites

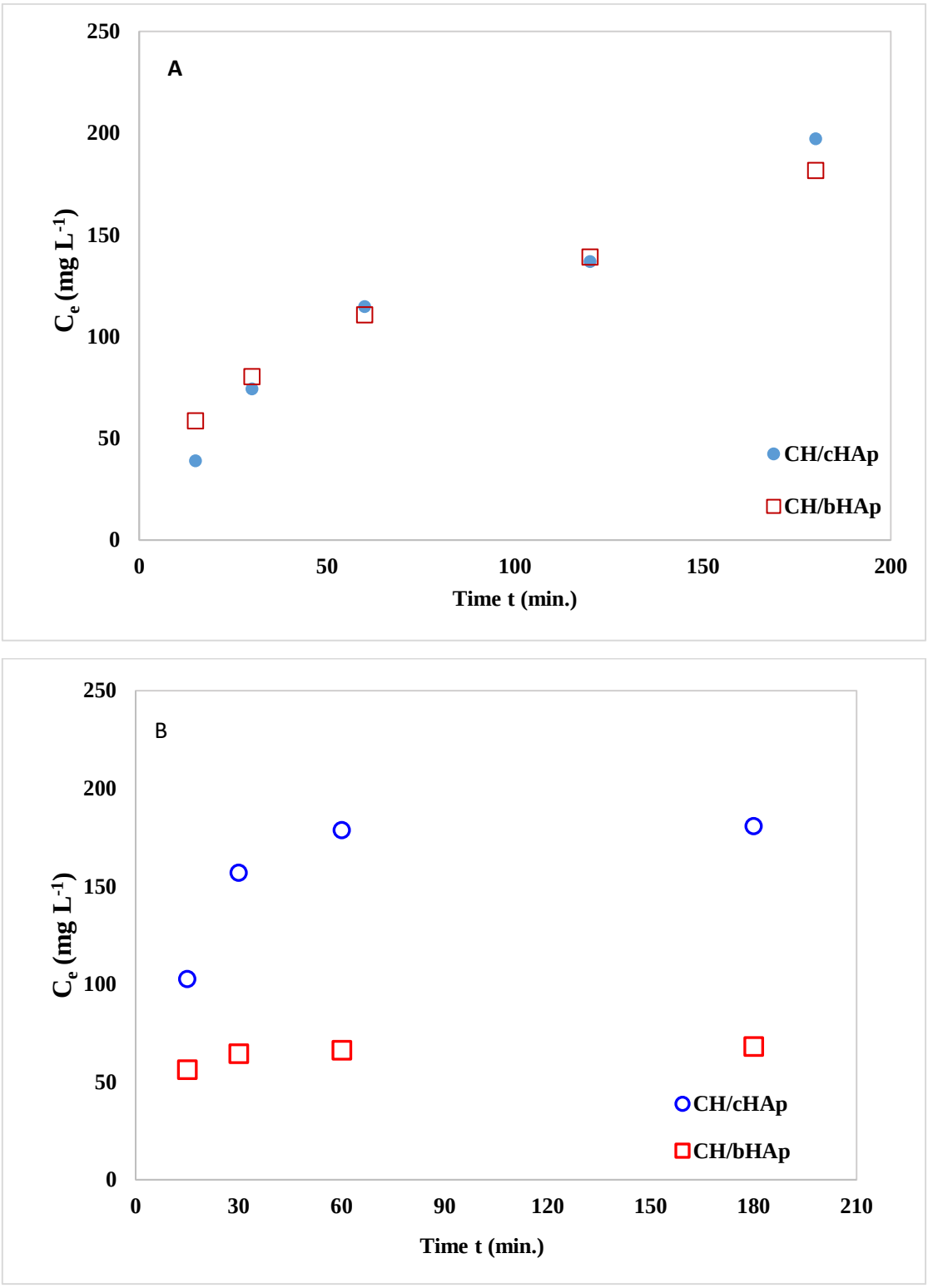

Figure 6-13: The concentration of phosphorus as analysed using ICP-MS in the industrial input stream solution exposed to the CH/HAp composites at doses of (A) 0.01 g (B) 0.1 g

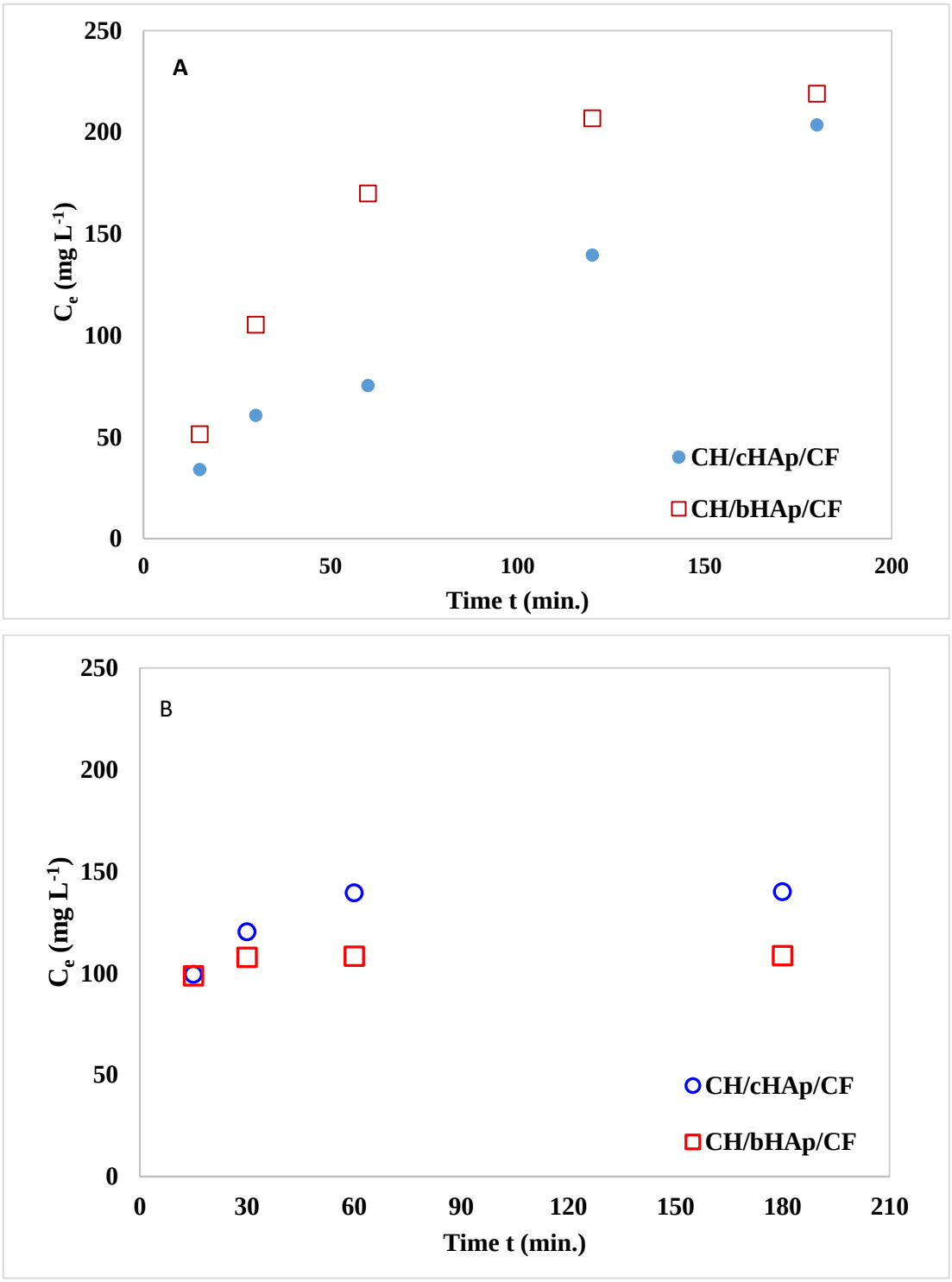

Figure 6-14: The concentration of phosphorus as analysed using ICP-MS in the industrial input stream solution exposed to the CH/HAp/CF composites at (A) 0.01 g, (B) 0.1 g of adsorbent doses

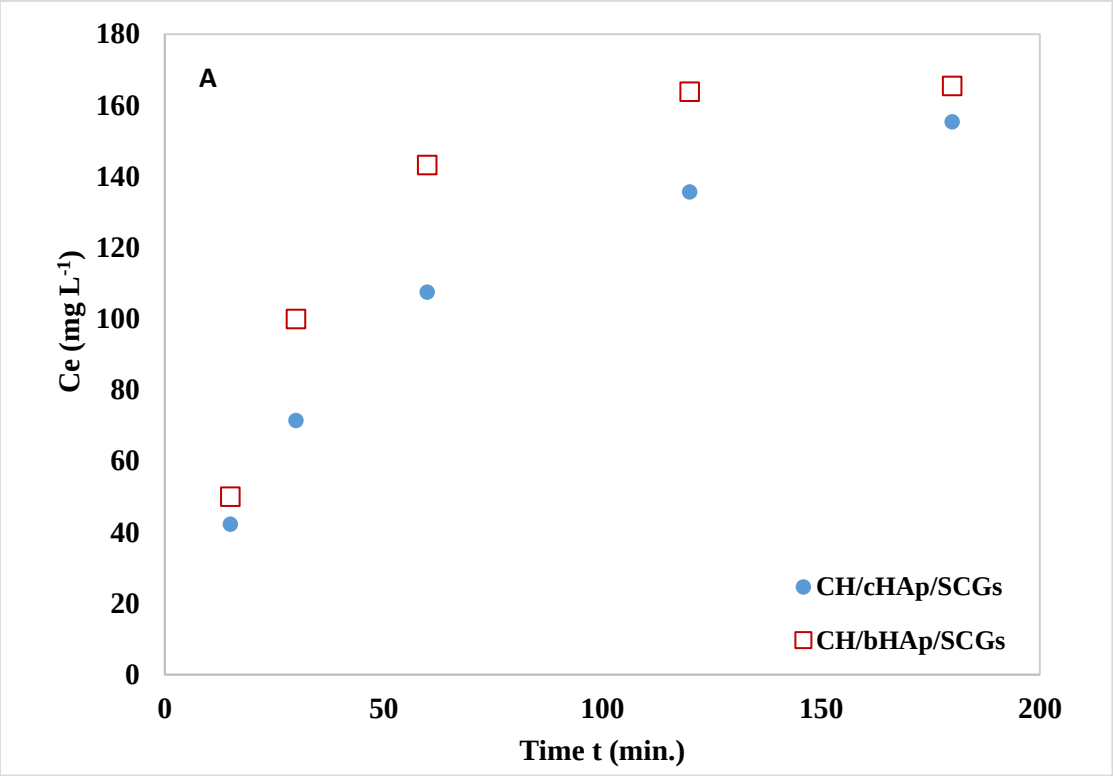

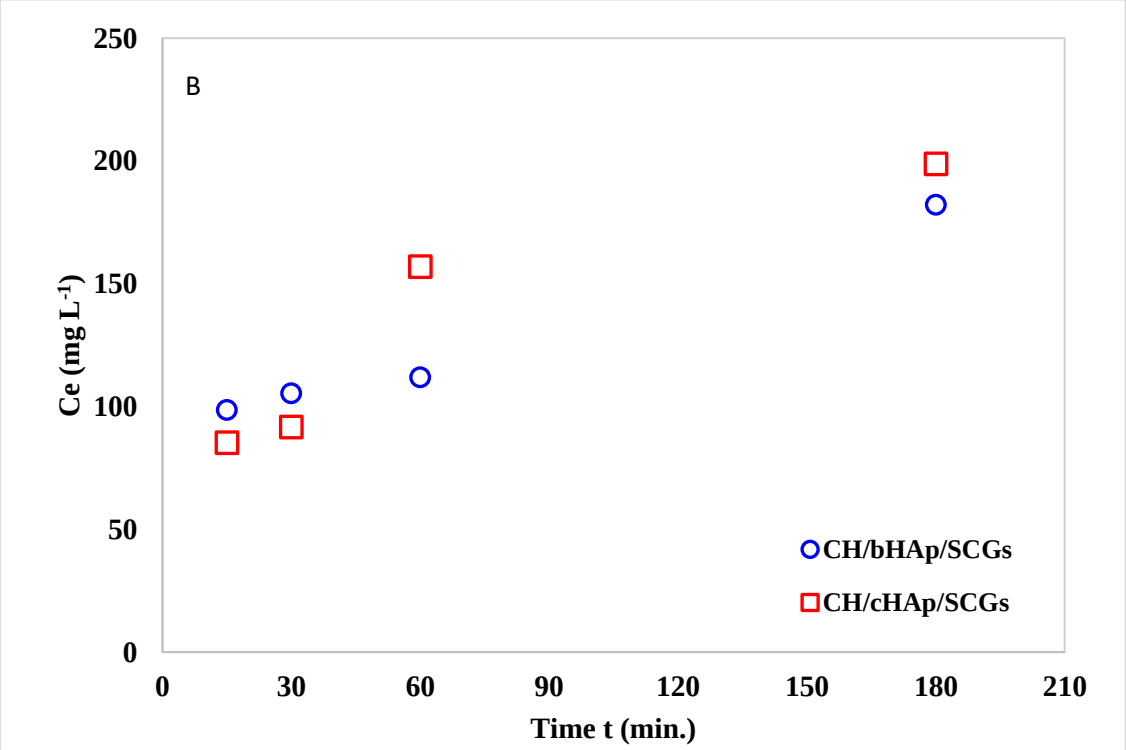

Figure 6-15: The concentration of phosphorus as analysed using ICP-MS in the industrial input stream solution exposed to the CH/HAp/SCGs composites at (A) 0.01 g, (B) 0.1 g of adsorbent doses

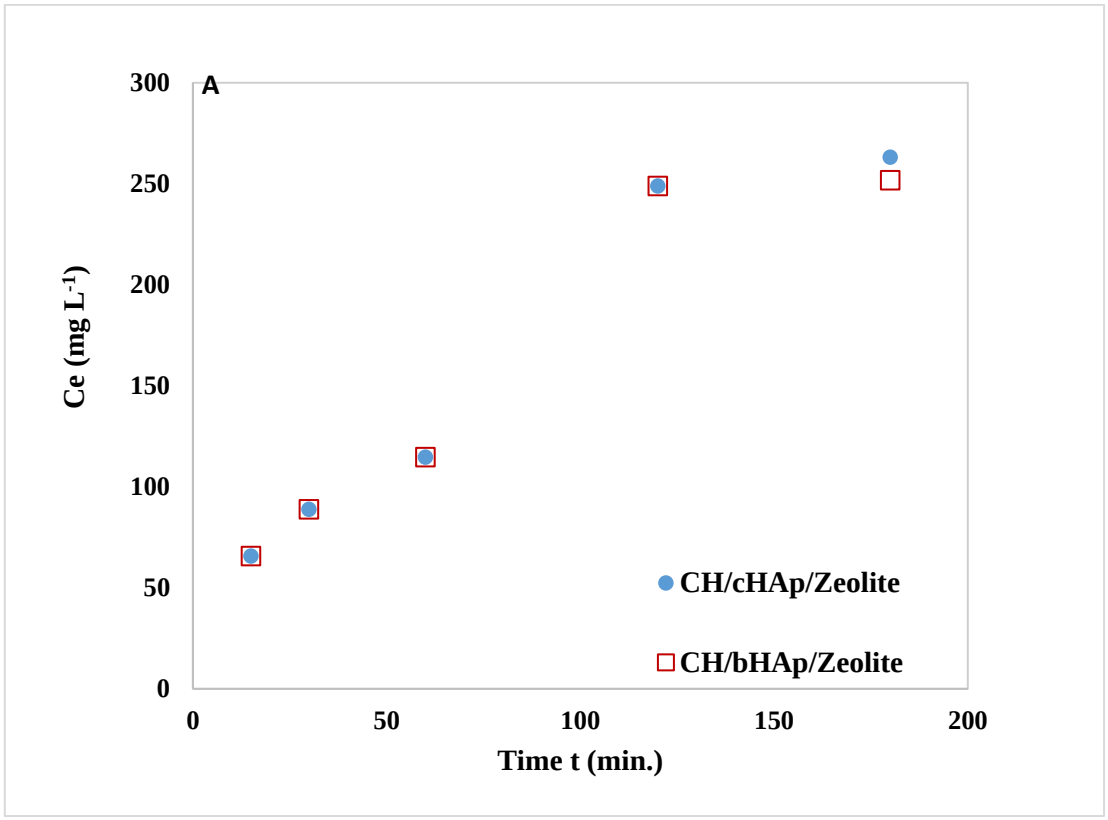

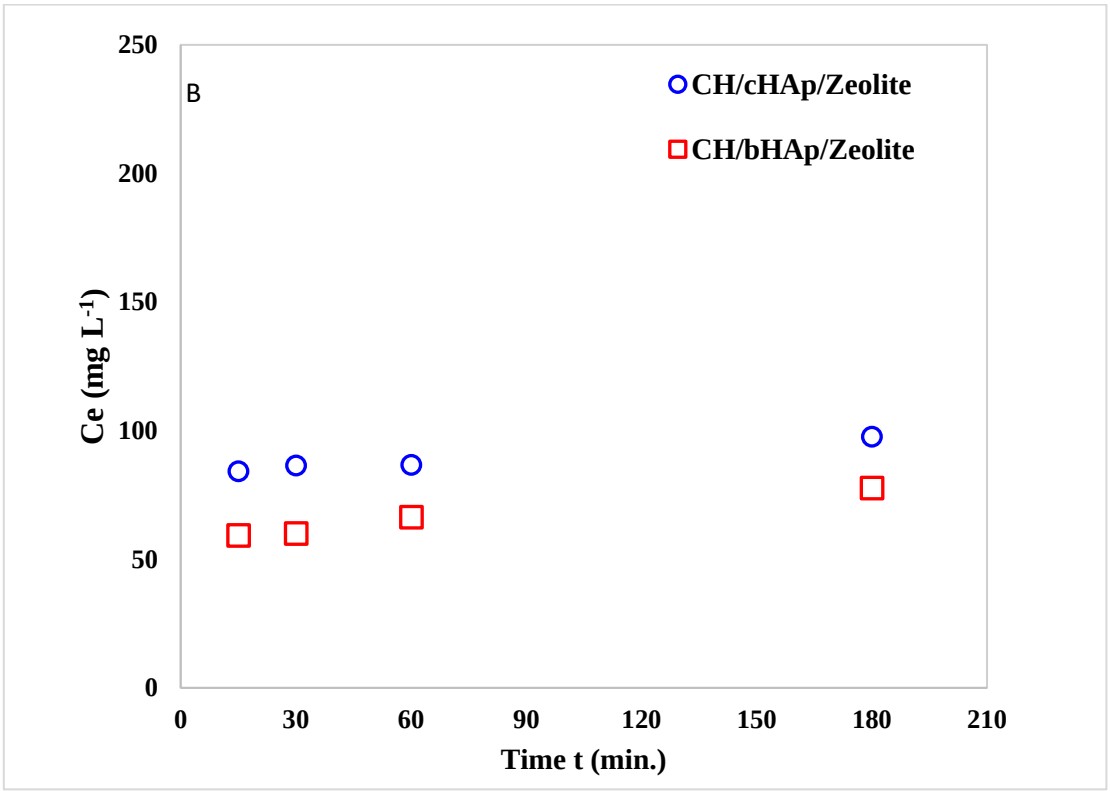

Figure 6-16: The concentration of phosphorus as analysed using ICP-MS in the industrial input stream solution exposed to the CH/HAp/zeolite composites at (A) 0.01 g, (B) 0.1 g of adsorbent doses.

Table: 6.1: The isotopic concentrations of the elements recorded by ICP-MS analysis in industrial input stream water sample before the exposure to the composite systems

Elements	C_o (ppm)	Elemental isotope	C_o (ppm)	Elemental isotope	C_o (ppm)	Metal ions	C_o (ppm)
11 B	1.67	^{56}Fe	5.21	$^{31\text{-}47}$P	32.65	$^{75\text{ -}91}$ As [$N_2O + H_2$]	1663.421
23 Na	9425.75	^{59}Co	0.89	$^{34\text{-}50}$S	96.33	^{111}Cd	4.91
24 Mg	51.39	^{60}Ni	2.30	^{51}V	20.30	^{137}Ba	17.04
27 Al	66.78	^{63}Cu	999.81	^{52}Cr	1682.61	^{206}Pb	94.68
39 K	261.67	^{65}Cu	979.83	^{53}Cr	1620.97	^{207}Pb	87.50
43 Ca	242.14	^{66}Zn	230.40	^{55}Mn	3.33	^{208}Pb	88.69
44 Ca	277.96	^{68}Zn	219.27	^{107}Ag	200.93		